A Study of the Feasibility of Connecting Large Offshore Wind Turbines in Electrical Clusters

Douglas W Elliott

2014

Doctor of Philosophy

Centre for Doctoral Training in Wind Energy Systems

Department of Electronic and Electrical Engineering

University of Strathclyde

This thesis is the result of the author's original research. It has been composed by the author and has not been previously submitted for examination which has led to the award of a degree.

Signed:

Date:

Acknowledgements

I would like to thank Professor Stephen Finney for his supervision and guidance throughout this work and also the Directors of the Centre for Doctoral Training in Wind Energy Systems, Professor Bill Leithead and Professor David Infield, who gave me the opportunity to conduct this research. In addition I would like to extend my thanks to Charles Croser for his guidance while developing the laboratory test rig.

This work was funded by the EPSRC, grant number EP/G037728/1.

I have enjoyed my time in the CDT for Wind Energy Systems tremendously and for that I have to thank my fellow PhD students, in particular the class of 2009. Also I am very grateful for the help, advice and chat of Drew Smith without whom the CDT would not operate. Cheers lads...it's been a ball!

Last, but not least, I would like to thank Mhairi for her continued support and understanding for the long hours that I have devoted to this work that I should have been spending with you...fancy a holiday?

Abstract

A comprehensive study of the motivation and methods of implementing electrical clusters of up to five wind turbines is presented. The merits and pitfalls of three potential technologies for implementing such clusters are investigated through the extensive simulation of each, from which it is concluded that passively rectifying the outputs of PM generators and connecting them in parallel, using a multi-terminal DC collection network, is the preferred option; allowing a degree of independence to occur between the turbines, whilst maintaining a high energy transfer efficiency. The process of generator output rectification is investigated thoroughly, demonstrating that the distortion of the generator terminal voltages allows the generator speeds to slip by up to 33% from the cluster synchronous speed (derived from the cluster common point voltage). The maximisation of the rectifier commutation overlap length to increase the generator slip capability is demonstrated to reduce the generator power factor, but also reduce the winding current and torque total harmonic distortion at maximum power output. In addition it is found that the use of the commutation overlap voltage distortion to provide generator slip, allows a significant energy transfer efficiency benefit to be achieved over the use of additional resistance for the same purpose. The resulting generator slip capability is proven to benefit the energy capture efficiency of the clustered turbines and also provide sufficient damping of the wind turbine drive-train natural oscillations. The operation of the system and the capability of the wind turbine rotational speeds to slip from the cluster synchronous speed are verified experimentally using a bench scale test-rig, incorporating two small wind turbine generators.

Table of Contents

Table of Figures

Abbreviations and symbols

Abbreviations		General Symbols	
AC	Alternating current	ΔT	Temperature differential [°]
Cp	Power Coefficient	AEP	Annual energy production [Wh]
CSC	Current source converter	a_n	nth harmonic Fourier series sine term coefficients
D1	Diode 1	b_n	nth harmonic Fourier series cosine term coefficients
D2	Diode 2	C	Capacitance [F]
D3	Diode 3	$C_{chopper}$	Chopper capacitance [F]
D4	Diode 4	C_{pmax}	Maximum power coefficient
D5	Diode 5	C_{snub}	Snubber capacitance [F]
DC	Direct Current	D	Modulation index
DFIG	Double-fed induction generator	E	Emf magnitude [V]
HV	High voltage	E_a	Phase A emf [V]
HVDC	High voltage direct Current	E_b	Phase B emf [V]
IG	Induction generator	E_c	Phase C emf [V]
IGBT	Insulated gate bi-polar transistor	E_{LL}	Line to line emf magnitude [V]
KVL	Kirchhoff's voltage law	E_{off}	Device switch off energy loss [Ws]
MTBF	Mean time before failure	E_{on}	Device switch on energy loss [Ws]
MTTF	Mean time to failure	E_{sync}	Equivalent emf to the synchronous speed [V]
MTTR	Mean Time to repair	f_e	electrical frequency [Hz]
MV	Medium voltage	GBR	Gearbox ratio
PCC	Point of common coupling	I	Turbulence intensity
PMDC	Permanent magnet direct current	I_6	6th current harmonic component magnitude [A]
PMG	Permanent magnet generator	I_a	Phase A current [A]
PSS	Power system stabiliser	I_b	Phase B current [A]
T1	Turbine 1	I_c	Phase c current [A]
T2	Turbine 2	I_{comm}	Commutation current [A]
T3	Turbine 3	I_d	D-axis generator stator current [A]
T4	Turbine 4	I_{dc}	DC current [A]
T5	Turbine 5	Iin	Input current [A]
VSC	Voltage source converter	Iinave	Average input current [A]
		IinB	Boundary input current [A]

General symbols

I_{inmax}	Maximum input current [A]
I_{out}	Output current [A]
I_p	Primary winding current [A]
I_q	Q-axis generator stator current [A]
I_r	Generator rotor current [A]
I_s	Secondary winding current [A]
$I_{winding}$	Winding current [A]
J_{gen}	Generator moment of inertia [kg.m^2]
J_T	Wind turbine rotor moment of inertia [kg.m^2]
K_{eq}	Equivalent shaft stiffness
K_i	Integral gain
K_p	Proportional gain
K_s	Shaft stiffness
L	Stator inductance [H]
L_{branch}	Branch cable inductance [H]
L_{common}	Common cable inductance [H]
L_l	Cable inductance [Ω]
L_m	Magnetising inductance [H]
L_p	Inductance referred to primary side of the transformer [H]
L_s	Inductance referred to secondary side of the transformer [H]
m	Modulation index
n	Number of turbines
N_p	Number of secondary winding turns
N_s	Number of primary winding turns
N_t	Transformer ratio
$N_{turbines}$	Number of turbines
P	Power [W]
P_{Aeroin}	Aerodynamic input power [W]
P_{BrLoss}	Branch cable power loss [W]
$P_{ClusterOut}$	Cluster output power [W]
$P_{CommLoss}$	Common cable power loss [W]

General symbols

$P_{GenLoss}$	Total generator power loss [W]
$P_{LossConduction}$	Device conduction power loss [W]
$P_{LossRextra}$	Extra resistance power loss [W]
$P_{LossSwitch}$	Device switching power loss [W]
P_{meas}	Power measured [W]
P_{nLoss}	nth Harmonic power loss [W]
$P_{nominal}$	Generaot nominal power [W]
P_{out}	Generator power output [W]
$P_{outCluster}$	Cluster power output [W]
P_{ref}	Power reference [W]
$P_{thermal}$	Thermal power loss [W]
P_{wind}	Power captured from the wind [W]
r	Radius [m]
R_{branch}	Branch cable resistance [Ω]
R_c	Equivalent core power loss resistance [Ω]
R_{common}	Common cable resistance [Ω]
R_{equiv}	Equivalent resistance [Ω]
R_{extra}	Extra resistance [Ω]
R_l	Cable resistance [Ω]
R_{lmax}	Maximum load resistance [Ω]
rms	Root mean squared
R_r	Rotor resistance [Ω]
R_{th}	Thermal resistivity [°/W]
$R_{thDiode}$	Diode thermal resistivity [°/W]
R_{thHs}	Heatsink thermal Resistivity [°/W]
R_{thIGBT}	IGBT thermal resistivity [°/W]
$R_{thmodule}$	IGBT module case thermal resistivity [°/W]
T_{aero}	Aerodynamic torque [Nm]
$T_{ambient}$	Ambient temperature [°]
$T_{DiodeJunctBoost}$	Boost converter diode junction temperature [°]
T_{gen}	Generator torque [Nm]

General symbols

t_{off}	Switch off time [s]
t_{on}	Switch on time [s]
T_s	Switching period length [s]
T_{shaft}	Shaft torsional torque [Nm]
TSR_{opt}	Optimal tip-speed ratio
v	Wind speed [m/s]
V_c	Capacitor voltage [V]
V_{c_ref}	Capacitor voltage reference [V]
V_{cave}	Average capacitor terminal voltage [V]
$V_{CE\ IGBT}$	IGBT collector-emitter voltage [V]
V_{comm}	Commutation voltage drop [V]
$V_{control}$	Controller voltage [V]
V_{dc}	DC voltage [V]
V_{dcCont}	Controller voltage [V]
V_{dcConv}	Converter terminal DC voltage [V]
V_{DCGen}	Equivalent DC generator voltage [V]
V_{dcPCC}	Point of common coupling DC voltage [V]
V_{dcRect}	Rectifier output DC voltage [V]
V_f	IGBT forward conduction voltage drop [V]
V_{in}	Input voltage [V]
$V_{in\ ave}$	Average input voltage [V]
V_{inref}	Voltage input reference [V]
V_{la}	Voltage across ph A inductance [V]
V_{lb}	Voltage across ph B inductance [V]
V_{lc}	Voltage across ph C inductance [V]
$V_{LClosed}$	Voltage across inductance switch closed [V]
V_{LOpen}	Voltage across the inductance when switch open [V]

General symbols

$V_{nominal}$	Generator nominal voltage [V]
V_{out}	Output voltage [V]
V_p	Primary winding nominal voltage [V]
V_{Ra}	Voltage across ph A resistance [V]
V_{Rb}	Voltage across ph B resistance [V]
V_{Rc}	Voltage across ph C resistance [V]
V_{Rextra}	Voltage across extra resistance [V]
V_{ripple}	Ripple voltage magnitude [V]
V_s	Secondary winding nominal voltage [V]
V_{Ta}	Phase A terminal voltage [V]
V_{Tb}	Phase B terminal voltage [V]
V_{Tc}	Phase C terminal voltage [V]
Z_{comm}	Commutation impedance [Ω]
Z_{gen}	Generator impedance [Ω]
Z_{TFP}	Primary winding impedance [Ω]
Z_{TFS}	Secondary winding impedance [Ω]
α	Commutation angle of advance start [rad]
δ	Commutation length [rad]
ζ	Damping coefficient
θ	Current phase angle [A]
θ_g	Generator angle of rotation [rad]
θ_r	Rotor angle [rad]
θ_s	Shaft angle of torsion [rad]
θ_T	Rotor angle of rotation [rad]
λ	Tip-speed ratio
λ_{opt}	Optimal tip-speed ratio
ρ	Air density [kg/m^3]

General Symbols

σ	Standard deviation of wind speed [m/s]
Ψ_f	Generator field flux [Wb]
ω	Rotational speed [rad/s]
ω_e	Electrical frequency [rad/s]
ω_{gen}	Generator rotational speed [rad/s]

Chapter 2 cont

Φ_{ag}	PM generator air-gap flux [Wb]
Φ_r	PM generator rotor flux [Wb]
Φ_s	PM Generator stator flux [Wb]
λ_{ds}	D-axis stator flux [Wb]
λ_{qm}	Q-axis mutual flux [Wb]

ω_n	Natural frequency [rad/s]
ω_r	Rotational speed [rad/s]
ω_s	Synchronous speed [rad/s]
ω_{sync}	Synchronous speed [rad/s]
ω_T	Turbine rotor rotational speed [rad/s]

Chapter 2 Induction generator and Synchronous generator model symbols

D	Generator rotor diameter [m]
emf	Electro motive force [V]
E_r	PM generator rotor emf [V]
E_s	PM generator stator emf [V]
I_{dr}	D-axis rotor current [A]
I_{ds}	D-axis stator current [A]
I_{qr}	Q-axis rotor current [A]
I_{qs}	Q-axis stator current [A]
J	Momnent of inertia [kg.m^2]
l	Rotor length [m]
L_{lr}	Rotor leakage inductance [H]
L_{ls}	Stator leakage inductance [H]
L_m	Mutual inductance [H]
p	Pole Pairs
R_{ds}	D-axis stator resistance [Ω]
R_{qs}	Q-axis stator resistance [Ω]
R_s	Stator resistance [Ω]
T_e	Generator torque [Nm]
T_r	Mechanical input torque [Nm]
V_{ds}	D-axis voltage [V]
V_{qs}	Q-axis voltage [V]
V_t	PM generator terminal voltage [V]
X	PM generator stator reactance [Ω]
δ	Load angle [°]
λ_{dm}	D-axis mutual flux [Wb]
λ_{dr}	D-axis rotor flux [Wb]
λ_{qr}	Q-axis rotor flux [Wb]
λ_{qs}	Q-axis stator flux [Wb]

Chapter 4 synchronous generator with damper windings model symbols

I_d	D-axis generator stator current [A]
I_{kd}	Q-axis damper winding inductance [H]
I_{kq}	D-axis damper winding inductance [H]
I_q	Q-axis generator stator current [A]
L_{ad}	D-axis generator stator inductance [H]
L_{aq}	Q-axis generator stator inductance [H]
L_{ld}	D-axis leakage inductance [H]
L_{lq}	Q-axis leakage inductance [H]
R_{kd}	D-axis damper winding resistance [Ω]
R_{kq}	Q-axis damper winding resistance [Ω]
V_d	D-axis generator terminal voltage [V]
V_{kd}	D-axis damper winding voltage [V]
V_{kq}	Q-axis damper winding voltage [V]
V_q	Q-axis generator terminal voltage [V]
Ψ_f	Generator field flux [Wb]
ω_r	Generator rotational speed [rad/s]

Chapter 7 DC converter extra symbols

I_c	Capacitor current [A]
R_l	Load resistance [Ω]
V_{dc}	Converter voltage [V]

Chapter 1 Introduction

The commercial development of wind energy as an alternative method of electricity generation began in the 1980s and has accelerated significantly over the past two decades. When contrasted with traditional methods of generating electricity such as burning oil, gas or coal, wind energy offers a bountiful energy resource that does not produce greenhouse gas emissions. The clean credentials of wind energy have been seized upon by governments worldwide as justification for investing huge sums of money in developing wind energy technology, with the hope of producing a sustainable, non-polluting source of electricity for many years to come.

Figure 1-1: Danish concept, horizontal axis, three bladed wind turbine [1].

Figure 1-2: Vertical axis wind turbine [2].

1.1 Origins of wind energy

The first wind turbines intended for generating electricity were developed and constructed around the middle of the last century, however it was not until the early 1980's that the first wind turbine, of the form recognised today, was developed. The generally accepted design of a wind turbine is based around the so called "Danish concept", which is a horizontal axis machine, usually with three blades, as shown in Figure 1-1. Other designs which are based around a vertical rotating axis also exist, Figure 1-2.

Wind turbines have developed from machines capable of generating in the range of 200kW, to machines that are capable of generating up to 7.5MW of power. This development in power output capacity has also seen turbines physically grow to hub heights in excess of 100m and blade lengths of 75m or more [3]. The global development of wind energy has seen a dramatic acceleration over the last 10 years going from 31.1GW of installed capacity in 2002 to 282.4GW of installed capacity by the end of 2012, as shown in Figure 1-3. While Asian and North American markets are beginning to dominate the

onshore sector, Europe and more specifically the UK are leading the development of offshore wind, with 2,948MW of installed capacity at the end of 2012 [4].

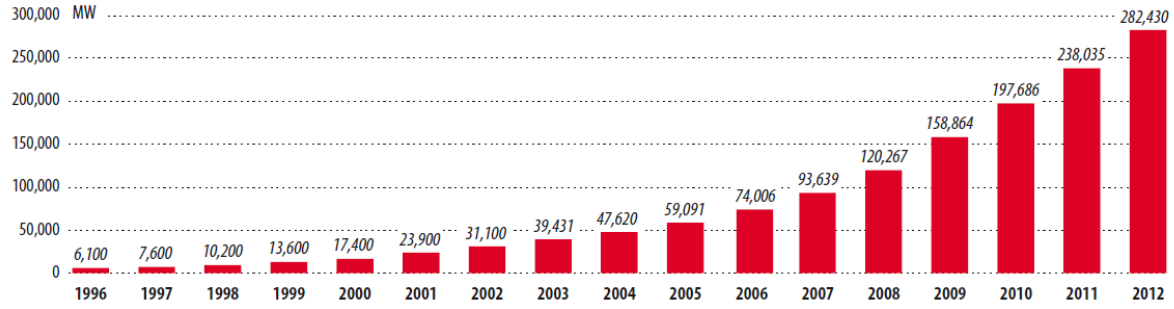

Figure 1-3: Global cumulative installed wind capacity 1996-2012 [4].

The largest of the turbines developed to date by manufacturers such as Siemens, Enercon, Repower, and Samsung, to name a few, are all aimed at the offshore market, whereas generally each manufacturer also produces a slightly smaller offering aimed at the onshore sector. A study conducted in 2012 highlighted that "the larger the turbines become the greener the electricity they produce, becomes" [5]. Therefore it is inevitable that over the next decade at least, the size of wind turbines will continue to grow.

1.2 Government energy policy and wind energy

In 2007 the European Commission agreed a target for 20% of all energy consumed to be produced from renewable sources by 2020 [6]. This target marked a continuation of a previous European target set in 1997 to generate 12% of energy from renewable sources by 2010. In 2009, the European Commission set out the Renewable Energy Roadmap, in response to the 2020 target, in which each member state was set a mandatory national target for the proportion of its energy consumption that should be sourced from renewable sources by 2020 [6]. The UK target for renewable energy was set at 15% of all energy consumed [7]. To meet this target the current UK

government set out its own Renewable Energy Roadmap in 2011 describing how it intends to meet its 2020 renewable energy target [8]. Within this document the Department for Energy and Climate Change (DECC) presents analysis concluding that between a 9GW and 13GW increase in onshore wind capacity is required by 2020 and that between a 10GW and 18GW increase of offshore wind capacity is required; therefore generating 30% of Britain's electricity from renewable energy sources by 2020, thereby meeting its target. These figures are put in context by the current levels of 6.7GW of onshore wind generation capacity and 3.7GW offshore wind generation capacity [9]. To achieve these capacity levels will require annual growth rates of 13% and 30% respectively from 2011 levels [8].

1.2.1 Subsidising the renewable energy industry

Since the inception of wind energy it has been clear that the costs involved with developing a large amount wind energy generation capacity are significantly higher than for the traditional generation technologies, even once fuel costs are taken into consideration. Therefore government energy policy has emerged to provide subsidies for the development of more expensive, clean electricity generation technologies. The Renewables Obligation has been the back bone of the subsidy regime in the UK for the past decade and the process has begun, as part of the 'Electricity Market Reform', to implement its replacement in the form of Contracts for Difference.

Renewables obligation

In 2002, HM Government established the Renewables Obligation with the aim of providing a support mechanism for the development of renewable energy projects in the UK [10]. The Renewables Obligation (RO) places an onus on suppliers of energy to source an increasing proportion of the

electrical energy they sell, from renewable sources. To facilitate the RO, Renewable Obligation Certificates (ROCs) were introduced to accredit each MWh of energy produced by an eligible generator, for use to offset the obligation target. The proportion of energy that the RO requires energy suppliers to supply from renewable sources has increased from 3%, in 2002, up to 10.4% in 2011 and will increase to 15.4% by 2016 [10] [11]. To encourage the development of other renewable electricity generation technologies, The Renewables Obligation Order 2009 set out bands within which certain technologies are awarded more than one ROC per MWh of energy generated [12]. For example: Tidal, Wave and Solar electricity generators are awarded two ROCs per MWh generated and Offshore Wind generators are awarded 1.5 ROCs per MWh generated.

Contracts for difference

Contracts for Difference were first proposed in the Coalition Government's Energy Bill in autumn 2012 as part of the Electricity Market Reform which is intended to attract £110billion of investment; it is anticipated that this amount is required to replace current generation capacity and upgrade the electricity grid by 2020 [13]. The purpose of Contracts for Difference is to provide an efficient and long term mechanism for the support of low carbon generation, thereby reducing the risks faced by generation developers by providing greater certainty to future revenues [14]. They work by paying a generator a 'top-up' on the wholesale price they receive for selling the energy they produce to a pre-agreed 'strike price'. Contracts for Difference also work the other way should the wholesale market price for energy exceed the 'strike price', in which case a generator will pay back the difference and therefore reduce consumer energy costs. The strike prices have initially been set to be consistent with the subsidy levels provided by the Renewables

Obligation, but it is envisaged that the strike prices will fall as the Contracts for Difference will allow reduced finance costs. The proposed initial strike prices for onshore and offshore wind energy generation are: £100/MWh and £155/MWh respectively [14]. It is expected that the first Contracts for Difference will be signed in 2014, initiating the move away from the Renewables Obligation.

1.3 The shift towards offshore wind energy

The shift towards offshore wind energy development has been driven by the prospect of better wind resource, less objection due to visual intrusion and the promise of the opportunity to install a greater number of wind turbines compared to onshore developments. A further driving force behind offshore wind energy development has been the recognition that there are not a sufficient number of potential wind farm sites onshore to allow the generation capacity required to meet the 2020 targets, to be built.

The first offshore wind farm in the UK was built at Blyth, Northumberland, in 2001, comprising of two turbines. Since then the UK Government has issued licenses for a potential 48GW worth of offshore wind farm development; of which only a portion will be operational by 2020 [15].

The Crown Estates, on behalf of the Government, has issued consent for offshore wind farms in three rounds. The first of which consisted of a relatively small number of sites close to shore, which were intended to demonstrate the concept of offshore wind energy. The second round of consents consisted of 15 sites within three main areas: Thames estuary, Greater Wash, and the north west, of which two are outside of UK territorial waters. Round Three of offshore consents, issued in 2007, started the ball

rolling on a potential 25GW of offshore wind farms to be built around the UK in more distant waters [16].

1.3.1 Challenges posed by the offshore environment

The construction of offshore wind farms poses significant challenges, most of which are different to those faced when developing onshore wind farms. To name a few, the challenges are: construction and installation of subsea foundations, the availability of suitable ships for construction and access, laying and repairing subsea cables and the availability of suitable windows of calm weather and sea state. The wind turbines themselves used in initial offshore wind farms were fairly similar to those used onshore with some modifications for use in a marine environment. Several manufacturers are now producing wind turbines specific for the offshore market which are larger than their onshore counterparts. Perhaps the biggest challenge of all is the provision of maintenance to an offshore wind farm. Wind turbines are like any electric / mechanical system, and require periodic maintenance to ensure a full operational life is achieved. Experience from onshore wind turbines has also indicated that major component failures do occur on occasion. The ability to gain access to a wind turbine to conduct either routine maintenance or take remedial action in the event of a failure is severely restricted by the weather in an offshore environment, where access is impossible during periods when the significant wave height exceeds 1.5m [17]. This means that a large emphasis is being placed upon the reliability of offshore wind turbines and the subsystems that are imperative to their operation, in an attempt to reduce the need for access to turbines.

One other major engineering challenge for offshore wind farms has been their connection to the onshore electrical transmission system. Onshore wind farms are generally connected to the transmission system via a

relatively short cable link, indeed the availability of an electrical connection close-by is often a major factor in the selection of onshore wind farm sites. However, offshore wind farm development sites are not commonly in the vicinity of the required electrical connection; therefore this has led to the use of often very lengthy subsea cables to transmit the generated electricity to the onshore electrical system. As the development of offshore wind farms moves towards the Round Three sites, challenges to the operability and economics of the technology used to provide this subsea electrical link begin to arise. Round Three offshore sites are situated considerably further from shore than previous sites and have much larger generation capacities; the transmission of large amounts of energy over long distances by subsea cables poses challenges to conventional techniques, but also presents the opportunity for alternative transmission techniques to be employed.

1.4 Focus and objectives of the thesis

This thesis focuses on the investigation of electrical network architectures for use within an offshore wind farm itself, known as "Collection Networks". In particular this thesis will focus on investigating the feasibility of a hybrid collection network, where a wind farm is separated into small groups of five wind turbines, known as "Clusters", within which they are electrically connected in parallel and controlled collectively. The potential opportunities and pitfalls of implementing such a network will be investigated in the context of the functionality of the wind turbines and also in terms of energy captured. Three methods of implementing clusters are developed based upon using induction and permanent magnet generators connected by either AC or DC electrical networks. The functionality of each method is investigated through the studying of the theoretical principles and the development of simulation models. One method in particular is focussed upon: Permanent magnet generators with rectified outputs connected in parallel by a DC network. The investigation of this technology studies in detail the commutation of the DC output current between the generator windings, the harmonics introduced to the system by rectification and the energy transfer efficiency. A bench scale test rig is also developed to verify the practical operation of this system.

This thesis presents the first study of the motivation and feasibility of implementing such a system. In particular the use of passive rectification to achieve slip between the generator rotational speeds of the wind turbines and the cluster synchronous speed is novel; providing the capability for adjacent turbines to operate with different rotational speeds when they are subject to continuously varying, different wind speeds.

1.5 Publications

The work presented in this thesis has been the subject of presentations at the following conferences. Each presentation has been accompanied by a technical paper.

D. W. Elliott, S. J. Finney, C. Booth – *Single Converter Interface for a Cluster of Offshore Wind Turbines*, IET Renewable Power Generation Conference, Edinburgh, 2011.

D. W. Elliott, C. E. Jones, S. J. Finney – *Offshore Wind Farm Cluster Based DC Collection Network – Operation and Design Considerations* – IET ACDC Conference, Birmingham, 2012.

D. W. Elliott, C. E. Jones, S. J. Finney – *A Comparison of Technologies for the Clustering of Multiple Wind Turbines* – European Wind Energy Agency Conference, Vienna, 2013.

Furthermore the paper presented at the IET ACDC conference has been developed further to be published in a new IET online reference publication.

D. W. Elliott, C. E. Jones, S. J. Finney – *Offshore Wind Farm Cluster Based DC Collection Network – Operation and Design Considerations*, 2013.

Throughout the period of study of the work presented in this thesis, the author has also been the main contributor to the following journal article and consultancy projects:

D. Elliott, D. Infield – *An Assessment of the Impact of Reduced Averaging Time on Small Wind Turbine Power Curves, Energy Capture Predictions and Turbulence Intensity Measurements*, Wiley Wind Energy, 2014.

D. Elliott, S. Finney – *A Review of Current Literature Relating to the Performance of AC Power Cable Insulation Compounds in Wet Environments*, for Atkins, 2010.

D. Elliott, C. E. Jones, S. Finney – *Torque Ripple in DC Collection Networks for Tidal Stream Generators*, for RES, 2012.

D. Elliott, K. Bell, S. Finney – *Transmission Requirements for Offshore wind Integration – A Study of the Merits of AC and HVDC Transmission Connection Options*, for the Electric Power Research Institute (EPRI), 2013.

1.6 Summary of thesis

Chapter 2 provides a review of relevant published literature to the electrical systems of wind farms and relevant theoretical principles.

Chapter 3 reviews the potential layouts of cluster based collection networks, investigates the economic motivation for introducing clustering and introduces the three cluster collection network topologies that will be studied in the latter chapters.

Chapter 4 uses the extensive simulation of each of the cluster topologies to determine and trade off the merits and pitfalls of each.

Chapter 5 reviews the theory of passive rectifier commutation, including the derivation of the harmonic components that result, the production of the cluster control characteristic and the representation of the system by a simplified model.

Chapter 6 aims to answer the following questions through theoretical explanation and the simulation of the system operation in different operating scenarios.

- How much slip can be achieved and how?
- How much generator slip is required?
- What are the effects of collective control on the operation of the wind turbines?

Chapter 7 describes the design and implementation of the bench scale test rig and experimentally verifies the operational characteristics of the system that are observed in simulation.

Chapter 8 provides the conclusions of this thesis, summarises the contribution to knowledge and lists potential topics for further work.

1.7 References

1. Pure Energy Centre. 2013; Available from: http://pureenergycentre.com/50kw-to-mw-wind-turbine/.
2. Barnard on wind. 2013; Available from: http://barnardonwind.com/2013/02/23/why-arent-vertical-axis-wind-turbines-more-popular/.
3. Wind Power Monthly. *The 10 Biggest Turbines in the World*. 2013; Available from: http://www.windpowermonthly.com/10-biggest-turbines.
4. Global Wind Energy Council, *Global wind statistics 2012*, 2013.
5. Caduff, M., et al., *Wind Power Electricity: The Bigger the Turbine, The Greener the Electricity?* Environmental Science & Technology, 2012. 46(9): p. 4725-4733.
6. *Communication from the commission to the council and the European Parliament - Renewable Energy Road Map - Renewable energies in the 21st century: building a more sustainable future.*, 2007, European Parliment: European Parliment.
7. *Directive 2009/28/EC Of The European Parliament and of The Council of 23rd April 2007 on the promotion of the use of energy from renewable sources and amending and subsequently repealing Directives 2001/77/EC and 2003/30/EC.*, in *2009/28/EC*2009, European Commission: European Commission.
8. DECC, *UK Renewable Energy Roadmap*, 2011.
9. Renewable UK. *UK Wind Energy Database*. 2013; Available from: http://www.renewableuk.com/en/renewable-energy/wind-energy/uk-wind-energy-database/index.cfm/map/1/.
10. *The Renewables Obligation Order 2002,*, in *2002 No. 914*2002: UK.
11. *The Renewables Obligation Order 2006*, in *2006 No. 1004*2006: UK.
12. *The Renewables Obligation Order 2009*, in *2009 No. 785*2009: UK.
13. DECC. *The Energy Bill*. 2012; Available from: https://www.gov.uk/government/collections/energy-bill#group_449.
14. DECC, *Electricity Market Reform: Delivering UK Investment.* 2013.
15. The Crown Estate. *The Crown Estate*. Available from: http://www.thecrownestate.co.uk.
16. The Beatrice Wind Farm Demonstrator Project. *The Beatrice Wind Farm Demonstrator Project*. Available from: http://www.beatricewind.co.uk.
17. Tavner, P., *Offshore Wind Turbines - Reliability, availability and maintenance*. Renewable Energy2012: IET.

Chapter 2 Wind Farm Electrical Systems

The electrical system of a wind farm provides the means of exporting the generated power from the wind turbines and provides the capability to control them. There are number of subsystems and components within the electrical system; the most important of which are the generators which provide the conversion between rotational kinetic energy to electrical energy for export. Secondary to these are the networks of cables that transfer the electrical energy from the turbines to the grid and onwards to the consumer. Of equal importance in some designs of wind turbine is the frequency converter, which couples the generator to the cable network. The frequency converter acts to suitably condition the generator electrical output for export and also provides a degree of control over the reaction torque produced by the generator, which can be beneficial to the operation of a turbine.

This chapter will review the different types of wind turbine that have emerged over the past three decades, giving their advantages and disadvantages relative to one another. The electrical network architectures that are commonly used to export power are also reviewed along with alternative network designs that have been proposed. This chapter will also provide an introduction to the hybrid collection network concept that is the focus of this thesis and the different architectures that could allow such a network to be implemented.

2.1 Wind turbine technology

Wind turbine technology has progressed significantly since the first commercial turbines became available in the 1980s. This progression has largely been driven by the growth of the physical size of turbines, which has increased their power output, and the desire to capture the maximum amount of energy per unit cost of the turbines. The earliest wind turbines were directly connected to electrical networks which meant their rotational speeds were fixed by the electrical frequency. Early turbines also used the blade aerofoils to limit their power extraction in high wind speeds by allowing the air flow over them to stall. Wind turbine technology has since developed with the introduction of active pitch control and variable rotational speed operation.

2.1.1 Wind turbine operation

Since the inception of wind energy equation (2.1) has been fundamental:

$$P = \frac{1}{2} \cdot \rho \cdot \pi \cdot r^2 \cdot v^3 \cdot c_p(\lambda) \tag{2.1}$$

This equation gives the power output from a wind turbine as a function of the wind speed, v; where ρ is the air density (1.225kg/m^3), C_P is the power coefficient, r is the rotor radius, and λ is the tip speed ratio of the machine. The power coefficient of a wind turbine dictates the fraction of the power in the wind that the wind turbine will extract. This coefficient is proportional to the ratio between the wind speed and the rotational speed of the turbine, referred to as the tip-speed ratio, λ, equation (2.2).

$$\lambda = \frac{\omega \cdot r}{v} \tag{2.2}$$

The relationship between the tip speed ratio and the power coefficient is governed by the design of the wind turbine blades, however the maximum

possible value of C_P was found to be 0.593 by Albert Betz [1]. This limit arises not through deficiency in blade design, but through the extraction of kinetic energy from the wind by the turbine rotor causing a reduction of the wind speed downstream of the rotor. This reduction in wind speed causes a blockage to the flow of air through the rotor; the greater the amount of kinetic energy that is extracted from the wind, the greater this blockage becomes. Alfred Betz determined the maximum amount of energy that can be extracted from the wind before this blockage causes air to flow around the wind turbine rotor, instead of through it. The definition of the power coefficient is:

$$C_p = \frac{Power\ extracted}{Power\ available} = \frac{Power\ extracted}{\frac{1}{2} \cdot \rho \cdot \pi \cdot r^2 \cdot v^3} \tag{2.3}$$

Although, the so called "Betz limit" states that the maximum proportion of energy that can be extracted is 59.3% of the energy available, no wind turbine design has achieved this level. This is due to imperfections in blade design and energy lost due to blade tip losses and drag. The relationship between λ and C_P for each different wind turbine design is described by its C_P - λ curve; an example of which is shown in Figure 2-1. Note that the maximum C_P achieved by this wind turbine is approximately 0.47, occurring when $\lambda \approx 7.5$.

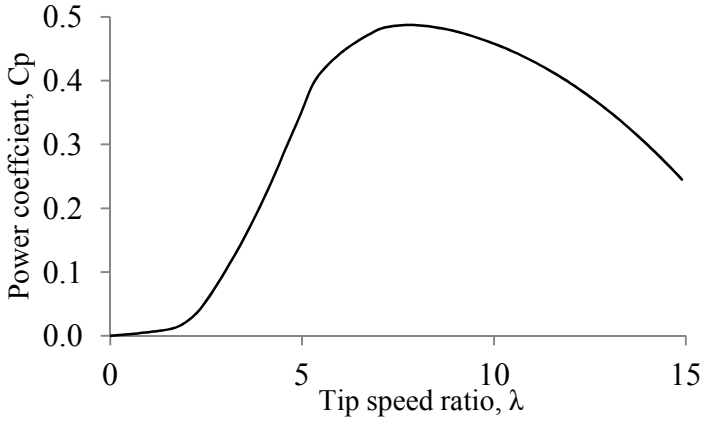

Figure 2-1: An example Cp - λ curve for a 5MW wind turbine [2].

The power output from a wind turbine is shown to be proportional to the cube of the wind speed by equation (2.3). Therefore the range of power output between low wind speeds and high wind speeds is large. It is generally accepted that the Weibull distribution is a good approximation of the probability density function of the wind speed at a specific site, with a specific mean wind speed [3]. Figure 2-2 shows an example Weibull distribution for a site with a mean wind speed of 7m/s; it is clear from this that the probability of the wind speed exceeding 12m/s is quite low. The rated output power of the generator is usually prescribed to roughly match the power output of the wind turbine at this point; as it is not economic to design a turbine to extract optimum power at higher wind speeds, as they occur infrequently. The point where the rated power of the generator is extracted from the wind is labelled as the "rated wind speed" of the wind turbine. If the wind speed were to be larger than the rated wind speed of the turbine, the generator is not capable of producing any more power; therefore a mechanism of restricting the power extracted from the wind is employed. Throughout the development of wind turbines two such mechanisms have emerged; stall regulation and pitch regulation [4]. Under the influence of either stall or pitch regulation, the relationship between the power output of a wind turbine and the wind speed is described by the "power curve" of a turbine, an example of which is given in Figure 2-3.

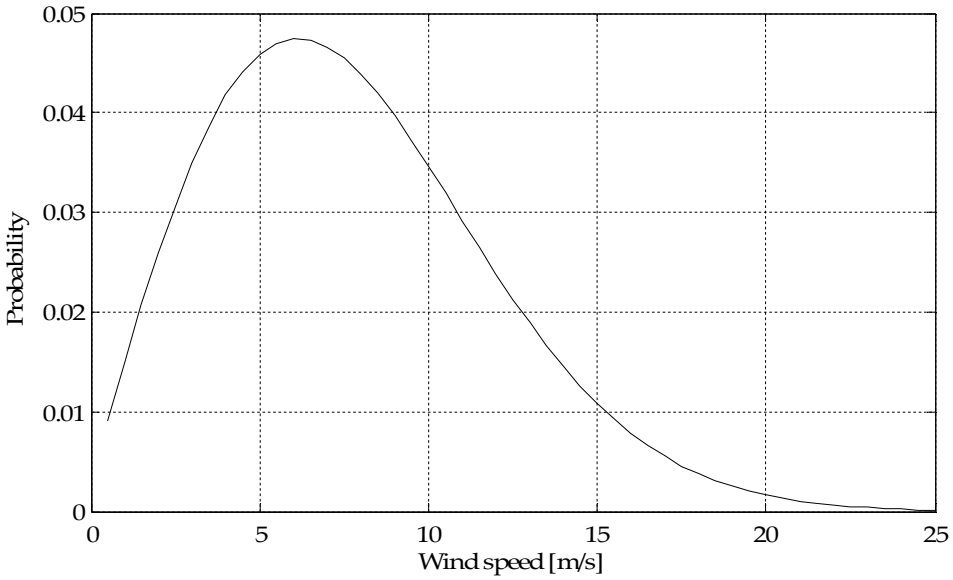

Figure 2-2: Weibull distribution for a site with mean wind speed of 7m/s.

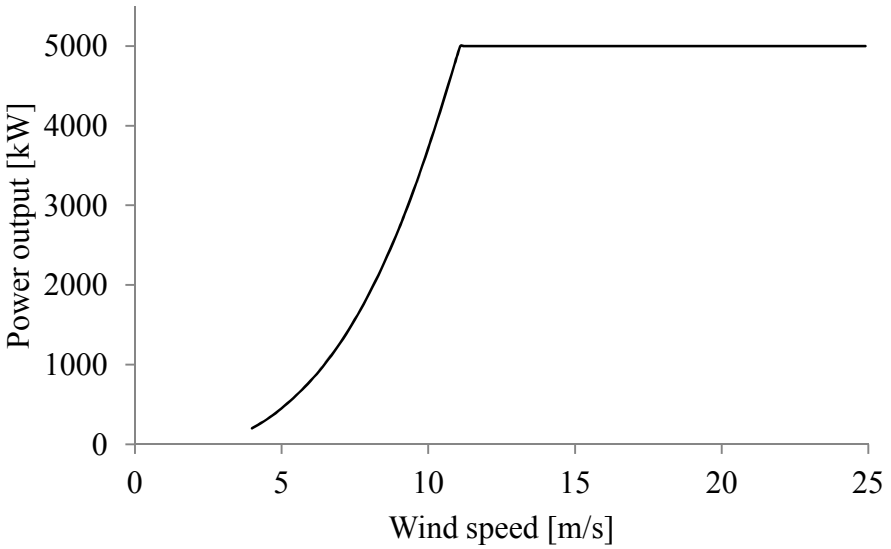

Figure 2-3: A typical wind turbine power curve.

2.1.2 Fixed speed stall regulated wind turbines

The generators in early wind turbines were connected directly to electrical networks; this meant that their rotational speeds were fixed by the electrical frequency. It can be observed from Figure 2-1 that a wind turbine rotor develops peak efficiency (Cp) at one particular tip speed ratio; therefore when the rotational speed is fixed, a turbine will spend a very little time

operating at optimum efficiency. For all other wind speeds the turbine will be operating sub-optimally. Early fixed speed turbines also relied upon the stalling of the air flow over the blades to limit the power they capture in high wind speed conditions. Stall reduces the lift force on the blades and increases the drag, thereby limiting the output power of the turbine. The use of stall regulation to limit the power output is not perfect as it relies heavily on the air flow conditions; additional energy is lost due to the premature onset of stall when the wind speed is in the proximity of the rated value. A further disadvantage is uncertainty introduced by stall to predictions of the structural loads placed on the blades, which leads to suboptimal blade design [3].

2.1.3 Pitch regulation

Active pitch regulation provides an alternative method of limiting the power capture of the turbine above the rated wind speed, by rotating the blade on its longitudinal axis to reduce the angle of attack, reducing lift [3]. Using active pitch regulation on a fixed speed wind turbine provides a marginal energy capture efficiency improvement. It does however allow for a more effective method of limiting the power capture in high wind speed conditions, without requiring the blades to enter stall; thereby allowing improved predictions of the structural loads on the blades, allowing better design. The range of pitch variation required for effective power control is typically from 0° to 35°, whereas the blades can be pitched to 90° for aerodynamic braking purposes when the turbine is required to come to a halt [3].

2.1.4 Variable speed wind turbines

To maximise the energy capture of a wind turbine when it is operating in wind conditions below rated wind speed, optimum λ must be maintained; this can be achieved by varying the rotational speed of the turbine. Early methods of achieving variable speed operation involved switching the number of generator stator pole windings in use during operation and allowing a variable amount of slip to occur within an induction generator by varying the generator rotor winding resistance [3]. Latter methods of achieving variable speed operation have involved the use of frequency converters to decouple the rotational speed of the generator from the network frequency [5]. Frequency converters have been employed in two different ways: to couple the generator rotor winding of an induction generator to the network, while the stator winding remains directly connected, and to couple stator windings to the network. In the first case a speed variation range of +/-30% about the synchronous speed can be achieved, whereas in the latter case the rotational speed can be varied from zero to the full rated speed of the generator.

While variable speed operation allows improvements to be made to the energy capture capability of the turbines, the use of frequency converters also introduces additional losses to the electrical system, offsetting some of the gain. The use of frequency converters in either case however, allows for control over the generator reaction torque, allowing the inertia of the wind turbine rotor to smooth out fluctuations of the wind speed; thereby reducing the stress applied to the mechanical drivetrain of the turbines. Using frequency converters also allows for the control of the turbine output power factor.

Combining both variable speed operation and active pitch control brings the benefits of both to a wind turbine design; principally allowing its operation to be actively controlled so that energy captured is maximised, while keeping mechanical loads induced by varying wind speeds under control. Both aspects do however add considerably to the complexity of a wind turbine, which may affect its reliability.

2.1.5 Wind turbine drivetrains

The drivetrain in a wind turbine is the mechanical system that links to the turbine rotor with the generator. Traditionally a wind turbine drive train consists of a gearbox and two drive shafts, as shown in Figure 2-4. The gearbox is required to step-up the rotational speed of the turbine rotor, which is of the order of 15-30rpm, to a speed that is suitable for standard generators (approximately 1500rpm) requiring a ratio of between 1:50 and 1:100 [3]. In most cases the step-up of the rotational speed is achieved using a three stage gearbox, each stage with ratios of between 1:3 or 1:5. In modern designs of wind turbine, efforts have been made to eliminate the gearbox from the drivetrain and directly couple the generator to the rotor of the turbine using a single drive shaft, as shown in Figure 2-5. This has been achieved by the bespoke design of generators that are capable of operating at the low speeds. Such wind turbines are given the name: "Direct Drive" wind turbines, after the direct coupling of the turbine rotor to the generator. The motivation behind the development of direct drive wind turbines is the need to improve the availability of the wind turbine subassemblies; as operational experience has shown that following the failure of the gearbox in a wind turbine, a significantly longer time period is required to repair it, in comparison to other components [6] [7].

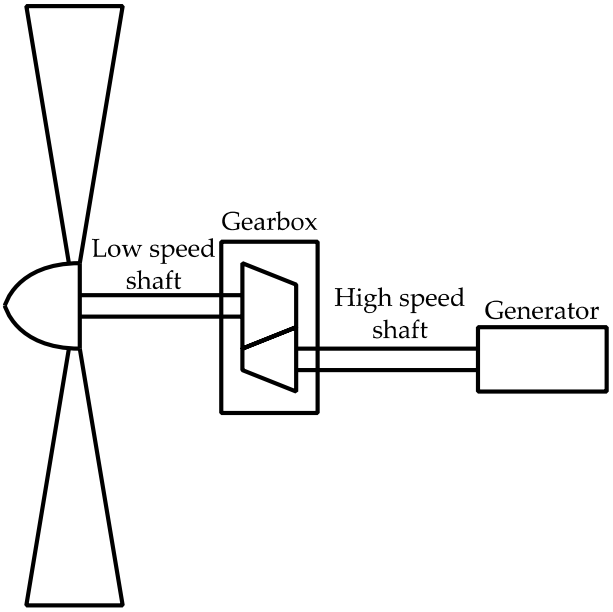

Figure 2-4: Wind turbine drive train which includes a gearbox.

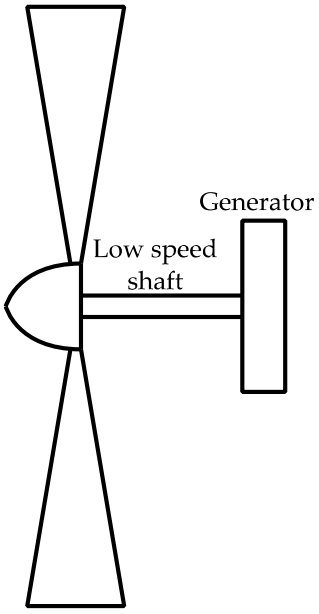

Figure 2-5: Direct drive wind turbine drive train.

2.2 Wind farm electrical networks

The electrical network associated with a wind farm consists of two sections: the collection network and the grid connection. The collection network allows for the output of each turbine to be aggregated and the grid connection exports the aggregated power output to the wider grid for transfer to the consumer.

2.2.1 Collection networks

A collection network bears many similarities to a distribution network used to deliver electrical energy to consumers. The collection network within a wind farm generally consists of multiple electrical feeders with a voltage level of 33kV and capacity of approximately 30MVA, collecting electrical energy from multiple wind turbines before connecting together at a central bus [8]. A transformer is usually present in the base of each wind turbine to step-up the output voltage of the generator, approximately 1kV, to the collection network voltage of 33kV. Figure 2-6 shows a diagram of an example radial collection network. The cable layout of a collection network has been the subject of a substantial amount of work to identify the most economic design; taking into account the availability benefits of an electrical ring based system versus the extra cost of installing the additional cable capacity [9]. The exploration of the trade-off between electrical ring and radial based systems carries more significance in offshore wind farm design, because the installation costs of cables are greater, but so too are the potential penalties that result from a fault; as the repair of a subsea cable takes significantly longer and is more expensive than the same operation onshore. The location of the substation within the wind farm, where all of the feeders connect together, also has a significant bearing on the design of collection

network. In an offshore wind farm the substation is placed on a platform, similar to those used by the oil industry, amongst the wind farm.

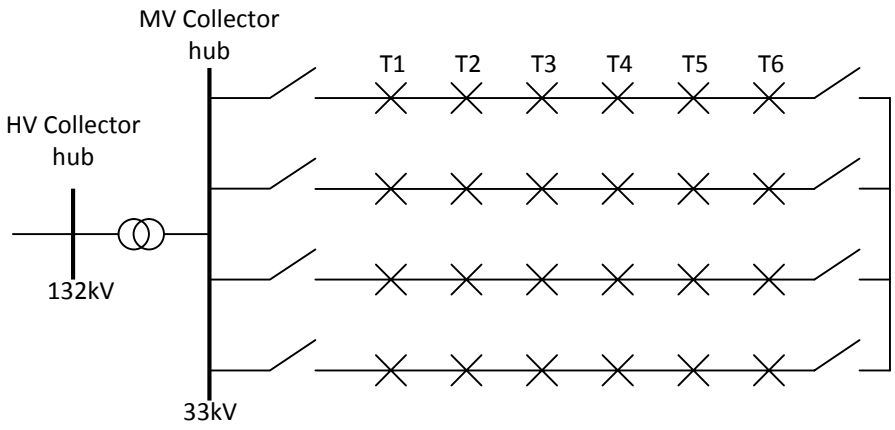

Figure 2-6: An example intra wind farm collection network [10].

2.2.2 Grid connections

The development of grid connection technologies has followed the growth of wind farm output capacities and also the deployment of wind farms offshore. The connection that links many onshore wind farms to the wider grid, where the connection distance is not usually greater than a few kilometres, consists of a single transmission cable usually with a voltage rating of 132kV. Indeed the proximity of a wind farm site to a suitable grid connection is a major factor when potential sites are identified.

The early wind farms that were constructed offshore have followed a similar philosophy, as they are located no further than 12 miles offshore (UK territorial waters). In most cases a single cable runs from the substation platform directly to an onshore substation. The licensing of offshore wind farm development areas, by the Crown Estate, that are much further from shore as part of the third round of consents, is driving the development of alternative grid connection technologies. The use of traditional transmission

technologies is limited to distances of approximately 80km by the cost of providing extra cable capacity to allow for the flow of reactive power produced by the cables, as well as the active power produced by the wind farm [11]. Reactive power is generated by the high capacitance of a cable and is proportional to its length. Therefore if such a cable were used for long distances, a greater proportion of its capacity would be taken up by the flow of reactive power rather than by active power, which is not justifiable economically.

High Voltage Direct Current (HVDC) transmission technology is mooted as the solution to the transfer of the generated energy from distant offshore wind farms. HVDC uses direct current to transfer energy and therefore does not generate reactive power and is theoretically capable of transferring electrical energy over many hundreds of kilometres. HVDC transmission has been in existence for many years in the form of current source converter (CSC) transmission used to interconnect different electrical systems [12] [13] [14] [15]. This however is only capable of transporting energy between two strong electrical systems as the conversion process between AC and DC is naturally-commutating, requiring strong voltage sources at either end of the link. In recent years voltage source converter (VSC) based HVDC transmission has come to the fore with the advancement of power electronic devices that are self-commutating; allowing a VSC to forcibly commutate the current passing through each device according to a control signal [15]. This enables the connection of an electrical network that is weak (a wind farm) via such a transmission system. To enable the use of HVDC transmission technology a power electronic converter is required at each point of interface with a conventional AC electrical network. In the context of a wind farm which has an internal AC collection network, a power electronic converter is

required to convert the AC output of the wind farm to DC for transmission and then to convert it back again so that it can be fed into the onshore grid. The requirement for such converters significantly increases the costs, complexity and losses of the transmission system. VSC based HVDC transmission is a relatively young technology and to date only the BorWin 1 wind farm in the North Sea, commissioned in 2012, has been connected using such technology, although it has been used to provide interconnections between different networks in the USA and Europe, for example: the Cross Sound Cable Project between New England and New York which was commissioned in 2003, and the Gotland link in Sweden commissioned in 1999 [16] [17] [18].

Alongside the development of HVDC transmission technology, there remains a significant industrial emphasis on investigating methods of extending the reach of traditional AC transmission. Such research is focussing on compensating for the reactive power production of a long subsea cable at different points along its length. The hope is that this will provide a lower cost solution for the transfer of energy from middle distance (50-200km) offshore wind farms [19] [20].

It is widely recognised however that only HVDC technology has the capability of transmitting power from wind farms located beyond 200km, such as those proposed in Round 3 of the Crown Estate's offshore wind programme. As a result there is also a significant body of research underway investigating methods of implementing an offshore HVDC grid in the North Sea, where multiple wind farms are connected together in a meshed system. Such a system will reduce the number of expensive power electronic

converters that are required and provide greater flexibility as to where on the onshore grid the generated power is fed in [21].

2.2.3 Alternative electrical networks

The electrical architecture of the collection network in an offshore wind farm has largely followed the systems used in onshore wind farms. However, the increasing size of wind turbines that are proposed for offshore use and the use of HVDC transmission, which decouples the collection network from the onshore fixed frequency grid, is driving research into alternative collection network architectures. Alternatives that are emerging involve variable, high or low frequency networks and also multi-terminal DC electrical networks. Architectures that encompass both AC and DC technology in a hybrid collection network are also under investigation. Indeed the bulk of the work within this thesis focusses on one part of how such a hybrid collection network could be implemented.

Alternative AC collection networks

In contrast to the use of an AC collection network with a fixed frequency, alternatives are being investigated that include using a fixed frequency that is higher or lower than onshore networks or allowing the frequency to vary [22]. The impedance introduced to an electrical network by the inductive and capacitive elements is directly related to the electrical frequency, and therefore so is the reactive power production and consumption of these elements. Higher electrical frequencies are often used in the electrical systems of aircraft and also on-board ships, as higher cable impedances are acceptable when cable lengths are particularly short, also lowering fault levels [23] [24]. Higher frequencies also bring the advantage of allowing the physical size of magnetic components, such as transformers, to be reduced.

A lower electrical frequency has the opposite effect, lowering the impedance of the cables but increasing the physical size of transformers.

Using either a higher or lower electrical frequency would bring advantages to a wind farm collection network: a higher frequency would allow the transformers in each turbine and also on the wind farm substation platform to have a smaller mass, and a lower frequency would lower the impedance of the collection network cables and therefore reduce reactive power flow, reducing losses. However both bring disadvantages that are the opposite of each other, namely; higher cable impedances and larger transformers, both of which would be a detriment to a collection network. So in actual fact the advantages of using a frequency other than that used already in onshore networks are limited.

A variable frequency collection network raises the prospect of achieving variable speed operation of the turbines in a wind farm without the requirement for individual frequency converters. In such an instance the frequency of the collection network would be regulated so that it changes with the average wind speed across the wind farm. This would allow for the wind turbines to be simplified considerably, by removing individual frequency converters, lowering their capital costs. However, the variation of the wind speeds experienced by each of the individual wind turbines in a wind farm, and their common rotational speed, could reduce the energy capture performance of the wind turbines, offsetting the potential advantages of a variable frequency network. On the face of it this is the most plausible AC alternative to the fixed frequency systems used at present, and some of the operating principles of such a system are adopted within the cluster based collection network that is the main subject of this thesis.

Multi-terminal DC collection networks

The use of multi-terminal DC collection networks has been the subject of much research [25] [26] [27] [28]. Such a network would only use half of the frequency converter in a wind turbine to convert the generator output to DC; the DC output of each turbine could then either be connected in series or parallel, as shown in Figure 2-7 and Figure 2-8. Connection in series would allow the output voltages of each turbine to be summed providing a much larger voltage at the terminals of the network and lower currents. Parallel connection allows the aggregation of the output currents of each turbine leading to potentially very high currents being transferred back to the wind farm substation. Therefore it is likely in such a case that an additional voltage step-up converter stage would be required in each turbine to lower the currents and therefore reduce conduction losses. The advantage of using DC is that there is no reactive power flow, reducing the cost of the cables required to transfer the energy to the wind farm substation. In either case a further step-up conversion stage will be required at the wind farm substation to increase the DC voltage for transmission [29]. The addition of extra power electronic conversion stages to the collection network adds significantly to complexity of such networks. The cost of this extra complexity is likely to be poorer reliability, which in an offshore scenario is a major factor. Therefore such technologies require more development before they are likely to be deployed within an offshore wind farm.

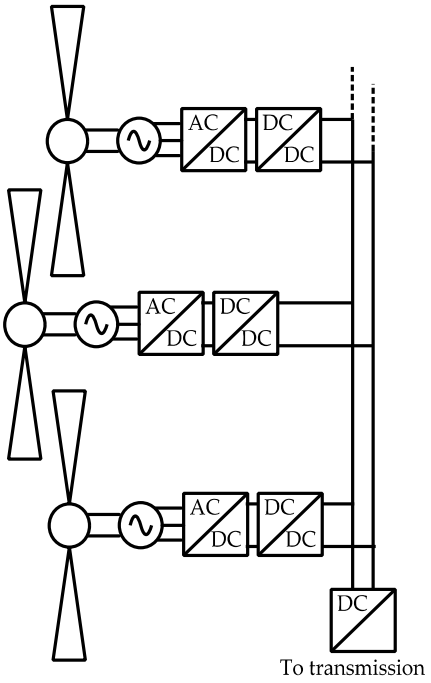

Figure 2-7: Wind farm parallel connected multi-terminal DC collection network.

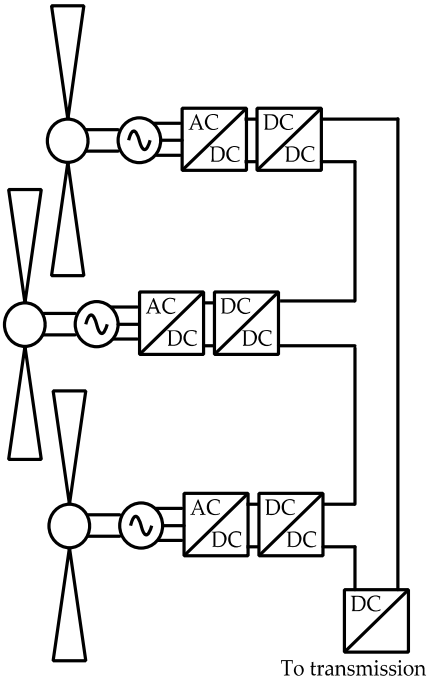

Figure 2-8: Wind farm series connected multi-terminal DC collection network.

Hybrid collection networks

A hybrid collection network splits the network into two different levels: the first of which connects a small number of turbines together in clusters and the second connects together multiple clusters that make up the wind farm. One of the advantages of variable frequency collection networks is the potential capability to achieve variable speed operation of the turbines in a wind farm without requiring frequency converters in each turbine. A hybrid collection network takes this idea but implements it on a smaller scale by using a single frequency converter to control a small group of turbines instead of the whole wind farm. The difference this makes is that the rotational speeds of the turbines in each cluster can be better matched to their local wind speeds, whilst still simplifying the subsystems within each turbine by allowing the removal of the frequency converter. The second

level of the collection network could use either an AC or DC network to aggregate the output power of each of the clusters, subject to the merits and pitfalls set out for each above.

The focus of this thesis is to investigate the implementation of the first level of a hybrid collection network. As stated above this part of the collection network could be implemented using a variable frequency AC network where the frequency is controlled by the cluster converter; such a system could also be implemented using a multi-terminal DC network. The system topographies that could be used to implement a cluster of turbines will be covered in greater detail in the next chapter of this thesis.

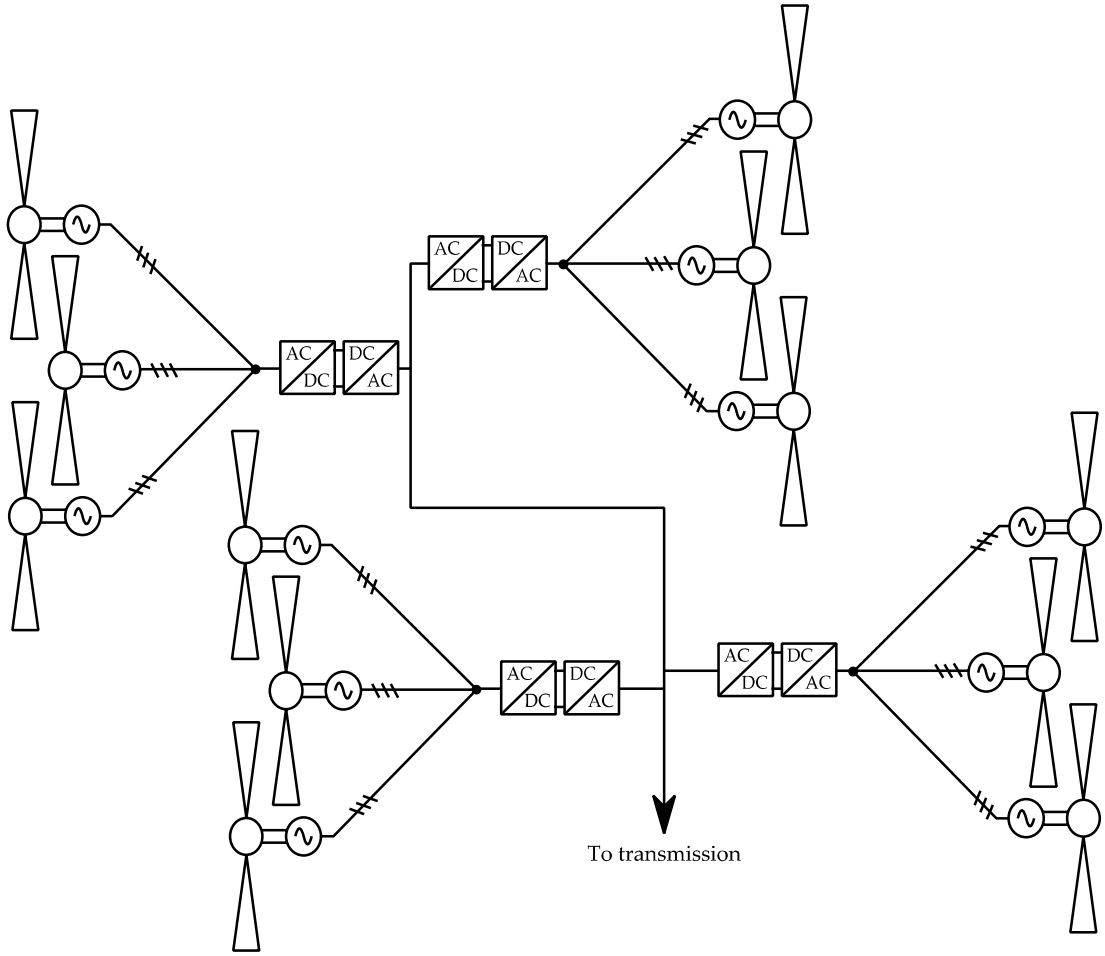

Figure 2-9: Two level hybrid collection network.

2.3 Wind turbine generator technology

The most critical aspect of a wind farm electrical system is the generator which converts the kinetic energy of the wind turbine rotor to electrical energy. Early wind turbines used induction generators to provide this conversion as they are capable of allowing a small amount of rotational speed variation which is beneficial when the wind speed changes. The advent of variable speed wind turbines has seen the use of induction generators (IG), doubly fed induction generators (DFIG) and permanent magnet generators (PMG) combined with frequency converters. DFIGs use a frequency converter to actively control the rotor currents and rotor magnetic field allowing the rotational speed of the turbine to vary by as much as 30% [3]. Whereas using a frequency converter with IGs and PMGs, allows for the generators to be completely decoupled from the fixed frequency of the electrical network.

This section will set out the operational theory behind IGs and PMGs, as it is plausible that either could be used to implement a cluster of turbines within a hybrid collection network.

2.3.1 Induction generators

Induction generators fall into two categories; squirrel cage and wound rotor. A squirrel cage induction generator has an autonomous rotor winding that is completely isolated from any electrical connection. At start up, the currents flowing in the stator windings produce a magnetising flux; this flux induces a voltage into the rotor winding. The rotor winding is short circuited, therefore allowing a current to flow as a result of the induced voltage. This rotor current sets-up a second flux in the machine which opposes the stator flux, producing the generator torque. Operating as a generator, the rotor

shaft is driven by the prime mover (wind turbine rotor). The generator torque acts against the input torque and is directly proportional to the active power output from the generator. The autonomous nature of the rotor winding requires the magnetising flux to setup the rotor flux; to achieve this magnetisation a reactive component is added to the stator currents. To ensure that a current is always present in the machine rotor, the rotational speed of the rotor must never equal the synchronous speed of the machine. The ratio of the speed difference between the rotational and synchronous speed is referred to as the machine slip, described by equation (2.4); where ω_s is the synchronous speed of the machine and ω_r is the rotor rotational speed. When operating as a generator, the rotor speed is greater than the synchronous speed, therefore the slip is negative.

$$\text{slip} = \frac{\omega_s - \omega_r}{\omega_s} \tag{2.4}$$

The introduction of an insulated three phase winding to the rotor of an induction machine forms a wound rotor machine. This rotor winding is connected via slip rings to a stationary circuit which allows control over the machine torque by regulating the rotor losses. Alternatively, the rotor winding can be connected to a power electronic converter and operated as a DFIG to implement control over the machine torque. The presence of power electronics also allows the recovery of the rotor loss energy, feeding it back to the stator or electrical source.

In normal operation, when connected to a stiff electrical grid, an induction generator is very robust and stable. Under a light driving torque the slip is low and torque will increase with the slip. The major issue with induction machines is the magnetising current supplied to the stator. This current is

wholly reactive and subsequently has a detrimental impact on the power factor at the machine terminals; compensation is commonly provided for this by parallel capacitor banks. In early wind turbines the squirrel cage induction generator was connected directly to a fixed frequency grid which meant it was effectively uncontrolled; therefore fluctuations in the shaft power fed into the machine from the turbine rotor are generally passed straight on to the electrical grid, causing voltage flicker [30]. The introduction of the frequency converter in a DFIG added a means of control, which has been extended where frequency converters are used to completely decouple the generator from the fixed network frequency. In such systems vector control algorithms are employed to provide full control over the generator torque [31] [5]. This removes the ability of an induction generator to autonomously change its generator torque in response to changes of the input torque, but does allow the rotational speed to change which is desirable in variable speed wind turbines.

Induction generator dynamic model

The dynamic model of an induction machine is vital to understanding its behaviour during operation. The dynamic model is expressed in terms of a two axis, rotating reference frame in Figure 2-10 and Figure 2-11 and by equations (2.5) to (2.12) [32]. The model consists of three sets of equations: voltage equations, flux equations and electromagnetic torque equations. The rotational speed of the two axis reference frame is ω rad/s, whereas the rotational speed of the machine rotor is ω_r rad/s. The terms $\omega\lambda_s$ and $(\omega-\omega_r)\lambda_r$ on the right hand side of equations (2.5) – (2.8) are referred to as the speed voltages, which arise due to the rotation of the reference frame, and λ denotes a magnetic flux. The model is usually implemented on a

synchronous rotating frame where ω is equal to ω_e, the machine stator electrical frequency.

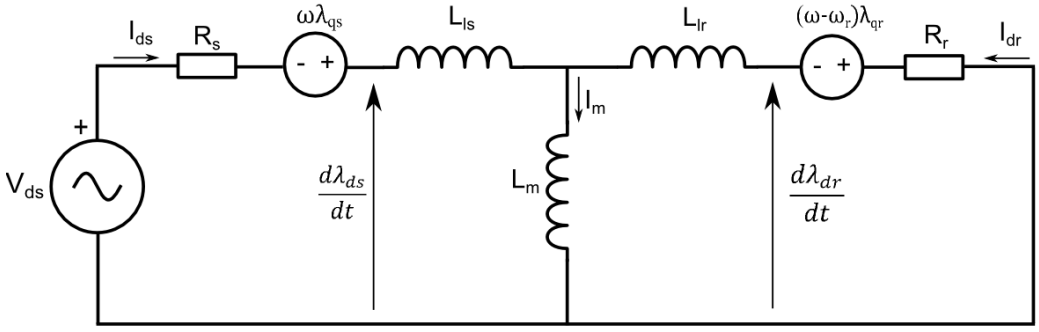

Figure 2-10: D-axis induction machine dynamic model [32].

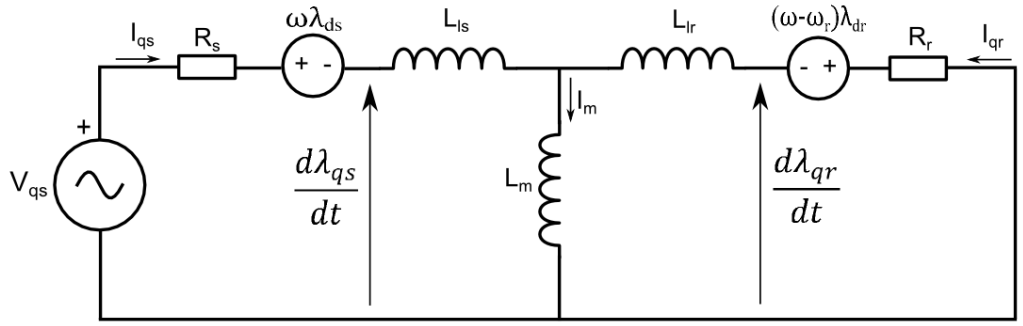

Figure 2-11: Q-axis induction machine dynamic model [32].

Voltage equations:

$$V_{ds} = R_s I_{ds} + \frac{d\lambda_{ds}}{dt} - \omega\lambda_{qs} \tag{2.5}$$

$$V_{qs} = R_s I_{qs} + \frac{d\lambda_{qs}}{dt} + \omega\lambda_{ds} \tag{2.6}$$

$$V_{dr} = R_r I_{dr} + \frac{d\lambda_{dr}}{dt} - (\omega - \omega_r)\lambda_{qr} \tag{2.7}$$

$$V_{qr} = R_r I_{qr} + \frac{d\lambda_{qr}}{dt} + (\omega - \omega_r)\lambda_{dr} \tag{2.8}$$

Flux linkage equations:

$$\lambda_{ds} = L_{ls} I_{ds} + L_m(I_{ds} + I_{dr}) \tag{2.9}$$

$$\lambda_{qs} = L_{sl} I_{qs} + L_m(I_{qs} + I_{qr}) \tag{2.10}$$

$$\lambda_{dr} = L_{lr}I_{dr} + L_m(I_{ds} + I_{dr}) \tag{2.11}$$

$$\lambda_{qr} = L_{lr}I_{qr} + L_m(I_{qs} + I_{qr}) \tag{2.12}$$

Where L_{ls} and L_{lr} are the stator and rotor leakage inductances, L_m is the magnetizing inductance.

To implement the model of the machine stator, equations (2.5) and (2.6) are rearranged and the current components derived from equations (2.9) and (2.10) by substituting in the mutual flux, which is:

$$\lambda_{dm} = L_m(I_{ds} + I_{dr}) \qquad \lambda_{qm} = L_m(I_{qs} + I_{qr})$$

Stator model:

$$\frac{d\lambda_{ds}}{dt} = [V_{ds} - R_sI_{ds} + \omega\lambda_{qs}] \tag{2.13}$$

$$\frac{d\lambda_{qs}}{dt} = [V_{qs} - R_sI_{qs} + \omega\lambda_{ds}] \tag{2.14}$$

Stator currents:

$$I_{ds} = \frac{(\lambda_{ds} - \lambda_{dm})}{L_{ls}} \tag{2.15}$$

$$I_{qs} = \frac{(\lambda_{qs} - \lambda_{qm})}{L_{ls}} \tag{2.16}$$

Similarly to implement the rotor model, equations (2.7) and (2.8) are rearranged and the currents derived from equations (2.11) and (2.12) by substituting in the mutual flux.

Rotor model:

$$\frac{d\lambda_{dr}}{dt} = [V_{dr} - R_rI_{dr} + (\omega - \omega_r)\lambda_{dr}] \tag{2.17}$$

$$\frac{d\lambda_{qr}}{dt} = [V_{qr} - R_rI_{qr} + (\omega - \omega_r)\lambda_{qr}] \tag{2.18}$$

Rotor currents:

$$I_{ds} = \frac{(\lambda_{dr} - \lambda_{dm})}{L_{lr}} \tag{2.19}$$

$$I_{qs} = \frac{(\lambda_{qr} - \lambda_{qm})}{L_{lr}} \tag{2.20}$$

The mutual fluxes are then calculated as functions of the stator and rotor fluxes, where $L_{ad} = L_{aq} = \frac{1}{\left(\frac{1}{Lm}+\frac{1}{L_{lr}}+\frac{1}{L_{ls}}\right)}$

$$\lambda_{dm} = L_{ad}\left[\frac{\lambda_{dr}}{L_{lr}} + \frac{\lambda_{ds}}{L_{ls}}\right] \tag{2.21}$$

$$\lambda_{qm} = L_{aq}\left[\frac{\lambda_{qr}}{L_{lr}} + \frac{\lambda_{qs}}{L_{ls}}\right] \tag{2.22}$$

The electromagnetic torque produced by the machine is given by

$$T_e = \frac{3p}{2}\left(I_{qs}\lambda_{ds} - I_{ds}\lambda_{qs}\right) \tag{2.23}$$

Where p is the number of pole pairs in the machine.

The mechanical model of the generator equates the electromagnetic torque produced by the machine with the input torque, T_r. This gives the generator acceleration as a result of the balance of the torques, where J = the inertia of the rotating components (kg.m^2).

$$\frac{J}{p}\frac{d\omega_r}{dt} = T_e - T_r \tag{2.24}$$

The dynamic model allows the response of the generator currents, fluxes, torque and rotational speed to be determined when changes of the terminal voltage, input torque or stator frequency occur. This model provides the basis for the simulation of the operation of an induction generator used in a wind turbine, in Chapter 4 of this thesis.

2.3.2 Permanent magnet generators

A PM generator is a form of synchronous generator where the rotor magnetic field is provided by permanent magnets. The rotation of the generator rotor rotates the magnetic field in the machine relative to the stator windings. This results in a changing magnetic flux linking with the stator winding, inducing a voltage. When the stator windings are part of a closed circuit, the induced voltage causes a current to flow; which in turn produces a second magnetic

flux in the generator. The phasor diagram in Figure 2-12, demonstrates the relationships between the voltages, currents and fluxes in the machine [33]. For simplicity of presentation the stator flux is aligned with the stator current, making it possible to show the fluxes, currents and voltages on one diagram. It is shown in Figure 2-12 that the load angle, δ, forms between the air-gap and rotor fluxes; this angle is directly related to the torque produced by the machine. The rotor and stator fluxes link with the stator windings to produce voltage components in the stator winding; which combine to give the terminal voltage of the machine, which is in quadrature to the air-gap flux. The voltage component related to the stator flux is effectively the voltage drop across the stator reactance, due to the stator current, I_a. In a PM generator the magnitude of the rotor flux, ϕ_r, is constant and therefore the output power factor will only change with the magnitude of V_t. Figure 2-12 shows the generator to be overexcited, therefore producing reactive power. The torque that is produced by the generator is given by equation (2.25); where it is a function of the voltage, E_r, induced by the rotor flux linkage ϕ_r, the terminal voltage, V_t, the stator reactance, X, and the load angle, δ. Maximum pull-out torque from the generator is achieved when δ = 90°.

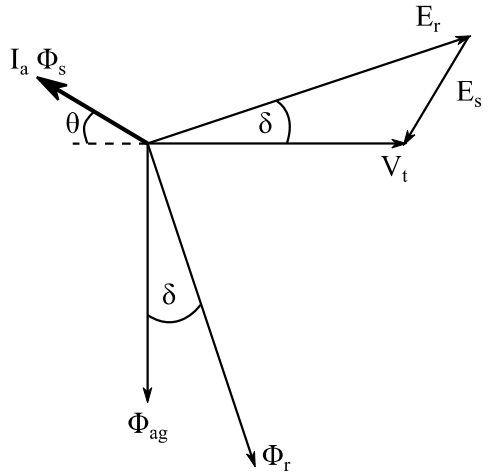

Figure 2-12: Combined electrical phasor and magnetic flux diagram for a PMG.

$$T_e = \frac{3.V_t.E_r.sin\delta}{\omega.X} \quad (2.25)$$

The relationship between the induced voltage in the stator and the rotational speed of the rotor leads to the electrical frequency equalling the rotational speed; therefore the rotor and stator fields are "synchronised". If such a generator were connected directly to a fixed frequency electrical network its rotational speed would be locked to the network frequency. The advantage of PM generators, in contrast to more conventional synchronous generators, is that the rotor magnetic field is naturally occurring within the magnetic material of the rotor and therefore it does not require an external current source for excitation. This also provides a significant advantage over induction generators, as it allows for a PM generator to operate with a greater efficiency [34].

There is a significant drive from wind turbine manufacturers to produce direct drive wind turbines, where the gearbox is not required between the turbine rotor and the generator. This requires bespoke generator designs that can operate at high power when rotating at low speeds. The power output capacity, P, of a generator can be described by equation (2.26); which shows that it is a function of the generator rotor diameter D, the length of rotor, l, and its rotational speed, ω, where K is a constant [3].

$$P = K.D^2.l.\omega \quad (2.26)$$

It can be observed from this equation that for low rotational speeds the generator must either be lengthened or its diameter increased so that the same power can be produced. Since the power is proportional to the square of the diameter, a smaller change of diameter can be made to achieve the necessary power, compared to length. Therefore most emerging designs of

direct drive generator in modern wind turbines have large diameters, of the order of 3 to 9 metres depending on the magnetic flux direction as it crosses the air-gap between the rotor and stator [35].

Permanent magnet generator dynamic model

To provide a dynamic model of a PMG, a two axis model operating in a rotating reference frame, synchronised with the rotor of the machine, is used [33]. The d and q axes are aligned so that the rotor flux acts on the d axis, as shown in Figure 2-13. Equations (2.27) and (2.28) give the rate of change of the d and q axis winding currents, I_{ds} and I_{qs}, as functions of the axis voltages, V_{ds} and V_{qs}, inductances, L_{ds} and L_{qs}, resistances, R_{ds} and R_{qs}, and the flux of the permanent magnets of the machine rotor, ϕ_r. Equation (2.29) gives the torque produced by the machine, T_e, as a function of the axis currents and rotor flux. The rotational acceleration of the machine is governed by equation (2.30), which balances the machine torque and the input mechanical torque, T_r. Also taken into account in this equation is the inertia, J, of the rotating components; which, in a wind turbine would be the sum of the generator inertia and wind turbine rotor inertia, referred to the high speed side of the gearbox (where a gearbox is present). The rotor of the PM generator can be salient or round (non-salient); by assuming a round rotor, the inductances L_{ds} and L_{qs} will be equal to each other.

$$\frac{di_{ds}}{dt} = \frac{V_{ds} + L_{qs}\omega_e i_{qs} - i_{ds}R_{ds}}{L_{ds}} \tag{2.27}$$

$$\frac{di_{qs}}{dt} = \frac{V_{qs} - L_{ds}\omega_e i_{qs} - i_{qs}R_{qs} - \Phi_r\omega_r}{L_{qs}} \tag{2.28}$$

$$T_e = \frac{3p}{2}\left[i_{ds}i_{qs}\left(L_{ds} - L_{qs}\right) + \Phi_r i_{qs}\right] \tag{2.29}$$

$$\frac{d\omega_r}{dt}J = (T_e - T_m) \tag{2.30}$$

From these equations it can be observed that the torque produced by the generator is a function of the q axis current only (when the generator rotor is non-salient). The voltage that is induced in the stator windings of the generator will always lead the field by 90°; however the output current phasor angle will vary in relation to the terminal voltage depending upon the loading and power factor of the generator. This mathematical model provides the basis for the PM generator used in the wind turbine modelled in Chapter 4 of this thesis.

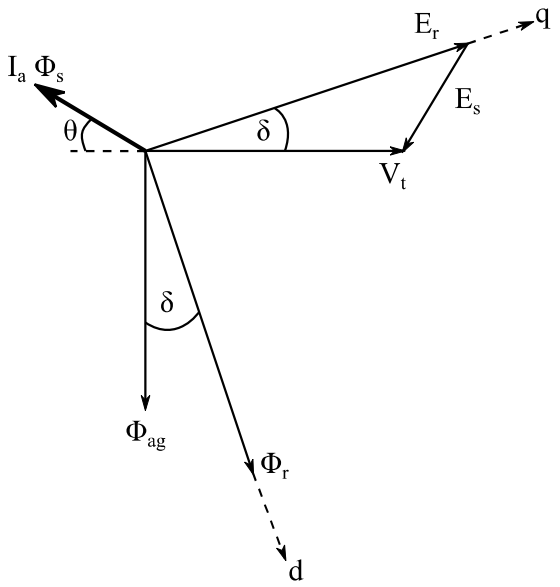

Figure 2-13: Combined electrical phasor and magnetic flux diagram for a PM generator, showing the d and q axes used in the dynamic model.

2.4 Power electronic converter reliability

Power converter reliability is an important subject in all applications. The definition of reliability is "the probability of a system to perform its purpose adequately under the operating conditions encountered for the period of time intended" [36]. The two key phrases in this definition are: "perform its purpose adequately under the operating conditions encountered" and "period of time intended". By relating these phrases to the deployment of power converter in wind turbines, the following observations can be made: the operating conditions that a wind turbine power converter must endure are dictated by the continuously changing wind speeds which manifest themselves as cyclic power flows through the converter; and the expected period of operation of a wind turbine converter is effectively continuous for potentially the whole life of a wind turbine, 20-25 years. The reliability of wind turbine power converters can be assessed in two different ways: 1) statistical analysis of operational data where the reliability is assessed on the basis of the number of observed failures over a period of time; and 2) stress analysis where the various failure modes of the converters are analysed in tandem with predictions of the operating conditions [37].

The analysis of operational data to determine reliability of wind turbine components has been conducted quite extensively in the literature [7, 38-40]. Critical to these analyses is the availability of significant amounts of operational data, ideally for the whole lifetime of a wind turbine. Herein lies the limitation to these analyses, as relatively speaking the wind generation industry is quite young and few turbines have completed their operational lives. Wind turbine technology has also advanced significantly over recent years, which further restricts the availability of consistent and comparable data for assessment. The assessments in the literature give conclusions based

on data from relatively few sources, namely the Windstats newsletter from Denmark [41] and LWK from Germany and Denmark [42]. These studies cover the whole range of wind turbine subsystems, but struggle to reflect the impact of various factors affecting reliability. There have also only been limited attempts to separate data reflecting the reliability of power converters from other components, mainly because of difficulties attributing a failure to a particular component.

Stress analysis is a method that is used quite extensively to assess the reliability of electrical components [43]. This method must be adapted for application to wind turbine power converters to reflect the operational states of a converter, as suggested in [37], and relies upon knowledge of the component breakdown of a converter; therefore allowing estimation of the failure rate of each individual component based upon the heat cycling it experiences. The failure rates of each component are then combined to provide estimates of the failure rate of the whole converter.

The significance of the reliability of wind turbine components is highlighted by the shift of wind farm development offshore by [44]. The example given, states that an onshore wind farm, consisting of 150 2MW wind turbines, requires at least 600 visits in one year for the wind farm to achieve an availability of 98%. This does not present a major problem onshore as turbines can be assessed anytime for maintenance. However if the accessibility of a wind farm were reduced to 65% by the availability of weather windows suitable for vessel access, the availability of wind farm falls to 90% [44]. Therefore if the reliability of the subsystems within a wind turbine can be improved, the required number of visits to each turbine can be reduced, mitigating some of the effects of lower accessibility to the turbines.

Power converter reliability data

The two methods used in the literature to assess the reliability of power converters and other electrical equipment in a wind farm, have produced a range of figures. A summary of these figures are as follows.

- [45] gives the failure rates of the major elements of a wind farm electrical network, replicated in Table 2-1. An estimate of the mean time to repair (MTTR) for each element in an offshore wind farm is also given. MTTR is dominated by the access time for inspection and repair, depending on the type of failure and time of year. This dataset does not include the power converter.

Table 2-1: Failure rates of various electrical components [46].

Equipment	*Failure rate [1/year]*	*MTTR [h]*
Medium-voltage breaker	0.025	240
Medium-voltage switch	0.025	240
Low-voltage contactor	0.0667	240
Nacelle Transformer	0.0131	240
5km feeder cable	0.015	1440
1.2km tower-tower cable	0.015	1440

- [7] Presents failure data from two different wind turbine converters and compares them with failure data for similar converters used in other industries. The failure data for the converter in this case has been aggregated with the data for its sub-assemblies to overcome difficulties in recording. From general industrial experience, the failure rate of converters was found to range from 0.045 - 0.2 failures per year. Whereas data collected from wind turbine converters with

operational life of 11 years and 9 years suggests the failure rates to be approximately 0.3 failures per year.

- [47] gives estimates of power converter failure rates differentiated by the type of generator used within the turbine. Where an induction generator is used the power converter failure rate is found to about 0.47 failures per year, and where a PM generator is used 1.03 failures per year occur. Figures are also given for the failure rate of the generators themselves: 0.06 and 0.22 failures per year for induction generators and PM generators respectively. The data set used in this study comprises of an uneven split by generator technology, 73% induction generator based, 27% PM generator; of the PM generators studied 23% are direct drive. This reflects the relative infancy of PM generator use in wind turbines, at the time of writing of the article, which is suggested as a contributory factor to the high failure rates of converters working with them. It is also likely that the induction generator wind turbines are smaller than those with PM generators, and therefore would exert less stress on the converters. The figures produced by this study are based upon operational data from the German 250MW wind test program [48], Windstats newsletter [41] and the LWK survey [42].
- [39] gives a comparison of failure data for geared and direct drive based wind turbines based on four different turbines, 2 geared and 2 direct drive. One turbine of each type is chosen to have a rating in the range of 500kW and one of 1.5MW. The geared turbines also all use DFIGs and the direct drive turbines use synchronous generators with either wound rotors or permanent magnets. It is found by this study that the power converters in the geared turbines have failure rates of

0.254 and 0.357 failures per year for the 500kW and 1.5MW turbines respectively, and the direct drive turbine converters have failure rates of 0.317 and 0.287 failures per year, respectively. The figures produced by this study are based upon operational data from the Windstats newsletter [41] and the LWK survey [42].

- [37] presents data calculated by a stress analysis of the components within a 2MW wind turbine converter, consisting of a four quadrant back to back converter. The data has been produced using wind speeds measured at two sites in Holland, with averages of 6.67m/s and 5.3m/s, to give a representation of the range and frequency of the converter output power levels. For the 6.67m/s site the failure rate is given as 0.4527 failures/ year and for the 5.3m/s site the failure rate is given as 0.2273 failures per year.

Table 2-2: Summary of converter failure rates from different sources.

Source	Converter Failure Rate (Failures / year)	Comments
[7]	0.3	
[25]	0.47	Induction generator
[25]	1.03	PM generator
[17]	0.254	~500kW geared turbine
[17]	0.357	1.5MW geared turbine
[17]	0.317	~500kW direct drive turbine
[17]	0.287	1.5MW direct drive
[15]	0.4527	6.67m/s average wind speed
[15]	0.2273	5.3m/s average wind speed
	0.4463	**Average all included**
	0.349	**Average excluding PM generator figure from [25]**

The data that has been identified from the different sources, summarised in Table 2-2, gives an average failure rate of 0.4463 failures per year. (Where the figure of 1.03 failures / per year from [25], that is significantly larger than the others, is neglected the average failure rate is 0.349 failures per year). Comparing these figures to those presented in Table 2-1 for the other electrical components within a wind farm, highlights that even the best case failure rate for a power converter is significantly higher than any other electrical component. Reflecting on the two key aspects to reliability set out that the beginning of the section highlights that the current power converters used in wind turbines are not particularly good at surviving for the intended life of a wind turbine and that, as shown by the fatigue analysis in [37], their reliability varies with their operating conditions.

2.5 References

1. Betz, A., *Schraubenpropeller mit geringstem energieverlust, as cited by Burton. T, Wind Energy Handbook.* 1919.
2. Jonkman, J., et al., *Definition of a 5MW reference wind turbine for offshore system development*, 2009, NREL.
3. Burton. T, et al., *The Wind Energy Handbook*. Vol. 1. 2008: Wiley.
4. Burton. T, S.D., Jenkins. N, Bossanyi E, *The Wind Energy Handbook*2008: Wiley.
5. Iov, F. and F. Blaabjerg. *Power electronics and control for wind power systems*. in *Power Electronics and Machines in Wind Applications, 2009. PEMWA 2009. IEEE*. 2009.
6. Feng, Y., P.J. Tavner, and H. Long, *Early experiances with UK Round 1 offshore wind farms.* Proceedings of the Intsitution of Civil Engineers : energy, 2010. 163.
7. Spinato, F., et al., *Reliability of wind turbine subassemblies.* Renewable Power Generation, IET, 2009. 3(4): p. 387-401.
8. Franken, B., et al. *Collection grid topologies for off-shore wind parks*. in *Electricity Distribution, 2005. CIRED 2005. 18th International Conference and Exhibition on*. 2005.
9. Lumbreras, S. and A. Ramos, *Offshore wind farm electrical design: a review.* Wind Energy, 2012: p. n/a-n/a.

10. Quinonez-Varela, G., et al., *Electrical collector system options for large offshore wind farms.* Renewable Power Generation, IET, 2007. 1(2): p. 107-114.
11. B. Van Eeckhout, et al., *Economic comparison of VSC HVDC and HVAC as transmission system for a 300 MW offshore wind farm.* European Transactions on Electrical Power, 2010. 20(5): p. 661-671.
12. Caillez, H., et al., *Design and construction of the cross-channel d.c. interconnector.* Electrical Engineers, Proceedings of the Institution of, 1963. 110(3): p. 603-618.
13. Foley, A.M., P. Leahy, and E.J. McKeogh. *Wind energy integration and the Ireland-Wales interconnector*. in *Sustainable Alternative Energy (SAE), 2009 IEEE PES/IAS Conference on*. 2009.
14. Teeuwsen, S.P. and R. Rossel. *Dynamic performance of the 1000 MW BritNed HVDC interconnector project*. in *Power and Energy Society General Meeting, 2010 IEEE*. 2010.
15. Rudervall, R., *High Voltage Direct Current (HVDC)Transmission Systems Technology Review Paper*, 2000.
16. Bodin, A. *HVDC Light - A preferable power transmission system for renewable energies*. in *Energetics (IYCE), Proceedings of the 2011 3rd International Youth Conference on*. 2011.
17. B. D. Railing, J.J.M., P. Steckley, G. Moreau, P. Bard, L. Ronstrom, J. Lindberg, *Cross Sound Cable Project second generation VSC technology for HVDC.* CIGRE B4-102, 2004.
18. Axelsson, U., et al. *The Gotland HVDC Light project-experiences from trial and commercial operation*. in *Electricity Distribution, 2001. Part 1: Contributions. CIRED. 16th International Conference and Exhibition on (IEE Conf. Publ No. 482)*. 2001.
19. R. Hodges, S. Dixon, and G. Bathurst, *Management of low frequency resonances for large scale offshore wind power plants with long AC cable connections*, in *12th Wind Integration Workshop*2013: London.
20. C. Zhang. *Developing Efficient & Secure Grid Connection in Deeper Waters, Further Offshore by Optimising Electrical Design & Transmission Technologies*. in *Deeper Water Offshore Wind Conference – Lowering Costs Together*. 2013.
21. Vrana, T.K., et al. *The North Sea Super Grid - a technical perspective*. in *AC and DC Power Transmission, 2010. ACDC. 9th IET International Conference on*. 2010.
22. Bauer, P., et al. *Evaluation of electrical systems for offshore windfarms*. in *Industry Applications Conference, 2000. Conference Record of the 2000 IEEE*. 2000.

23. Beno, J.H., R.E. Hebner, and A. Ouroua. *High-frequency power generation and distribution in multi-megawatt power systems*. in *Electric Ship Technologies Symposium (ESTS), 2011 IEEE*. 2011.
24. Eid, A., et al. *Constant frequency aircraft electric power systems with harmonic reduction*. in *Industrial Electronics, 2008. IECON 2008. 34th Annual Conference of IEEE*. 2008.
25. Prasai, A. and D. Divan. *DC Collection for Wind Farms*. in *Energy 2030 Conference, 2008. ENERGY 2008. IEEE*. 2008.
26. Robinson, J., et al., *Analysis and Design of an Offshore Wind Farm Using a MV DC Grid.* Power Delivery, IEEE Transactions on, 2010. 25(4): p. 2164-2173.
27. Max, L., T. Thiringer, and O. Carlson, *Control of a wind farm with an internal direct current collection grid.* Wind Energy, 2011: p. n/a-n/a.
28. Meyer, C., et al. *Control and Design of DC-Grids for Offshore Wind Farms*. in *Industry Applications Conference, 2006. 41st IAS Annual Meeting. Conference Record of the 2006 IEEE*. 2006.
29. C Zhan, C.S., A Crane, A bullock, D Grieve, *DC Transmission and Distribution System for a Large Offshore Wind Farm*, in *IET AC DC 2010*2010: Savoy Place, London.
30. Bossanyi, E., Z. Saad-Saoud, and N. Jenkins, *Prediction of flicker produced by wind turbines.* Wind Energy, 1998. 1(1): p. 35-51.
31. Domi, et al. *Vector control of squirrel cage induction generator for wind power*. in *Electrical Machines (ICEM), 2010 XIX International Conference on*. 2010.
32. Wu, B., *High-Power Converters and AC Drives*2006: Wiley Inter-Science.
33. Say, M.G., *Alternating Current Machines*. 5th ed1983: John Wiley & Sons.
34. Liserre, M., et al., *Overview of Multi-MW Wind Turbines and Wind Parks.* Industrial Electronics, IEEE Transactions on, 2011. 58(4): p. 1081-1095.
35. Zavvos, A., et al. *Structural comparison of permanent magnet direct drive generator topologies for 5MW wind turbines*. in *Power Electronics, Machines and Drives (PEMD 2012), 6th IET International Conference on*. 2012.
36. Roy Billinton, R.N.A., *Reliability evaluation of engineering systems: concepts and techniques*. 2nd ed1996.
37. Kaigui, X., J. Zefu, and L. Wenyuan, *Effect of Wind Speed on Wind Turbine Power Converter Reliability.* Energy Conversion, IEEE Transactions on, 2012. 27(1): p. 96-104.

38. Arabian-Hoseynabadi, H., H. Oraee, and P.J. Tavner, *Wind turbine productivity considering electrical subassembly reliability.* Renewable Energy, 2010. 35(1): p. 190-197.
39. Arabian-Hoseynabadi, H., P.J. Tavner, and H. Oraee, *Reliability comparison of direct-drive and geared-drive wind turbine concepts.* Wind Energy, 2010. 13(1): p. 62-73.
40. Tavner, P.J., J. Xiang, and F. Spinato, *Reliability analysis for wind turbines.* Wind Energy, 2007. 10(1): p. 1-18.
41. *Windstats Newsletter*, 1999-2001.
42. *Eggersglub: Windenergie X Praxisergebnisse, Landwwirtschaftskammer Schleswig-Holstein*, 1995 - 2004.
43. Abdi, B., et al., *Reliability Considerations for Parallel Performance of Semiconductor Switches in High-Power Switching Power Supplies.* Industrial Electronics, IEEE Transactions on, 2009. 56(6): p. 2133-2139.
44. G.J.W. van Bussel, M.B.Z., *Offshore wind energy, the reliability dilemma*, in *The First World Wind Energy Conference*2002: Berlin.
45. Ambra Sannino, H.B., Erik Koldby Nielsen, *Reliability of Collection Grids for Large Offshore Wind Parks*, in *9th International Conference on Probabilistic Methods Applied to Power Systems*2006: Stockholm.
46. Ambra Sannini, H.B., Erik Koldby Nielsen, *Reliability of Collection Grids for Large Offshore Wind Parks*, in *9th International Conference on Probabilistic Methods Applied to Power Systems*2006: Stockholm.
47. E. Echavarria, B.H., G. J. W. van Bussel, T. Tomiyama, *Reliability of Wind Turbine Technology Through Time.* Journal of Solar Energy Engineering, 2008. 130.
48. ISET, *Wind energy report Germany 2006*, 2006.

Chapter 3 Cluster Based Collection Networks

Cluster based collection networks form one part of a hybrid collection network architecture. The objective of such a network is to allow variable speed operation of a small group of wind turbines without each requiring an individual power converter. It was alluded to in the previous chapter that a cluster system could be implemented using a variable frequency AC network; in addition, a DC electrical network could also be used by incorporating simple and robust passive rectification of the generator output. A cluster collection network connects the generators of the turbines in parallel via lengths of cable at a point of common coupling (PCC), from where a single cable runs to the cluster power converter. The cluster power converter facilitates the variable speed operation of the turbines by either regulating the electrical frequency of the AC network or the common point voltage, in a DC network. It is anticipated that the removal of the power

converters from each individual wind turbine and the use of a single power converter for a group of turbines, will reduce the number of converter failures in a wind farm. This will be particularly beneficial to an offshore wind farm because the number of visits required to each turbine to carry out remedial action, following the failure of the power converter, will be significantly reduced. However, the resultant close relationship between the rotational speeds of the turbines in a cluster will prevent each turbine operating at its optimal rotational speed for its local wind conditions, introducing an energy capture penalty. The use of a cluster based system will require the redesign of a typical wind farm electrical system so that the turbines are connected in a star formation, instead of the radial network designs that are currently preferred [1]. This will allow the positioning of the converters for multiple clusters at one or more common location, depending on the size of the wind farm; which in an offshore wind farm would be located on substation platforms. A second level of collection network would also be required to connect the converter substations with the grid connection substation. Figure 3-1 shows a diagram of the electrical layout of a wind farm which is based upon clusters of turbines.

The aim of this chapter is to investigate the potential benefits to the availability of a wind farm brought by implementing a cluster based collection network; it will also investigate the size of the energy capture penalty introduced by the close association between the rotational speeds of the clustered turbines, in comparison to where the turbines are independent. Finally this chapter will describe the different technologies that could be used to implement the cluster collection network, how it is envisaged they would operate and the merits and pitfalls of each.

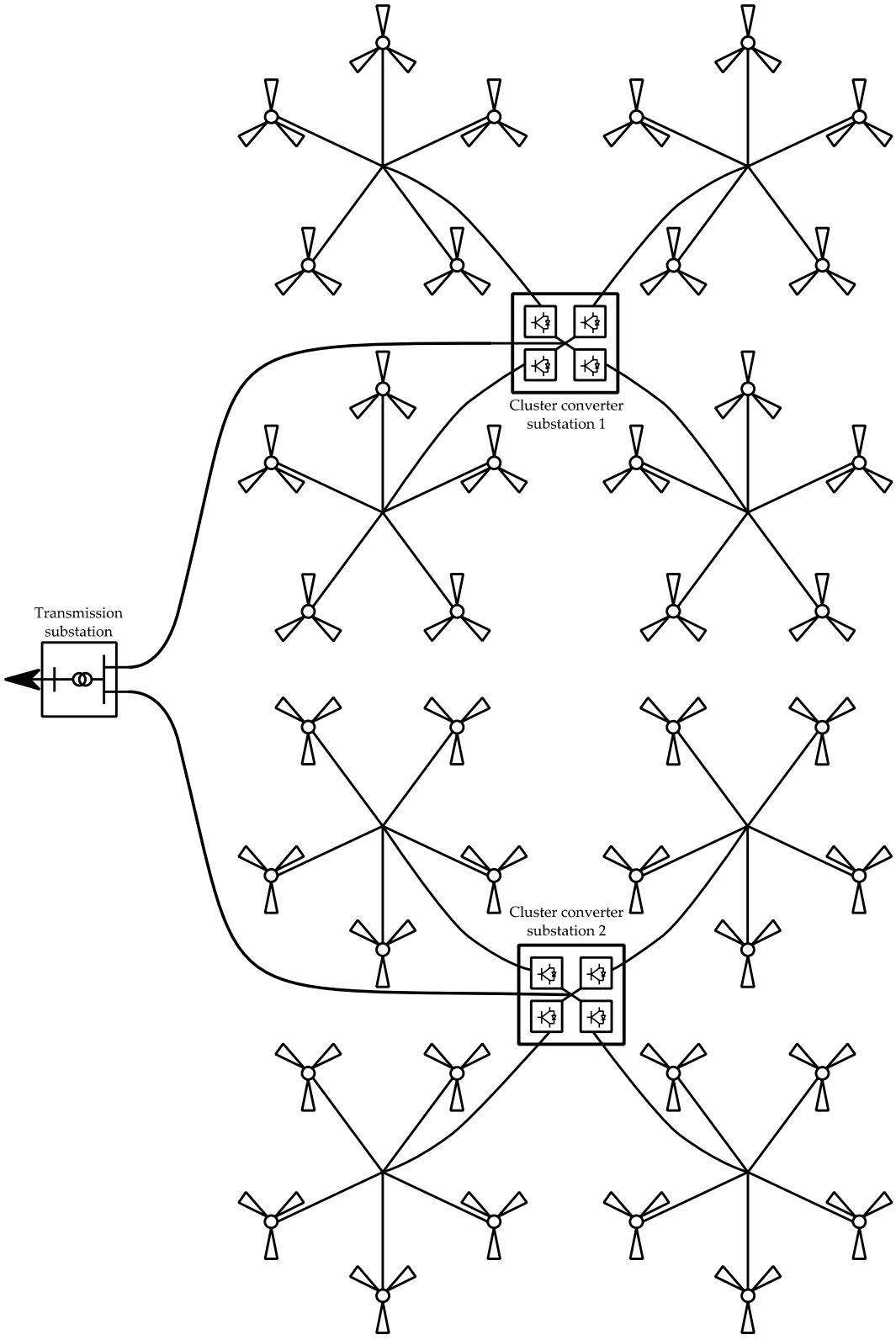

Figure 3-1: An example of a possible wind farm electrical layout based around clusters of five wind turbines.

3.1 Wind turbine availability

The availability of a wind turbine can be described in two ways: Technical Availability, which describes the amount of time a turbine is available to generate electricity as a percentage of the theoretical maximum, or Commercial Availability, which describes the amount of time a turbine is available to generate as a percentage of a contracted maximum, which makes some allowances for maintenance and repair downtime [2]. To determine the availability of a wind turbine, the failure rate of the turbine which takes into account the failure rate of all of the individual components, and the repair time for each failure are required.

The aim of this investigation is to determine the impact of using a cluster based collection network on the availability of a group of turbines, where a single power converter is required for a group of turbines over the case where each turbine has an individual power converter. To enable this, the effect on the turbine availability of the different number and location of the converters has to be separated from the effect of the reliability of the other components in the system. This can be achieved by assuming the failure rates of all other components and subsystems in a wind turbine and wind farm would not be affected by the change of the electrical layout used, therefore they will not influence the results of this analysis.

The key basis for this investigation is adequate data describing the reliability of a power converter and also the repair times. Data describing the reliability of power converters in wind turbines has been set out in Table 2-2. Difficulty sourcing suitable data that differentiates between converter type and size requires, for the purposes of this study, for it to be assumed that the reliability of the power converters in the individual and cluster cases are

equal. There is precedent however for high power converters to incorporate redundancy in their designs which may improve their fault tolerance and resilience, however such converters have so far been produced in smaller numbers, therefore their designs may be less mature which may have the opposite effect [3] [4]. Although the introduction of redundancy and the development of a larger converter are likely to involve additional costs, the benefit of additional resilience to the failure rates of the fewer larger power converters within a cluster based offshore wind farm could be merited.

The repair time of a converter is a function of the particular mode of failure, the availability of a replacement part, manpower to make the repair and also the accessibility of the turbine. It is assumed that the availability of replacement parts and manpower would be equal in either case and therefore has no influence on the result of this analysis. In reality it is possible that the repair time of a larger converter could be greater as a result of their being less experience working with such converters and also because the availability of spare parts may be worse, due to the smaller number of converters in operation and higher cost of components. [5] gives a figure of 73 repairs per year for the repair rate of power converters in an onshore wind farm, which indicates the number of converters that can be repaired annually with near 100% accessibility.

The remaining aspect that affects the repair time of a converter in either case is access to the location of the failed converter, either in a turbine nacelle / tower or on a substation platform. Data describing the accessibility rate of an offshore wind farm is scarce in the public domain, however [2] indicates that wave heights must not be more than 1.5m for safe access to a turbine by boat and [6] gives an accessibility of 65% for the proportion of time the turbines in

Horns Rev wind farm, Denmark, are accessible. For the purposes of this investigation it is also assumed that the accessibility of a substation platform is the same as that of a turbine.

Using this data and the smaller average of the converter failure rates calculated in the previous chapter, 0.349 failures per year, the technical availability of a group of five turbines with individual converters or operating in a cluster can be determined by firstly calculating the Mean Time to Failure (MTTF) of the converters in the group, then calculating the Mean Time to Repair of a single converter (MTTR) and the Mean Time Between Failures (MTBF); equations (3.1) - (3.8).

For a group of five wind turbines with individual converters:

$$MTTF = \frac{1}{failure\ rate \times no.converters} = \frac{1}{0.349 \times 5} = \mathbf{0.573\ years} = \mathbf{209 days} \tag{3.1}$$

$$MTTR = \frac{1}{repair\ rate\ \times accesibility} = \frac{1}{73\ \times 0.96} = \mathbf{0.0211\ years} = \mathbf{7.7\ days} \tag{3.2}$$

$$MTBF = MTTF + MTTR = \mathbf{0.5941\ years} \tag{3.3}$$

Therefore the technical availability of five turbines with individual converters is:

$$Technical\ Availability = \frac{MTTF}{MTBF} = 0.9645 = \mathbf{96.45\%} \tag{3.4}$$

For a group of five turbines connected together in a cluster with a single converter:

$$MTTF = \frac{1}{failure\ rate} = \frac{1}{0.349} = \mathbf{2.87 years} = \mathbf{1048\ days} \tag{3.5}$$

$$MTTR = \frac{1}{repair\ rate\ \times accesibility} = \frac{1}{73\ \times 0.96} = \mathbf{0.0211\ years} \quad (3.6)$$
$$= \mathbf{7.7\ days}$$

$$MTBF = MTTF + MTTR = \mathbf{2.89\ years} \quad (3.7)$$

The technical availability of five turbines connected together with a single converter is therefore:

$$Technical\ Availability = \frac{MTTF}{MTBF} = 0.993 = \mathbf{99.3\%} \quad (3.8)$$

It is shown by this analysis that reducing the number of converters by clustering the wind turbines together improves the technical availability of the group of five turbines by 2.85%. These values of availability refer to the readiness of all five turbines in a cluster to generate electricity together; it does not consider the possibility of fewer than five turbines being operable, as may be the case when they have individual converters. It should also be noted that reducing the number of converters reduces the overall number of failures in the group from 1.74 failures per year to 0.349, therefore reducing the number of visits to a wind farm to repair the converters within this group five-fold.

In addition, the effects of the reduced availability on the energy captured by the group of wind turbines should also be considered; taking into account the fact that the failure of the cluster power converter will require the shutdown of all five wind turbines. In order to observe the effects of this, the annual energy production (AEP) of a single wind turbine, with 100% availability, is required along with a figure representative of the amount of energy a turbine would not produce over the 7.7 day period required for the

power converter repair. To determine the AEP the turbine parameters detailed in Chapter 4 are used to produce the turbine power curve, which is then combined with the Weibull Distribution, produced with an average wind speed of 8m/s and shape factor of 2, to give the annual probability distribution of each wind speed across the normal operating range of a wind turbine (4m/s – 25m/s in 0.5m/s steps) [7]. The average amount of energy a turbine will produce over a period of 7.7 days is then determined by dividing the AEP by the number of 7.7 day periods in a year (47.4). Both are given in Table 3-1.

Table 3-1: Annual energy production of a single turbine and the average energy produced over a 7.7day period.

Annual	7.7 days
17.5GWh	369.196MWh

Therefore by combining the annual number of failures of the individual power converters and the cluster converter, with the amount of energy lost each time there is a failure, the resultant annual energy production of the group of turbines can be determined, shown in Table 3-2. These figures indicate that clustering has no impact on their annual energy production. However, if the failure rate of the cluster converter were lower than the converters used in the individual turbines, clustering would improve the energy production of the group turbines.

Table 3-2: Resultant annual energy capture taking into account the energy lost following the failure of a power converter.

Converters per group	Energy loss per failure	MTTF	No. failures	Energy lost
5	369.196MWh	0.573yr	1.745/yr	644.25MWh
1	1,846MWh	2.865yr	0.349/yr	644.25MWh

Resultant AEP	% Reduction
16,856MWh	3.681%
16,856MWh	3.681%

The analysis so far has been conducted for a single group of five wind turbines; however offshore wind farms are made up of many hundreds of turbines. Therefore the benefits of using a cluster based collection network will be significantly larger in terms of the availability of a whole wind farm. To demonstrate this, a case study is analysed based upon the Dogger Bank Creyke Beck A wind farm.

3.1.1 Case study: Dogger Bank Creyke Beck A

Dogger Bank is an area of the North Sea earmarked for the development of a wind farm by the Forewind consortium [8]. Forewind have split the Dogger Bank area up into smaller zones, the first two that will be developed are Creyke Beck A and B; each will have a generating capacity of 1.2GW and are located 131km from shore at their nearest point. For this case study only Creyke Beck A will be considered and it is assumed that each turbine will have an output capacity of 5MW (information regarding the actual turbines that will be used is not publicly available), therefore the wind farm will consist of 240 turbines. Following the same method as above, the availability of the wind farm and the AEP have been calculated where each wind turbine

has an individual power converter and where the wind farm is separated into 48 clusters of 5 wind turbines, requiring one power converter per cluster. The same data regarding the failure and repair rates of the converters and the wind farm average wind speed is used, as above.

For Creyke Beck A wind farm with 240 individual turbines and converters:

$$MTTF = \frac{1}{failure\ rate \times no.converters} = \frac{1}{0.349 \times 240} = \mathbf{0.0119\ years} = \mathbf{4.34\ days} \tag{3.9}$$

$$MTTR = \frac{1}{repair\ rate\ \times accesibility} = \frac{1}{73\ \times 0.96} = \mathbf{0.0211\ years} = \mathbf{7.7\ days} \tag{3.10}$$

$$MTBF = MTTF + MTTR = \mathbf{0.033\ years = 12.05days} \tag{3.11}$$

Therefore the technical availability of the 240 turbines is:

$$Technical\ Availability = \frac{MTTF}{MTBF} = 0.3606 = \mathbf{36.06}\% \tag{3.12}$$

For Creyke Beck A wind farm with 240 individual turbines separated in to 48 clusters of 5 turbines, with a single converter per cluster:

$$MTTF = \frac{1}{failure\ rate \times no.converters} = \frac{1}{0.349 \times 48} = \mathbf{0.0588\ years} = \mathbf{21.5\ days} \tag{3.13}$$

$$MTTR = \frac{1}{repair\ rate\ \times accesibility} = \frac{1}{73\ \times 0.96} = \mathbf{0.0211\ years} = \mathbf{7.7\ days} \tag{3.14}$$

$$MTBF = MTTF + MTTR = \mathbf{0.0799\ years = 29.16days} \tag{3.15}$$

Therefore the technical availability of the 48 clusters of turbines is:

$$Technical\ Availability = \frac{MTTF}{MTBF} = 0.736 = \mathbf{73.6}\% \tag{3.16}$$

Table 3-3 gives the calculated values of the wind farm AEP, indicating that it is not affected by the improved availability, as above.

The figures calculated here indicate that reducing the number of power converters in the wind farm brings a clear benefit to the technical availability, but also that the reduced number of power converters has no impact on the wind farm AEP. While the figures give an indication of the improved availability, it is possible that the rate of repair of the power converters will be significantly higher in reality, as it is likely that it would be worth the extra investment by the wind farm operator to employ extra maintenance crews to carry out more repairs in such a large wind farm, where each crew could potentially repair at least 73 converters per year.

Table 3-3: Resultant annual energy capture taking into account the energy lost following the failure of a power converter, for the Creyke Beck A wind farm.

Converters per group	Energy loss per failure	MTTF	No. failures	Energy lost
5	369.196MWh	0.01194yrs	83.76/yr	30,923MWh
1	1,846MWh	0.0597yrs	16.75/yr	30,923MWh

Resultant AEP	% Reduction
4,169.28GWh	0.736%
4,169.28GWh	0.736%

3.1.2 Sensitivity study of availability figures

Limited information is available regarding the man power, repair rates and accessibility of most modern offshore wind farms; therefore the sensitivity of the calculated figures to greater repair rates and lower failure rates of the converters and also greater accessibility to the turbines is investigated. The following plots show the sensitivity of the availability figures calculated for the Creyke Beck A wind farm to these factors, when the turbines have individual power converters and when they are grouped together into clusters with a single power converter per cluster and controlled collectively.

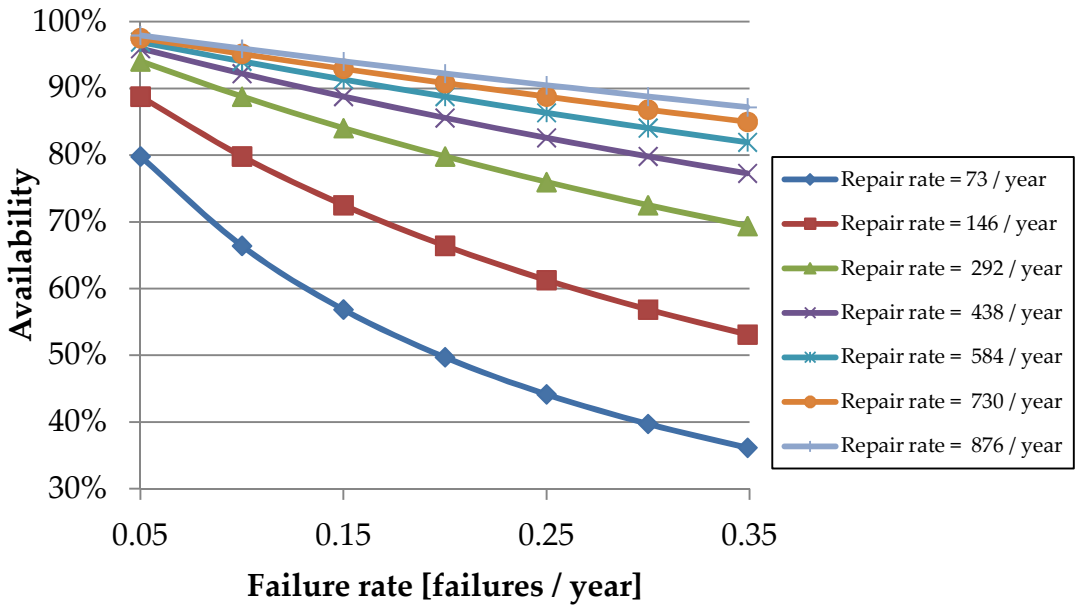

Figure 3-2: Availability of the wind farm where the turbines have individual power converters and their failure and repair rates are varied; assuming a constant turbine accessibility of 65%.

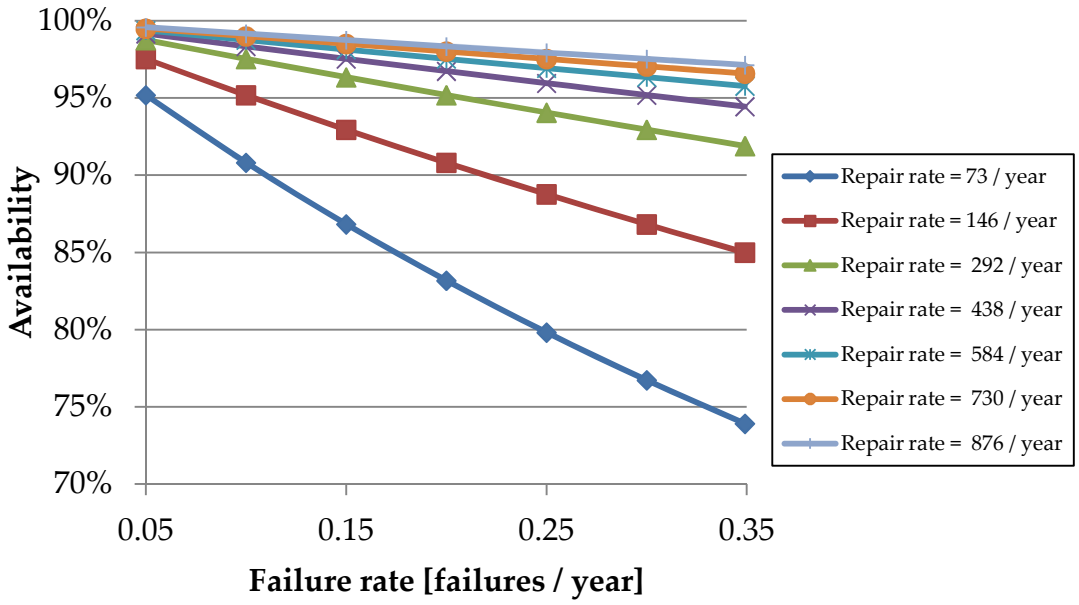

Figure 3-3: Availability of the wind farm where the turbines are clustered together with a single power converter per cluster and their failure and repair rates are varied; assuming a constant turbine accessibility of 65%.

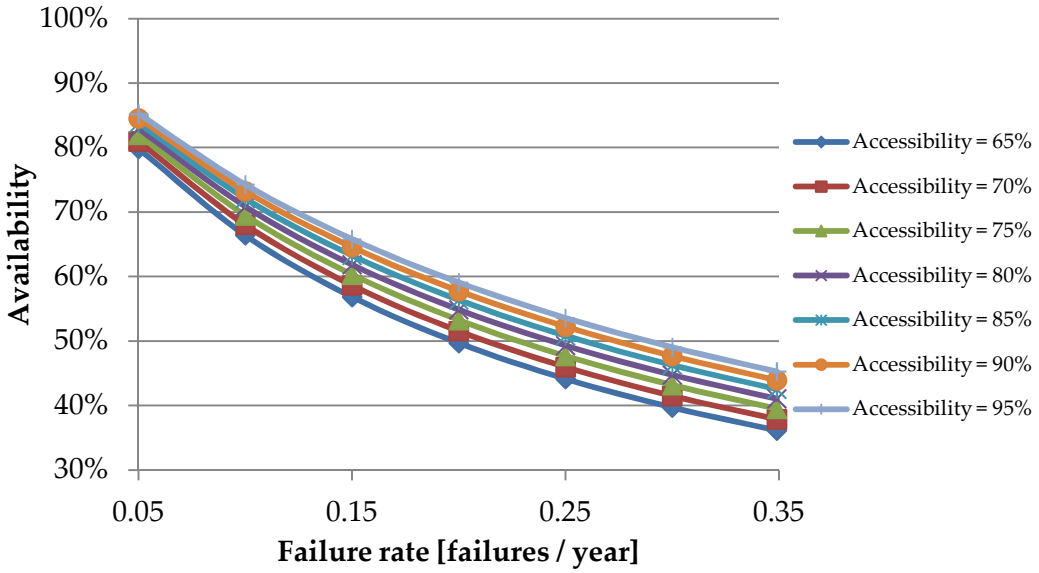

Figure 3-4: Availability of the wind farm where the turbines have individual power converters and the failure rate and proportion of time the turbines are accessible are varied; assuming a constant repair rate of 73 converter repairs per year.

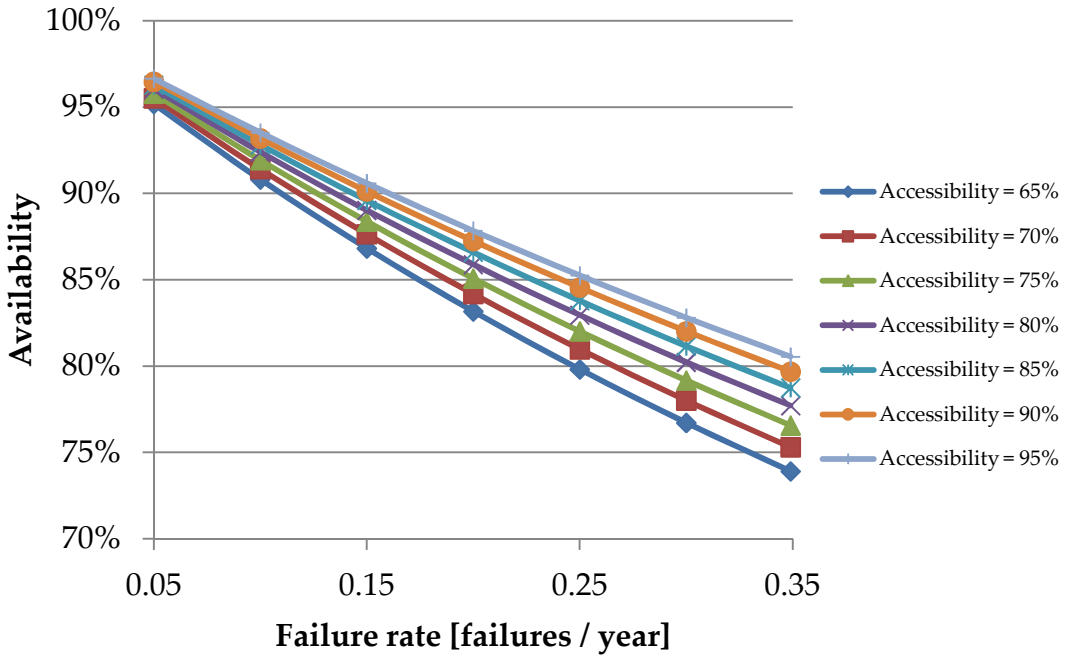

Figure 3-5: Availability of the wind farm where the turbines are clustered together with a single power converter per cluster and the failure rate and proportion of time the turbines are accessible are varied; assuming a constant repair rate of 73 converter repairs per year.

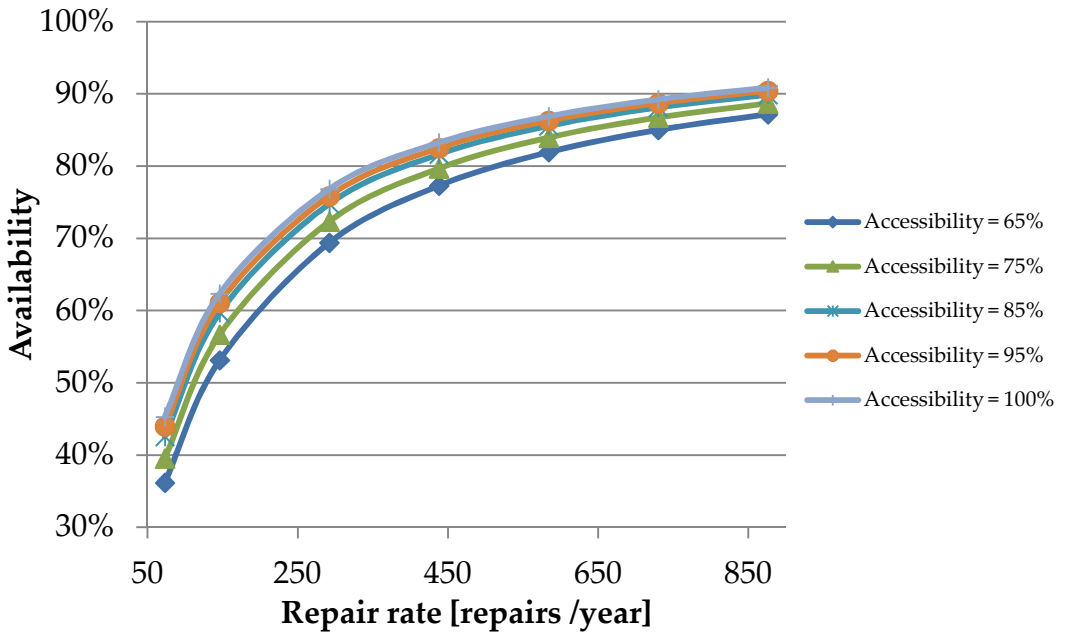

Figure 3-6: Availability of the wind farm where the turbines have individual power converters and the repair rate and proportion of time the turbines are accessible are varied; assuming a constant converter failure rate of 0.349 failures per year.

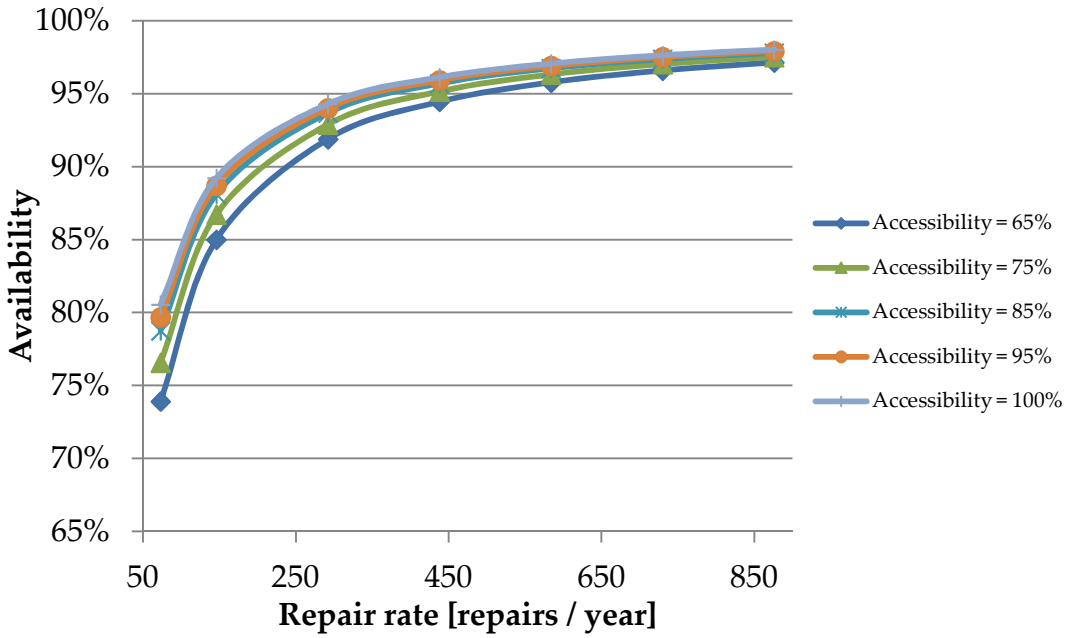

Figure 3-7: Availability of the turbines in the cluster where the turbines are clustered together with a single power converter per cluster and the repair rate and proportion of time the turbines are accessible are varied; assuming a constant converter failure rate of 0.349 failures per year.

Figure 3-2 and Figure 3-3 show the impact of improved failure and repair rates on the wind farm availability. It can be observed that where the failure rate of the converters is lower, the availability of the wind farm is substantially higher, and also that increasing the rate of repair of the converters increases the availability substantially, whilst decreasing the impact of the improved failure rates. By comparing the data in each figure on the basis of whether the turbines are connected in clusters or not, reveals that the overall availability of the wind farm is improved significantly where the turbines are clustered, regardless of the failure and repair rates.

Figure 3-4 and Figure 3-5 show the impact of turbine accessibility, in addition to the decreasing failure rate; where it can be observed that the improved rate of accessibility benefits the availability of the wind farm, but only by

10% where the turbines have individual converters and 15% where they are clustered. The advantage in terms of availability, of grouping the turbines into clusters, is demonstrated by comparing the two plots; which highlights that the clustered case allows for a generally higher availability of the wind farm.

The final pair of plots, Figure 3-6 and Figure 3-7, show the effects of improved turbine accessibility, also with improved converter repair rates; indicating that an improved repair rate substantially improves availability. It can also be observed, as in Figure 3-4 and Figure 3-5, that improved accessibility to the turbines provides a limited improvement to the availability. Finally, it is once again demonstrated that improved availability of the wind farm is achieved where the turbines are connected in clusters.

It can be concluded from this sensitivity study that the influence on the availability of the failure and repair of the power converters can be significantly reduced by increased rates of repair of the converters and also by grouping of the turbines into clusters. Improvements to the reliability of the converters themselves would also benefit the wind farm availability; whereas improved accessibility has a smaller impact. The results shown here back-up the assertion made earlier that for a wind farm of this size it is worthwhile, in terms of availability, for the wind farm operator to employ more maintenance teams and thereby increase repair rates from those suggested by [5], which gave the original repair rate figure.

3.1.3 Conclusions

Overall the analysis presented here demonstrates that the number of converter failures can be reduced significantly, from 83.76 failures/year to 16.75 failures/year for the case study investigated, therefore reducing the

repair requirements and improving the availability of the wind farm. It is also demonstrated however that the improved availability does not benefit the annual energy production of the wind farm, as a result of the greater consequences of a single power converter failure negating the effects of a lower number of failures. It should however be noted that with a reduced number of larger converters in a wind farm, the inclusion of redundancy within their design and the provision of a redundant converter alongside those in operation on a centralised converter platform could be warranted; therefore acting to reduce the failure rate of the converters and also the downtime of the clustered wind turbines following a failure. In which case the assumption made here that the failure and repair rates of the individual and cluster converters are equal would no longer be valid; benefiting the availability of the cluster based wind farm and also increasing its annual energy production.

This study has focused solely on the impact on the availability of a wind farm due to failure of the power converters. It has not taken into account the impact of the failure of other components within the wind turbines or wider wind farm systems; such as the gearboxes or collection network cables. Therefore the figures produced here provide only indicative predictions of the availability of Creyke Beck A wind farm.

3.2 Wind turbine and cluster operation

The connection of neighbouring wind turbines into clusters removes the independence that each turbine normally enjoys when it has its own dedicated power converter. The result of which is that the previously independent variation of the rotational speed of each turbine, with respect to its local wind conditions, is no longer possible to the same extent. In Chapter 2 the concept of a variable frequency collection network was introduced with the prospect of achieving variable speed operation of the turbines in a wind farm without the need for individual power converters. However, this concept was dismissed because of the likelihood that the wind farm would incur a large energy capture penalty due to the restriction of the rotational speeds of the turbines to an average that is suitable for the whole wind farm. The hybrid collection network concept is proposed as a compromise between having a converter in each individual turbine and the variable frequency concept, as it separates a wind farm into smaller clusters of adjacent turbines that will then rotate at approximately the same speed; which will allow more diversity between the rotational speeds of the turbines across a wind farm. It is envisaged that this compromise will reduce the size of the energy capture penalty, and it has been demonstrated in the previous section that this will also require fewer failure prone converters within a wind farm. It is anticipated that this reduction in energy capture loss will occur because the difference between the wind speeds incident on each turbine will be smaller in a cluster, since the turbines are located closer together.

The objective of this section is to analyse how a cluster of turbines would be operated and the likely effect on the overall annual energy captured, in comparison to where the turbines are independent.

3.2.1 Operation of a cluster of wind turbines

In order to achieve the maximum energy capture from the wind, the power coefficient, Cp, of a wind turbine must be maximised throughout operation. As stated in Chapter 2, the power coefficient is related to the design of the turbine blades and also to the tip-speed ratio. To achieve maximum Cp, the tip-speed ratio must be optimised and maintained throughout operation. Equation (3.17) shows that the tip-speed ratio, λ, is a function of the rotational speed, ω, the turbine radius, r, and the wind speed, V.

$$\lambda = \frac{\omega . r}{V} \tag{3.17}$$

Therefore to maintain the optimum tip-speed ratio, the rotational speed must change with the wind speed incident of the turbine rotor. A variable speed wind turbine is controlled by regulating the reaction torque the generator places on the drive-train in opposition to the input torque from the wind. It does this by taking a measurement of the rotational speed of the turbine and applying the torque that would be required for the incident wind speed which corresponds to the turbine operating at its optimum tip-speed ratio. Newton's second law of motion then governs the acceleration or deceleration of the turbine by the balance of the generator and input torques. It should be noted that this method of control only applies when the turbine is operating between its maximum and minimum rotational speeds; once either is reached, the speed is held constant regardless of the optimum operating point. Figure 3-8 shows the operating curve of a wind turbine; there are three clear operating regions: the first fixed speed region where the turbine is operating at a minimum speed, the variable speed region where the rotational speed is regulated so that the optimum tip speed ratio is achieved,

and the 2nd fixed speed region where the rotational speed is held constant at the maximum speed of the turbine. Once rated torque is achieved the turbine pitch system acts to limit the torque.

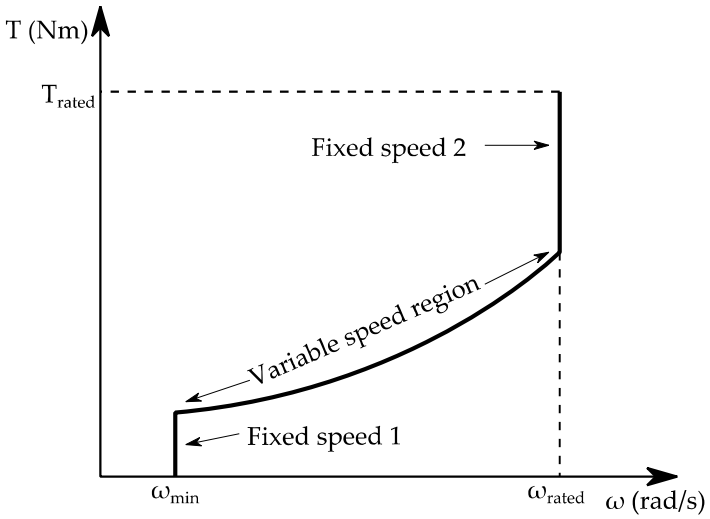

Figure 3-8: Torque speed operating characteristic of a variable speed wind turbine.

Ordinarily this method of control, during the variable speed region, performs well, keeping the tip speed ratio close to the optimum for maximum energy capture [9]. The ability of a turbine to maintain the optimum tip-speed ratio when it is operated as part of a cluster is restricted because each turbine no longer has the capability to regulate the reaction torque applied by its generator to the drive train. The implication of this is that the rotational speed of each turbine will no longer follow changes of the wind speed as before, preventing the optimum tip-speed ratio being maintained.

The cluster power converter provides the control capability for each wind turbine in the cluster; however it controls the turbines collectively, not individually. Therefore the converter is not able to directly regulate the torque produced by the generator in each turbine; instead it must do so

indirectly by controlling system parameters such as electrical frequency or DC voltage. It therefore controls these parameters to allow the turbines to rotate at the average of the optimum speeds for each turbine in the cluster. The nature of the generators used could allow a degree of independent rotational speed variation by each turbine in accordance with local wind speeds (this will be explored later in this chapter); however the rotational speeds of the turbines in a cluster will be largely the same. Therefore all of the turbines will operate with suboptimal rotational speeds and therefore not achieve maximum energy capture from the wind.

3.2.2 Estimation of the energy capture penalty

To make an assessment of the viability of the hybrid collection network concept, an estimate of the energy capture loss is required. To produce this estimate a statistical approach is used; based around the principles of wind energy resource assessment at a potential wind farm site.

Energy capture loss estimation process

When an assessment of the wind resource at a particular wind farm site is made, measurements of the wind speed are recorded over a particular measurement period (6 months to 2 years) with a resolution of 1 second. The recorded data is then averaged over 10 minute periods to remove the short term influence of high frequency wind variations and sorted into 'bins' of 0.5m/s over the operating range of a wind turbine (4m/s - 25m/s). The resulting number of measurements in each bin gives the distribution of the wind speeds that occurred over the measurement period. The shape of this distribution can be approximated by the Weibull distribution, an example of which is shown in Figure 3-9. The spread of the wind speed measurements in each bin, about the bin mid-point, can be regarded as Gaussian and

therefore represented by the normal distribution; where the standard deviation, σ, of the distribution is related to the site turbulence intensity, I, equation (3.18) (where $\overline{V}$ is the site mean wind speed [m/s]). Turbulence intensity is a measure of the variation of a wind farm site's wind speed about the mean wind speed, and is approximately 8-9% for an offshore wind farm site and 14-16% for an onshore wind farm site [10, 11]. This measure of wind speed variation does not take into account the wake effects of upwind turbines; however wake effects will increase the variation of the wind speed about the mean, and therefore the consideration of the 14-16% range of turbulence intensity which represents a wind farm site with a greater amount of wind variation, in addition to the 8-9% range, gives a indication of their impact.

$$I = \frac{\sigma}{\overline{V}} \tag{3.18}$$

To determine the energy capture loss when a group of five adjacent turbines are operated as a cluster instead of individually, a wind speed dataset covering a period on one year is required. To produce this, the wind speed distribution at the wind farm is assumed to be represented by the Weibull distribution based around the site mean wind speed. This allows the number of 10 minute periods in a year that the wind speed falls into each 0.5m/s bin to be determined; an example of this distribution is shown in Figure 3-10. By assuming that the mean wind speed across the cluster in each 10 minute period is constant, it can also be assumed that the wind speeds experienced by the individual turbines will be normally distributed about that mean. Therefore a wind speed can be assigned to each turbine in the cluster randomly from within the normal distribution. This process is repeated until

a wind speed is generated for each turbine for every 10 minute period across the Weibull distribution. The random nature of the wind speed assigned to each turbine in each 10 minute period causes the wind speed associated with each turbine to be different from that of its neighbour, representing the likely difference between the wind speeds experienced by adjacent turbines. The data generated by this process is used as the basis for determining the power output from each turbine in each period when it is either operating independently or as part of a cluster; allowing a comparison to be made between the two scenarios and giving an estimate of the energy capture loss where the turbines are operated as a cluster.

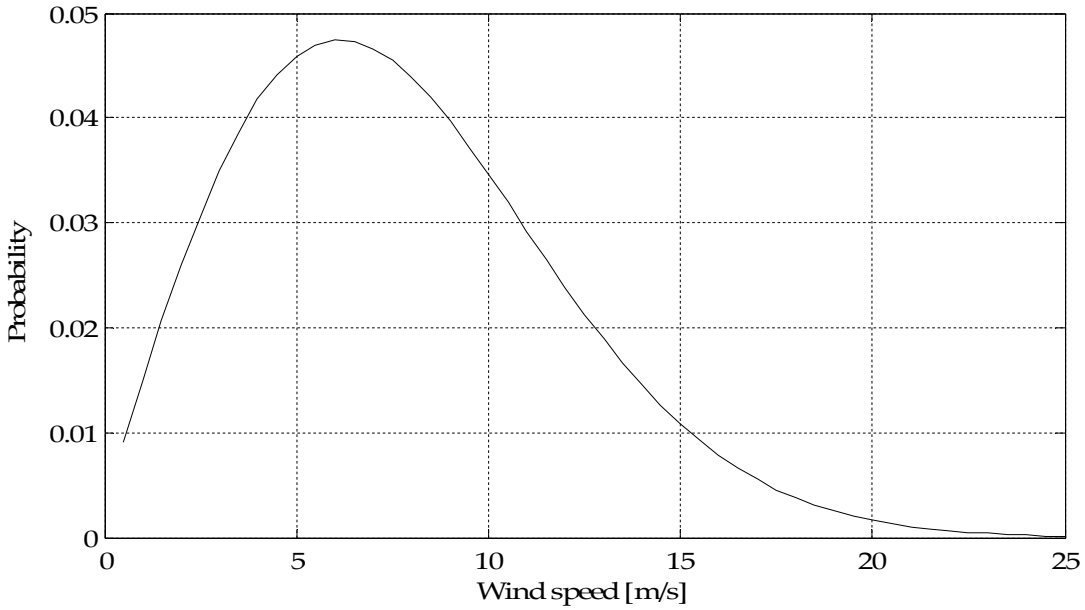

Figure 3-9: Weibull probability distribution of wind speed for a site with a mean wind speed of 8m/s.

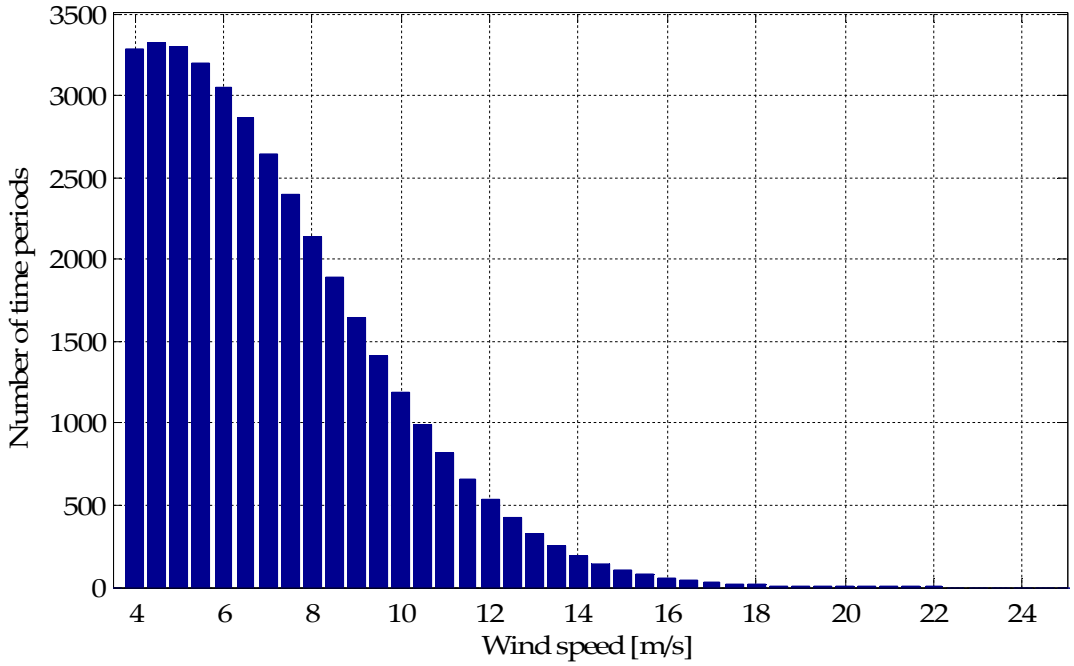

Figure 3-10: Distribution of the number of 10 minute periods in a year that the wind speed falls into each 0.5m/s bin.

To determine the power output of each turbine in response to the wind speed, the power coefficient, Cp, is required. To obtain a figure for the Cp of each turbine in each time period, consideration has to be given to the tip speed ratio of the turbine and therefore the rotational speed. An example operating curve for a variable speed wind turbine is shown in Figure 3-8, indicating that the rotational speed of a turbine is allowed to vary over a certain range as the input torque from the wind changes. When a turbine has the capability to operate independently of its neighbours, it operates very close to the optimum rotational speed for the incident wind speed and therefore the tip speed ratio is also near optimal, allowing the Cp to be maximised. However, where the turbines are operating as a cluster, the rotational speeds of the adjacent wind turbines will change only with the average wind speed across the cluster; therefore each turbine will operate slightly away from the optimum speed for its individual wind speed, causing a sub-optimal tip-speed ratio and reduced Cp. The impact of clustering the

turbines together on energy capture is only felt when the turbines are operating in the variable speed region of their operating curve, as away from this region all of the turbines would ordinarily have equal and constant rotational speeds.

For this analysis, where the turbines are operating independently and within the variable speed operating region, it is assumed that they are operating with the maximum power coefficient. Where the turbines are operating as a cluster, the individual tip-speed ratio of each turbine is determined using the individual wind speeds and the cluster rotational speed. This allows the Cp to be determined using the Cp-λ curve, which is the same for all of the turbines (assuming the turbines are identical). Therefore the average power produced by each turbine in each 10 minute period over a year can be determined; the summation of which gives the overall annual energy capture for the turbines in the group. Calculation of the annual energy capture of the turbines when they are operating individually and as a cluster, allows for the difference between the two scenarios to be determined, giving the energy capture loss incurred when operating the turbines as a cluster. The random assignment of wind speeds to each turbine leads to marginally different results every time the analysis is completed; therefore to achieve a consistent result the analysis is repeated 100 times and the results of each repetition averaged.

Estimation of energy capture loss for a 5MW offshore wind turbine

To produce an estimate of the energy capture loss, the parameters and operating characteristics of a 5MW wind turbine are used, given in Table 3-4 and Figure 3-11. The analysis is also repeated over a range of site mean wind speeds, from 6m/s to 9m/s in steps of 0.5m/s, and site turbulence intensities

of 9%, which is realistic of an offshore site, and 15%, which is representative of an onshore site, to investigate the sensitivity of the result to increased spread of the wind speeds between turbines [10] [11].

Table 3-4: Parameters of the 5MW wind turbine used for the energy capture analysis [12].

Generator Power Rating	5MW
Rotor diameter	63m
Minimum rotational speed	6.9rpm
Maximum rotational speed	12.1rpm
Optimal tip speed ratio, λ	7.8
Maximum power coefficient, Cp	0.4873

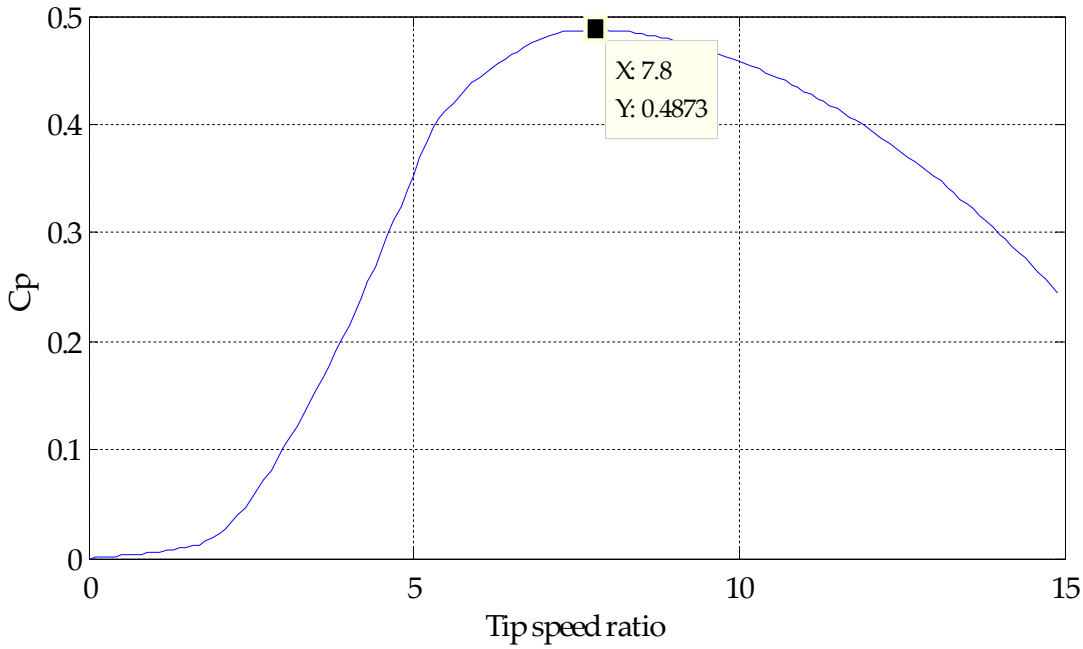

Figure 3-11: Cp – λ curve for the 5MW turbine used in this analysis [12].

Following the process above, the Weibull distribution has been used to determine the spread of the wind speeds across the operating range of site mean wind speeds. Figure 3-12 and Figure 3-13 show the distribution of the 10 minute measurement periods across the operating range; it can be observed that increasing the site mean wind speed spreads the

measurements further across the range, and also leads to a higher most common wind speed.

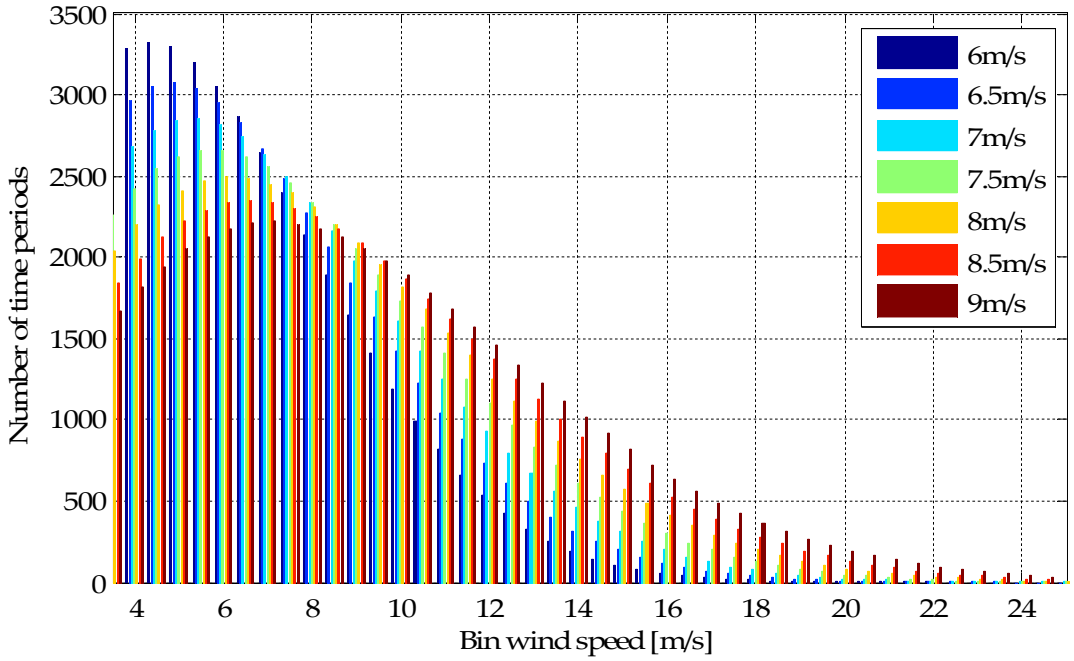

Figure 3-12: Histogram showing the spread of 10 minute measurement periods across the range of bin wind speeds, where the site mean wind speed is increased.

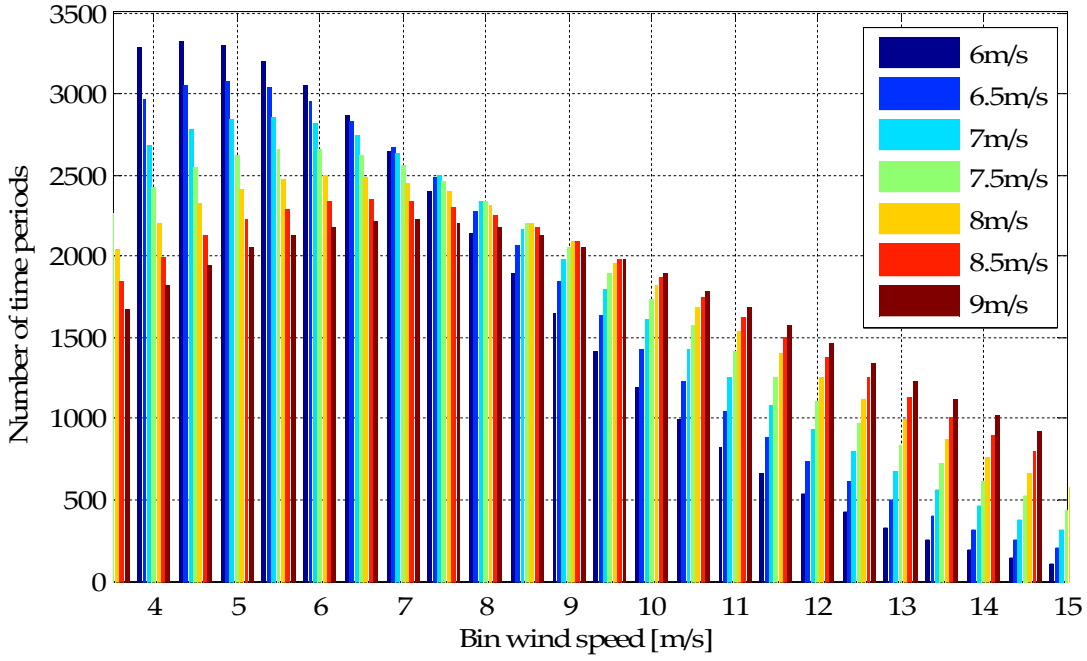

Figure 3-13: Enlarged histogram showing the spread of 10 minute measurement periods across the range of bin wind speeds, where the site mean wind speed is increased.

By comparing these plots with the ideal rotational speed characteristic in Figure 3-14, it is clear that as the site mean wind speed increases, the proportion of time the turbines will spend in the variable speed region of the operating curve will change. The significance of this becomes clearer when considering the difference between the energy captured per bin by a single turbine, when the group operate independently and as a cluster, in Figure 3-15 and Figure 3-16.

The energy lost per bin is greatest for the site mean wind speeds that are in the middle of the range, and lowest for the outermost site mean wind speeds. It can also be observed that the largest amount of energy is lost when the wind speed is between 7m/s and 9m/s, corresponding to the variable speed operating range of the turbines. The larger site turbulence intensity also results in a generally greater amount of energy being lost, which is observed by comparing Figure 3-15 and Figure 3-16. This is also reflected in Figure 3-17 where the difference between the total annual energy production of the group of turbines, when they are operated individually and as a cluster, is plotted against changing site mean wind speed. It is clear from all of these plots that a greater amount of energy is lost over the middle of the range site mean wind speeds, and where the turbulence intensity is larger. Also when the total energy lost is represented as a percentage of the annual total energy produced by the turbines in Figure 3-18, similar trends occur.

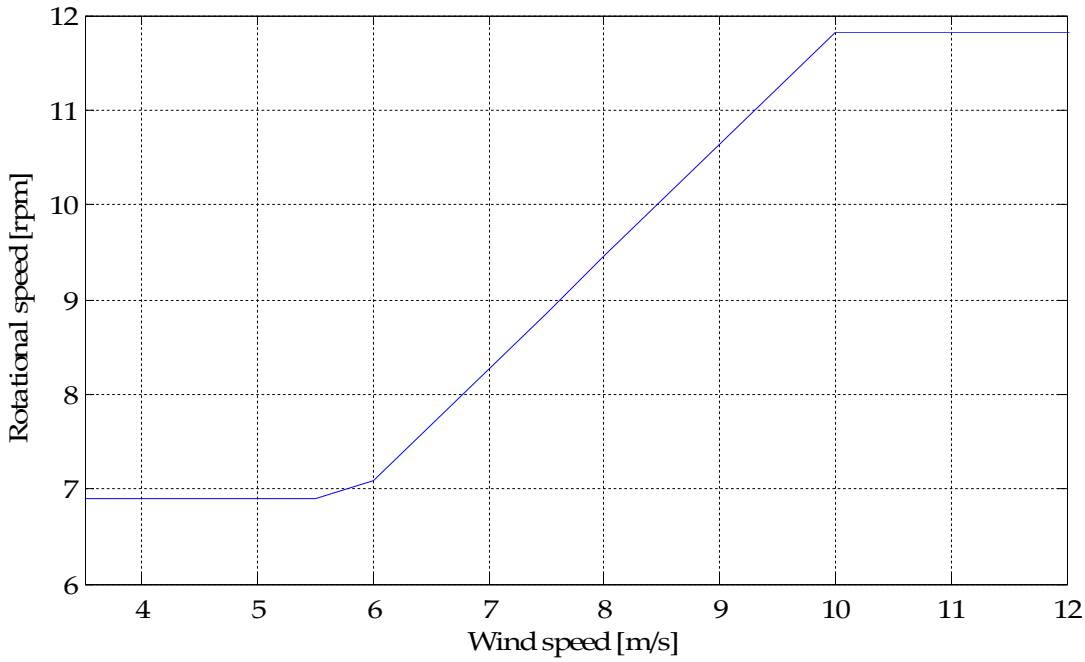

Figure 3-14: Rotational speed operating characteristic of a variable speed wind turbine.

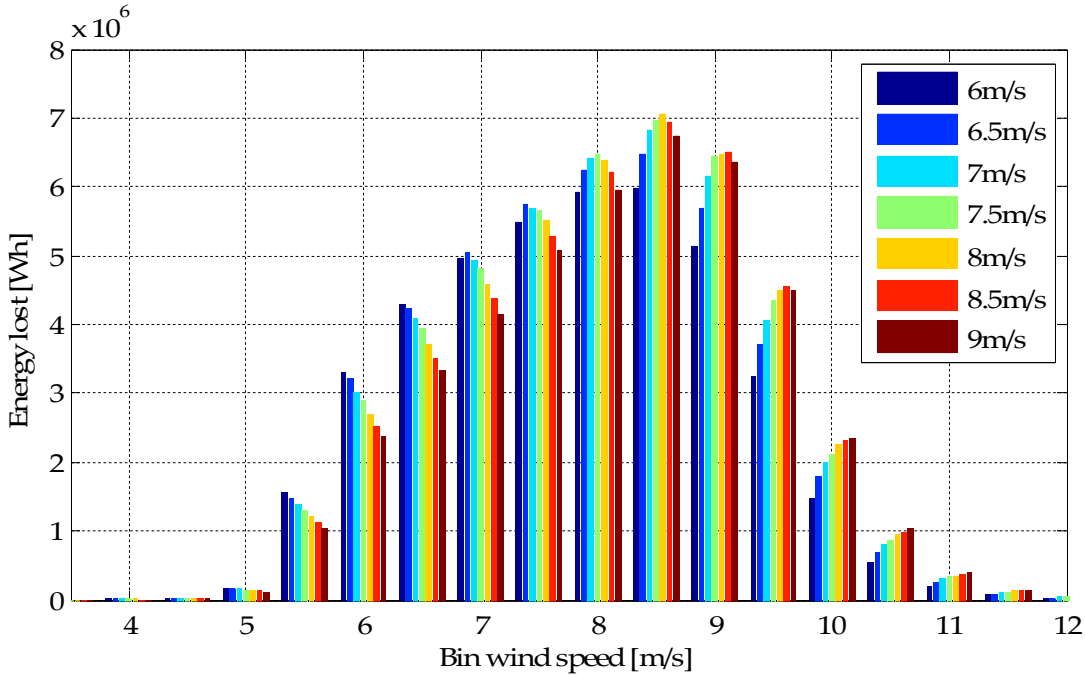

Figure 3-15: Energy lost by a single wind turbine per wind speed bin as the site mean wind speed is increased, with a site turbulence intensity of 9%.

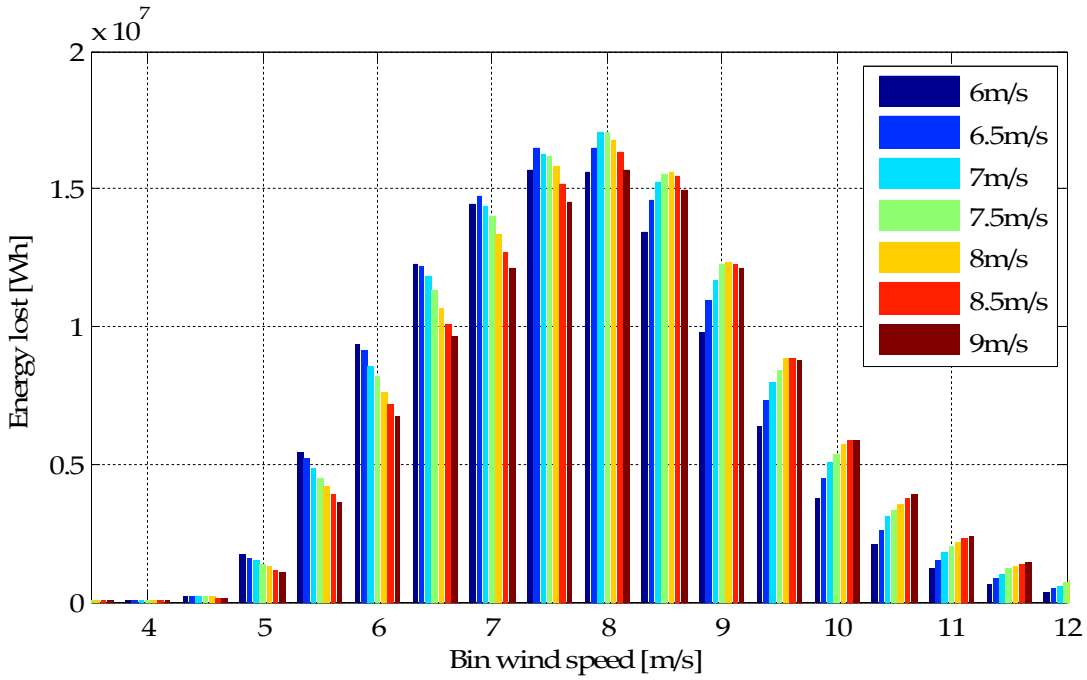

Figure 3-16: Energy lost by a single wind turbine per wind speed bin as the site mean wind speed is increased, with a site turbulence intensity of 15%.

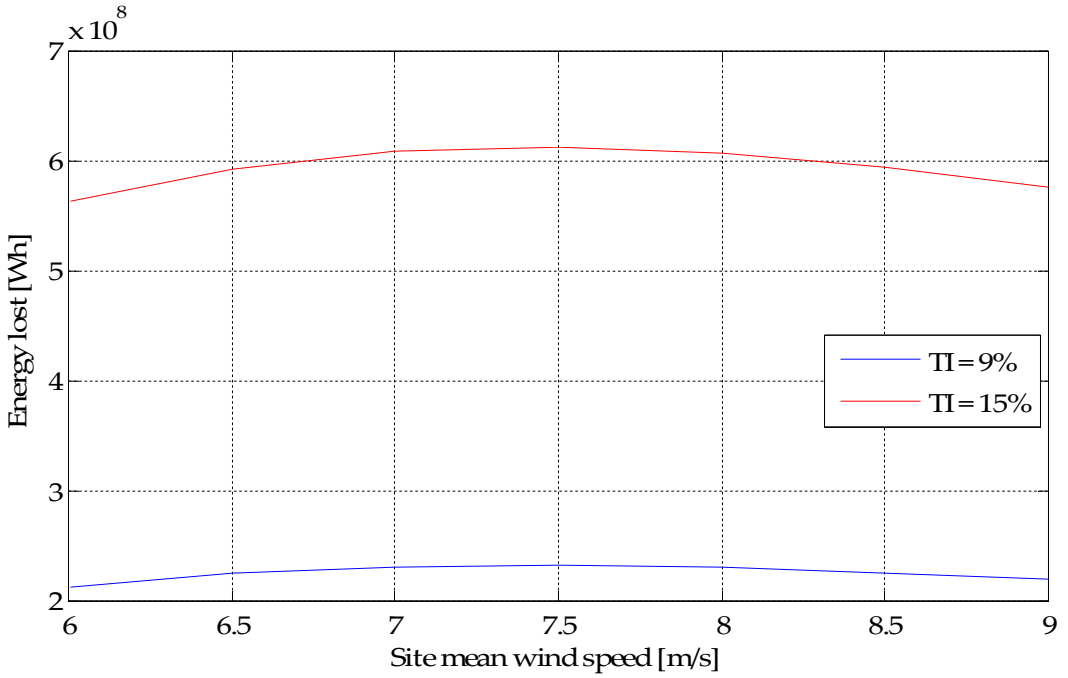

Figure 3-17: Total annual energy loss due to operating a group of turbines as a cluster with increasing site mean wind speeds, for site turbulence intensities (TI) of 9% and 15%.

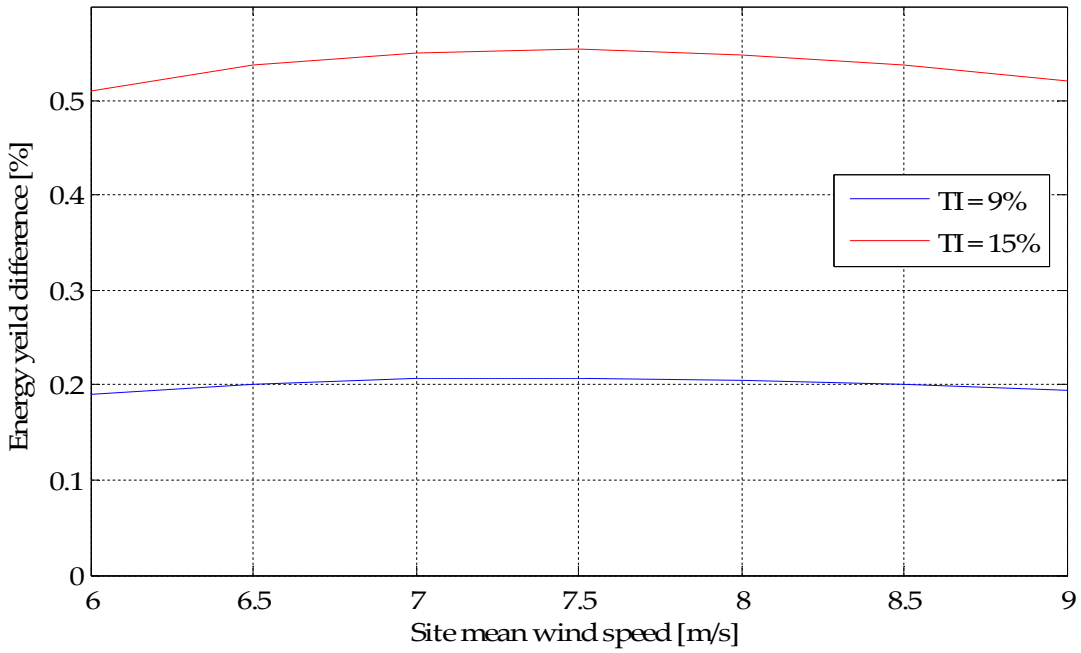

Figure 3-18: Energy loss as a percentage of the overall annual energy production of a group of turbines with increasing site mean wind speed, for site turbulence intensities (TI) of 9% and 15%.

3.2.3 Conclusions

It can be concluded from this analysis that the energy capture loss that occurs as a result of operating a group of five turbines as a cluster is less than 0.25% of the total energy captured by the turbines when the turbulence intensity is 9%, and less than 0.55% for a turbulence intensity of 15%; which although small is still a significant loss. It is notable from these figures that the energy capture loss is greatest for the middle of the range site mean wind speeds and also that it increases when there is a result of higher amount of wind speed variation between turbines, which is highlighted by the figures produced with larger turbulence intensity. More energy is lost over the middle range site mean wind speeds because the turbines spend proportionately more time operating in the variable speed region of their operating curves compared to the outermost site means.

The approach used here is based purely upon statistical predictions of the wind speed variation, averaged over 10 minute time periods, over the course of a year. [13] suggests a method of predicting the power production of a wind farm based around the power spectral density of the wind speeds incident on a wind turbines and also incorporates coherence functions that link together the wind speeds of adjacent turbines. This method may provide an alternative approach to conducting the analysis completed here.

3.3 Clustering technologies

Three potential technologies have been identified that could be used to implement a cluster of turbines; key to all is the type of generator used. The two most common types of generator used within wind turbines are induction and permanent magnet generators; the operating principles of each were described in the previous chapter. In addition to the generators in a cluster system is a network of cables and the cluster converters. It has been alluded to above that the electrical network could be implemented using either an AC or a DC system; in each case the principles of operation of the cluster are slightly different. This section will describe the three potential ways a cluster could be implemented, using: induction generators with an AC network, PM generators also with an AC network, and PM generators with rectified outputs and a DC network.

3.3.1 Induction generators with an AC network

An induction generator requires an alternating terminal voltage to set up the magnetic fields within the machine; therefore it must be connected to an alternating current (AC) electrical system. The rotational speed of an induction generator is closely linked to the frequency of the electrical network; therefore it is possible to control the rotational speed by regulating the electrical frequency. Figure 3-19 shows the torque speed characteristic of an induction generator, where the point of zero torque corresponds to the synchronous frequency of the electrical system. Therefore in order for the machine to produce a torque onto the drive-train of the wind turbine, in opposition to the input torque from the wind, the rotational speed, ω_r, must not equal the synchronous speed, ω_s. An induction machine in a wind turbine functions as a generator, therefore the rotational speed will always be

greater than the synchronous speed, and the torque generated by the machine, T_{gen}, will have a negative polarity.

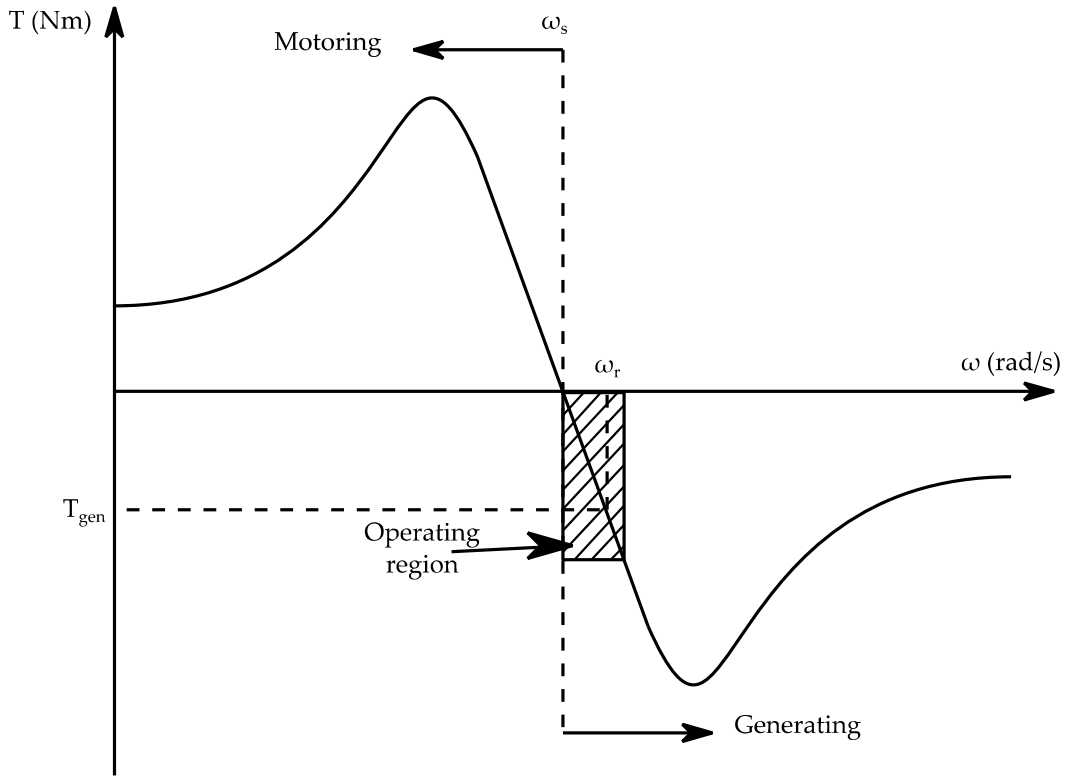

Figure 3-19: Torque speed characteristic of an induction machine operating as a generator.

Where the synchronous frequency of the electrical system is constant (if a turbine were directly connected to a large AC electrical system) only very small rotational speed variations will occur; these arise due to changes of the input torque, T_m, from the wind turbine rotor with changes of wind speed. During steady state operation the rotational speed of the turbine is constant, therefore the generator torque (reaction torque), T_e, applied to the turbine drive train will equal the input torque, satisfying Newton's second law of motion, equation (3.19). In response to a change of the input torque, caused by a variation of wind speed, the rotational speed accelerates or decelerates due to the now unbalanced torques; this change of rotational speed relative to the synchronous speed produces a change of the generator torque,

continuing until the torques become balanced, halting the acceleration. The relationship between rotational speed and torque is demonstrated by the torque speed characteristic in Figure 3-19; which, during the operating range, is approximately linear. If the rotational speed increases beyond the operating range, the maximum torque of the generator is exceeded and the rotational speed will accelerate uncontrollably. The slope of this relationship, during the operating range, governs the rotational speed variation required for the generator torque to match the input torque; the slope itself is a function of the electrical resistance of the generator rotor windings, R_r, as shown by equation (3.20); which can be chosen by the designer of the machine to allow a certain slope. The proportionality of the rotational speed and the synchronous speed is described by the slip of the generator, equation (3.21).

$$J.\frac{d\omega_r}{dt} = T_m - T_e \tag{3.19}$$

$$T = \frac{3.I_r^2.R_r}{(\omega_s - \omega_r)} \tag{3.20}$$

$$Slip = \frac{\omega_s - \omega_r}{\omega_s} \tag{3.21}$$

J = moment of inertia [kg.m^2], I_r = rotor current [A], R_r = Rotor resistance [Ω]

The use of induction generators within a cluster of variable speed wind turbines requires the rotational speed of the generators to vary, allowing the tip-speed ratio of the turbine rotors to be optimised for the average wind conditions across the cluster. This is achieved by varying the electrical frequency, which in turn shifts the zero torque point of the generator torque speed characteristic (the synchronous speed). A shift of the synchronous

speed causes an instantaneous change to the reaction torque applied by the generator to the drive train, allowing the turbine rotor to accelerate or decelerate, as demonstrated in Figure 3-20. When the frequency changes it is important to avoid the saturation of the magnetic components of the machine, therefore the terminal voltage must be regulated in proportion to the frequency; this control method is referred to as scalar or Voltage/Frequency control [14].

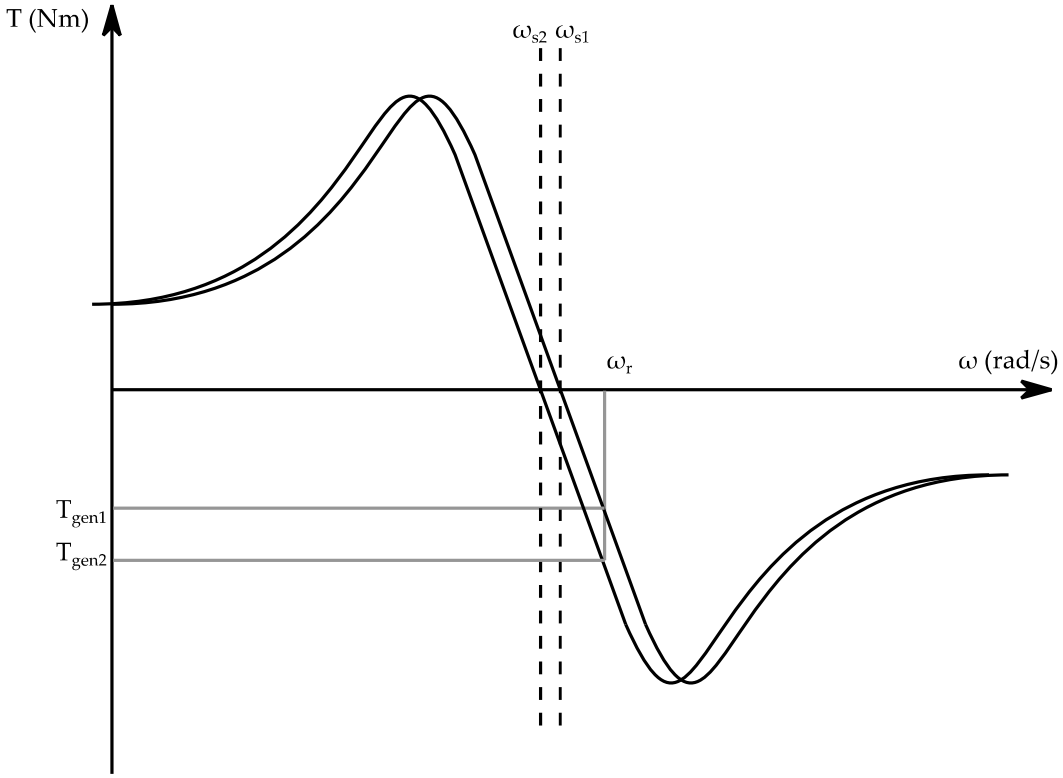

Figure 3-20: Induction machine torque speed characteristic indicating the effects of a reduction of the synchronous speed.

The implementation of a cluster collection network using such a system will require the cluster converter to regulate the electrical frequency. The generators would then be connected in parallel with each other and be synchronised to the same network frequency. A diagram of the system is shown in Figure 3-21. When faced with changing inputs torques from the wind, the generators will move along their individual generator torque

speed curve to produce the necessary reaction torque. The cluster converter will act to vary the network frequency according to the average wind speed across the group of turbines. It will aim to do this relatively slowly so that the frequency does not respond to abrupt short term turbulent wind speed changes on a single machine, and so that the operating points of the turbines change gradually. It would be preferable to use generators where the slope of the torque speed operating characteristics allow for at least 10% slip to be achieved between the synchronous and rotational speeds. This will allow a degree of independent variation of the rotational speeds in response to changes of the input torque from the wind. This is a similar philosophy to the design of the generators used in fixed speed wind turbines, where the slip is relied upon to damp the oscillations of the mechanical drive train due to the varying input torque from the wind [15]. The large amount of slip however requires a relatively large rotor winding resistance which also reduces the efficiency of the generator. The requirement for external excitation of induction machine leads to the machine absorbing significant amounts of reactive power; this also contributes to lower machine efficiency.

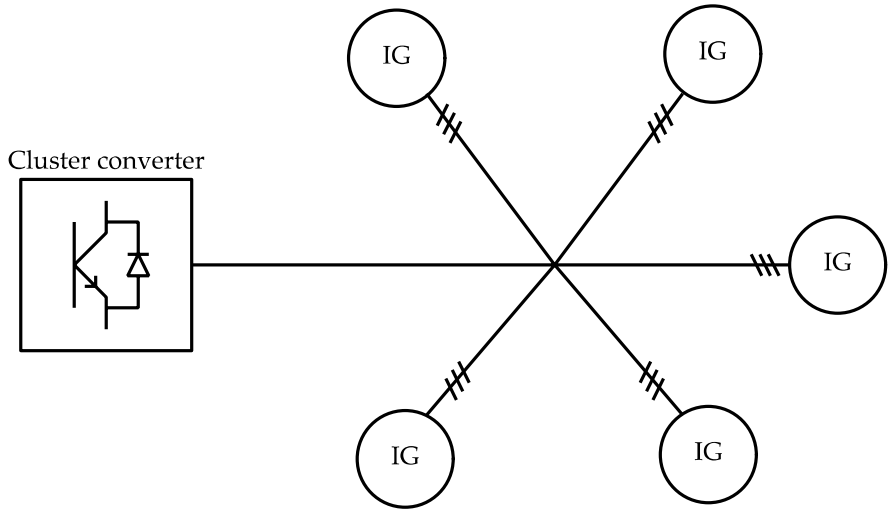

Figure 3-21: Induction generator (IG) based cluster with a three phase variable frequency network.

3.3.2 PM generators with an AC network

Permanent magnet generators have a natural means of providing a magnetic field; therefore such a generator can be connected to either an AC electrical network or a DC network through a rectifier. In this case the connection of PM generators to an AC network will be considered.

As stated in Chapter 2, the electrical frequency of the electrical network is directly related to the rotational speed of a PM generator, and the torque applied by the generator onto the turbine drive train is a function of the angle between the air-gap magnetic flux and the stator magnetic flux (load angle). In response to changes of input torque from the wind, the load angle will change, whilst the rotational speed remains constant. To maintain the constant rotational speed, the generator torque must follow the input torque closely. Therefore the response of the generator to changes of the input torque is very stiff, as a small change of load angle produces a big change of generator torque. During operation the required torque must also not exceed the maximum pull out torque of the generator which arises when the load angle equals 90˚, allowing synchronism to be maintained within the machine. The operating characteristic of a PM generator is governed by equation (3.22), which relates the generator torque to the magnitude of the internal EMF, E, the terminal voltage, V_t, the stator reactance, X, electrical frequency, ω_e, and the load angle of the generator, δ.

$$T = \frac{E.V_t.sin\delta}{X \ .\omega_e} \tag{3.22}$$

Where PM generators are the basis of a cluster system, the regulation of the rotational speeds is achieved by controlling the frequency of the electrical network and each turbine within the cluster will rotate at the same speed.

Differences between the wind speeds incident on each turbine will produce different input torques; therefore the load angle of each generator will be different. A common result of the stiff reaction of synchronous generators to changes of electrical or mechanical load, are oscillations of the generator rotor with respect to the prime mover (wind turbine rotor) due to the flexibility and twisting of the drive shafts between the two. Oscillations also arise due to interactions between the power flows of generators that are electrically adjacent. In a large power system such oscillations are controlled by damper windings in the generators and by power system stabilisers (PSS), which control the excitation of the generator rotor (where the excitation of the generator rotor is provided by an external source). Damping in a PM generator coupled to an AC electrical network can only be provided by the damper windings of the generator rotor. Therefore oscillations that occur due to the change of the input torque may have a significant bearing on the operability of a cluster collection network based on this arrangement.

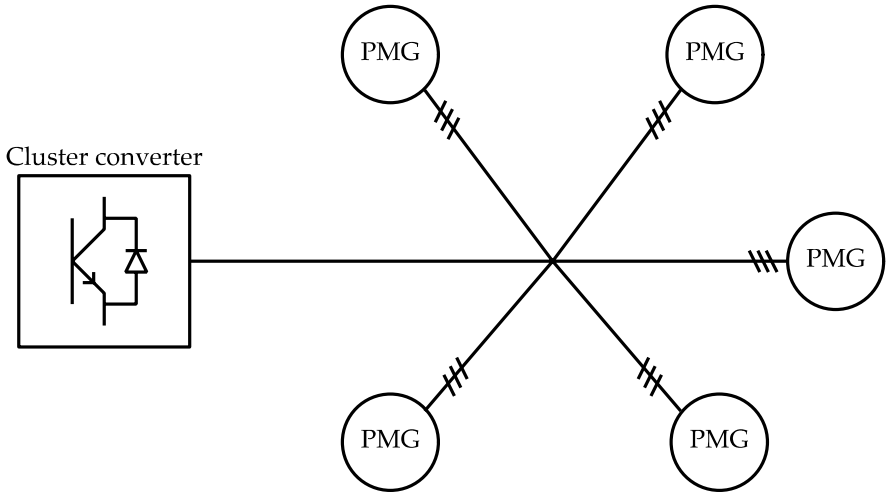

Figure 3-22: PM generator (PMG) based cluster of with a three phase variable frequency network.

The self-excitation of a PM generator allows it to operate with a higher efficiency, in comparison to an induction generator, with only conduction

losses in the stator windings of significance. The electrical arrangement of the AC network is this case is very similar to the induction machine case above, where the cluster controller regulates the synchronous frequency. Figure 3-22 shows a schematic of the cluster collection network with PM generators.

3.3.3 PM generators with a DC network

The use of a PM generator in conjunction with a rectifier allows it to be connected to a DC electrical network. Therefore, although the electrical frequency of the generator output is still directly related to the rotational speed of the machine, the relationship between the terminal voltage magnitude and the rotational speed, given by equation (3.23), becomes the most important. Rectifiers can be implemented using a selection of different semiconductor components, each introducing a different capability: controlled switch on and natural switch off, controlled switch on and controlled switch off and natural switch on and natural switch off. To maintain the simplicity and robustness of a cluster electrical system, diodes are used as the main constituent component of the rectifiers used here. A diode will naturally switch on when the voltage between its anode and cathode becomes positive, it will then switch off again when this voltage reverses and the current passing through it falls to zero. The action of a diode rectifier is referred to as being passive because no outside switching input is required, which therefore allows a diode rectifier to be more robust than an actively controlled power converter.

$$E = \Psi_f . \omega_r \tag{3.23}$$

$$\overline{V_{dc}} = \frac{3.\sqrt{3}.V_t}{\pi} \tag{3.24}$$

The action of a rectifier samples the sinusoidal terminal voltage of the generator to produce the DC output voltage; the magnitude of which is directly proportional to terminal voltage magnitude, V_t, and therefore the rotational speed of the generator, ω_r , by equation (3.24) (Ψ_f = Generator magnetic flux constant). The terminal voltage of the generator is related to the emf, E, generated in the stator windings by the rotating field and the voltage drop across the stator winding impedance. When the rectifier is connected to a closed circuit, a direct current flows from the rectifier, which shifts the output current between pairs of the generator windings depending on which pair gives the largest phase to phase voltage. The flow of real power through the DC network is therefore directly proportional to the reaction torque produced by the generator onto the wind turbine drive train, and therefore it is possible to regulate the torque of the generator by actively controlling the flow of real power through the DC network. In order to control the power flow through the DC circuit a controllable voltage source is required, which can be provided by a DC voltage converter. The power flow through the DC network is a function of the voltage difference between the terminals of the rectifier and the voltage source; which are separated by the cable impedance which connects the generator and rectifier to the DC converter. Control over the rotational speed of the generator is indirectly achieved by the voltage source because the voltage at the terminals of the rectifier must be greater than the controlled voltage; therefore by specifying a particular DC voltage, the generator will accelerate until its terminal voltage is sufficient to allow the transfer of power corresponding to the input from the wind.

The use of such a system to implement the clustering of a number of turbines will require a rectifier at the terminals of each generator; the turbines will then be interconnected by a network of DC cables. A diagram of a cluster collection network using this approach is shown in Figure 3-23. The cluster converter acts to control the voltage at the common point where all of the turbines are connected together. The real power output and therefore the torque produced by each generator onto the turbine drive train are determined by the voltage differences between the terminals of the individual rectifiers and the common point. Therefore as the input torque to each generator changes with the wind speed, the generators will accelerate or decelerate, naturally regulating their power output and torque. In order to optimise the rotational speeds of the generators to the wind conditions across the cluster of turbines, the cluster converter will vary the voltage at the common point in the network and therefore influence the power flow and torques of each generator, causing their rotational speeds to accelerate or decelerate as required. Differences between the rotational speeds of the turbines will occur due to differing input torques from the wind incident on each turbine. The degree of difference is proportional to the size of the voltage difference between the rectifier outputs and the cluster common point required to drive the necessary power flow. The resistance of the cables between these two points therefore plays a key role in this. In addition, the capacitance of the cables will restrict the rate of change of the DC voltages in the system which could limit the change of the turbine speeds; however if the cable lengths are relatively short the capacitances will not have a significant impact; it is also probable that the large turbine rotor inertia will be the most significant factor affecting the rate change of turbine rotational speed.

An analogy can be drawn between the operation of this system and that of an induction machine; where the synchronous speed in the system is related to the voltage at the common point and to allow each of the generators to produce torque their rotational speeds must be greater than the synchronous speed. Therefore the proportionality between the synchronous speed and rotational speed of each turbine can be described as the slip of each generator, similarly to an induction machine.

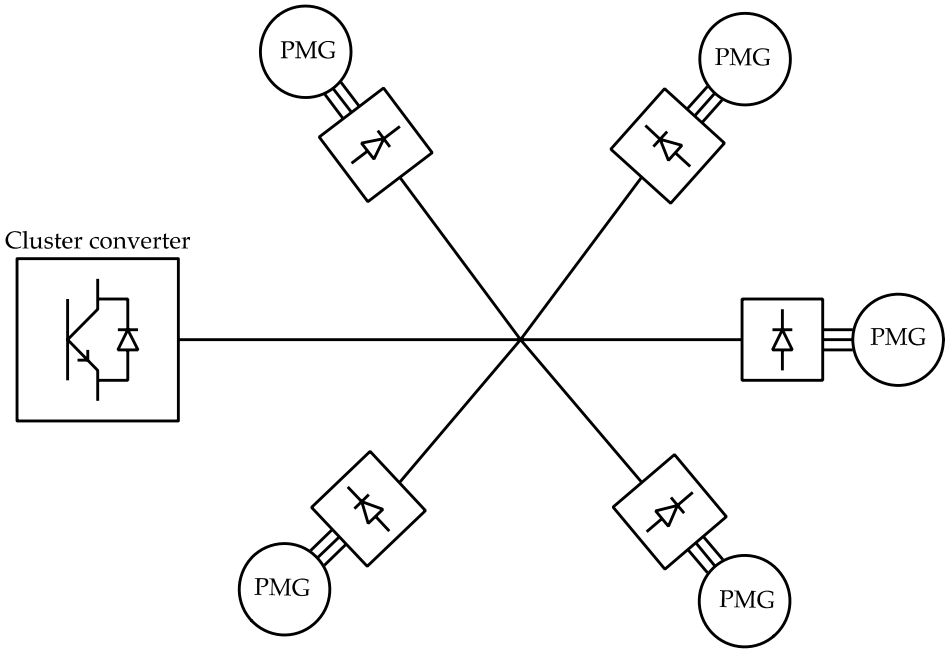

Figure 3-23: PM generator and DC electrical network based cluster.

The ideal operation of a PM generator with a rectifier would allow the transfer of the output current instantaneously between the phase windings of the generator, as shown in Figure 3-24[i]. However in reality the inductance of the generator stator windings makes this impossible. Therefore the transfer of the output current between the windings of the generator takes a finite amount of time, Figure 3-24[ii]; a process referred to as the commutation of the current between the windings, the time it takes for the full transfer of the current is referred to as the commutation time. The imperfect commutation of the output current between the windings of the

generator also leads to the distortion of the generator terminal voltages and therefore the output voltage of the rectifier, as shown in Figure 3-24[iii]. This distortion is reflected onto the voltage on the DC side of the rectifier and has the effect of reducing the average DC output voltage of the rectifier slightly; referred to as the commutation voltage drop. This voltage distortion therefore introduces an additional voltage drop component which lowers the average of the voltage at the DC terminals of the rectifier, which directly affects the flow of real power from the generator. This voltage drop therefore contributes to the voltage difference that allows the rotational speed of the generator and the cluster synchronous speed to be different. It should be noted that the voltage drop introduced by commutation does not result in an additional loss of power, as would be the case with a resistive voltage drop; this property is critical to maintaining the high efficiency that using PM generators brings to the system. The commutation process introduced here will be dealt with in greater detail later in this thesis.

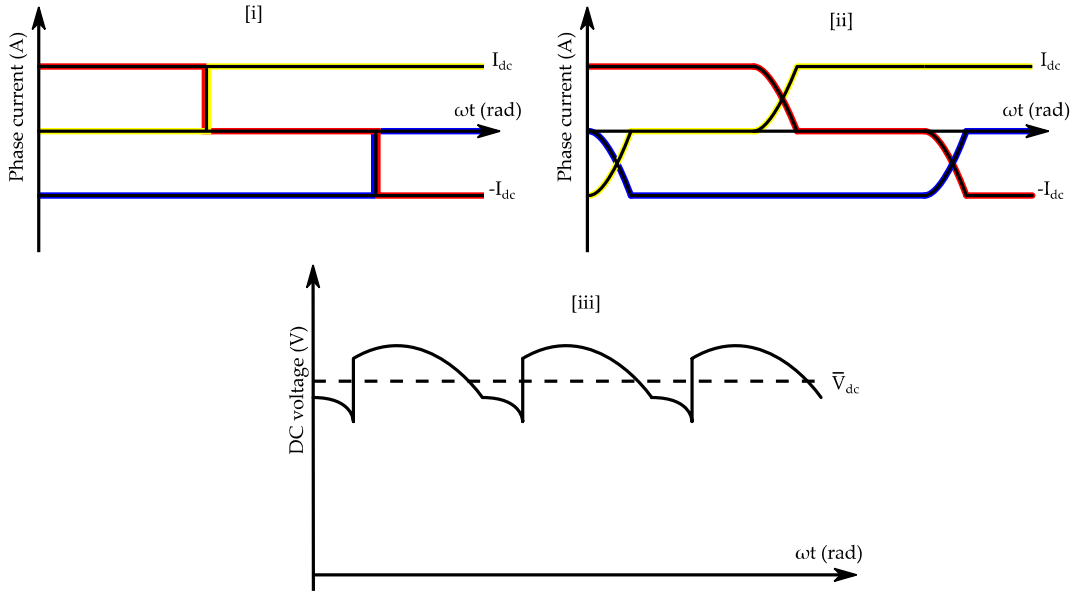

Figure 3-24: [i] Ideal transfer of the DC output current between the generator windings by the rectifier; [ii] Non-ideal transfer of the DC output current between the generator windings by the rectifier; [iii] Distorted rectifier output voltage as a result of the finite rectifier commutation overlap.

3.4 Discussion and conclusions

The studies presented in this chapter have investigated the impact of electrically clustering groups of five wind turbines on their availability and on their annual energy capture, which influence the two major economic factors of the operation of an offshore wind farm: the maintenance costs and the revenue produced from the sale of the generated electrical energy. It has been found that connecting five wind turbines in a cluster reduces the overall number of power converter failures within a wind farm and as such increases their availability; however it has been demonstrated that when a failure does occur the greater consequences, in terms of lost energy production, counteract the potential energy capture benefits of the improved availability. The reduced number of failures, from 83.76/yr to 16.75/yr for the Creyke Beck A wind farm, in itself however brings a significant benefit to the operation of an offshore wind farm because it will directly reduce the maintenance costs. It should also be noted that assuming the failure rate of the cluster converter equals that of the individual power converters, causes the prediction of the impact of clustering five wind turbines together on their annual energy production to be conservative, and therefore any improvement of the failure rate of the cluster converter, in comparison to the individual turbine converters, will benefit overall energy production of the wind farm.

Secondly it has been found that the requirement for the turbines in an electrical cluster to rotate with a common speed, chosen to be the optimum for the average of the wind speeds across the clustered turbines, causes a reduction of the energy capture efficiency of each of the turbines and therefore lowers the wind farm annual energy production by between 0.25% and 0.55%, depending upon the severity of the variations of wind speed

across the cluster. This will have a direct impact upon the revenue produced from the sale of energy generated by the wind farm. However, the magnitude of this energy capture loss could be lessened if it were possible for the individual turbines to maintain a certain degree of independence, allowing them to vary their rotational speeds about the cluster synchronous speed in response to locally changing wind speeds. Therefore it can be concluded from the two studies conducted in this chapter that the implementation of electrical clusters of wind turbines will lower the maintenance costs of the wind farm but also slightly reduce revenue from the sale of the energy.

Lastly, this chapter has introduced the different methods by which a cluster of wind turbines could be implemented, highlighting the potential merits and pitfalls of each. In particular the mechanisms, or lack of, through which each method of implementation allows the individual turbines to retain a degree of independence, even though they are controlled collectively, have been highlighted.

3.5 References

1. Lumbreras, S. and A. Ramos, *Offshore wind farm electrical design: a review.* Wind Energy, 2012: p. n/a-n/a.
2. Tavner, P., *Offshore Wind Turbines - Reliability, availability and maintenance*. Renewable Energy2012: IET.
3. Siemens, *Robicon Perfect Harmony - The Drive of Choise for Highest Demands*.
4. Hiller, M., R. Sommer, and M. Beuermann. *Converter Topologies and Power Semiconductors for Industrial Medium Voltage Converters*. in *Industry Applications Society Annual Meeting, 2008. IAS '08. IEEE*. 2008.
5. Arabian-Hoseynabadi, H., H. Oraee, and P.J. Tavner, *Wind turbine productivity considering electrical subassembly reliability.* Renewable Energy, 2010. 35(1): p. 190-197.
6. G.J.W. van Bussel, M.B.Z., *Offshore wind energy, the reliability dilemma,* in *The First World Wind Energy Conference*2002: Berlin.
7. Burton. T, S.D., Jenkins. N, Bossanyi E, *The Wind Energy Handbook*2008: Wiley.
8. Forewind. *Dogger Bank Creyke Beck*. 2013; Available from: www.forewind.co.uk/projects/dogger-bank-creyke-beck.html.
9. Bossanyi, E.A., *The Design of closed loop controllers for wind turbines.* Wind Energy, 2000. 3(3): p. 149-163.
10. Barthelmie, R., et al., *Ten Years of Meteorological Measurements for Offshore Wind Farms.* Journal of Solar Energy Engineering, 2005. 127(2): p. 170-176.
11. Burton. T, et al., *The Wind Energy Handbook*. Vol. 1. 2008: Wiley.
12. Jonkman, J., et al., *Definition of a 5MW reference wind turbine for offshore system development*, 2009, NREL.
13. Sørensen, P., et al., *Modelling of power fluctuations from large offshore wind farms.* Wind Energy, 2008. 11(1): p. 29-43.
14. Krause, P.C., *Analysis of Electric Machinery and Drive systems*. 2nd ed2002: IEEE.
15. Kumar, K.V., A.N. Rao, and M.P. Selvan. *Mitigation of output power fluctuations in wind farms with Opti-slip induction generator*. in *Sustainable Alternative Energy (SAE), 2009 IEEE PES/IAS Conference on*. 2009.

Chapter 4 Initial modelling of clusters

To investigate the operation of the different wind turbine cluster concepts, introduced in Chapter 3, a time domain dynamic model is required for each. The Matlab Simulink environment has been chosen for the development of these models, with the aid of the SimPowerSystems blockset. In order to develop models of each concept, a number of sub-models are required that represent the individual components, such as: a model of a wind turbine rotor and its interaction with the wind, a drive train and generator model, and a model of the electrical system including the cable network, the cluster converter and the controller. In addition to these models test operating scenarios are required that cover the likely operating conditions that a cluster of turbines would be expected to operate in; these scenarios will take the form of a number of different wind speed conditions where the winds are

continuously varying; although constant wind speed conditions and step changes will also be used to aid the investigations.

This chapter will describe the layout of the models developed for each of the cluster technology concepts, including each of the sub-models. It will then demonstrate the operation of each of the concepts under a number of operating conditions, chosen to highlight the particular features of each technology. The merits and pitfalls of each technology will then be discussed, concentrating on the applicability of each technology concept for connecting and operating a group of wind turbines as a cluster. Potential alterations that could offer improvements to each concept will also be put forward.

4.1 Wind turbine model

A model of the wind turbine rotor and its interaction with the wind are critical to determining the torque input to the generator. The relationship between the power in the wind and that extracted by a wind turbine was set out in chapter 2; to employ this in a model, the physical parameters of an example wind turbine are required. These parameters are taken from the reference wind turbine developed by the US National Renewable Energy Laboratory (NREL) for development of offshore wind systems [1], given in Table 4-1. The characteristic that is key to determining the power captured and therefore the input torque to the generator, is the Cp – λ curve; using the parameters of the NREL turbine and in particular the geometry of its blades this curve has been produced using the Bladed software package from DNV GL (formerly Garrad Hassan), which models the aerodynamics of the wind turbine in detail; the resultant Cp – λ curve is shown in Figure 4-1.

Using these parameters and the equation for power captured from the wind given in chapter 2, a basic model of the wind turbine has been developed that takes the wind speed and rotational speed of the generator as inputs, and produces the input torque to the generator as an output. Equation (4.1) forms the basis of this model in conjunction with a look-up table holding the Cp – λ curve of the turbine rotor; the gearbox ratio is taken into account in the derivation of this equation to give the torque input to the generator as a function of the generator speed, as opposed to the low speed shaft torque and turbine rotor speed. The blade pitch mechanism that limits the power captured by the turbine rotor once the maximum power output of the generator has been reached is not included in the model; therefore this model is valid only for use with wind speeds below the turbine rated wind speed. A block diagram of the model is shown in Figure 4-2, where the function f(u) is given in equation (4.2).

Table 4-1: Wind turbine model parameters [1] .

Generator power rating	5 MW	Hub Height	90 m
Rotor orientation	Upwind	Cut-in wind speed	3 m/s
Number of blades	3	Rated wind speed	11.4 m/s
Rotor diameter	126 m	Cut-out wind speed	25 m/s
Minimum rotational speed	6.9 rpm	Rated rotational speed	12.1 rpm
Blade second mass moment of inertia	11,776,047 kg.m^3	Gearbox ratio	97:1
Rated generator rotational speed	1174 rpm		

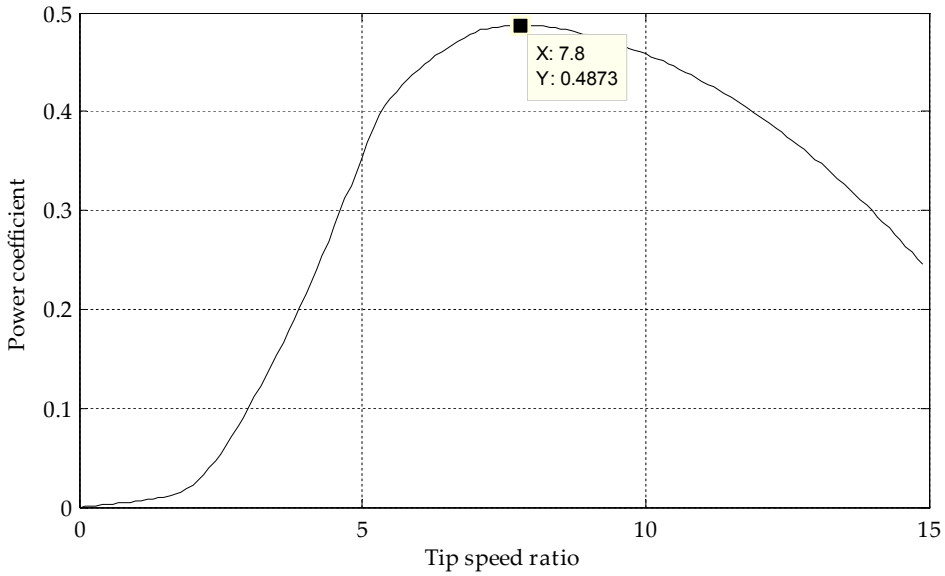

Figure 4-1: Wind turbine Cp - λ operating curve, with the maximum Cp and its associated tip-speed ratio highlighted.

$$T_{gen} = \frac{\rho . \pi . r^2 . V^3 . C_p}{2 . \omega_{gen}} \quad (4.1)$$

$$T_{Aero} = \frac{\rho . \pi . r^3 . V^2 . C_p}{2 . \lambda} \quad (4.2)$$

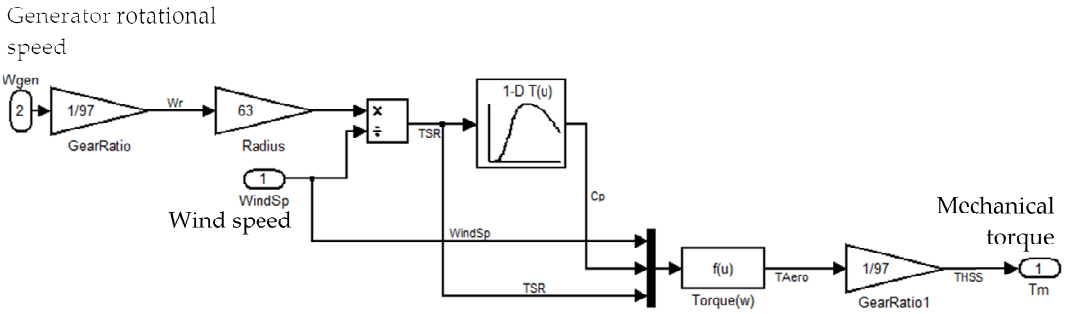

Figure 4-2: Wind turbine model block diagram.

4.2 Test operating conditions for modelling

The operating conditions that a cluster of wind turbines would be subject to are mainly dependant on the variation of the wind speeds incident on each turbine. However, the operating condition of the electrical network is also important. To investigate the operation of a cluster of turbines here, only the variation of the wind speeds is considered; it is assumed that the electrical network is always available and in good condition.

As discussed in the previous chapter, the individual wind speeds experienced by each wind turbine are likely to be different due to turbulent variations of the wind; although the wind speeds experienced by adjacent wind turbines will follow a similar average wind variation pattern over long periods of time. Wind turbulence also introduces variations of the wind speed across the swept area of the wind turbine rotor; the wind speed that is said to produce the torque on to the wind turbine drive train is the 'effective wind speed', which is an average of the wind speed across the rotor swept area [2] [3]. The inertia of the turbine rotor also acts as a low pass filter, removing the effects of high frequency changes of wind speed. To simulate realistic operating conditions for a group of turbines, a number of different effective wind speed data sets have been produced taking into account these effects. These data sets have been produced using the method set out in [2], which has been developed into a Simulink model by David Thompson, of the Industrial Control Centre at the University of Strathclyde.

The use of the wind profiles however could potentially 'cloud' some of the characteristics of each of the cluster technology concepts. Therefore scenarios are also applied where the wind speed inputs to each turbine are held constant and equal to each other, constant and different to each other

and where step changes of wind speed are applied to individual turbines. The step changes of wind speed will allow the transient response of the machines to be investigated, along with the effect of a change of wind speed on one turbine on the others in the cluster; the constant but different wind speeds between turbines will allow the steady state interactions of the machines to be studied.

Traces of the effective wind speed time series that have been produced for are shown in Figure 4-3. A mean wind speed of 7m/s is used in each case with a turbulence intensity of 10%, which is representative of an offshore wind farm site [4]. Figure 4-4 shows the constant wind speeds and associated step changes that are applied to allow the study of the transient behaviour of the turbines.

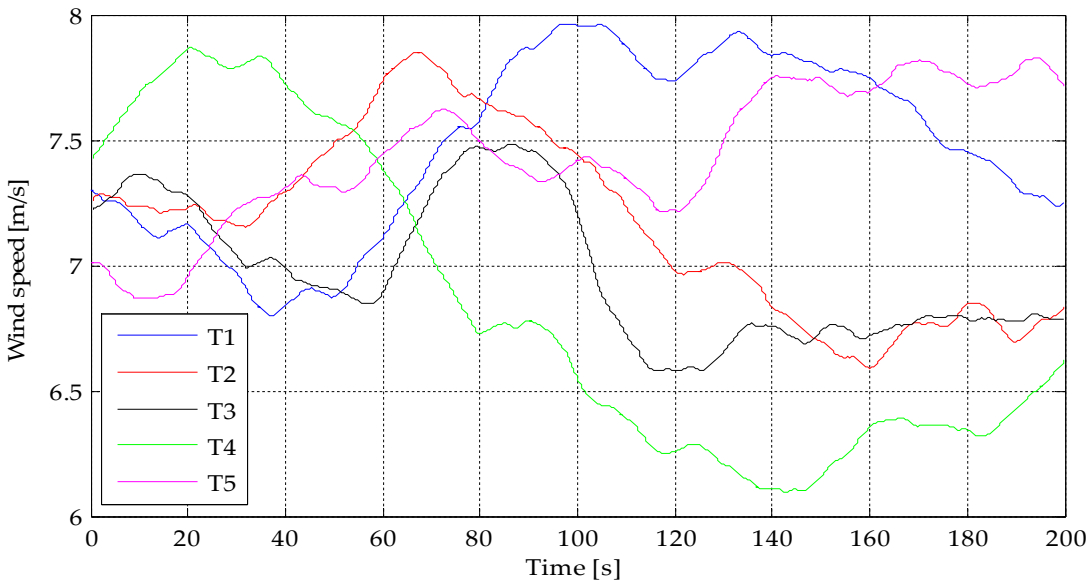

Figure 4-3: Continuously varying wind speed profiles generated for five wind turbines.

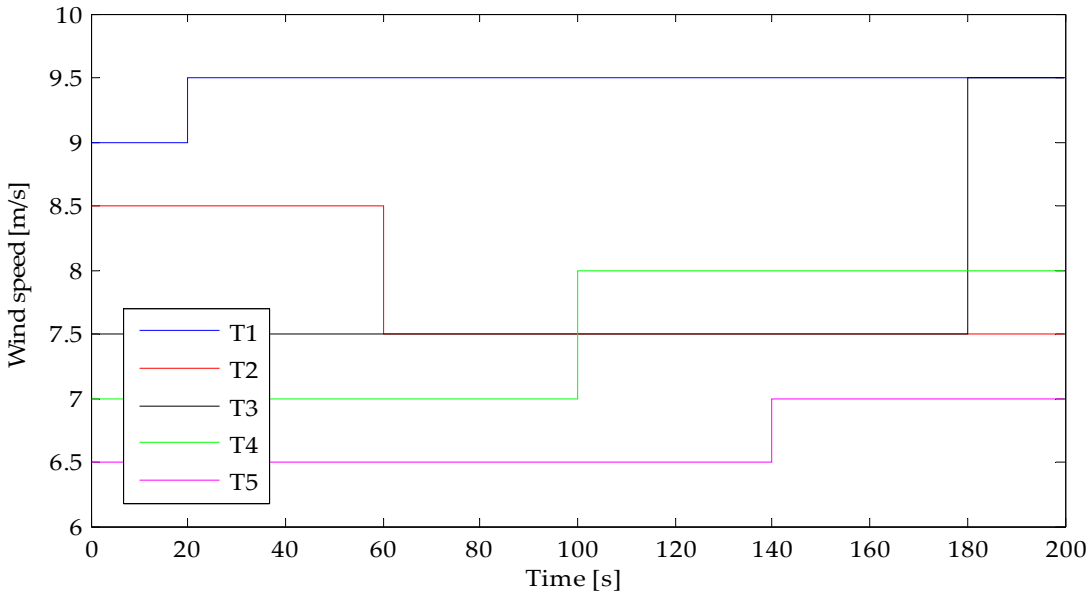

Figure 4-4: Wind speed profiles where the wind speed input to each turbine is constant but different initially, then a step change is applied to each.

4.3 Induction generator wind turbines with an AC electrical network

In this case, the generators within each wind turbine are induction machines; therefore the electrical network connecting them together is a three phase AC system, so that reactive power can be supplied for excitation.

The system model has been broken down into the following sub-models: wind turbine and generator, electrical network with cluster converter and the cluster controller.

4.3.1 Wind turbine and induction generator sub-model

The first sub-model includes the wind turbine model developed above, driving the induction generator model. The induction generator model is based upon the mathematical model set out in Chapter 2 and takes the mechanical torque from the wind turbine model as an input and connects to the three phase electrical network. The model of an induction generator acts as a current source to the electrical network. Measurements of the rotational speed and generator torque are also output from the model and fed back to the wind turbine model.

The make-up of the induction machine model is shown in Figure 4-5 to Figure 4-10 along with references to the corresponding equations given in Chapter 2; the induction generator parameters used in the model are shown in Table 4-2, where the inertia, J, applied to the generator is the summation of the generator's own inertia and the inertia of the wind turbine rotor referred to the high speed side of the gearbox, which is three times the individual blade second mass moment of inertia given in Table 4-1. The electrical parameters have been taken from previous induction generator based wind turbine studies and scaled up to 5MW [5] [6]. In particular the generator voltage has been increased from 690V to 3.3kV to cater for the higher power

level, and the magnetising inductance has been increased to maintain a reasonable output power factor at this higher voltage.

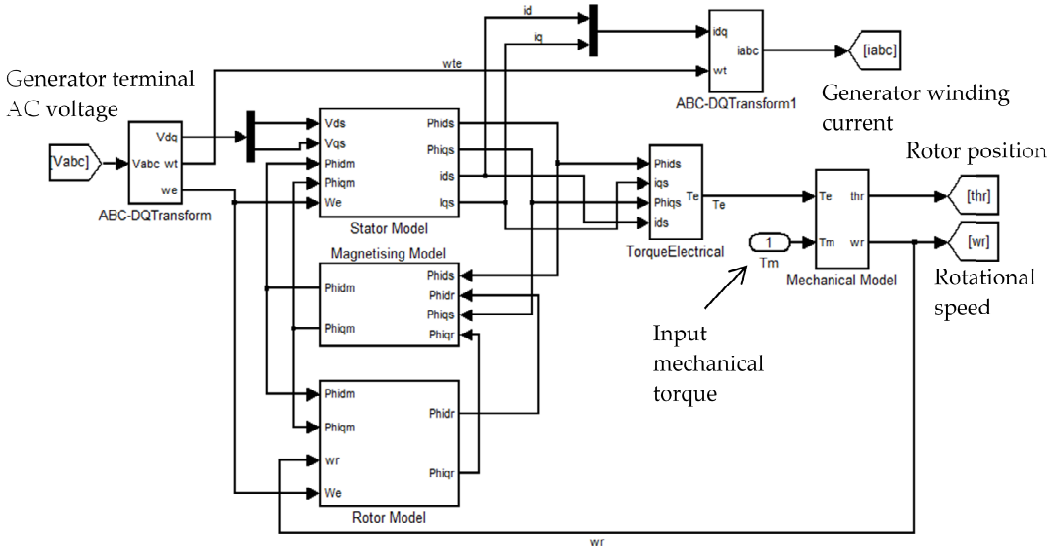

Figure 4-5: Induction generator model overall block diagram, each constituent subsystem is shown in Figure 4-6 to Figure 4-10.

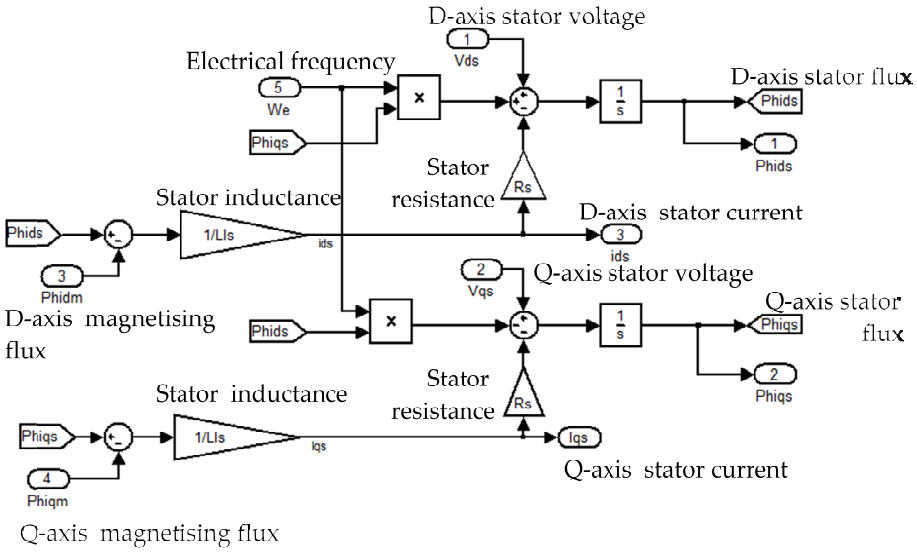

Figure 4-6: Induction generator stator model based on equations (2.13) and (2.14).

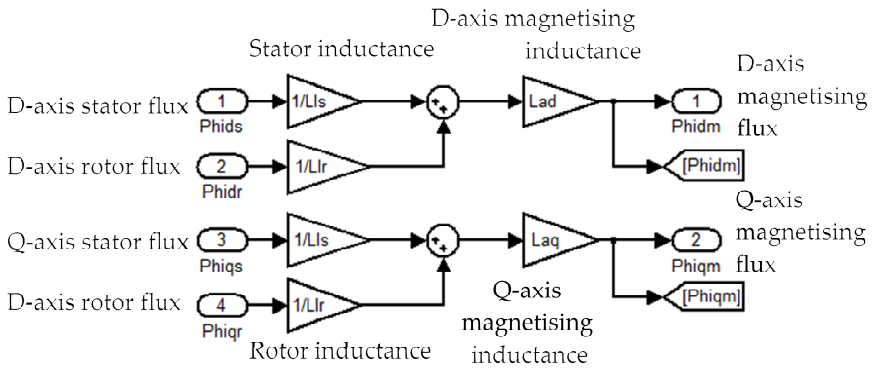

Figure 4-7: Induction generator magnetisation model based on equations (2.11) and (2.12).

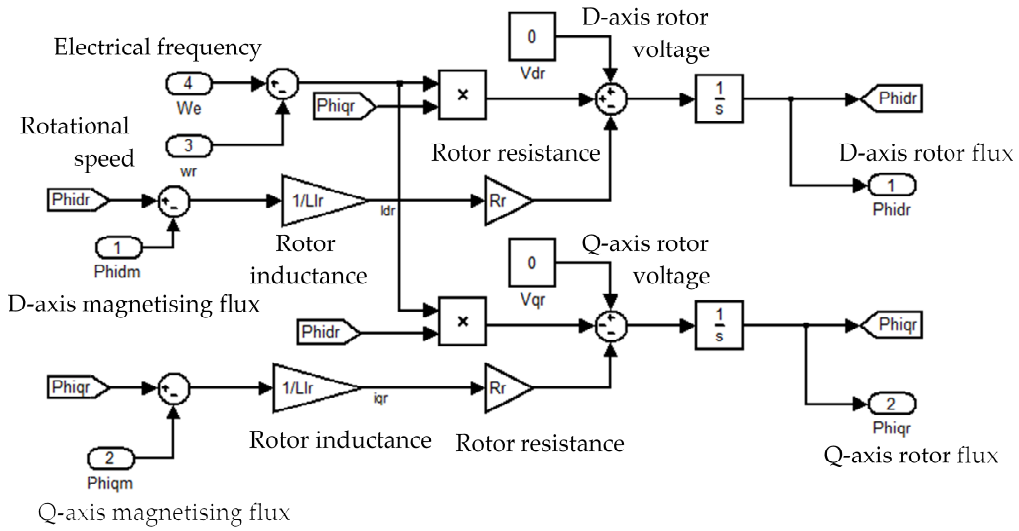

Figure 4-8: Induction generator rotor model block diagram based on Equations (2.17) to (2.18).

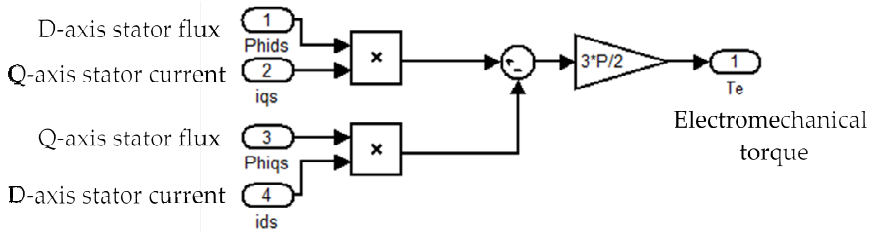

Figure 4-9: Induction generator torque model block diagram, based on Equation (2.23).

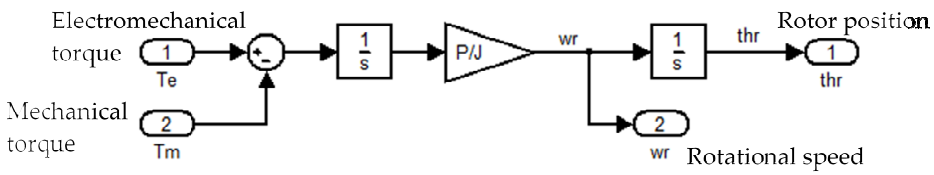

Figure 4-10: Induction generator mechanical model block diagram, based on Equation (2.24).

The torque slip characteristic for the generator is shown in Figure 4-11, which also gives the characteristic where the rotor winding resistance is increased by a factor of four; the purpose of this will be discussed later in this section. The arrangement of the wind turbine and induction generator model is shown in Figure 4-12. In addition to the generator, a parasitic resistive load is included at the terminals of the generators, this is required as Simulink does not allow elements that are effective current sources (generators and inductances) to be connected in series; a three phase parallel load is required, with high resistance of 200Ω, to mitigate this.

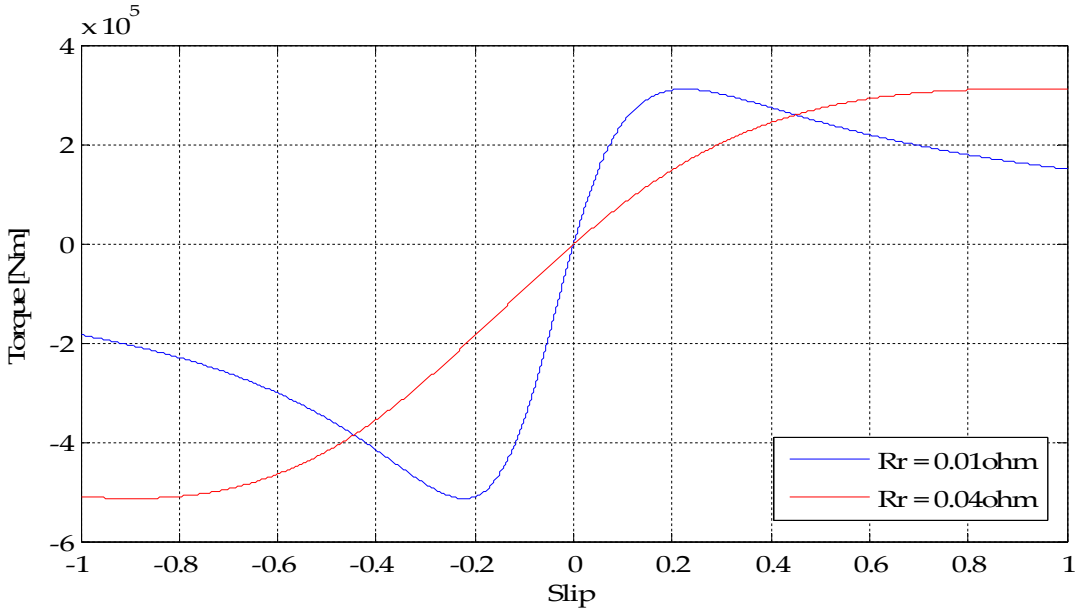

Figure 4-11: Torque slip characteristic of the induction generator used for different generator rotor winding resistance.

Table 4-2: Induction generator parameters.

$V_{nominal}$ (rms)	3,300V	Stator resistance	0.011Ω
$P_{nominal}$	5,000kW	Stator inductance	0.0568mH
$Frequency_{nominal}$	50Hz	Rotor resistance	0.01Ω
Pole Pairs	2	Rotor inductance	0.091mH
Combined inertia	4300.7 kg.m^2	Magnetising inductance	11.52mH

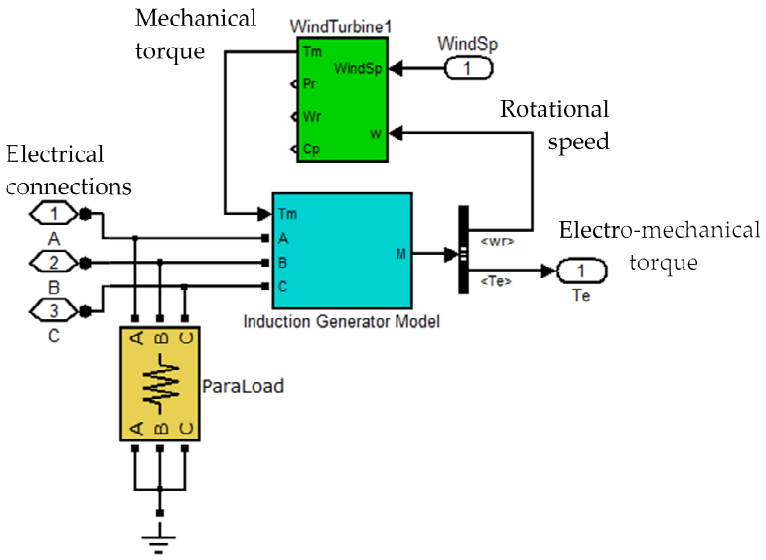

Figure 4-12: Wind turbine and induction generator model block diagrams.

4.3.2 Electrical network and cluster converter sub-model

The second sub-model includes the electrical network that couples the turbines together and the cluster converter. The cluster converter is based on the operating principles of a voltage source converter (VSC), which, for simplicity is modelled as a three phase set of ideal voltage sources, displaced 120° from each other. A step-up transformer is also included at the terminals of the generators to enable the transfer of the necessary power through the cables. The lengths of the branch cables (between the generators and the point of common coupling, PCC) are 10km, and the length of the common cable (between the PCC and the cluster converter) is also 10km. The 10km branch cables are longer than would be expected in an actual wind farm and will therefore exaggerate the effects of their impedance on their end-to-end voltage drop; this will however help to highlight any effects caused by this voltage drop. It is also assumed that the cross-section of the all of the cables is 500mm² for simplicity; however in reality the common cable will be rated to transport the aggregate maximum power output of the five turbines. The

impedance parameters of the cables and transformers are shown in Table 4-3 and a schematic of the electrical network is shown in Figure 4-13.

Table 4-3: Transformer and cable parameters, where the LV winding of the transformer is taken as the primary winding [7] [8].

Transformer rated power	5MVA	Nominal Frequency	40Hz
V_{HV} transformer nominal	33kV	Transformer HV winding leakage inductance	115mH (0.1327pu)
V_{LV} transformer nominal	3.3kV	Transformer HV winding resistance	1.82Ω (0.0083pu)
Transformer magnetisation inductance	4.33H (500pu)	Transformer LV winding leakage inductance	1.15mH (0.1327pu)
Transformer core loss equivalent resistance	1089Ω (500pu)	Transformer LV winding resistance	0.0182Ω (0.0083pu)
Cable series inductance	0.3mH/km	Cable conduction resistance	0.0366Ω/km

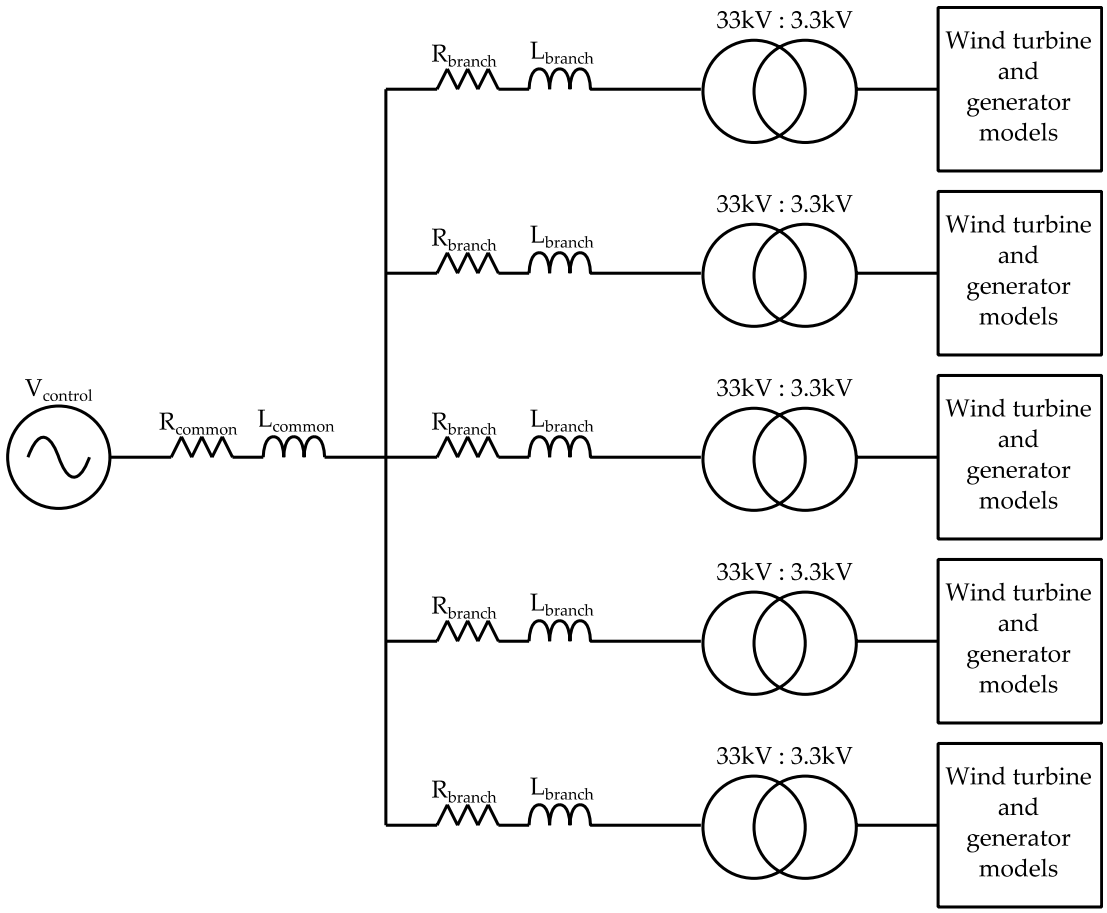

Figure 4-13: AC cluster electrical network schematic.

4.3.3 Cluster controller sub-model

The aim of the cluster controller is to regulate the frequency of the electrical network, therefore indirectly controlling the rotational speeds of the turbines. Since the cluster converter controls the turbines collectively, it acts as if the group of turbines are in actual fact one large wind turbine, with a power output that is equal to the aggregated power output of the individual turbines. Ideally measurements of the wind speed would be taken at each turbine and the average used to control the cluster frequency. However representative measurements of the wind speed are difficult and therefore the control of the system must be achieved without it. To allow the controller to understand the current operating point of the cluster, the active power output from the whole cluster is measured at the input terminals of the converter. This measurement is compared with a reference which gives the optimum power output of the cluster for the current network frequency; the result of which is used to drive the change of the network frequency until the reference power matches the measured power, at which point the turbines will be operating at the optimum rotational speed for the average wind speed across the cluster. The actual rotational speeds of the individual wind turbines will vary slightly from that of the large wind turbine due to local differences in wind speed requiring each turbine to operate at a different point on the generator slip curve.

The power reference values are determined using Equations (4.3) and (4.4), taking into account the value of tip-speed ratio, λ_{opt}, which allows the turbine rotor to operate at its peak power coefficient, C_{pmax}, taken from Figure 4-1. A block diagram of the cluster controller is shown in Figure 4-14; a proportional integral (PI) controller is used to drive the network frequency according to the error between the measured and reference powers. Since

the system is non-linear the bandwidth of the controller will vary with the operating point; the maximum bandwidth however is designed to be approximately 0.5Hz, which is small enough to remove high frequency changes of power output, but sufficient to follow the general change of the average wind speed. Limits to the range of rotational speed variation and therefore network frequency are also applied, as given in Table 4-1; integral anti wind-up is included for when the frequency is limited.

$$P = \frac{\rho . \pi . r^5 . \omega_r^3 . C_{pmax} . N_{turbines}}{\lambda_{opt}^3} \tag{4.3}$$

$$f_e = \frac{\omega_r . GBR . p}{2\pi} \tag{4.4}$$

(GBR = gear box ratio, p = pole pairs, $N_{turbines}$ = number of turbines in a cluster, ρ= density of air (kg/m^3), r = turbine rotor radius (m), f_e=electrical frequency (Hz)).

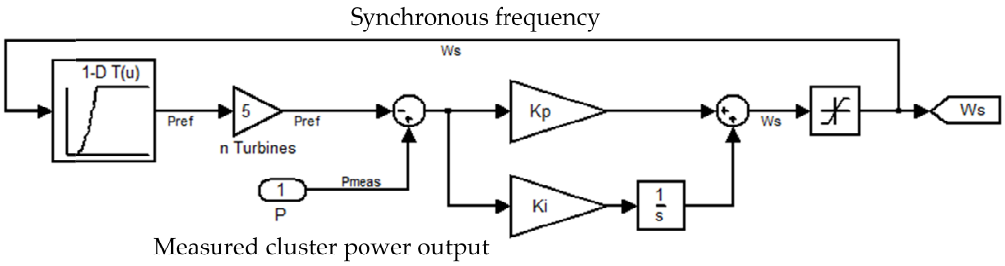

Figure 4-14: Cluster controller outline block diagram.

4.3.4 Simulation results

To gain an understanding of the operation of this system when faced with the wind speed scenarios detailed in Section 4.2; two simulations have been run using each of the sets of wind profiles for a run time of 200 seconds.

Continuously varying wind speeds

It is shown by Figure 4-15 that, in response to the varying winds, in Figure 4-3, incident on each turbine, the rotational speeds of the generators vary

slightly in comparison to each other as well as in relation to the cluster synchronous speed, which is directly related to the electrical frequency. The variation of the rotational speeds relative to the synchronous speed is a result of the slip required in each induction generator to produce a reaction torque to match the input torque; therefore when the wind speed peaks, the slip also peaks producing the necessary torque. The variation of turbine 1s input and generator torques in relation to each other are shown in Figure 4-16; where it can be observed that the turbines accelerate or decelerate as a result of the mismatch between the torques. (A negative input torque drives the induction machine as a generator; therefore the generator reaction torque is also negative so that it acts against the input torque).

The aggregate power output of the cluster, shown in Figure 4-17, gives an indication of the average wind speed across the cluster of turbines. This measurement is used to regulate the electrical frequency, and therefore the frequency follows the change of the cluster output power, as shown in Figure 4-18. The effectiveness of the controller at regulating the rotational speeds of the turbines is indicated by the proximity of each of the instantaneous rotor power coefficients to the maximum for the rotor design, 0.4873. This is shown to be good in Figure 4-19 as the power coefficients of each turbine do not stray more than 2.5% from the maximum.

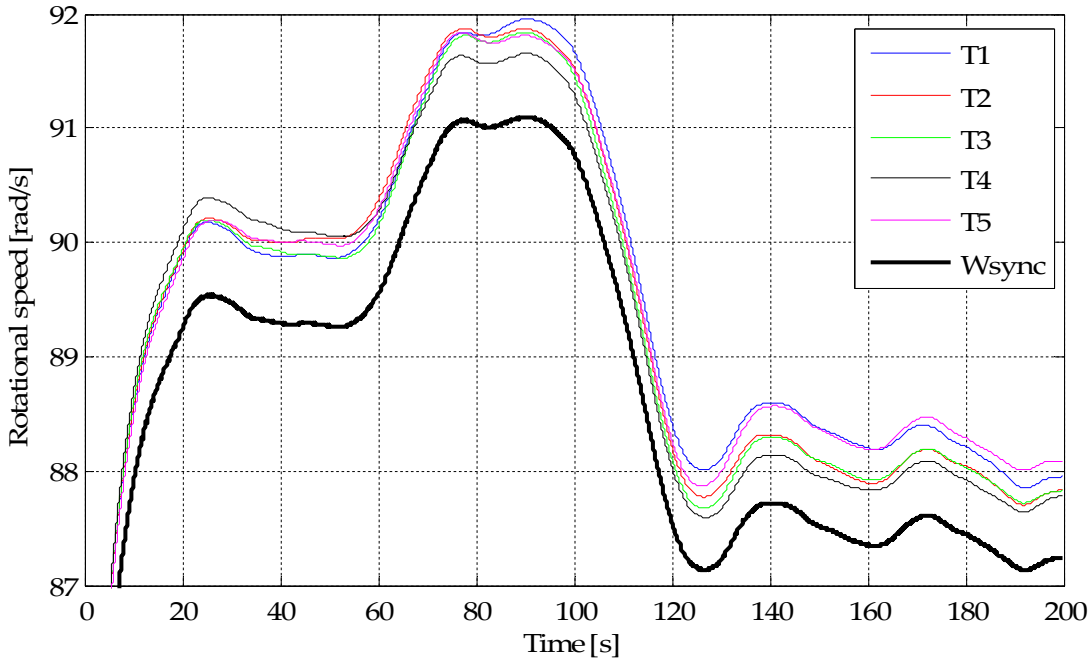

Figure 4-15: Generator rotational speeds and cluster synchronous speed in response to continuously varying input wind speeds.

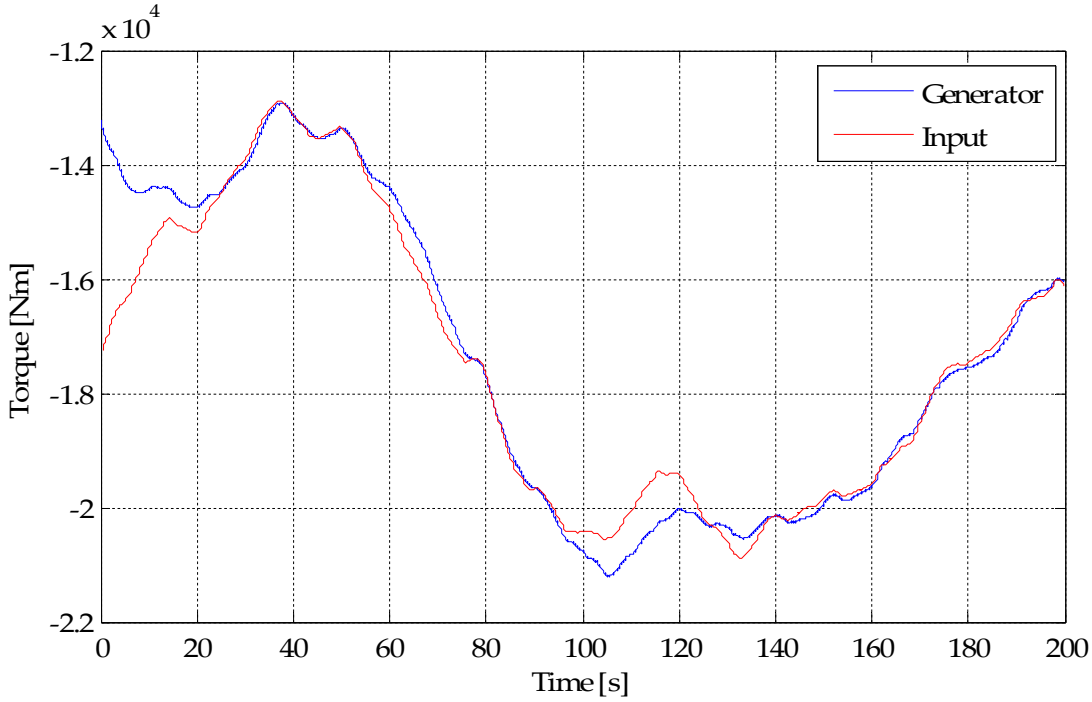

Figure 4-16: Generator and input torque of turbine 1 in response to the continuously varying wind speed.

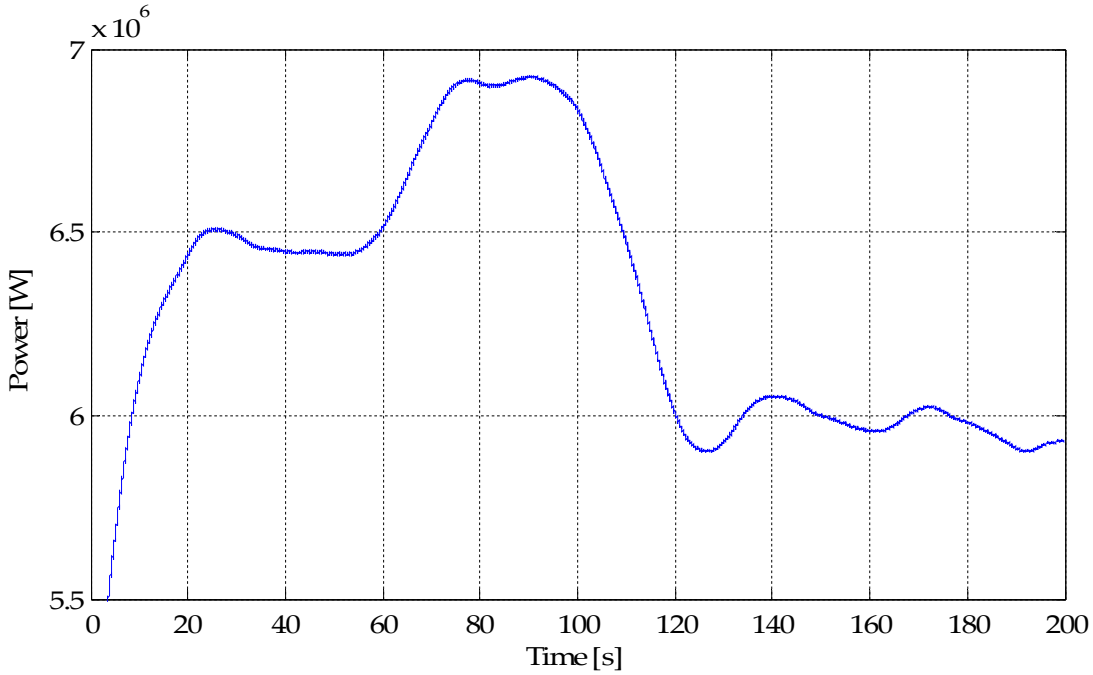

Figure 4-17: Aggregated active power output from the cluster in response to continuously varying wind speeds on each turbine.

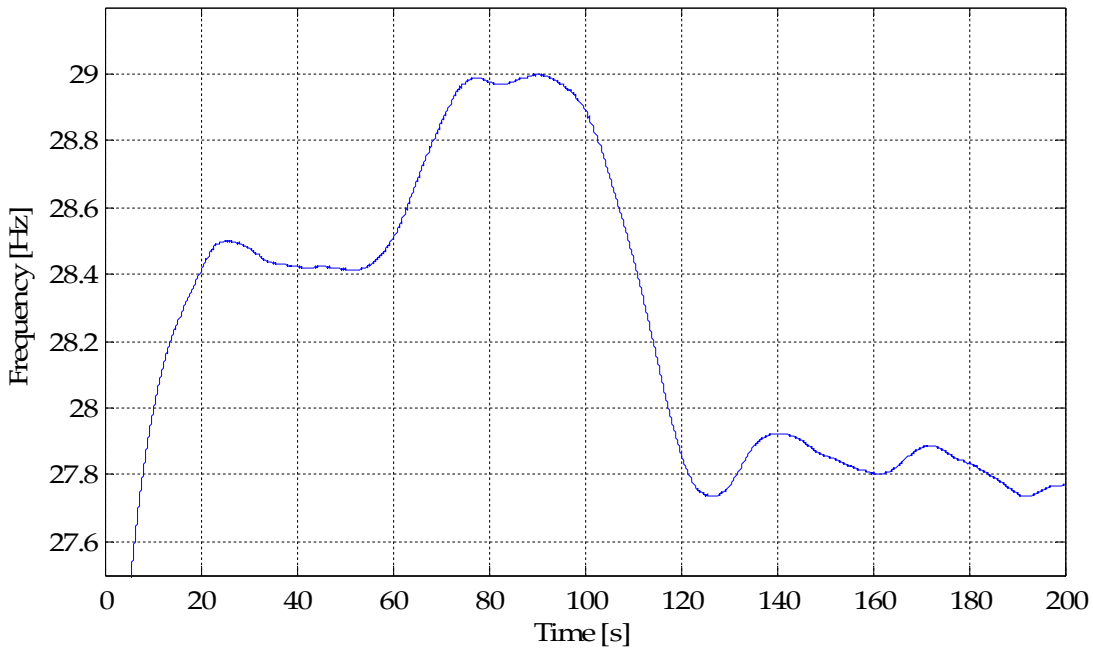

Figure 4-18: Cluster electrical frequency driven by the cluster controller in response to the variation of the aggregate cluster output power.

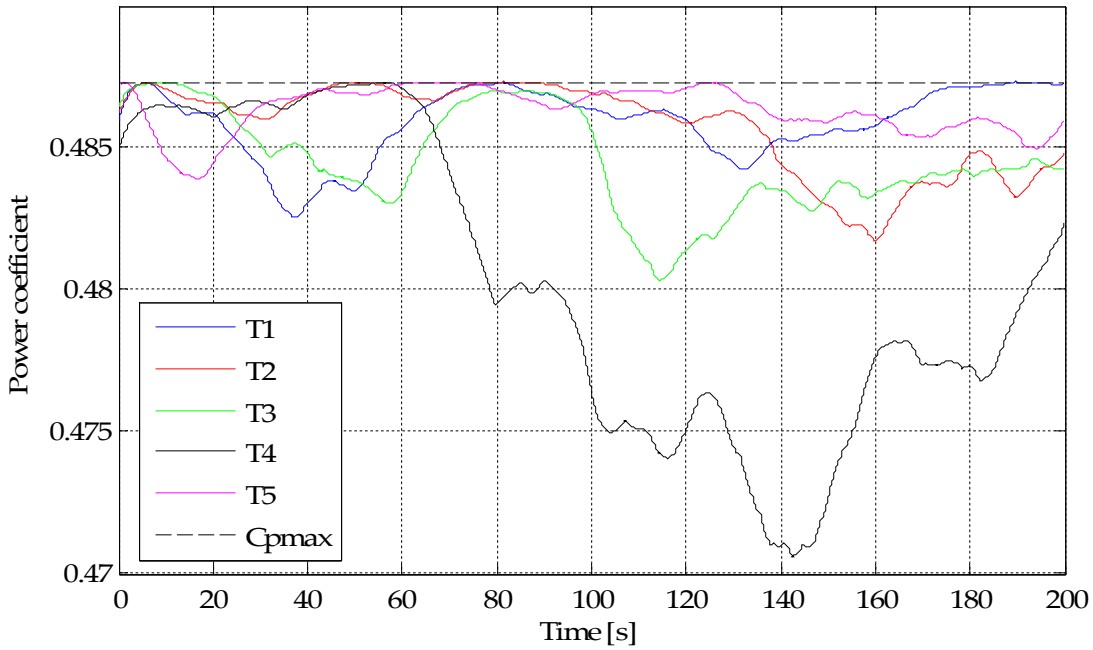

Figure 4-19: Power coefficient of each turbine in comparison to the maximum Cp possible for the turbine rotor.

Constant but different wind speeds with step changes

When the wind speeds follow the profiles in Figure 4-4, the effects of different wind speeds between turbines and the transient response of the each turbine in the cluster to an abrupt change of wind speed on a single turbine are observed. In the first instance where constant but different wind speeds are applied to each turbine, prior to the 20 second point, the rotational speeds of each turbine are different, shown in Figure 4-20, allowing the generators to produce the necessary reaction torques to match the input torque. When a step change is applied to turbine 1, at 20 seconds, its input torque responds immediately and the generator torque follows with a slightly slower rate of change, as shown in Figure 4-21; the input torque increases furthest and the resulting imbalance between the torques causes the rotational speed of the generator to increase. The increase of the rotational speed subsequently causes the generator slip to increase, shown in Figure 4-23, causing the torques to eventually converge, allowing the rotational speed to reach a new steady state. In addition to the change of generator slip, in response to the input change, the increased power output from the cluster causes the controller to alter the system frequency, which also changes the slip. The slip is observed to reach a steady state very soon after the input change is applied, yet the torque continues to change; this occurs as a result of the change of the overall power throughput, and since power is proportional to the torque multiplied by the rotational speed, when the power throughput reaches its new level the rotational speed will continue to increase until the torques become equal, shown in Figure 4-21 and Figure 4-22.

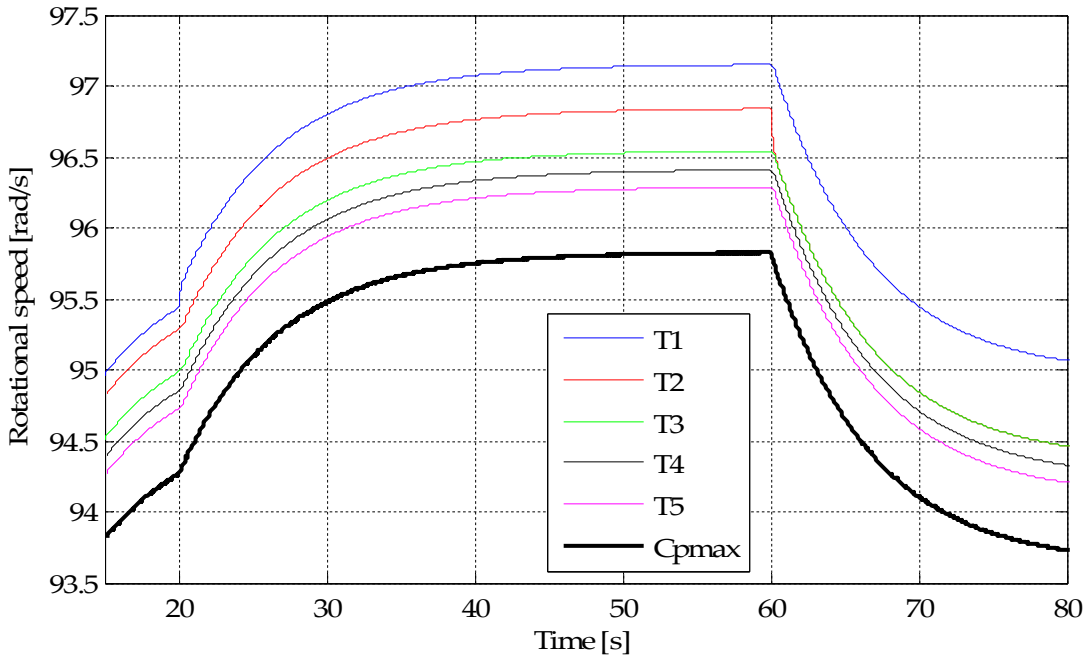

Figure 4-20: Generator rotational speeds and cluster synchronous speed when the turbines are subjected to the wind speed variations in Figure 4-4.

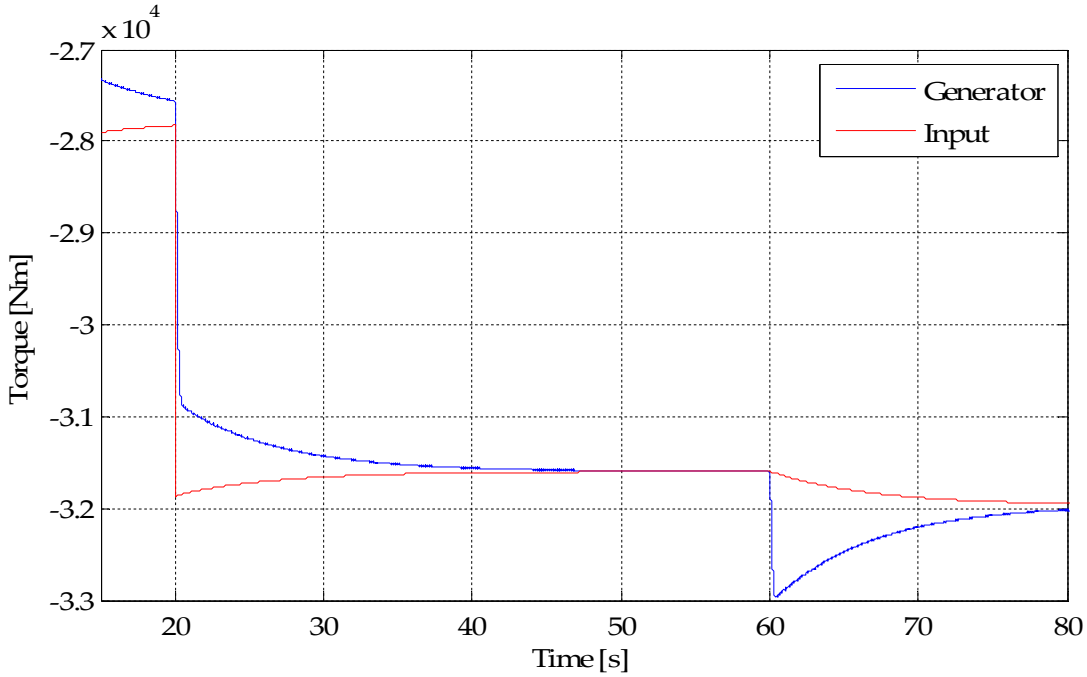

Figure 4-21: Generator and input torque of turbine 1 in response to the step changes of wind speed in Figure 4-4. A step change of wind speed is applied to this turbine at 20 seconds and turbine 2 at 60 seconds.

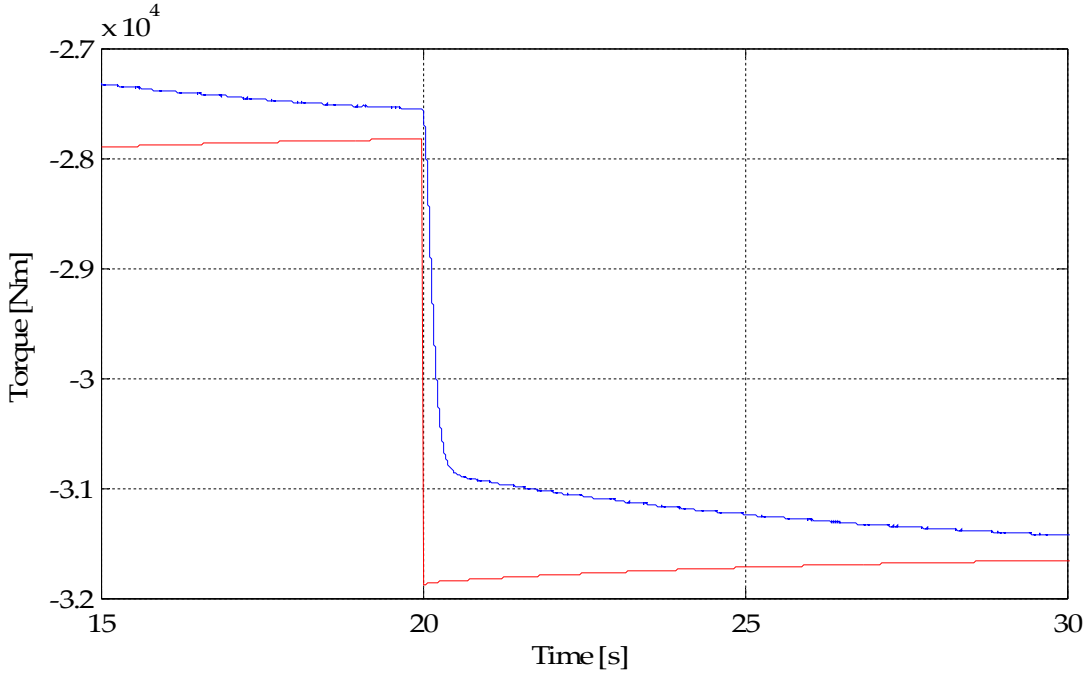

Figure 4-22: Enlarged generator and input torque of turbine 1 in response to the step change of wind speed in Figure 4-4.

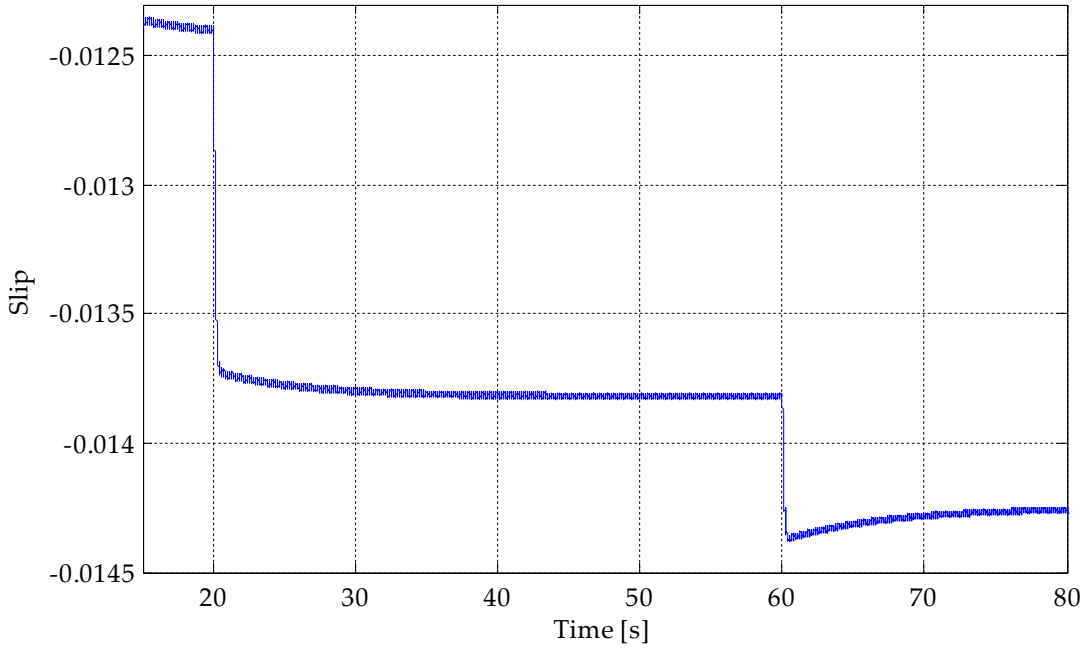

Figure 4-23: Turbine 1 generator slip in response to the step changes of wind speed in Figure 4-4. A step change of wind speed is applied to this turbine at 20 seconds and turbine 2 at 60 seconds.

The response of turbine 1 to a step change of wind speed on an adjacent turbine is shown in Figure 4-20 and Figure 4-21, after 60 seconds when a step reduction of wind speed is applied to turbine 2. It is shown that in response to this, the rotational speed of turbine 1 and indeed all of the turbines decrease, driven by increases of the generator torques, as shown in Figure 4-24. The torque changes of the turbines with constant wind speed are driven by the controller changing the electrical frequency and subsequently the point of zero generator torque. This produces an increase of generator torque if the wind speed on the adjacent turbine decreases and vice versa if the wind speed increases, causing the rotational speeds of the generators to either accelerate or decelerate. After a period of time the torques balance and the rotational speeds reach a new steady state.

Following the wind speed change the cluster controller acts to alter the cluster frequency to optimise the turbine rotational speeds for optimum energy capture. The changes of the cluster frequency and power coefficient of each turbine are shown in Figure 4-25 and Figure 4-26, where it can be observed that the controller is effective at keeping the majority of the individual turbine power coefficients close to the maximum (within approx. 2.5%). The power coefficients of turbines 1 and 5 are least optimal because their wind speeds are furthest from the cluster average. This is in contrast to the tighter spread of the power coefficients in Figure 4-19, where the wind speeds are continuously varying, but don't differ by more than 2m/s. This highlights that when there are greater differences between the wind speeds on each turbine, the ability of the cluster controller to optimise the rotational speed of each turbine to achieve maximum Cp is diminished, the effects of which were discussed in the previous chapter.

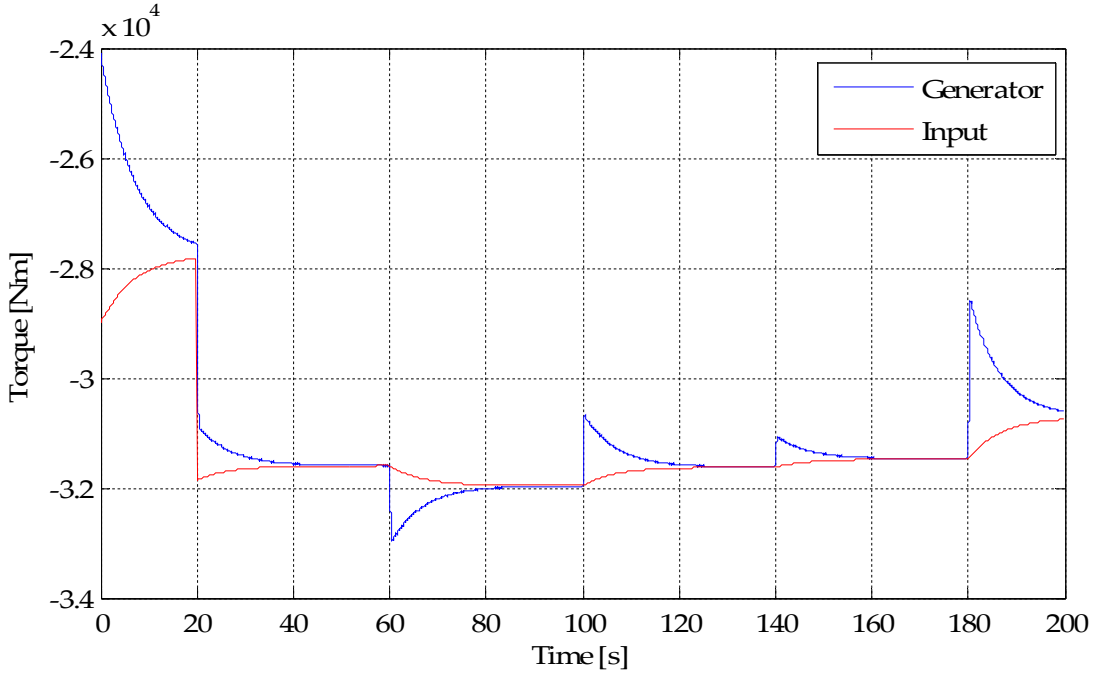

Figure 4-24: Turbine 1 generator and input torque in response to the step changes of wind speed in Figure 4-4.

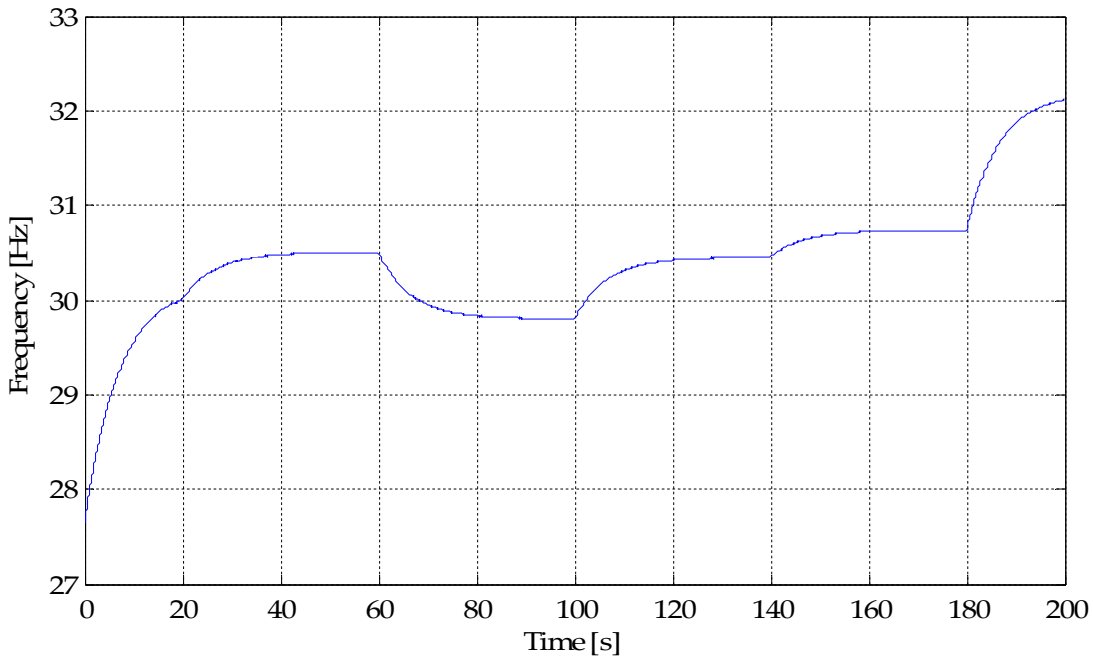

Figure 4-25: Cluster electrical frequency responding to the wind speed changes in Figure 4-4.

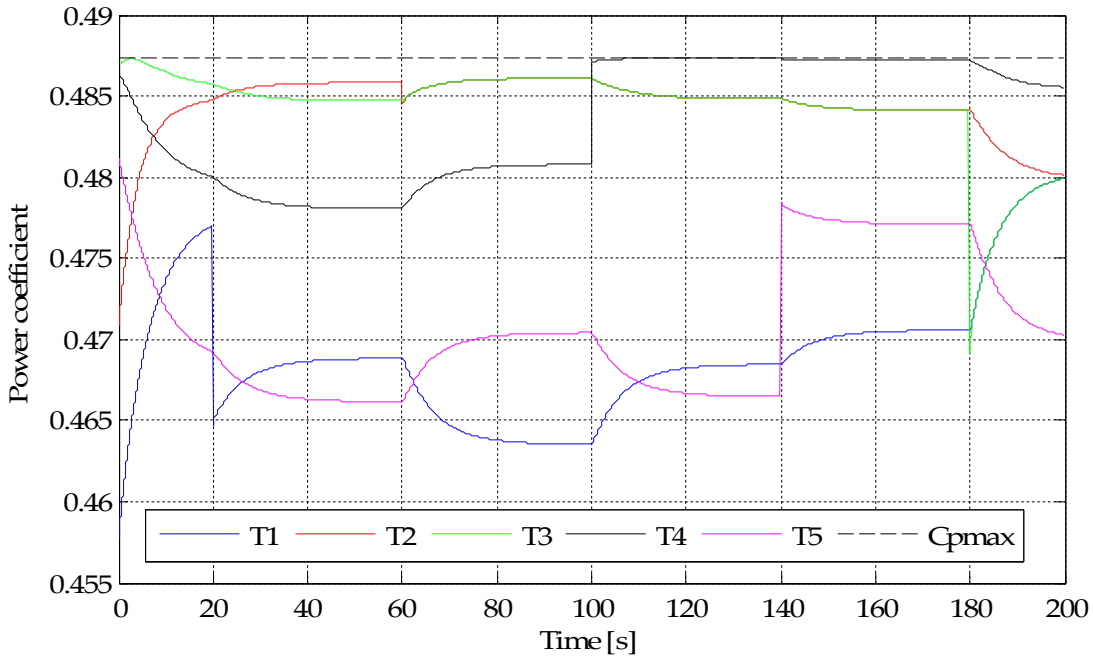

Figure 4-26: Power coefficient of each turbine in the cluster as a result of the wind speed changes in Figure 4-4.

The impact of a shallower slip slope

The amount the rotational speed of each turbine varies about the synchronous speed is related to slope of the generator slip curve, which itself is a function of resistance in the generator rotor winding, as mentioned in the previous chapter. When a group of previously independent induction generator based wind turbines are operated as a cluster, the independence of each turbine is significantly reduced; in fact the only independence that remains is the ability for each turbine to operate at a different point on the generator slip slope (assuming the generators are identical). A degree of independence between turbines is important so the generators can produce the necessary reaction torque to balance the input torque from their local wind conditions and also so that the individual turbine tip-speed ratios can be as near to optimal as possible. By reducing the gradient of the slip slope

the rotational speed of each generator can be granted a greater range of variation for a particular change of generator torque; this can be achieved by increasing the generator rotor winding resistance. An indication of the impact of this is observed by increasing the winding resistance by an arbitrary factor of four and applying the same wind speed profiles, in Figure 4-4. The impact of the rotor resistance increase on the generator torque slip characteristic is shown in Figure 4-11.

$$Energy\ transfer\ efficiency\ (\%) = \left(\frac{P_{outCluster}}{P_{AeroIn}}\right) \times 100 \qquad (4.5)$$

Comparing the turbine rotational speeds in Figure 4-27 with Figure 4-20 demonstrates the effect of the reduced gradient of the slip slope, where it can be observed that the speeds are higher in relation to the synchronous speed, indicating a greater slip. The benefit this brings to the operation of the turbines is identified by comparing Figure 4-28 with Figure 4-26, which, for the same changes of wind speed, show that the power coefficients of the turbines are closer to the maximum, particularly turbine 1. The limited improvement experienced by turbine 5 is due to it experiencing the lowest wind speed relative to the cluster average, giving it less influence over the cluster operating point. As a result of the improved power coefficients the turbine rotors extract power from the wind with greater efficiency; this is offset however by the added losses in the extra rotor winding resistance required to achieve the shallower slip slope. The energy transfer efficiency, equation (4.5), of the generators and electrical system for the different simulation runs with the initial and reduced gradient slip slopes are shown in Figure 4-29, where it can be observed that the efficiency of the system is a few percent lower as a result of the additional rotor winding resistance.

Therefore it can be concluded that the extra energy lost is greater than the energy capture gained by improving the turbine power coefficients.

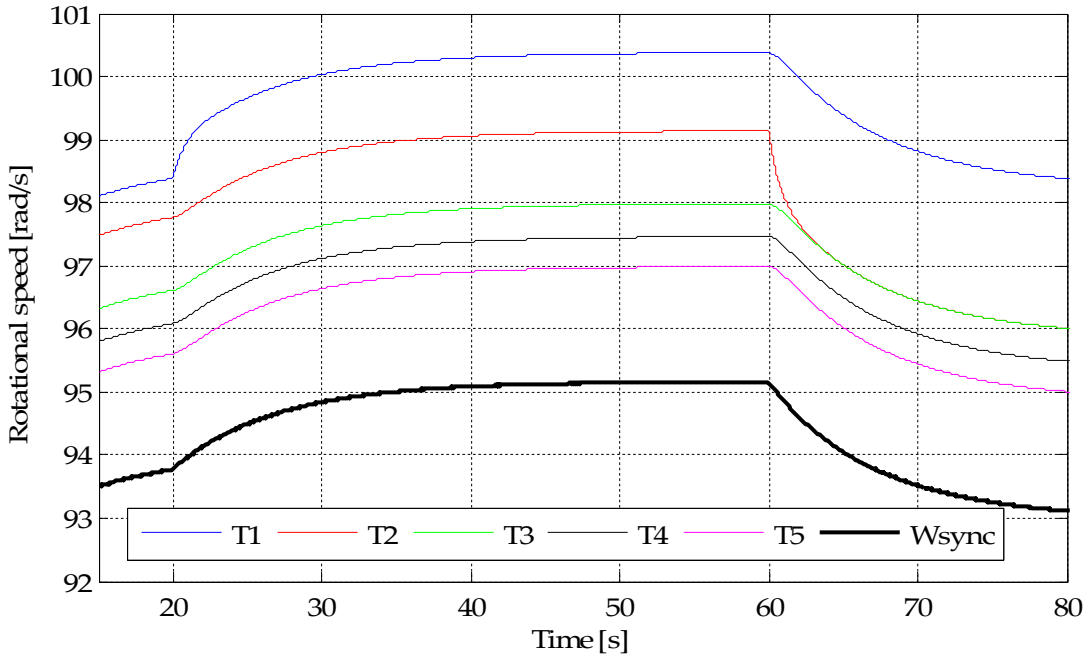

Figure 4-27: Generator rotational speeds and cluster synchronous speed when the turbines are subjected to the wind speed variations in Figure 4-4 and the rotor winding resistance is increased by a factor of four.

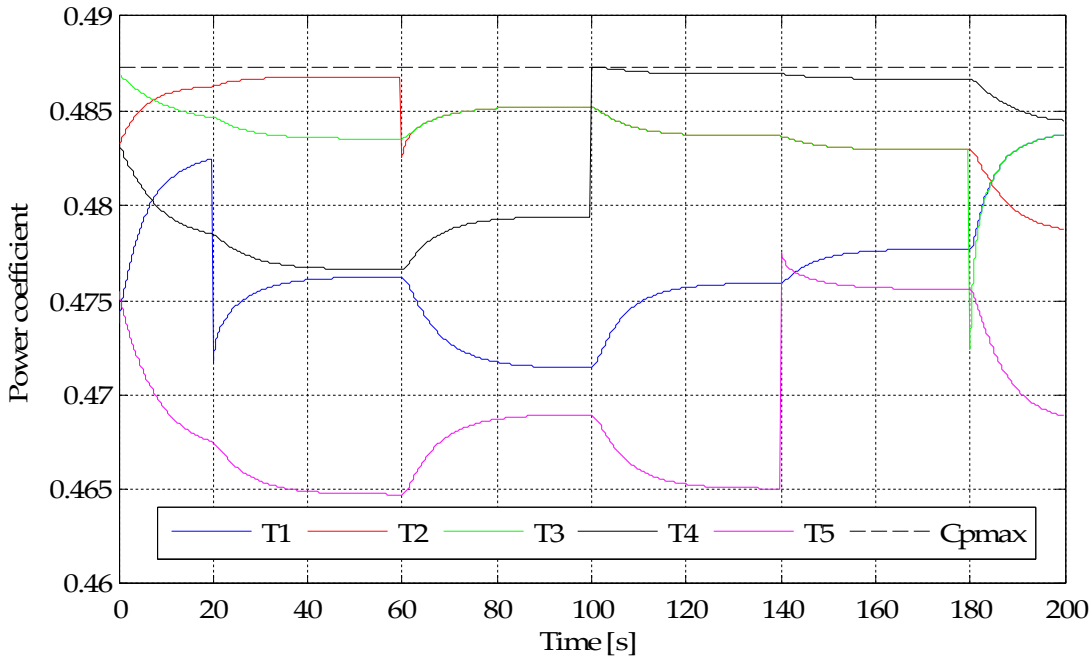

Figure 4-28: Power coefficient of each turbine in a cluster as a result of the wind speed changes in Figure 4-4 and where the generator rotor resistance has been increased by a factor of four.

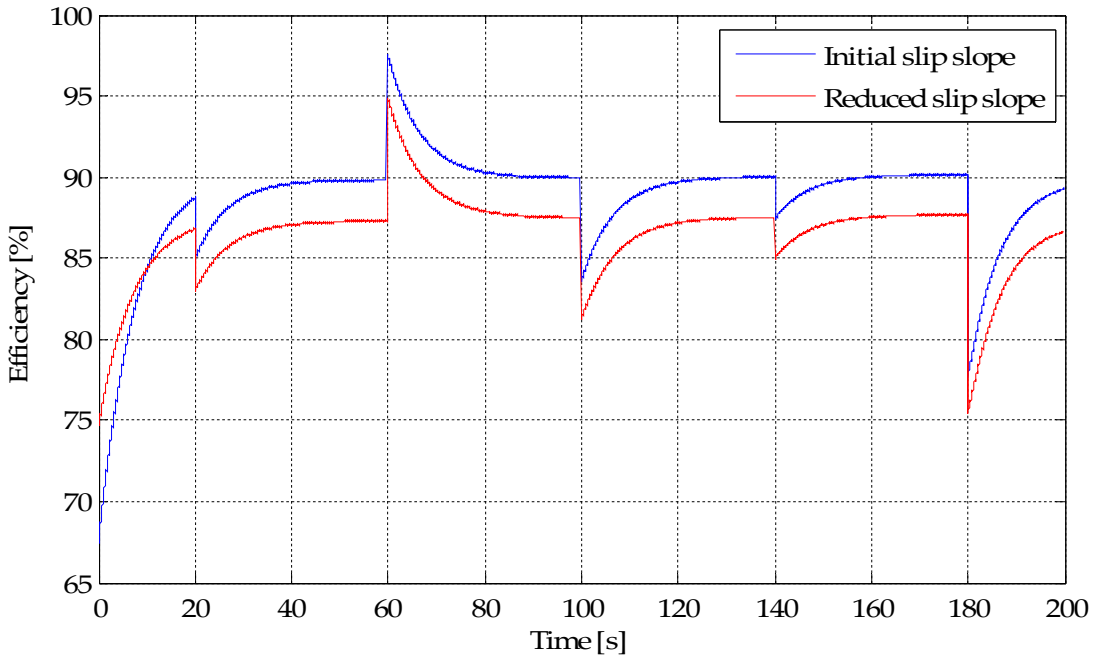

Figure 4-29: Energy transfer efficiency of the generators and electrical system when the initial slip slope of the generators is used and where the gradient has been reduced. The turbines are subject to the wind speed changes in Figure 4-4.

4.4 PM generator based wind turbines with an AC electrical network

The use of PM generators within a cluster based collection network can be achieved by either directly connecting the generators to the electrical network, in which case the network must be based on AC principles, or by rectifying the generator outputs and connecting them to a DC electrical network. The case where the PM generators are directly connected to an AC network is investigated here, and the electrical network topography is very similar to the network used with the induction generators, above shown in Figure 4-13.

To investigate the characteristics of a cluster of wind turbines which incorporate PM generators, a system model that comprises of similar sub-models to the induction machine case has been developed. The constituent sub-models are: the wind turbine and PM generator sub-model, the electrical network and cluster converter sub-model and the cluster controller sub-model. Only the first sub-model is different to the induction machine case.

4.4.1 Wind turbine and PM generator sub-model

The model of the PM generator is based on the mathematical model set out in Chapter 2 and is used in conjunction with the wind turbine model developed in Section 4.1. The generator model takes the mechanical torque produced by the wind turbine model as an input and when the generator is coupled to an AC electrical network it rotates with a speed directly related to the electrical frequency. The generator model also produces a measurement of the rotational speed which is fed back to the wind turbine model. The generator parameters are given in Table 4-4; these parameters have been sourced from previously published work and the rotational inertia and wind turbine parameters are the same as those used in section 4.3 [9]. Block

diagrams of the constituent parts of the PM generator model are given in Figure 4-30 to Figure 4-33; the overall layout of the wind turbine and PM generator sub-model is similar to that shown in Figure 4-12. Also, to allow the model to be simulated, a parasitic load is included at the terminals of the generators, similar to that used in the induction machine case above.

Table 4-4: PM generator parameters.

$V_{nominal}$ (rms)	3,300V	Stator resistance, R	0.002Ω
$P_{nominal}$	5,000kW	Stator inductance, $L_{ad,aq}$	1.6mH
$Frequency_{nominal}$	50Hz	Magnetic flux constant, Ψ_f	7.7487
Pole Pairs	2	Combined inertia, J	4300.7 kg.m^2

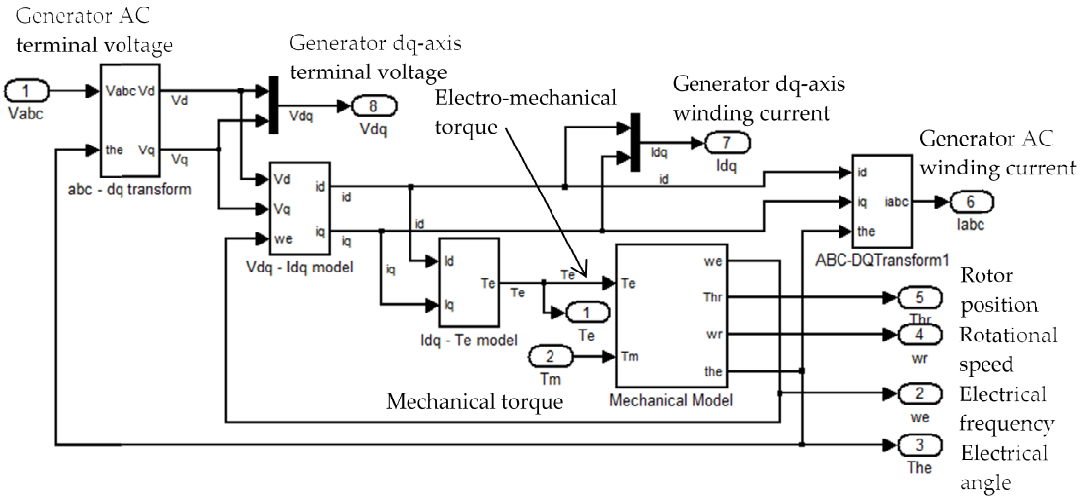

Figure 4-30: PM generator model block diagram. Each constituent sub-model is shown in Figure 4-31 to Figure 4-33.

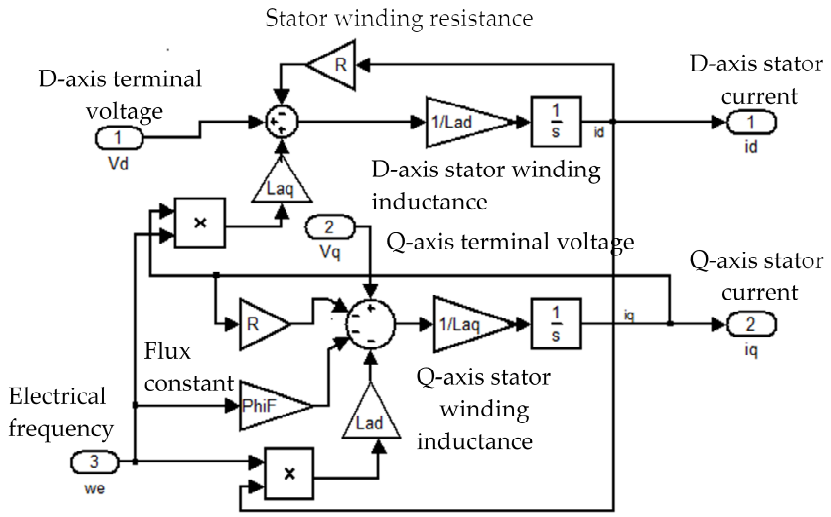

Figure 4-31: PM generator stator model block diagram based on equations (2.27) and (2.28).

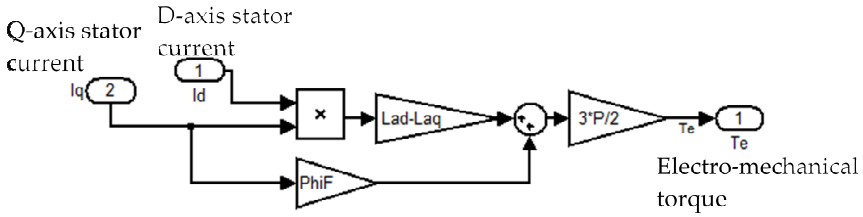

Figure 4-32: PM generator torque model block diagram based on equation (2.29).

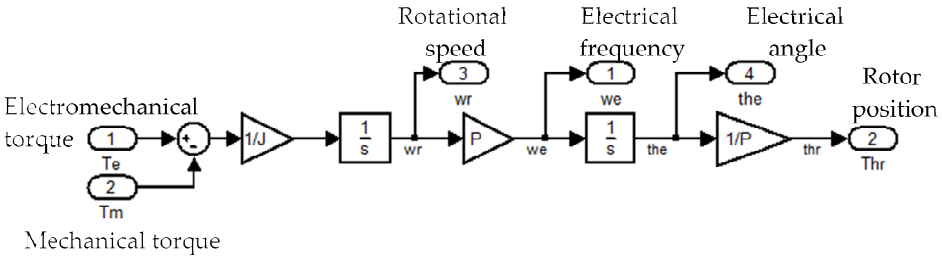

Figure 4-33: PM generator mechanical model block diagram based on equation (2.30).

4.4.2 Electrical system and cluster controller sub-models

The electrical network model in this case is identical to the induction machine case, consisting of a step-up transformer at the terminals of each generator, a network of three phase cables running to a point of common coupling and a single cable running from this point to the cluster converter,

as shown in Figure 4-13. The cluster controller acts with the same principles as above to regulate the electrical frequency of the network. In contrast to the induction machine case however, the rotational speeds of the generators are synchronised by the electrical frequency without any slip provision, therefore the controller directly regulates the rotational speeds of the turbines and each turbine in the cluster will rotate with equal speed.

4.4.3 Simulation results

To gain an understanding of the operability of a cluster of turbines where PM generators are used in each turbine, the following wind speed conditions are applied: initial equal wind speeds of 8m/s on all turbines with a step increase to 9m/s of the wind speed of turbine 1, and the wind speed profiles set out in Figure 4-3 and Figure 4-4.

Constant equal wind speeds and a step change

By applying equal wind speeds to each turbine then introducing a step change to turbine 1, the effect of different input torques on the adjacent turbines can be observed. This has been modelled where the initial wind speed incident on all turbines is 8m/s and then a step increase to 9m/s is applied to turbine 1. It can be observed in Figure 4-34 that initially the rotational speeds of each turbine are equal, and when the wind speed on turbine 1 is increased, the rotational speeds of the turbines also increase. The rise in rotational speeds is due to the response of the cluster controller to the increase in power output from the cluster, as shown by the change of the cluster synchronous speed.

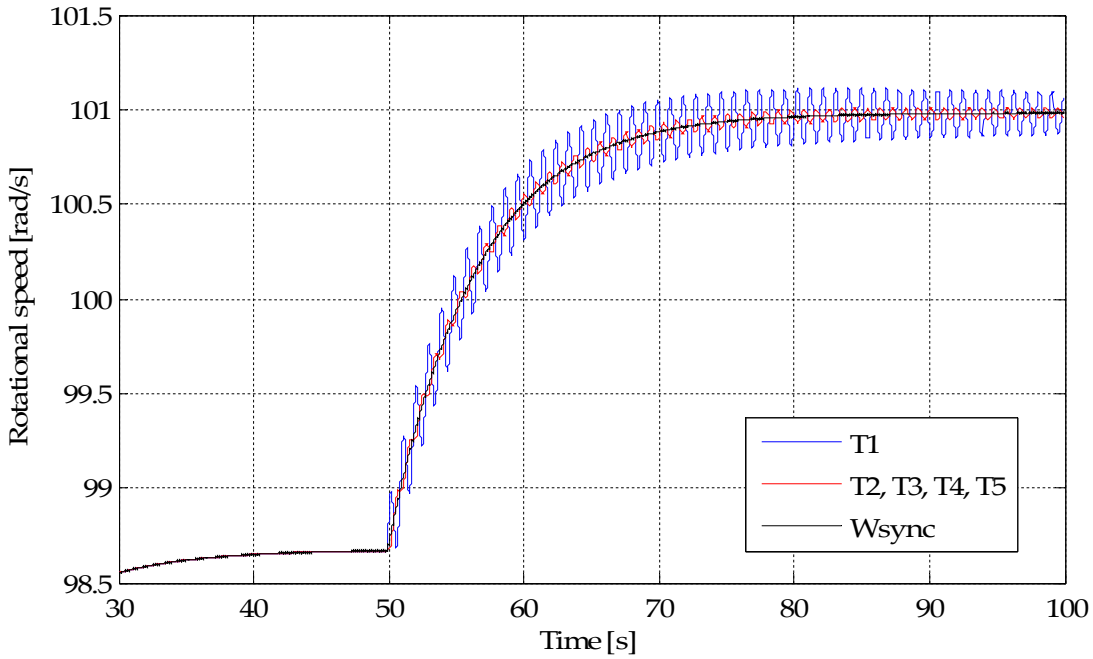

Figure 4-34: Turbine rotational speeds and the cluster synchronous speed, where the wind speed is initially equal on all turbines at 8m/s, then turbine 1 sees an increase to 9m/s at 50 seconds.

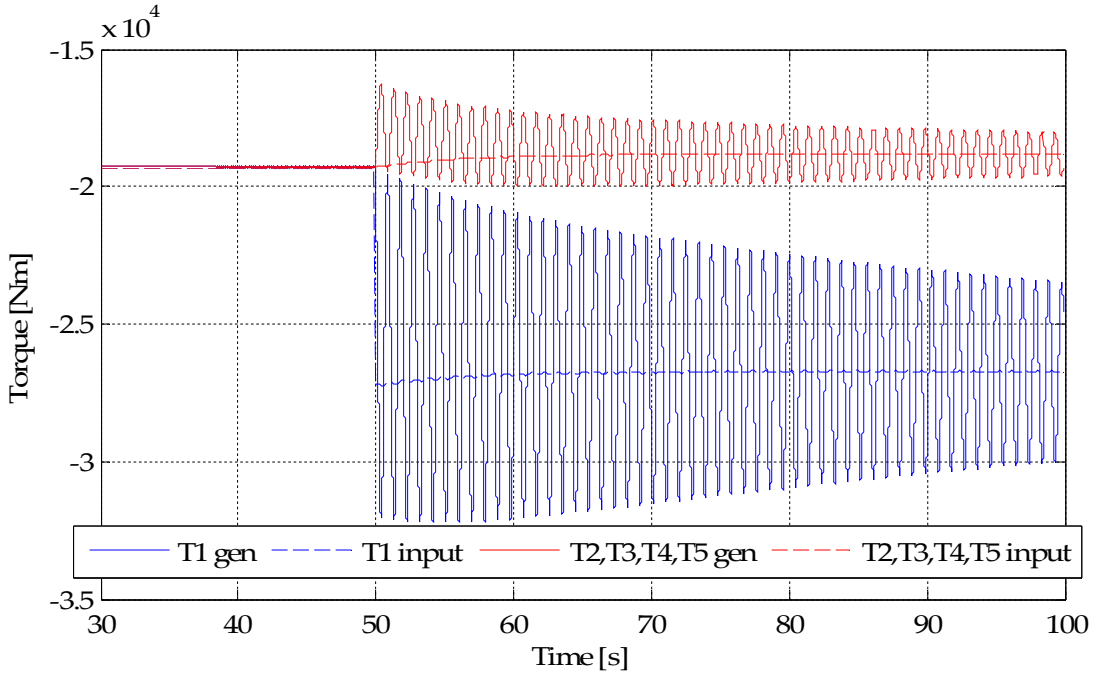

Figure 4-35: Generator and input torques of each generator, where initially the wind speed on each turbine is equal at 8m/s then a step increase to 9m/s is applied to turbine 1 at 50 seconds.

In addition to this general behaviour, the rotational speed of turbine 1 can be observed to oscillate following the change of wind speed; indeed the rotational speeds of the other machines also oscillate but with smaller magnitudes. These oscillations are observed more clearly on the generator torques in Figure 4-35 and arise due to the change of the generator rotor angles caused by the changing input torque. The differential equation that represents the mechanical dynamics of a PM generator is given by equation (2.30) and can be rewritten as equation (4.6), where the generator torque is a direct function of the rotor angle, θ_r, by the constant k, and $\omega_r = \frac{d\theta_r}{dt}$. This equation is a second order equation but does not contain any first order terms; therefore by comparing it with the standard dynamic equation for a second order system, equation (4.7), it can be observed that it has a damping coefficient (ζ) of zero; and therefore the system is an under-damped second order system. The lack of damping in the system leads to the continued oscillations shown in Figure 4-35.

$$T_m = -\frac{d\theta_r^2}{dt}J + k.\theta_r \tag{4.6}$$

$$U(t) = \frac{1}{\omega_n^2}.\frac{d^2y(t)}{dt} + \frac{2.\zeta}{\omega_n}.\frac{dy(t)}{dt} + y(t) \tag{4.7}$$

The oscillations of the adjacent turbine speeds and torques are a result of the generators in the cluster interacting; therefore the oscillations have the opposite polarity to those of turbine 1. This behaviour indicates that the generators are swinging against one another, which is a common feature of the small signal stability of large power systems. In such systems additional measures are often taken to assist a generator in achieving a steady state rotor angle following either abrupt load or input changes; these measures

include the use of a Power System Stabiliser and damper windings within the generator [10].

A Power System Stabiliser adds damping to generator rotor oscillations in large synchronous generators by controlling the generator excitation. Damping is achieved by providing a reaction torque component that is in phase with the rotor speed deviations [10]. The synchronous generators proposed for use in wind turbines are excited by permanent magnets, and therefore it is not possible to actively control the excitation to provide the damping torque component required in this manner.

Damper windings in the rotor of a generator take the form of copper rods embedded in the pole face that are connected to end rings forming short circuited windings, similar to those in a squirrel cage induction generator. Their purpose is to damp speed oscillations within the generator and therefore enable a steady state rotor angle to be achieved [10] [11]. Damping is achieved by the relative motion of the generator rotor and the stator flux, which induces an emf in the damper windings. This emf causes currents to flow which produce their own flux in the air-gap of the generator which interacts with the stator flux to produce a torque that is in phase with the speed oscillations, therefore acting to damp them out. In effect these windings act like an induction generator within a synchronous generator, where the size of the torque component produced is proportional to the speed difference between the stator flux and the generator rotor. The damping these windings provide, if they were included within a PM generator, is significant as it is a form of natural damping within the generator that does not require external active control.

4.4.4 Modification of PM generator model to include damper windings

In wind turbines to date PM generators have been accompanied by fully rated power converters and therefore damping is achieved actively by the control system. The inclusion of damper windings in these generators has not been prevalent due to the small pole pitches required to accommodate the large numbers of poles [12]. Some consideration has however been given to the use of PM generators that are directly connected to fixed frequency electrical systems that require some ability to damp mechanical oscillations: [13] proposes incorporating a part rated power converter between the generator and the star connection point that is capable of actively applying damping; [14] proposes placing the generator on flexible mounts so that the damping can be provided externally; and [15] studies the use of damper windings within the rotor of the generator.

To demonstrate the effect of adding damping to the mechanical system, damper windings have been added to the PM generator model used above. To include damper windings in the generator model, extra elements are required that represent the induced voltages and currents in the damper windings and also the fluxes they produce. The modified mathematical model of a PM generator that includes damper windings is given by [11]; the equations giving the damper winding currents, the modified stator winding currents and the generator torque are shown in equations (4.8) to (4.12) and the implementation of the model is shown in Figure 4-36 to Figure 4-39, and the impedance parameters of the damper windings are given in Table 4-5.

Damper winding currents:

$$\frac{di_{kd}}{dt} = V_{kd} - R_{kd}i_{kd} + L_{ad}\frac{di_d}{dt}L_{ad} + L_{kd} \tag{4.8}$$

$$\frac{di_{kq}}{dt} = \frac{V_{kq} - R_{kq}i_{kq} - L_{aq}\frac{di_q}{dt}}{L_{aq} + L_{kq}} \tag{4.9}$$

Stator winding currents:

$$\frac{di_d}{dt} = \frac{V_d - R_d i_d - L_{ad}\frac{di_{kd}}{dt} + L_{aq}\omega_r i_{kq} + \left(L_{aq} + L_{lq}\right)\omega_r i_q}{L_{ad} + L_{ld}} \tag{4.10}$$

$$\frac{di_q}{dt} = \frac{V_q - R_q i_q - L_{aq}\frac{di_{kq}}{dt} - \Psi_f\omega_r - L_{ad}\omega_r i_{kd} - (L_{ad} + L_{ld})\omega_r i_q}{L_{aq} + L_{lq}} \tag{4.11}$$

Generator torque:

$$T_e = -L_{aq}i_d\left(i_{kq} + i_q\right) + i_q\Psi_f + L_{ad}i_q(i_{kd} + i_d) + \left(L_{ld} - L_{lq}\right)i_d i_q \tag{4.12}$$

Where: $V_{kd,kq}$ = damper winding voltages which are short circuited and therefore equal zero, $R_{kd,kq}$ = damper winding resistance, $L_{kd,kq}$ = damper winding inductances, $L_{ld,lq}$ = stator winding leakage inductances, which are assumed to equal zero.

Table 4-5: Damper winding impedance parameters.

Damper winding inductance $\left(L_{kd}\text{ and }L_{kq}\right)$	1.5mH	Damper winding resistance $\left(R_{kd}\text{ and }R_{kq}\right)$	0.02Ω

The effects of the damper windings can be observed by comparing Figure 4-40 and Figure 4-41 with Figure 4-34 and Figure 4-35 where equal wind speeds are applied. It can be observed that, where the damper windings are present, the oscillatory component of the rotational speed is removed and the generator torque oscillations are damped out within 5 seconds of the step change of wind speed being applied. The general behaviour of the rotational speeds is similar to before, following the change of the synchronous frequency that is driven by the cluster controller. It is also observed that the

input and generator torques do not balance initially, therefore allowing the rotational speeds of the generators to accelerate as required.

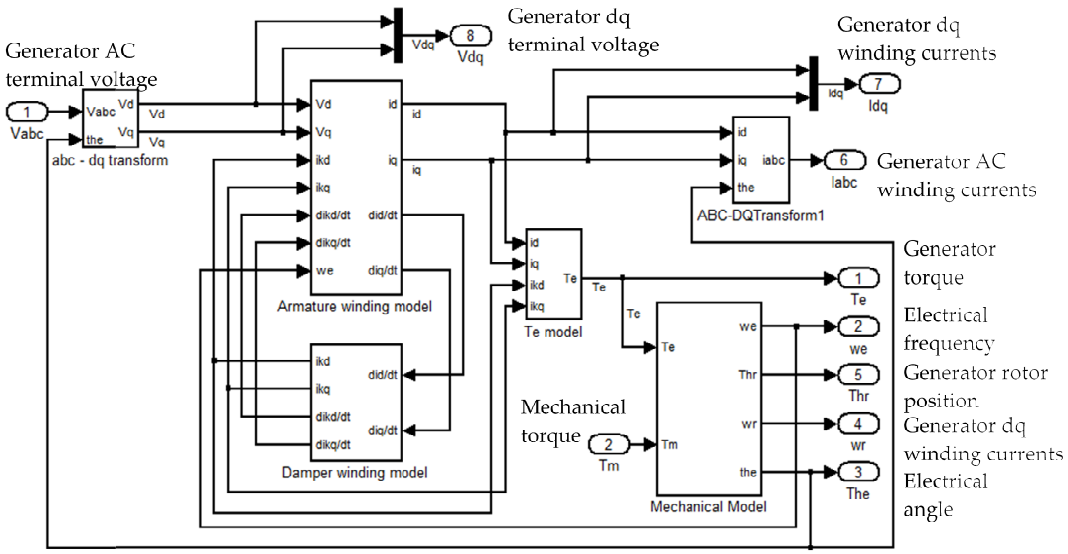

Figure 4-36: PM generator model block diagram with damper windings.

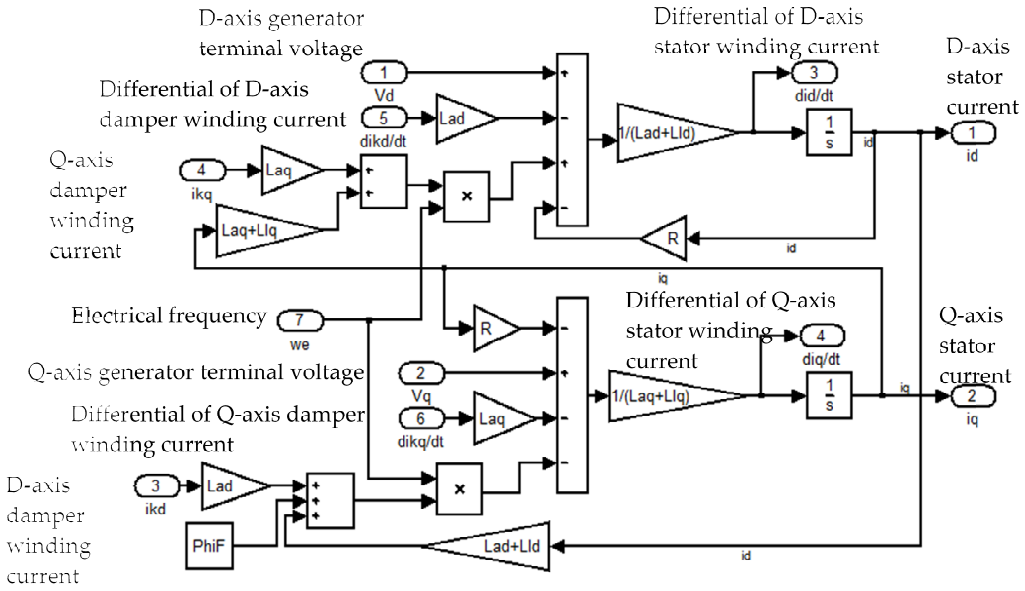

Figure 4-37: PM generator stator (armature) model with damper windings based on equations (4.10) and (4.11).

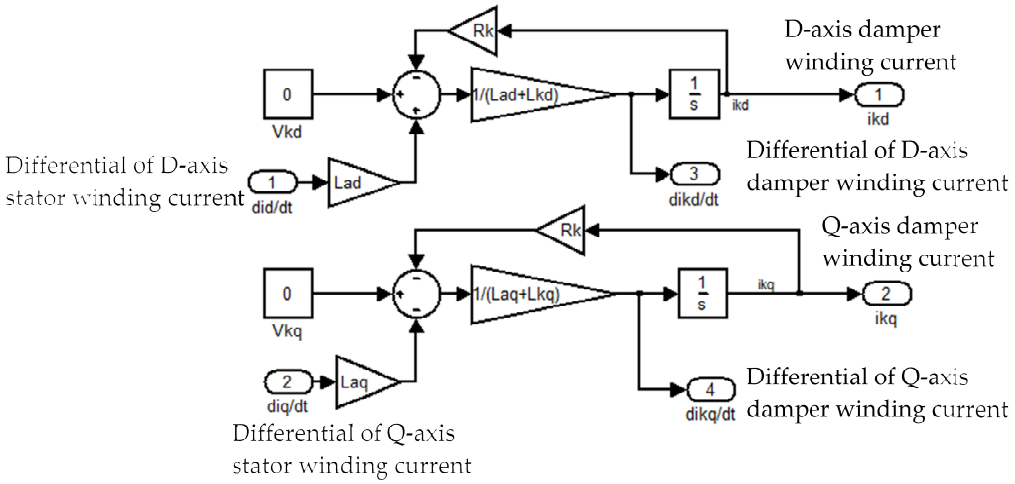

Figure 4-38: PM generator damper winding model based on equations (4.8) and (4.9).

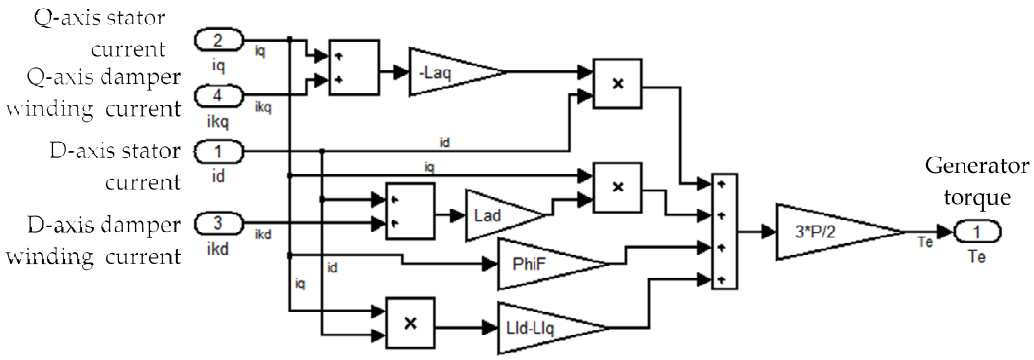

Figure 4-39: PM generator with damper windings torque calculation based on equation (4.12).

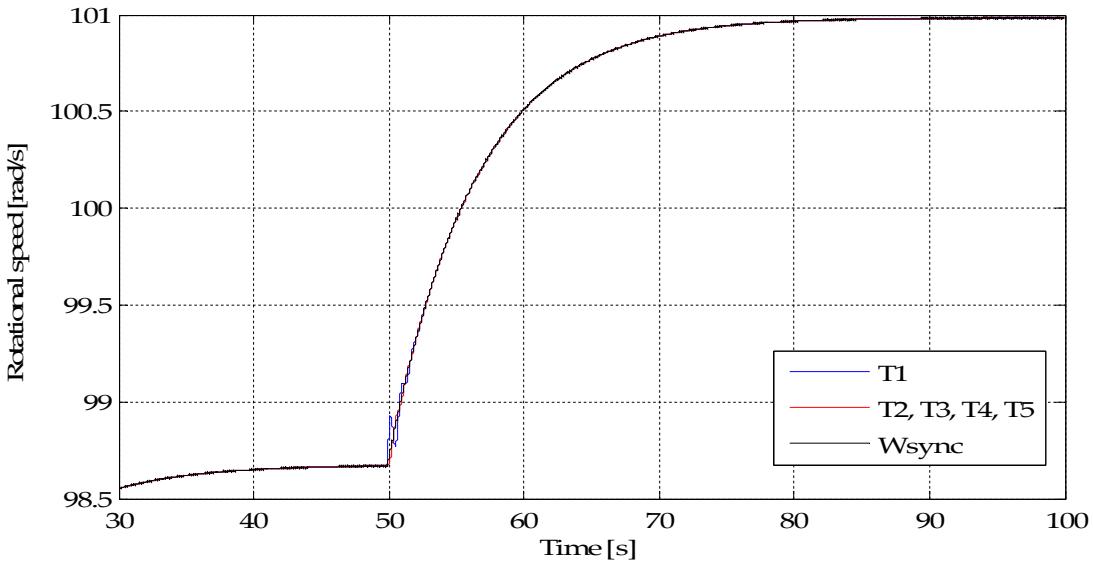

Figure 4-40: Turbine rotational speed and the cluster synchronous speed, where damper windings are included in the generators and the wind speed is initially equal on all turbines at 8m/s, then increasing on turbine 1 to 9m/s.

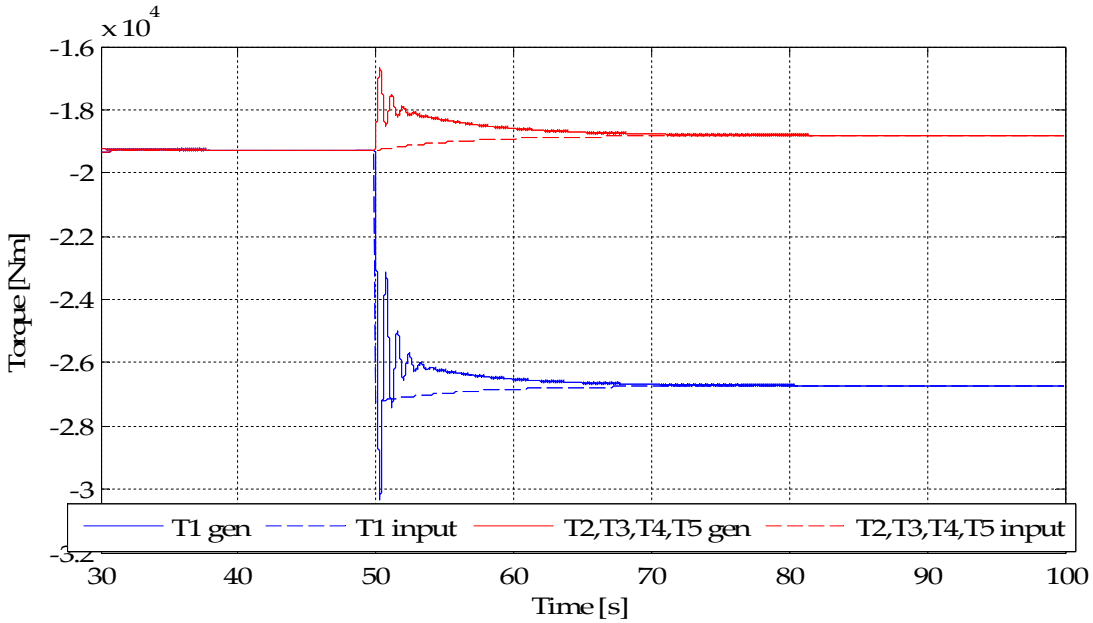

Figure 4-41: Generator and input torques of each generator, where initially the wind speed on each turbine is equal at 8m/s then a step increase to 9m/s is applied to turbine 1.

It can be concluded from this investigation that in order for a PM generator and AC network based cluster to operate without oscillation, some form of additional damping must be included. The inclusion of damper windings

within the generators presents a straight forward and proven method of providing this ability; although it may present challenges to the design of the generators where a small pole pitch is required.

Constant but different wind speeds with step changes

To investigate the operation of the cluster of turbines that incorporate PM generators in the wind conditions given by the profiles in Figure 4-4, the PM generator model which includes the damper windings has been used. Figure 4-42 shows the generator speeds where the wind speeds are initially different and step changes are applied to turbines 1 and 2, as in Figure 4-4.

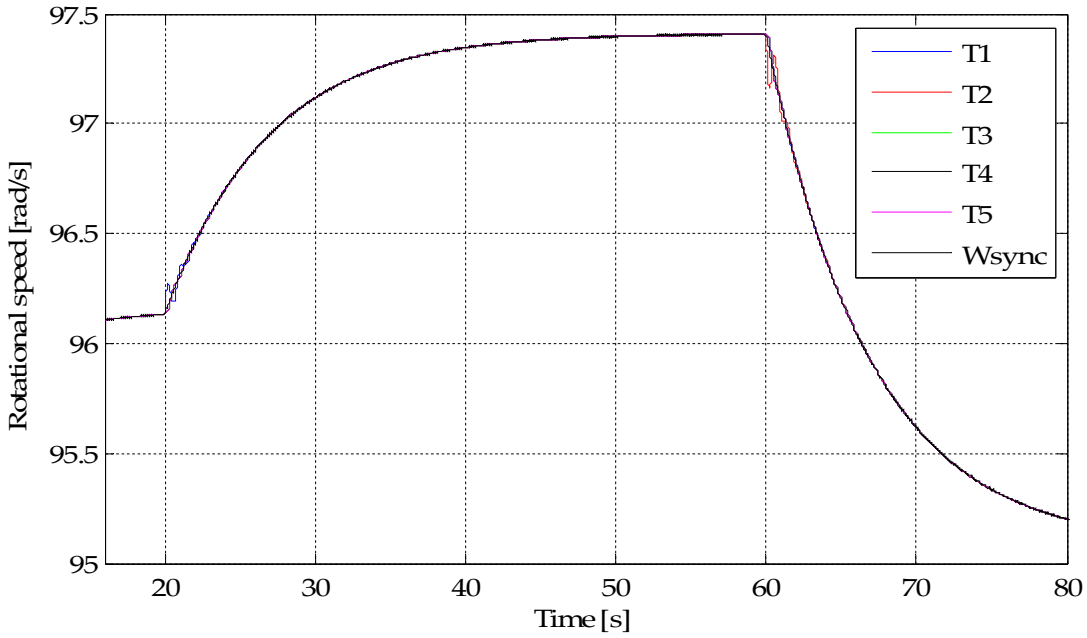

Figure 4-42: Rotational speeds of each of the turbines along with the cluster synchronous speed in response to the wind speeds in Figure 4-4.

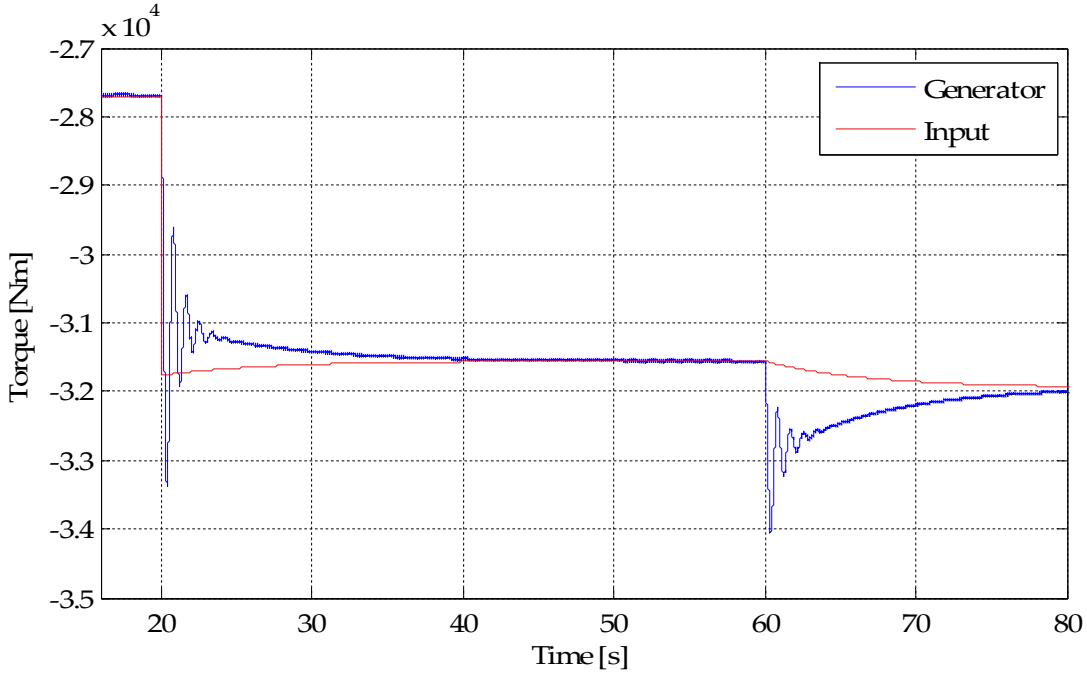

Figure 4-43: Input and generator torque on turbine 1 following a step increase in wind speed at 20 seconds and responding to a step change on turbine 2 at 60 seconds, as in Figure 4-4.

The most significant effect of using PM generators, as opposed to induction generators, is on the rotational speeds of the generators. It can be observed in Figure 4-42 that the rotational speeds of the turbines are always equal to each other and to the synchronous speed of the network. This is not a surprise, as the rotational speeds of any synchronous generator are always synchronised to the cluster electrical frequency. In response to the step increase of wind speed on turbine 1, after 20 seconds, and the step down on turbine 2, after 60 seconds, the rotational speeds accelerate and decelerate respectively, driven by the reaction of the cluster controller to the change of the cluster power output. Figure 4-43 shows the input and generator torques of turbine 1, showing that in response to the changes of wind speed and the action of the cluster controller, the torques move out of balance to drive the change of the turbine rotational speeds. It can also be observed that the step

changes of wind speed initiate generator torque oscillations that are damped out quickly within a few seconds due to the action of the damper windings. The changes of the input and generator torques of turbine 1 are shown in Figure 4-44 over the full range of wind speed changes in Figure 4-4; it can be observed from this that their variation is similar to the induction machine case, providing the necessary torque imbalances to accelerate and decelerate the turbines. It can also be observed that oscillations of the generator torque are initiated by each change of wind speed and are damped out quickly.

It is evident from the traces of the generator torque in Figure 4-44 that turbine 1 not only responds to the changes of its own wind speed but also to wind speed changes on the adjacent turbines. As noted above, this comes about due to the controller reaction to the overall change of the cluster power output; this response is classed an interaction between the turbines in the cluster and is a natural feature of clustering the turbines, resulting from the change of the common system frequency.

The energy capture efficiencies of the turbines are shown in Figure 4-45; by comparing this plot to Figure 4-26 and Figure 4-28, it can be observed that the synchronised nature of the turbine rotational speeds causes a reduced energy capture efficiency compared to the induction generator case where extra resistance is added to the rotor windings. It should also be noted however that comparing these power coefficients to the case where the induction generators have the original slip slope, shows that there is little difference between them. This arises because the amount of independence between the turbines, where the original induction machine slip slope is used, is very limited. Figure 4-45 shows that turbines 1 and 5 experience the

worst energy capture efficiencies, this occurs because their respective wind speeds are furthest from the cluster mean wind speed.

It can be concluded from these comparisons that the use of PM generators does not particularly reduce the energy capture efficiency of the turbines in comparison to the induction machine case with the original parameters, and only minor deficiencies arise compared to the induction machine case with the larger rotor winding resistance.

Figure 4-46 shows the energy transfer efficiency of the PM generators and electrical system. Comparing this efficiency with that shown in Figure 4-29, indicates that using PM generators improves the energy transfer efficiency by approximately 5%. In Figure 4-46 it can also be observed that the system efficiency is greater than 100% for a short period; this is caused by the action of the cluster controller to slow the rotational speed of the turbine, which requires the extraction of some of the stored kinetic energy from the turbine rotor and its inertia, in addition to the power captured from the wind.

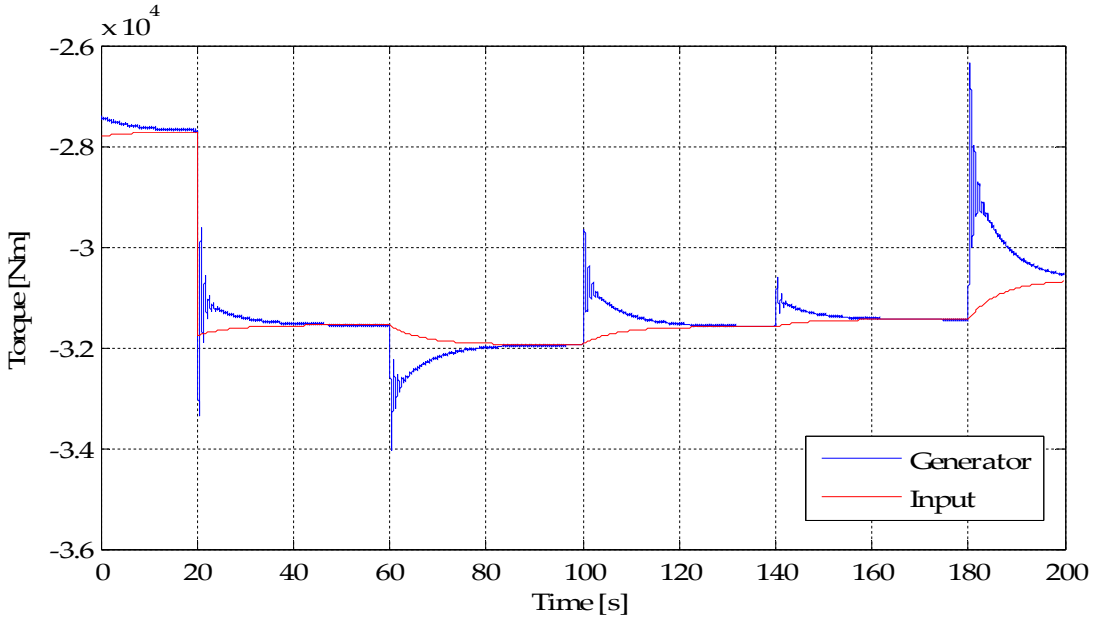

Figure 4-44: Generator and input torque of turbine 1 in response to the wind speed changes in Figure 4-4.

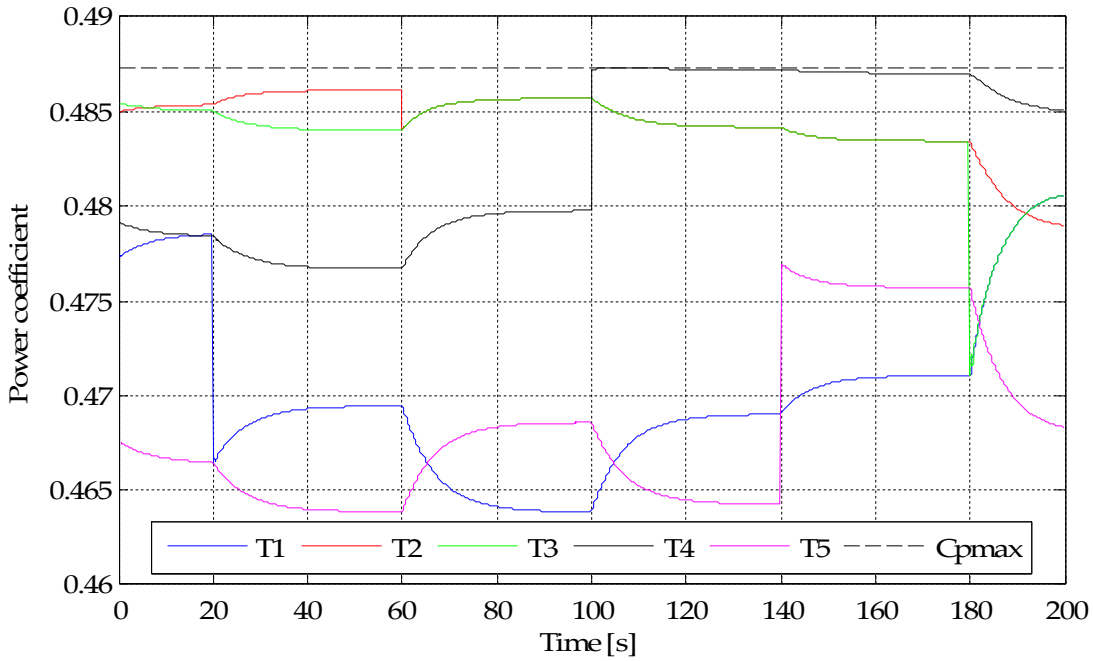

Figure 4-45: Power coefficiencts of each turbine in the cluster in comparison to the turbine C_{pmax}, where PM generators are used.

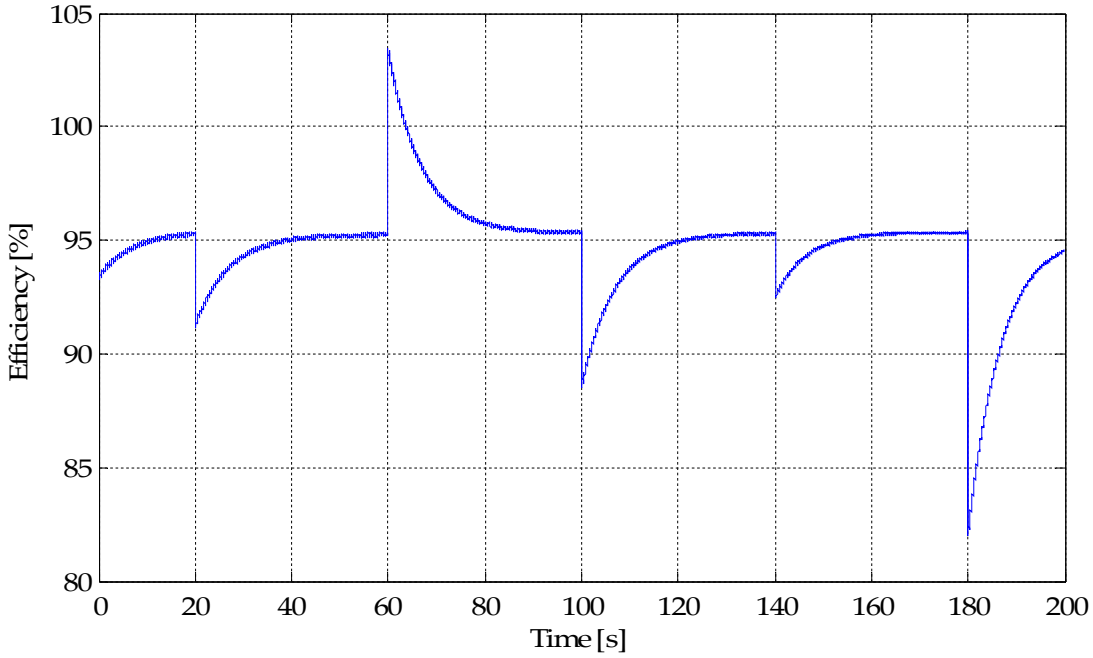

Figure 4-46: Energy transfer efficiency of the generators and cluster electrical system in response to the wind speed changes in Figure 4-4.

Continuously varying wind speeds

To observe the operation of the PM generator based wind turbines and cluster when the wind speeds continuously vary, as in Figure 4-3, the generator model that incorporates damper windings is again used. It can be observed from Figure 4-47 that, as expected, the rotational speeds of all of the turbines are equal and also that the generator and input torques, in Figure 4-48, vary in relation to each other to drive the changes of the rotational speeds. It can also be observed from both the rotational speeds and the torques that the oscillations that were present above, before the damper windings were added, are not present here; it is also notable that the variations of wind speed do not initiate the oscillations because they are relatively smooth in comparison to the abrupt step changes applied before.

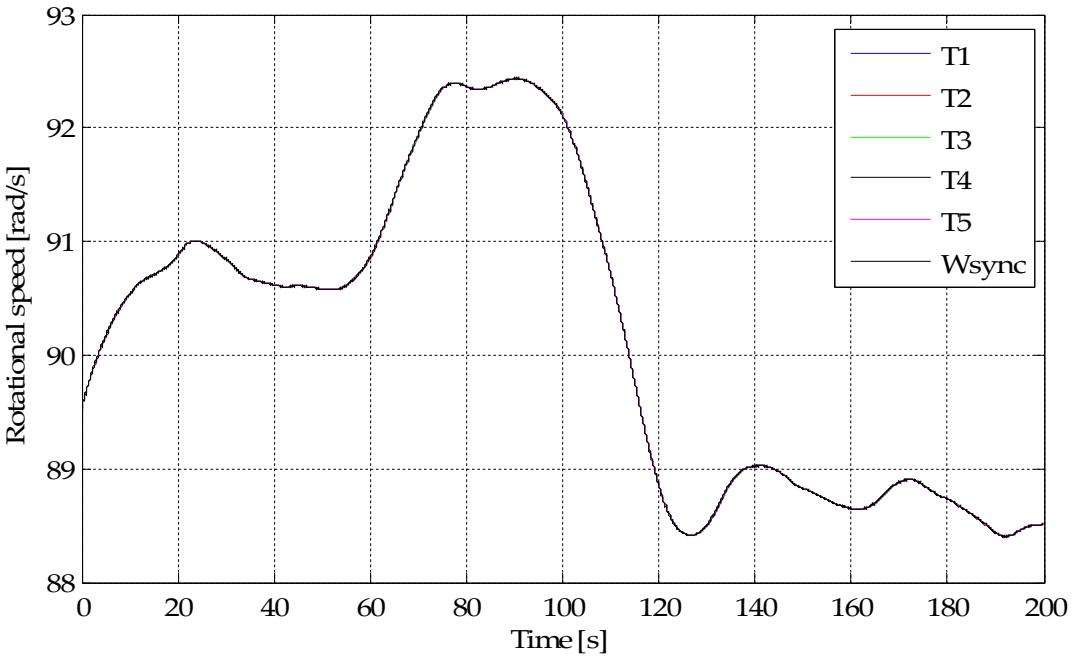

Figure 4-47: Rotational speeds of each generator and the cluster synchronous speed where the turbines are subjected to the continuously varying wind speeds in Figure 4-3.

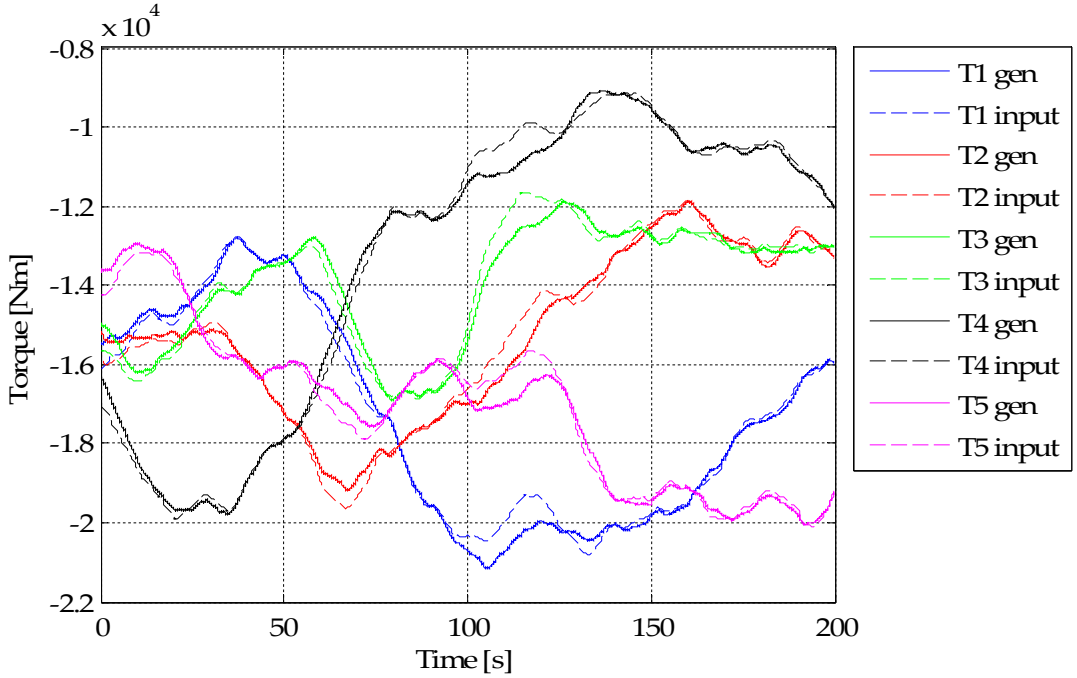

Figure 4-48: Generator and input torques of each turbine where they are subjected to the continuously varying wind speeds in Figure 4-3.

4.5 Rectified PM generator based wind turbines and DC electrical network

An alternative method of incorporating PM generators in a cluster of turbines is to rectify their outputs and connect them together using a multi-terminal DC electrical network. PM generators are excited by the magnetic material fixed to their rotors and therefore they do not require external excitation. This aspect lends itself to the rectification of their outputs as the generator will effectively provide an independent AC electrical voltage source. Diode rectifiers are the simplest method of rectifying a generator output, however power flow can only pass from the generator to the DC network and not vice versa.

The model developed for simulating this system is based around the same wind turbine and generator model as above (without the generator damper windings); however the electrical system is quite different, consisting of a full bridge diode rectifier and a DC electrical network. The cluster converter takes the form of a DC-DC converter so that the voltage level of the DC network can be controlled. The cluster controller is based on similar operating principles to the AC cases; however the controlled system variable is voltage instead of frequency. The simulation model is separated into the following sub-models: the wind turbine and generator sub-model, the rectifier, electrical network and cluster converter sub-model and the cluster controller sub-model.

4.5.1 Wind turbine and PM generator sub-model

The wind turbine and PM generator model used in this case are very similar to that developed in Section 4.4; the PM generator model does not include the damper windings. The layout of this model is similar to that shown in

Figure 4-12, and the parameters used are largely the same as those given in Table 4-1 and Table 4-4; however, in this case the nominal peak terminal voltage of the generator is increased to 5.4kV giving a generator magnetic flux constant of 12.67. This increased voltage and flux constant are required to lower the maximum output current of the generator so that, with the generator and transformer parameters stated, the length of the rectifier commutation overlap is less than $\pi/3$ radians (the relationship between the generator current output, impedance and rectifier commutation overlap length will be dealt with in Chapters 5 and 6). In order to allow the model to be simulated successfully a parasitic load is also included at the terminals of the generators, similarly to above.

4.5.2 DC electrical network and cluster converter sub-model

The electrical network model incorporates the step-up transformer, the diode rectifier, the electrical cable network and the cluster converter. The diode rectifier consists of six diodes arranged to form a three phase full bridge rectifier as shown in Figure 4-49. The rectifier at the terminals of each generator feeds into a DC branch cable, modelled as an inductance with series resistance element to account for conduction losses. The branch cables connect together at a point of common coupling (PCC) from where a single cable runs to the cluster converter. As above, each of the cable elements have equal 10km lengths and it is assumed that each of the cables has a conductor cross-section of 500mm^2; the per-unit length impedances are given in Table 4-6. In this case, as with the AC network cases, it is assumed that the common output cable has the same cross-section as the branch cables, and therefore the same per-unit length impedances. Step-up transformers at the terminals of the generators are included to reduce the magnitudes of the output currents flowing through the cluster network and therefore keep

conduction losses to a minimum. The transformer parameters are similar to those in Table 4-3 where the step-up ratio of 1:10 is used, which in this case gives a voltage ratio of 5.4kV : 54kV. The layout of the cluster cable network is shown in Figure 4-50, where forward and return paths are required for each turbine to form closed DC circuits. The cluster converter is modelled as an ideal controllable DC voltage source for simplicity.

Table 4-6: DC cable per unit impedance parameters [7].

Cable resistance	0.0366Ω/km	Cable inductance	0.55mH/km

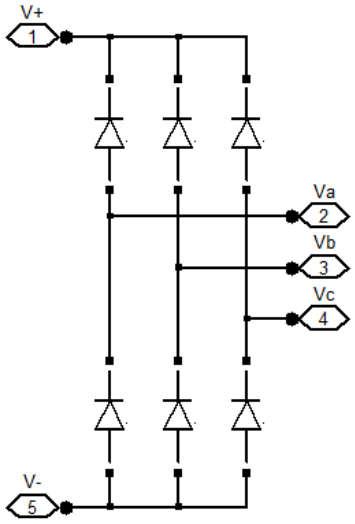

Figure 4-49: Full bridge diode rectifier.

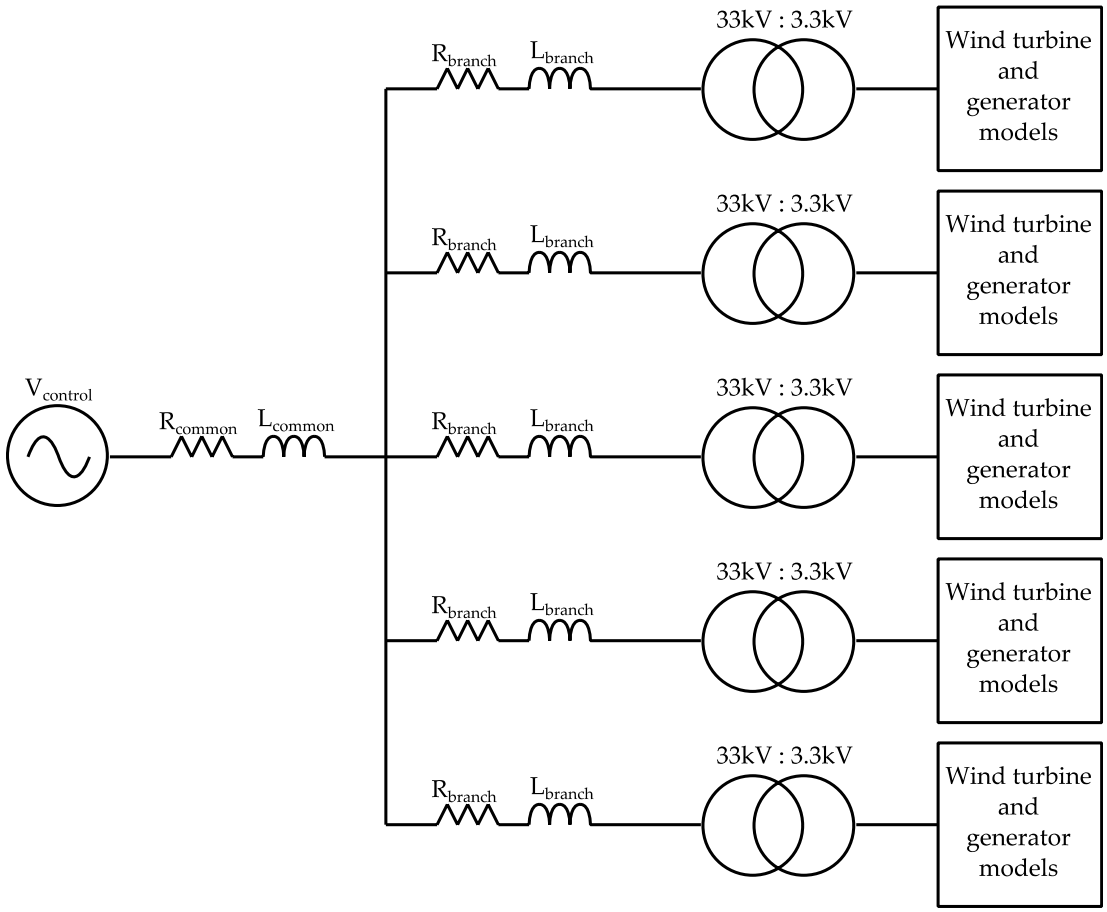

Figure 4-50: Multi-terminal DC cluster electrical layout.

4.5.3 Cluster controller sub-model

The cluster controller model is based on similar principles to those used in the AC cases: a measurement of the active power flowing into the cluster converter is taken and compared with a reference power. The main difference between this case and the AC cases is that the controlled system variable is the electrical system voltage instead of the frequency. The operating principles of the rectified PM generators were introduced in the previous chapter of this thesis, where the importance of the relationship between the rotational speeds of the generators and the DC network voltage was highlighted. Using this relationship it is possible for the rotational speeds of the generators to be controlled indirectly by the regulation of the DC voltage at the terminals of each of the rectifiers. In this case, the

rotational speeds of the turbines are allowed to continue to increase with wind speed beyond the rated speed stated in Table 4-1, therefore maintaining the optimum tip-speed ratio until the power output of the turbine reaches its rated value; this allows for the controller design to be kept simple; in reality the rotational speeds of the turbines would be capped at the turbine rated speed by limiting the controller output voltage. Once the rated power output is achieved the controller will maintain a constant output voltage, therefore holding the rotational speed constant.

In order to achieve the appropriate rectifier voltages the voltage drops across the cable resistances between the rectifiers and the cluster converter must be considered. The magnitude of these voltage drops can be determined using the known resistances of the cables and by deriving the currents flowing through them from the measured cluster output power. The calculated voltage drops are used in addition to the instantaneous converter output voltage to predict the rotational speeds of the turbines, which are then used to determine the reference power output from the cluster, assuming optimal turbine rotational speeds for the local wind speeds.

In addition to the voltage drops introduced to the system by the resistive elements of the cables, the rectifiers also introduce a voltage drop as a result of the distortion caused by the commutation overlap of the output currents between generator windings. The exact process behind this voltage drop will be explored in the next chapter of this thesis; however it must be compensated for at this stage when predicting the rotational speeds of the turbines. The commutation voltage drop is a function of the instantaneous DC output current from the rectifier, the electrical frequency of the generator output and the stator winding inductance. The magnitude of this voltage

drop, as a proportion of the pre-commutation rectified machine terminal voltage, increases approximately linearly with the turbine output and therefore is approximated by equation (4.13) here (P_{out} = generator active power output (W)).

$$V_{comm}(\%) = 3.5 \times 10^{-5}.P_{out} - 153.6 \qquad (4.13)$$

The cluster controller is based around a proportional integral controller, shown in Figure 4-51, where the bandwidth of the control system will change with the operating point as the system is non-linear. The controller gains have been chosen so that the maximum bandwidth is approximately 0.5Hz.

The controller acts to drive the system voltage to the point where the reference power used in the initial comparison equals the measured power. By doing so it also causes the turbines to accelerate or decelerate, improving their tip-speed ratios and subsequently their power coefficients. The controller takes a measurement of the aggregate power output from the turbines, which is equivalent to the power produced by the average wind speed across the cluster; it therefore acts to optimise the synchronous speed to the average cluster wind conditions. Since it is unlikely that the local wind conditions of each wind turbine will equal the cluster average, the individual turbines will not operate with the optimal tip-speed ratio for their local wind conditions; the effects of which on energy capture loss were discussed in the previous chapter of this thesis.

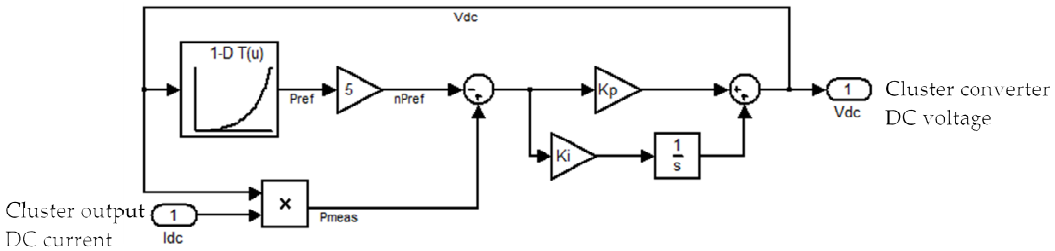

Figure 4-51: Cluster controller block diagram.

4.5.4 Simulation results

To investigate the operational characteristics of this method of implementing a cluster of turbines and provide comparisons with the previous two methods, the wind speed conditions in Figure 4-3 and Figure 4-4 have been applied to the model.

Continuously varying wind speeds

The rotational speeds of the turbines in this case, in response to continuously varying input wind speeds, vary significantly in relation to the synchronous speed, shown in Figure 4-53. The cluster synchronous speed is derived from the voltage that is common to each turbine at the point of common coupling, V_{PCC}, using equation (4.14), and is driven by the cluster controller action. This equation is similar to equation (3.24) which relates the rectifier output voltage to the generator speed. (Ψ_f=is the generator field constant and p = generator pole pairs).

$$\omega_{sync} = \frac{V_{dcPCC}.\pi}{3.\sqrt{3}.\Psi_f.p} \tag{4.14}$$

$$slip = \frac{\omega_{sync} - \omega_{gen}}{\omega_{sync}} \tag{4.15}$$

Comparing the synchronous speed to the rotational speeds of the individual turbines, it can be observed that the rotational speeds are generally always greater than the synchronous speed but that they generally follow its variations. An analogy can be drawn between the relationships of the rotational and synchronous speeds in this case, with the relationship of the same variables in the induction machine case in Section 4.3; because in either case a differential between the two is required for the generator to produce torque. This speed differential, as a proportion of the synchronous speed, is referred to as the slip of the generator and is calculated in the same manner

in this case as with induction generators, using equation (4.15), where ω_{gen} is the turbine rotational speed. The difference between this case and the induction generator case is that the slip in the system comes about due to the voltage drops between the generators and the point of common coupling, instead of the requirement for a changing magnetic flux cutting the generator rotor windings. Therefore the amount of independent variation of the individual turbine rotational speeds is related to the size of the commutation and cable resistive voltage drops, which in turn are functions of the output of each turbine. The change of the combined voltage drop with the output current of each generator is approximately linear and therefore so is the relationship between the reaction torque produced by each generator and the slip, shown in Figure 4-52. This therefore completes the analogy between this case and the induction machine case, as the torque slip characteristic of an induction machine is linear also, within its normal operating range. The linearity of the relationship between torque and slip is reflected by the similarity between the traces of generator reaction torque and generator slip in Figure 4-54 and Figure 4-55 respectively. Also, shown by Figure 4-54 is the relationship between the input torque and generator torque which drives the acceleration and deceleration of the turbine rotational speed.

By comparing Figure 4-53 with Figure 4-15 it can be observed that there is a much larger difference between the synchronous speed and the rotational speeds of each turbine; indicating that the gradient of the linear relationship between the slip and torque of each generator in this case is smaller, compared to the induction generators used in Section 4.3. The smaller slip slope gradient allows each turbine, in this case, to have a significantly greater ability to vary its rotational speed according to its local wind conditions; which brings the benefit of improving the turbine energy capture efficiency

by allowing them to achieve a tip-speed ratio that is closer to the optimum; this is demonstrated by the improved proximity of the power coefficients of the turbines to the maximum in Figure 4-56.

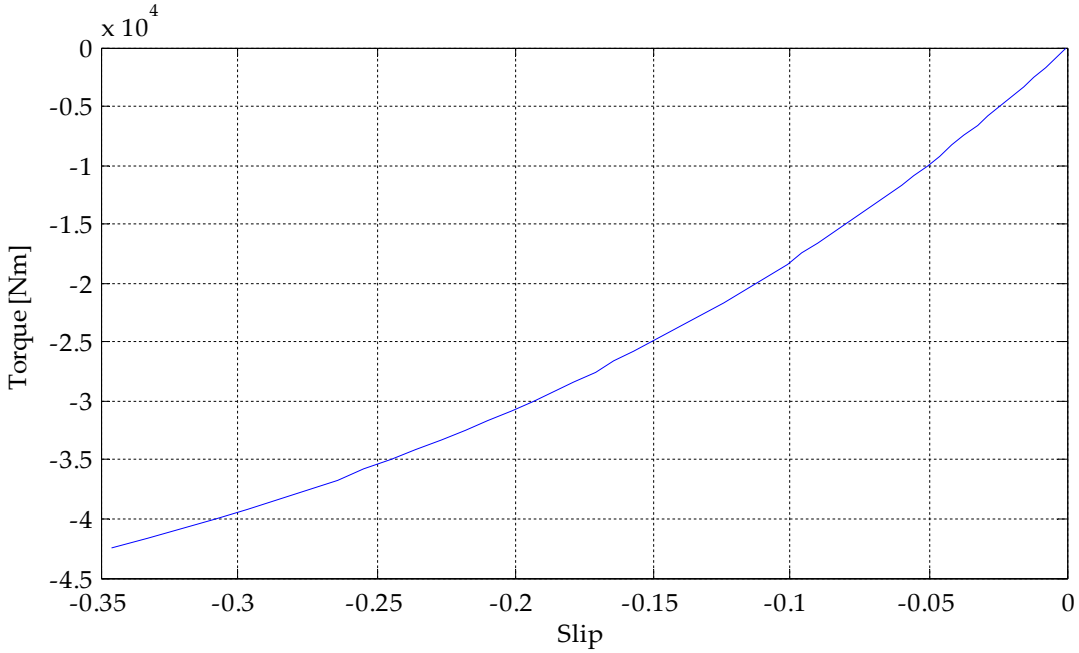

Figure 4-52: Torque slip characteristic.

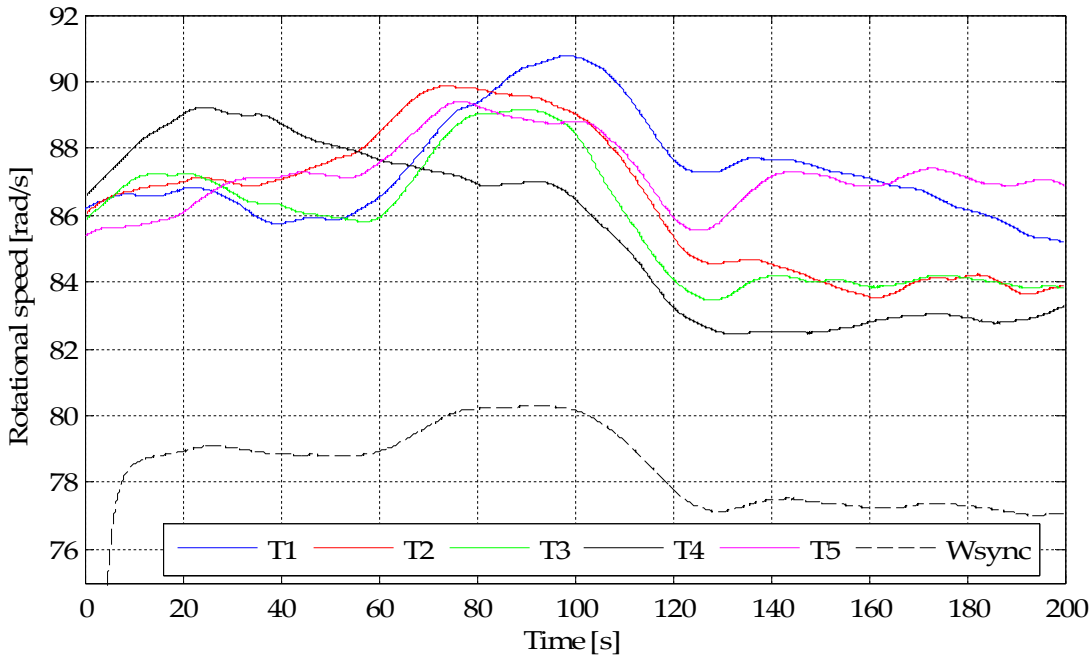

Figure 4-53: Generator rotational speeds and cluster synchronous speed when the continuously varying wind speed profiles in Figure 4-3 are input to the turbine models.

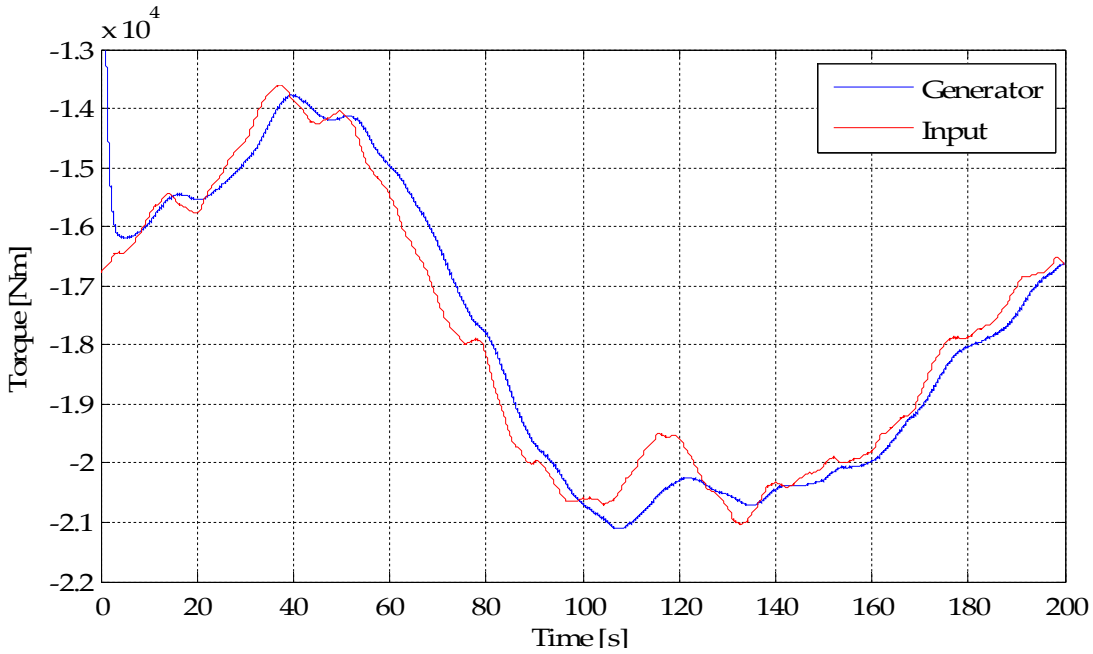

Figure 4-54: Turbine 1 input and generator torques in response to the wind speed variation in Figure 4-3. (Note: the generator torque has been filtered to remove high frequency harmonics for clarity of presentation).

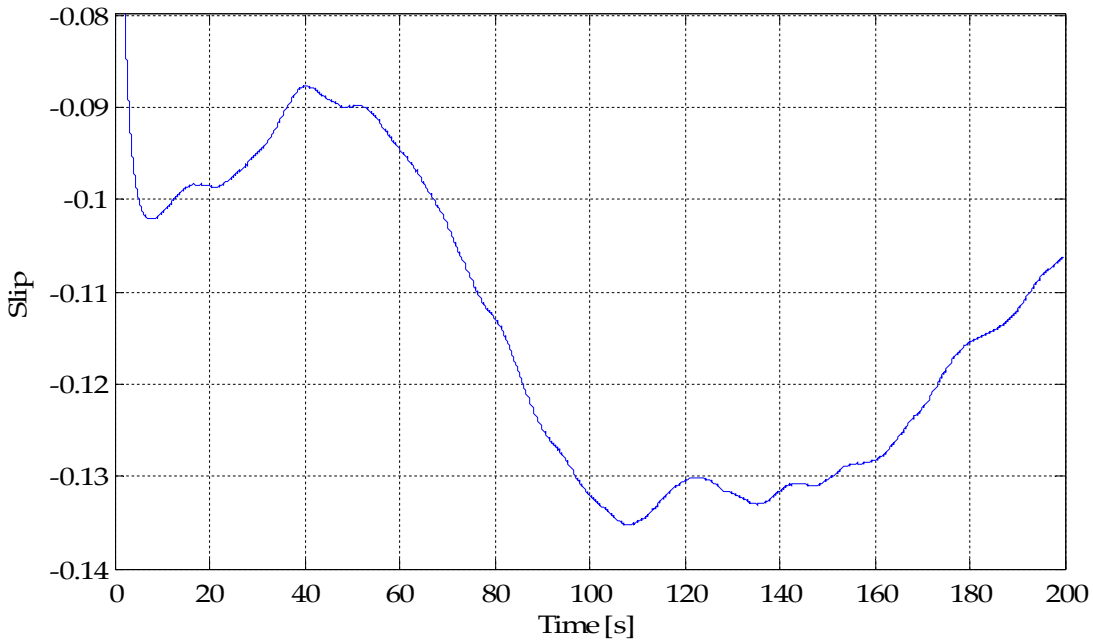

Figure 4-55: Generator slip of turbine 1 in response to the continuously varying wind speeds in Figure 4-3.

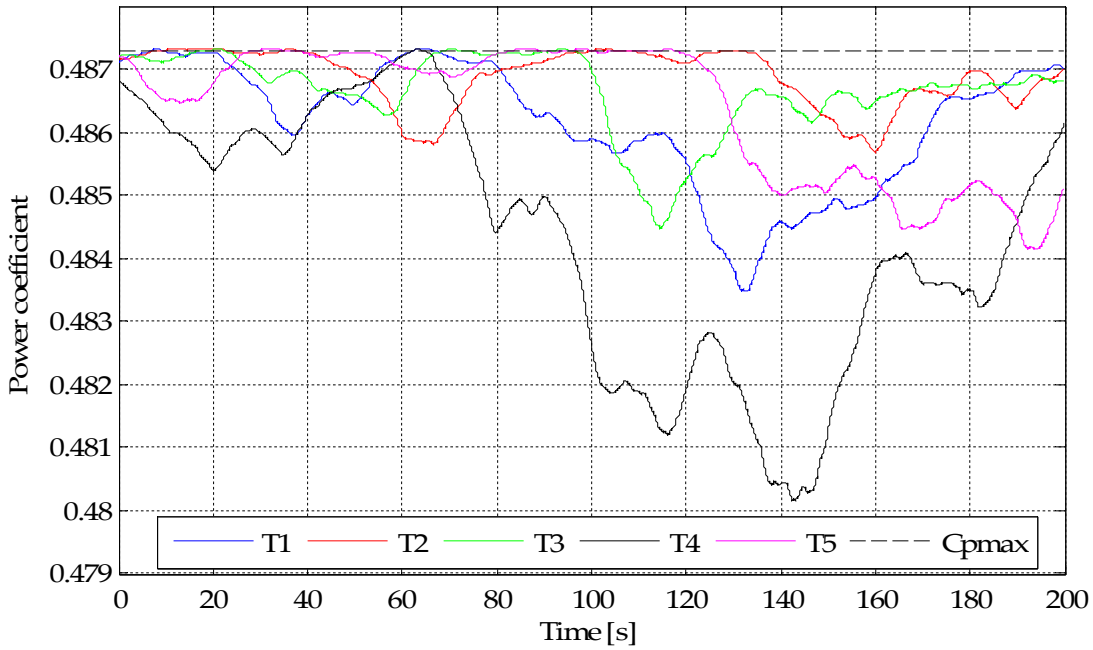

Figure 4-56: Power coefficients of each of the turbines in comparison to the Cp maximum, for the wind speeds in Figure 4-3.

In section 4.3 the effect of decreasing the gradient of the torque slip curve was investigated and proven to be beneficial to the turbine energy capture as it has here. In order to achieve the reduced slip curve gradient where induction machines were used, extra resistance was added to the generator rotor windings, which negated the energy capture benefit achieved by improving the turbine power coefficients. The gradient of the torque slip relationship in this case is a function of the combined voltage drops of the cable resistances and the commutation distortion, the key property of which is that only the cable resistances cause a loss of energy in the system. Therefore the exploitation of the commutation voltage drop presents the opportunity to allow for a lower gradient of the torque slip relationship without increasing the losses in the system. The process that causes the commutation voltage drop will be investigated in more detail later in this thesis, however the energy transfer efficiency of the system is shown in

Figure 4-57, indicating that despite the lower gradient torque slip relationship, the losses in the system are small. The efficiency peaks above 100% during a period where the controller is acting to slow the turbine speeds; this is achieved by drawing more power from the turbines than is input from the wind.

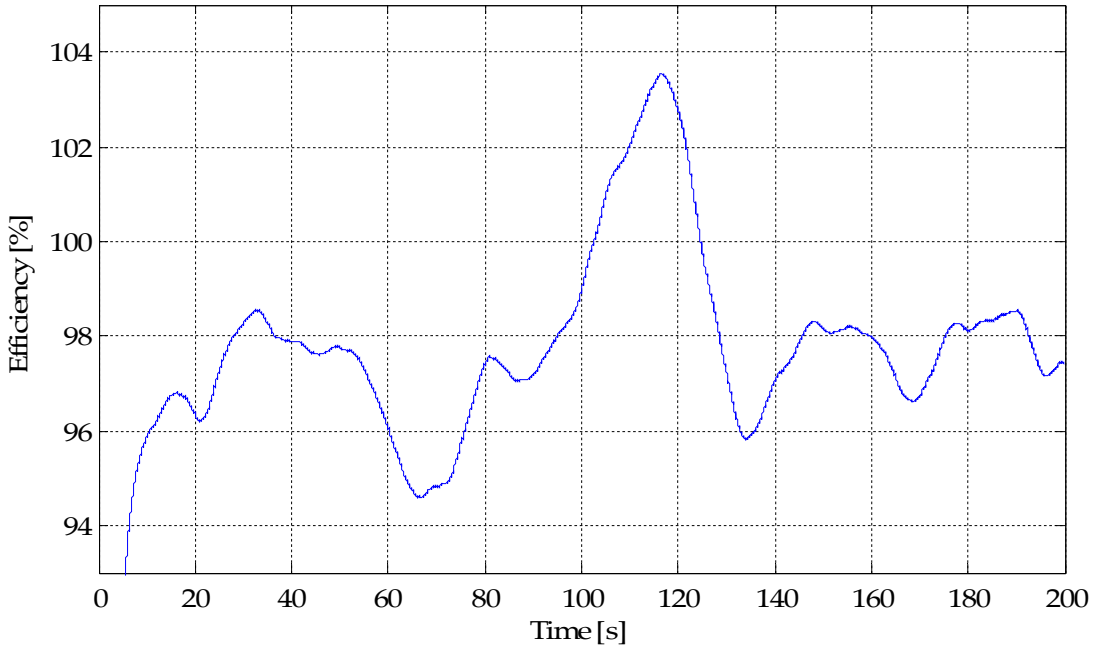

Figure 4-57: Power transfer efficiency of the generators and cluster network when the wind speeds in Figure 4-3 are incident on each turbine.

Constant wind speeds with step changes

When the turbines are subject to the wind speeds in Figure 4-4 it is clear that once again significant differences occur between the rotational speeds, Figure 4-58. The rotational speeds are also greater than the cluster synchronous speed, derived from the common point voltage using equation (4.14). The general behaviour of the turbines in this case confirms the observations made when the turbines are subject to continuously varying wind speeds: the torque produced by each of the turbines is proportional to the slip that occurs between the synchronous and rotational speeds, highlighted by

comparing Figure 4-59 and Figure 4-60; the extra ability of the rotational speeds to follow their individual wind speed changes, allow the turbines to operate with power coefficients that are closer to the maximum, shown by Figure 4-61; and the energy transfer efficiency that is achieved by combining the PM generators with rectifiers and a DC network is substantially better than the induction machine case and slightly better than where the PM generators are directly connected to an AC electrical system, shown by Figure 4-62.

It is also highlighted by the change of the rotational speeds, torques and slip that the turbines respond to changes of wind speed on adjacent turbines as well as to wind speed changes of their own. These interactions between the turbines are dominated by the action of the cluster controller to the cluster power output change, but are also a result of the proportionality of the common point voltage (and cluster synchronous speed) to the current flow through the cluster common cable. It is also clear that the resulting changes of rotational speed of the turbines that do not directly see the wind speed change are significantly smaller than the change of rotational speed of the turbine that does see the wind speed change. This is a consequence of the resistive and commutation voltage drops of the turbine experiencing the wind speed change following the change of power output; whereas the other turbines change only with the common voltage.

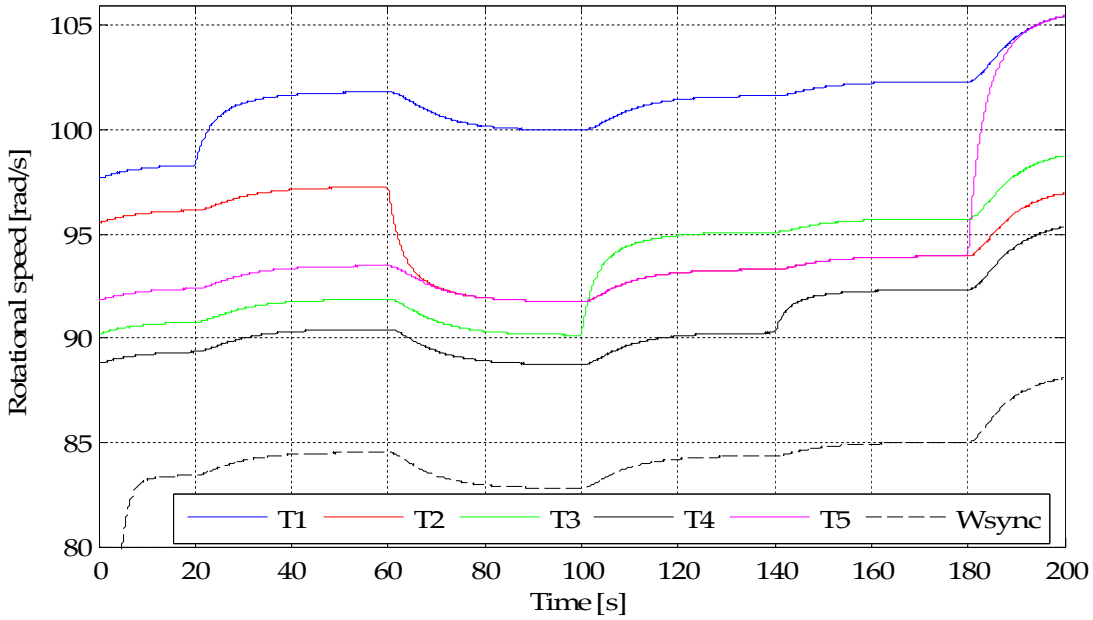

Figure 4-58: Rotational speeds of each of the turbines and the cluster synchronous speed, where the turbines are subject to the wind speeds in Figure 4-4.

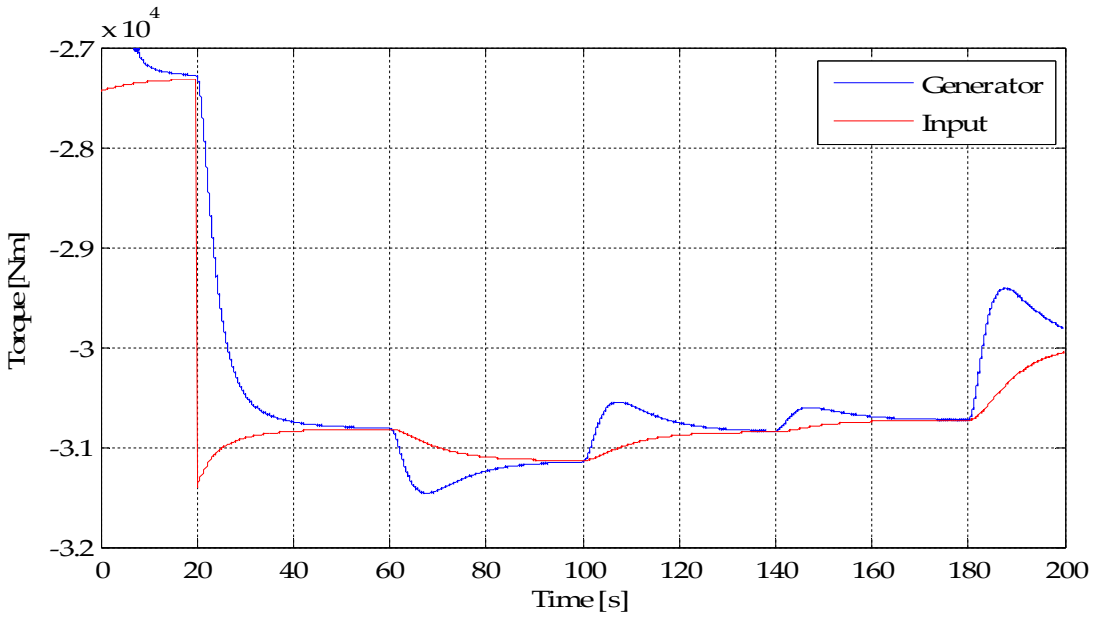

Figure 4-59: Generator and input torque of turbine 1 in response to the wind speed profiles in Figure 4-4. (Note: the generator torque trace has been filtered to remove high frequency harmonic components for clarity of presentation).

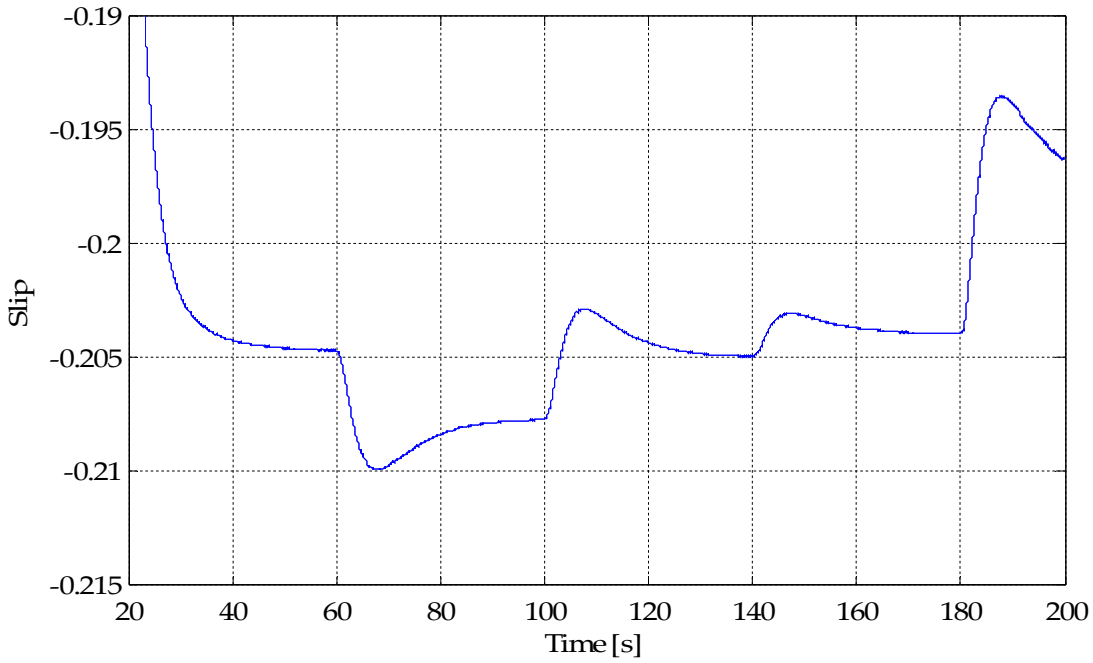

Figure 4-60: Generator slip of turbine 1 in response to the wind speed profiles in Figure 4-4.

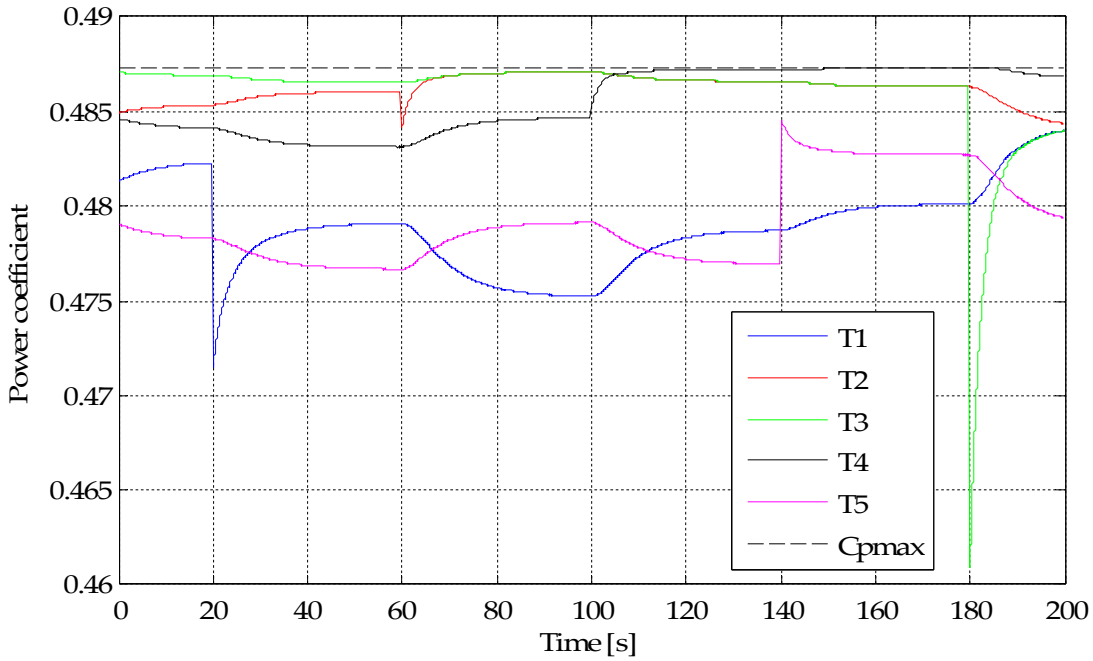

Figure 4-61: Individual turbine power coefficients in comparison to the C_{pmax}, where the turbines are subject to the wind speeds in Figure 4-4.

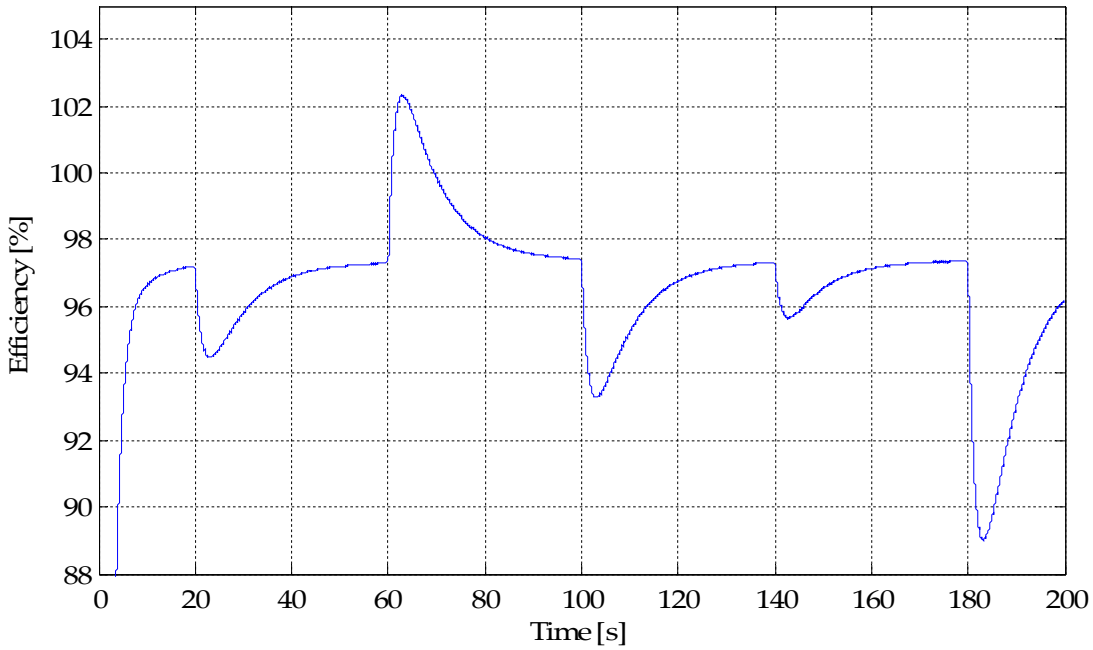

Figure 4-62: Energy transfer efficiency of the cluster of turbines when they are subject to the wind speeds in Figure 4-4.

Looking in more detail at the torques produced by the generators in each turbine reveals that a high frequency harmonic sinusoidal component is present. This component can be observed in Figure 4-63 where the wind speed on turbine 1 is constant; the magnitude of which, as a proportion of the average torque, can be represented by calculating the total harmonic distortion of the torque. The total harmonic distortion (THD) is determined by measuring the magnitude of the harmonic component and the average torque, and then inserting both into equation (4.16); the resulting THD is 5.98%.

$$THD[\%] = 100 \times \frac{Harmonic\ magnitude}{\sqrt{2}\ .\ Average\ Torque} \tag{4.16}$$

This harmonic component is a consequence of the commutation of the output current between the generator windings, in addition to the commutation voltage drop discussed earlier. The three phase nature of the generator

output means that the output current commutates between windings six times per cycle, therefore the harmonic that is present on the generator torque has the frequency of the 6th harmonic of the generator rotational speed. The harmonic content acts about the average torque that is applied to the generator and therefore does not have an impact on the general operation of the system; its main effect is to introduce vibration to the mechanical drive train that could potentially excite structural resonances within the wind turbine drive train, it will also generate considerable audible noise. In addition to the torque harmonic components, harmonics are also introduced to the DC side voltages and currents as a result of the rectification process; a detailed investigation of the harmonics that are present on the generator torque and DC currents and voltages will be conducted later in this thesis.

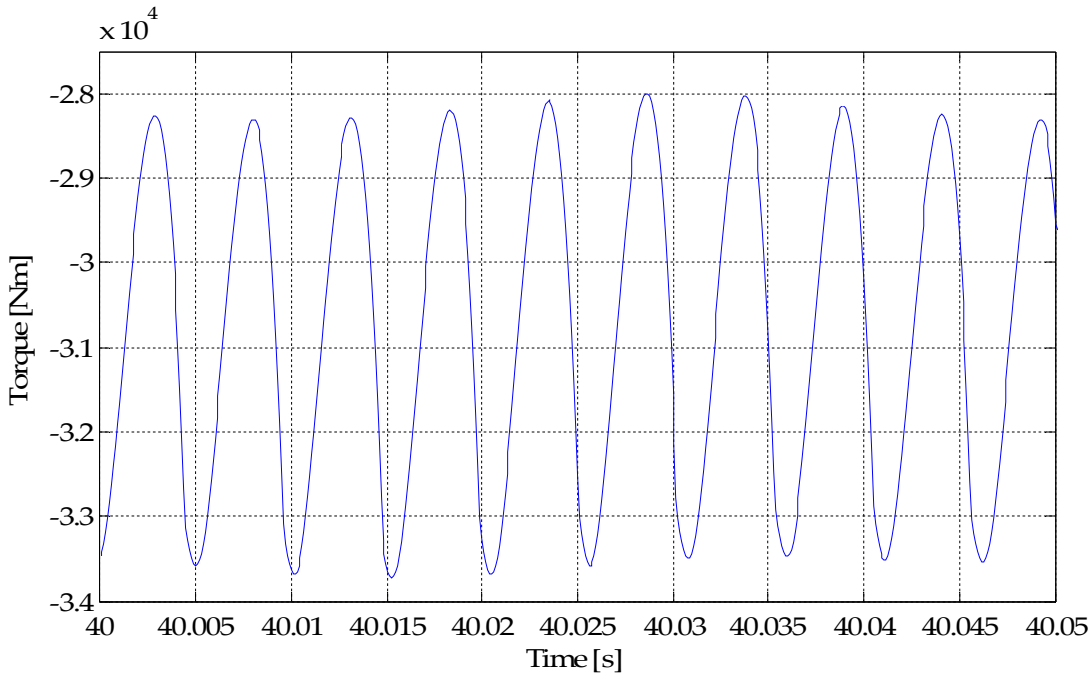

Figure 4-63: Enlargement of turbine 1 generator torque, showing the 6th harmonic component that is present.

4.5.5 Alternative designs of PM generator

Although the use of three phase, sinusoidally wound PM generators is exclusive in this work, alternative generator designs could be advantageous to reducing the harmonic magnitudes introduced by the rectifiers.

The production of perfectly smooth instantaneous torque by a generator relies on the design of the generator and also the ability of the generator drive to produce ideal current and voltage waveforms. The torque pulsations that have been observed in Figure 4-63 result from using a sinusoidally wound stator with rectangular or trapezoidal shaped currents. To produce a perfectly smooth torque with this machine the winding currents must also be perfectly sinusoidal. An alternative to using sinusoidally wound generators is to use a generator that is designed to produce trapezoidal shaped currents through the concentration of the windings or to increase the number of phases in the system. The minimisation of the torque pulsations in either case however still requires the perfect matching of the currents and the machine design. Many methods have been pursued to reduce torque pulsations, ranging from modification of machine designs to compensating for machine and current imperfections through cancellation of the pulsating torque components using control techniques [16].

The design and application of concentrated winding generators has been extensively researched for applications where the output of the generator is rectified; indeed these machines are commonly referred to as brushless permanent magnet DC generators (PMDC) [17] [18] [19] [20] [21]. The stator windings of such machines are arranged so that they are uniformly distributed over 60° arcs, therefore producing rectangular output emfs and

currents. It is also possible to design generators to provide trapezoidally shaped currents, which are beneficial where the commutation of the generator output current is unlikely to be instantaneous. The exact designs of such machines have different merits and pitfalls in comparison to a conventional sinusoidally wound generator, for example: the peak air-gap voltage and phase currents must be reduced in magnitude to maintain equal air-gap flux and rms current; rectangular or trapezoidally wound currents will reduce the magnitudes of the harmonics introduced to the generator torque, and DC voltages and currents; and the power density of such machines is often improved [19] [18]. Although a reduction in torque harmonic magnitude is produced by using these machines, it is not however removed completely; the finite commutation overlap of the output current between the generator windings still has some effect [19]. The generalised operational behaviour of such machines however is very similar to conventional machines, where the peak terminal voltage is proportional to the rotational speed of the generator. The rectangular shaped voltages also mean that the rectified DC voltage, which is equal to the generator line to line voltage, is simply equal to twice the phase voltage. The magnitudes of the harmonics are also a function of the generator output [20].

Alternatively the use of multiphase generators (machines with more than three phases) has been proven to also provide reduced torque harmonic magnitudes [19]. The use of higher numbers of phases increases the torque ripple frequency, whilst also reducing the amplitude, because the proportion of the current that is transferred between windings in each commutation is less. Therefore multi-phase machines also provide improved power densities, machine efficiencies and the potential for improved fault resilience [22].

The advantages presented by both the use concentrated windings or multi-phase machines has also led to the investigation of multi-phase concentrated winding machines, which combine the advantages of both cases, namely the reduction of the torque pulsations whilst also reducing the phase current magnitudes [23].

4.6 Discussion and conclusion

The preceding sections of this chapter have set out the results of preliminary investigations into the operation of each of the three technologies that could be used to implement an electrical cluster of wind turbines. Each technology has been tested with wind speed scenarios that represent the likely normal operating conditions of a group of wind turbines, with steady but different wind speeds and also with step changes of wind speed. It can be concluded from these investigations that it is technically possible to implement a cluster of turbines using any of the three technologies; however there are particular merits and pitfalls to the use of each. The primary indices of comparison of the technologies are: the ability to achieve the highest possible turbine rotor power coefficient and therefore capture the most amount of energy from the wind; and the efficiency by which the energy captured by the wind turbines is transferred through the cluster electrical system and onwards to the consumer. In addition to these indices there are also specific technical aspects of each technology that bring particular advantages and disadvantages to the operation of the system. The indices considered here allow the technical costs and implications to be highlighted; each of the technologies could also be compared based upon their capital costs, however this has not been conducted here.

4.6.1 Maximisation of energy capture

The capability of a turbine to operate at the best possible power coefficient and therefore capture the most amount of energy from the wind is related to its ability to allow its rotational speed to vary with wind speed. The nature of a cluster based electrical system removes the independence previously enjoyed by wind turbines where they each have individual power converters; however it has been shown by two of the technologies studied

that a degree of independence between the rotational speeds of the turbines can actually be retained. It is also possible, in all three of the cases studied, for the cluster controller to regulate the synchronous speed of the cluster to follow the average wind speed across the turbines; this in itself has been shown to be effective in allowing the power coefficients to be maintained within 5% of the maximum of the rotor design.

It has been observed that both the induction generator and rectified PM generator technologies allow for some degree of independence to be achieved between the turbines. In either case this is related to the ability of the generator speeds to slip from the cluster synchronous speed. Modelling of the induction generator case has revealed, where the original generator parameters are used, that the amount of generator slip that can be achieved is actually small (less than 1.5%), limiting the ability of the turbines to independently vary their rotational speed, shown by Figure 4-15 and Figure 4-20. The limited slip is a result of the steep gradient of the generator torque slip curve; however, by increasing the generator rotor winding resistance the gradient of the slip slope can be reduced, allowing the generators to achieve a greater slip and therefore allow the rotational speeds to vary by a greater amount from the synchronous speed. The benefit of reducing the gradient of the torque slip characteristic can be observed by the comparison of the power coefficients of the turbines in Figure 4-26 and Figure 4-28. The modelling of the rectified PM generator case has revealed that there is a significant natural ability within the system for the rotational speeds to vary independently. This ability results from the relationship between the slip of the turbines and the resistive and commutation voltage drops, which provides a torque slip characteristic gradient that is substantially smaller than either of the induction machine cases. The effects of this can be observed in Figure 4-60

where the maximum generator slip that is achieved, in the applied wind conditions, is approximately 21%. The benefit of this capability is again reflected by the closer proximity of the turbine power coefficients to the maximum in Figure 4-56 and Figure 4-61 compared to the induction generator cases.

It was anticipated that the use of PM generators directly connected to an AC electrical network would prevent the turbines from achieving any independent speed variation from each other because they must be synchronised to the electrical frequency. This was confirmed by the modelling of the system and is demonstrated in Figure 4-42 and Figure 4-47. As with the other two cases however the regulation of the cluster synchronous speed allows for the rotational speeds of the turbine to change with the average wind speed across the cluster of turbines and therefore still allow the turbines to achieve power coefficients within 5% of the maximum. It is shown however, by comparing the turbine power coefficients in this case with those of the other two cases, that the energy capture efficiency of the turbines remain lower in this case because of the lack of a degree of independent rotational speed variation between the turbines.

4.6.2 Energy transfer efficiency

The energy transfer efficiency of the generators and cluster electrical network is important so that the maximum amount of the energy captured by the wind turbine is transferred onwards to the consumer. The energy transfer efficiency has been calculated for each of the three cluster technology cases. By comparing each of the efficiencies in response to the constant wind speeds and step changes in Figure 4-29, Figure 4-46, and Figure 4-62, it has been identified that both of the cases which incorporate PM generators achieve

average efficiencies of approximately 95% and 98% for the AC and DC network cases respectively, whereas the induction generator case achieves an average efficiency of between 87% and 90%, depending on the rotor winding resistance used. This gives a clear indication that using PM generators is advantageous to the efficiency of the system over induction generators. The differences arise due to the different methods of excitation used by each generator; where the induction generators consume reactive power for excitation, but PM generators are excited by the magnetic material attached to their rotors. It is also notable that when the output of the PM generators is rectified that the system is marginally more efficient than when directly connected to an AC network; it is possible however that the greater generator voltage rating used in this case causes this, lowering the magnitudes of the currents.

4.6.3 Technical considerations

In addition to the aspects discussed above, each of the technologies has exhibited particular characteristics that can either be beneficial or detrimental to the operation of a cluster based collection network.

The requirement of external excitation for induction generators is a substantial disadvantage; this flow of reactive power not only affects the efficiency of the system but also requires the components within the system to be capable of operating with relatively low power factors whilst still transferring the active power output of the turbine; the uprating of system components to allow for this will add to the capital costs. It is common however, in wind farms based on directly connected fixed speed wind turbines, that local capacitive compensation is used to provide some power

factor correction within each turbine; the capability of this however would vary with the electrical frequency.

The requirement for damper windings within a PM generator that is connected directly to an AC network, provides a disadvantage to their use. The inclusion of damper windings within the rotor of a PM generator has not been a common feature of PM generator design to date because of the high numbers of poles and the small pole pitches that result. Although proven in the above investigations that their presence is beneficial, the design of a generator which incorporates such windings is problematic.

Where a PM generator is used in conjunction with a rectifier, damper windings are no longer required; however the production of harmonic torque components as a result of the rectification process could potentially pose a challenge to their use. Alternative designs of PM generators based on multi-phase designs and concentrated windings that produce trapezoidal instead of sinusoidal output currents have been briefly reviewed. This review has highlighted that the use of such machines could prove beneficial to reducing the magnitude of the harmonics produced.

4.6.4 Conclusions of initial investigations

In can be concluded from the investigations conducted in this chapter that a cluster of turbines could be implemented using any of the three technologies proposed. However the third technology where the outputs of PM generators are rectified is the most appropriate for the implementation of a cluster of wind turbines, because it provides a high energy transfer efficiency and also naturally allows a significant degree of independence to be achieved between the rotational speeds of the generators through the provision of slip; allowing for the turbines to achieve improved energy capture efficiencies.

From this point forward the focus of this thesis will be the investigation of the detailed operational aspects of this technology, with the aim of providing a comprehensive study of the feasibility of its use in a cluster collection network.

4.7 References

1. Jonkman, J., et al., *Definition of a 5MW reference wind turbine for offshore system development*, 2009, NREL.
2. Neilson, V.W., *Individual blade control for fatigue load reduction of large-scaled wind turbines: theory and modelling.*, in *Department of Electronic and Electrical Engineering*2010, University of Strathlcyde: Glasgow.
3. Burton. T, et al., *The Wind Energy Handbook*. Vol. 1. 2008: Wiley.
4. Barthelmie, R., et al., *Ten Years of Meteorological Measurements for Offshore Wind Farms.* Journal of Solar Energy Engineering, 2005. 127(2): p. 170-176.
5. Dusonchet, L., F. Massaro, and E. Telaretti. *Effects of electrical parameters of induction generator on the transient voltage stability of a fixed speed wind turbine*. in *Universities Power Engineering Conference, 2008. UPEC 2008. 43rd International*. 2008.
6. Tohidi, S., A. Rabiee, and M. Parniani. *Influence of model simplifications and parameters on dynamic performance of grid connected fixed speed wind turbines*. in *Electrical Machines (ICEM), 2010 XIX International Conference on*. 2010.
7. ABB, *XLPE Land Cable System - Users Guide*.
8. ABB, *XLPE Submarine Cable Systems - Attachement to XPLE Land Cable Systems -Users guide (rev 5)*.
9. Muyeen, S.M., et al. *Transient stability enhancement of variable speed wind turbine driven PMSG with rectifier-boost converter-inverter*. in *Electrical Machines, 2008. ICEM 2008. 18th International Conference on*. 2008.
10. Kundar, P., *Power system stability and control*1994: McGrawhill.
11. Say, M.G., *Alternating Current Machines*. 5th Edition ed1983: John Wiley & Sons.
12. Spooner, E. and A.C. Williamson, *Direct coupled, permanent magnet generators for wind turbine applications.* Electric Power Applications, IEE Proceedings -, 1996. 143(1): p. 1-8.
13. Grabic, S., N. Celanovic, and V. Katic. *Fixed speed wind turbine topology based on actively damped PMSG*. in *Power Electronics and Motion Control Conference (EPE/PEMC), 2010 14th International*. 2010.

14. Westlake, A.J.G., J.R. Bumby, and E. Spooner, *Damping the power-angle oscillations of a permanent-magnet synchronous generator with particular reference to wind turbine applications.* Electric Power Applications, IEE Proceedings -, 1996. 143(3): p. 269-280.
15. Kamiev, K., J. Nerg, and J. Pyrhonen. *Design of damper windings for direct-on-line permanent magnet synchronous generators*. in *EUROCON 2009, EUROCON '09. IEEE*. 2009.
16. Jahns, T.M. and W.L. Soong, *Pulsating torque minimization techniques for permanent magnet AC motor drives-a review.* Industrial Electronics, IEEE Transactions on, 1996. 43(2): p. 321-330.
17. Bose, B., *Power Electronics and Variable Frequency Drives:Technology and Applications*1997: Wiley-IEEE Press
18. Lipo, T.A. and F.X. Wang, *Design and Performance of a Converter Optimized AC Machine.* Industry Applications, IEEE Transactions on, 1984. IA-20(4): p. 834-844.
19. Jahns, T.M., *Torque Production in Permanent-Magnet Synchronous Motor Drives with Rectangular Current Excitation.* Industry Applications, IEEE Transactions on, 1984. IA-20(4): p. 803-813.
20. Krishnan, R. and R. Geun-Hie, *Modeling, simulation, and analysis of variable-speed constant frequency power conversion scheme with a permanent magnet brushless DC generator.* Industrial Electronics, IEEE Transactions on, 1990. 37(4): p. 291-296.
21. Pillay, P. and R. Krishnan, *Modeling, simulation, and analysis of permanent-magnet motor drives. II. The brushless DC motor drive.* Industry Applications, IEEE Transactions on, 1989. 25(2): p. 274-279.
22. Parsa, L. *On advantages of multi-phase machines*. in *Industrial Electronics Society, 2005. IECON 2005. 31st Annual Conference of IEEE*. 2005.
23. Parsa, L. and H.A. Toliyat, *Five-phase permanent-magnet motor drives.* Industry Applications, IEEE Transactions on, 2005. 41(1): p. 30-37.

Chapter 5 Rectifier commutation

Key to the operation of a cluster collection network based on rectified PM generators is the commutation of the output current by the rectifier, which transfers the output DC current between the phase windings of the generator. Ideally this process would occur instantaneously with no overlap, however the generator winding inductance restricts the rate of change of the phase currents and therefore the commutation takes a finite period of time, during which both the outgoing and incoming phase windings are conducting. The period where both windings are conducting is referred to as the commutation overlap; a consequence of which is the distortion of the phase terminal voltages of the generator, as a result of the windings involved in the commutation being effectively short circuited for the duration. The distortion of the voltages is reflected on the output DC voltage of the rectifier and therefore reduces the average. This reduction of average voltage is convenient within a cluster based collection network because it contributes to

the voltage difference between the generators and the cluster common point, which produces slip.

This chapter will cover in detail the process of rectifier commutation, including the derivation of the commutation overlap length as a function of generator winding impedance and rotational speed, and the average DC voltage reduction introduced by the distortion of the generator terminal voltage. An analysis of the harmonics that are present in the generator winding current will then be conducted with the aim of determining the displacement power factor of the generator output, the power losses in the generator windings and the total harmonic distortion of the generator torque caused by the commutation process. All of these factors will then be taken into account to produce the cluster controller operating curve that links the cluster output voltage to the converter voltage and turbine rotational speeds. The effects of the step-up transformer on the commutation process will also be considered along with a simplified model representation of the overall system.

5.1 The process of rectifier commutation

A diode rectifier operates by conducting current through the pair of diodes that have the largest forward voltage across them. The sinusoidal variation of a PM generators three phase emf means that at any instant two diodes are forward biased and conducting, whereas the others are reverse biased and not conducting. Figure 5-1[i] shows the three phase emf of the generator and that diodes 1 and 6 conduct during period (a) since the voltage between the red and blue phases is greatest; it is also shown that during period (b) diodes 3 and 6 conduct since the voltage between the yellow and blue phases is greatest. The DC output voltage of the rectifier, V_{dc}, follows the phase to

phase emf of the conducting phases, and the DC current can be assumed to be constant. The commutation process shown here is ideal because the output current transfers between the generator windings instantaneously, therefore the current waveform of each winding is perfectly rectangular; conducting the forward current for a period of $2\pi/3$ radians, then not conducting for $\pi/3$ radians, and then conducting the reverse current for $2\pi/3$ radians and so on.

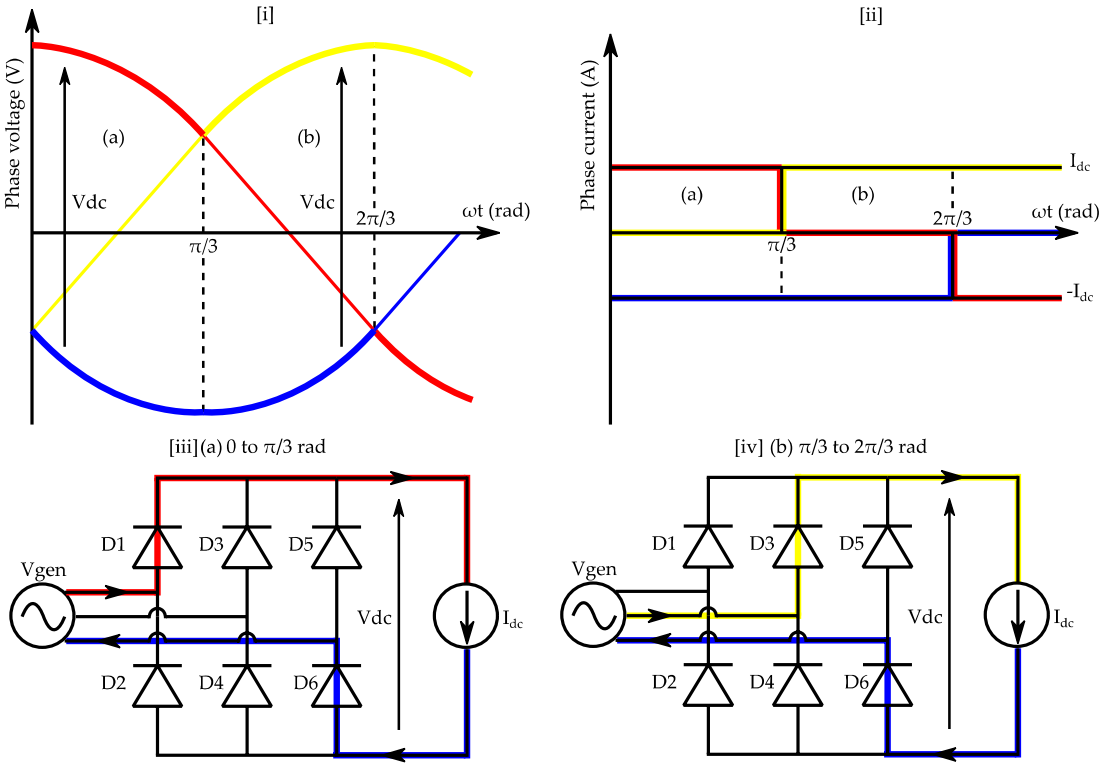

Figure 5-1: [i] Three phase generator emfs, where the thicker lines indicate the pair of voltages with the greatest difference between them; [ii] generator phase winding currents; [iii] diode rectifier indicating the path of the current during period (a); [iv] diode rectifier indicating the path of the current during period (b).

The ideal commutation shown in Figure 5-1 will not to occur in reality because of the impedance of the generator stator windings. Accounts of the commutation process, giving consideration to the influence of the stator inductance on the commutation process, are given in [1] and [2]. These are

reviewed here because the process of commutation and the voltage drop it introduces are particularly significant to the operation of a cluster collection network based on rectified PM generators. In addition to the generator winding inductances, the effects of the generator winding resistance is also considered.

The presence of inductance in the generator stator windings slows the rise and fall of the current at the beginning and end of each pulse. By assuming the output DC current remains constant throughout the commutation, the instantaneous incoming and outgoing winding currents must sum to equal the DC current. Figure 5-2[ii] shows the commutation between phases A and B, where the current transfers from diode 1 to diode 3. Since only diodes 1 and 3 are involved in the commutation, and diode 4 is conducting the return current, the circuit can be simplified to that shown in Figure 5-2[iii].

The commutation begins when the emfs E_a and E_b become equal, at which point diode 3 begins to conduct current. Since the sum of I_a and I_b must always equal I_{dc}, when diode 3 begins to conduct, the forward current through diode 1 must also begin to fall. Therefore a component of current effectively flows from phase B to phase A, labelled as I_{comm} in Figure 5-2, which is also equal to I_b. The commutation continues until I_{comm} equals I_{dc}, at which point I_a is zero and I_b also equals I_{dc}. The angular displacement that occurs while this process takes place is δ radians, referred to as the commutation length. During commutation, the terminals of generator windings A and B are effectively short circuited and therefore the voltage at point P, where they connect together, is equal to the average of the phase voltages. This voltage reduces in magnitude throughout the commutation as the phase voltages change relative to each other, but remains equal to the

average until the commutation is complete. As a result of the effective short circuit between the windings, the terminal voltages of both windings are distorted for this period, as shown in Figure 5-2[i]. Once the commutation is complete and diode 1 stops conducting, phase A no longer influences the voltage at P which is therefore equal to E_b.

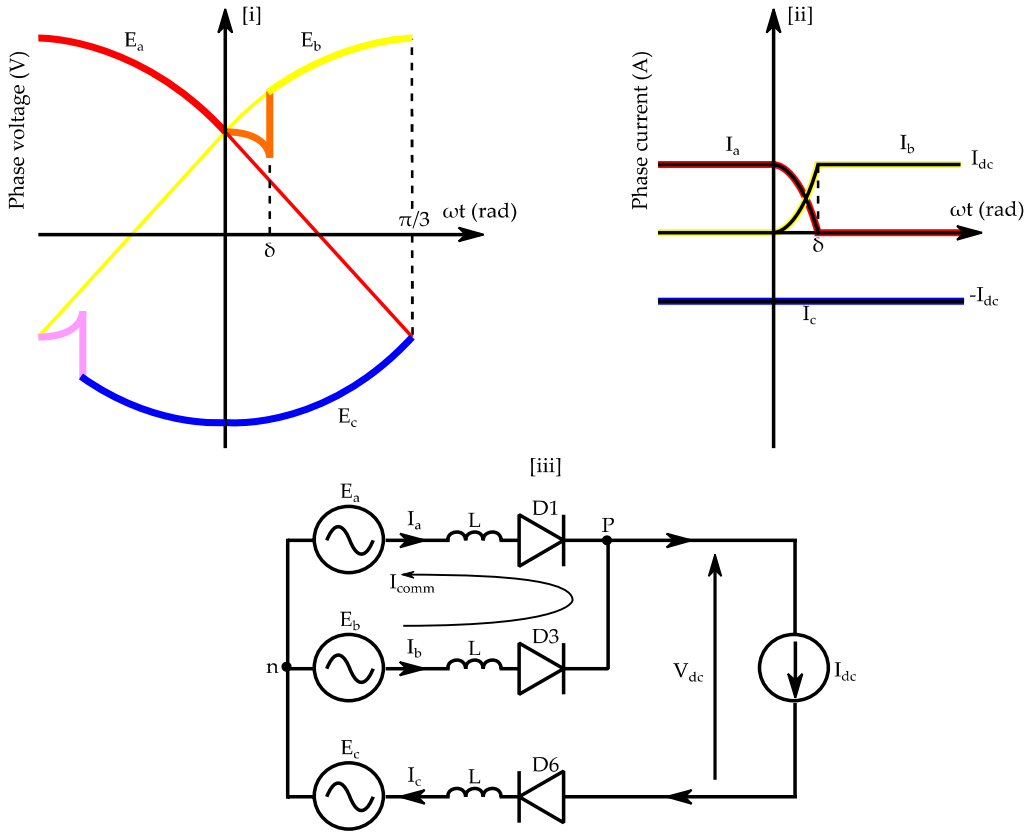

Figure 5-2: [i] Three phase generator terminal voltages for the commutation from phase A to phase B, showing the distortion that results; [ii] generator phase winding currents during the commutation; [iii] simplified rectifier circuit only showing the diodes that are involved in the conduction of current [1].

5.1.1 Commutation length with stator inductance

The length of the commutation process is important when determining the effects of the voltage distortion on the average DC rectifier output voltage. It is influenced by both the inductive and resistive components of the generator

stator windings; however initially here the stator winding conduction resistance is neglected to simplify the analysis.

During commutation the currents in each generator winding involved are:

$$I_a = I_{dc} - I_{comm} \tag{5.1}$$

$$I_b = I_{comm} \tag{5.2}$$

Therefore the voltages across each of the winding inductances are:

$$V_{La} = L.\frac{dI_a}{dt} = -L.\frac{dI_{comm}}{dt} \qquad \text{since } \frac{dI_{dc}}{dt} = 0 \tag{5.3}$$

$$V_{Lb} = L.\frac{dI_b}{dt} = L.\frac{dI_{comm}}{dt} \tag{5.4}$$

During commutation the windings involved are effectively short circuited at their terminals and therefore the circuit diagram can be simplified further to that shown in Figure 5-3.

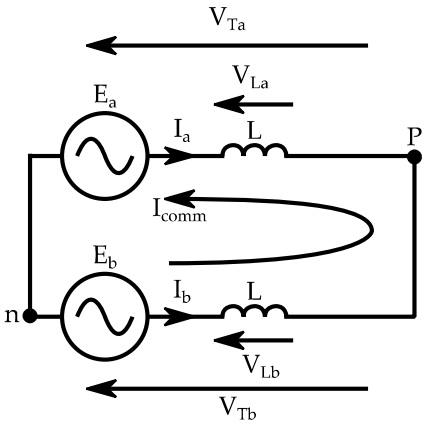

Figure 5-3: Simplified electrical circuit during commutation.

The voltages in this circuit will sum to zero by KVL, therefore:

$$V_{Ta} = V_{Tb} \tag{5.5}$$

$$\therefore E_a - V_{La} = E_b - V_{Lb} \tag{5.6}$$

$$\therefore E_b - E_a = V_{Lb} - V_{La} \tag{5.7}$$

Where $V_{La} = L.\frac{dI_a}{dt} = -L.\frac{dI_{comm}}{dt}$ and $V_{Lb} = L.\frac{dI_b}{dt} = L.\frac{dI_{comm}}{dt}$ (5.8)

$$E_b - E_a = 2.L.\frac{dI_{comm}}{dt} \tag{5.9}$$

At the beginning of the commutation $I_{comm} = 0$ and at the completion of the commutation $I_{comm} = I_{dc}$; therefore the length of the commutation, δ, can be determined by solving equation (5.9) to find the point when $I_{comm} = I_{dc}$, as follows:

Rearranging (5.9) and multiplying both sides by the electrical frequency, ω_e, to find the commutation length as an angular displacement:

$$\omega_e.L\int_0^{I_{dc}} dI_{comm} = \int_0^{\delta} \frac{E_b - E_a}{2} d\omega_e t \tag{5.10}$$

$$\therefore \omega_e.L.I_{dc} = \int_0^{\delta} \frac{E_b - E_a}{2} d\omega_e t \tag{5.11}$$

Where the origin is located at the beginning of the commutation, as shown in Figure 5-2, and $E_a = E.\cos\left(\omega t + \frac{\pi}{3}\right)$ and $E_b = E.\cos\left(\omega t - \frac{\pi}{3}\right)$.

$$E_b - E_a = \sqrt{3}.E.\sin(\omega t) \tag{5.12}$$

$$\therefore \omega_e.L.I_{dc} = \int_0^{\delta} \frac{\sqrt{3}.E.\sin(\omega t)}{2} d\omega t \tag{5.13}$$

$$\therefore \omega_e.L.I_{dc} = \frac{\sqrt{3}.E.(1-\cos\delta)}{2} \tag{5.14}$$

$$\therefore \cos\delta = 1 - \left(\frac{2.\omega_e.L.I_{dc}}{\sqrt{3}.E}\right) \tag{5.15}$$

Therefore the commutation length, δ, is a function of the electrical frequency, ω, the stator inductance, L, the line-line voltage, $\sqrt{3}.E$, and the DC output

current, I_{dc}; and will not exceed $\pi/3$ radians so that one commutation can end before the next begins.

5.1.2 Commutation length with stator inductance and resistance

When the conduction resistance of the stator windings is considered in addition to the inductance, a more accurate prediction of the length of the commutation overlap can be produced.

The currents in either of the phase windings involved in the commutation are in this case the same as in equations (5.1) and (5.2) and the DC current remains constant; however the commutation circuit now includes the resistive elements, as shown in Figure 5-4.

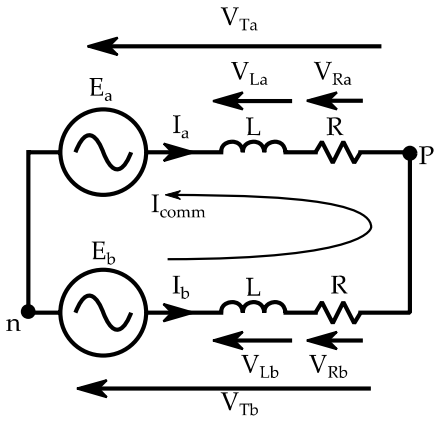

Figure 5-4: Simplified electrical circuit during commutation, including both stator resistances and inductances.

The voltages in the circuit will again sum to zero by KVL, therefore:

$$V_{Ta} = V_{Tb} \tag{5.16}$$

$$E_a - V_{La} - V_{Ra} = E_b - V_{Lb} - V_{Rb} \tag{5.17}$$

$$\therefore E_b - E_a = V_{Lb} + V_{Rb} - V_{La} - V_{Ra} \tag{5.18}$$

Where: $V_{La} = L.\frac{dI_a}{dt} = -L.\frac{dI_{comm}}{dt}$, $V_{Lb} = L.\frac{dI_b}{dt} = L.\frac{dI_{comm}}{dt}$,
$V_{Ra} = I_a.R = (I_{dc}.R - I_{comm}.R)$ and $V_{Rb} = I_b.R$.

Therefore:

$$E_b - E_a = 2.L.\frac{dI_{comm}}{dt} + 2.I_{comm}.R - I_{dc}.R \tag{5.19}$$

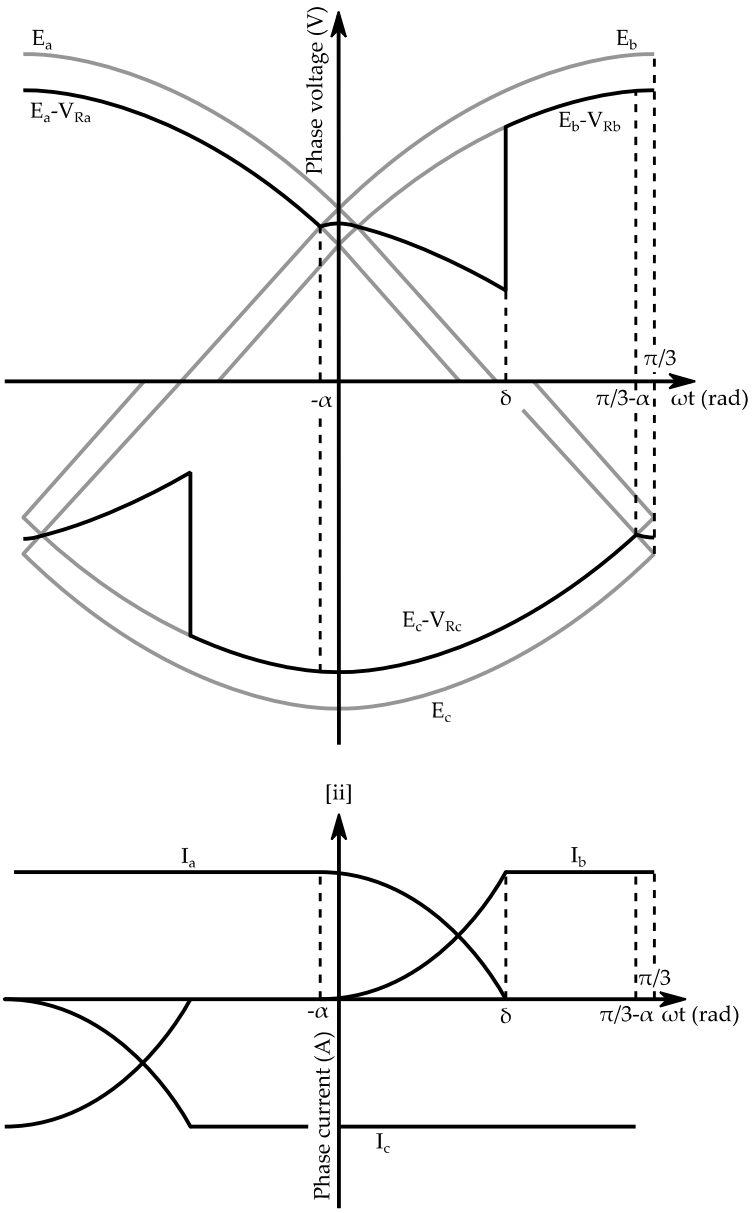

Figure 5-5: [i] Generator emfs and terminal voltages, taking into account the voltage drops across the stator resistances; [ii] Generator phase currents before, during and after commutation.

The presence of the stator winding conduction resistances causes the commutation process to begin earlier, at the point where the terminal voltage of phase A, V_{Ta}, which is the winding emf minus the voltage drop across the

resistance, is equal to the terminal voltage of winding B, V_{Tb}, which is equal to the emf of winding B; note that at the beginning of the commutation I_b is zero and therefore so is V_{Rb}. The winding emfs and terminal voltages are shown in Figure 5-5[i] before, during and after the commutation process.

The presence of the winding resistance means that the commutation will begin at the angle $-\alpha$ radians and will continue until I_{comm} equals I_{dc} at δ radians. In order to accurately predict the length of the commutation, the earlier start must be taken into account. The relationships between the phase winding currents are the same as those in equations (5.1) and (5.2); therefore the commutation length can be determined by a similar process, but by first calculating the angle at which it starts, $-\alpha$, by finding the angle at which $E_a - V_{Ra} = E_b$, as follows:

$$E_a - V_{Ra} = E_b \tag{5.20}$$

$$\therefore E.\cos(\omega t + \frac{\pi}{3}) - I_{dc}.R = E.\cos(\omega t - \frac{\pi}{3}) \tag{5.21}$$

$$\therefore \sin(-\alpha) = \frac{I_{dc}.R}{\sqrt{3}.E} \tag{5.22}$$

Rearranging equation (5.19) and substituting in equation (5.12), phase shifted by $-\alpha$ radians, gives:

$$\therefore \frac{\sqrt{3}.E.\sin(\omega t - \alpha)}{2.L} + \frac{I_{dc}.R}{2.L} = \frac{dI_{comm}}{dt} + \frac{I_{comm}.R}{L} \tag{5.23}$$

Equation (5.23) can then be solved for I_{comm} using Laplace transforms, where $I_{comm}(0) = 0$, giving equation (5.24).

$$I_{comm}(\omega t) = \frac{I_{dc}}{2} - \frac{I_{dc}.e^{-\left(\frac{R}{\omega.L}.\omega t\right)}}{2} + \frac{\sqrt{3}.E.\omega.\cos(-\alpha).e^{-\left(\frac{R}{\omega.L}\omega t\right)}}{2.L.\left(\omega^2 + \left[\frac{R}{L}\right]^2\right)}$$
$$+ \frac{\sqrt{3}.E.\sin(-\alpha).\sin(\omega t)}{2.L.\omega} - \frac{\sqrt{3}.E.\cos(-\alpha).\cos(\omega t)}{2.L.\left(\omega^2 + \left[\frac{R}{L}\right]^2\right)} \quad (5.24)$$
$$+ \frac{\sqrt{3}.E.R.\sin(-\alpha).\cos(\omega t)}{2.L^2.\left(\omega^2 + \left[\frac{R}{L}\right]^2\right)} + \frac{\sqrt{3}.E.R.\cos(-\alpha).\sin(\omega t)}{2.L^2.\left(\omega^2 + \left[\frac{R}{L}\right]^2\right)}$$
$$- \frac{\sqrt{3}.E.R.\sin(-\alpha).e^{-\left(\frac{R}{\omega.L}.\omega t\right)}}{2.L^2.\left(\omega^2 + \left[\frac{R}{L}\right]^2\right)} - \frac{\sqrt{3}.E.R^2.\sin(-\alpha).\sin(\omega t)}{2.L^3.\omega.\left(\omega^2 + \left[\frac{R}{L}\right]^2\right)}$$

The commutation length, δ, can be determined from equation (5.24) by finding the angle, ωt, where $I_{comm} = I_{dc}$. As stated above the maximum commutation length is π/3 radians.

5.1.3 Voltage distortion due to commutation overlap

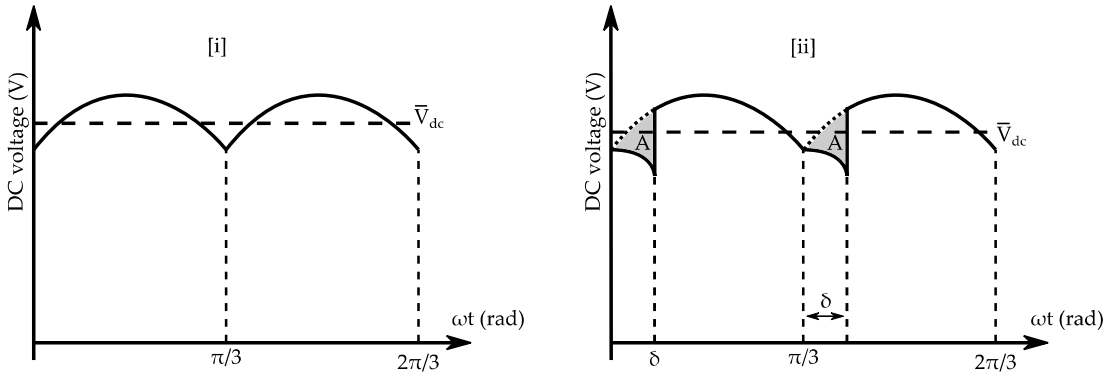

Figure 5-6: [i] Ideal DC voltage; [ii] DC voltage including distortion introduced by commutation overlap.

Knowledge of the commutation length allows the impact of the commutation voltage distortion on the average DC voltage to be determined. The DC voltage at the output terminals of the rectifier will always follow the line to line voltage between the generator terminals that is greatest; therefore it changes between windings six times per cycle as shown in Figure 5-6. The

average of the DC voltage is important because it is this that drives the current flow through the DC network and not the instantaneous voltage. The average voltage in the ideal case, before the distortion is considered, is equal to the generator line-line voltage averaged over a 6th of a cycle, or π/3 radians, given by Equation (5.25) and shown in Figure 5-6[i]; where the line-line voltage is determined as follows:

$E_b - E_c = \sqrt{3}.E.\cos(\omega t - \frac{\pi}{6})$, where $E_c = -E.\cos(\omega t)$.

$$\overline{V_{dc}} = \frac{3}{\pi}\int_0^{\frac{\pi}{3}} \sqrt{3}.E.\cos\left(\omega t - \frac{\pi}{6}\right).d\omega t \tag{5.25}$$

When the distortion due to the commutation overlap is taken into account a similar process is followed, however the area A in Figure 5-6[ii], must be subtracted from the integral before averaging.

Voltage drop due to stator inductance distortion

The distortion of the generator terminal voltages when the stator inductance is present, results from the voltage drop across the inductances during the commutation process. The voltage at point P during the commutation process can be determined as a function of the winding emfs involved; calculated here initially where only the inductance of the stator windings is considered:

$$V_{Pn} = E_a - L.\frac{dI_a}{dt} \tag{5.26}$$

$$V_{Pn} = E_b - L.\frac{dI_b}{dt} \tag{5.27}$$

Taking the average of equations (5.26) and (5.27) gives:

$$2.V_{Pn} = (E_a + E_b) - L.\frac{d(I_a + I_b)}{dt} \tag{5.28}$$

From equations (5.1) and (5.2) $I_{dc} = I_a + I_b$, and where $E_a + E_b = E.\cos(\omega t)$, and $\frac{dI_{dc}}{dt} = 0$, equation (5.28) can be simplified to:

$$V_{Pn} = \frac{E.\cos(\omega t)}{2} = V_{comm} \tag{5.29}$$

The area A can therefore be calculated by integrating the voltage V_{Pn} over the commutation period, between 0 and δ radians, and subtracting it from the integral of E_b over the same period, as shown in equation (5.30).

$$A = \int_0^{\delta} (E_b - V_{Pn})\, d\omega t = \int_0^{\delta} E.\cos\left(\omega t - \frac{\pi}{3}\right) d\omega t - \int_0^{\delta} \frac{E.\cos(\omega t)}{2} d\omega t \tag{5.30}$$
$$= \frac{\sqrt{3}.E}{2}(1 - \cos\delta)$$

By substituting in equation (5.14), equation (5.30) can be reduced to:

$$A = \omega.L.I_{dc} \tag{5.31}$$

Therefore the average DC voltage, taking into account the commutation distortion, can be determined by subtracting the area A from the integral of the line-line voltage between the two conducting windings, B and C, before averaging, as shown by equation (5.32).

$$\overline{V_{dc}} = \frac{3}{\pi}\left[\int_0^{\frac{\pi}{3}} \sqrt{3}.E.\cos(\omega t - \frac{\pi}{6})\, d\omega t - \omega.L.I_{dc}\right] \tag{5.32}$$

Therefore the reduction of the average DC voltage that results from the commutation overlap distortion is:

$$\Delta\overline{V_{dc}} = \frac{3.\omega.L.I_{dc}}{\pi} \tag{5.33}$$

Voltage drop due to stator inductance and resistance distortion

When the generator stator resistance is considered in addition to the stator inductance, determining the reduction of the average DC voltage due to the commutation overlap is more complex. It was noted above, and shown in Figure 5-5[i], that the presence of the stator resistances causes the commutation to start early. Therefore to calculate the average DC voltage over a $\pi/3$ radian period, the integral of the difference between the winding terminal voltages must be determined between the start of the commutation at $-\alpha$ radians and $\pi/3 - \alpha$ radians. The calculation of this integral is performed by separating the area between the voltages into smaller sections which can be calculated separately, before summing the results. The smaller sections of area are labelled A, B and C in Figure 5-7.

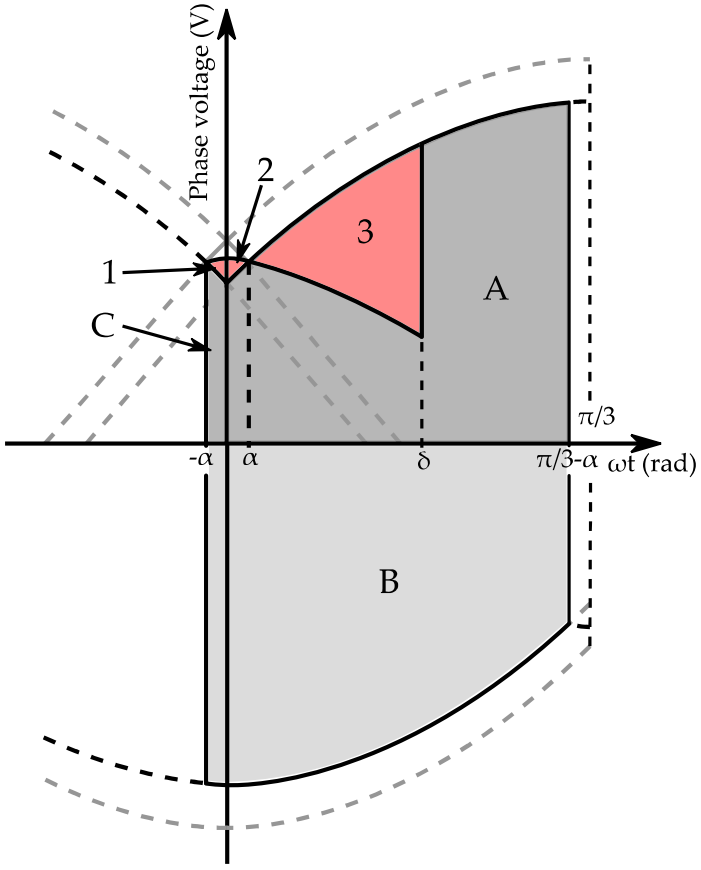

Figure 5-7: Areas between the winding voltages for integration.

The areas shaded red (1, 2 and 3) are the result of the commutation distortion. Area 3 is similar to the area A calculated above and will be subtracted from the overall integration result. Areas 1 and 2 arise from the advance start of the commutation and are added to the overall integral area.

The voltage at the terminals of the windings involved in the commutation, V_{comm}, is determined in a similar manner to above, as follows:

$$V_{Pn} = E_a - L.\frac{dI_a}{dt} - I_a.R \tag{5.34}$$

$$V_{Pn} = E_b - L.\frac{dI_b}{dt} - I_b.R \tag{5.35}$$

Taking the average of equations (5.34) and (5.35), gives:

$$2.V_{Pn} = (E_a + E_b) - L.\frac{d(I_a + I_b)}{dt} - R.(I_a + I_b) \tag{5.36}$$

From equations (5.1) and (5.2) $I_{dc} = I_a + I_b$, where $E_a + E_b = E.\cos(\omega t)$, and $\frac{dI_{dc}}{dt} = 0$, therefore equation (5.36) can be simplified to:

$$V_{Pn} = \frac{E.\cos(\omega t)}{2} - \frac{R.I_{dc}}{2} = V_{comm} \tag{5.37}$$

Therefore each of the individual areas can be calculated as follows:

$$Area\ A = \int_0^{\frac{\pi}{3}-\alpha} (E_b - I_d.R)\, d\omega t = E.\left(\sin(-\alpha) + \frac{\sqrt{3}}{2}\right) - I_{dc}R.\left(\frac{\pi}{3} - \alpha\right) \tag{5.38}$$

$$Area\ B = \int_{-\alpha}^{\frac{\pi}{3}-\alpha} (E_c - I_d.R)\, d\omega t = -E.\left(\sin\left(\frac{\pi}{3} - \alpha\right) - \sin(-\alpha)\right) + \frac{I_{dc}.R.\pi}{3} \tag{5.39}$$

$$Area\ C = \int_{-\alpha}^{0} (E_a - I_d.R)\, d\omega t = E.\left(\frac{\sqrt{3}}{2} - \sin\left(-\alpha + \frac{\pi}{3}\right)\right) - I_{dc}.R.\alpha \tag{5.40}$$

$$Area\ 1 = \int_{-\alpha}^{0} [V_{comm} - (E_a - I_{dc}.R)]\, d\omega t$$
$$= \frac{I_{dc}.R.\alpha}{2} - \frac{E}{2}.\sin(-\alpha) + I_{dc}.R.\alpha - E.\left(\frac{\sqrt{3}}{2} - \sin\left(-\alpha + \frac{\pi}{3}\right)\right) \quad (5.41)$$

$$Area\ 2 = \int_{0}^{-\alpha} [V_{comm} - (E_b - I_{dc}.R)]\, d\omega t$$
$$= \frac{I_{dc}.R.\alpha}{2} + \frac{E}{2}.\sin(\alpha) + I_{dc}.R.\alpha - E.\left(\sin\left(\alpha - \frac{\pi}{3}\right) + \frac{\sqrt{3}}{2}\right) \quad (5.42)$$

$$Area\ 3 = \int_{\alpha}^{\delta} [(E_b - I_{dc}.R) - V_{comm}]\, d\omega t$$
$$= E.\left[\sin\left(\delta - \frac{\pi}{3}\right) - \sin\left(\alpha - \frac{\pi}{3}\right)\right] - \frac{E.[\sin(\delta) - \sin(\alpha)]}{2} \quad (5.43)$$
$$- \frac{I_{dc}.R.(\delta + 3.\alpha)}{2}$$

The reduction of the average voltage over a 6th of a cycle, due to the distortion, can be determined by calculating the average DC voltage where the commutation overlap caused by the inductances is neglected and then by subtracting the average DC voltage where the commutation overlap is included, using equations (5.44) and (5.45) respectively. Areas 1 and 2 are included in both equations because they are a result of the voltage drops across the stator resistances which cause the commutation to begin earlier.

Average DC voltage before distortion is included:

$$\overline{V_{dc1}} = \frac{3.(Area\ A + Area\ B + Area\ C + Area\ 1 + Area\ 2)}{\pi} \quad (5.44)$$

Average DC voltage including the commutation distortion:

$$\overline{V_{dc2}} = \frac{3.(Area\ A + Area\ B + Area\ C + Area\ 1 + Area\ 2 - Area\ 3)}{\pi} \tag{5.45}$$

Therefore the change of the average DC voltage due to the commutation distortion is:

$$\therefore \Delta\overline{V_{dc}} = \overline{V_{dc1}} - \overline{V_{dc2}} = \frac{3.Area\ 3}{\pi} \tag{5.46}$$

The reduction of the average DC voltage, $\Delta\overline{V_{dc}}$, is referred to as the commutation voltage drop.

The key characteristic of this voltage reduction is that it occurs without the loss of energy normally associated with a resistive voltage drop. The commutation overlap does however decrease the power factor of the generator output, because the rectifier effectively absorbs reactive power. The flow of this reactive power will therefore slightly increase the losses within the winding conduction resistances.

The absorption of reactive power by the rectifier is caused by the changing of the fundamental winding current component phase angle, as a result commutation process. Figure 5-8 and Figure 5-9 show the current waveforms for a single generator winding with and without the influence of the winding inductances. To achieve the rectangular or trapezoidal shape of the current pulses, higher order harmonic components are present in addition to the fundamental. If these harmonics are removed, only the fundamental sinusoidal component will remain, as shown. The fundamental component of the current transfers the majority of the output power from the generator and therefore the phase shift of this component, as a result of the commutation overlap, causes the rectifier to absorb reactive power.

Comparing the fundamental components in Figure 5-8 and Figure 5-9 gives an indication of the phase shift that occurs; to determine the exact phase shift the Fourier series of the winding current pulses must be determined; this will be conducted later in this chapter.

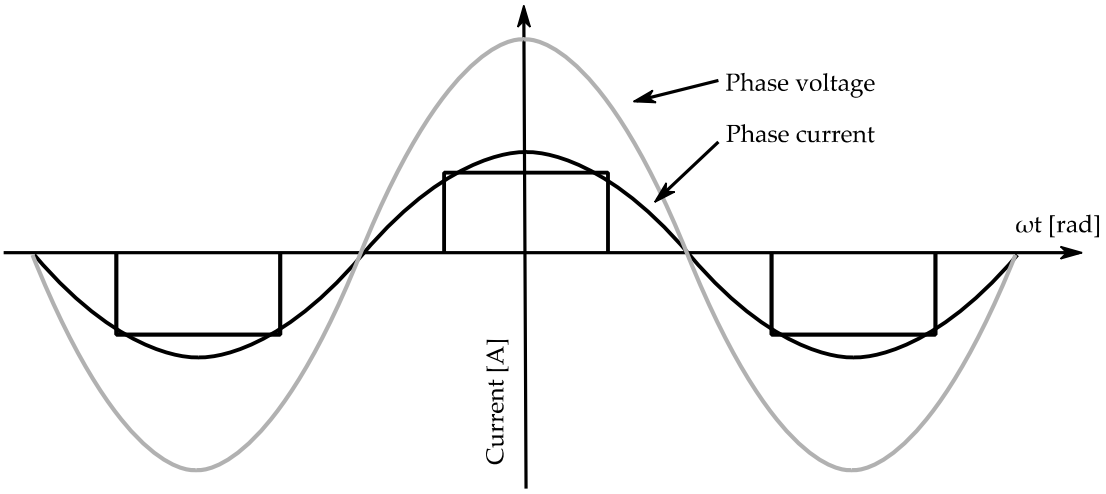

Figure 5-8: Rectangular current pulses where no commutation overlap occurs, along with the fundamental current harmonic component; with phase voltage for reference.

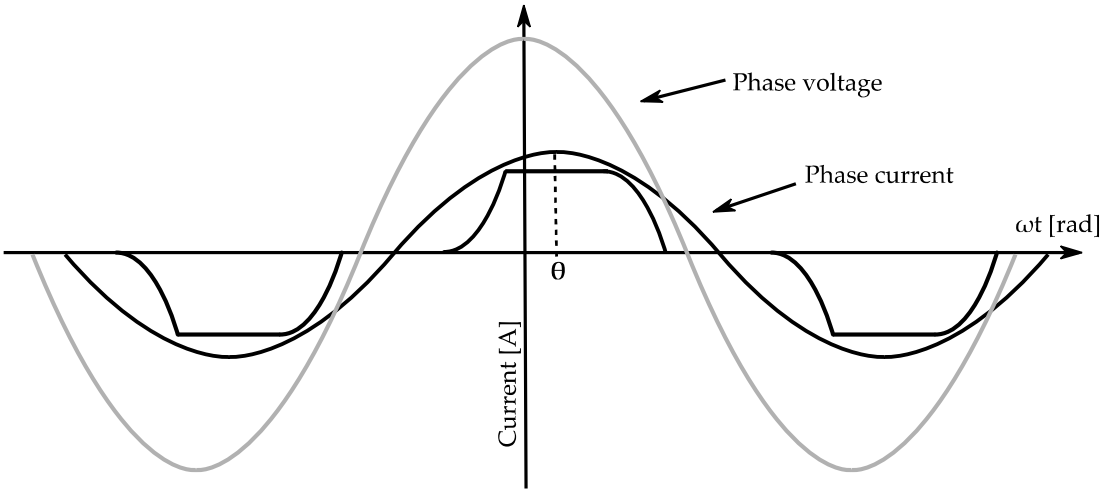

Figure 5-9: Current pulses including the effects of commutation overlap, along with the fundamental current harmonic which is phase shifted by the overlap; with phase voltage for reference.

Commutation voltage drop as an equivalent resistance

The commutation voltage drops determined in equations (5.33) and (5.46) can be represented by equivalent resistances; the values of which are determined by dividing the voltage drops by the DC output current, shown by equation (5.47). This allows the rectified PM generator to be represented by a DC voltage source with a source resistance. Care should be taken however when representing this voltage drop by an equivalent resistance, because it is frequency dependent and the losses that would normally be associated with a resistance do not occur in the actual system.

$$R_{eqiv} = \frac{\Delta\overline{V_{dc}}}{I_{dc}} \tag{5.47}$$

5.1.4 Verification of commutation predictions

To verify the process of predicting the length of the commutation overlap and the effects of it on the average DC voltage set out in section 5.1.2; the system is simulated in Simulink and a comparison is made between the simulation and the predictions of the winding currents, generator terminal voltages and rectifier DC output voltage before, during and after the commutation. The measurements of the simulated generator winding currents, terminal voltages and DC voltage are captured using the system model set out in the previous chapter, reduced to include just one turbine, without the step-up transformer. A prediction of the incoming winding current is produced using equation (5.23), the voltages at the terminals of the windings involved in the commutation are predicted using equation (5.37) and the DC voltage is predicted by determining the line-line voltage between the generator windings that are conducting. The average of the measured simulation DC voltage is also compared with the prediction produced using

equation (5.46). The wind speed that is applied in this instance to the turbine in the system model is 8m/s and the level of current where commutation overlap ceases (where $I_{comm} = I_{dc}$) is measured to be 471 Amps.

Figure 5-10 shows that the prediction of the incoming winding current matches the simulation measurement throughout the commutation overlap period, and Figure 5-11 shows that the predictions of the voltages that occur at the terminals of the generator windings involved in the commutation also match the simulation measurements. In addition, Figure 5-12 shows that the predicted rectifier output DC voltage waveform is similar to the simulated waveform and that the average of the simulation voltage matches the prediction.

It can be concluded from these comparisons that the predictions and the measurements of the current and voltages correlate well; therefore the analysis set out above is valid.

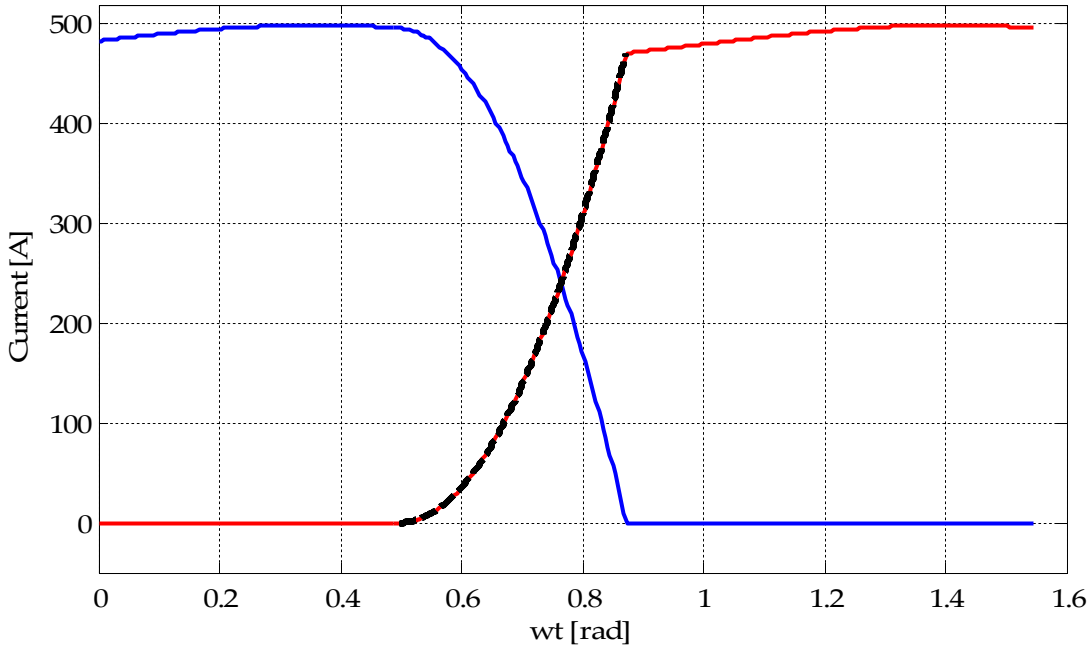

Figure 5-10: Simulated generator winding currents (blue and red lines) before, during and after the commutation overlap and the predicted incoming winding current during commutation (dashed black line).

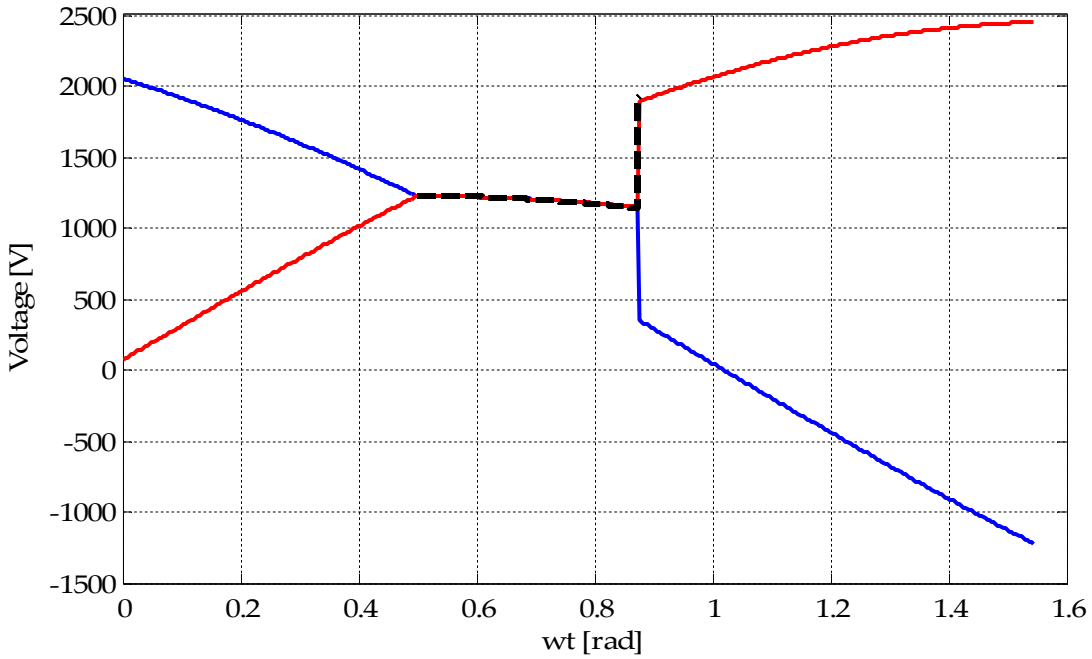

Figure 5-11: Measurements of the simulated generator terminal voltages (blue and red lines) before, during and after the commutation overlap and the predicted terminal voltage during commutation (dashed black line).

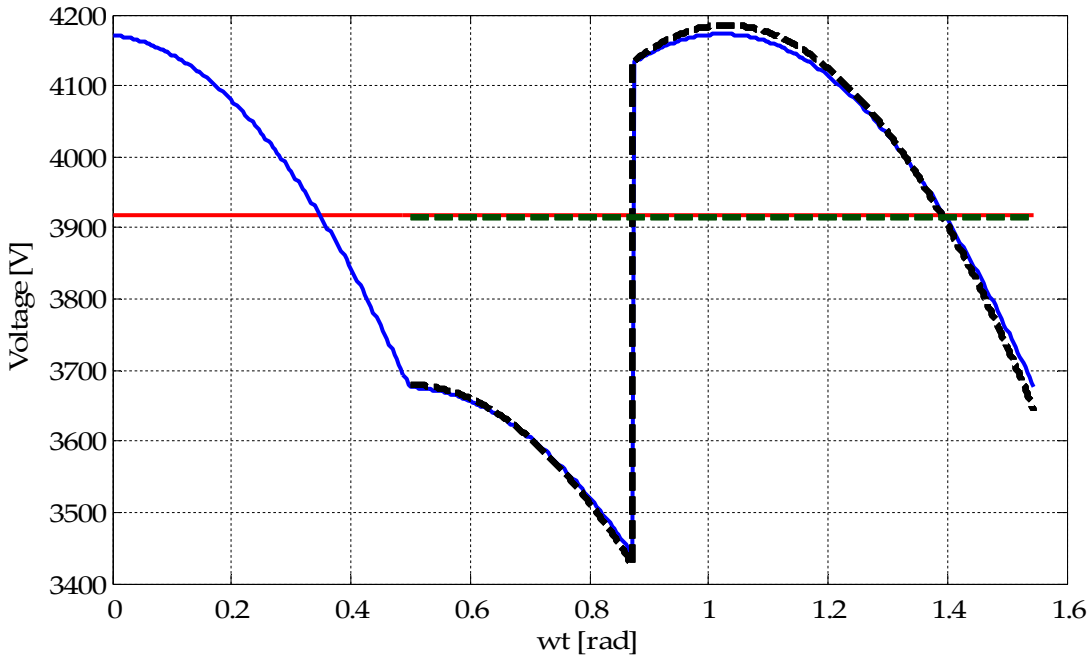

Figure 5-12: Simulated and predicted rectifier DC output voltage (blue line and dashed black line respectively) before, during and after commutation and the average simulated and predicted rectifier DC output voltage (red line and dashed green line).

5.2 Harmonics introduced by commutation

The rectification of the PM generator output requires each phase winding to produce pulses of output current. The rectangular or trapezoidal shape of these pulses requires higher order harmonic current components to be present in addition to the fundamental sinusoid. The presence of these higher order harmonics is felt not just on the winding currents of the generator but also on the torque applied by the generator onto the mechanical drive train of the wind turbine. In addition to the current harmonics, the sampling of the generator winding line-line voltage by the rectifier also causes a 6^{th} harmonic component to be present. Since the DC voltage gives rise to the DC current and because the DC side inductance is relatively small, this voltage harmonic also introduces a harmonic onto the DC output current of the rectifier.

To determine which harmonic components are present within the generator windings, their relationship to the output DC current of the rectifier, and how they are reflected onto the generator torque, the Fourier series of the current pulses can be calculated. The Fourier series also allows the phase of the fundamental current component to be determined, allowing an indication of the generator output power factor to be produced.

It has been shown in the previous section that the shape of the winding current pulses is affected by the rectifier commutation overlap, causing the current pulses to take up a trapezoidal shape instead of rectangular, as shown in Figure 5-8 and Figure 5-9. It should also be noted that the 6^{th} harmonic component that is present on the DC output current is also reflected onto the winding currents and therefore the rectifier output current

cannot be regarded here as perfectly constant, as was the case in the previous section.

Initially the Fourier series is calculated for the rectangular pulses, neglecting the effects of the commutation overlap; the harmonic component of the DC output current is also included in this study. This provides a clear indication of the major harmonic components present within the winding current pulses and also of the impact of these harmonic components on the generator torque.

Secondly, the Fourier series of the winding current is calculated taking into account the effects of the rectifier commutation overlap. This allows the impact of the commutation overlap on the phase of the fundamental current component to be determined, and therefore the extent to which the commutation overlap reduces the output power factor of the generator. To enable this, the winding current during the commutation is approximated by assuming it rises and falls with a constant rate of change to simplify the analysis. The harmonic component of the DC output current is not included in this case. Knowledge of the current harmonic magnitudes calculated in this case will also allow the generator torque to be derived as a function of the current harmonics and the effects of the rectifier commutation; it will also allow the power lost due to the generator winding resistance to be determined.

In both of the cases studied here, the winding current waveforms must be defined clearly for a single cycle to allow the Fourier series' to be calculated. Figure 5-13 shows the current waveform for the first case, where the winding currents are rectangular and Figure 5-14 shows the winding current waveform for the second case where the commutation overlap is considered.

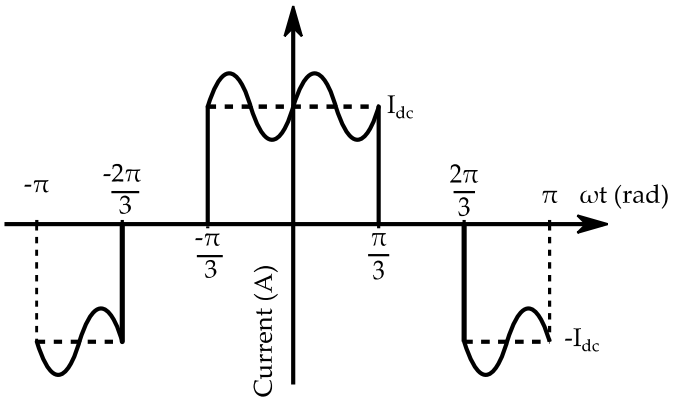

Figure 5-13: Rectangular winding current for the initial Fourier series study.

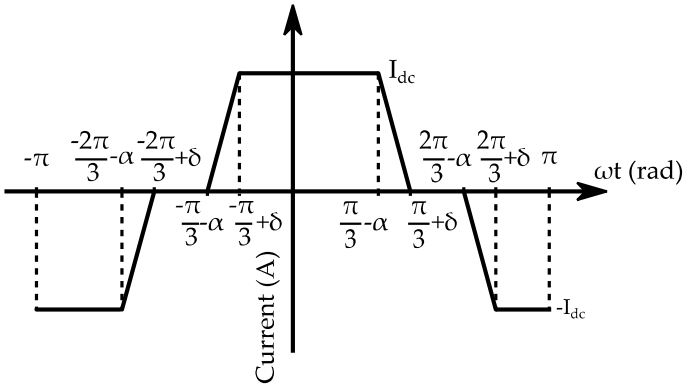

Figure 5-14: Trapezoidal winding current for the second Fourier series study.

5.2.1 Winding current Fourier series without commutation overlap

The Fourier series coefficients are calculated by separating the waveform into sections, each with an explicit equation describing the current waveform. The equation describing the waveform in each section is multiplied by both the sine or cosine waveform at each harmonic frequency, and then integrated to determine the harmonic coefficients. In this case the harmonic coefficients comprise of three different integrals representing the three regions where the winding current in non-zero in Figure 5-13. The cosine and sine coefficients, a_n and b_n respectively, are determined using equations (5.48) and (5.49), where I_6 is the magnitude of the 6th harmonic component present on the DC current and n is the harmonic number. This analysis highlights that the most significant harmonics in the winding current are the fundamental, the 5th

harmonic and the 7th harmonic; the coefficients for which are given in Table 5-1.

$$\begin{aligned} a_n = \frac{1}{\pi}\int_{-\frac{\pi}{3}}^{\frac{\pi}{3}}(I_{dc} + I_6.\sin(6\omega t)).\cos(n\omega t)\,d\omega t \\ -\frac{1}{\pi}\int_{-\pi}^{-\frac{2\pi}{3}}(I_{dc} + I_6.\sin(6\omega t)).\cos(n\omega t)\,d\omega t \\ -\frac{1}{\pi}\int_{\frac{2\pi}{3}}^{\pi}(I_{dc} + I_6.\sin(6\omega t)).\cos(n\omega t)\,d\omega t \end{aligned} \tag{5.48}$$

$$\begin{aligned} b_n = \frac{1}{\pi}\int_{-\frac{\pi}{3}}^{\frac{\pi}{3}}(I_{dc} + I_6.\sin(6\omega t)).\sin(n\omega t)\,d\omega t \\ -\frac{1}{\pi}\int_{-\pi}^{-\frac{2\pi}{3}}(I_{dc} + I_6.\sin(6\omega t)).\sin(n\omega t)\,d\omega t \\ -\frac{1}{\pi}\int_{\frac{2\pi}{3}}^{\pi}(I_{dc} + I_6.\sin(6\omega t)).\sin(n\omega t)\,d\omega t \end{aligned} \tag{5.49}$$

$$\begin{aligned} I_a(\omega t) = a_1.\cos(\omega t) + b_1.\sin(\omega t) + a_5.\cos(5\omega t) + b_5.\sin(5\omega t) \\ + a_7.\cos(7\omega t) + b_7.\sin(7\omega t) + \cdots \end{aligned} \tag{5.50}$$

Table 5-1: Most significant a_n and b_n harmonic coefficients of the winding current in Figure 5-13.

n	a_n	b_n
1	$\frac{2\sqrt{3}.I_{dc}}{\pi}$	$-\frac{12\sqrt{3}.I_6}{35\pi}$
5	$-\frac{2\sqrt{3}.I_{dc}}{5\pi}$	$\frac{12\sqrt{3}.I_6}{11\pi}$
7	$\frac{2\sqrt{3}.I_{dc}}{7\pi}$	$\frac{12\sqrt{3}.I_6}{13\pi}$

Knowledge of these coefficients allows the phase winding current waveform to be reconstructed using equation (5.50). The resulting winding current waveform is shown by the blue line in Figure 5-15, which takes up the general shape of the winding current; however the inclusion of further

higher order harmonics is required to refine the shape of the waveforms, as shown by the red line which includes harmonics up to the 100th component.

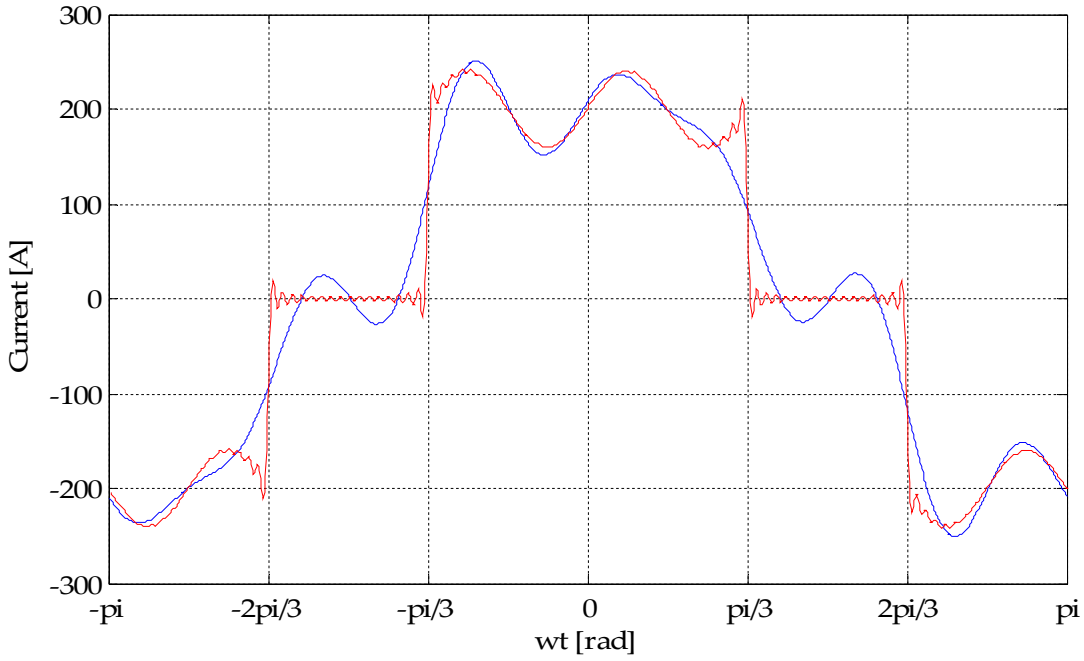

Figure 5-15: Winding current waveforms reconstructed from the Fourier series in equation (5.50); the blue line includes only the components up to the 7th harmonic, and the red line includes the components up to the 100th harmonic (I_{dc}=200A and $I_{6magnitude}$=40A).

To observe the impact of the winding current harmonics on the generator torque, the Fourier series of each of the three phase generator winding currents is required. The additional winding currents are determined using the harmonic coefficients in Table 5-1 and by altering equation (5.50) to account for the respective phase shifts of each phase current. The three phase currents must then be referred to the rotating two axis reference frame in which the generator is modelled using the Parks transformation. The resulting direct and quadrature axis components of the currents are given by equations (5.51) and (5.52), including the fundamental, 5th and 7th harmonics only:

$$I_d(\omega t) = [a_5.\sin(6\omega t) - b_5.\cos(6\omega t) - a_7.\sin(6\omega t) + b_7.\cos(6\omega t)] \quad (5.51)$$

$$I_q(\omega t) = [a_1 + a_5.\cos(6\omega t) + b_5.\sin(6\omega t) + a_7.\cos(6\omega t) + b_7.\sin(6\omega t)] \quad (5.52)$$

The generator torque can then be determined by substituting the direct and quadrature current components into equation (2.29), which gives the generator torque as a function of the harmonic component coefficients as shown in equation (5.53) (it is assumed the generator is non-salient, therefore $L_d = L_q$). It can be observed from this equation that the torque component due to the DC output current is dominant and also that the harmonic torque component is a function of both the average DC current output and the 6th harmonic on the DC current. The current harmonics of a higher order than the 7th harmonic that are present to refine the winding current waveform shown in Figure 5-15, although not included here, will also be present on the generator torque as multiples of the 6th harmonic, i.e. 12th, 18th, 24th and so on.

$$\begin{aligned} Torque &= \frac{3}{2}.p.\Psi_f(a_1 + (a_5 + a_7).\cos(6\omega t) + (b_5 + b_7).\sin(6\omega t)) \\ &= p.\Psi_f\left[I_{dc}.\left(\frac{6\sqrt{3}}{2\pi} - \frac{6\sqrt{3}}{35\pi}.\cos(6\omega t)\right) + \frac{432\sqrt{3}.I_6}{143\pi}.\sin(6\omega t)\right] \end{aligned} \quad (5.53)$$

5.2.2 Winding current Fourier series including the commutation overlap

A similar process is followed to determine Fourier series coefficients of the winding current waveform that includes the effects of the commutation overlap, shown in Figure 5-9. However, in this case the waveform must be separated into seven parts where each has an explicit equation describing the current. The additional parts are required to take into account the commutation overlap, in particular the advance start of the commutation represented by the angle α and the commutation length represented by the angle δ. During the commutation periods the winding currents are

approximated by straight lines to simplify the algebra. The winding current during each region in Figure 5-14 is given by equations (5.54) to (5.60); these equations are used to determine the cosine and sine Fourier series harmonic coefficients, a_n and b_n respectively, using equations (5.61) to (5.64).

$$-\pi \leq \omega t \leq -\frac{2\pi}{3} - \alpha \qquad I_{winding} = -I_{dc} \tag{5.54}$$

$$-\frac{2\pi}{3} - \alpha \leq \omega t \leq -\frac{2\pi}{3} + \delta \qquad I_{winding} = \frac{I_{dc}}{\delta + \alpha}.\omega t + I_{dc}.\left(\frac{2\pi + 3\alpha}{3\delta + 3\alpha} - 1\right) \tag{5.55}$$

$$-\frac{\pi}{3} - \alpha \leq \omega t \leq -\frac{\pi}{3} + \delta \qquad I_{winding} = \frac{I_{dc}}{\delta + \alpha}.\omega t + I_{dc}.\left(1 + \frac{\pi - 3\alpha}{3\delta + 3\alpha}\right) \tag{5.56}$$

$$-\frac{\pi}{3} + \delta \leq \omega t \leq \frac{\pi}{3} - \alpha \qquad I_{winding} = I_{dc} \tag{5.57}$$

$$\frac{\pi}{3} - \alpha \leq \omega t \leq \frac{\pi}{3} + \delta \qquad I_{winding} = -\frac{I_{dc}}{\delta + \alpha}.\omega t + I_{dc}.\left(1 + \frac{\pi - 3\alpha}{3\delta + 3\alpha}\right) \tag{5.58}$$

$$\frac{2\pi}{3} - \alpha \leq \omega t \leq \frac{2\pi}{3} + \delta \qquad I_{winding} = -\frac{I_{dc}}{\delta + \alpha}.\omega t + I_{dc}.\left(\frac{2\pi + 3\delta}{3\delta + 3\alpha} - 1\right) \tag{5.59}$$

$$\frac{2\pi}{3} + \delta \leq \omega t \leq \pi \qquad I_{winding} = -I_{dc} \tag{5.60}$$

$$
\begin{aligned}
a_n = \frac{1}{\pi}\int_{-\pi}^{-\frac{\pi}{3}-\alpha} & -I_{dc}.\cos(n\omega t)\,d\omega t \\
& + \frac{1}{\pi}\int_{-\frac{2\pi}{3}-\alpha}^{-\frac{2\pi}{3}+\delta}\left[\frac{I_{dc}}{\delta+\alpha}.\omega t + I_{dc}.\left(\frac{2\pi+3\alpha}{3\delta+3\alpha}-1\right)\right]\cos(n\omega t)\,d\omega t \\
& + \frac{1}{\pi}\int_{-\frac{\pi}{3}-\alpha}^{-\frac{\pi}{3}-\delta}\left[\frac{I_{dc}}{\delta+\alpha}.\omega t + I_{dc}.\left(1+\frac{\pi-3\alpha}{3\delta+3\alpha}\right)\right]\cos(n\omega t)\,d\omega t \\
& + \frac{1}{\pi}\int_{-\frac{\pi}{3}+\delta}^{\frac{\pi}{3}-\alpha} I_{dc}.\cos(n\omega t)\,d\omega t \\
& + \frac{1}{\pi}\int_{\frac{\pi}{3}-\alpha}^{\frac{\pi}{3}+\delta}\left[-\frac{I_{dc}}{\delta+\alpha}.\omega t + I_{dc}.\left(1+\frac{\pi-3\alpha}{3\delta+3\alpha}\right)\right]\cos(n\omega t)\,d\omega t \\
& + \frac{1}{\pi}\int_{\frac{2\pi}{3}-\alpha}^{\frac{2\pi}{3}+\delta}\left[-\frac{I_{dc}}{\delta+\alpha}.\omega t + I_{dc}.\left(\frac{2\pi+3\delta}{3\delta+3\alpha}-1\right)\right]\cos(n\omega t)\,d\omega t \\
& + \frac{1}{\pi}\int_{\frac{2\pi}{3}+\delta}^{\pi} -I_{dc}.\cos(n\omega t)\,d\omega t
\end{aligned}
\tag{5.61}
$$

$$
\begin{aligned}
b_n = \frac{1}{\pi}\int_{-\pi}^{-\frac{\pi}{3}-\alpha} & -I_{dc}.\sin(n\omega t)\,d\omega t \\
& + \frac{1}{\pi}\int_{-\frac{2\pi}{3}-\alpha}^{-\frac{2\pi}{3}+\delta}\left[\frac{I_{dc}}{\delta+\alpha}.\omega t + I_{dc}.\left(\frac{2\pi+3\alpha}{3\delta+3\alpha}-1\right)\right]\sin(n\omega t)\,d\omega t \\
& + \frac{1}{\pi}\int_{-\frac{\pi}{3}-\alpha}^{-\frac{\pi}{3}-\delta}\left[\frac{I_{dc}}{\delta+\alpha}.\omega t + I_{dc}.\left(1+\frac{\pi-3\alpha}{3\delta+3\alpha}\right)\right]\sin(n\omega t)\,d\omega t \\
& + \frac{1}{\pi}\int_{-\frac{\pi}{3}+\delta}^{\frac{\pi}{3}-\alpha} I_{dc}.\sin(n\omega t)\,d\omega t \\
& + \frac{1}{\pi}\int_{\frac{\pi}{3}-\alpha}^{\frac{\pi}{3}+\delta}\left[-\frac{I_{dc}}{\delta+\alpha}.\omega t + I_{dc}.\left(1+\frac{\pi-3\alpha}{3\delta+3\alpha}\right)\right]\sin(n\omega t)\,d\omega t \\
& + \frac{1}{\pi}\int_{\frac{2\pi}{3}-\alpha}^{\frac{2\pi}{3}+\delta}\left[-\frac{I_{dc}}{\delta+\alpha}.\omega t + I_{dc}.\left(\frac{2\pi+3\delta}{3\delta+3\alpha}-1\right)\right]\sin(n\omega t)\,d\omega t \\
& + \frac{1}{\pi}\int_{\frac{2\pi}{3}+\delta}^{\pi} -I_{dc}.\sin(n\omega t)\,d\omega t
\end{aligned}
\tag{5.62}
$$

$$\therefore a_n = \frac{2.I_{dc}}{n^2.\pi.(\delta+\alpha)}.\left[\sin\left(\frac{2n\pi}{3}\right)+\sin\left(\frac{n\pi}{3}\right)\right].[\sin(n\delta)+\sin(n\alpha)] \quad (5.63)$$

$$\therefore b_n = \frac{2.I_{dc}}{n^2.\pi.(\delta+\alpha)}.\left[\sin\left(\frac{2n\pi}{3}\right)+\sin\left(\frac{n\pi}{3}\right)\right].[\cos(n\alpha)-\cos(n\delta)] \quad (5.64)$$

Knowledge of these coefficients allows the Fourier series of the waveform in Figure 5-14 to be determined using equation (5.50). The resulting waveform that the Fourier series represents is shown in Figure 5-16 and is similar to Figure 5-14, confirming the validity of the Fourier coefficients in equations (5.63) and (5.64).

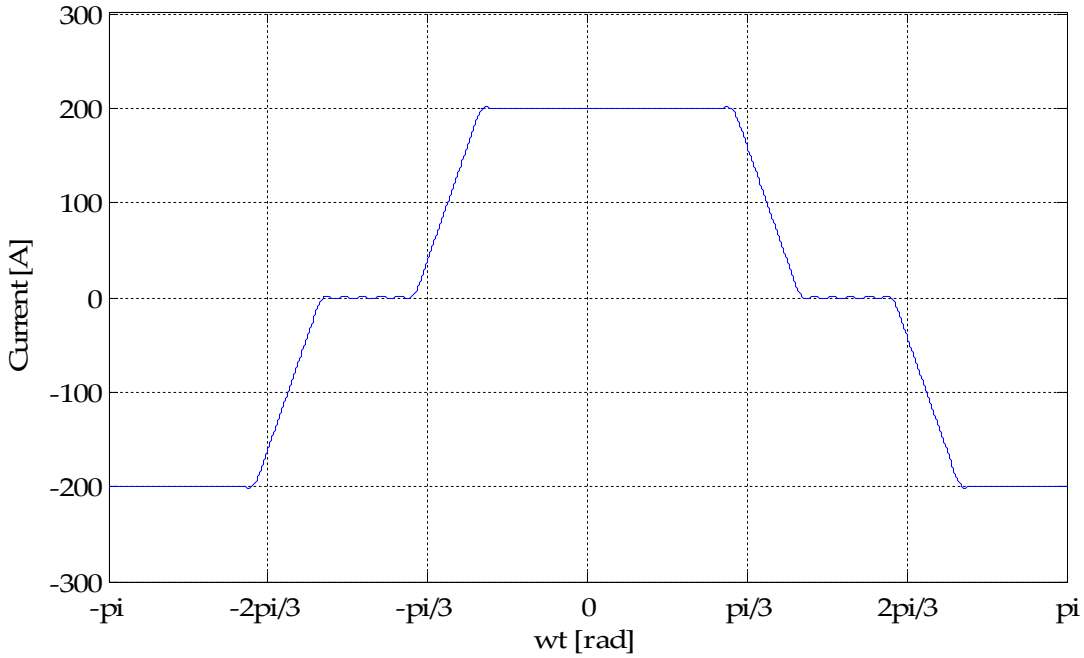

Figure 5-16: Winding current waveform reconstructed from the Fourier series, including the effects of the commutation overlap; components up to the 50th harmonic are included (I_{dc}=200A, $\delta = \pi/9$ radians and $\alpha = \pi/36$ radians).

The purpose of determining the Fourier series of this waveform is to investigate the effect of the commutation overlap on the phase angle of the fundamental current component relative to the generator winding terminal voltage, and therefore the output displacement power factor of the generator.

In addition, the harmonic components of the generator torque and the power lost in the generator windings due to each harmonic current component can be determined.

The phase angle of the fundamental current component can be determined by calculating the phase angle of the resultant phasor between the cosine and sine Fourier coefficients, a_n and b_n, using equation (5.65). This gives the phase angle as a function of the harmonic order, n, the commutation overlap, δ, and the commutation advance start angle, α, from which the generator output displacement power factor can be determined using equation (5.67) where n=1.

$$\tan\theta = \frac{b_n}{a_n} \tag{5.65}$$

$$\theta = \frac{n.(\delta - \alpha)}{2} \tag{5.66}$$

$$Displacement\ Power\ Factor = \cos(\theta) \tag{5.67}$$

The generator torque can be determined in a similar manner to the previous section by determining each of the winding currents as a function of the harmonic components then referring them to the rotating reference frame to give the direct and quadrature axis currents. The coefficients of the most significant harmonic components are shown in Table 5-2; using these and the quadrature axis current, the torque can be determined using equation (2.29), as shown in equation (5.68), (Where $L_d = L_q$).

$$\begin{aligned} Torque = \frac{3.\sqrt{3}.p.\Psi_f.I_{dc}}{\pi.(\delta+\alpha)}\Bigg[&\sin\delta + \sin\alpha \\ &+ \sin(6\omega t).\left[\frac{1}{49}.(\sin(7\delta) + \sin(7\alpha) + \cos(7\delta) - \cos(7\alpha))\right. \\ &\left.+ \frac{1}{25}.(\sin(5\delta) + \sin(5\alpha) + \cos(5\delta) - \cos(5\alpha))\right]\Bigg] \end{aligned} \tag{5.68}$$

The torque is therefore shown to be a function of the DC output current, the commutation advance start angle, α, and length, δ, and consists of a DC and a 6th harmonic component, similarly to above.

Table 5-2: Most significant generator winding current harmonic component coefficients.

n	a_n	b_n
1	$\frac{2.\sqrt{3}.I_{dc}}{\pi.(\delta+\alpha)}[\sin(\delta)+\sin(\alpha)]$	$\frac{2.\sqrt{3}.I_{dc}}{\pi.(\delta+\alpha)}[\cos(\alpha)-\cos(\delta)]$
5	$-\frac{2.\sqrt{3}.I_{dc}}{25.\pi.(\delta+\alpha)}[\sin(5\delta)+\sin(5\alpha)]$	$-\frac{2.\sqrt{3}.I_{dc}}{25.\pi.(\delta+\alpha)}[\cos(5\alpha)-\cos(5\delta)]$
7	$\frac{2.\sqrt{3}.I_{dc}}{49.\pi.(\delta+\alpha)}[\sin(7\delta)+\sin(7\alpha)]$	$\frac{2.\sqrt{3}.I_{dc}}{49.\pi.(\delta+\alpha)}[\cos(7\alpha)-\cos(7\delta)]$

The power lost in the generator windings due to each harmonic current component can be determined by calculating the rms of each and then applying equation (5.69), where n is the harmonic number and R is the generator winding resistance. The total power lost in the generator windings can then be found using equation (5.70).

$$P_{n\,Loss} = 3.I_{n\,rms}^2.R \tag{5.69}$$

$$P_{GenLoss} = \sum_{n=1}^{\infty} P_{n\,Loss} \tag{5.70}$$

5.2.3 Verification of generator power factor, torque and winding power loss predictions

To verify the predictions made of the generator output power factor, generator torque and the power losses in the generator windings, the same simulation of the system with a wind speed of 8m/s used in section 5.1.4 is used here. To predict the generator output power factor using equation (5.67) the commutation overlap length and the commutation advance start

angle are required. To provide these values, a measurement of the average DC output current is taken from the simulation and used directly in the harmonic analysis and also to predict the commutation length and advance start angle using the method in section 5.1.2. The simulation values of the average DC output current, $\overline{I_{dc}}$, the predicted commutation length, δ, and advance angle, α, used are given in Table 5-3. The predicted value of the fundamental current component phase angle, relative to the generator terminal voltage, and the resultant power factor are given in Table 5-4.

Table 5-3: Values of average DC output current, $\overline{I_{dc}}$, commutation length, δ, and commutation advance angle, α, used to predict the generator output power factor.

$\overline{I_{dc}}$	485A
δ	0.378rad (21.66°)
α	2.2784×10^{-4} rad (0.013°)

Table 5-4: Predicted values of the winding current phase angle, relative to the generator terminal voltage, and the generator output power factor, generated using the procedure in section 5.2.2.

θ	0.1889rad (10.82°)
Power factor	0.9822 lagging

To provide a measurement from the simulation of the fundamental winding current phase angle for comparison, Fast Fourier Transform (FFT) analysis is performed to determine the magnitudes and phase angles of the winding current harmonic components. This is conducted using the PowerGui FFT Analysis tool in Matlab Simulink. The resultant winding current fundamental phase angle, relative to the generator terminal voltage, is given in Table 5-5, along with the resulting power factor. The current harmonic magnitudes and the power losses in the generator windings due to each harmonic component, calculated using equation (5.69), are given in Table 5-6.

Also in this table are the predicted winding current harmonic component magnitudes that have been produced using the analysis in section 5.2.2, and the subsequent power losses due to each.

Table 5-5: Simulated values of the fundamental winding current phase angle, relative to the generator terminal voltage, and the generator output power factor.

θ	0.190rad (10.89°)
Power factor	0.9819 lagging

By comparing the power factor in Table 5-5 to that in Table 5-4, it is clear that the simulated and predicted values are similar. In addition, it can be observed from Table 5-6 that the simulated and predicted power losses in the generator windings, due to each harmonic component, are also similar; giving rise to values of total power loss in the generator windings that are much the same.

It can be concluded from this exercise that the method set out in section 5.2.2 provides a good prediction of the generator output power factor and power loss within the generator windings. The small differences that do arise are likely to be caused by the approximation of the winding currents by assuming a constant rate of change during commutation which allowed the Fourier series analysis to be simplified.

Table 5-6: Simulated and predicted winding current harmonic magnitudes and the power lost in the generator winding as a result of each.

		Simulated		Predicted	
Harmonic No.	**Freq (Hz)**	**Mag (Amps)**	**P_{Loss} (W)**	**Mag (Amps)**	**P_{Loss} (W)**
1	30.5	535.046	858.822	531.607	847.818
5	152.5	99.039	29.426	91.717	25.236
7	213.5	53.420	8.561	55.960	9.395
11	335.5	24.267	1.767	20.403	1.249
13	396.5	14.702	0.648	10.562	0.335
17	518.5	5.776	0.100	0.717	0.002
19	579.5	3.480	0.036	3.418	0.035
23	701.5	1.787	0.010	4.998	0.075
25	762.5	1.110	0.004	4.524	0.061
29	884.5	0.408	0.000	2.409	0.017
31	945.5	0.110	0.000	1.202	0.004
Total generator power loss (W)			**899.375**		**884.227**

To verify the predictions of the generator torque produced using equation (5.68), the torque waveform is reconstructed from its Fourier series and plotted alongside a trace of the generator torque taken from the model. The reconstructed torque waveform is observed, in Figure 5-17, to possess a similar average to that produced by the model; however the actual waveform shapes exhibit some differences. These differences arise as a result of the following approximations of the winding current waveform made when deriving the Fourier series: firstly, the straight line approximations of the outgoing and incoming winding currents during commutation cause the

incoming winding to begin transferring power earlier in the commutation period, since its current has a quicker rise from zero and has the larger instantaneous voltage magnitude, therefore overestimating the minimum point of the generator torque harmonic; secondly the omission of the 6th harmonic current component from the waveforms, in the periods between commutations, also omits the alternating torque component it produces, therefore underestimating the peak of the torque harmonic component. Both of these factors contribute to the underestimation of the torque harmonic magnitude shown and to that also reflected by the underestimation of the generator torque total harmonic distortion measured from the model waveform, by the THD of the Fourier series waveform; both measured from Figure 5-17 and calculated using equation (4.16) and shown in Table 5-7.

Table 5-7: Predicted and simulated total harmonic distortion of the generator torque.

Prediction	5.69%
Simulated	7.71%

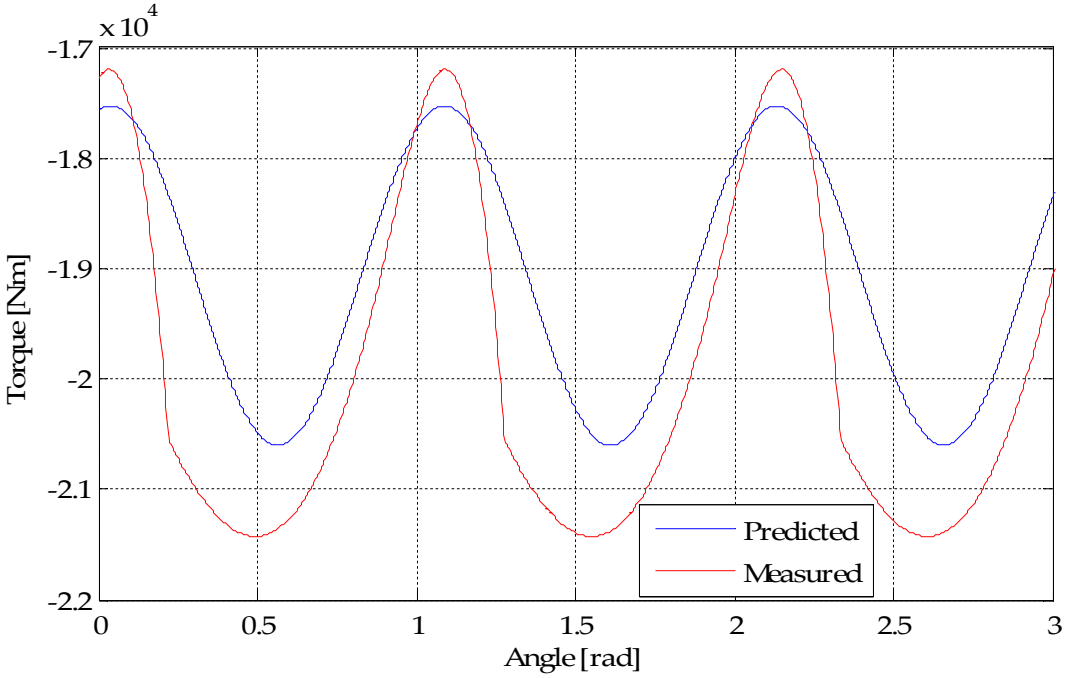

Figure 5-17: Predicted and measured simulation generator torque waveforms.

It can be concluded from these comparisons that calculating the Fourier series of the generator winding currents using the approximations made and taking into account the commutation angle of advance start and overlap length, is a valid method of predicting the generator output power factor, average torque and winding power loss. However it slightly underestimates the magnitude of the generator torque harmonic component and therefore the total harmonic distortion.

5.3 The inclusion of a step-up transformer

In this chapter so far, the rectifier has been coupled directly to the terminals of the generator and therefore the output DC voltage, which is a function of the generator terminal line to line voltage, has been of the order of 5.4kV when the generator is operating at rated rotational speed. This voltage level leads to an output current of the order of 925Amps from a single turbine when it is generating maximum power output of 5MW. When a cluster of five turbines in considered, the maximum output current from the cluster would be five times this level, which would in turn cause prohibitively high conduction losses in the cluster common output cable, if it were physically possible for a cable to conduct this much current; the maximum current carrying capacity of a subsea cable at present is approximately 2200Amps, for a cable with a conductor cross-section of 2400mm^2, designed for use in HVDC transmission schemes [3]. Therefore, to reduce the output current from each turbine to more manageable levels step-up transformers must be employed. The parameters of the transformers used are set out in Chapter 4 of this thesis and allow the increase of the voltage ten-fold, reducing the output current by the same amount.

The use of a step-up transformer between the generator and rectifier also affects the commutation process of the rectifier because the operating voltage of the rectifier is now ten-times greater than previously, the current is ten-times less and it also introduces extra impedance to the AC side of the rectifier. The process of commutation continues to occur in the same way as described in section 5.1; however these effects along with that of the transformer step-up ratio on the effective AC side impedance that governs the length the commutation overlap, must be now considered.

The relationships that link the voltages, currents and impedances across a transformer are given by equations (5.71) to (5.73) and the basic equivalent circuit of a transformer is given in Figure 5-18, comprising of the winding impedances and the parallel magnetising impedance [4]. The circuit has been simplified by referring the secondary winding impedances to the primary side using equation (5.73). (N_p, N_s, V_p, V_s, I_p, I_s, Z_{TFP} and Z_{TFS} are the primary and secondary number of winding turns, voltages, currents and impedances respectively).

$$V_p = V_s . \frac{N_p}{N_s} \tag{5.71}$$

$$I_p = I_s . \frac{N_s}{N_p} \tag{5.72}$$

$$Z_p = \frac{V_P}{V_s} = \frac{\left(V_s . \frac{N_p}{N_s}\right)}{\left(I_s . \frac{N_s}{N_p}\right)} . = Z_s . \left(\frac{N_p}{N_s}\right)^2 \tag{5.73}$$

$$Z_s = Z_p . \left(\frac{N_s}{N_P}\right)^2 \tag{5.74}$$

$$Z_{comm} = \left(Z_{TFP} + Z_{gen}\right) . \left(\frac{N_p}{N_s}\right)^2 + Z_{TFS} \tag{5.75}$$

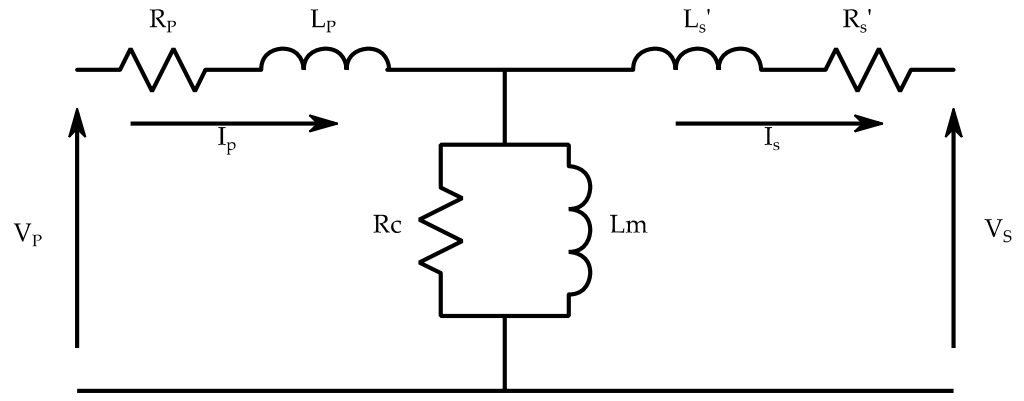

Figure 5-18: Step-up transformer circuit diagram; where the subscript, P, denotes the primary side parameters, subscript, S, denotes the secondary side parameters and R_c and L_m are the core loss and magnetising parameters [4].

In order to determine the effects of the transformer on the rectification process, which occurs on the secondary side of the transformer, the primary impedances are referred to the secondary side, using equation (5.74). The impedance on the primary side of the transformer consists not just of the transformer winding impedance but also of the generator winding impedance and the transformer parallel magnetising impedance. However, since the parallel magnetising impedance is significantly larger than the combined winding impedances, it can be neglected. Therefore the impedance that affects the commutation of the output current by the rectifier is the sum of the generator and transformer winding impedances, referred to the secondary side of the transformer, plus the transformer secondary winding impedance, as shown by equation (5.75) where Z_{TFP} and Z_{TFS} are the primary and secondary transformer winding impedances and Z_{gen} is the generator winding impedance. This impedance is now significantly larger than before the transformer was introduced, potentially prolonging the current commutation beyond the maximum length of $\frac{\pi}{3}$ radians; the increased impedance however, is offset by the reduction of the rectifier DC output current and the increase of the voltage by the transformer. Therefore, all things being equal, the length of the commutation overlap should be equal to that prior to the introduction of the transformer; however the addition of the transformer winding impedances to the generator winding impedances increases the overall AC side impedance, elongating the commutation overlap.

The phase voltages at the input to the rectifier can be determined by multiplying the generator terminal voltages by the transformer step-up ratio; this allows the rectifier DC output voltage and commutation overlap distortion to be determined by the process set out in section 5.1.

Comparing Figure 5-19 with Figure 5-10, before and after the transformer is included, shows that the commutation overlap is longer where the transformer in present, 0.5724rad as opposed to 0.378rad as expected.

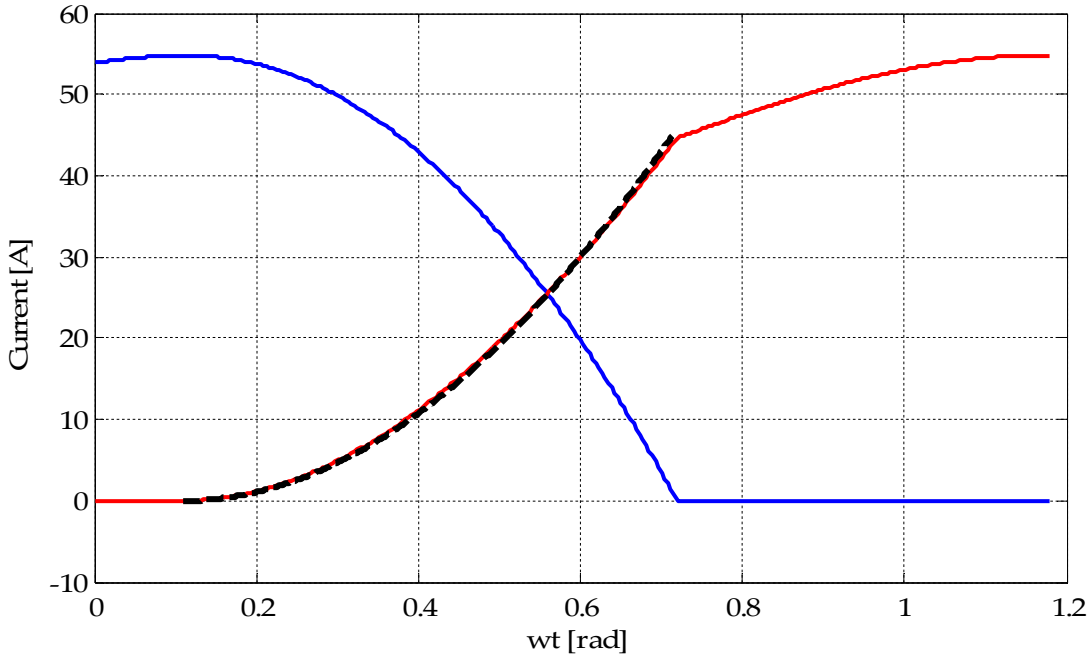

Figure 5-19: Measured simulation rectifier AC side phase current (blue and red lines) where the transformer is included and the predicted incoming phase current (dashed black line).

5.4 Cluster controller operating curve

In the previous chapter, the design of the cluster controller was discussed; noting that knowledge of the drop in voltage between the generators and the point of common coupling is important to ensuring the cluster converter voltage is such that the turbine rotational speeds are optimal for the wind conditions. The voltage drop is made up of two components: the voltage drop across the cable resistive elements and the commutation voltage drop. These voltage drops must be accounted for within the control curve which links the instantaneous converter output voltage to the expected power output of the cluster, used as the reference power in the controller.

The control curve for the cluster can be determined using the known parameters of the generators, cables and wind turbine rotor and the resulting curve fed into the controller as a look-up table. To produce the operating curve an algorithm has been developed which predicts the power output of the cluster across the full range of operating wind speeds by assuming the turbines are operating with optimal tip-speed ratios and therefore capturing power from the wind at maximum efficiency.

The use of a single converter to control multiple wind turbines means that the controller acts as if the cluster is a single large turbine, with an output equal to the aggregate of the individual turbine outputs. The control curve is therefore produced by calculating the power output of this large turbine across the wind speed operating range using the optimal tip-speed ratio. This also allows the optimal rotational speed of the turbine for each operating wind speed to be determined; which, by the process outlined in section 5.1, can be used to determine the DC voltage required at the rectifier output terminals to achieve it. Knowledge of the required rectifier terminal

voltage also allows the common point voltage and cluster converter voltage to be determined by subtracting the cable resistive voltage drops. The cluster converter voltage is limited to a value which allows the turbine speed to remain optimal up until the maximum cluster output power is achieved; thereafter holding the rotational speed constant while the turbine pitch system (not modelled here) acts to hold the power captured by each turbine constant at the maximum value.

The measured cluster output power is effectively a measurement of the average wind conditions across the cluster. The cluster control curve therefore allows the controller to compare the measured cluster power output to the power output it expects for the instantaneous cluster voltage. The result of this comparison tells the controller whether or not the current operating voltage is appropriate for the current wind conditions. If it is not appropriate the measured and expected (reference) powers will not match and the controller will act to correct the cluster voltage. The design of the cluster controller was discussed in Chapter 4 of this thesis and is shown again in Figure 5-20.

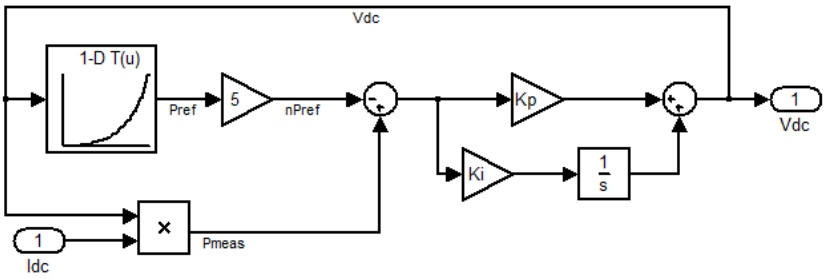

Figure 5-20: Cluster controller block diagram.

Although the controller acts as if the cluster of turbines is a single large wind turbine, the actual individual turbine speeds will vary about the operating point set by the controller according to their individual wind speeds. The

amount by which the rotational speed of each turbine will vary about the common point voltage is related to the variation of the commutation and resistive voltage drops, which are both functions of the power output of each individual turbine, giving rise to the slip between the generators.

5.4.1 Control curve algorithm

The operating curve of the cluster is dependent upon the relationship between the rectifier DC output voltage, the generator rotational speed and output power. To produce this curve the DC output current, the subsequent length of the commutation overlap and the power lost within the generator, transformer and cables must be determined. These aspects are interdependent because the currents are functions of the voltages and the voltages are functions of the currents; therefore an iterative approach is required.

The main steps to produce the control curve are as follows, the initial steps are conducted by focusing on a single turbine (Figure 5-22 shows the process in a flow diagram and the Matlab script implementation of the algorithm is included in Appendix A):

1. Determine the rotational speed and power captured by the wind turbine for each wind speed over the turbine operating range, assuming that the tip-speed ratio is optimal and the turbine is operating with the maximum power coefficient.

Using the calculated power values, the following iterative process for each rotational speed operating point can be conducted:

2. Calculate the rectifier average output voltage by assuming the AC side resistances and the commutation overlap distortion have no impact, using the analysis in section 5.1.

3. Determine the DC output current using the power captured from the wind, calculated in step 1, and the average DC voltage calculated in step 2.
4. Calculate the length of the commutation overlap and re-calculate the rectifier average DC output voltage.
5. Determine the magnitude of each winding current harmonic component that results from the commutation process using the commutation advance start and length angles calculated in step 4, using the analysis in section 5.2.
6. Calculate the power lost in the generator and transformer winding resistances due to each current harmonic component, using the analysis in section 5.2.
7. Re-calculate the DC output current using the power captured minus the winding losses.

Steps 3 to 7 should be repeated and the difference between the output current calculated in the present and previous iterations determined. Over a number of iterations the difference should fall as they converge. Once the difference has fallen below $1x10^{-6}$, the iteration process can cease and the values of DC output current, rectifier DC voltage and the losses produced by the last iteration can be taken as outputs. ($1x10^{-6}$ is an arbitrary number, but one that is small enough to ensure that the quantities calculated are accurate to several decimal places).

The calculated values of the DC output current, generator and transformer winding losses and the rectifier DC output voltage can then be used to determine the voltage drops through the branch cables from the turbines to the point of common coupling and also the conduction losses.

By assuming that each turbine in the cluster is producing the same output, the voltage drop and losses in the cluster common output cable can be determined by multiplying the output current by the number of turbines in the cluster (five). Therefore predictions of the required cluster converter voltage to allow the turbines to rotate at the optimum speed for each wind speed in the operating range can be produced along with predictions of the output power from the cluster. The resulting control curve that is produced linking the instantaneous cluster converter voltage with the expected power output from the cluster is shown in Figure 5-21.

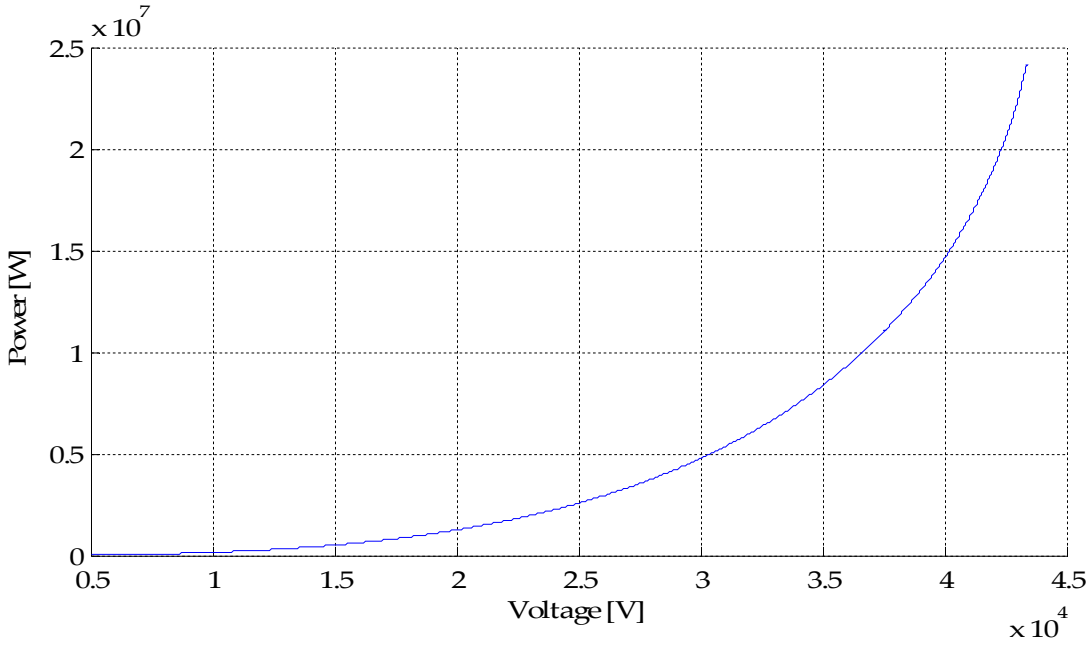

Figure 5-21: Control curve of the cluster linking the DC converter output voltage to the measured cluster output power.

The algorithm developed here to determine the cluster control curve also allows for the relationship between the wind speed incident on a turbine and predictions of the commutation overlap length, the commutation advance angle, the slip between the cluster synchronous speed and the turbine rotational speeds and the generator power factor to be determined, as shown in Figure 5-23, Figure 5-24, Figure 5-25 and Figure 5-26. These relationships

are produced over only the first half of the operational wind range of the turbines because beyond the rated wind speed of the turbines, approx. 11.5m/s, the electrical power output and rotational speed of the turbines are held constant by the turbine pitch control.

Figure 5-23 and Figure 5-24 show that both the length of the commutation and the angle of commutation advance start increase with wind speed and the subsequent increase in turbine power output. It is also shown by Figure 5-25 that the slip between the turbine and cluster synchronous speed, derived from the voltage at the cluster common point, increases with the turbine output and that almost 30% slip can be achieved at maximum turbine output power. Finally Figure 5-26 shows that the generator output power factor decreases with wind speed as a result of increasing length of the commutation overlap, causing the rectifier to absorb larger amounts of reactive power.

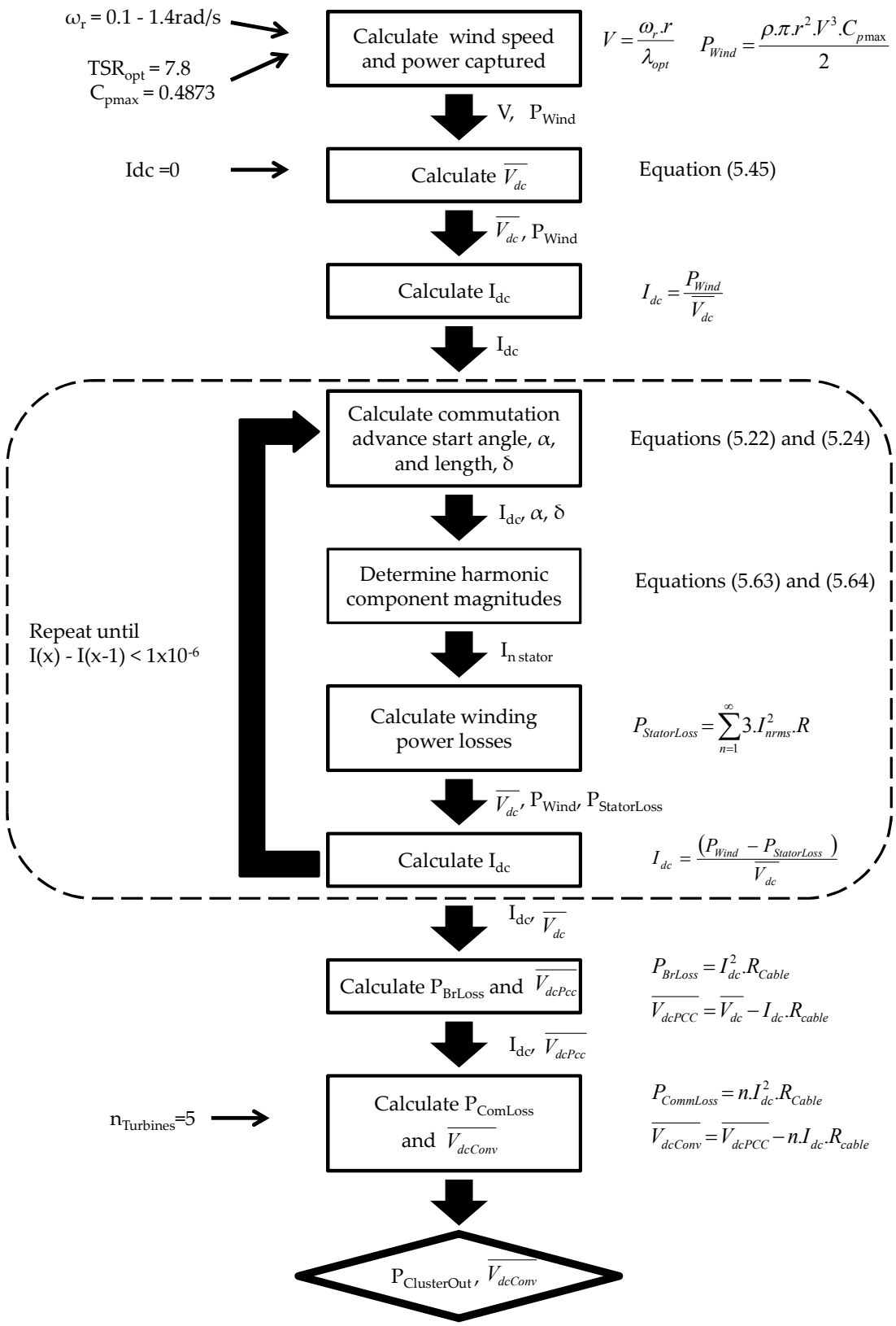

Figure 5-22: Flow diagram of the algorithm that produces the cluster control curve.

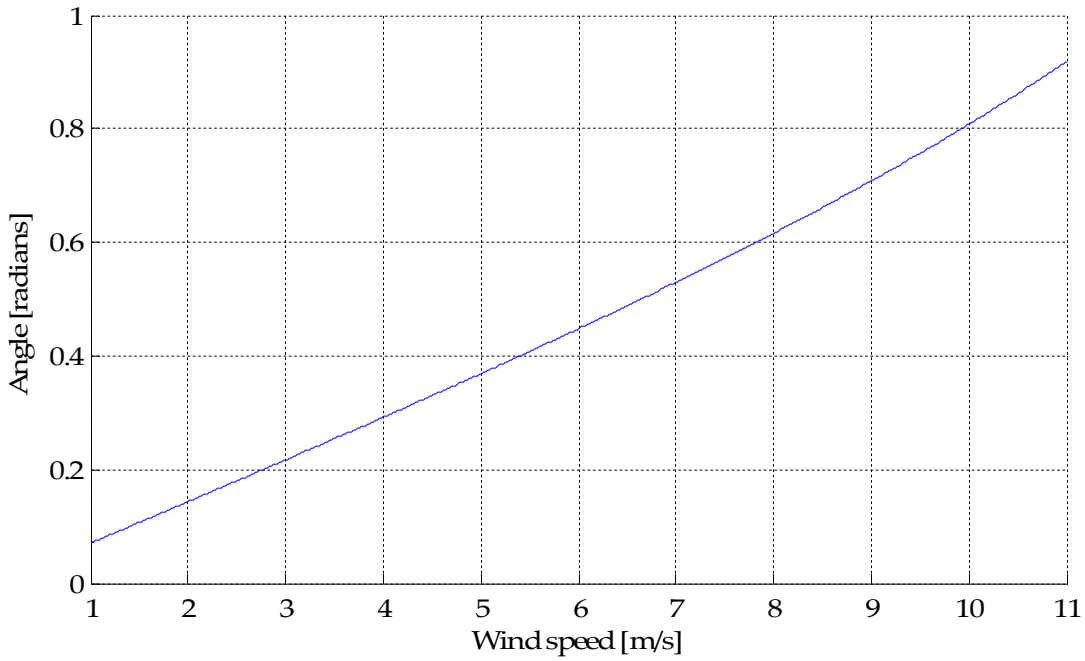

Figure 5-23: Length of the rectifier commutation overlap with incident wind speed.

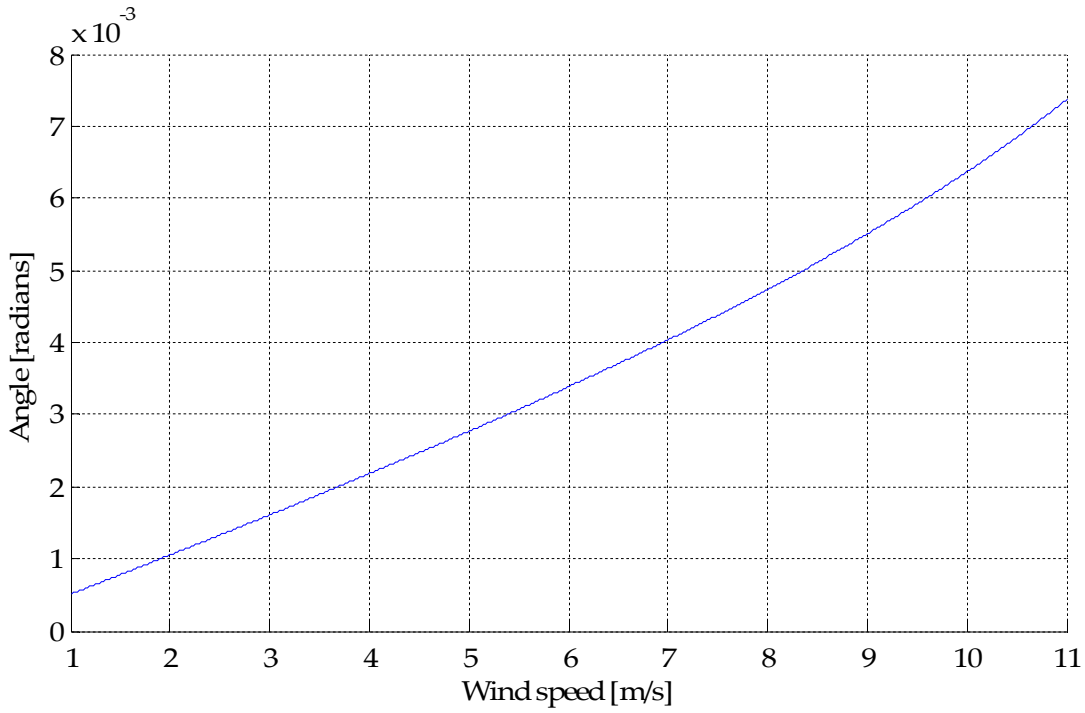

Figure 5-24: Commutation advance start angle with the incident wind speed.

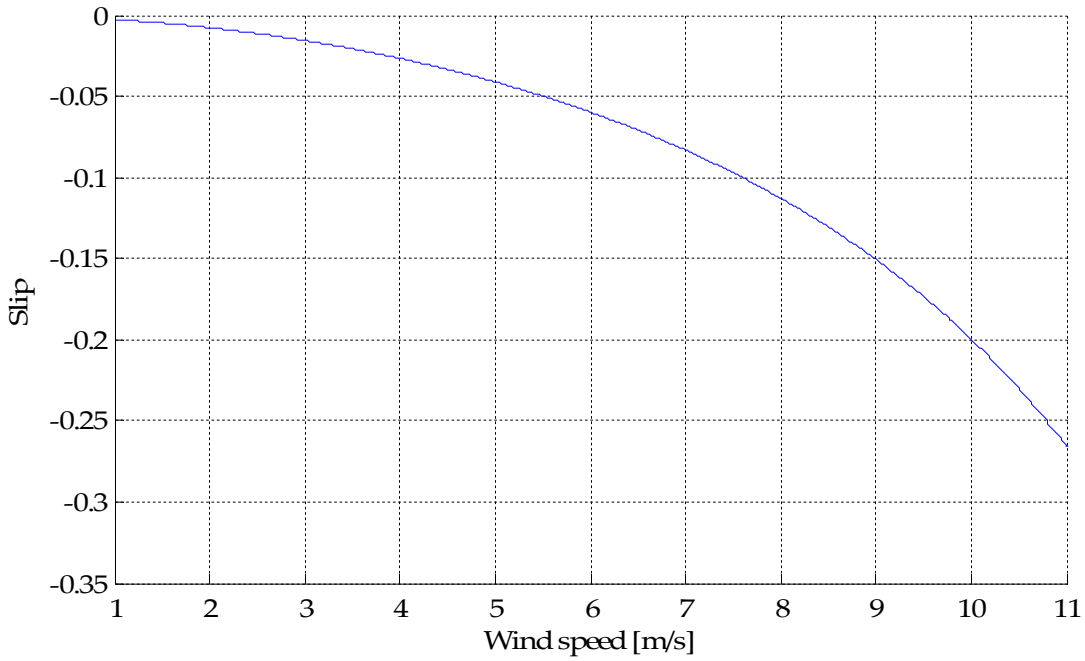

Figure 5-25: Generator slip with incident wind speed.

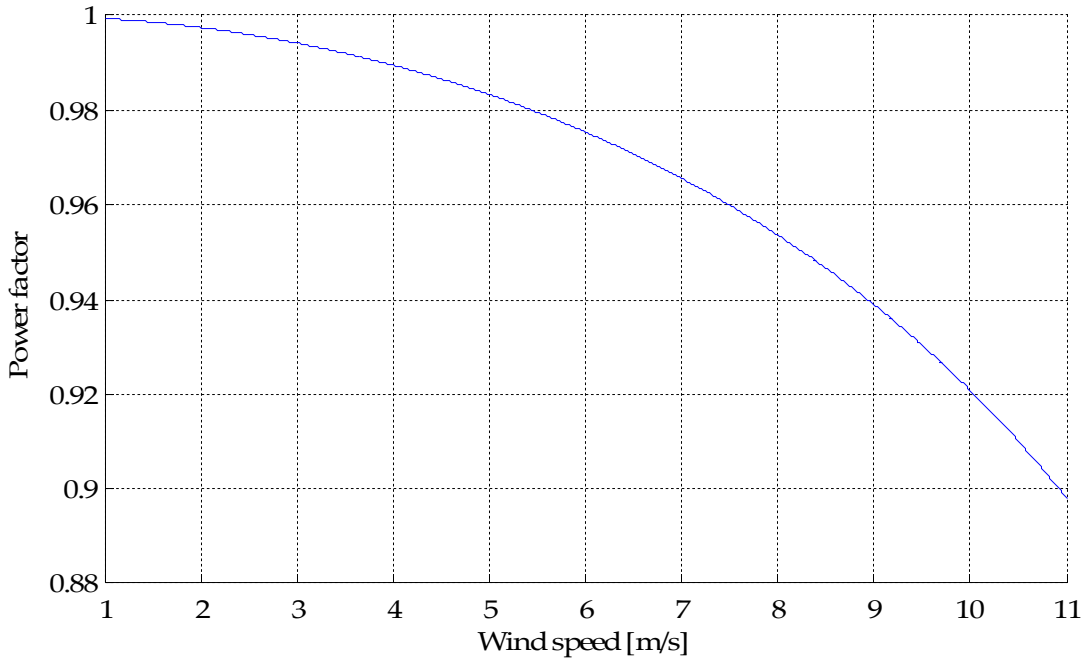

Figure 5-26: Lagging generator power factor with incident wind speed.

5.5 Simplified representation of a cluster electrical system

The analysis conducted so far in this chapter has set out the principles upon which a cluster of wind turbines, based on PM generators with rectified outputs and a multi-terminal DC network, operates; in particular the presence of the commutation overlap, the resulting distortion of the generator terminal voltages and the associated average DC voltage drop have been discussed. The understanding gained of the average DC voltage drop allows its magnitude to be predicted as a function of the turbine power output and the electrical frequency, which is directly related to the rotational speed. The ability to predict the magnitude of the average voltage drop allows a simplified representation of the system to be formed, where the detail surrounding the action of the rectifier can be removed. In particular, the simplified system allows the harmonics introduced to the generator and DC currents and voltages to be removed, along with the harmonic component introduced to the generator torque and as a consequence the general behaviour of the turbines can be observed with greater clarity.

The simplification of the electrical system is achieved by representing the PM generator, the rectifier and its associated voltage drop by an equivalent DC generator. The characteristic equations of such a generator that relate its rotational speed to its output DC voltage, before the commutation voltage drop is considered, and the generator torque to its output current are given by equations (5.76) and (5.77); a diagram of the simplified system is also given in Figure 5-27.

The average voltage drop introduced by the rectifier commutation occurs without the corresponding power loss that would be associated with a resistive voltage drop; therefore to include it in the simplified representation

of the system it must take the form of a voltage source in opposition to the DC generator output, as shown in Figure 5-27. The system can be further simplified by combining the generator output and the commutation voltage drop, as shown in Figure 5-28, where the generator output voltage is given by equation (5.78).

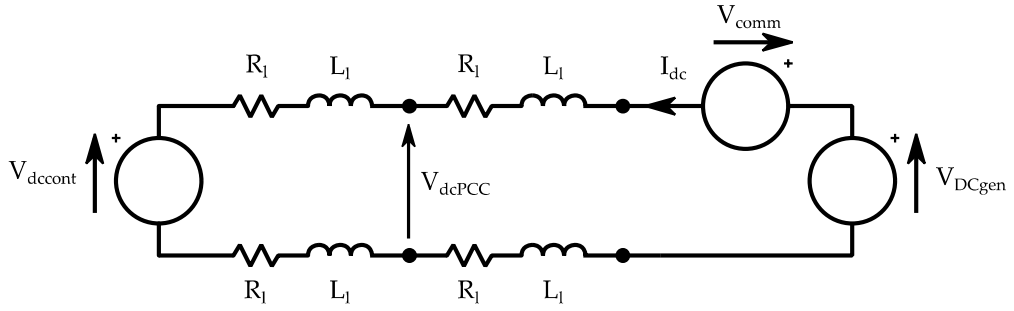

Figure 5-27: Circuit diagram of the simplified system model where V_{comm} is shown as a voltage source in opposition to V_{dcgen}.

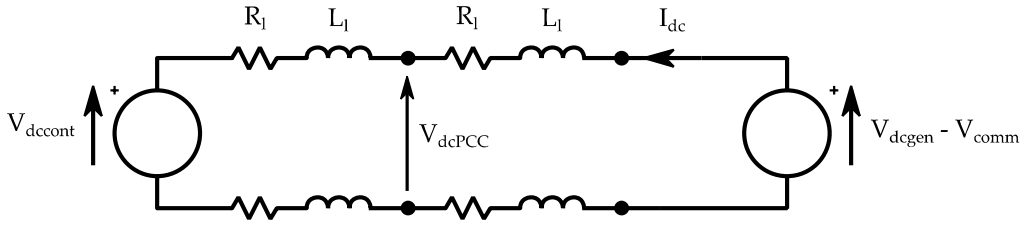

Figure 5-28: Circuit diagram of the simplified system model where V_{comm} is combined with V_{dcgen}.

The rectifier commutation voltage drop has been proven to be a function of the DC output current and the electrical frequency of the PM generator output by equation (5.33); therefore to include it in the simplified model it must be able to change with the operating point of the generator. By assuming that the rotational speed of the generator is always optimised for the current wind speed, a characteristic between the commutation voltage drop and the DC output current can be formed by the same process that produces the cluster control curve, set out in the previous section; Figure 5-29 shows this relationship across the operating output current range for a single

turbine. The assumption that the turbine is operating with the optimal rotational speed for the wind speed conditions allows the corresponding rotational speed to each level of output current to be known and therefore taken into account when producing the characteristic in Figure 5-29.

The remainder of the simplified model, including the DC cables and the DC converter, are exactly the same as those in the full model of the system. Therefore the action of the cluster controller to regulate the voltages in the system and the rotational speeds of the turbines will match the action where the actual generator and rectifier are present.

$$V_{DCgen} = \frac{3.\sqrt{3}.\Psi_f \omega_{gen}.p}{\pi} \tag{5.76}$$

$$T_{gen} = \frac{3.\sqrt{3}.\Psi_f.I_{dc}.p}{\pi} \tag{5.77}$$

$$V_{DCgen} = \frac{3.\sqrt{3}.\Psi_f \omega_{gen}.p}{\pi} - V_{comm} \tag{5.78}$$

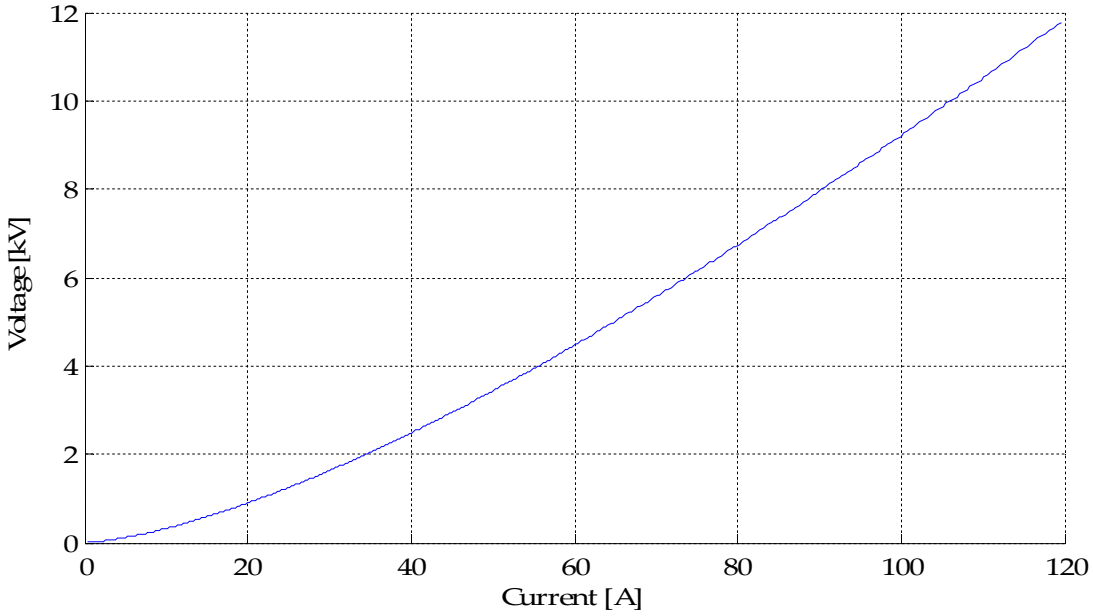

Figure 5-29: Commutation voltage drop with DC output current characteristic.

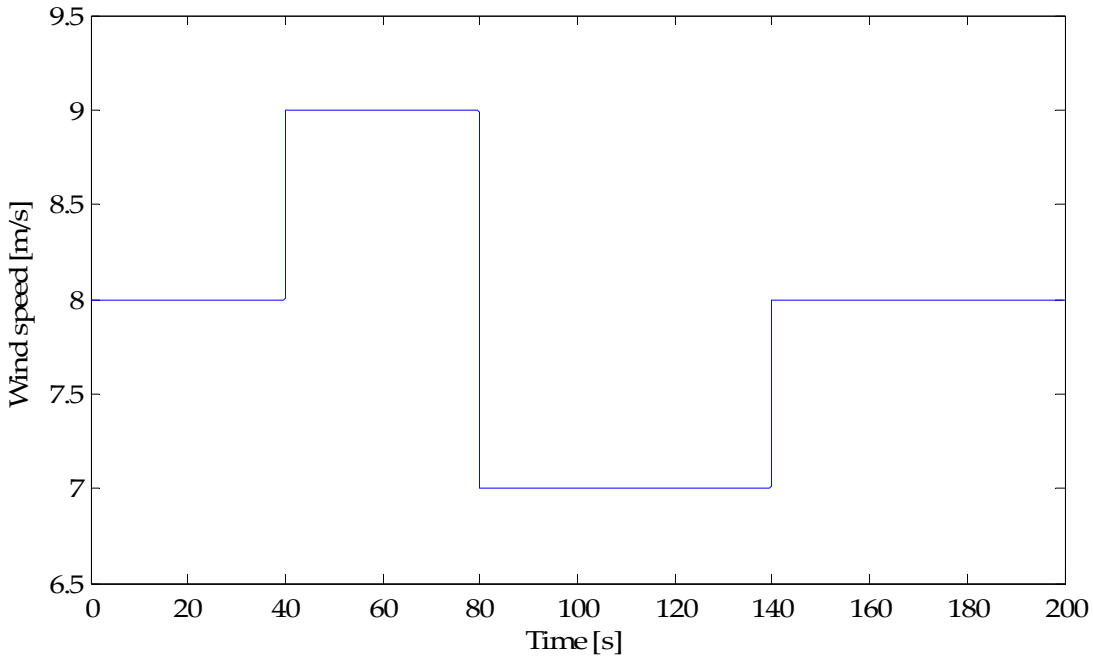

Figure 5-30: Wind speed step changes used for verification of the simplified model with the full system model.

To verify the operation of the simplified model with that of the full system model, both have been reduced to include only a single turbine and are simulated with the wind conditions shown in Figure 5-30.

It is shown in Figure 5-31 that the rotational speed of the turbines in either model are very similar, as are the cluster converter voltages shown in Figure 5-32. When comparing the output voltage of the equivalent generator, in the simplified model, with the rectifier output voltage, in the full system model in Figure 5-33, it is also observed that the averages of both are similar; however the rectifier output voltage also incorporates the harmonics described previously. The same is true of the power output and generator torques in either case, shown by Figure 5-34 and Figure 5-35, where the averages are similar but the waveforms from the full system model also include the high frequency harmonics. It can be concluded from this comparison that the simplified model provides a good approximation of the system.

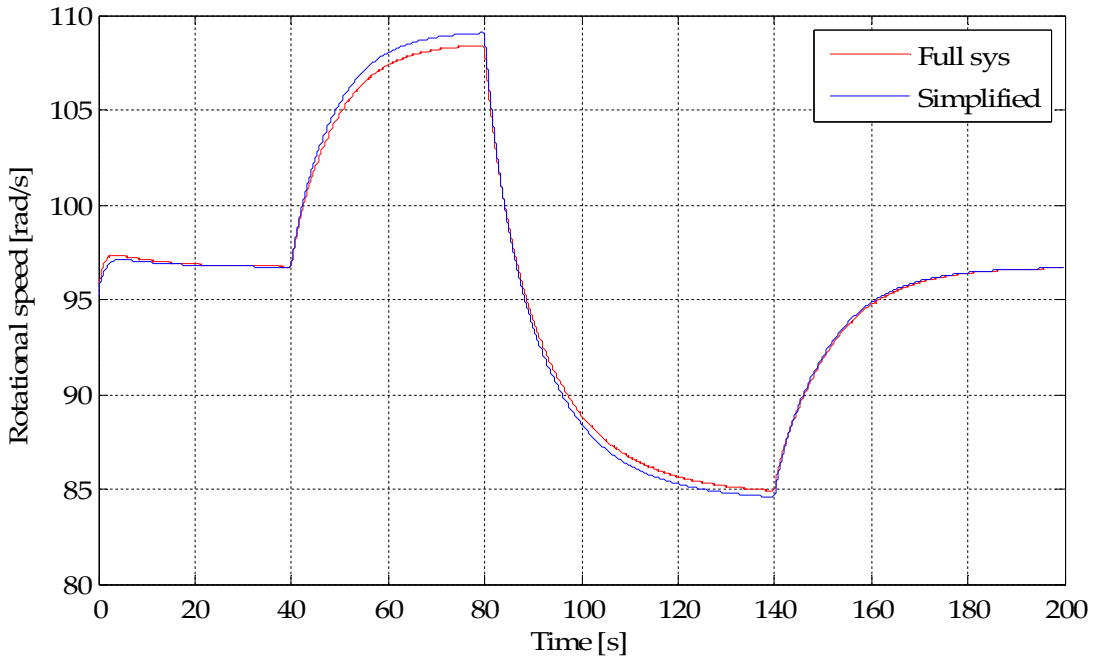

Figure 5-31: Rotational speeds of the generators in the simplified and full system models in response to the wind conditions in Figure 5-30.

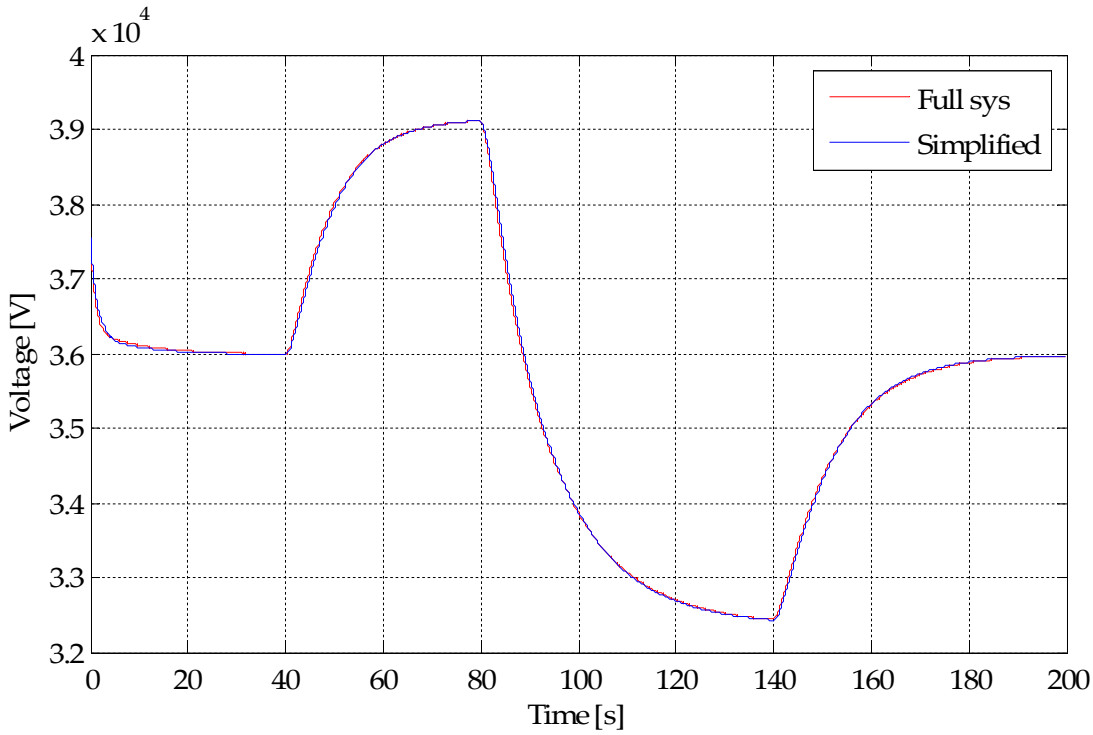

Figure 5-32: Cluster converter voltages in the simplified and full system model in response to the wind conditions in Figure 5-30.

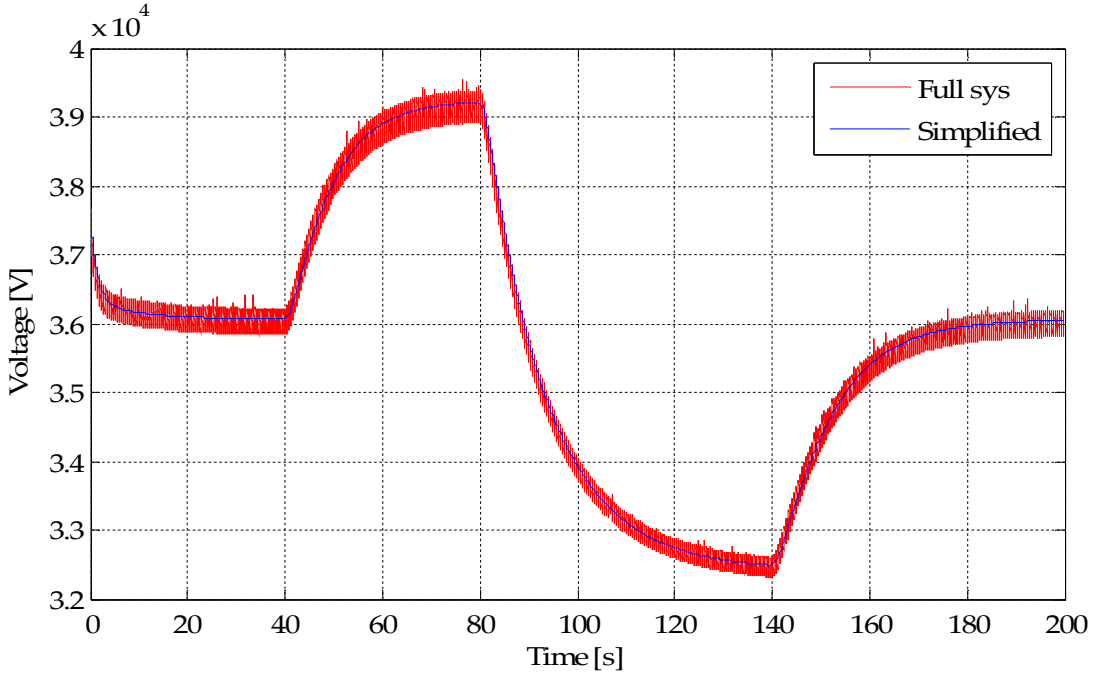

Figure 5-33: Output voltage of the equivalent generator in the simplified model and the DC rectifier output voltage in the full system model, in response to the wind conditions in Figure 5-30.

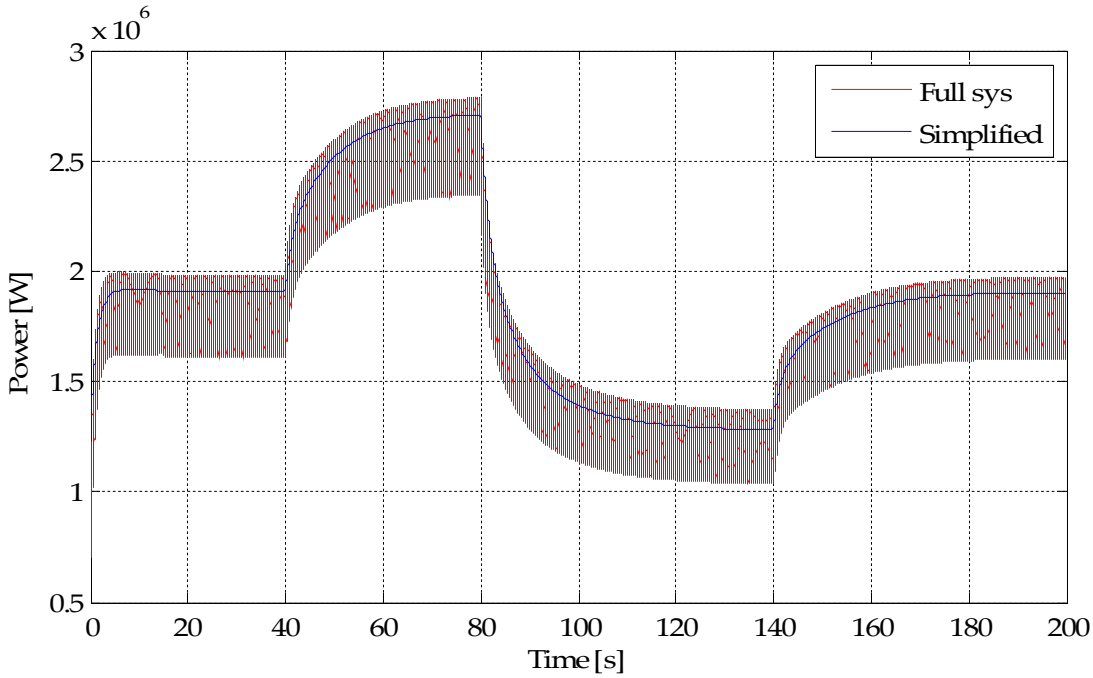

Figure 5-34: Cluster power output from both the simplified and full system models in response to the wind conditions in Figure 5-30.

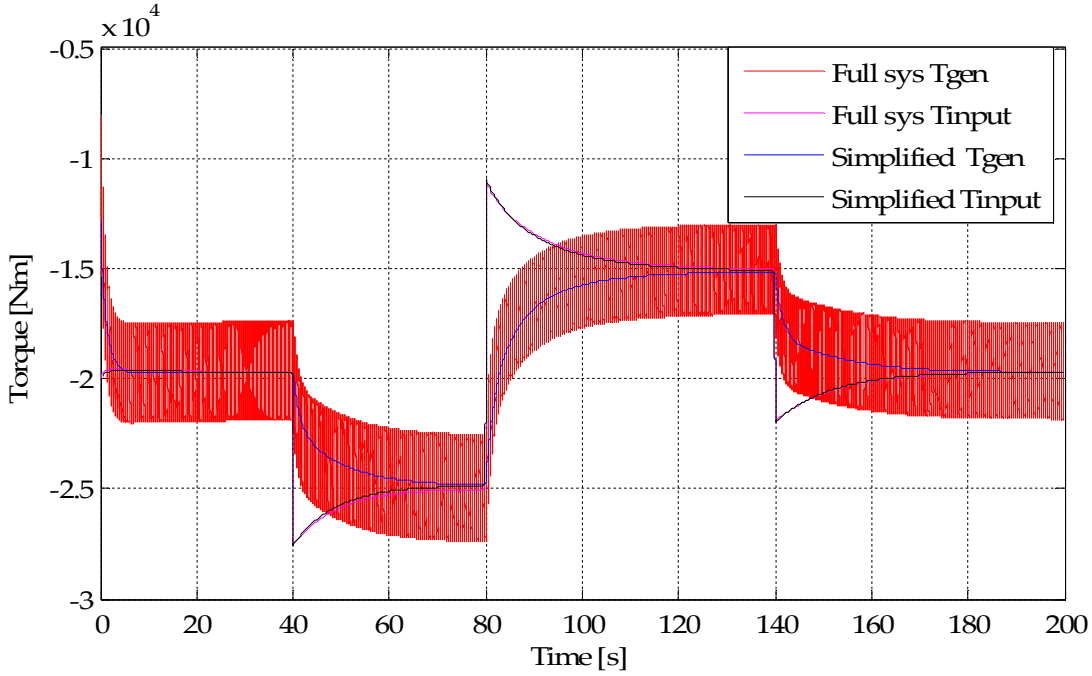

Figure 5-35: Input and generator torques for the simplified and full system models in response to the wind conditions in Figure 5-30.

5.6 References

1. Mohan, N., T.M. Undeland, and W. Robbins, *Power Electronics - Converters, Applications and Design*. 3rd ed2003: John Wiley & Sons.
2. Kimbark, E.W., *Direct current transmission*. Vol. 1. 1971: Wiley-Interscience.
3. ABB, *Its time to connect - Technical description of HVDC light technology*, 2008.
4. J. Duncan. Glover, M.S.S., *Power System Analysis and Design*. 3rd ed2001: Brooks / Cole.

Chapter 6 Optimal Operation of a Cluster of Turbines

The operation of a wind turbine can be regarded as optimal when it is extracting the maximum amount of power from the instantaneous wind conditions, for the lowest cost; where the costs are of a physical nature caused by the stress and fatigue placed on the various system components during operation. To optimise the operation of a group of wind turbines, electrically connected in a cluster, both the capability of each turbine to extract the maximum amount of power from the wind and its ability to alleviate mechanical stresses on the turbine drive train must be investigated. To investigate these aspects of the clustered electrical system, with the system characteristics highlighted so far in this thesis, the following questions are asked:

- How much generator slip can be achieved and what is the best way of achieving it?
- How much generator slip is required for achieving the optimal operation of the individual turbines?
- What effect does the collective control of the wind turbines have on their ability to achieve optimal operation?

The provision of a considerable amount of generator slip is a significant benefit of the preferred clustering technology over the other two possible technologies studied in Chapter 4. The generator slip allows a degree of independence between the turbines which is important so that their rotational speeds can follow their local wind conditions. In the previous chapter the process of rectifier commutation was investigated, in particular the voltage drop caused by the commutation overlap. This voltage drop is one of two potential methods of achieving the generator slip; the second method requires the addition of extra resistance between the rectifier terminals and the cluster common point. To determine the viability of both methods, the capability of each and the associated side effects will be investigated.

Secondly, an assessment of the amount of generator slip that is required to allow the turbines to achieve optimal operation, in wind conditions representative of reality, will be conducted. The metrics upon which this assessment will be based include: the ability of the individual turbines to maximise the amount of power extracted from the wind, therefore maximising overall cluster output, and the ability of the cluster electrical system to provide damping to the mechanical drive train of the wind

turbines, therefore preventing the oscillation of the different mechanical components causing irreparable damage.

Lastly, investigations into the impact of operating a group of turbines as a cluster will be conducted; in particular investigating the effects of controlling the turbines collectively and investigating the effects of interactions between the turbines that occur as a result of their parallel connection.

This chapter will answer these questions by further investigating the capability of the system to provide generator slip and the secondary effects of doing so, by assessing how much slip is required by each turbine to maximise its power capture from the wind, and by determining the effects of controlling the turbines collectively.

6.1 How much slip can be achieved and how?

Earlier in this thesis the importance of the direct relationship between the generator slip capability and the voltage difference between the generator and cluster common point was introduced. This relationship occurs as a result of the proportionality of a PM generator's emf and its rotational speed. The larger the voltage difference between the generator and the cluster common point, the further the generator rotational speed can slip from the cluster synchronous speed.

A voltage difference between the generator and the cluster common point can be achieved in two ways: by the rectifier commutation voltage drop, or by the addition of extra resistance. The merits and pitfalls of each of these methods will be investigated in this section.

6.1.1 The limits of the commutation voltage drop

To assess the viability of using the commutation voltage drop to provide the generator slip, first of all the maximum amount of voltage drop that can be achieved must be determined. The commutation voltage drop is a function of the length of the rectifier commutation overlap, which itself is a function of the generator output current, the generator stator winding impedance and the rotational speed of the generator. The use of a rectifier with a three phase PM generator causes the current to commutate between generator windings six times per cycle; therefore the absolute maximum commutation length that can be achieved is $\pi/3$ radians, which therefore dictates the maximum voltage drop that can be achieved.

The analysis set out in section 5.1 allows the commutation voltage drop to be determined with and without the influence of the generator winding resistance. In the case studied here the generator winding resistance is ignored. The maximum commutation voltage drop is therefore determined by taking the average of equation (5.30), where the commutation length, δ, is equal to π/3 radians, and is therefore a function of the generator emf only, as shown by equation (6.1).

$$\Delta\overline{V_{dc}} = \frac{3.\sqrt{3}.E}{2\pi}(1-\cos\delta) = \frac{3.\sqrt{3}.E}{4\pi} \tag{6.1}$$

The maximum commutation voltage drop, as a proportion of the ideal rectifier average output voltage, where there is no commutation overlap, is found to be 25% by equation (6.3), where:

$$\overline{V_{dc}} = \frac{3}{\pi}[V_b - V_c] = \frac{3}{\pi}\left[\int_0^{\frac{\pi}{3}} \sqrt{3}.E.\cos(\omega t - \frac{\pi}{3})\, d\omega t\right] = \frac{3.\sqrt{3}.E}{\pi} \tag{6.2}$$

$$\frac{\Delta\overline{V_{dc}}}{\overline{V_{dc}}} = \frac{\left(\frac{3.\sqrt{3}.E}{4\pi}\right)}{\left(\frac{3.\sqrt{3}.E}{\pi}\right)} = \mathbf{\frac{1}{4}} \tag{6.3}$$

Figure 6-1 shows the extent of the rectifier output voltage distortion caused by maximising the commutation overlap, as well as the effect on the average rectifier output voltage.

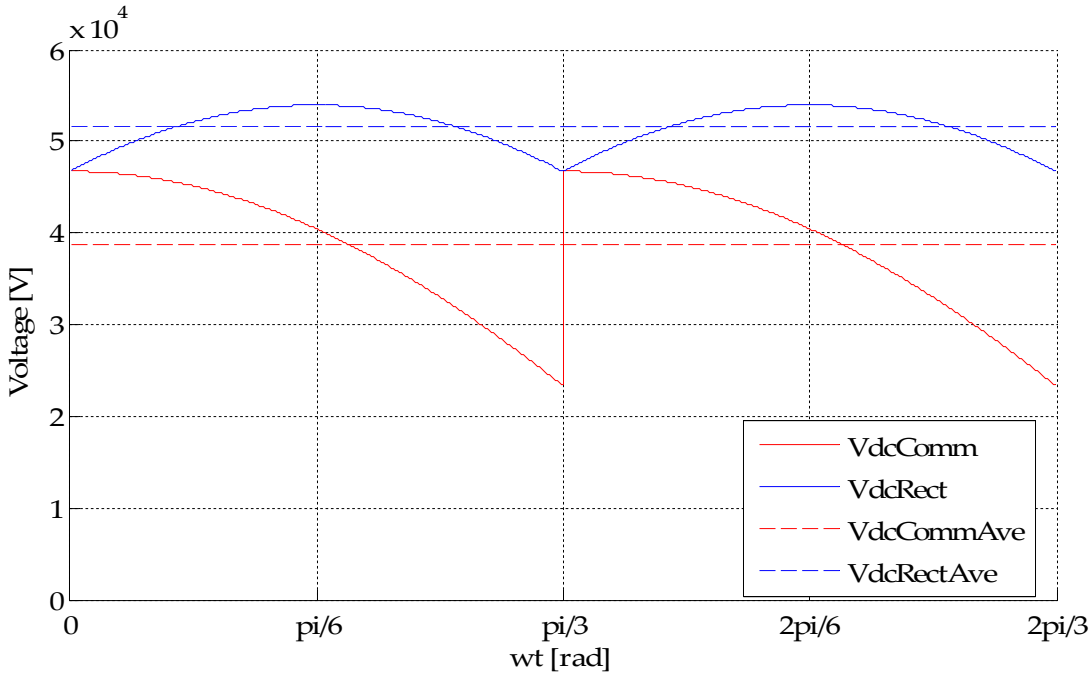

Figure 6-1: Rectifier DC output voltage waveforms with (red lines) and without (blue lines) the distortion caused by the commutation overlap, and their associated averages (dashed lines).

The maximum commutation voltage drop that can be achieved using the generator parameters set out in the earlier chapters of this thesis, taking into consideration the presence of the step-up transformer, where the turbine is rotating at the optimum rotational speed for maximum power production (132.2rad/s) is given by (6.4).

$$\Delta\overline{V_{dc}} = \frac{3.\sqrt{3}.E}{2\pi}(1-\cos\delta) = \mathbf{13,841.1\ V} \tag{6.4}$$

The generator slip that results from the maximisation of the commutation voltage drop can be determined as follows (ignoring the cable resistive voltage drop since it is negligible in comparison):

$$slip = \frac{\omega_{sync} - \omega_{gen}}{\omega_{sync}} \tag{6.5}$$

Where the cluster synchronous speed is derived from the average voltage at the cluster common point, $\overline{V_{PCC}}$, by rearranging equation (6.2) and using the relationship between the emf, E, and rotational speed of a PM generator in equation (6.6), as shown by equation (6.7); where N_t is the transformer step-up ratio, Ψ_f is the generator flux constant, and p = the number of generator pole pairs.

$$E = \Psi_f . p . N_t . \omega \tag{6.6}$$

$$\omega_{sync} = \frac{\overline{V_{PCC}} . \pi}{3 . \sqrt{3} . E_{sync}} = \frac{\overline{V_{PCC}} . \pi}{3 . \sqrt{3} . \Psi_f . p . N_t} \tag{6.7}$$

The generator rotational speed can also be written as a function of the rectifier output voltage, before the commutation distortion is considered in equation (6.2):

$$\omega_{gen} = \frac{\overline{V_{dc}} . \pi}{3 . \sqrt{3} . E_{gen}} = \frac{\overline{V_{dc}} . \pi}{3 . \sqrt{3} . \Psi_f . p . N_t} \tag{6.8}$$

Therefore substituting equations (6.7) and (6.8) into (6.5) allows the slip to be determined in terms of the common point voltage and the rectifier output voltage.

$$slip = \frac{\overline{\overline{V_{pcc}}} - \overline{V_{dc}}}{\overline{V_{pcc}}} \tag{6.9}$$

The voltage difference between the generator and the common point, neglecting the cable resistance, is therefore solely a result of the commutation voltage drop; and the average voltage at the cluster common point, as a function of the generator emf and the commutation length, can be found by subtracting equation (6.1) from equation (6.2) as follows:

$$\overline{V_{pcc}} = \frac{3.\sqrt{3}.E}{\pi} - \frac{3.\sqrt{3}.E}{4\pi} = \frac{9.\sqrt{3}.E}{4.\pi} \tag{6.10}$$

Therefore by substituting equation (6.10) and (6.2) in to equation (6.9), the maximum amount of slip that can be achieved by maximising the commutation voltage drop is found to be 33.33%, by equation (6.11).

$$slip = \frac{\overline{\frac{9.\sqrt{3}.E}{4.\pi}} - \frac{3.\sqrt{3}.E}{\pi}}{\frac{9.\sqrt{3}.E}{4.\pi}} = -\mathbf{\frac{1}{3}} \tag{6.11}$$

In order for the generator in a wind turbine to achieve this level of slip, the generator winding impedance, output current and rotational speed must be optimised to allow the maximum commutation length to occur. The rotational speed of the generator however is constrained by the requirement for the turbine to rotate at the optimal speed for maximum energy capture from the wind, and the current will fluctuate with the power output; therefore the only remaining variable that can be optimised is the generator winding inductance. The winding inductance must therefore be optimised for when the turbine is producing maximum output power and rotating at maximum speed. To determine the level of winding inductance that allows this to occur, the analysis set-out in section 5.1 can again be applied.

Equation (5.15) gives the commutation length as a function of the generator DC output current, winding inductance, emf and rotational speed. By rearranging this equation and substituting in the maximum generator rotational speed, the maximum emf and the output current that allows it to generate its maximum power, it can be solved to find the winding inductance at which the commutation length is maximised. In actual fact by substituting equation (6.6) into (5.15) the optimum inductance becomes a

function of the generator output current only, as shown in equation (6.12); noting that ω in equation (5.15) is the electrical frequency which is the rotational speed multiplied by the number of pole pairs, p, in the generator.

$$L = \frac{\sqrt{3}.\Psi_f.N_t.(1-\cos\delta)}{2.I_{dc}} \tag{6.12}$$

However, the output current is still a function of the total output power and the rectifier output voltage. Therefore the output current from the generator when it is producing maximum power (5MW) and rotating at its maximum speed (132.1rad/s) must be calculated in advance, using equation (6.13), by neglecting the cable resistance and assuming the rectifier terminal voltage that drives the output current is equal to the common point voltage given by equation (6.10).

$$I_{dc} = \frac{P_{out}}{\overline{V_{PCC}}} = \frac{P_{out}.4.\pi}{9.\sqrt{3}.E} = \frac{P_{out}.4.\pi}{9.\sqrt{3}.\Psi_f.p.N_t.\omega_{max}} = \mathbf{120.42A} \tag{6.13}$$

Therefore the generator winding inductance, required to maximise the commutation length and voltage drop when the turbine is operating at full output can be determined using equation (6.12) as follows:

$$L_s = \frac{\sqrt{3}.\Psi_f N_t.}{4.I_{dc}} = \mathbf{0.456H} \tag{6.14}$$

This value appears to be very large; but it should be noted that this is the generator winding inductance referred to the secondary, high voltage, side of the step-up transformer. The actual generator winding inductance is determined by referring this value back to the primary side of the transformer using equation (6.15), giving a much more realistic result, as follows:

$$L_p = \frac{L_s}{N_t^2} = \mathbf{4.56mH} \tag{6.15}$$

Conclusions

So far in this section, the inductance involved in the commutation process has been referred to as the generator stator winding inductance; however in actual fact this inductance can be the sum the generator winding inductance and the transformer winding inductance, and indeed an additional inductive choke could be included between the generator and the transformer. The combined primary side inductance of the generator and transformer windings used in the system models developed so far in this thesis is 3.9mH, therefore the inductance which is naturally in the system is not too far from the inductance required to maximise the commutation length and voltage drop.

When the turbine is operating in wind conditions that do not allow it to produce its maximum power output, the commutation length will be shorter and therefore the commutation voltage drop smaller. Figure 6-2 and Figure 6-3 show the commutation length and voltage drop respectively over the lower half of the wind turbine operating wind speed range, where the turbine produces less than its maximum power output. It can clearly be observed that, even though the generator parameters are chosen to maximise the commutation length and generator slip at full power output, when the turbine output is less than the maximum the generator slip will be significantly smaller. Therefore a drawback of using the commutation voltage drop to produce the generator slip is that it can only be maximised when the turbine is producing its maximum output, and when the output is less than the maximum the generator slip is somewhat smaller. This should

be contrasted however with the fact that it does not involve the same power loss as that is associated with a resistive voltage drop of the same magnitude.

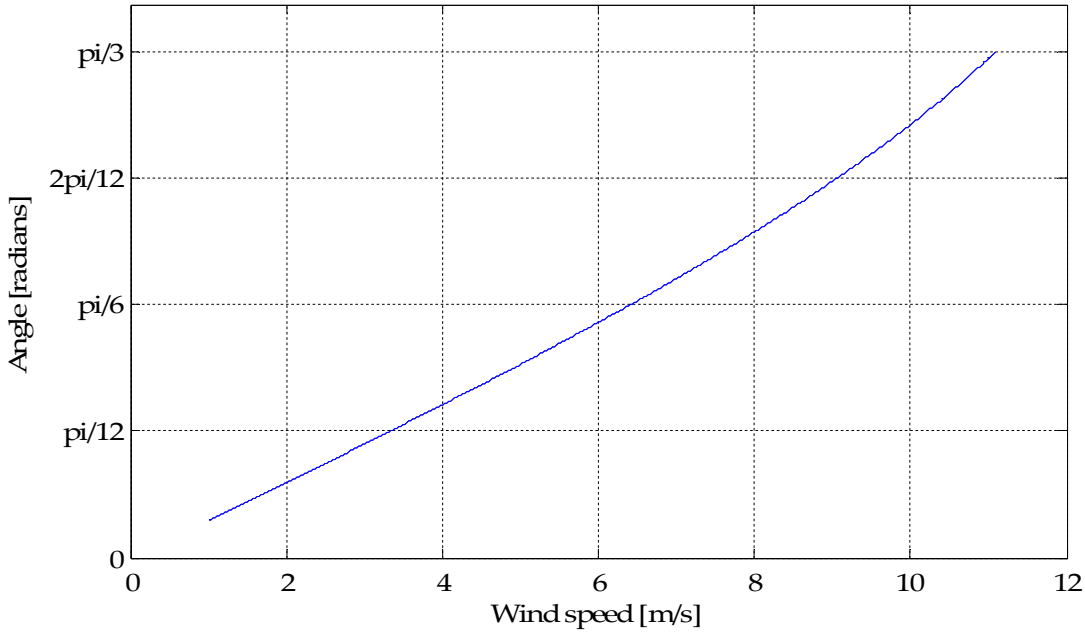

Figure 6-2: Commutation overlap length, where the generator winding inductance is optimised to achieve the maximum commutation length at rated wind speed.

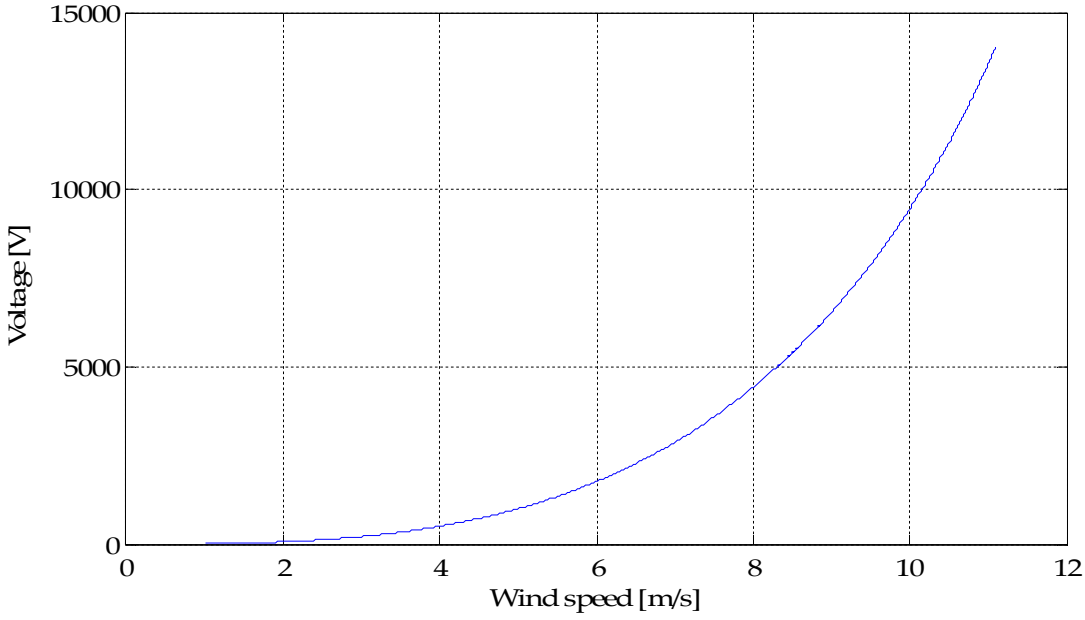

Figure 6-3: Commutation voltage drop with wind speed, where the generator winding inductance is optimised to achieve the maximum commutation length at rated wind speed.

6.1.2 The additional effects of using the commutation voltage drop to provide generator slip

The analysis conducted in Chapter 5 highlights that the length of the commutation overlap also affects the generator output power factor and the winding current harmonic component magnitudes; therefore affecting the power losses in the generator and the size of the generator torque harmonic component. To understand how the maximisation of the commutation length affects these aspects, the analysis in section 5.2 can be applied with the inductance value that is the sum of the generator and transformer winding inductances used so far in the system models (referred to as the base value of inductance) and with the inductance value calculated above, that maximises the commutation length at the maximum output from the generator (referred to as the maximum value of inductance).

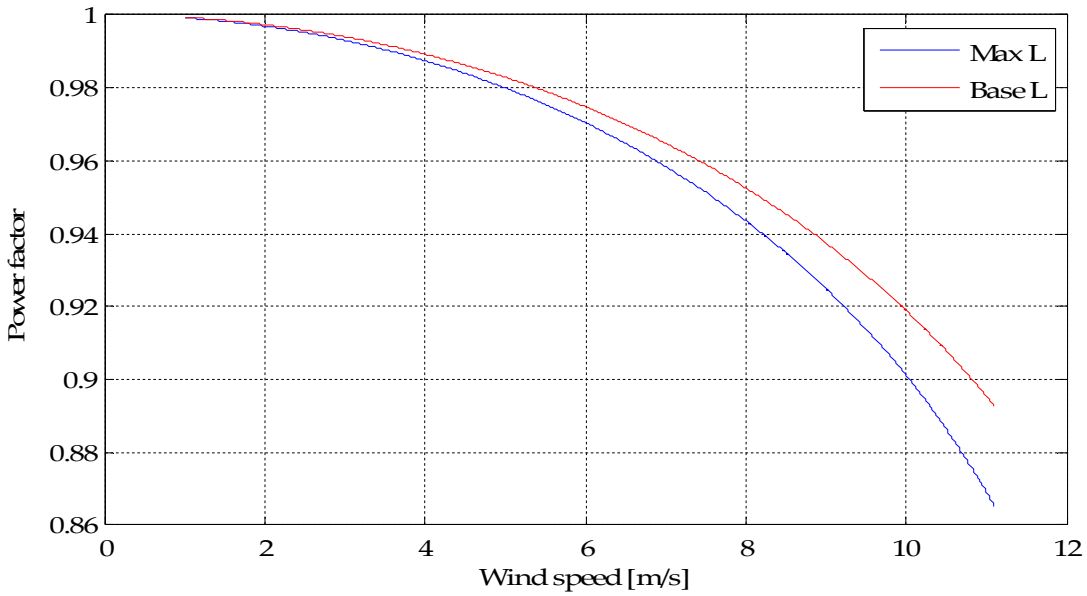

Figure 6-4: Generator output power factor with wind speed; where the base value of inductance (L) is the sum of the generator and transformer winding inductances and the maximum value of inductance is the value calculated above which maximises the commutation length.

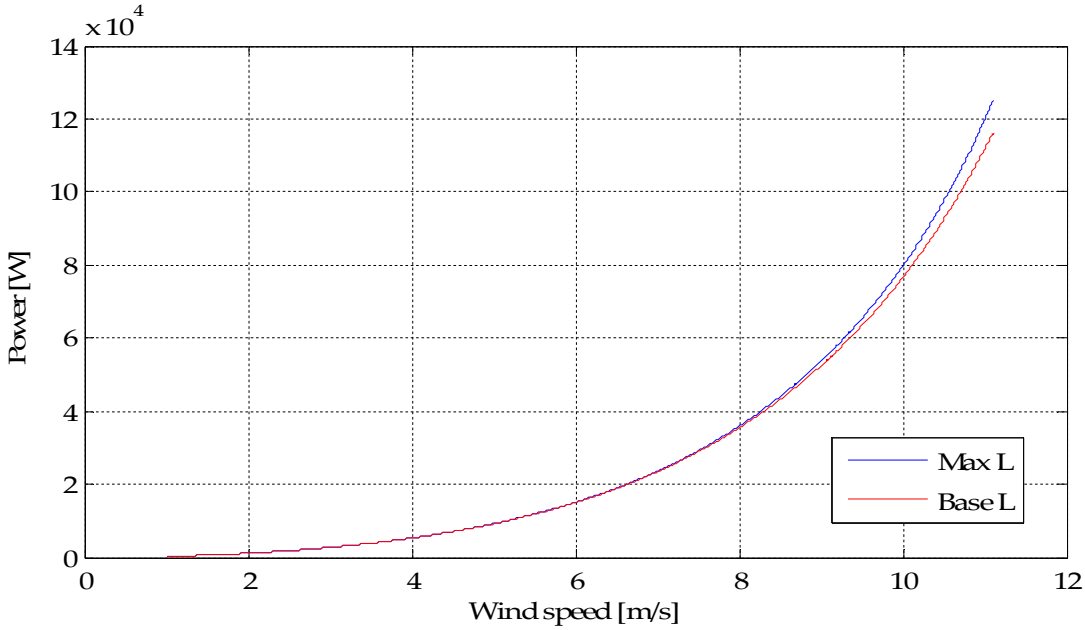

Figure 6-5: Power lost in the generator and transformer windings with wind speed; where the base value of inductance (L) is the sum of the generator and transformer winding inductances and the maximum value of inductance is the value calculated above which maximises the commutation length.

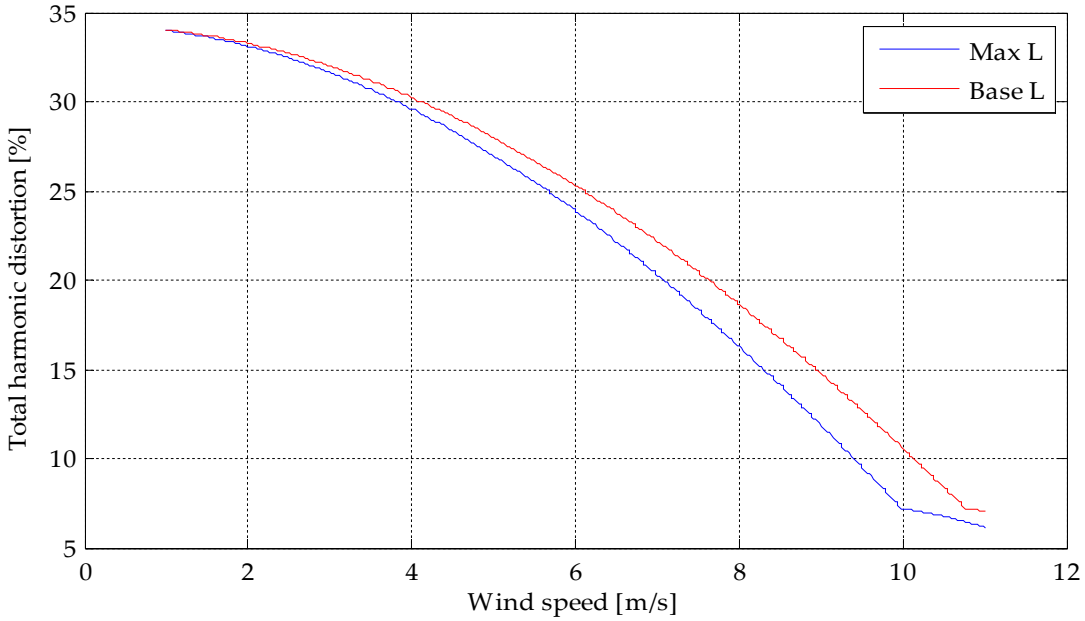

Figure 6-6: Total harmonic distortion of the generator winding current with wind speed; where the base value of inductance (L) is the sum of the generator and transformer winding inductances and the maximum value of inductance is the value calculated above which maximises the commutation length.

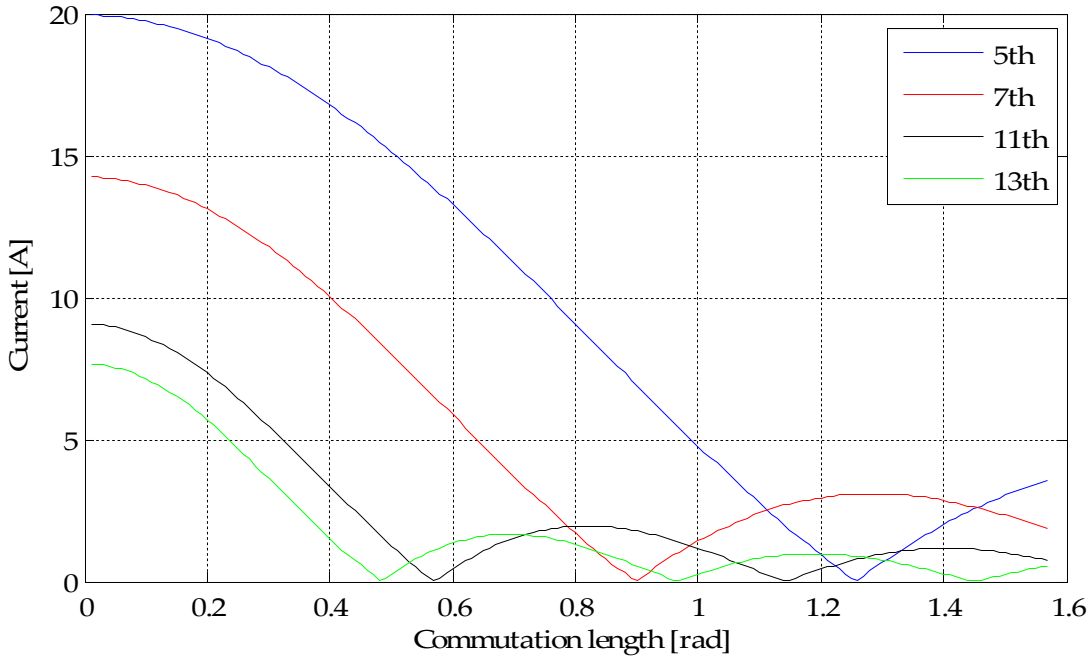

Figure 6-7: Winding current harmonic magnitudes with commutation length, where the DC current output of the rectifier is constant at the level when the wind speed is 10m/s at the start of the kink in Figure 6-6 (90.42A).

It can be observed from Figure 6-4 and Figure 6-5 that the maximisation of the commutation length lowers the generator output power factor, which therefore increases the power losses within the generator and transformer windings due to the increased reactive power flow.

In Figure 6-6 it can also be observed that the total harmonic distortion (THD) of the generator winding current falls with increasing wind speed and that it falls quicker when the inductance is larger (only the 5^{th} and 7^{th} harmonics are considered in the calculation of the THD). In addition, towards the high end of the wind speed range a kink can be observed in the THD curve, which is a result of the changing magnitude of each current harmonic component with the rectifier commutation length. Figure 6-11 shows the change of the winding current THD where the current magnitude is held constant; the TDH falls to zero where the sine and cosine components of each harmonic

cancel out at a particular commutation length angle; the kink in Figure 6-6 corresponds to the cancellation of the 7th harmonic components. The angle at which the cancellation occurs is independent of the current harmonic magnitudes, and therefore the THD of the winding current has a fixed relationship with the commutation length that can be determined using equation (6.16) and is shown in Figure 6-8. The increase of the generator inductance, which causes the commutation length to increase quicker with wind speed in Figure 6-9, will cause the cancelation point of each harmonic component to occur at a lower wind speed, as shown in Figure 6-6.

$$THD(\%) = 100.\left[\frac{\left(-\frac{\sin 5\delta}{25}\right)^2 + \left(-\frac{1-\cos 5\delta}{25}\right)^2 + \left(\frac{\sin 7\delta}{49}\right)^2\left(\frac{1-\cos 7\delta}{49}\right)^2}{(\sin\delta)^2 + (1-\cos\delta)^2}\right] \qquad (6.16)$$

The maximum possible length of the commutation, $\pi/3$ radians (1.047 radians), means that only the 7th current harmonic component cancellation point occurs within the operating range of the rectifier, the cancelation of the 5th harmonic component occurs at 1.26 radians as shown in Figure 6-7. The cancellation points of the harmonic components of a higher order than the 7th also occur within the rectifier operating range as shown in Figure 6-7; however these have not been included in the calculation of the total harmonic distortion. If they were included they would cause additional kinks to occur at the wind speeds corresponding to their points of cancelation.

The THD of the generator torque has a similarly constant relationship with the rectifier commutation length to the winding current THD, given by equation (6.17) and plotted in Figure 6-10. However in this case it can be

observed that this relationship causes the THD to rise to a peak at a commutation length of 0.61 radians and then falls back again; highlighting that the peak level of distortion occurs when the generator is only part loaded.

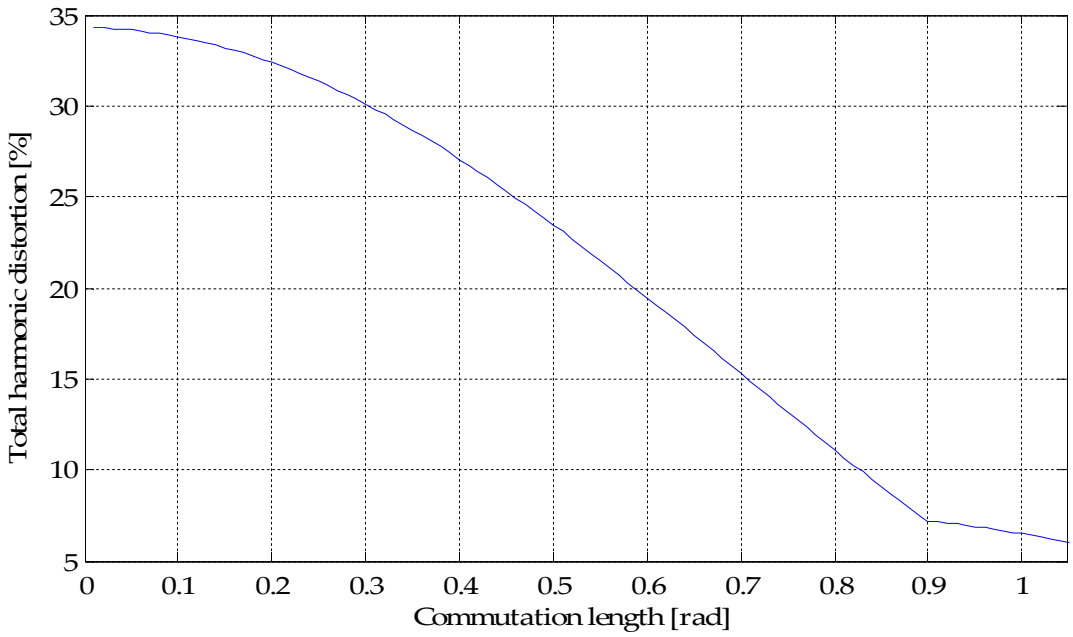

Figure 6-8: Generator winding current total harmonic distortion (including only the 5th and 7th harmonic components) with commutation length.

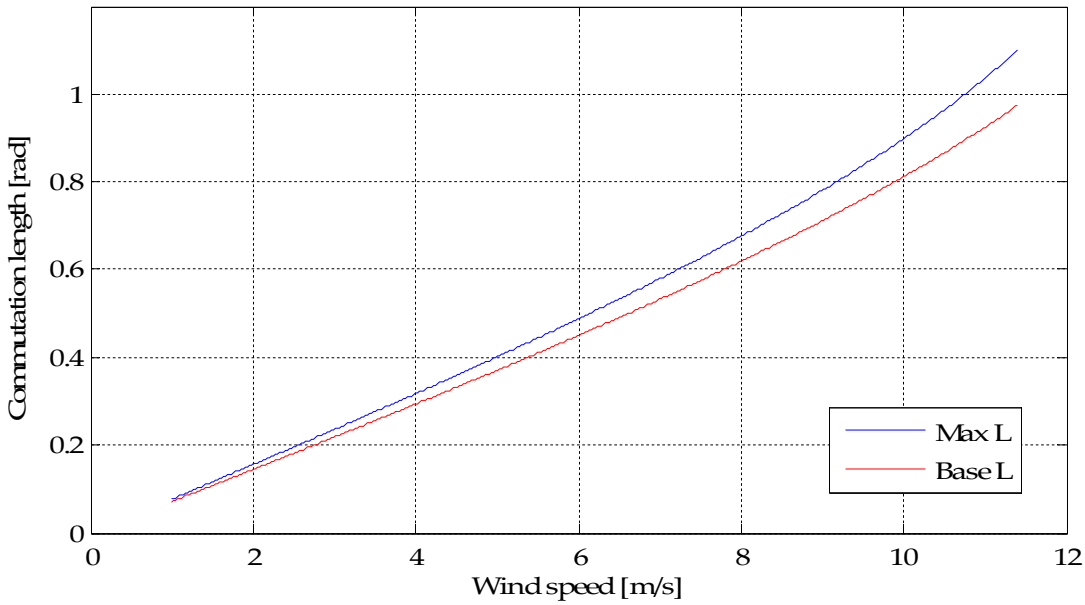

Figure 6-9: Rectifier commutation length with wind speed; where the base value of inductance (L) is the sum of the generator and transformer winding inductances, and the maximum value of inductance is the value calculated above which maximises the commutation length.

When the generator is producing maximum torque (where the commutation length will be longest) the distortion caused by the harmonic content is almost equal to that when the rectifier commutation is ideal (δ=0 radians).

It can further be observed in Figure 6-11 that the change of generator torque THD with wind speed is dependent upon the generator stator winding inductance. This relationship occurs because of the increased commutation lengths for each wind speed that are associated with the larger inductance, shown in Figure 6-9. The combination of this relationship with the fixed relationship of the THD and commutation length means that when the inductance is larger, the peak THD occurs at a lower wind speed and therefore the THD when the generator is operating at full load, at rated wind speed, is smaller.

$$THD(\%) = 100.\left[\frac{\left(-\frac{\sin 5\delta}{25}\right)^2 + \left(-\frac{1-\cos 5\delta}{25}\right)^2 + \left(\frac{\sin 7\delta}{49}\right)^2 \left(\frac{1-\cos 7\delta}{49}\right)^2}{(\sin\delta)^2}\right] \quad (6.17)$$

Conclusions

This analysis highlights the importance of the relationship between the generator winding inductance, rectifier commutation length, generator output power factor and the distortion of the generator winding currents and torque. It is concluded that although increasing the generator winding inductance reduces the power factor, it is actually beneficial to reducing the distortion of the winding currents and therefore the torque produced by the generator.

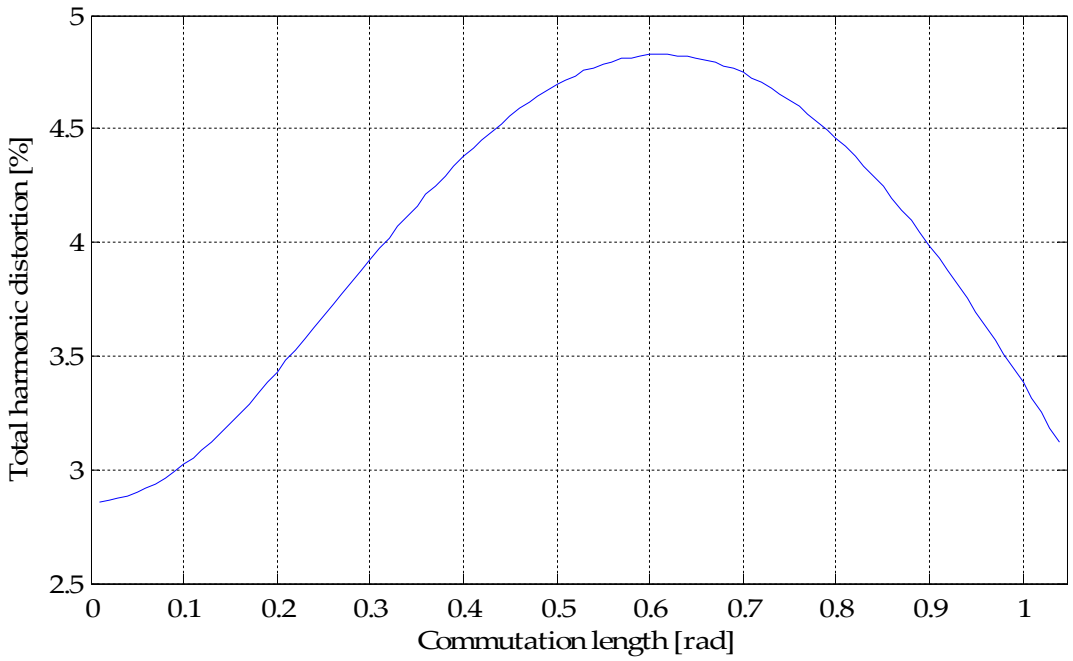

Figure 6-10: Generator torque total harmonic distortion (including the effects of only the 5th and 7th current harmonic components) with commutation length.

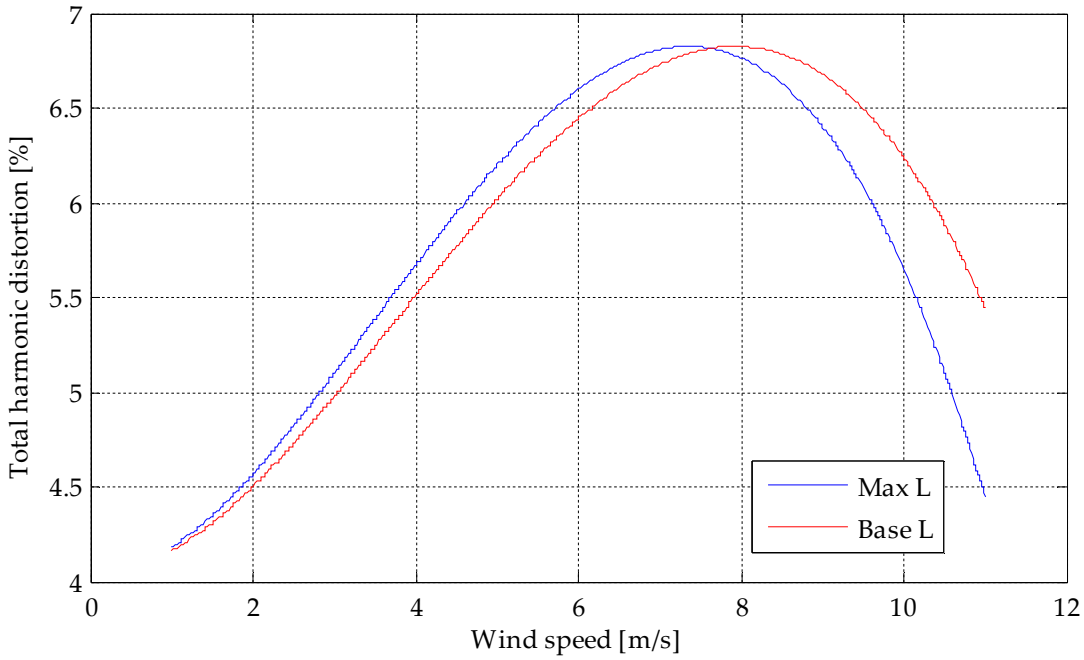

Figure 6-11: Generator torque total harmonic distortion with wind speed; where the base value of inductance (L) is the sum of the generator and transformer winding inductances, and the maximum value of inductance is the value calculated above which maximises the commutation length.

6.1.3 Using extra resistance to achieve slip

The second method of providing the generator slip is to achieve the necessary voltage drop across a resistance connected at the output of the rectifier, as shown in Figure 6-12. The voltage drop across this extra resistance will add to the voltage drop that occurs as a result of the commutation process, before the generator winding inductance was maximised above. (Some level of commutation voltage drop will always be present so long as there is a finite inductance within the generator and transformer windings). The voltage drop across the resistance can be determined using Ohms Law and therefore the total slip inducing voltage drop can be found using equation (6.18).

$$\Delta\overline{V_{dc}} = V_{Rextra} + \overline{V_{comm}} = R_{extra}.I_{dc} + \frac{3.\sqrt{3}.E}{2\pi}(1 - \cos\delta) \tag{6.18}$$

Where δ is the length of the commutation overlap caused by I_{dc} and the inductance that is naturally present in the generator and transformer windings.

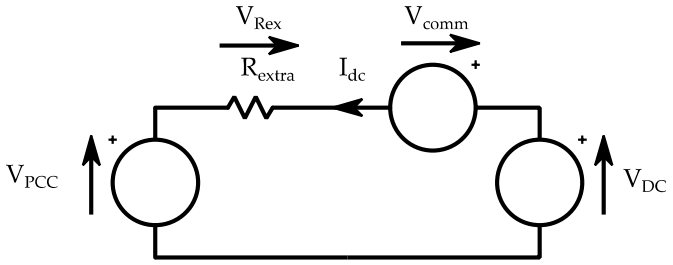

Figure 6-12: Simplified circuit diagram including the rectifier output voltage V_{dc}, commutation voltage drop V_{comm}, the extra resistance introduced to increase the generator slip, R_{ex}, and the cluster common point voltage V_{pcc}.

The amount of generator slip that can be achieved with the added resistance is determined using equation (6.9), where $\overline{V_{dc}}$ is given by equation (6.2) and where $\overline{V_{pcc}}$ is determined as follows:

$$\overline{\overline{V_{pcc}}} = \overline{V_{dc}} - \overline{V_{comm}} - R_{extra}.I_{dc} \tag{6.19}$$

Where $\overline{V_{comm}}$ is determined by averaging equation (5.30) over π/3 radians:

$$\overline{V_{comm}} = \frac{3.\sqrt{3}.E}{2.\pi}.(1 - \cos\delta) \tag{6.20}$$

$$\therefore \overline{V_{pcc}} = \frac{3.\sqrt{3}.E}{2.\pi}.(1 + \cos\delta) - R_{extra}.I_{dc} \tag{6.21}$$

$$Slip = \frac{\left(3.\sqrt{3}.E.(\cos\delta - 1) - R_{extra}.I_{dc}.2\pi\right)}{\left(3.\sqrt{3}.E.(1 + \cos\delta) - R_{extra}.I_{dc}.2\pi\right)} \tag{6.22}$$

To determine the value of resistance that is required to produce the maximum level of generator slip as that determined as a sole result of the commutation voltage drop above, equation (6.22) should be solved for R_{extra} when the slip = -1/3. The rectifier output current, I_{dc}, is required to do this and can be determined by dividing the maximum generator power output by the voltage at the rectifier terminals, taking into account the commutation voltage drop but not the voltage drop across the extra resistance, using equation (6.23).

$$I_{dc} = \frac{P_{out}}{(\overline{V_{dc}} - \overline{V_{comm}})} = \frac{P_{out}.2\pi}{3.\sqrt{3}.E.(1+\cos\delta)} \tag{6.23}$$

Therefore the extra resistance can be calculated by equation (6.24).

$$R_{extra} = \frac{-3.\sqrt{3}.\left[\omega.L.I_{dc} - slip.\left(\sqrt{3}.E - \omega.L.I_{dc}\right)\right]}{\sqrt{3}.I_{dc}.\pi.(1-slip)} = \mathbf{24.061\Omega} \tag{6.24}$$

This value appears large, but when viewed in perspective with the rated voltage (54kV) and rated current (92.6A) and presented in per unit, 0.04pu, is reasonable.

Conclusions

A key characteristic of this method of achieving generator slip is that it effectively has no limit, whereas the commutation voltage drop is limited by the maximum length of the commutation overlap, to 33.33%. To reflect this, generator slip can be calculated across the wind speed range with resistance values of 24Ω, 36Ω and 48Ω, as shown in Figure 6-13. This indicates that by doubling the extra resistance, the slip can be extended to approximately 47%. The downside to adding additional resistance however is an increase in the

system losses and the subsequent reduction of the energy transfer efficiency; which will be investigated in the next section.

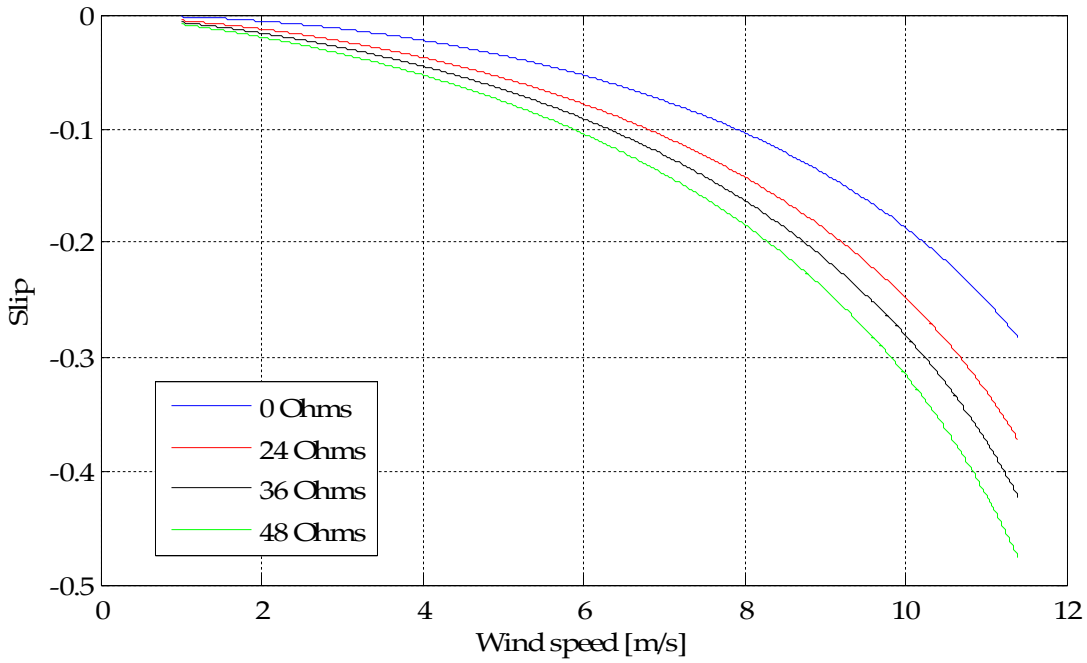

Figure 6-13: Generator slip achieved using additional resistances of 24Ω, 36Ω and 48Ω.

6.1.4 Additional effects of using extra resistance to provide generator slip

As a result of using extra resistance to provide additional generator slip, the power lost within the electrical system will increase. However, locating the extra resistance at the output of the rectifier means that it will have no impact on the commutation process and therefore the generator power factor and winding current and torque harmonics will be unaffected. To investigate the additional power lost within the system as a result of adding extra resistance, equation (6.25) is used to determine the losses as a function of the rectifier output current across the wind speed range used above, for resistance values of 24Ω, 36Ω and 48Ω.

$$P_{lossRextra} = I_{dc}^2 . R_{extra} \tag{6.25}$$

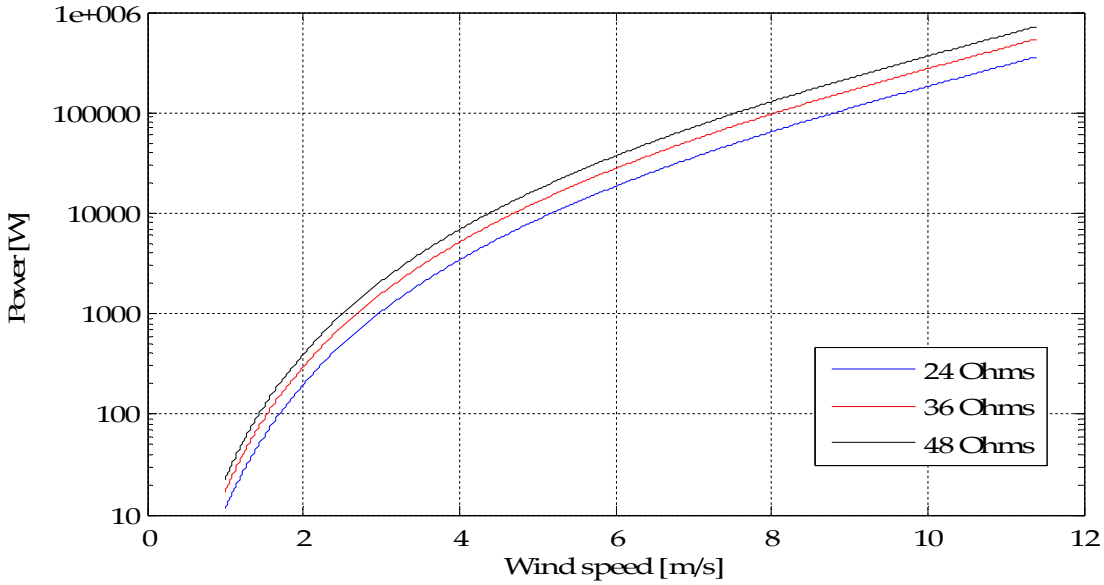

Figure 6-14: Power lost through the extra resistance plus the turbine branch cable resistance, where three different values of extra resistance are applied.

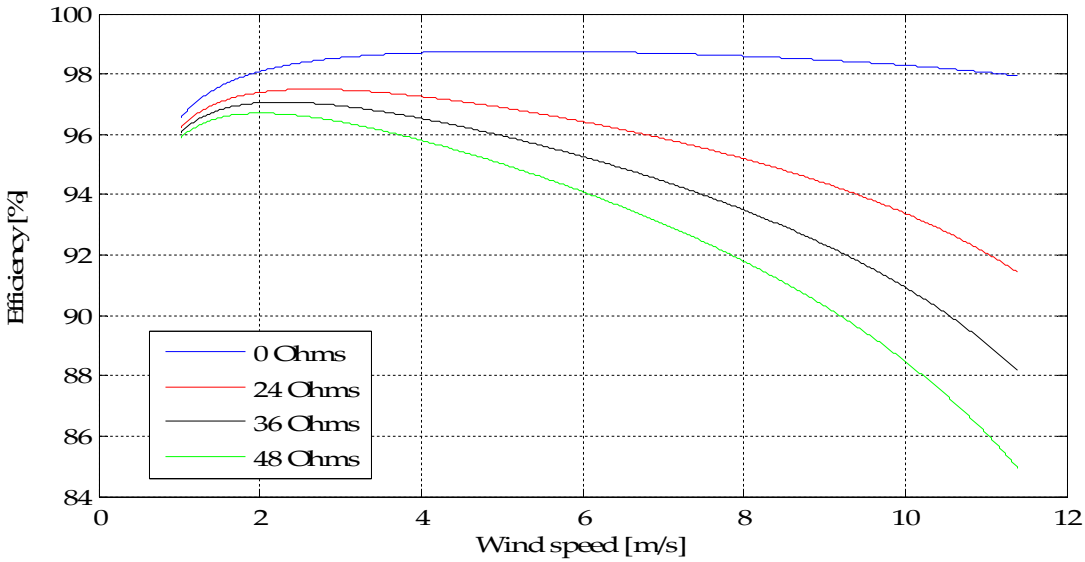

Figure 6-15: Energy transfer efficiency between the wind turbine rotor and the terminals of the cluster converter with wind speed, where the value of extra resistance is increased in three steps.

It can be observed from Figure 6-14 that the power loss across the wind speed range increases as the size of the extra resistance is increased, peaking at approx. 500kW for the 24Ω resistance and rising to approx. 900kW for the 48Ω resistance. This extra energy loss has a significant impact on the energy

transfer efficiency, shown in Figure 6-15, which is calculated between the captured power from the wind by the rotor and power output from the electrical network; with the efficiency dropping below 92% when the 24Ω resistance is used and falling further to 85% with the 48Ω resistance. These values can be compared to the base case efficiency in section 6.1.2 (the blue line in Figure 6-15) where no extra resistance is present; from which it can be observed that the efficiency is reduced by between 6 and 13% by the addition of extra resistance. It should be noted that the power lost within the generator and transformer windings is also taken into account in these efficiency calculations.

Conclusions

This analysis highlights a significant disadvantage when extra resistance is added to increase the generator slip. It can therefore be concluded from the investigations into both methods of increasing generator slip that increasing the generator winding inductance is the preferred method, because the increase of the power losses in the system caused by the extra resistance are significantly larger. A possible drawback of this method however is that the maximum level of generator slip is limited by the maximum length of the rectifier commutation overlap, to 33.33%; to achieve generator slip greater than this, additional resistance must be added at the output of the rectifier and the additional power loss introduced by doing so, accommodated. An additional advantage that has been highlighted by investigating the impact of increased generator winding inductance on the harmonics in the system is that the total harmonic distortion of the generator torque when the generator is operating under full load can be reduced slightly.

6.2 How much generator slip is required?

Generator slip has been highlighted so far as a key feature of the cluster electrical system based on rectifying the outputs of PM generators; investigation of the capabilities of such a system has shown that there is scope for more than 33.33% slip to be achieved if extra resistance is added. In order to understand how much slip is actually required within the system, the effects of slip on the operation of the turbines must be investigated. The aim of this section is to investigate the effects of generator slip on the ability of each turbine to maximise the amount of energy it captures from the wind and to understand the capability of the generators and electrical system to provide damping to the wind turbine mechanical drive train.

6.2.1 Maximising wind turbine energy capture

The effectiveness of a wind turbine at capturing the maximum amount of energy from the wind is related to its ability to maximise its rotor power coefficient. The power coefficient is directly linked to the rotor tip-speed ratio, which relates the incident wind speed to the rotational speed. To maximise the energy capture, the tip-speed ratio must be optimised by allowing the rotational speed of the rotor to follow the constantly changing wind speed. Where the turbines are electrically clustered, their rotational speeds are regulated collectively and therefore the ability of each turbine to match its rotational speed to its wind speed, to optimise its tip-speed ratio, is limited; the effects of which on energy capture performance are discussed in Chapter 3. The presence of generator slip however allows the rotational speed of each turbine to retain a degree of independence and offset some of the effects of the collective control.

To investigate the effect of generator slip on the ability of each turbine to achieve the optimal tip-speed ratio; the simplified system model set out in section 5.5 is used. This model allows the generator slip capability to be easily varied over a wide range, whilst also removing harmonics introduced to the generator currents and torque by the rectification process, improving clarity. A cluster of five wind turbines is modelled and the ability of each turbine to achieve the optimum tip-speed ratio is investigated when they are subject to two sets of wind speed data: the first set is produced with a turbulence intensity of 10% and the second set is produced with turbulence intensity of 20%, shown in Figure 6-16 and Figure 6-17 respectively. The two different sets of wind speed data allow the operation of the system to be investigated with different amounts of variation between the wind speeds incident on each turbine; a turbulence intensity of 10% is similar to that of an offshore wind farm site, whereas the 20% turbulence intensity represents a wind farm site with particularly severe turbulent wind speeds [1] [2].

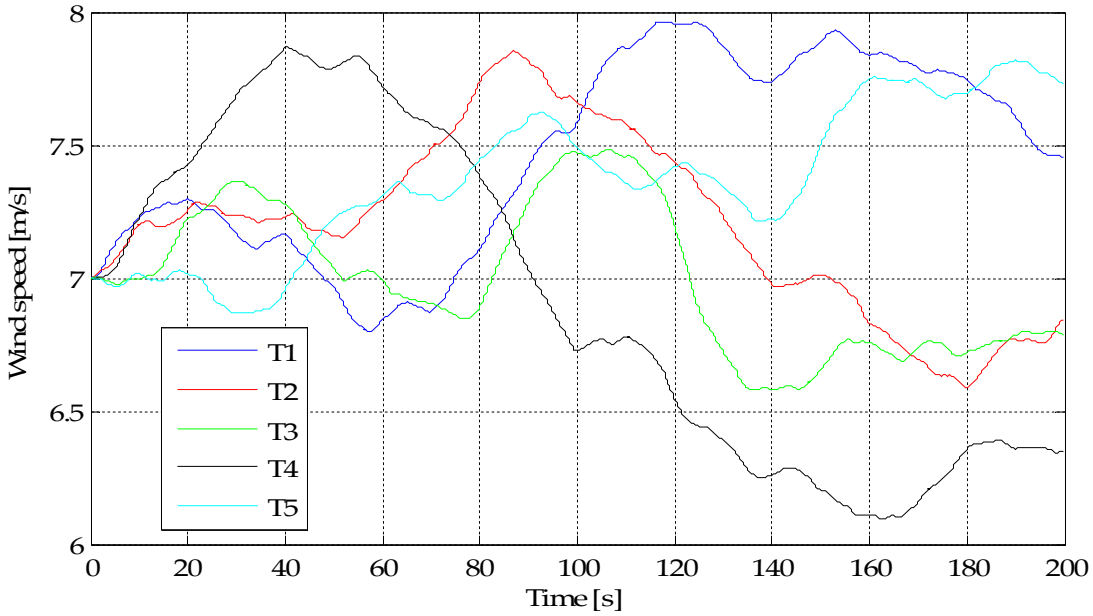

Figure 6-16: Wind speed profiles generated with mean wind speed of 7m/s and turbulence intensity of 10%.

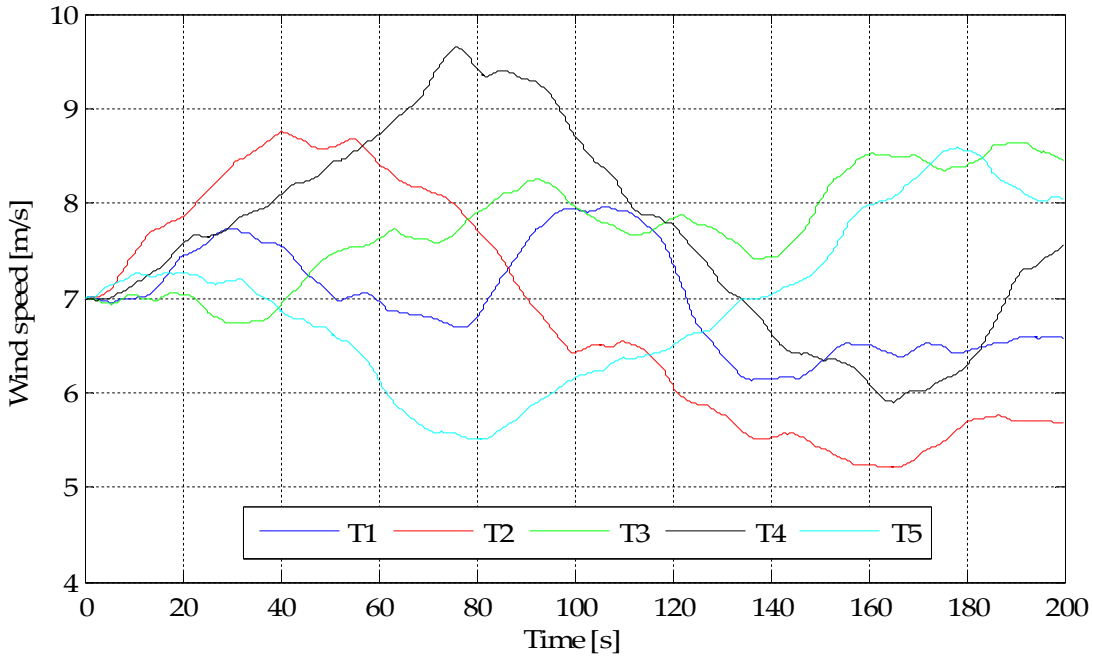

Figure 6-17: Wind speed profiles generated with mean wind speed of 7m/s and turbulence intensity of 20%.

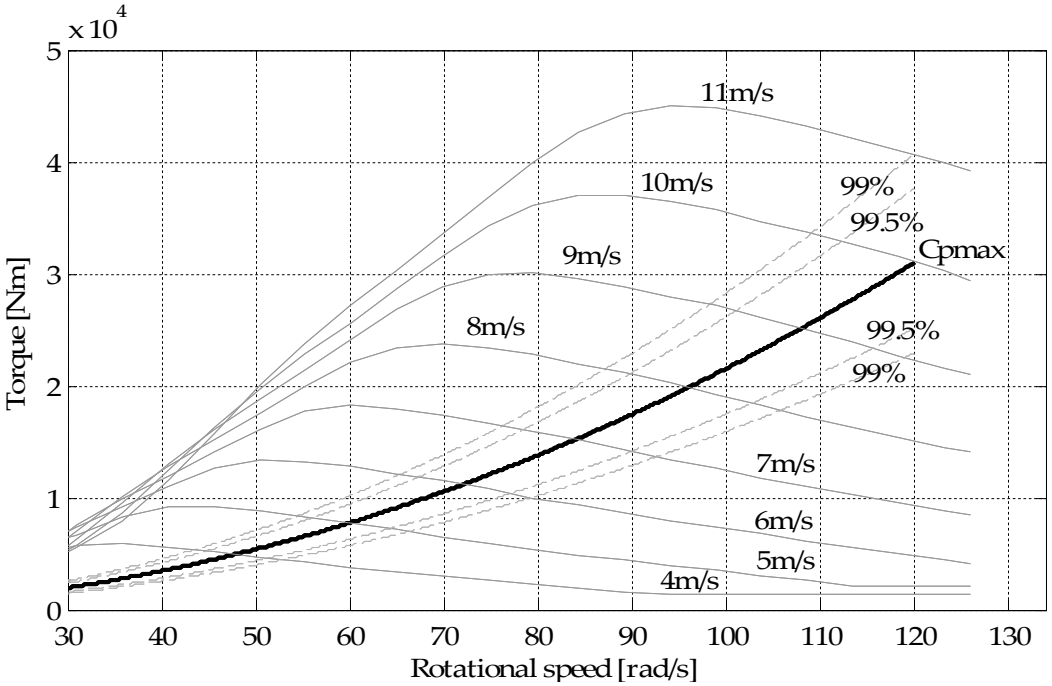

Figure 6-18: Ideal generator torque speed characteristic that allows the turbine rotor to operate with maximum power coefficient (Cpmax). Along with torque speed characteristics when the turbine is operating at 99% and 99.5% of the Cpmax and fixed wind speed torque speed characteristics across the wind speed range of 4m/s to 11m/s (grey lines).

The capability of a wind turbine to achieve the optimum rotational speed for its instantaneous wind speed can be observed by plotting the generator torque against its rotational speed and the turbine optimal torque speed characteristic. The torque speed operating characteristic of a wind turbine was introduced in Chapter 3 and the characteristic of the wind turbine modelled in this thesis is shown in Figure 6-18; highlighting the optimum relationship between generator torque and rotational speed required for the turbine to achieve the maximum power coefficient (Cpmax). Additional characteristics for the turbine operating between 99% and 99.5% of the maximum power coefficient are also shown in Figure 6-18 and will be used to help gauge the turbine energy capture performance; the closer the turbine

rotational speed and torque follow the Cpmax relationship, the better the efficiency with which the turbine will capture energy from the wind. The characteristic plotted in Figure 6-18 assumes that the rotational speed of the turbine is not limited at any point; in reality however limits will be applied according to the turbine design.

Table 6-1: System model parameters and associated maximum generator slip for the different cases modelled to investigate the effects of different levels of generator slip.

Case (1)	No commutation voltage drop.	Maximum slip = 1.5%
Case (2)	Commutation voltage drop due to half of the generator and transformer combined inductance, 1.95mH.	Maximum slip = 13%
Case (3)	Commutation voltage drop due to the total generator and transformer combined inductance, 3.9mH.	Maximum slip = 26%
Case (4)	Maximum commutation voltage drop due to an increased inductance of 4.56mH.	Maximum slip = 34%

To investigate the effects of different amounts of generator slip on the ability of each turbine to operate with the best possible power coefficient for their respective wind speeds, simulations have been run for the cases shown in Table 6-1 with both sets of wind speed data. Note that the cable impedances set out in Chapter 4 have been included in this model.

Case 1 – Maximum slip of 1.5%

In this case, where the generator slip is minimal, it can be observed in Figure 6-19 and Figure 6-20 that the rotational speeds of the turbines vary over a range of approximately 84 rad/s to 89 rad/s in response to the low variation wind speeds, and 80 rad/s to 93 rad/s in response to the high variation wind

speeds, and that the generator torque strays from the C_{pmax} curve by approximately 1% and 5% for each set of wind speeds respectively. The limited generator slip causes the relationship between the cluster synchronous speed and the turbine speeds to be close, as shown in Figure 6-21 and Figure 6-22; in fact it is shown that all of the turbines rotate at almost the same speed and vary only as a result of the controller action, which works to optimise the synchronous speed for the changing average wind speed across the cluster. The variation of the turbine operating points about the C_{pmax} curve shown in Figure 6-19 and Figure 6-20, are the result of the different wind speeds incident on each turbine producing differing input aerodynamic torques to the generators. The inability of the turbine speeds to follow the local wind speed requires the generator torques to vary quite considerably in order to balance the input aerodynamic torques, causing them to stray from the optimum curve. This causes quite wide variation of the turbine power coefficients, preventing each turbine from maximising its energy capture.

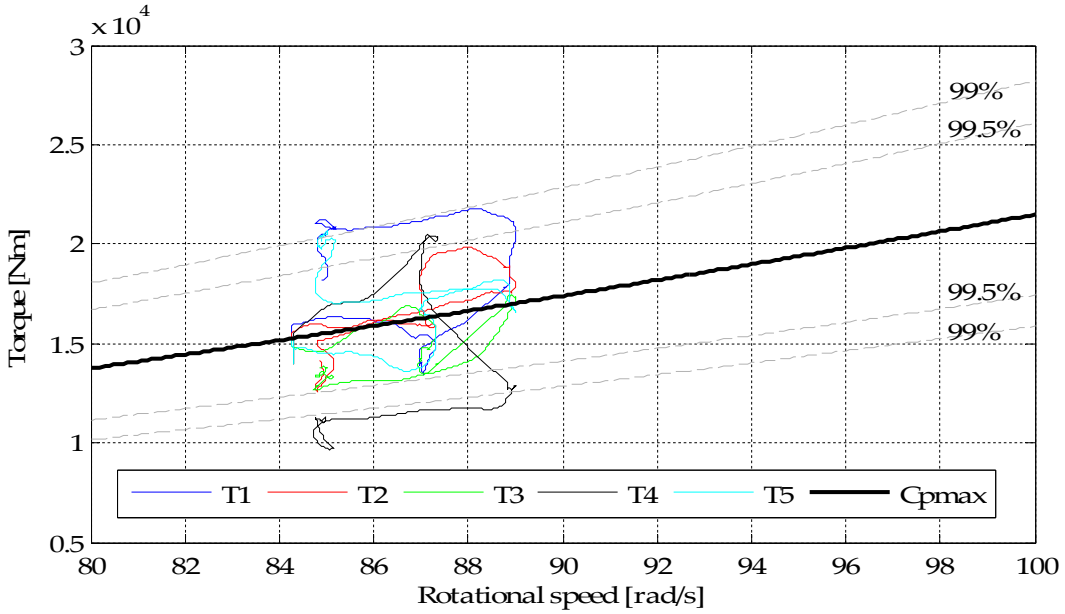

Figure 6-19: Generator torque with rotational speed for each turbine with maximum generator slip of 1.5% in response to the wind profiles with low variation; against the Cpmax, 99.5% and 99% of Cpmax operating characteristics.

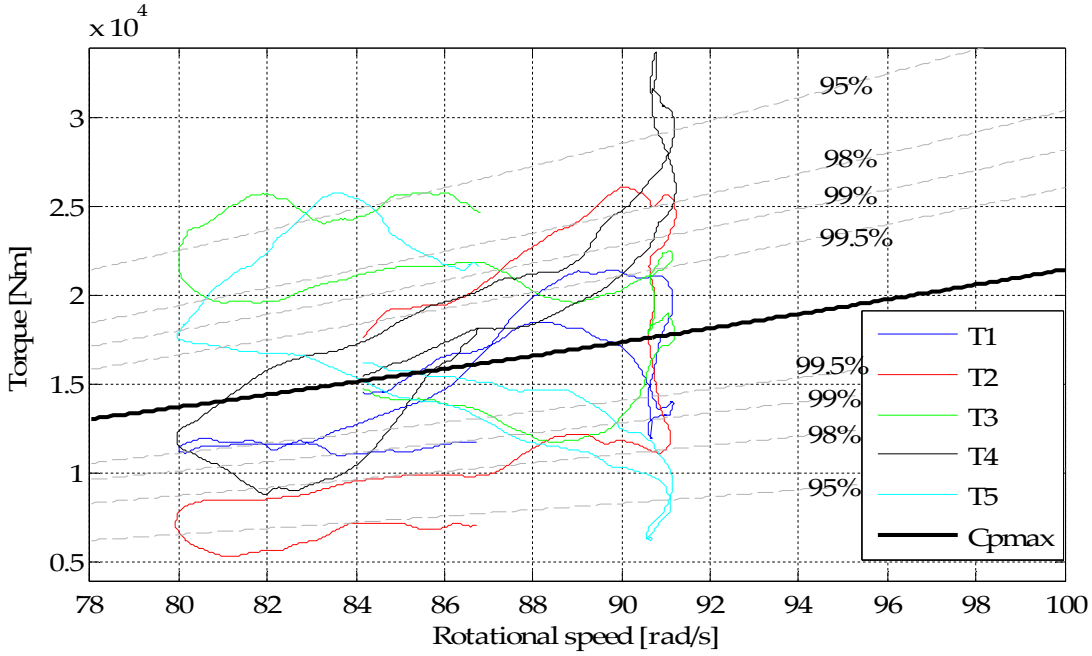

Figure 6-20: Generator torque with rotational speed for each turbine with maximum generator slip of 1.5% in response to the high variation wind profiles; against the Cpmax, and 95% to 99.5% of Cpmax operating characteristics.

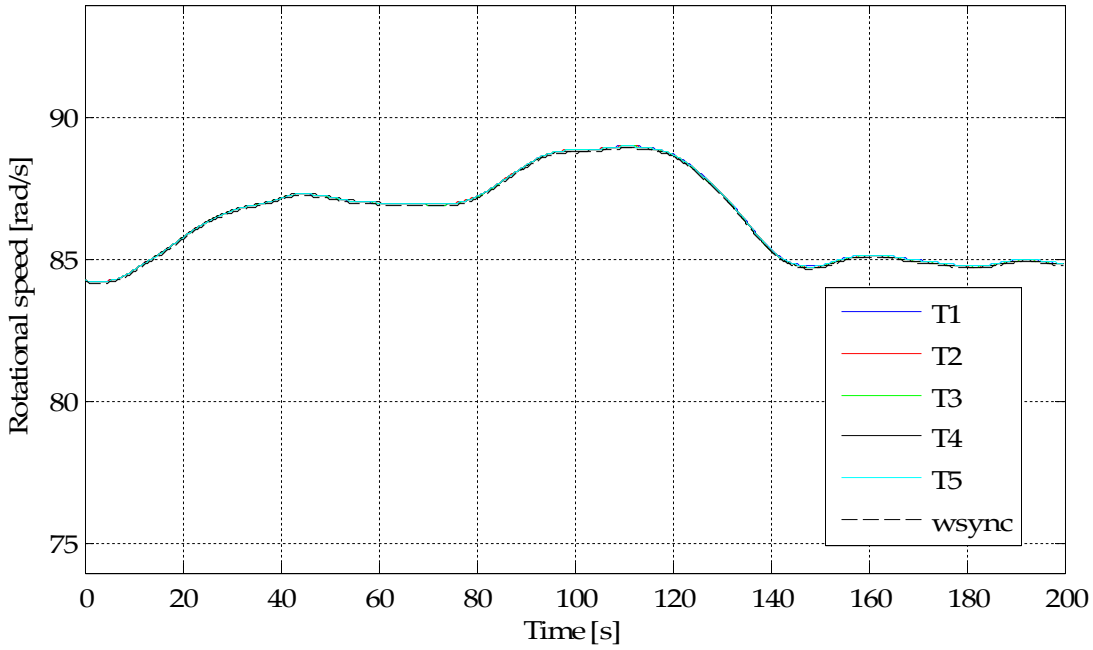

Figure 6-21: Turbine rotational speeds and cluster synchronous speed in response to the low variation wind profiles, where the maximum generator slip is 1.5%.

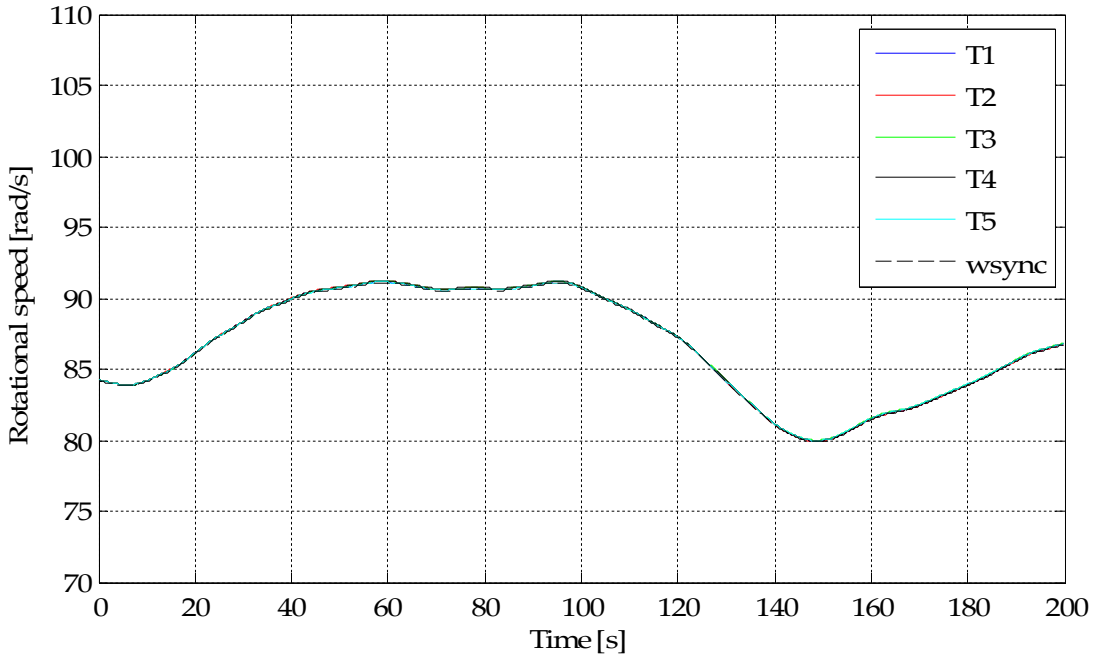

Figure 6-22: Turbine rotational speeds and cluster synchronous speed in response to the high variation wind profiles, where the maximum generator slip is 1.5%.

Case 2 – Maximum slip of 13%

The provision of a greater amount of generator slip allows for the rotational speed of each turbine to have greater freedom with respect to the cluster synchronous speed. This can be observed by comparing the operation of the turbines in this case, in Figure 6-23 and Figure 6-24, with their operation with minimal slip above. The larger generator slip allows the turbines to vary their rotational speeds over a greater range of approximately 81rad/s to 89rad/s, and from 77rad/s to 97rad/s, for each set of wind speeds respectively. This extended range reduces the spread of the generator torques about the C_{pmax} curve, allowing the turbines to operate mostly within 99%, for the first set of wind speeds, and within 95%, for the second set, of the optimum power coefficient. The improved performance of the turbines is caused by the extra freedom of the rotational speeds allowing them to follow their individual wind speeds much more closely, smoothing the generator torque required for the limitation of the rotor acceleration. The extra freedom of the turbine speeds is also demonstrated in Figure 6-25 and Figure 6-26 where the separation between the turbine speeds and the cluster synchronous speed is clearly evident; the ability for the individual turbine speeds to vary considerably and independently of each other can also be observed. Comparison of the operation of the turbines in this case with case 1 clearly indicates that the addition of extra slip is beneficial to their energy capture performances.

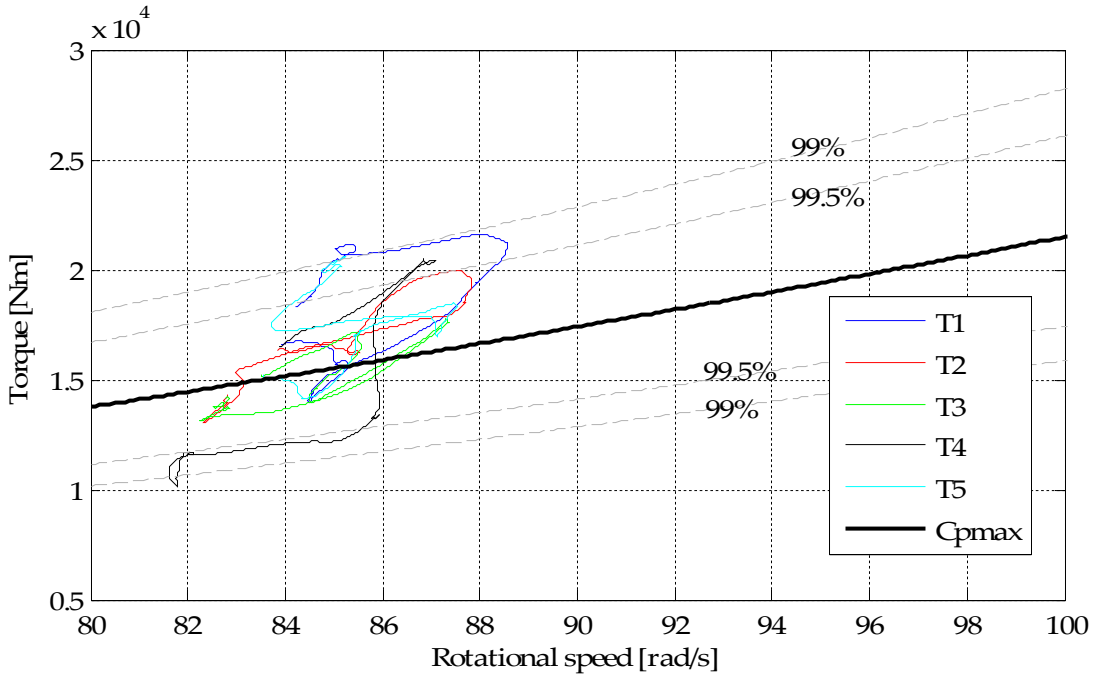

Figure 6-23: Generator torque with rotational speed for each turbine with maximum generator slip of 13% in response to the low variation wind profiles; against the Cpmax, and 99% to 99.5% of Cpmax operating characteristics.

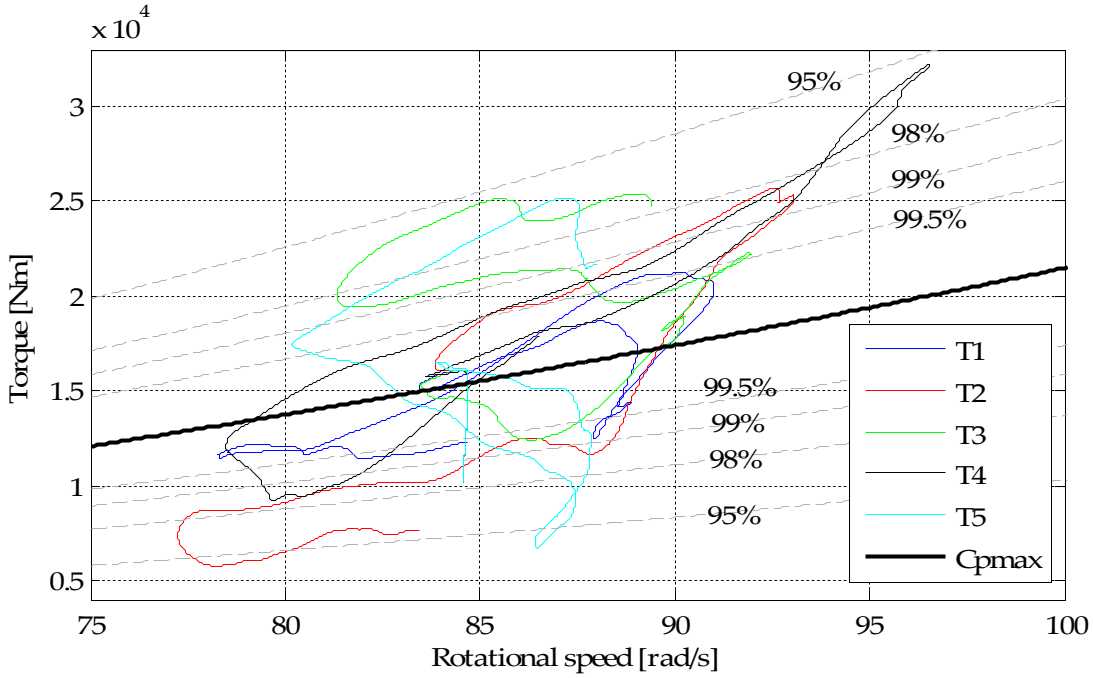

Figure 6-24: Generator torque with rotational speed for each turbine with maximum generator slip of 13% in response to the high variation wind profiles; against the Cpmax, and 95% to 99.5% of Cpmax operating characteristics.

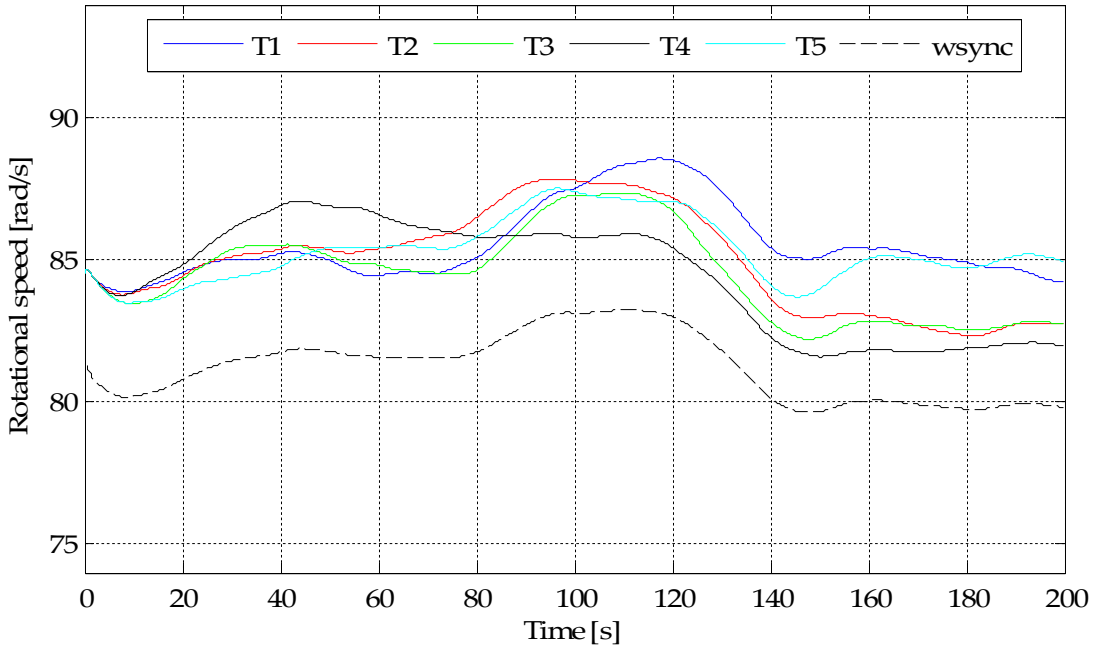

Figure 6-25: Turbine rotational speeds in response to the low variation wind profiles, along with the cluster synchronous speed, where maximum generator slip is 13%.

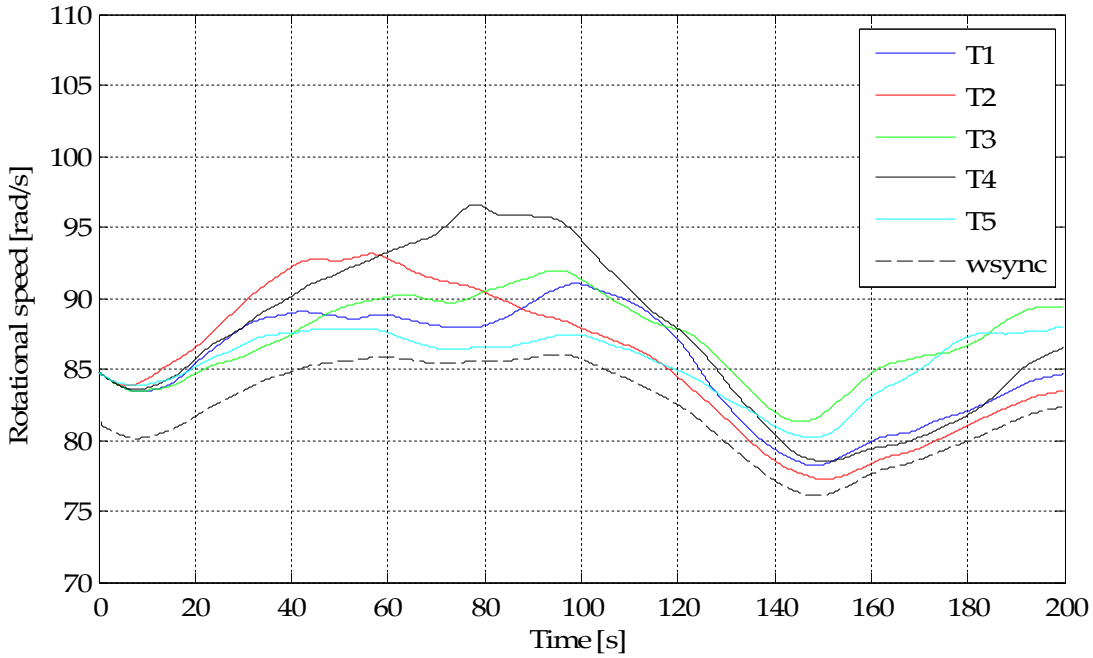

Figure 6-26: Turbine rotational speeds in response to the high variation wind profiles, along with the cluster synchronous speed, where maximum generator slip is 13%.

Case 3 – Maximum slip of 26%

By allowing a larger amount of generator slip the performance of the turbines can be improved further. In this case the maximum generator slip that would naturally occur in the system as a result of the commutation voltage drop is applied. The extra slip can be observed in Figure 6-27 and Figure 6-28 to allow the turbine speeds to vary over a greater range whilst also improving their energy capture performance. In particular the ranges of rotational speed variation in either case are approximately 82rad/s to 92rad/s, and 77rad/s to 106rad/s; and the turbine operating points are within 99.5% of the optimum for the low variation wind speeds and mostly within 98% of the optimum for the high variation wind speeds. The increased variation of the turbine rotational speeds relative to the synchronous speed and each other is also shown in Figure 6-29 and Figure 6-30. It is therefore concluded that the lengthening of the rotational speed ranges of variation and the improvement of the turbine performance caused by increasing the maximum generator slip by a factor of 2 to 26% improves the energy capture performance of each turbine in the cluster significantly.

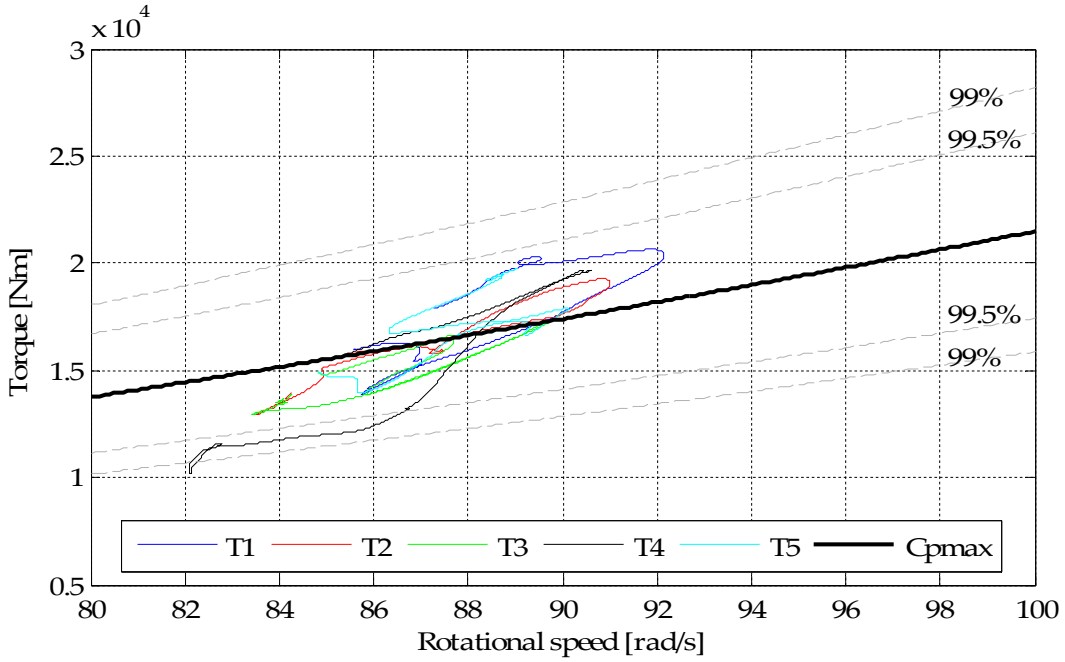

Figure 6-27: Generator torque with rotational speed for each turbine with maximum generator slip of 26% in response to the low variation wind profiles; against the Cpmax, and 99% to 99.5% of Cpmax operating characteristics.

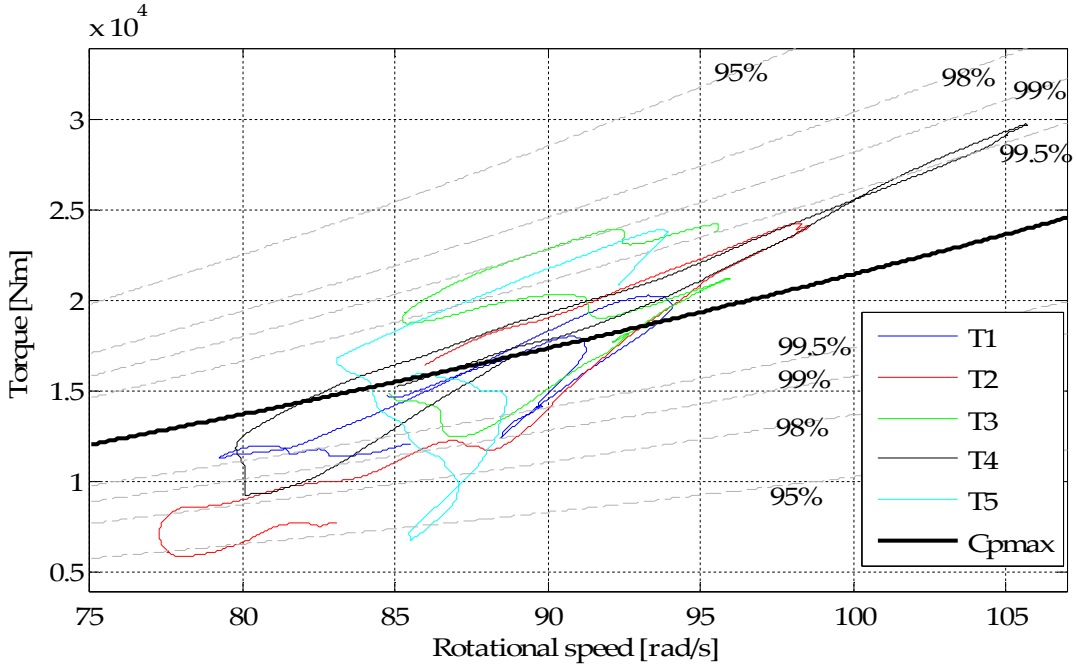

Figure 6-28: Generator torque with rotational speed for each turbine with maximum generator slip of 26% in response to the high variation wind profiles; against the Cpmax, and 95% to 99.5% of Cpmax operating characteristics.

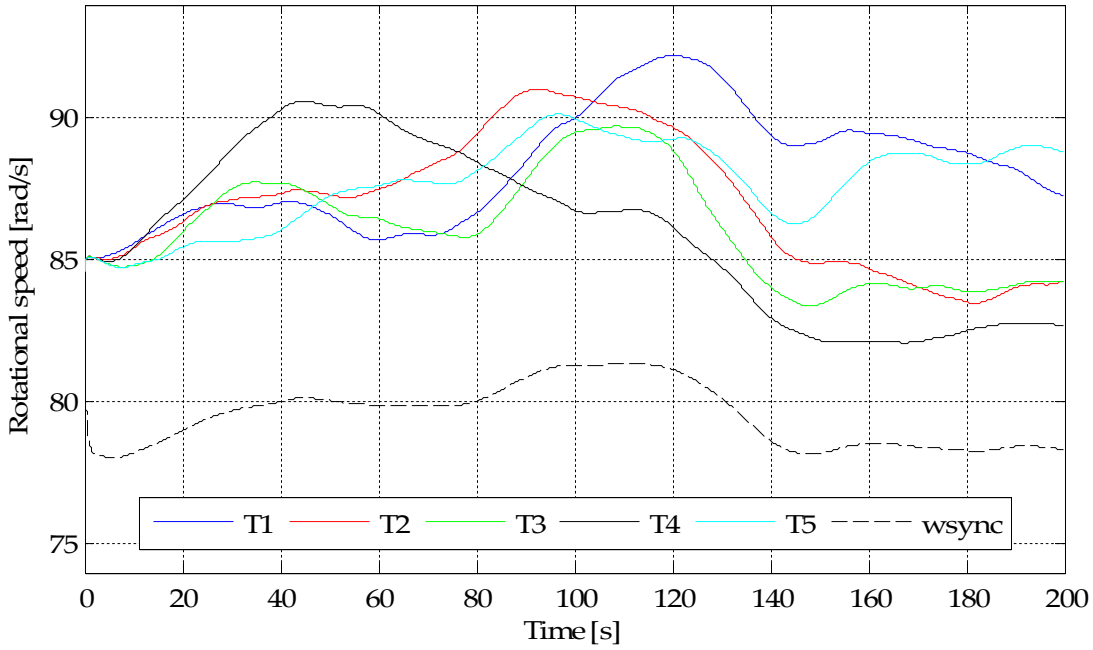

Figure 6-29: Turbine rotational speeds in response to the low variation wind profiles, along with the cluster synchronous speed, where maximum generator slip is 26%.

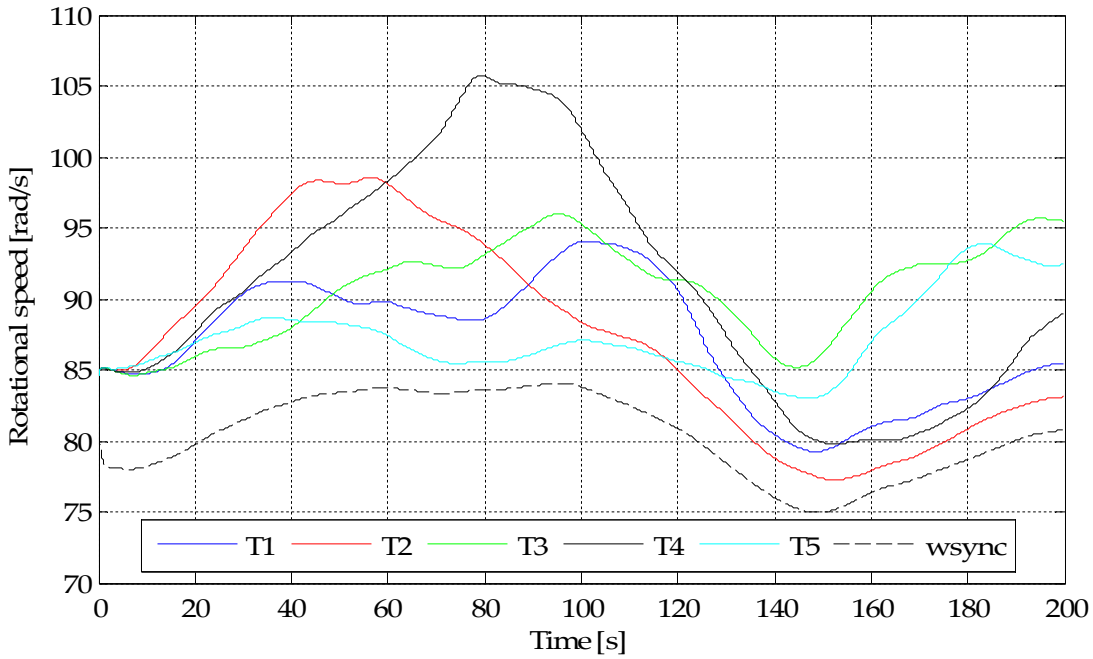

Figure 6-30: Turbine rotational speeds in response to the high variation wind profiles, along with the cluster synchronous speed, where maximum generator slip is 26%.

Case 3 - Maximum slip of 34%

The further increase of the generator slip provided by maximising the commutation voltage drop, further increases the freedom of the turbine speeds to follow the continuously changing wind speeds. This is reflected in Figure 6-31 and Figure 6-32 where the range of speed variation is slightly larger than the previous case. Slight improvements to the proximity of the generator torque to the optimum also occur as a result. However, the minimal improvement caused by this further increase of generator slip, in comparison the large improvements found in the previous cases, highlights that the continued increase of the generator slip capability brings only minor additional benefits to the energy capture performance of the turbines.

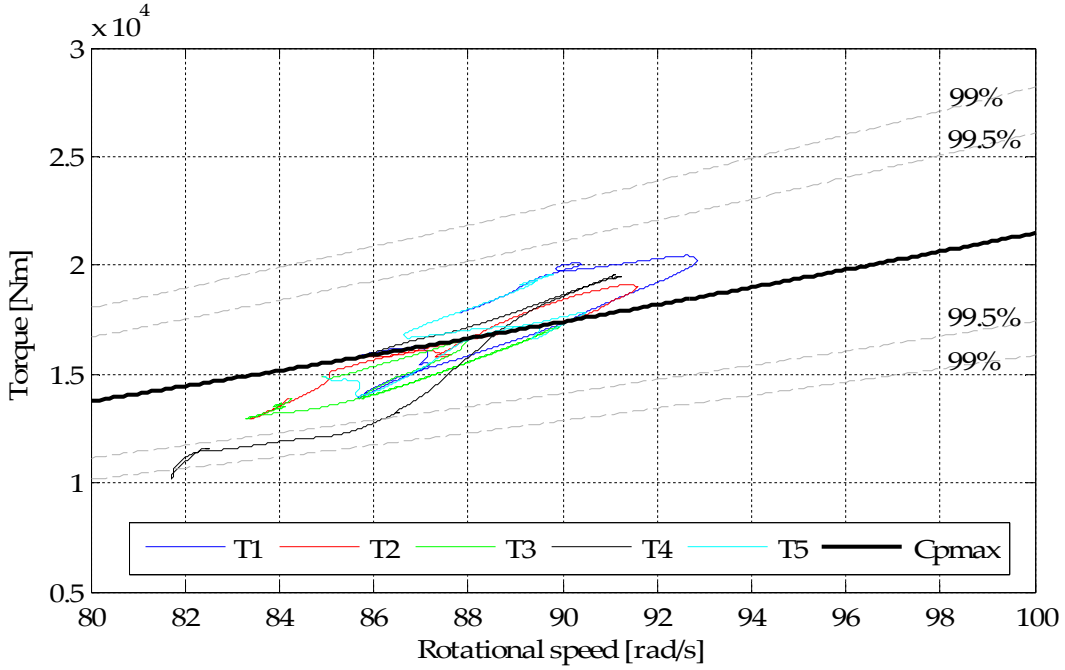

Figure 6-31: Generator torques with rotational speed for each turbine in response to the low variation wind profiles, where the generator inductance is 4.56mH; against the Cpmax, and 99% to 99.5% of Cpmax operating characteristics.

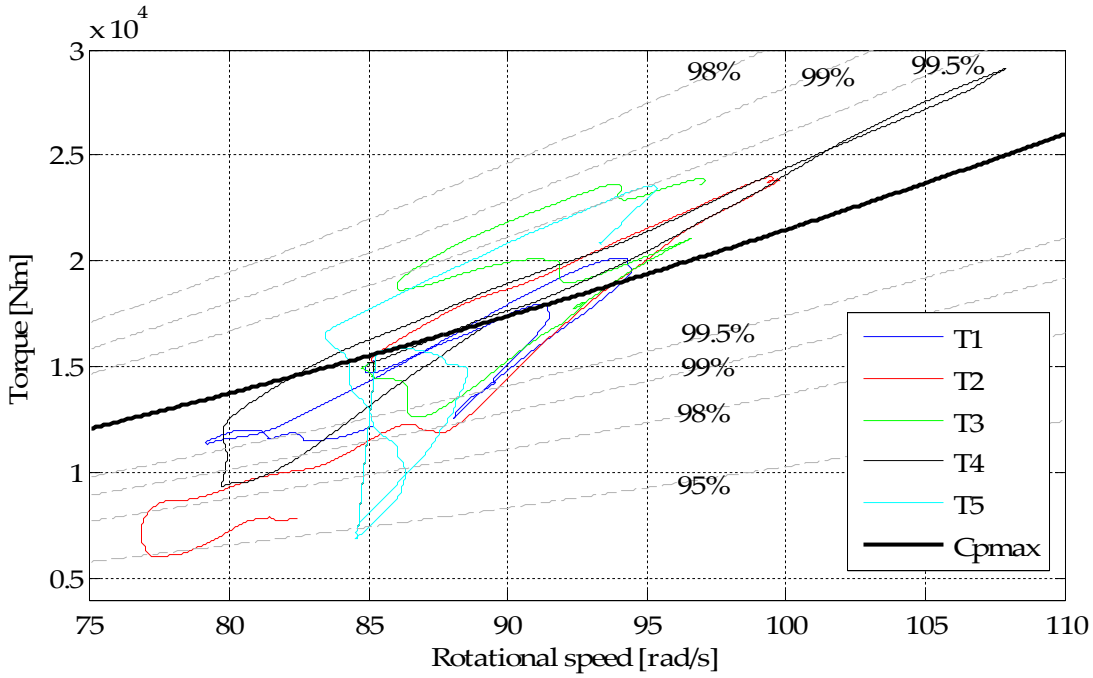

Figure 6-32: Generator torques with rotational speed for each turbine in response to the high variation wind profiles, where the generator inductance is 4.56mH; against the Cpmax, and 99% to 99.5% of Cpmax operating characteristics.

Conclusions

It can therefore be concluded that the increase of the generator slip, which grants each turbine the freedom to vary its rotational speed in response to the wind speed, is beneficial to the performance of the turbines connected together in a cluster. The performance improvement observed between the first case with limited slip, and the 2nd and 3rd cases with 13% and 26% maximum slip respectively, show that the greater the amount of slip that can be achieved the better the energy capture performance. This is further demonstrated by increasing the maximum slip to 34%; however the smaller size of the incremental improvement of performance achieved by this increase, relative to where the maximum slip is 26%, is minor. Therefore the pursuit of the maximum amount of slip within the system by maximising the

commutation voltage drop and potentially by adding extra resistance is not warranted by the small incremental improvement it provides.

It is therefore concluded that the generator slip that naturally occurs within the system, due to the rectifier commutation overlap caused by the combined transformer and generator inductances, is sufficient to bring significant improvements to the energy capture performance of the clustered turbines, in comparison to where the generator slip capability is minimal. This investigation further underlines the conclusion made in Chapter 4 that the ability of a cluster of turbines based upon rectified PM generators to use generator slip to improve their energy capture is a major advantage over both the induction generator and AC connected PM generator cases.

6.2.2 Damping of wind and mechanical oscillatory components

The wind that acts upon a wind turbine varies in both time and space due to wind turbulence. Wind turbulence is referred to as the passing of large circulating eddies of air flow that can be of a comparable size to the diameter of a wind turbine rotor and cause the torque produced by a wind turbine rotor to fluctuate periodically as the blades cut through the eddies as they rotate [3]. Fluctuations are also introduced by the turbine blades passing in front of the turbine tower, an effect referred to as tower shadow. These periodic rotor torque fluctuations pass through the turbine drive-train to the generator and onwards as output power fluctuations and have a frequency typically in the region of 1Hz, depending upon the size of the turbine rotor and its rotational speed [3]. Higher frequency variations of the turbine output power also occur due to the dynamics of the turbine drive-train and structure, with typical frequencies of a few Hz.

The different control strategies of wind turbines offer different methods for dealing with these torque and power fluctuations. Wind turbines that are directly connected to electrical networks and rotate at a fixed speed are very stiff in response to these fluctuations, transferring them straight through the turbine drive-train and onto the output power, causing the local electrical network voltage to flicker [3]. Such turbines use induction generators as the means of converting the rotating mechanical energy to electrical energy, which are also regarded as strong dampers to oscillatory fluctuations of torque, therefore the periodic fluctuations do not have a big impact of the turbine drive-train [4]. Variable speed wind turbines involve some degree of decoupling from the electrical network and therefore the large inertia of the turbine rotor soaks up high frequency variations of input torque, reducing the severity with which they appear on the turbine power output. The controller of a variable speed generator however prescribes the generator torque applied to the drive-train; therefore, although such turbines may also use induction generators the same damping is not applied [4]. The lack of drive-train damping in a variable speed wind turbine can result in quite significant oscillations due to the torsional twist of the drive shafts between the generator and the turbine rotor, and therefore can apply very large torques on to the gearbox, which sits in the middle, increasing its mechanical fatigue [4]. Such oscillations are often excited by changes of the mechanical load, for example due to large wind fluctuations, or due to changes of the electrical output caused by, for example, a network fault [5]. To circumvent these issues, the controllers of variable speed wind turbines are usually modified to provide damping by applying a small torque ripple at the drive-train natural frequency, in phase with the oscillations [4].

These considerations are also relevant to variable speed wind turbines that are connected together in a cluster. However, in this case the individual turbines do not have individual controllers and therefore damping cannot be applied to the drive-train in the same way.

So far in this section the capability of the generator slip to improve the energy capture of the turbines has been investigated; however the generator slip also provides the capability to damp the turbine drive-train to prevent the oscillations, described above, occurring. To investigate this ability a brief overview of the mechanical system dynamics will be given along with a description of the required damping. The link between the generator torque and the operation of the cluster electrical system, which allows the damping to be achieved, will then be described; and a model of a wind turbine drive train developed and integrated into the simplified cluster system model to demonstrate the damping capability of the generators with different amounts of generator slip.

Mechanical system dynamics and using generator torque for damping

To understand the damping capabilities of the cluster electrical system, first of all the dynamic equations of the drive-train are required. The drive-train of a wind turbine can be simplified and represented by two rotating masses, or inertias, coupled by a flexible driveshaft, as shown in Figure 6-33; where the inertias represent the wind turbine rotor and the generator respectively (At this stage the presence of the gearbox is not considered).

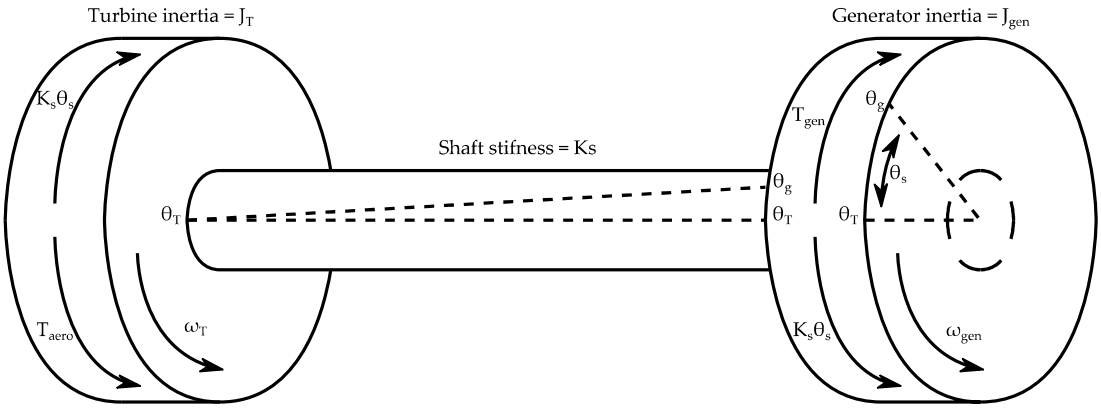

Figure 6-33: Simplified representation of a wind turbine drive-train, where the rotor is taken as the reference.

Both the turbine rotor and the generator exert torque on to each of the inertias in opposite directions to each other. The turbine rotor torque, referred to as the aerodynamic torque, T_{aero}, applies the input torque to the system, whereas the generator torque applies the resistive torque. The flexible shaft, which is in torsion between the inertias, also applies a torque component to each inertia, in opposing directions that are equal in magnitude related to the torsion angle of the shaft, θ_s, and its stiffness, K_s.

The equation of motion for each inertia, derived using Newton's second law, can be determined by taking the turbine rotor as the reference, as follows:
Turbine rotor equation of motion:

$$T_{aero}(t) = J_T.\frac{d\omega_T}{dt} + T_{shaft}(t) \tag{6.26}$$

Where $T_{shaft} = K_s.\theta_s$ and θ_s is determined by

$$\frac{d\theta_s}{dt} = \omega_T - \omega_{gen}, \text{ therefore } \theta_s = \theta_T - \theta_g \tag{6.27}$$

$$\therefore T_{aero}(t) = J_T.\frac{d\omega_T}{dt} + K_s.\theta_s(t) \tag{6.28}$$

Generator equation of motion:

$$T_{shaft}(t) = J_{gen}.\frac{d\omega_{gen}}{dt} + T_{gen}(t) \tag{6.29}$$

$$\therefore K_s.\theta_s(t) = J_{gen}.\frac{d\omega_{gen}}{dt} + T_{gen}(t) \tag{6.30}$$

Both equations can therefore be rewritten as second order differential equations, as follows:

$$T_{aero}(t) = J_T.\frac{d^2\theta_T}{dt^2} + K_s.\theta_s(t) \tag{6.31}$$

$$-T_{gen}(t) = J_{gen}.\frac{d^2\theta_{gen}}{dt^2} - K_s.\theta_s(t) \tag{6.32}$$

Comparing these equations with the general equation for a second order dynamic system, given in equation (6.33), it can be observed that there are no first order terms and therefore no damping in the system. This indicates therefore that the drive-train of a wind turbine is a naturally under-damped dynamic system.

$$U(t) = \frac{1}{\omega_n^2}.\frac{d^2y(t)}{dt} + \frac{2.\zeta}{\omega_n}.\frac{dy(t)}{dt} + y(t) \tag{6.33}$$

ω_n = natural frequency (rad/s), ζ = damping ratio.

In order to apply damping to the system the generator torque must also be a function of the first order differential of the angle of rotation θ, which can also be referred to as the rotational speed.

$$T_{gen} \propto \frac{d\theta}{dt} = \omega$$

In a fixed speed induction generator based wind turbine the generator torque is a function of the generator slip and therefore rotational speed, applying the necessary damping.

In order to determine damping capabilities of the rectified PM generators, the relationship between the generator torque and the rectifier output DC current, which is a function of the harmonic components of the winding current, is used, equation (5.68). To simplify this equation the 6th harmonic component is ignored to give just the average generator torque, as shown in equation (6.34). Also by assuming that the commutation advance start angle, α, equals zero and that the commutation length, δ, is small (allowing sin δ ≈ δ), the average generator torque can be approximated by equation (6.35).

$$Torque = \frac{3.\sqrt{3}.p.\Psi_f.I_{dc}}{\pi.(\delta+\alpha)}[\sin\delta + \sin\alpha] \tag{6.34}$$

$$Torque = \frac{3.\sqrt{3}.p.\Psi_f.I_{dc}}{\pi} \tag{6.35}$$

This simplified equation describes the torque produced by the DC generator used in the simplified system model and shows that it is a function of the DC output current.

To establish the link between the generator torque and rotational speed, required for the application of damping, the DC current and the rotational speed must also be related. Using Figure 6-34 as an aid, the DC current can be determined as a function of the DC output voltage of the generator, $\overline{V_{dc}}$, the rectifier commutation voltage drop, $\Delta\overline{V_{dc}}$, the cluster common point voltage, $\overline{V_{PCC}}$, and the cable resistance, R_l, as shown by equation (6.36).

By Kirchoffs voltage law:

$$\overline{V_{dc}} = \Delta\overline{V_{dc}} + I_{dc}.R_l + \overline{V_{PCC}} \tag{6.36}$$

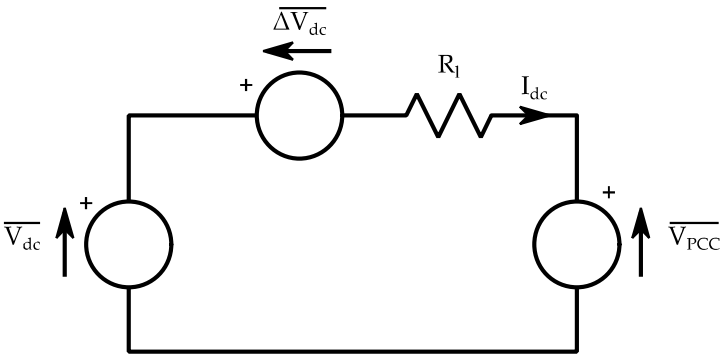

Figure 6-34: Circuit diagram of the simplified system model.

Therefore the rotational speed, output current and generator torque can be linked as follows:

Where from equation (5.33) $\Delta\overline{V_{dc}} = \frac{3.\omega_r.L.I_{dc}.p}{\pi}$

$$\overline{V_{dc}} - \overline{V_{PCC}} = \frac{3.\omega_r.L.I_{dc}.p}{\pi} + I_{dc}.R_l \tag{6.37}$$

$$\therefore I_{dc} = \frac{(\overline{V_{dc}} - \overline{V_{PCC}})}{\left(\frac{3.\omega_r.L.p}{\pi} + R_l\right)} \tag{6.38}$$

By substituting equation (6.38) into equation (6.36)

$$Torque = \frac{3.\sqrt{3}.p.\Psi_f.(\overline{V_{dc}} - \overline{V_{PCC}})}{\pi.\left(\frac{3.\omega_r.L.p}{\pi} + R_l\right)} \tag{6.39}$$

By substituting equation (6.2) into (6.39) and where $E = \Psi_f.\omega_r.p.N_t$

$$Torque = \frac{3.\sqrt{3}.p.\Psi_f.\left(\frac{3.\sqrt{3}.\Psi_f.\omega_r.p.N_t}{\pi} - \Delta\overline{V_{dc}}\right)}{\pi.\left(\frac{3.\omega_r.L.p}{\pi} + R_l\right)} \tag{6.40}$$

Equation (6.40) shows that generator torque is a function of rotational speed, ω_r, which appears on both the numerator and denominator. The term involving the rotational speed on the denominator is in actual fact equal to the equivalent resistance caused by the commutation voltage drop in equation (5.47) and because the effect of a small change of rotational speed on this resistance is limited, it can be assumed to be constant. Therefore the generator torque is given by equation (6.41) as a function of the turbine rotational speed, and will therefore provide the required damping to the wind turbine drive-train.

$$Torque = \frac{3.\sqrt{3}.p.\Psi_f.\left(\frac{3.\sqrt{3}.\Psi_f.\omega_r.p.N_t}{\pi} - V_{PCC}\right)}{\pi.\left(R_{equiv} + R_l\right)} \tag{6.41}$$

The generator torque can also be written in terms of the generator slip, by substituting equation (6.9) into equation (6.39), to give:

$$Torque = \frac{3.\sqrt{3}.p.\Psi_f.(-slip.V_{PCC})}{\pi.\left(R_{equiv} + R_l\right)} \tag{6.42}$$

Drive-train model

In order to demonstrate the damping capability of the rectified PM generators, a dynamic model of the wind turbine drive-train has been developed for use with the simplified system model. Representation of a wind turbine drive train by a multi-mass model is introduced by [6] and expanded upon by [7], which provides a comparison of 6-mass, 3-mass and 2-mass models of a wind turbine rotor and drive-train. It is concluded by [7] that a 2-mass model allows the mechanical dynamics to be expressed with a level of accuracy that is suitable for modelling the performance of a wind

turbine in electrical grid transient studies; therefore a 2-mass model will be used here.

The model developed is based around the equations of motion set out above, altered to include the gearbox. The gearbox is incorporated into the model by combining the gearbox and generator rotating masses, as shown in Figure 6-35. The effect of the ratio between the low speed and high speed sides of the gearbox on the inertias, speeds and shaft stiffness is included by referring them to the high speed side of the gearbox using equations (6.43), (6.44) and (6.45); where the referred quantities are primed (x'). The equivalent drive shaft linear stiffness in [8] is referred to the high speed of the gearbox using equation (6.46).

The gearbox of a wind turbine can be represented by two rotating masses, each with its own inertia, as shown in [7]. The combined inertia of the gearbox components is determined here as a proportion of the generator inertia using data given in [7] as a guide. The block diagram of the drive train model is shown in Figure 6-36 and the parameters of the various model components are given in Table 6-2. The mechanical damping of the drive shaft, given in [8], is negligible relative to the stiffness, therefore it is neglected in this model.

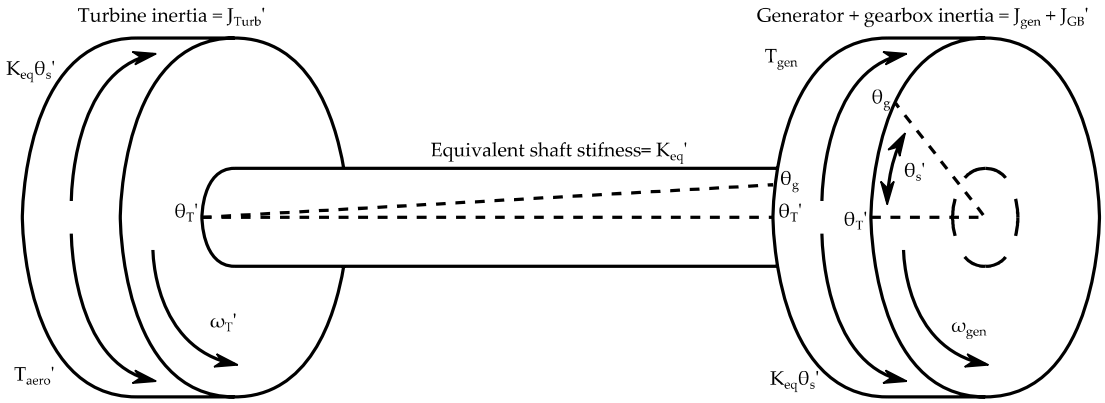

Figure 6-35: Two mass drive-train diagram showing the turbine quantities referred to the high speed side of the gearbox.

$$T'_{aero} = \frac{T_{aero}}{N_{GB}} \tag{6.43}$$

$$\omega'_T = \omega_T . N_{GB} \tag{6.44}$$

$$J'_{turb} = \frac{J_{turb}}{N_{GB}^2} \tag{6.45}$$

$$K'_{eq} = \frac{K_{eq}}{N_{GB}^2} \tag{6.46}$$

The equations of motion of the drive-train model, including the gearbox, are therefore given by equations (6.47) to (6.50).

Turbine rotor equation of motion:

$$T'_{aero} = J'_{turb} . \frac{d\omega'_T}{dt} + T'_{shaft} \tag{6.47}$$

$$J'_{turb} . \frac{d\omega'_T}{dt} = T'_{aero} - \theta'_s . K'_{eq} \tag{6.48}$$

Generator equation of motion:

$$T_{shaft} = \left(J'_{GB} + J_{gen}\right) . \frac{d\omega_{gen}}{dt} + T_{gen} \tag{6.49}$$

$$\left(J'_{GB} + J_{gen}\right).\frac{d\omega_{gen}}{dt} = \theta'_s.K'_{eq} - T_{gen} \tag{6.50}$$

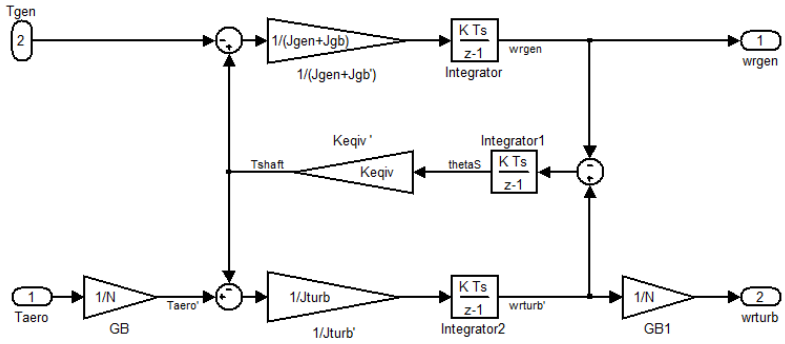

Figure 6-36: Dynamic wind turbine drive train model.

Table 6-2: Wind turbine mechanical drive-train parameters [8].

Generator inertia	534.1 kg.m^2	Referred turbine rotor inertia	3766 kg.m^2
Turbine rotor inertia	3.54x10 ^{7} kg.m^2		
Gearbox inertia	0.57 x Generator inertia	Equivalent shaft stiffness	9.21x10 ^{4} Nm/rad

Observations and conclusions

By inserting the drive-train model into the simplified system model, the damping applied to the drive-train by the slip capability can be demonstrated. To provide a benchmark for comparison where there is little damping in the system, the commutation voltage drop is removed from the simplified model and the DC line impedances reduced by a factor of 1000 to eliminate the influence the voltage drop across them may have. The step changes of wind speed used in the previous chapter to demonstrate the operation of the simplified model are again applied here.

It can be observed in Figure 6-37 that in the benchmark case there is a significant oscillation present on the generator torque. This oscillation is the

result of the under-damped 2nd order nature of the mechanical drive-train; the magnitude of the oscillation visibly decays with time due to the damping effect of the remaining DC line resistances, but overall the system remains severely under-damped. By comparing the benchmark system torques with those where the commutation voltage drop is included in the model, in Figure 6-38, it can be clearly observed that the inclusion of the commutation voltage drop provides sufficient generator slip to damp the drive train oscillation; therefore demonstrating that the generator slip is naturally capable of providing the required drive train damping, without any active controller influence.

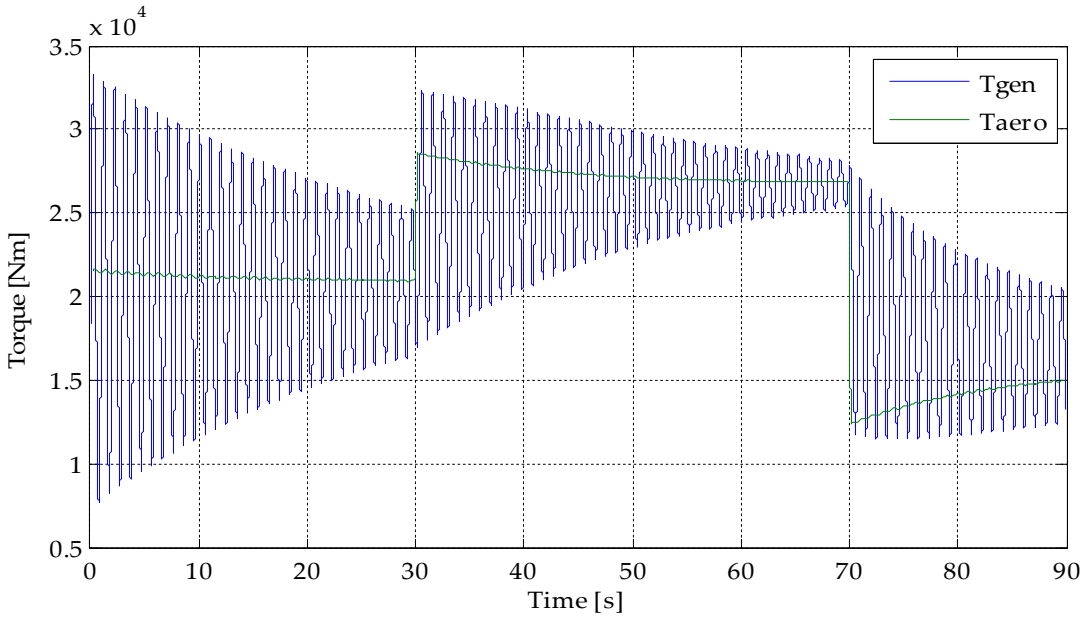

Figure 6-37: Benchmark generator and aerodynamic torque (referred to the high speed side of the gearbox) when the rectifier commutation voltage drop is not included in the simplified model.

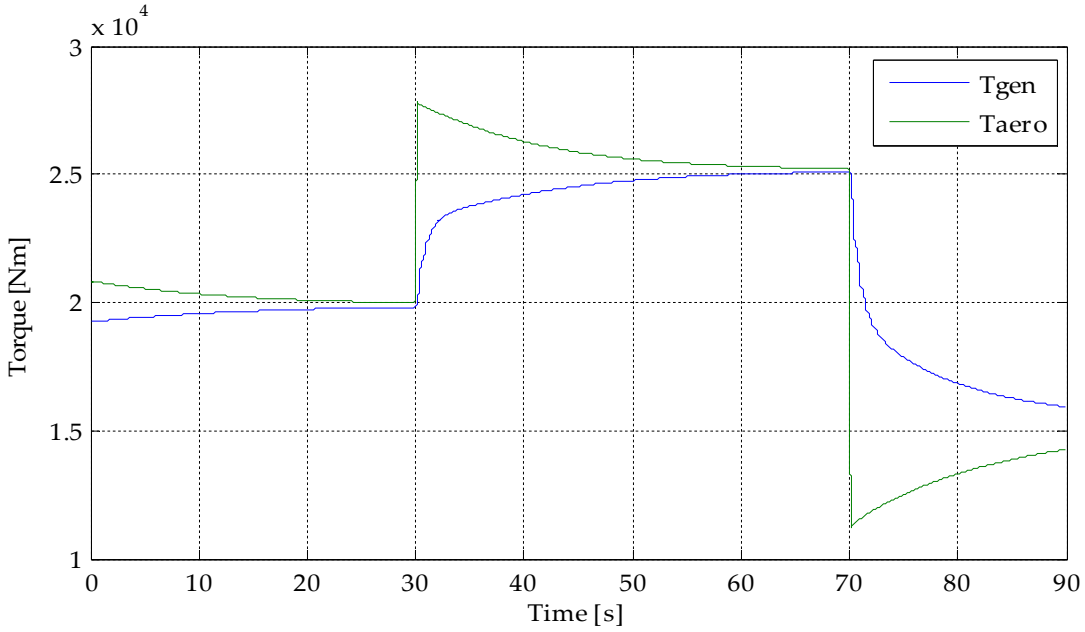

Figure 6-38: Generator and aerodynamic torque (referred to the high speed side of the gearbox) when the rectifier commutation voltage drop is included in the simplified model.

6.3 What are the effects of collective control on the operation of the wind turbines?

Connecting multiple wind turbines in an electrical cluster effectively removes their independence; causing their operation to become closely related. This section will investigate the impact of different cluster sizes and how the turbines interact on their operational performance. Firstly the effect of controlling the turbines in different sizes of cluster, collectively, on their performance will be investigated; then the interactions between the turbines when they are subject to different wind speeds will be studied. Lastly, an investigation into the superposition of the current harmonics produced by each turbine within the cluster common output cable will be performed.

6.3.1 Collective versus individual wind turbine control

The effects of collective control can be determined by observing the ability of the wind turbines to follow the optimum operating curve. The maximum number of wind turbines in a cluster considered in this thesis is five; therefore the operational performance of the clustered turbines will be investigated for cluster sizes of one, two and five turbines. Similarly to above, the performance of the turbines will be investigated when they are subject to the continuously varying wind speed profiles shown in Figure 6-16, and the generator torque and rotational speed of each turbine will be plotted against the optimum turbine torque speed characteristic.

Performance of a single turbine

It can be observed in Figure 6-39 that when a single turbine is controlled directly by the cluster controller, its operating point follows the optimum curve very closely. This behaviour demonstrates that the controller is capable of closely regulating the speed of the turbine so that it follows changes of the wind speed incident on the turbine, therefore maximising its energy capture efficiency.

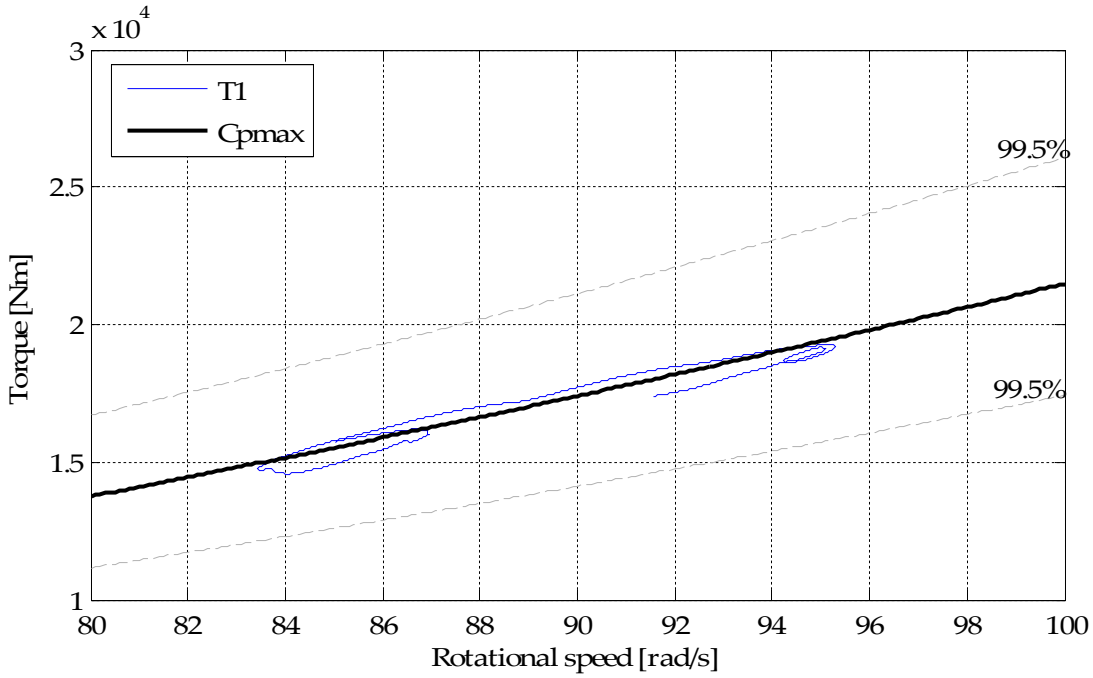

Figure 6-39: Single turbine cluster generator torque with rotational speed in response to continuously varying the wind profiles; against the Cpmax and 99.5% of Cpmax operating characteristics.

Performance of a two turbine cluster

When there are two turbines present in a cluster the operational behaviour of the turbines is slightly different. It can be observed in Figure 6-40 that the range of turbine rotational speed variation is more limited and the generator operating points stray further from the optimum. This demonstrates that the introduction of a second turbine diminishes the performance of the first turbine, whilst also preventing the optimum operation of the second turbine; highlighted in particular by comparing the operational performance of turbine 1, between this case and the previous case, since this turbine is subject to the same wind speed profile in both cases.

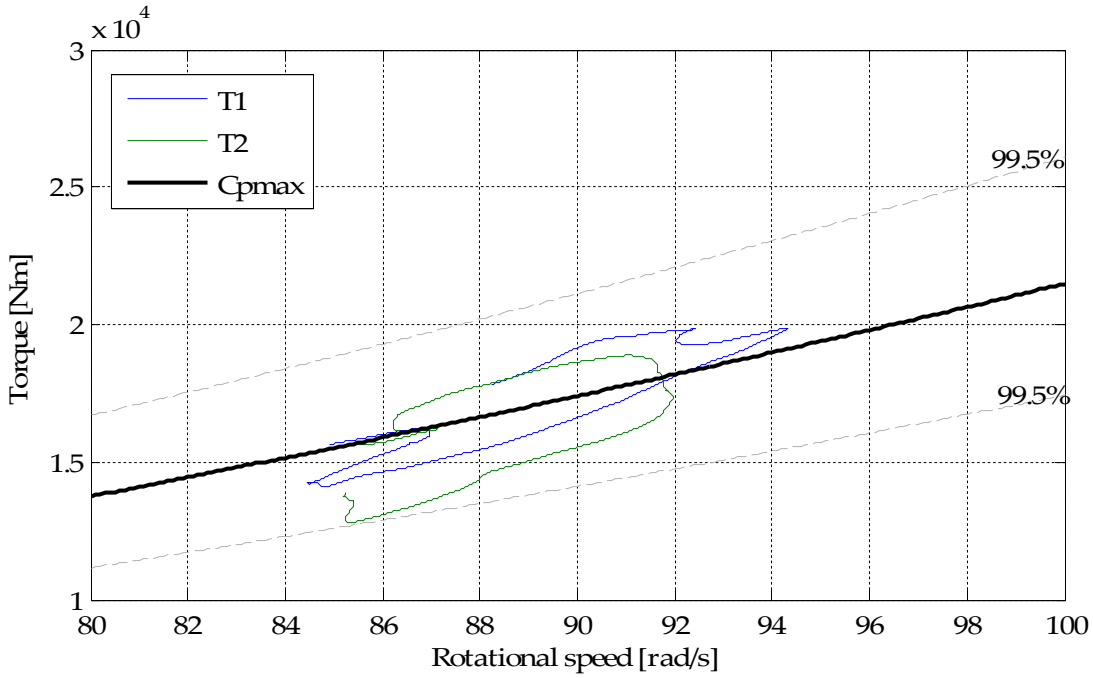

Figure 6-40: Two turbine cluster generator torque with rotational speed in response to continuously varying the wind profiles; against the Cpmax and 99.5% of Cpmax operating characteristics.

Performance of a five turbine cluster

Furthermore, when the cluster size is increased to five wind turbines it can be observed, by comparing Figure 6-40 and Figure 6-41, that the range of rotational speed variation is again slightly smaller, but that the proximity of the operating points to the optimum, does not significantly diminish further. This indicates that increasing the size of the cluster to five turbines has only a limited extra negative impact on the operational performance of the turbines.

However, by again comparing the performance of turbine 1 here with the first case, highlights that the collective control still has a significant detrimental effect on the operational performance of the turbines.

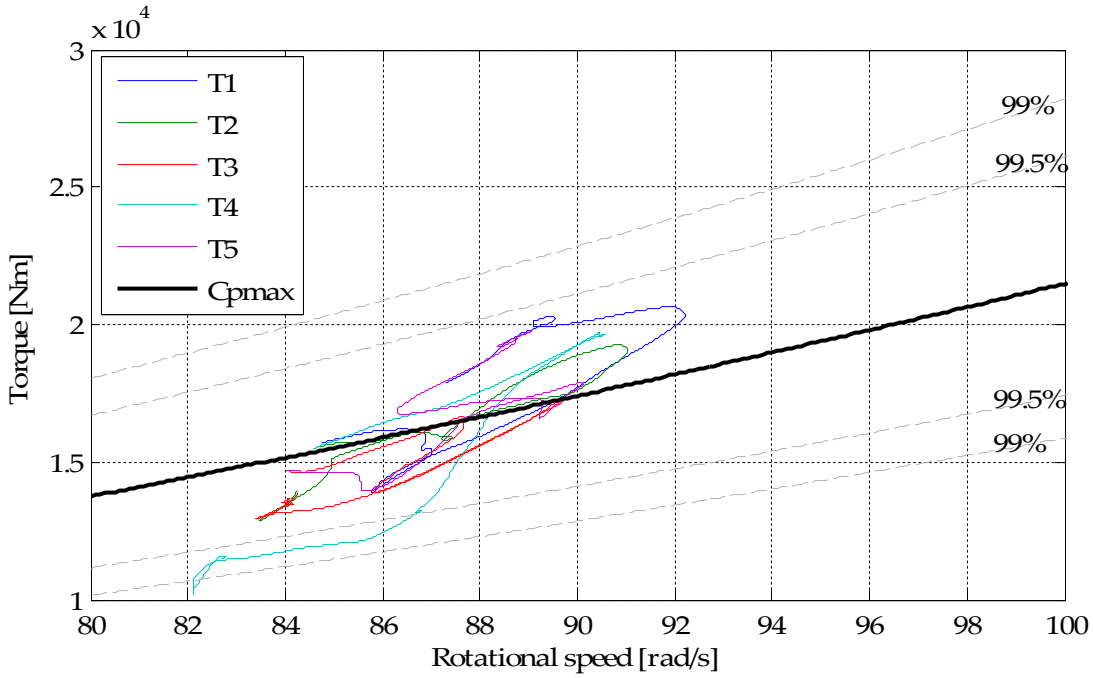

Figure 6-41: Five turbine cluster generator torque against rotational speed, in response to continuously varying the wind profiles; along with the Cpmax, 99.5% and 99% of Cpmax operating characteristics.

Conclusions

It is proven by this investigation that the operation of the turbines, and their capability to respond to the continuously changing wind speeds, is negatively affected by the collective control of the turbines. However, it is observed that the largest relative impact occurs when the cluster size is increased from one turbine to two, and that the relative impact of the extension of the cluster to include five turbines is limited. While it appears that the collective control of the turbines has an observable negative impact on the operation of the turbines, it should be noted that in all of the cases investigated, the turbine operating points largely remain within the 99.5% of the maximum rotor power coefficient, and therefore the impact on the overall total energy capture of the clustered turbines is small.

6.3.2 Interactions between the turbines in a cluster

The parallel connection of the clustered turbines provides the means for the turbines to interact. In particular the turbines will interact when they are each producing different amounts of power and rotating at different speeds as a result of different local wind speeds. The cluster common point voltage in a DC cluster has a key influence over each of the turbines, as it is the voltage difference between this point and the average rectifier output voltages that governs the output current and power flow from each turbine. Therefore the variation of this voltage with changes of power output from each turbine is the predominant cause of the interactions between the turbines.

There are two primary influences on the cluster common point voltage: the action of the controller, which regulates the cluster converter voltage and therefore the common point voltage, and also the voltage difference that arises across the cluster common output cable, as a result of its conduction resistance and the current flowing through it, which is the aggregate of the output current from each of the clustered turbines. The cluster converter voltage is regulated by the controller and responds to changes of the cluster output power; therefore if the power output from the cluster changes, as a result of a wind speed change on a single turbine, the cluster controller will change the converter voltage. Similarly if the output of a single turbine increases, the current flow through the cluster common cable will increase, driving up the voltage difference across its impedance. The effect of a change of the common point voltage, for example an increase, on the remaining turbines is a reduction of the voltage difference between the

common point and their individual rectifier terminals, lowering their output currents. This reduction of current is effectively caused by components of current circulating between the turbine whose wind speed has increased and the remaining turbines whose wind speeds are constant, causing the reduction of the output currents of these turbines. As shown earlier in this chapter, the output current of each turbine is directly related to the generator torque, and therefore as a result of the circulating current components the generator torque will fall, allowing the turbine rotational speeds to accelerate. This increase of rotational speed, however, increases the voltage at the rectifier terminals and therefore causes the output current of the turbines to rise again, also increasing the generator torque and slowing their acceleration as a result.

To determine the severity of the turbine interactions and to determine if either of the two possible causes of common point voltage change is the dominant cause of the interactions, two investigations are conducted: Firstly, the responses of turbines three to five to step changes of wind speed on turbines one and two is investigated, where both the cluster controller and the voltage difference across the common cable are allowed to influence the common point voltage; turbines three to five are each assigned a different wind speed that remains constant throughout the simulation run. Secondly, the cluster controller is disengaged and the cluster converter voltage held constant while the same changes of wind speed are applied, allowing just the effects of the voltage drop across the common cable to be observed. The spread of wind speeds across the turbines and the step changes applied, are shown in Table 6-3.

Table 6-3: Wind speeds used to investigate the interactions between the clustered turbines.

Turbine 1	8m/s increasing to 8.5ms/
Turbine 2	7.5m/s increasing to 8m/s
Turbine 3	7m/s constant
Turbine 4	6.5m/s constant
Turbine 5	6m/s constant

Case 1 – Cluster controller engaged

In response to the step changes of wind speed on turbines one and two, where the controller is free to regulate the cluster converter voltage, it is observed in Figure 6-42 that the rotational speeds of the turbines whose wind speeds are constant throughout, respond to the wind speed step changes on the adjacent turbines; confirming that the turbines in a cluster interact. The interactions are further highlighted by the variation of the voltage differences between the terminals of each rectifier and the cluster common point, shown in Figure 6-44 (plotted as a percentage of the voltage differences prior to the step change). It is observed that the step changes on turbines 1 and 2 cause their voltage differences to increase as a result of their greater power outputs; whereas the voltage differences of turbines three to five, enlarged in Figure 6-46, fall and settle to a new steady state level. This effect gives rise to the circulating current components flowing between turbines 1 and 2, and turbines 3 to 5, as a result of their increased power outputs.

The response of turbines 3 to 5 can be separated into two parts: a transient response and a steady state response. The transient response occurs as a result of the initial increase of the common point voltage, which causes

initially large circulating current components to flow which lower the net turbine output currents and therefore the generator torques allowing the turbines to accelerate, as shown in Figure 6-44.

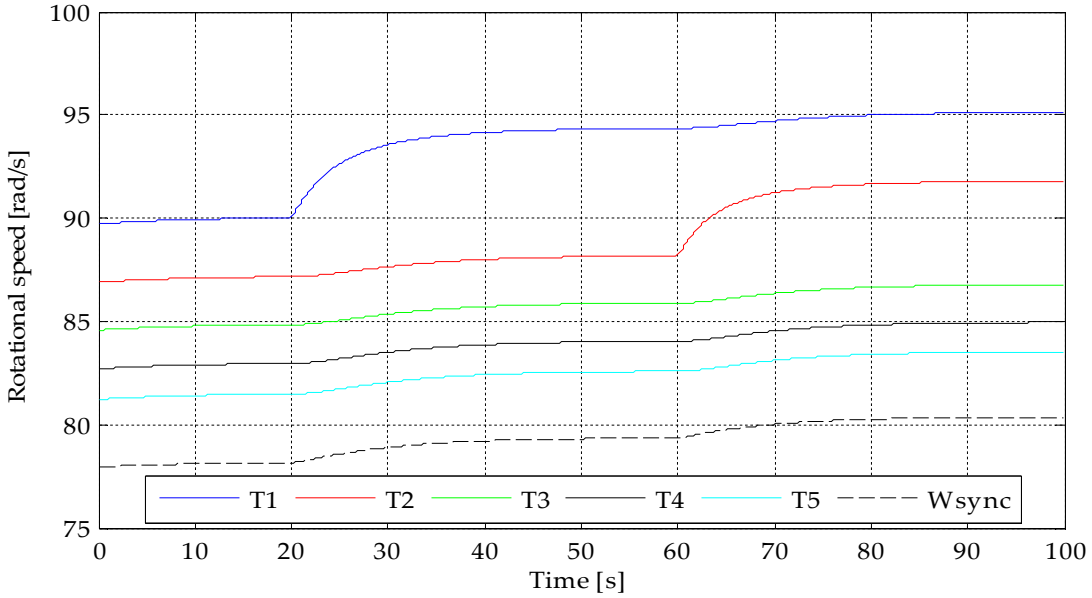

Figure 6-42: Turbine rotational speed and cluster synchronous speed when turbines 1 and 2 are subject to increases of wind speed after 20 and 60 seconds respectively.

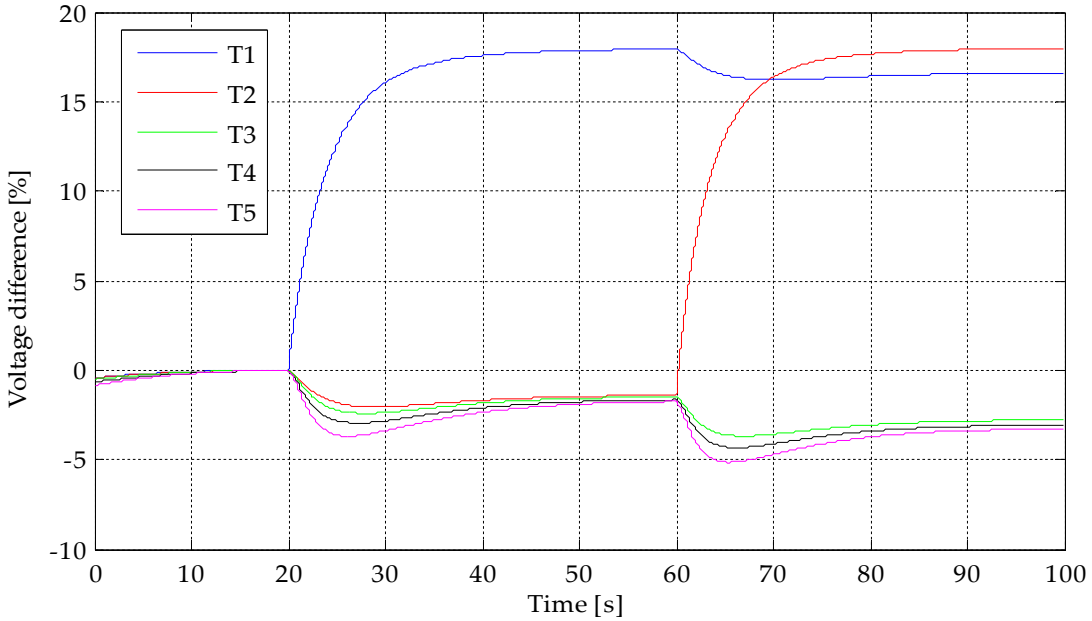

Figure 6-43: Voltage differences between the output terminals of each rectifier and the cluster common point, as a percentage of the voltage differences immediately prior to the first wind speed step change.

The steady state response is caused by the approximately constant power output of these turbines and their increased rotational speeds and rectifier terminal voltages, requiring a smaller current to transfer the same power. It is further shown by Figure 6-44 that the steady state response of turbine 5, whose wind speed is furthest from that of turbine 1, is greatest. This occurs because the circulating current component caused by its interaction with turbine 1 is a larger proportion of its overall current than for the other turbines, therefore lowering its generator torque by the greatest amount causing its rotational speed to increase furthest, as shown in Figure 6-45.

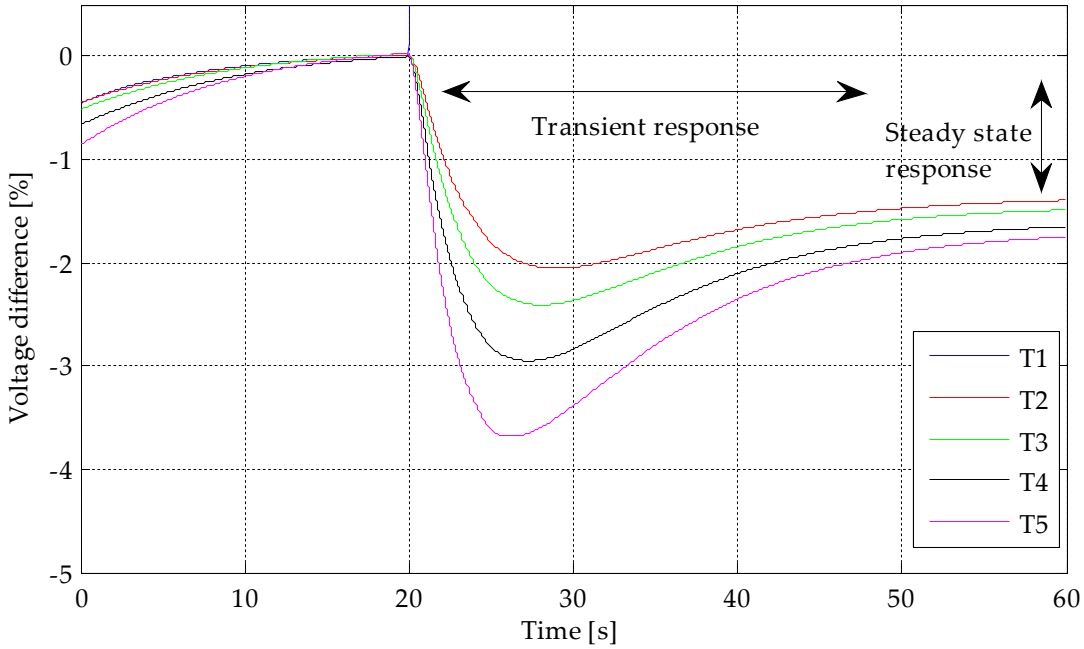

Figure 6-44: Enlarged percentage voltage differences between the output terminals of the rectifiers and the cluster common point, indicating the transient and steady state responses.

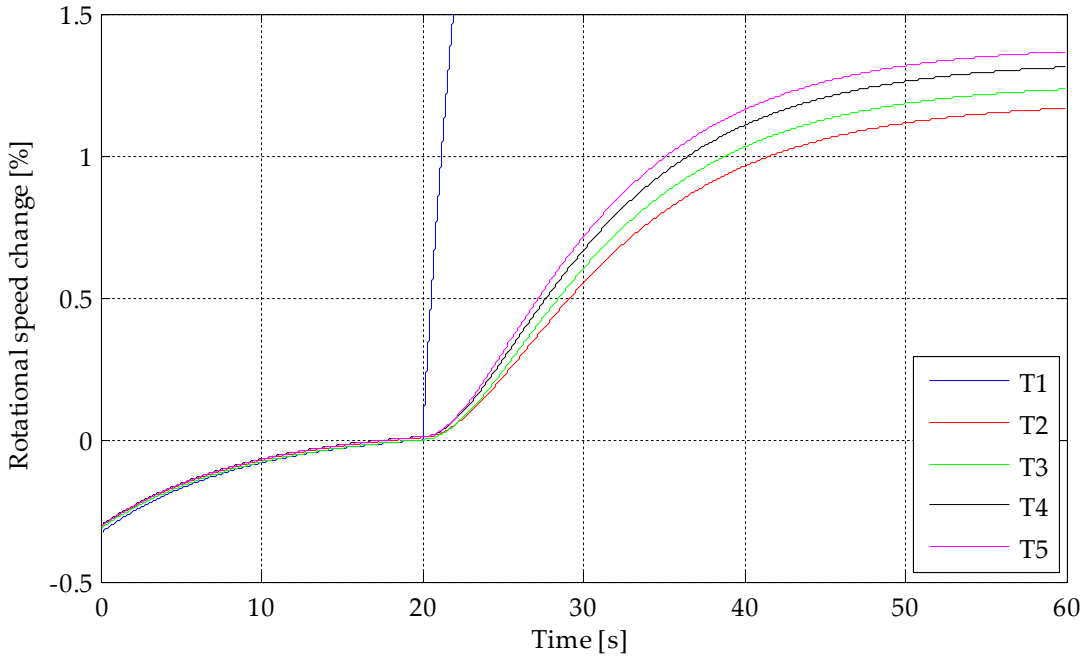

Figure 6-45: Turbine rotational speed change as a percentage of their rotational speeds before the wind speed step change to turbine 1 is applied.

Case 2 – Cluster controller disengaged and converter voltage fixed

Disengaging the cluster controller and holding the cluster converter voltage constant, allows the influence of the voltage drop across the cluster common output cable on the interactions between the turbines to be isolated. It is observed from Figure 6-46 and Figure 6-47 that as a result of applying the same wind speed step changes to turbines 1 and 2, the response of the remaining turbines is significantly smaller than those shown above. It is further shown by Figure 6-48 that the voltage differences between the cluster common point and each of the turbine rectifiers are not significantly affected. This indicates that the voltage drop across the cluster common output cable has a negligible influence on the interactions that occur between the turbines. The primary cause of this limited impact is the relatively small size of the current magnitude (approx. 200 - 215Amps), which, when multiplied by the

cable resistance (0.366Ω), gives a voltage drop 79V, which is approximately 0.24% of the converter voltage magnitude.

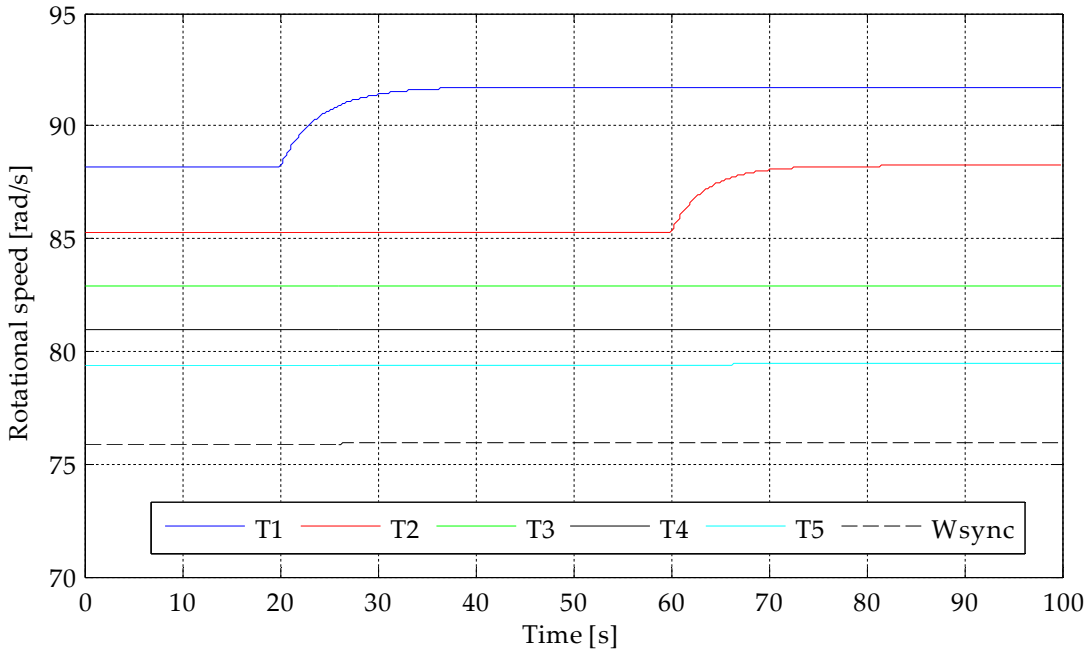

Figure 6-46: Turbine rotational speed and cluster synchronous speed when turbines 1 and 2 are subject to increases of wind speed, after 20 and 60 seconds respectively, where the cluster converter voltage is held constant.

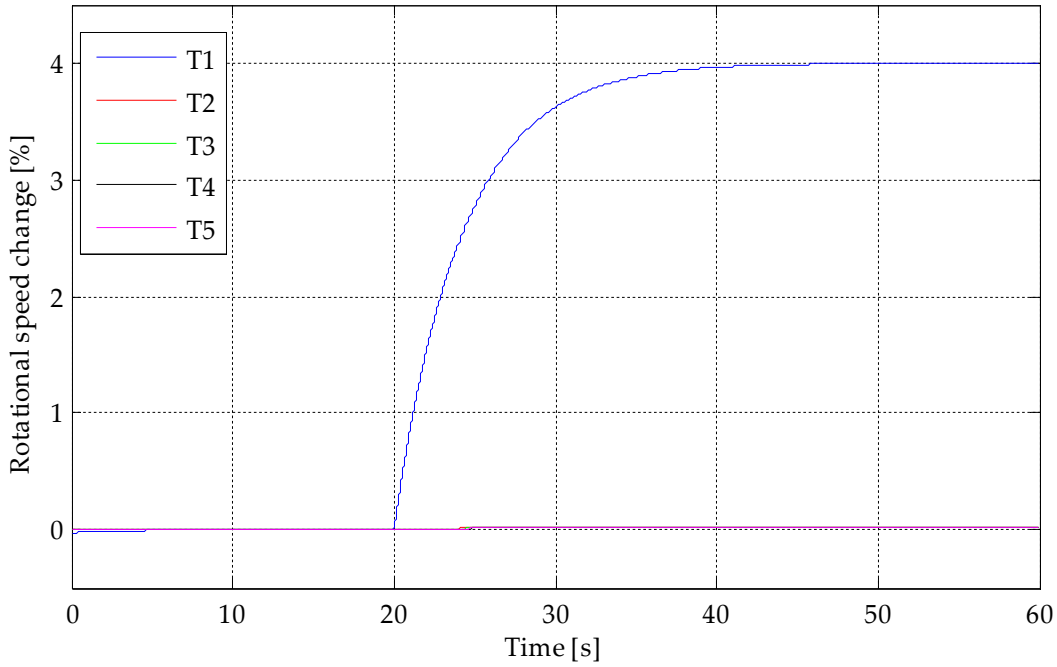

Figure 6-47: Change of turbine rotational speed as a percentage of their rotational speeds before the step change on turbine 1 is applied; where the cluster control voltage is fixed.

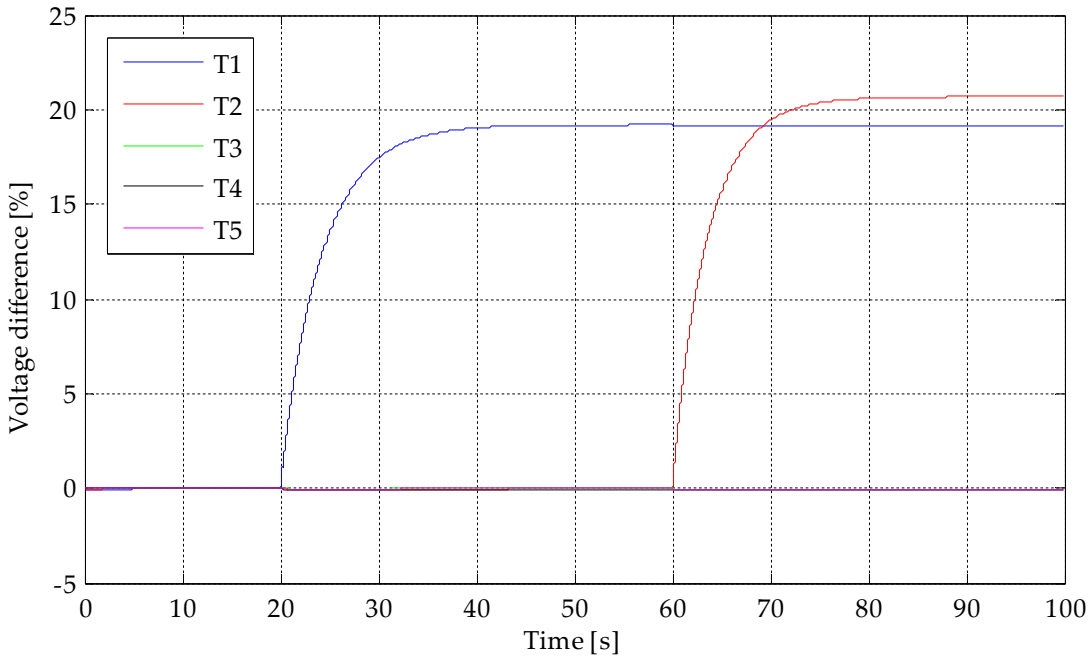

Figure 6-48: Voltage differences between the output terminals of each rectifier and the cluster common point, as a percentage of the voltage differences immediately prior to the first step change; where the cluster control voltage is fixed.

Conclusions

This investigation therefore proves that although there are two possible causes of the change of the cluster common point voltage, the impact of the controller action to optimise the converter voltage for the average wind speed across the cluster, is dominant. It is also proven that a change of cluster common point voltage, due to the increased output of one turbine, causes circulating current components to flow from this turbine towards the remaining turbines, reducing their generator torques and causing them to accelerate initially and then settle to new steady state operating points.

6.3.3 Harmonic superposition

Within the common cluster output cable the current and power produced by each turbine is aggregated. In addition, the harmonics that are present on the output DC currents of each turbine, as a result of the rectification process, are superimposed. The frequency of the current harmonics produced by the clustered turbines are likely to be different, since they are directly related to the turbine rotational speed which are unlikely to be equal. Therefore when the currents produced by each turbine are aggregated in the cluster output cable, the superposition of the harmonic components will produce a resultant harmonic component with a frequency equal to the difference between them. Where the rotational speeds of the turbines in the cluster are similar the difference between the harmonic frequencies will be small, therefore the frequency of the harmonic component that results from their superposition will also be small, and vice versa when the differences between the turbine rotational speeds are larger giving a higher frequency component.

This current harmonic component has the potential to influence the voltage at the cluster common point, since it is a function of voltage drop across the cluster common output cable, as mentioned above. It therefore also has the potential to influence the current outputs of each turbine and therefore the torque produced by the generators; potentially causing additional oscillations within the wind turbine mechanical drive trains.

To investigate the impact of this harmonic component on the operation of the cluster of turbines the full system model, detailed in Chapter 4, is used so that the harmonic emission of the rectifiers is included in the simulations. The model is reduced to include only two turbines to allow the superposition of the harmonic components to be observed with the greatest clarity.

To begin with the wind speeds incident on the turbines are equal at 7m/s, which causes the turbines to rotate with the same speed and therefore produce current harmonics with the same frequency. A step increase from 7m/s to 8m/s is then applied to turbine 1 so that they rotate with different speeds and produce different frequency current harmonics.

It can be observed from Figure 6-49 that initially, as expected, where the wind speeds incident on the turbines are equal, they rotate with equal speeds and produce current harmonics of the same frequency (161Hz); also it can be observed that the harmonic components superimpose perfectly and there is no resultant low frequency harmonic component. However, when the wind speeds are different, and the turbines rotate with different speeds, causing them to produce current harmonics with different frequencies (176.4Hz, 170Hz respectively), in Figure 6-50, the superposition is no longer perfect

and a lower frequency component is present (6.4Hz). As mentioned above the presence of this low frequency component will be reflected onto the voltage at the cluster common point, which is shown in Figure 6-51; however the relative magnitude of this harmonic to the average voltage at this point is quite small. Therefore the impact of this voltage harmonic on the currents produced by each of the turbines is also small; this is also indicated by the individual turbine output currents shown in Figure 6-50, which do not exhibit a low frequency component to match the low frequency component present on the overall cluster output current.

Conclusions

It is therefore shown by this investigation that the low frequency harmonic components, present within the cluster common output cable, do not have a significant impact on the output currents of the individual turbines and therefore do not affect the generator torques and the operation of the turbines.

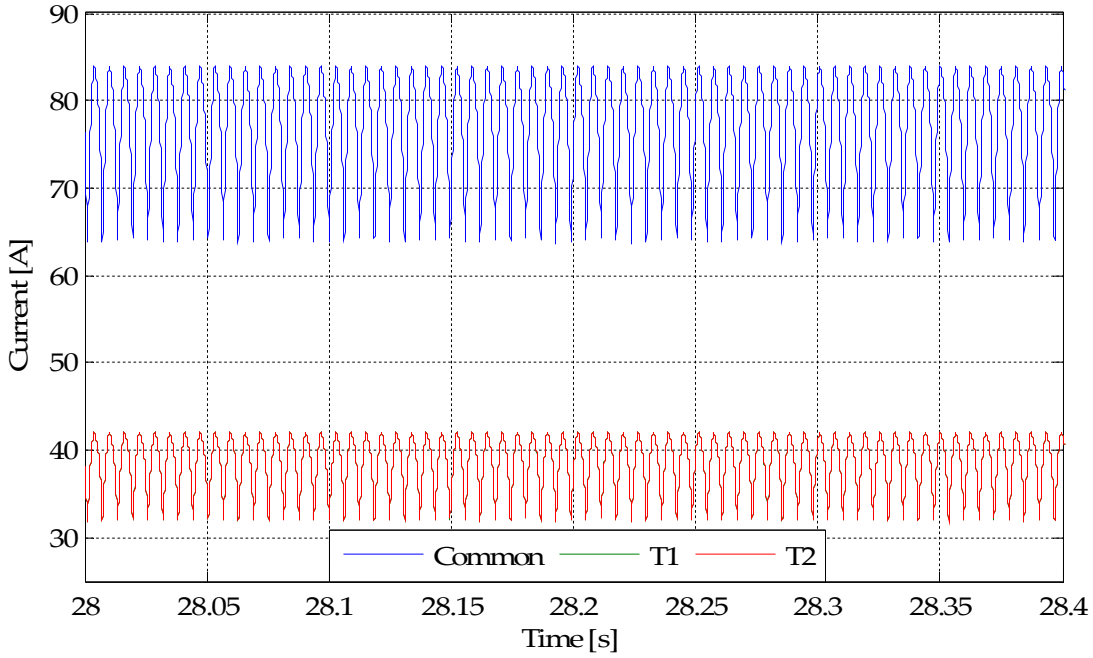

Figure 6-49: Cluster common cable and turbine currents where the wind speeds incident on each turbine are equal and they are rotating at the same speed.

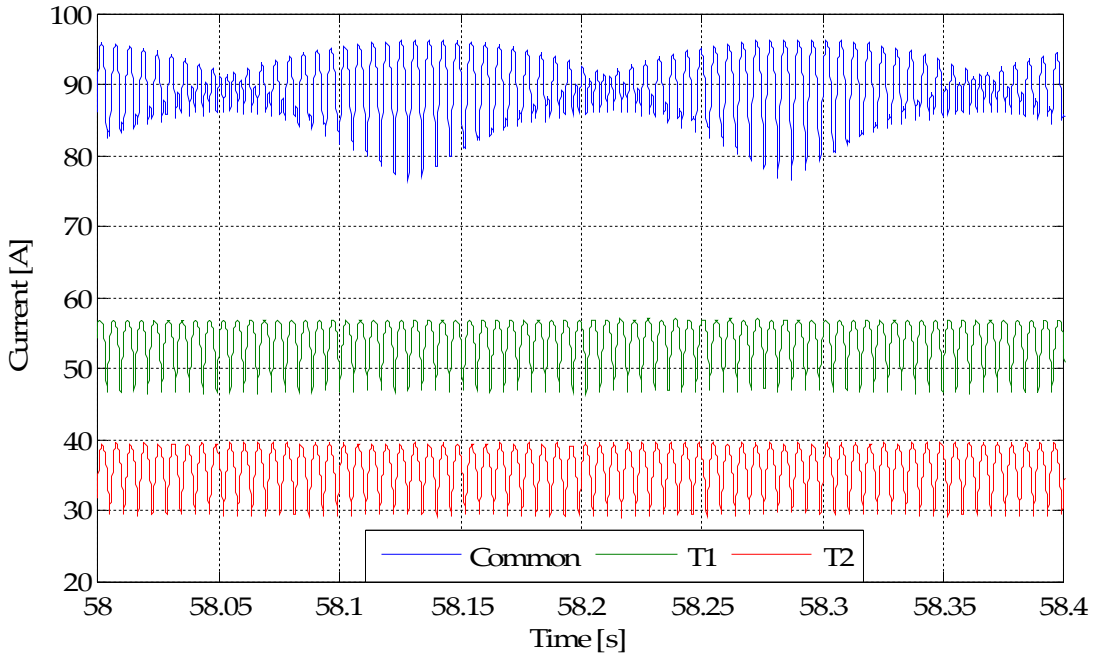

Figure 6-50: Cluster common cable and turbine currents where the wind speeds incident on each turbine are 8m/s and 7m/s respectively and they are rotating at different speeds.

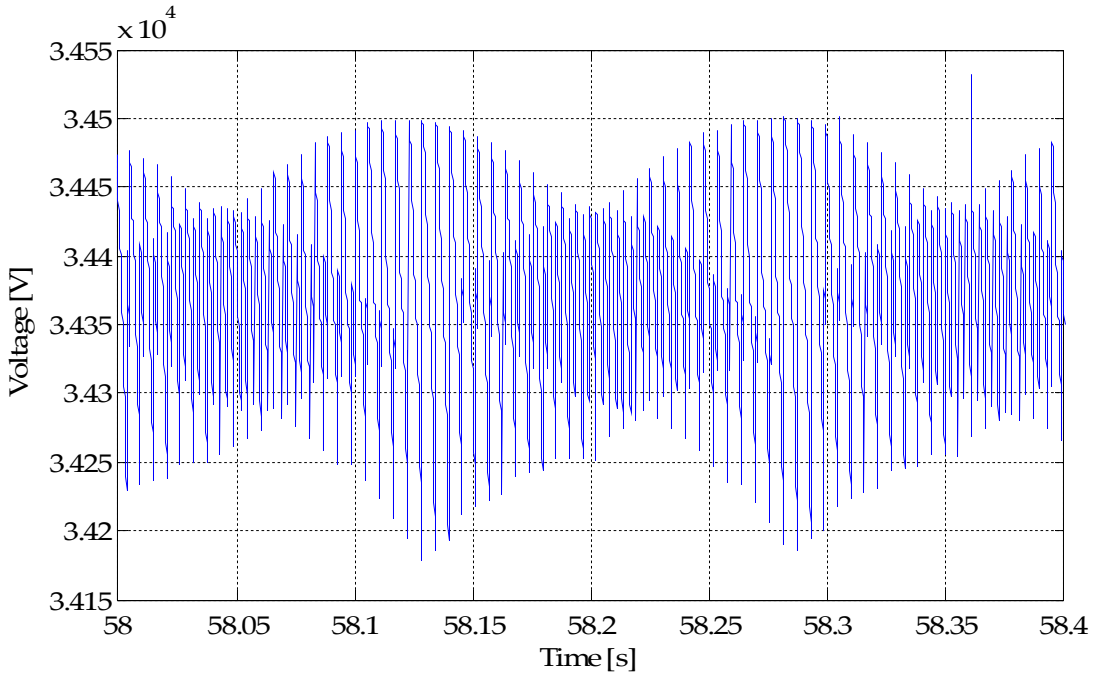

Figure 6-51: Cluster common point voltage when the wind speeds incident on each turbine are 8m/s and 7m/s respectively and they are rotating at different speeds.

6.4 Discussion and conclusions

The aim of this chapter has been to answer the following questions:

- How much generator slip can be achieved and what is the best way of achieving it?
- How much generator slip is required for achieving the optimal operation of the individual turbines?
- What effect does the collective control of the wind turbines have on their ability to achieve optimal operation?

It has been found that the generator slip of each turbine can be a function of both commutation overlap length and the size of any additional resistance added at the DC terminals of the rectifiers; therefore either can be used as a means to maximise the generator slip. However the maximum commutation length is limited to $\pi/3$ radians, which also limits the slip that can be produced by this method to 33.33%, and the introduction of additional resistance will significantly reduce the energy transfer efficiency of the electrical system. It has therefore been determined that the generator winding inductance required to maximise the commutation length, when the turbine is producing maximum power and to maximise the generator slip is 4.56mH which is not significantly larger than the inductance that is naturally present in the system, 3.9mH. The maximum generator slip that can be achieved without the addition of extra inductance is approximately 27%, which is close to the 33.33% maximum. It has also been proven that the maximisation of the voltage distortion caused by the commutation overlap has a negative impact upon the generator output power factor, but that it also proves beneficial to the reduction of the generator torque harmonic

distortion, causing the peak total harmonic distortion to occur at a lower level of power through-put (wind speed).

By investigating the effects of different amounts of generator slip on the operational performance of a cluster consisting of five wind turbines; it has been proven that up to approximately 33% slip is beneficial to their energy capture performance. In particular it has been proven that the 26% slip that can be achieved without adding additional inductance to the generator allows considerable amounts of freedom between the rotational speeds of adjacent turbines, improving their operational performance. However it has also been shown that the pursuit of greater amounts of slip, by the addition of extra inductive and resistive elements, will provide only limited further improvements to the energy capture performance. In addition the damping effect of generator slip on the mechanical drive train of a wind turbine has been proven to be advantageous, allowing the oscillation which naturally occurs due to its second order under-damped nature, to be sufficiently damped.

Lastly, it has been demonstrated that the collective control of different sizes of cluster diminishes the operational performance of the wind turbines; in particular the performance of a two turbine cluster exhibits the greatest detrimental effect in comparison to the operation of a single turbine controlled directly. It has also been shown that the increase of the cluster size to include five wind turbines does not cause the operational performance of the turbines to diminish significantly further. Through the simulation of the turbine responses when uneven wind speed changes are applied across the cluster, it has been shown that they interact; the dominant

cause of which is the action of the cluster controller to regulate the cluster common point voltage. In particular, the interactions have been found to be most prominent between the turbines whose wind speeds are furthest from the turbine experiencing the wind speed change, because the circulating current component is a larger proportion of its overall output current, prior the change of wind speed, than the other turbines. Finally is has been shown that the DC current harmonic components produced by the rectifiers of each turbine superimpose within the common cluster output cable producing a low frequency harmonic component. This harmonic component is reflected onto the cluster common point voltage, but its magnitude is small in comparison to the average voltage and therefore doesn't impact significantly upon the generator currents and torques of the turbines.

6.5 References

1. Barthelmie, R., et al., *Ten Years of Meteorological Measurements for Offshore Wind Farms.* Journal of Solar Energy Engineering, 2005. 127(2): p. 170-176.
2. T. Burton, D.S., N. Jenkins, E. Bossanyi, *Wind Energy Handbook*: J Wiley & Sons, Ltd.
3. Bossanyi, E., Z. Saad-Saoud, and N. Jenkins, *Prediction of flicker produced by wind turbines.* Wind Energy, 1998. 1(1): p. 35-51.
4. Bossanyi, E.A., *Wind Turbine Control for Load Reduction.* Wind Energy, 2003. 6(3): p. 229-244.
5. Geng, H., et al., *Comparison of oscillation damping capability in three power control strategies for PMSG-based WECS.* Wind Energy, 2011. 14(3): p. 389-406.
6. A. Hansen, P.S., F. Blaabjerg, *Dynamic modelling of wind farm grid interaction.* Wind engineering, 2002. 26(4): p. 191-208.
7. Muyeen, S.M., et al., *Comparative study on transient stability analysis of wind turbine generator system using different drive train models.* Renewable Power Generation, IET, 2007. 1(2): p. 131-141.
8. Jonkman, J., et al., *Definition of a 5MW reference wind turbine for offshore system development*. 2009, NREL.

Chapter 7 Experimental Validation

Up to this point, this thesis has focused on establishing the theoretical basis of the operation of a cluster collection network based upon rectified PM generators, and backing it up with computer simulations which demonstrate the various operational aspects of the system. While the computer simulation models developed have proven that the theoretical system operation is valid, the practicalities of implementing such a system are not taken into account. Therefore, in order to demonstrate that a cluster collection network can be implemented practically, the development of a laboratory scale test rig is detailed in this chapter. The simulation models of the system are based on the wind turbine specification set out in Chapter 4 which has a power output rating of 5MW; it is not possible to practically implement the system on this scale within the laboratory, therefore the test rig system is a scaled down version, by a factor of 2000, using 2.5kW generators.

This chapter will cover the development of the bench scale test rig, including a detailed description of its layout, the design decisions made and its operation. A scaled version of the simulation model developed in the previous chapters of this thesis will also be used alongside the test rig to allow comparisons to be drawn between the experimental and simulated operation of the test rig; with the aim of verifying the operational characteristics of the system, for example the production of generator slip.

7.1 Design of the bench scale test rig

The key components of a cluster collection network are the generators. The generators available for use in this test rig are taken from small wind turbines and are axial flux permanent magnet generators; two such generators are used and the parameters of which are given in Table 7-1. To provide the input torque to the generators induction motors are used in place of the wind turbine rotors, the use of which is not possible in the laboratory. Each induction motor is controlled by a proprietary three phase power electronic drive that allows the torque applied by the motor to the generator to be dictated by an external analogue input. The motor and drive parameters are also given in Table 7-1 and are rated to provide significant headroom over the generator rating. The motors and generators are coupled together through a gearbox and driveshaft.

Each generator produces a three phase sinusoidal output voltage and current when connected directly to a resistive load. Rectification of the generator voltages is conducted using three phase full bridge diode rectifiers that are self-contained, the components numbers of which are given in Table 7-1. In addition to the rectifiers a controllable DC voltage source is required; to provide this a two stage converter is developed and implemented, the design

and implementation of which will be described later in this chapter. The rectifiers and DC converter are connected together by single core cables and inductive and resistive elements are added to represent the properties of the cables that would be used in reality to couple the generators together.

The DC converter provides the primary means of control over the cluster of wind turbines; the control algorithm of the converter and the cluster collection system is implemented within a dSPACE microprocessor system which also provides the analogue torque reference input required by the induction motor drives. The dSPACE system allows the controller to be implemented using a Matlab Simulink model, therefore allowing the control algorithm developed in the system models to be transferred directly for use within the test rig; it also accepts analogue inputs which allow voltage and current measurements, produced by transducers placed throughout the test rig, to be read into the control algorithm. The overall layout of the mechanical and electrical subsystems of the test rig is shown in Figure 7-2; the location of the various transducers throughout the system is indicated by the dashed circles. In addition to the control algorithm, the model of the wind turbine rotor, which provides the link between wind speed and the aerodynamic input torque to the generator, developed in Chapter 4, is implemented within the dSPACE system to convert a numerical wind speed input into the equivalent aerodynamic torque for use as the torque reference inputs to the induction motors. The parameters of the small wind turbine from which the generators are taken are given in Table 7-1, its power coefficient vs tip-speed ratio characteristic is also given in Figure 7-1.

To aid the operation of the test rig, a user interface has been developed within the ControlDesk software that accompanies the dSPACE

microprocessor system. Using this interface it is possible to view and modify the parameters within the test rig control system in real-time; in particular it allows the wind speed that is applied to each turbine to be manually controlled. In addition, the user interface also allows the display of the voltage and current measurements provided by transducers placed throughout the system, both numerically and graphically. The user interface developed to aid the test-rig operation is shown in Figure B-4 in the Appendix.

Table 7-1: Test rig component parameters.

PM generator parameters			
Rated power output	2.5kW	Field constant (per phase)	1.626 V/rad^{-1}
Rated rotational speed	300rpm	Phase winding resistance	3.94Ω
Number of pole pairs	4	Phase winding inductance	32mH
RMS current rating	7.4A	**Motor Drive**	
Induction motor		Emerson Unidrive SP1405	
Leroy Somer LSMV 112MG		Power rating	4kW
Power rating	4kW	Rated current	8.8A
Rated voltage	400V	Rated voltage	400V
Rated rotational speed	1460rpm	**3 Phase Full Bridge Diode Rectifier**	
Gearbox ratio	3.09	Semikron SKD 2508	
Rated torque	84Nm	Rated current	20A
		Rated voltage	800V
Wind turbine			
Rated output power	2.5kW	Max Cp	0.4188
Rotor radius	1.893m	Opt tip-speed ratio	6.2

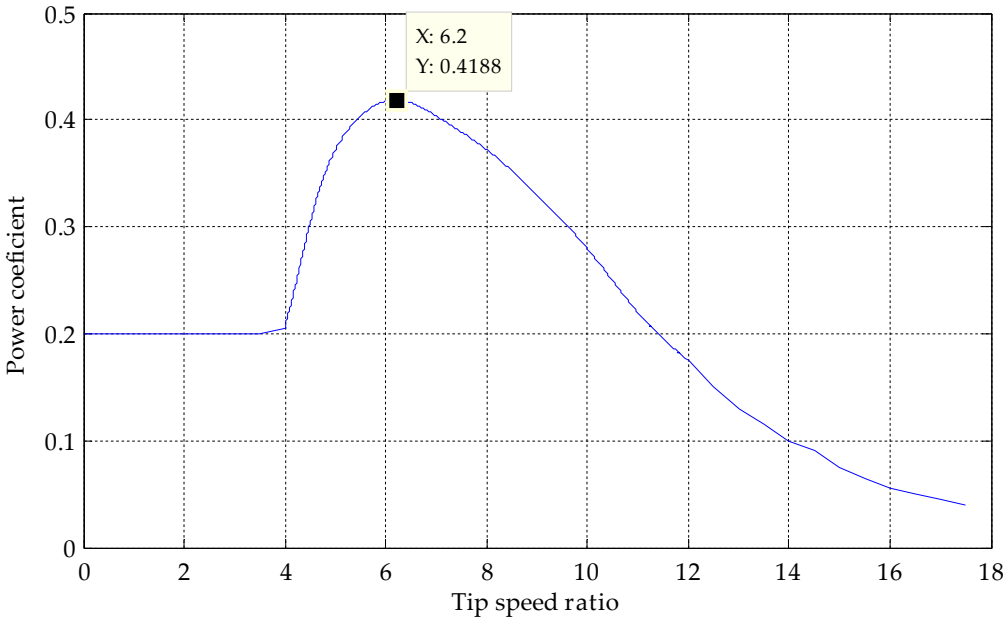

Figure 7-1: Test rig wind turbine tip speed ratio against power coefficient characteristic.

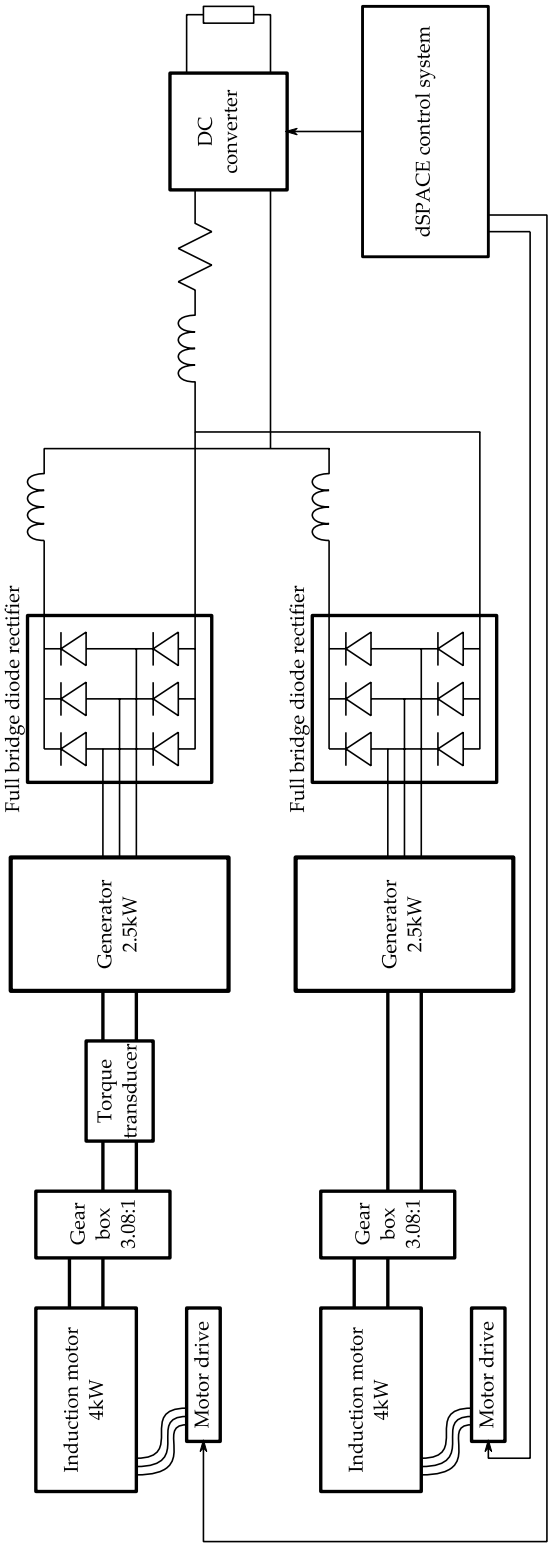

Figure 7-2: Test rig schematic diagram.

7.2 DC converter design and control

Within the system models, developed in the previous chapters of this thesis, an ideal controllable DC voltage source has been used to apply the main means of control to the system. To implement a controllable voltage source experimentally within the test rig a two stage DC-DC converter is developed and implemented. The primary objectives of this converter are to regulate the DC voltage of the collection cable network and to export the power generated by the turbines; by doing so it also indirectly regulates the rotational speeds of the generators. Within the laboratory the output power of the generators is fed into a resistive load, as shown in Figure 7-2.

7.2.1 DC-DC converter theoretical operation

The DC–DC converter is implemented by combining boost and chopper conversion stages. The boost converter acts to step-up the input voltage to a higher level, which in turn is kept constant by the chopper which modulates the current flowing into the load. Since the voltage on the output side of the boost converter is kept constant by the chopper, the boost converter is able to regulate the magnitude of its input voltage. The layout of the two conversion stages is shown in Figure 7-3.

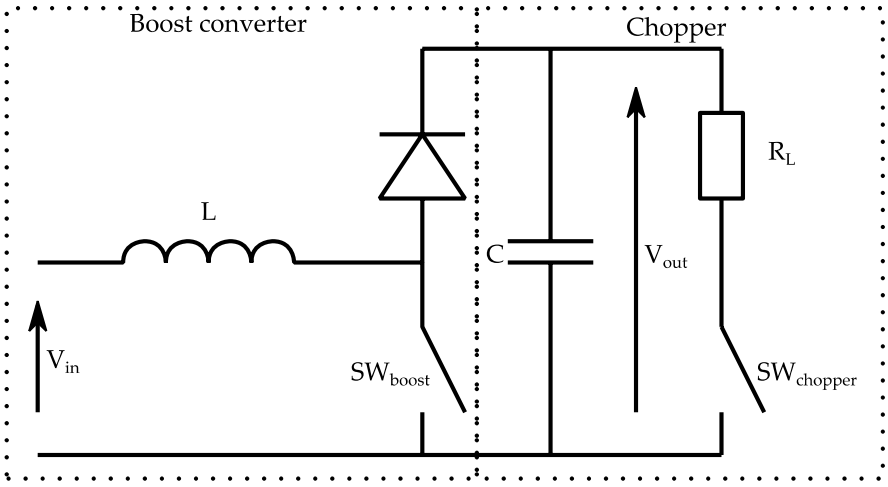

Figure 7-3: Schematic diagram of the DC converter.

Boost converter operation and design

The operation of a boost converter can be separated into two different states: switch closed and switch open [1]. When the switch is closed the diode is reverse biased and the input supplies energy to the inductor; when the switch is open the diode is forward biased and both the inductor and input supply energy to the output; it is assumed at this stage that the action of the chopper maintains a constant voltage at the output of the boost converter. The instantaneous voltage at the input terminals of the converter therefore changes depending upon the switch state: when the switch is closed the input voltage equals that across the inductor only, and when the switch is open the input voltage equals the output voltage minus the voltage across the inductor, as shown by the diagram and waveforms in Figure 7-4 and Figure 7-5. The average of the input voltage over one switching cycle gives the controlled voltage of the cluster; this voltage can be regulated by changing the converter modulation index, which dictates the proportion of a switching cycle the switch is closed to the proportion where it is open. The input voltage to the converter can be determined as a function of the output voltage using equation (7.2), where D is the modulation index of the converter, given by equation (7.1).

$$D = \frac{t_{on}}{T_S} = \frac{T_s - t_{off}}{T_s} \tag{7.1}$$

$$V_{in} = V_{out}.(1 - D) \tag{7.2}$$

A boost converter can operate in two different modes: where the input current is continuous or discontinuous; the converter used here is designed to operate in continuous conduction mode throughout the operating range of the cluster turbines.

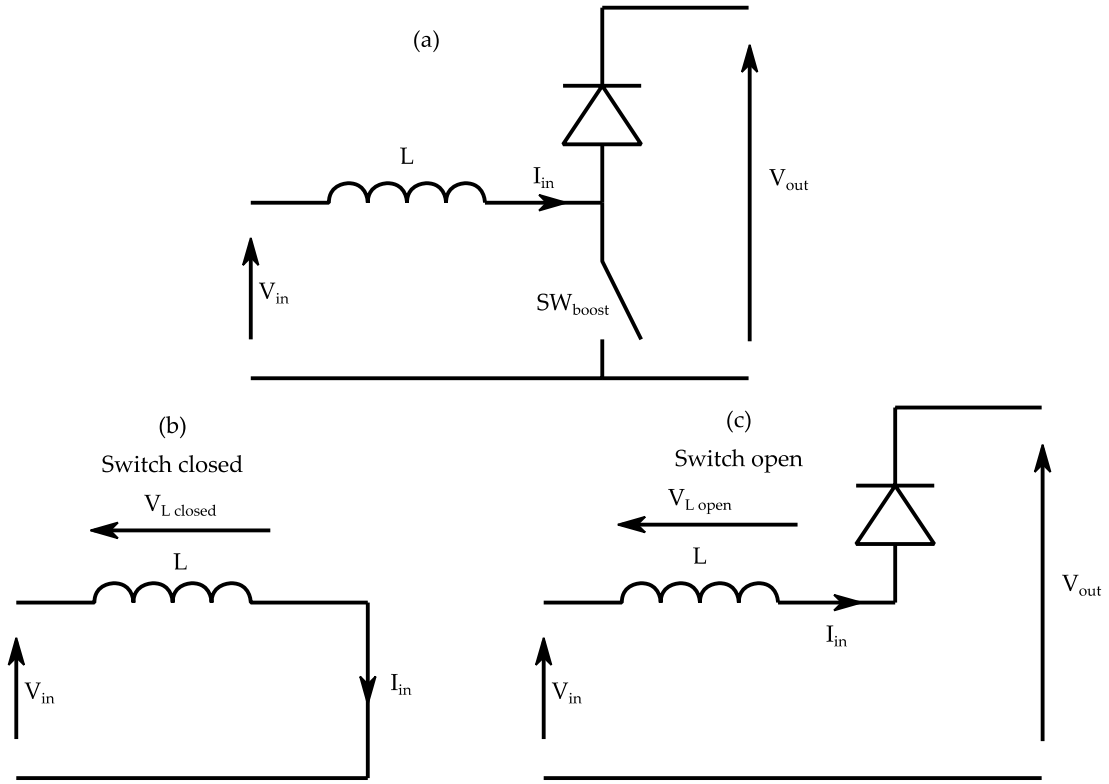

Figure 7-4: (a) Boost converter full circuit; (b) when switch is closed; (c) when switch is open [1].

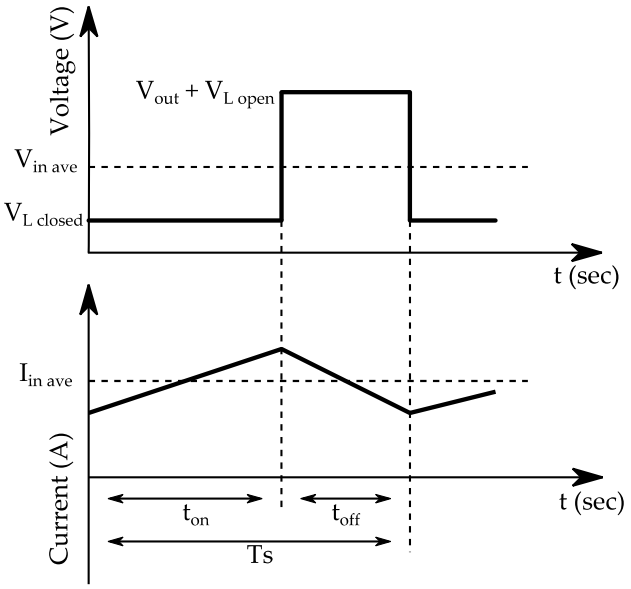

Figure 7-5: Boost converter input voltage and current during one switch cycle.

The average input current at which the operating mode of the converter passes between continuous and discontinuous current conduction is referred to as the boundary condition or boundary current [1]. This condition is a function of the size of the converter input inductance, L, the output voltage, V_{out}, the modulation index, D, and the switching cycle length, T_s; and can be determined using equation (7.3).

$$I_{inB} = \frac{V_{out}.T_s.D(1-D)}{2.L} \tag{7.3}$$

To ensure the converter operates in continuous conduction mode throughout the operating range of the wind turbines, the boundary current must be set below the minimum input current level and modulation index which corresponds to a single turbine in the system operating at its cut-in wind speed (4m/s) with optimal rotational speed. The optimum rotational speed of the turbine at this wind speed (13.1rad/s) is determined using the optimum tip-speed ratio for the turbine, given in Table 7-1. The required converter input voltage and currents that correspond to the turbine operation at this point are both functions of the generator field constant, the power captured from the wind and the voltage drops between the generator and the converter, including the commutation voltage drop. Therefore the algorithm developed in Chapter 5, with the parameters of the test rig in Table 7-1, is used to determine the characteristic between these quantities; the corresponding converter voltage, when only a single turbine is operating at its cut in wind speed, is 124.1V and the input current is 1.177A. The converter must therefore be designed so that the boundary current is below this level so that it remains is continuous conduction mode across its full operational range. A key factor in the converter design is the converter modulation index at which the minimum voltage and current occurs; this can

be calculated using equation (7.2), a process which also requires knowledge of the converter output voltage. The converter output voltage is optimised so that the turbines can rotate at the optimum speed for the wind speed at which is produces its maximum power output, 9.5m/s. The algorithm developed in Chapter 5 can again be used to calculate this voltage, taking into account the voltage drops in the system; the resulting maximum required converter input voltage is 242.6V. By allowing some headroom over this, the converter output voltage is chosen to be 350V; therefore the modulation index at which maximum operating point of the cluster occurs is 0.69. The inductor size and the switching cycle length that are therefore required to achieve a boundary current that is below the minimum operating condition can therefore be calculated using equation (7.3). The size of this inductor is limited by the equipment available for use in the laboratory and is therefore set to 25mH, leaving only the switching cycle length to be calculated by rearranging equation (7.3) and substituting in the variables. The minimum switch cycle length is therefore 0.735ms, which gives a switching frequency of 1361Hz; to provide some headroom between the boundary current and the minimum operating point, this frequency is rounded up to 1500Hz, which is still within the practical range of high capacity power converters.

Using these parameters and the control curve algorithm from Chapter 5, the modulation index required across the turbine operating wind speed range which allows the turbines to operate with optimum speed can be determined, as shown in Figure 7-6. Furthermore the input current to the converter across the operating wind speed range can be compared with the boundary current, confirming that the converter will maintain continuous

conduction mode across the full operating range of the turbine, as shown in Figure 7-7.

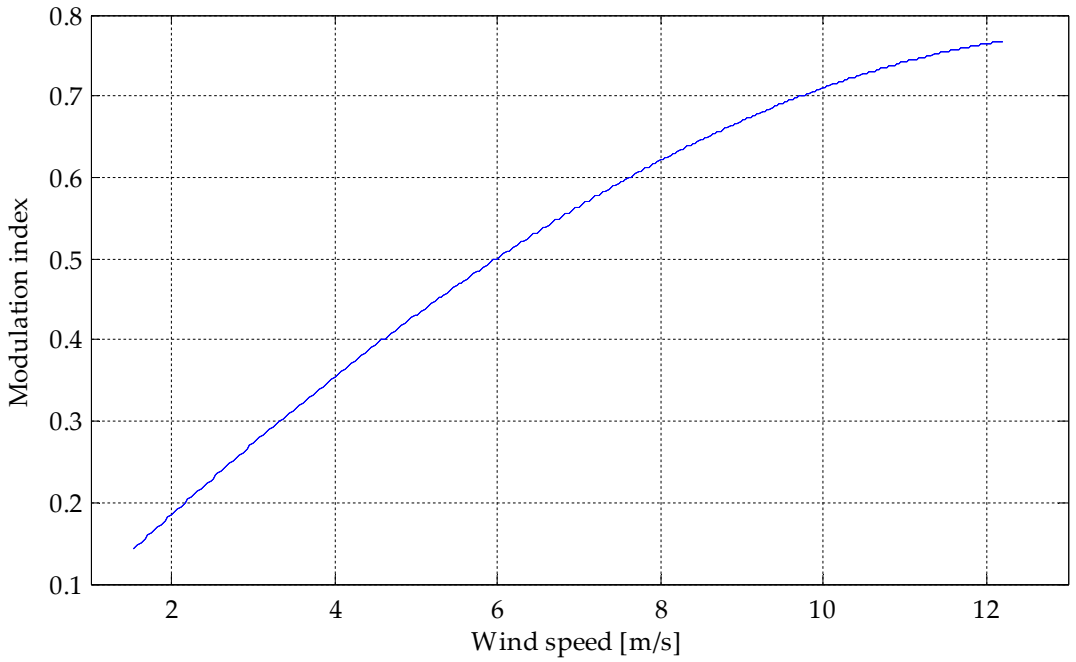

Figure 7-6: Boost converter modulation index required to optimise turbine rotational speed across the operating wind speed range.

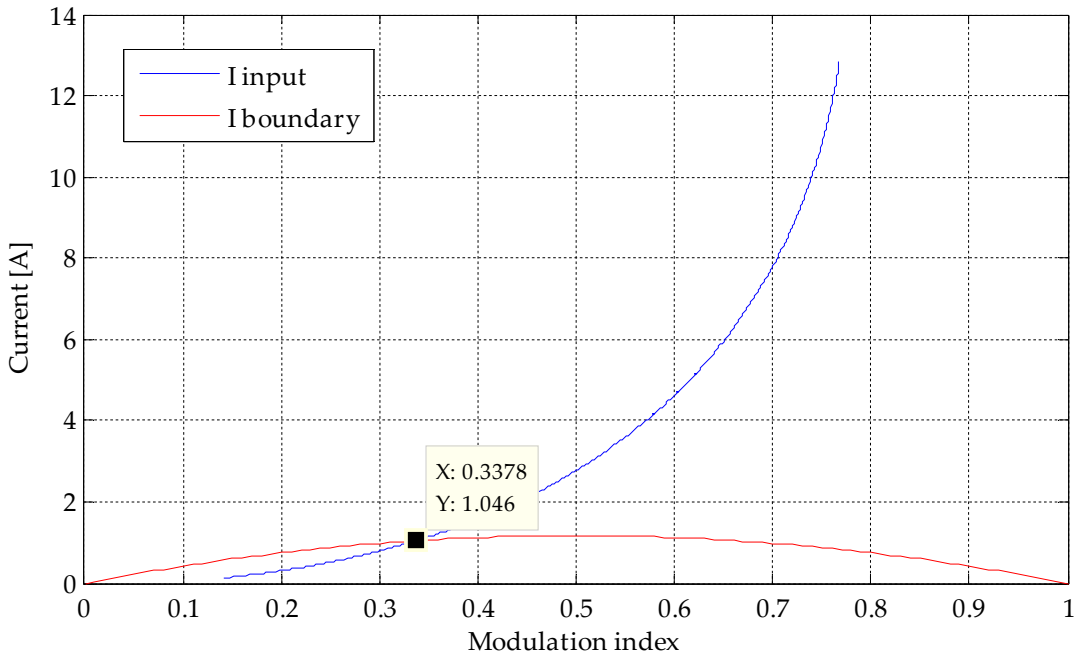

Figure 7-7: Boost converter average input and boundary current with modulation index; highlighting the converter input current and modulation index of the boundary condition. To produce the input current curve the wind turbine rotational speed is optimised for the wind speed across the full operating range.

To actively control the input voltage to the converter so that it matches the reference, a feedback control loop is implemented to regulate the converter modulation index. To provide the feedback voltage measurement for this controller a transducer is used to take a measurement of the voltage at the converter input. The control loop is based upon a proportional integral controller and acts to vary the modulation index between zero and one, as shown in Figure 7-8. The bandwidth of the controller is set to 5.4Hz and the bode plot of the closed loop transfer function of the converter is shown in Figure B-1 in the Appendix. Integral anti-wind-up is also included to disable the controller integral term when the modulation index is equal to either its maximum or minimum. The reference value towards which the converter controller must drive the input voltage is provided by the cluster controller, which is similar to that used in the system models in the previous chapters of this thesis. The bandwidths of the two controllers are separated by a factor of ten so that the cluster and converter controllers do not interfere.

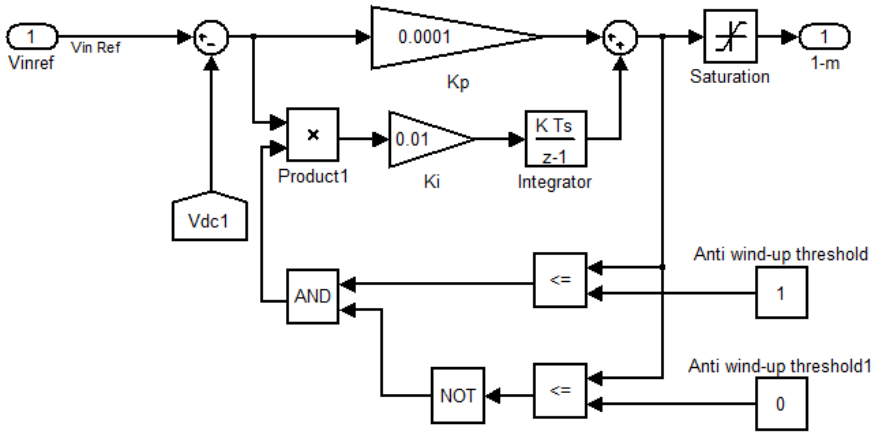

Figure 7-8: Boost converter controller, incorporating a PI controller and integral anti-wind-up.

To instruct the converter switch to open and close according to the modulation index it must be converted into a pulsed waveform. This is

achieved by pulse width modulation where the modulation index is compared with a triangular carrier waveform, with a frequency equal to the switching cycle length. When the magnitude of the carrier wave is greater than the modulation index a positive pulse closing the switch will occur, and when the carrier waveform is less than the modulation index a zero pulse opening the switch will occur, as shown in Figure 7-9. To allow the correct open and close signals to be given the modulation index must actually be subtracted from one, as shown in equation (7.2).

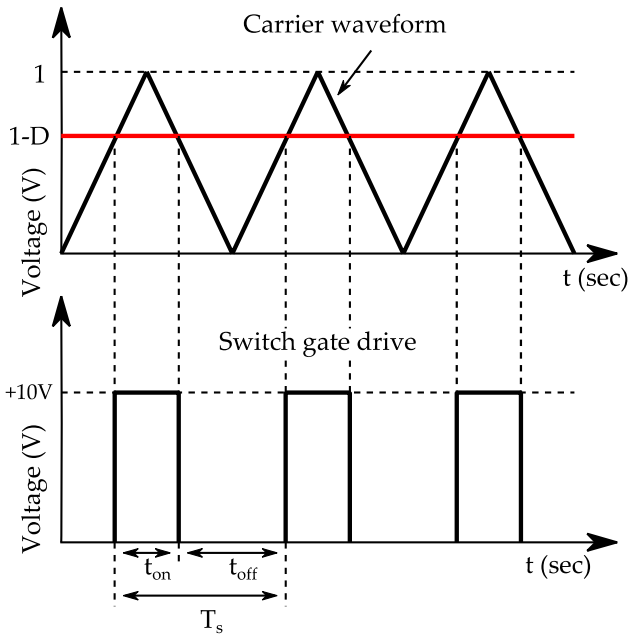

Figure 7-9: Comparison of 1-D controller output with the carrier waveform, to produce the gate drive pulses for the converter switch.

Chopper converter operation and design

The chopper converter regulates the output voltage of the boost converter by modulating the current flowing through the load. It does this by regulating the voltage across the capacitor, which is proportional to the current flowing into it, shown by equation (7.6). As with the boost converter, the chopper has two operational states: where the switch is open and closed, as shown in

Figure 7-10. When the switch is open the input current flows straight into the capacitor charging it up and increasing the voltage across it, Figure 7-11(b). When the switch is closed the capacitor current reverses and combines with the input current to flow through the load, Figure 7-11(c). The reversal of the capacitor current causes it to discharge, reducing the voltage across it. The amount by which the voltage across the capacitor varies is related to its size and the amount of time the converter spends in each state. The size of the capacitor and load resistance can be chosen to limit the ripple of the capacitor voltage to within a particular margin using equations (7.4) and (7.5); whilst also allowing the minimum output current to be twice the maximum input current to allow the converter to maintain a constant average voltage. The modulation index of the converter is regulated by a controller similar to that of the boost converter, shown in Figure 7-12, which changes the proportion of each switching cycle that the capacitor voltage increases and decreases, allowing the average of the voltage across the capacitor to be controlled to the reference level. The controller bandwidth of this converter is tuned to be approximately a factor ten greater than the boost converter to avoid interference (the closed loop transfer function bode plot of this converter is shown in Figure B-2 in the Appendix).

$$V_{ripple} = \frac{T_s.(I_{in}.(1-2.D) + I_{out}.D)}{C} \tag{7.4}$$

$$ripple\ (\%) = \frac{V_{ripple}}{V_{c\ ave}} \tag{7.5}$$

$$\frac{dV_c}{dt}.C = I_c \tag{7.6}$$

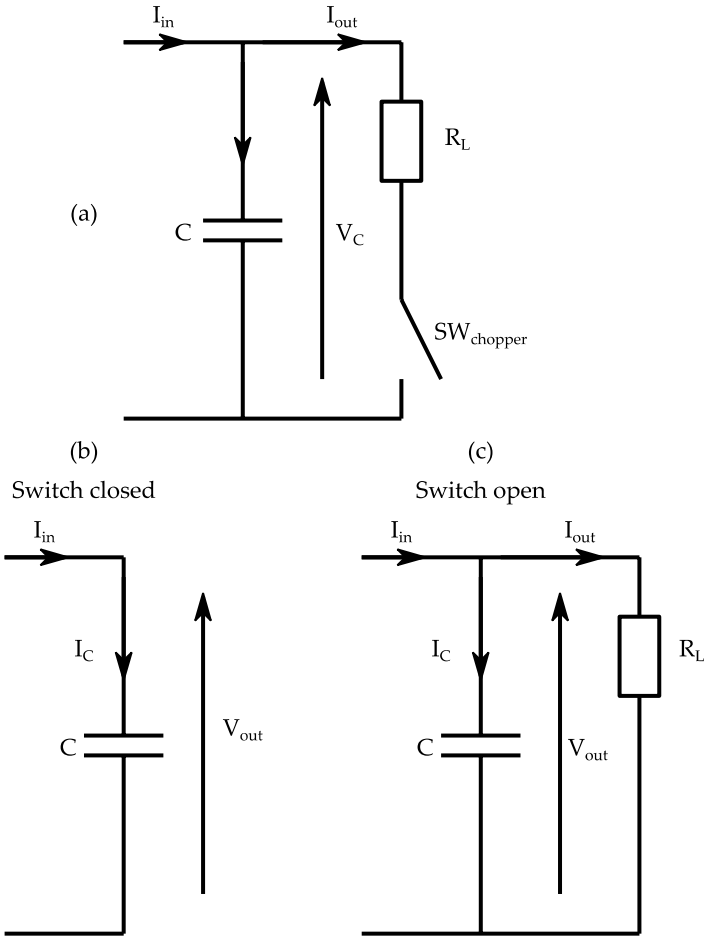

Figure 7-10: (a) Chopper converter full circuit; (b) when the switch is closed; (c) when the switch is open [1].

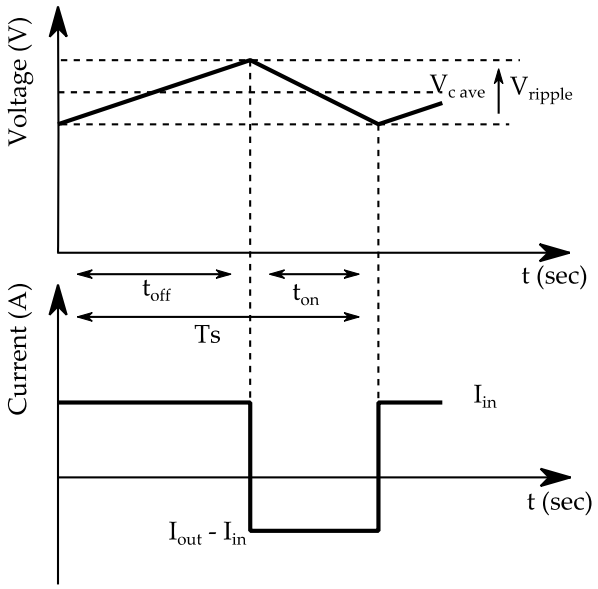

Figure 7-11: Chopper capacitor voltage and current across one switch cycle.

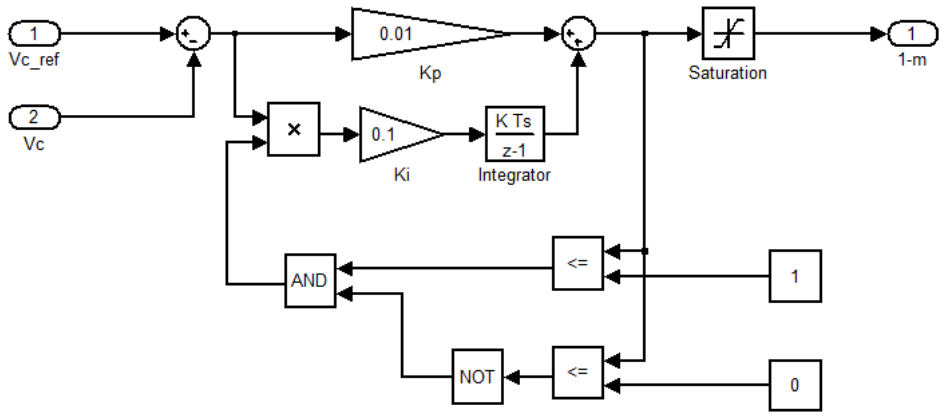

Figure 7-12: Chopper converter controller, incorporating a PI controller and integral anti-wind-up.

The voltage on the output side of the boost converter is to be held constant at 350V, as discussed above, it is also desired for the capacitor voltage ripple to be less than 5% across the operating range. The voltage ripple is a function of both the capacitance and the load resistance; the size of the capacitor is restricted by those available for use in the laboratory and is therefore chosen to be 1.1mF, and the maximum load resistance is restricted by the requirement for twice the maximum input current to flow through the load at the required voltage level; therefore allowing the capacitor discharge current to pass through the load in addition to the input current when the switch is closed. The maximum load resistance is therefore determined using equation (7.7) to be 11.6Ω; where peak input current, when both generators are producing maximum power, is approximately 15A. The change of the capacitor voltage ripple with modulation index is therefore determined for this maximum input current using equation (7.4), for load resistances up to 11.6Ω and where the switching cycle length is 1ms, as shown in Figure 7-13.

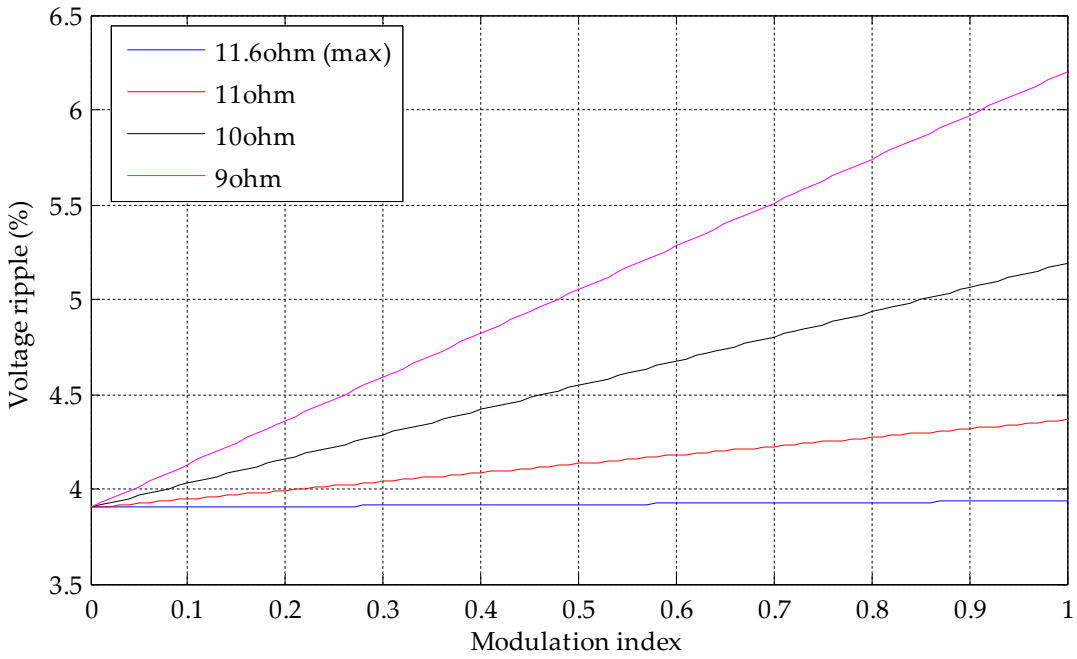

Figure 7-13: Chopper converter capacitor voltage ripple with modulation index for different load resistances and maximum input current.

It can be observed in Figure 7-13 that the smaller resistances cause the voltage ripple to be more severe; however if the resistance remains above approx. 10.2Ω, the maximum ripple is less than the 5% objective across the operating range. The value of resistance is therefore chosen to be 11Ω, allowing a small amount of headroom to the maximum resistance, whilst keeping the maximum voltage ripple below 5%.

$$R_{L\,max} = \frac{V_c}{2.\,I_{in\,max}} \tag{7.7}$$

7.2.2 DC-DC converter modelling

To verify the operation of the DC converter, a model based on the design detailed above has been developed using Insulated Gate Bi-polar Transistors (IGBT) to provide the switch action. The model is used to verify the main function of the converter, which is to regulate the voltage at its input and thereby indirectly control the rotational speeds of the generators; and to

verify that the voltage on the output side of the boost converter can be maintained at a constant level. The ability of the converter to remain in continuous conduction mode when the minimum input current is applied is also verified.

To test the ability of the boost converter to regulate the converter input voltage, a constant current of 7A is fed into the converter using an ideal current source, as shown in Figure 7-14; in addition a smoothing capacitor (1.1mH) is placed across the input terminals of the boost converter to attenuate the high frequency switching harmonics (a parasitic resistance of 1000Ω is also included to allow the simulation to execute). By applying a step change to the converter input reference voltage, from 150V to 200V, the action of the converter can be observed, as shown in Figure 7-16. The response of the converter input voltage to the change of reference is slightly over damped due to the relatively low controller bandwidth, but is otherwise satisfactory.

To test the ability of the converter to continuously conduct current when the system operating point is at its minimum, the current source is replaced by a voltage source with constant magnitude corresponding to that expected when a single generator is rotating at its minimum operational speed (13.1rad/s and 124.1V). In this case the smoothing capacitor and parasitic resistance introduced above are removed and replaced with a 1Ω series resistance between the voltage source and the converter terminals, as shown in Figure 7-15, to limit the size of the current transient that occurs in the initial stages of the simulation allowing the controllers to act. It can be observed in Figure 7-17 that in this case the converter input current is close to

the boundary between continuous and discontinuous mode, confirming the satisfactory operation of the converter in these conditions.

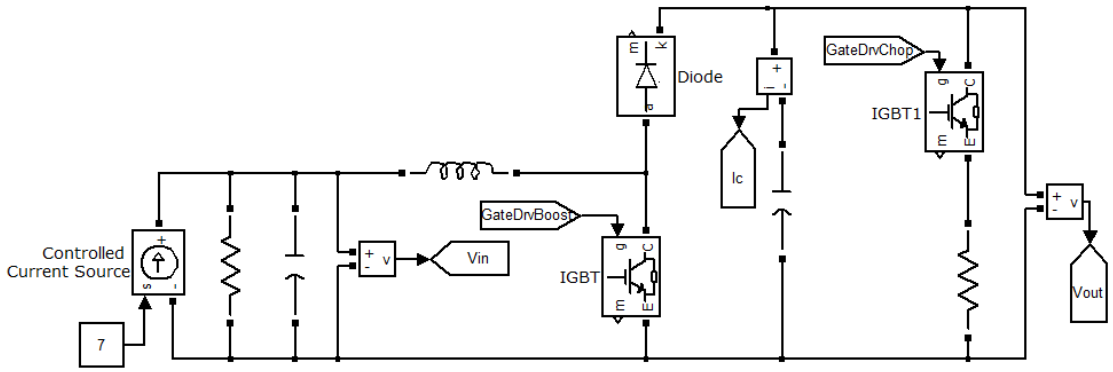

Figure 7-14: DC converter with a controllable current source input, smoothing capacitance and parasitic load.

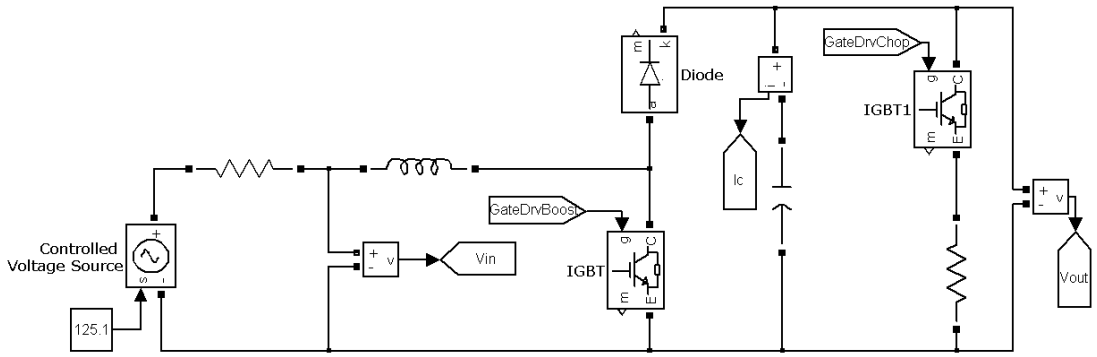

Figure 7-15: DC converter with a controllable voltage source input and series resistance.

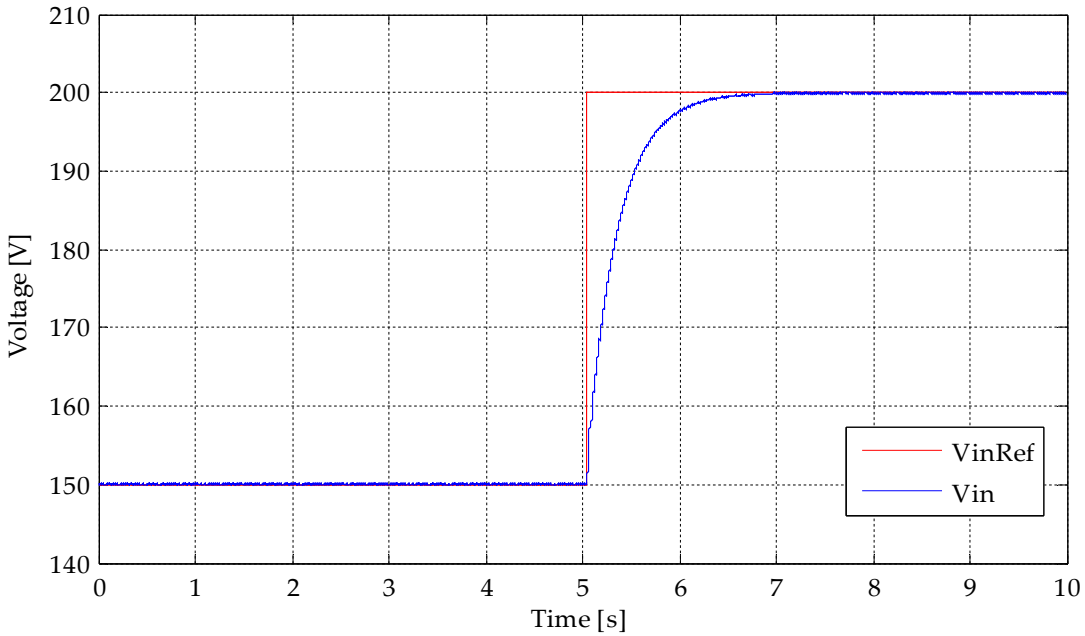

Figure 7-16: Boost converter input voltage response to the step increase of the voltage reference.

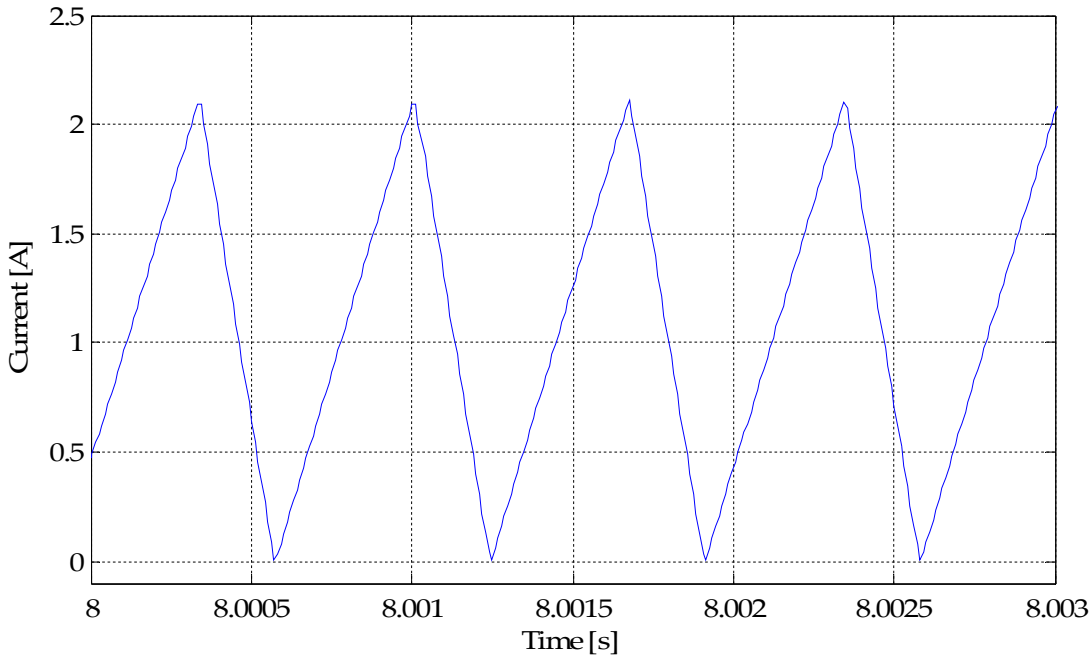

Figure 7-17: Boost converter input current minimum operating condition.

The ability of the chopper converter to maintain a constant voltage on the output side of the boost converter and to keep the voltage ripple within 5%, is also determined by applying a voltage source at the input to the converter;

in this case the input voltage that corresponds to when the generators are rotating at their maximum operational speed (242.6V) is applied. It can be observed from Figure 7-18 that the chopper maintains the average voltage satisfactorily at 350V, and also that in Figure 7-18 the voltage ripple is approximately 1.8% of the average voltage. It is also observed that the voltage ripple does not completely follow the anticipated triangular waveform shape shown in Figure 7-11; this occurs as a result of the combination of the chopper and boost converter actions which cause both the input and output current of the chopper to be discontinuous. Therefore when the closing of the boost converter switch and the opening of the chopper converter switch coincide, the voltage across the capacitor is momentarily constant, as current can neither flow in or out of the capacitor. This affects the charging and discharging of the capacitor and therefore restrains the ripple of the capacitor voltage slightly.

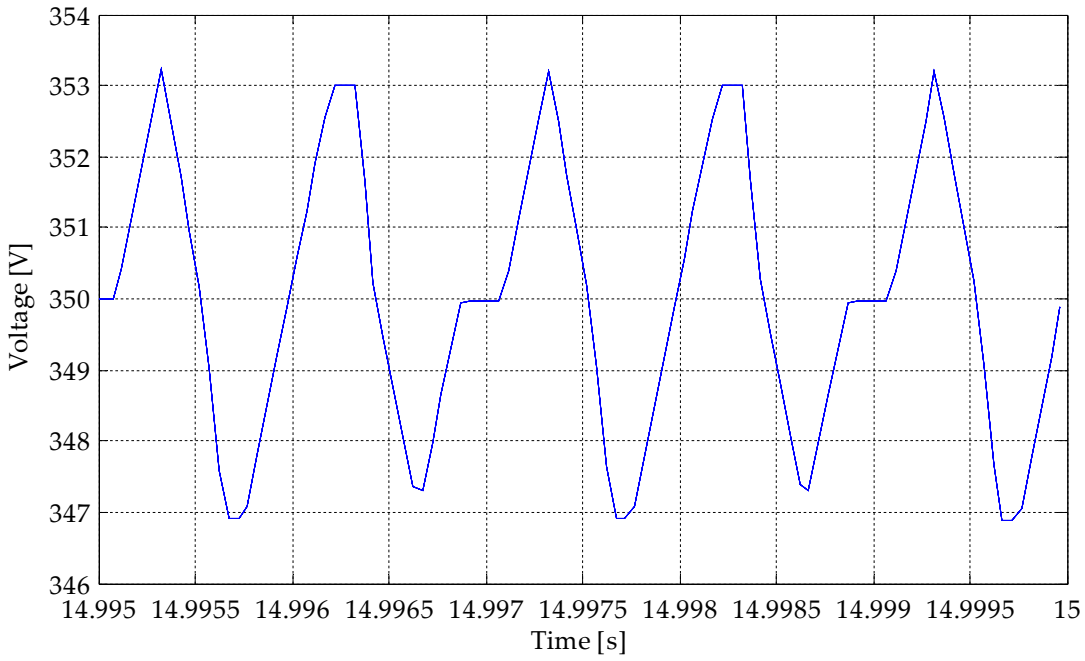

Figure 7-18: Boost converter output voltage, regulated by the chopper converter.

7.2.3 DC converter practical implementation

To develop the DC converter in the laboratory, a few other factors must be taken into consideration in the design, for example: the measurement of the currents and voltages in the electrical system to provide feedback to the controllers, the limitation of voltage stresses across the power electronic devices caused by the switching action, and the dissipation of the heat generated by the devices during operation to regulate the semiconductor junction temperatures. The operation of the resultant DC converter must also be verified against the simulation model to ensure it operates as intended.

Measurement of current and voltages

The dSPACE microprocessor system accepts analogue voltage inputs, therefore measurements of the voltages and currents from analogue voltage and current transducers can be read in. LEM voltage and current transducers are used which each produce a voltage signal that is proportional to either the input current or voltage. To ensure the output signals of these transducers are compatible with the dSPACE system they are also conditioned by an amplifier stage to be within the range of +/- 10V. The dSPACE system samples the analogue signals for numerical processing in the control software; these measurements are also filtered in software to remove high frequency noise before they are input to the various control loops. The placement of the voltage and current measurements throughout the system is shown in Figure 7-2. The measurement of the three phase generator output voltages also allows the rotational speeds of the generators to be determined using the Simulink SimPowerSystems Phase Locked Loop to determine the electrical frequency of the generator output. The rotational speed is used within the wind turbine rotor model to calculate the

aerodynamic torque instruction to the induction motor drive for the input wind speed.

Power electronic device voltage stress management

When using any power electronic device care must be taken to ensure that transient voltage spikes, caused by changes of current through stray inductances as a result of the switching action, do not apply excessive stress to the devices. In particular for the converters developed here the voltages that occur across the stray inductances will cause an overvoltage spike to occur during the switch off process. To mitigate these spikes a capacitor is placed across the terminals of the devices to slow the rate of increase of the voltages across them. This capacitor will limit the rate of change of voltage for a finite amount of time while it charges up, which is long enough for the currents through the stray inductances to reach zero. To allow the capacitor to be most effective it should be located as close as possible to the terminals of the devices. In theory the large capacitance that is present as part of the chopper converter could perform this role, however it is not possible to directly connect it across the device terminals due to its physical size. Therefore small snubber capacitors (0.1μF) are connected across the device terminals; the layout of the physical converter that includes these snubber capacitors is shown in Figure 7-19.

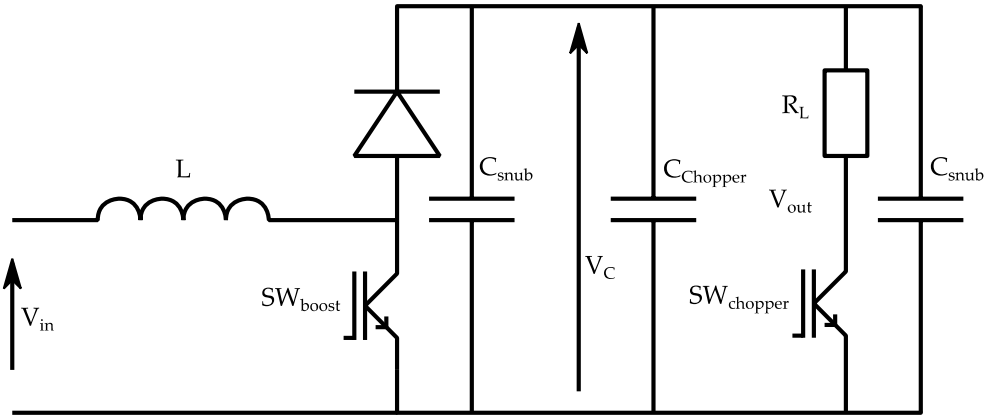

Figure 7-19: DC converter including snubber capacitors.

Device junction temperature management

The switching action and conduction of electrical current through the power electronic devices also causes a significant amount of energy to be lost as heat within each device, which can cause the temperature of the semiconductor junction to rise above its maximum operating temperature (125°C) and cause it to fail [1]. To ensure the junction temperatures remain within the operating range, the heat generated must be dissipated by fixing the devices to a heat sink. The ability of a heat sink to dissipate heat is a function of its size and also the thermal resistivity of its interface with the device. To ensure a sufficient amount of heat is dissipated to keep the junction temperatures within the operating range, the size of the heat sink and the transfer of energy through it must be carefully considered.

The power electronic devices used in the DC converter developed here are modules that consist of two IGBTs and two parallel diodes. Two such modules are required, one for each converter stage; a diagram of the device arrangement with the heat sink and the material interface thermal resistivities is shown in Figure 7-20. When determining the heat dissipation from the devices through the heat sink, the quantity of energy expelled by each device and the thermal resistivity of the interfaces of different materials

are important. The arrangement of the devices and the thermal resistivity of material interfaces can be represented by a simple diagram, analogous to an electrical circuit, shown in Figure 7-21. The change of temperature between the device semiconductor junctions and the ambient temperature is a function of the power dissipation of the devices and the thermal resistivity between the two, by equation (7.8). Knowledge of the thermal resistivities, the maximum power dissipated by each device and the ambient temperature, therefore allows the junction temperatures to be back calculated to ensure they are less than the operational maximum (125°C). Details of the heat sink available for use and of the device modules are given in Table 7-2.

$$\Delta T = P_{Thermal} . R_{TH} \tag{7.8}$$

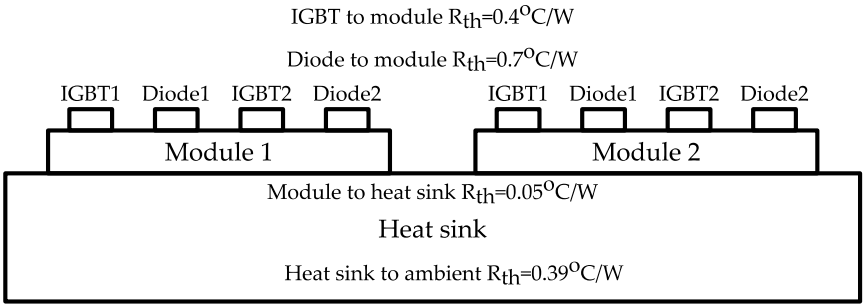

Figure 7-20: Arrangement of the power electronic devices, their modules and the heat sink, giving the thermal resistivity, R_{th}, of each interface.

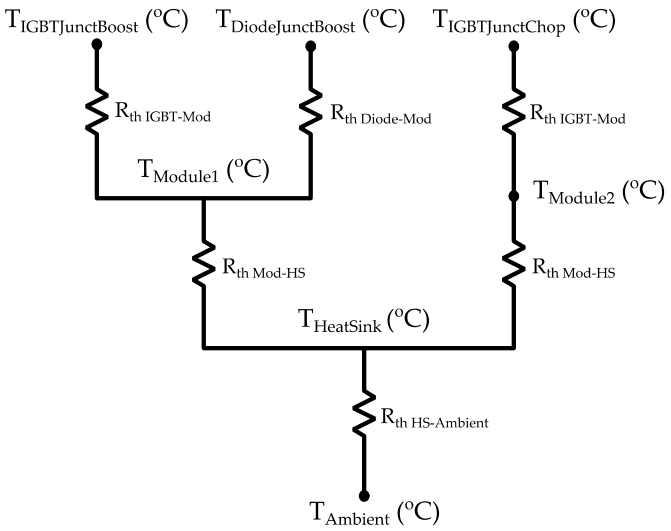

Figure 7-21: Thermal diagram of the converter semiconductor devices, modules and heat sink; omitting the devices that do not dissipate power.

Table 7-2: Test rig heat sink and IGBT module parameters [2] [3].

IGBT and diode modules			
Semikron SKM 50GB 123D		IGBT switch off energy loss, E_{off}	3.5mWs
Current rating	50A	Diode switch on energy loss, E_{on}	1.8mWs
$V_{CE\ IGBT}$	2.75V	Diode switch off energy loss, E_{off}	1.5mWs
$V_{f\ diode}$	1.5V	**Heat sink**	
$R_{th\ IGBT}$	0.4°C/W	Semikron P3	
$R_{th\ Diode}$	0.7°C/W	Dimensions	180mm / 125mm / 115mm
$R_{th\ module}$	0.05°C/W	Thermal resistivity (2 modules) R_{thHS}	0.39°C/W
IGBT switch on energy loss, E_{on}	5mWs	Ambient temperature	25°C

Where the maximum current flowing through the boost converter IGBT and diode is equal to the maximum input current from the generators, the conduction power loss and switching energy dissipation can be determined using the device characteristics given in Table 7-2, along with the switch modulation index in these conditions, 0.31. The maximum current flowing through the chopper IGBT is a function of the reference voltage of the chopper (350V), the load resistance (11Ω) and the maximum power input to the converter (5kW); therefore the conduction loss and switching energy dissipation in this device can also be determined using the data in Table 7-2 and the maximum operational modulation index, 0.476. The conduction losses and switch energy dissipation calculated for each converter are given in Table 7-3. This data therefore allows the junction temperatures to be calculated by combining the thermal resistivities of the various material interfaces and by applying equation (7.8), where the ambient temperature is assumed to be 25°C [1]. The resulting maximum junction temperatures that have been calculated are shown in Table 7-3, which indicate that the proposed heat sink will ensure the maximum operating temperature of the devices is well within the device maximum.

Table 7-3: Conduction losses and switch energy dissipation per switch cycle and the resultant device junction temperatures.

IGBT boost converter		**Diode boost converter**	
$P_{LossConduction}$	12.79W	$P_{LossCondunction}$	15.53W
$P_{LossSwitch}$	4.815W	$P_{LossSwitch}$	1.05W
$T_{IGBTJunct}$	61.55°C	$T_{DiodeJunct}$	66.12°C
IGBT chopper converter			
$P_{LossCondunction}$	32.13W	$T_{IGBTJunct}$	69.5°C
$P_{LossSwitch}$	4.96W		

The resulting DC–DC converter and its various components are shown in Figure 7-22, the input inductor and load resistance are not shown. It should be noted that the smoothing capacitor placed across the input to the converter, introduced above to test its functionality, is also included in the final converter. This capacitor removes the converter switching harmonics from the converter input voltage and therefore allows it to appear as an ideal voltage source to the cluster electrical system. The presence of this capacitor in close proximity to the converter input inductor however introduces a resonant frequency of approximately 190rad/s; to ensure this resonance is not excited the converter controller gains have been tuned to apply sufficient damping at this frequency, as shown by the system closed loop transfer function bode plot in Figure B-1 in the Appendix. The exclusion of this capacitor would lead to the switching harmonics propagating throughout the cluster electrical system, which, although won't impact on its operation, will disguise the actual voltage waveforms at the different points of the system, for example on the generator terminal voltages and the rectifier outputs.

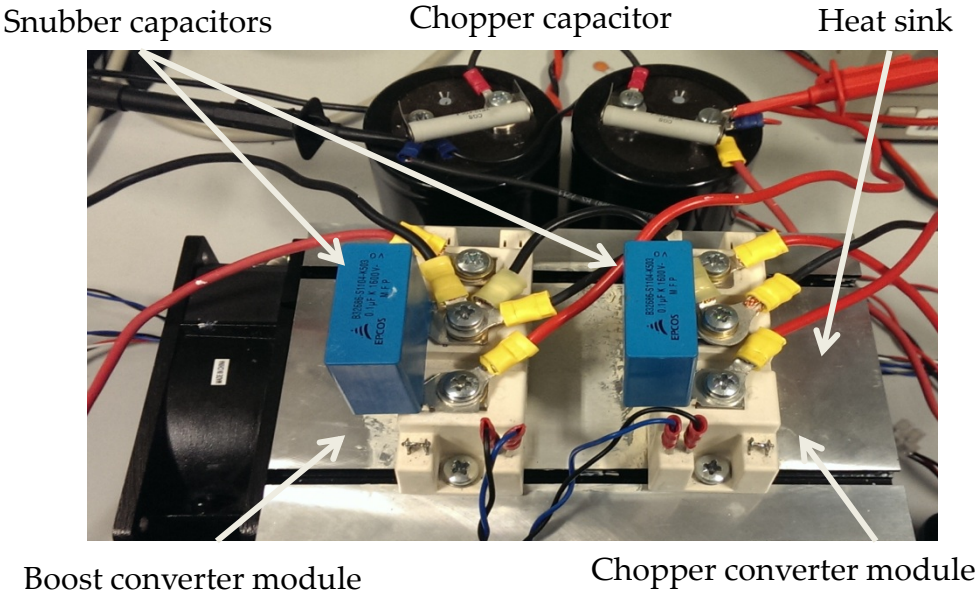

Figure 7-22: Test rig DC converter, highlighting the major components.

Verification of converter operation

To verify the operation of the DC converter the same tests are applied as those which tested the functionality of the model above. To provide the input to the converter both current and voltage sources are required; these are provided by an external DC source that has the capability to operate in both current and voltage controlled modes. The reference converter input voltage in each test case, along with the converter output voltage reference are set in the test rig user interface prior to the connection of the input source. Initially the DC source is used in current control mode to test the ability of the converter to regulate the converter input voltage. The DC source is set to provide an average current input to the converter of 7A, similarly to above, and initially the converter voltage reference is set to 150V. By applying a step change to the converter input voltage reference, from 150V to 200V, it is observed in Figure 7-23 that the controller reacts to the reference change by smoothly increasing the converter input voltage towards the new reference. Comparing this behaviour to that of the converter model in Figure 7-16 reveals that the responses to the step change correlate well.

Secondly, the DC source is used in voltage control model to test the ability of the converter to maintain continuous current conduction for the minimum expected average input current; the converter input reference voltage is set to 124.1V in this case, corresponding to the voltage that would allow the turbines to operate at their minimum rotational speed (13.1rad/s); the DC source voltage is set slightly higher to encourage current flow into the converter (125.1V). It can be observed from Figure 7-24 that the converter input current operates at the boundary condition and therefore maintains continuous conduction mode. By comparing the experimental converter input current to that in Figure 7-17 produced by the simulation, it can be

observed that the correlation between the test rig and the model behaviour under similar conditions, close to the boundary current, is good.

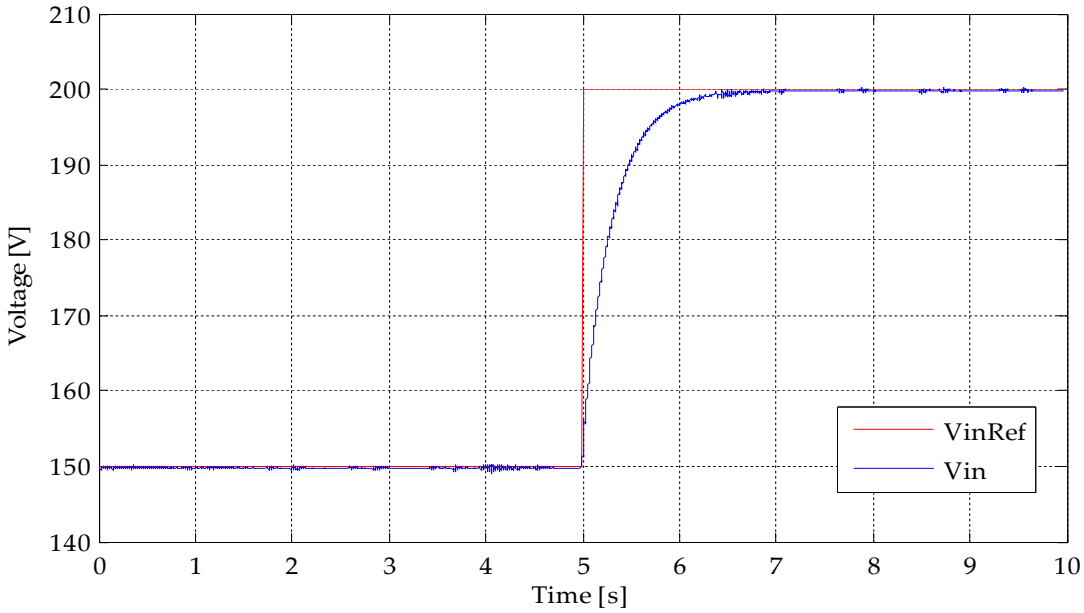

Figure 7-23: Boost converter experimental input voltage step response to a change of the voltage reference.

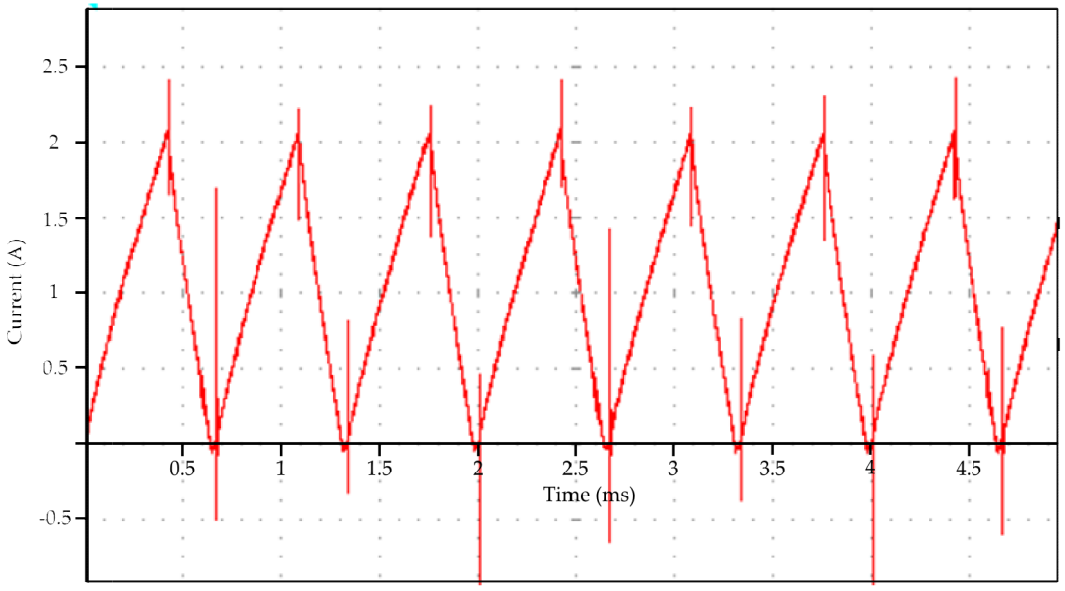

Figure 7-24: Test rig DC converter input current operating at its boundary condition.

To verify the ability of the chopper converter to maintain a constant voltage on the output side of the boost converter and to keep the voltage ripple within 5% of the reference, the input DC source is again used in voltage

control mode. However, in this instance the input voltage source is set to a voltage slightly above the maximum expected input voltage (242V), and the boost converter reference is set to the maximum required for the generators to rotate at maximum speed. This allows the current flowing into the converter from the voltage source to be representative of the current that would occur when the turbines are operating at their maximum power outputs. The average boost converter output voltage and ripple are shown in Figure 7-25, where it can be observed that the average is approx. 350V, matching the reference; the voltage ripple is also shown to be approximately 2.8% of the average voltage, which is within the 5% requirement. By comparing this voltage waveform with the same voltage from the system model, in Figure 7-18, it can be observed that they are again similar; exhibiting the same constant voltage periods where the boost converter switch is closed and the chopper converter switch is open.

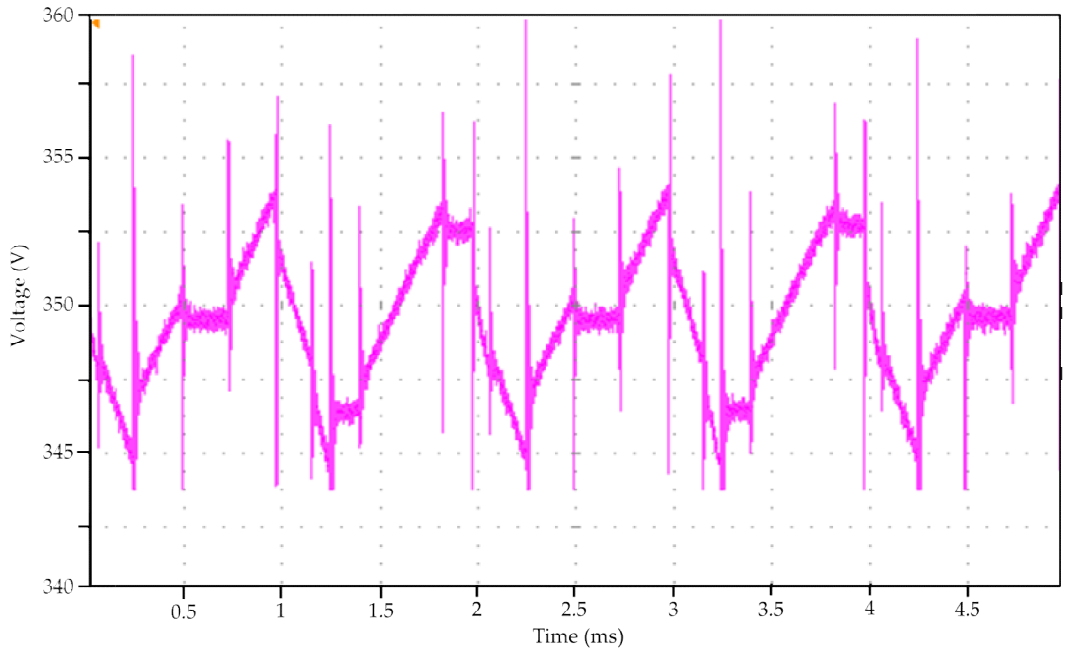

Figure 7-25: Test rig boost converter output voltage.

7.3 Scaled cluster system model

To provide direct comparisons between the operation of the test rig and the system models developed earlier in this thesis, the models are scaled down to be representative of the test rig system. In particular, the scaled down size of the test rig, in comparison to the full sized system, requires the modification of the generator electrical parameters and also lower power level does not merit the use of a step-up transformer. In addition the wind turbines from which the test rig generators are taken are intended to be direct drive, and therefore a gearbox is not required to step-up the rotational speed of the turbine rotor for electricity generation. Also, to ensure the best possible correlation between the test rig and the models, the model of the DC converter, developed above, is combined with the wider system model. The DC converter performs the same function as the controlled ideal voltage source used in the models so far, and therefore is used as a direct replacement; the smoothing capacitance on the converter input, introduced above to test its operation, is also included in the model to filter the converter switching harmonics from the rest of the system. The various parameters of the test rig components have been set out in Table 7-1; these parameters are also used in the model to ensure correlation between it and the test rig.

The modified system parameters used in the model are also used to calculate the cluster optimum control curve, using the algorithm developed in Chapter 5. These modifications are made primarily to reflect the different generator parameters on the rectifier commutation process, which is a key contributor to the slip that occurs between the generators and is therefore a key contributing factor to the operating characteristic of the cluster of turbines. Also, the availability of only two generators for use in the test rig requires the number of turbines included in the model to be reduced from five to two.

Despite the modification of the majority of the system parameters to match the test rig, the principles of the control of the cluster remain the same. In particular, the controller acts on the result of a comparison between the measured output power from the cluster (measured at the input to the DC converter) and a reference power level that corresponds to the instantaneous converter input voltage, given by the cluster control curve. As a result the controller bandwidth used in the full system models is maintained both in the test rig and the scaled system models. It should be noted however that the moment of inertia of the test rig generators is smaller than that of a 5MW wind turbine by several orders of magnitude; the inertia of the test rig has been calculated by measuring its dimensions and the estimating the rotating component masses, to give 2.9kg.m^2. As a result of the smaller generator inertia the response of the turbine rotational speeds to changes of the aerodynamic input torque, derived from the wind speed, will be significantly quicker than the full sized system. Therefore the response of the full sized system models and the test rig to changes of wind speed will not be comparable.

The system model that results from these modifications is shown in Figure 7-26 and Figure 7-27; the cluster control curve, produced with the parameters of the test rig, is also shown in Figure 7-28. Following the modification of the parameters used to produce this curve, it is also used within the test-rig controller implemented within the dSPACE microprocessor; this further ensures that the correlation of the test rig and the modified model will be as close as possible.

To gain an indication of the expected operational characteristics of the test rig system, the control curve algorithm is also used to provide predictions of the

amount of generator slip that will occur between the generators over the operating range of the test rig turbines, shown in Figure 7-29. It can be observed that a maximum generator slip of approximately 42% can be achieved between the turbines when they are operating at their rated wind speed, which is greater than the slip achievable by the full system. This increased slip capability is the result by the significantly larger generator winding resistance in comparison to the winding resistance of the 5MW generators modelled earlier. It can also be observed from Figure 7-28 that there is quite a significant difference between the power captured from the wind and the power input to the DC converter; this too is a result of the large generator winding resistances of the test rig generators, which cause a significant loss of power which is dissipated as heat.

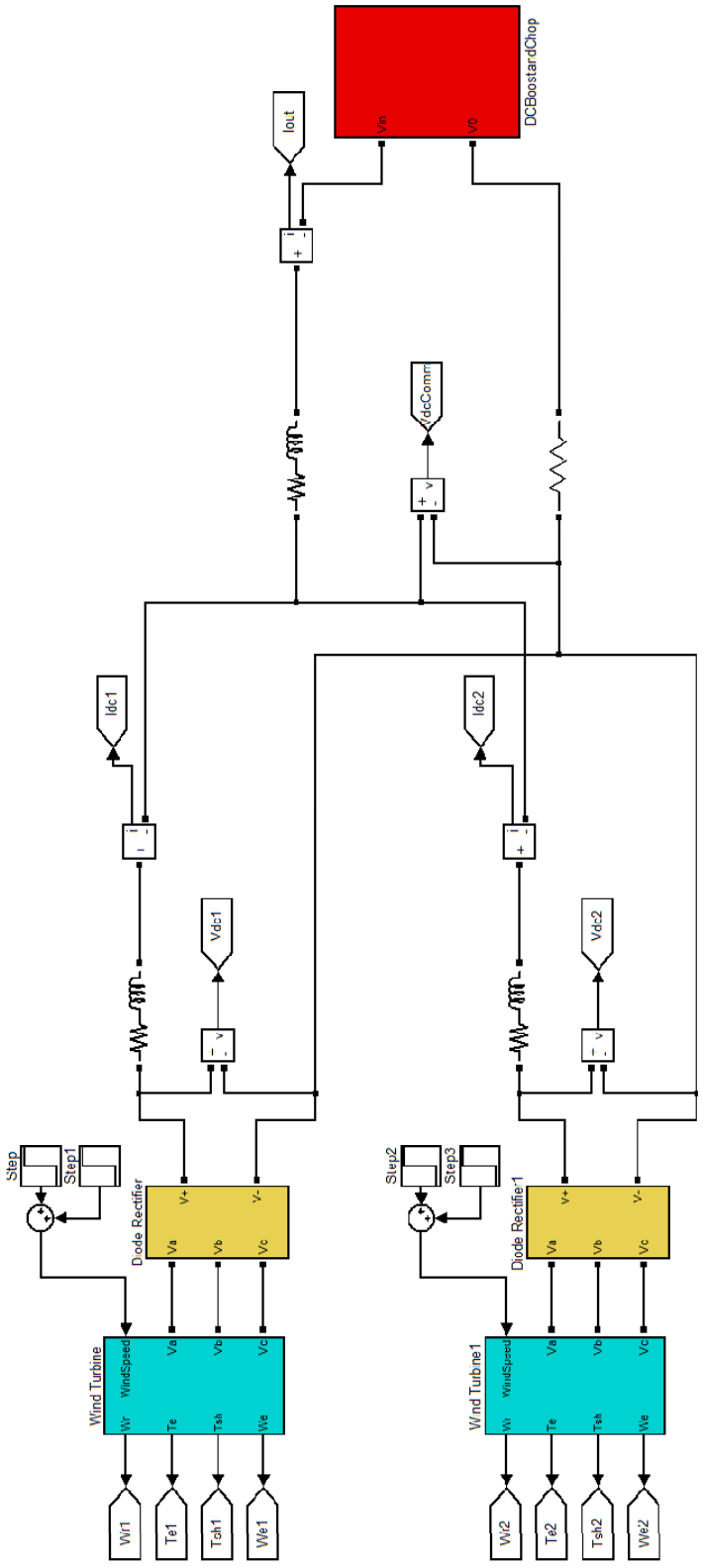

Figure 7-26: Test rig system model, including the DC converter.

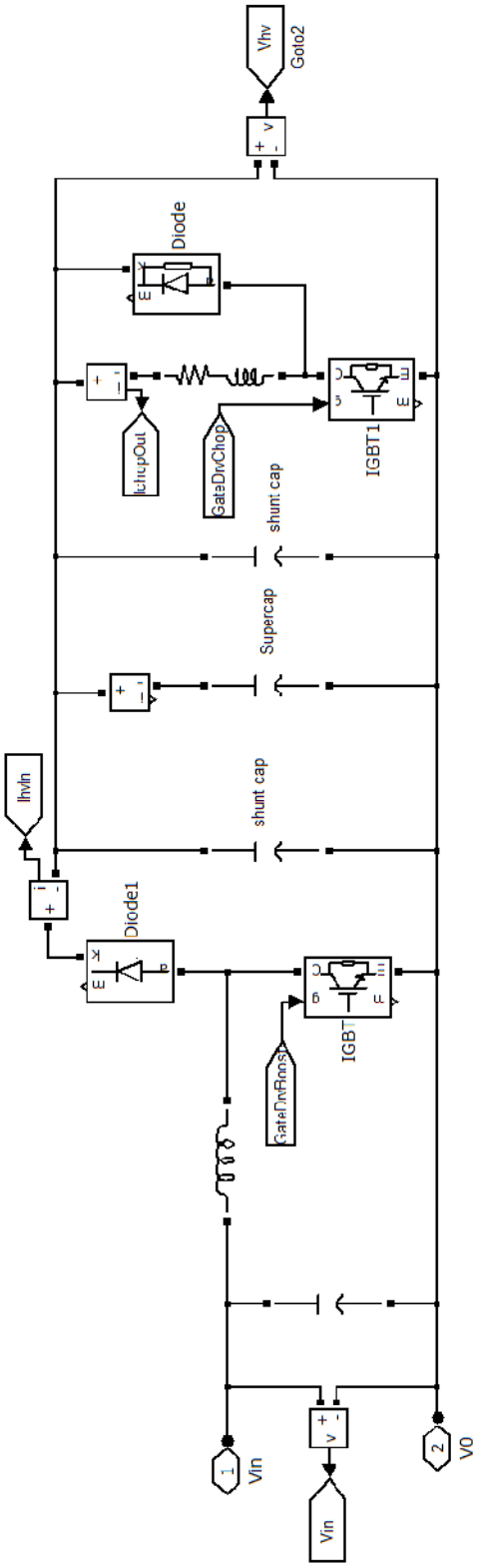

Figure 7-27: DC converter implemented within the DCBoostandChop block in the modified system model shown in Figure 7-26.

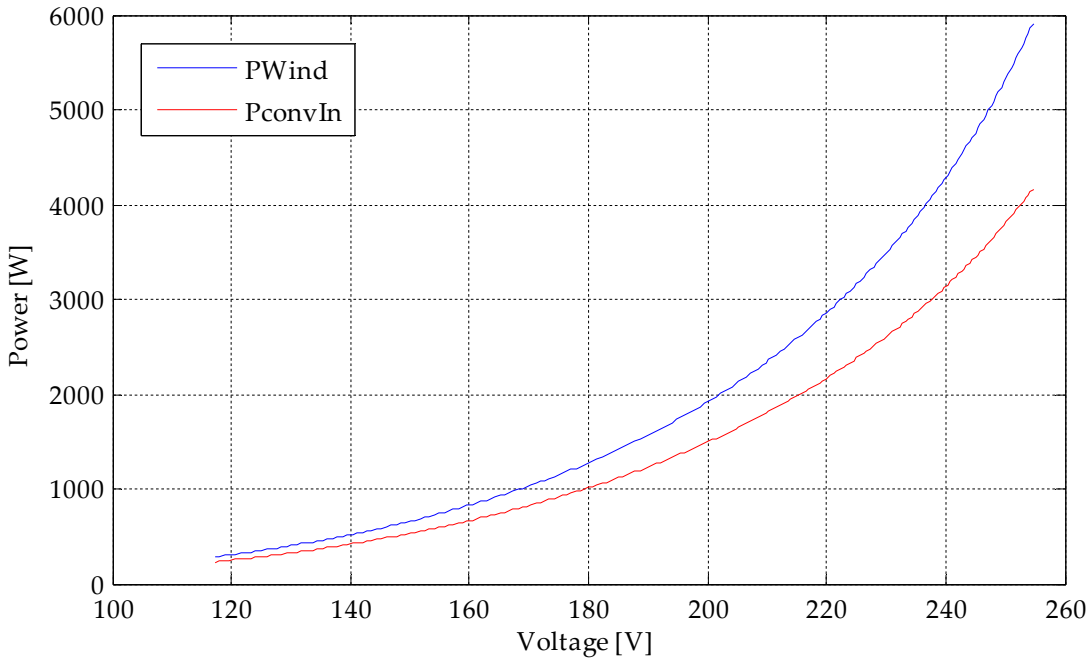

Figure 7-28: Test rig control curve between DC converter input voltage and power (PconvIn) and the power captured by the turbines from the wind (Pwind).

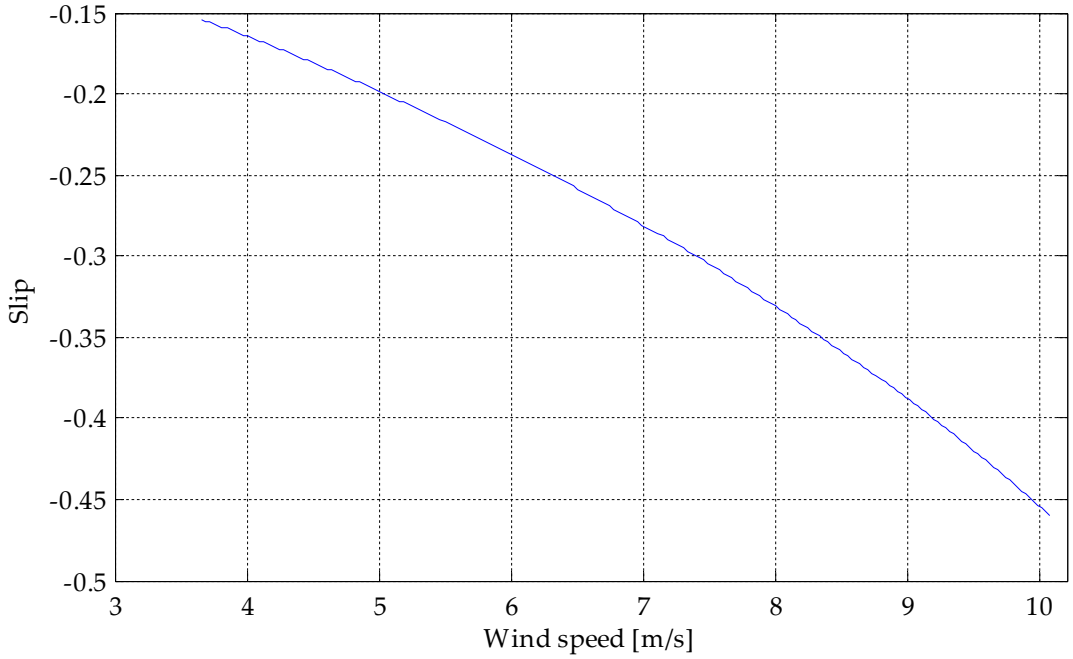

Figure 7-29: Test rig generator slip across the operating range.

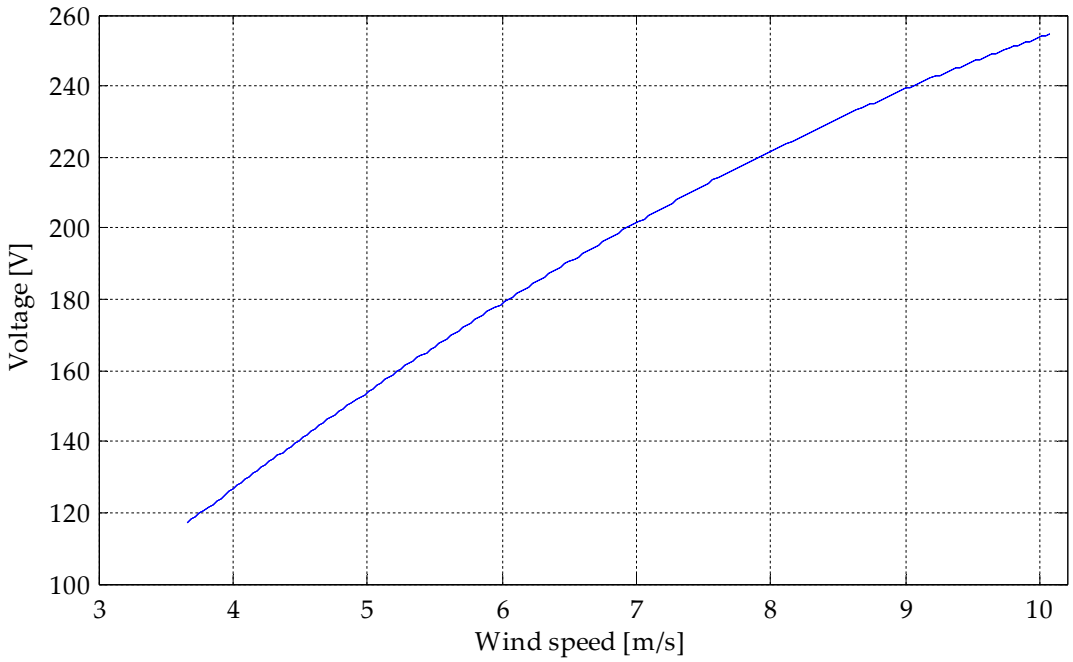

Figure 7-30: Test rig DC converter input voltage with wind speed.

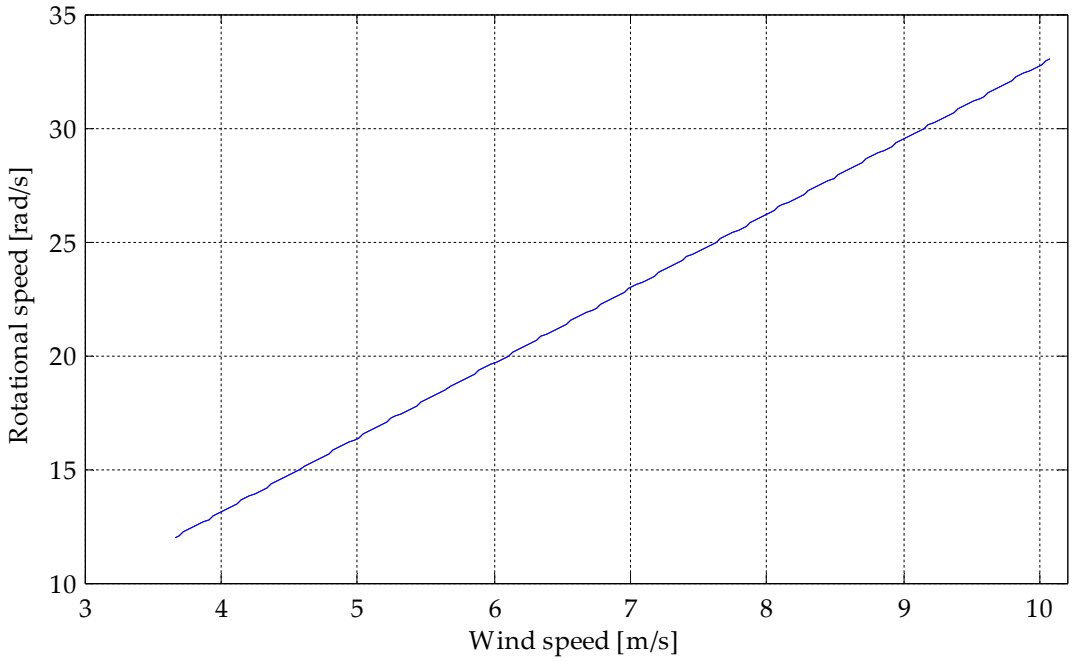

Figure 7-31: Test rig optimal turbine rotational speed with wind speed.

7.4 Experimental verification of system models

To verify the operation of the system models experimentally, a number of test scenarios are required. The most important feature of the system, which has been investigated intensively so far in this thesis, is the generator slip capability that results from the rectifier commutation overlap. To verify the ability of the generators to slip relative to the cluster synchronous speed (or common point voltage), a single turbine will be used initially with a constant wind speed. This will allow both the detail of the rectifier commutation process to be confirmed and the steady state generator slip to be investigated. In addition, a step change of wind speed will also be applied to a single turbine to investigate how the generator slip changes with wind speed.

Secondly, the harmonics that are introduced to the generator windings and the output DC currents and voltages by the rectification process will be investigated. This will allow the confirmation of the trapezoidal shape of the winding current, which results from the commutation process, in particular. In addition, the investigation of the generator DC output voltage and current harmonics will also provide confirmation of the harmonic superposition within the cluster common output cable and the subsequent the low frequency beat current harmonic that occurs as a result. To provide the clearest verification of the harmonics in the system, first of all only a single turbine will be used with a constant wind speed; the second turbine will then be introduced with both an equal and different wind speeds to investigate the superposition of the harmonics.

Verification of the interactions between the clustered turbines is also important; these interactions result from both the active response of the

cluster controller to a change of the cluster average wind speed and also from changes of the common point voltage (and cluster synchronous speed) which occur due to changes of the current flowing through the cluster common cable impedance. Two scenarios will therefore be applied for verification purposes: initially the cluster controller will be given the freedom to vary the control voltage in response to the change of the wind speeds, and secondly the cluster converter input voltage will be held constant. In both scenarios alternate step changes of wind speed will be applied to each turbine.

Lastly, the operation of the cluster of turbines when subject to different and continuously varying wind speeds will be demonstrated to highlight the stability of the system operation and the change of the generator slip in conditions that are representative of reality. This will also demonstrate the ability of the controller to optimise the cluster synchronous speed to the average wind speed across the cluster, therefore optimising the turbine rotational speeds as much as possible and maximising energy capture.

To conduct the above comparisons between the scaled system model and the test rig, the wind speed step changes shown in Figure 7-32 will be used where possible. To experimentally demonstrate the operation of the system when subject to continuously varying wind speed conditions, the wind speed profiles shown in Figure 7-46 will be applied.

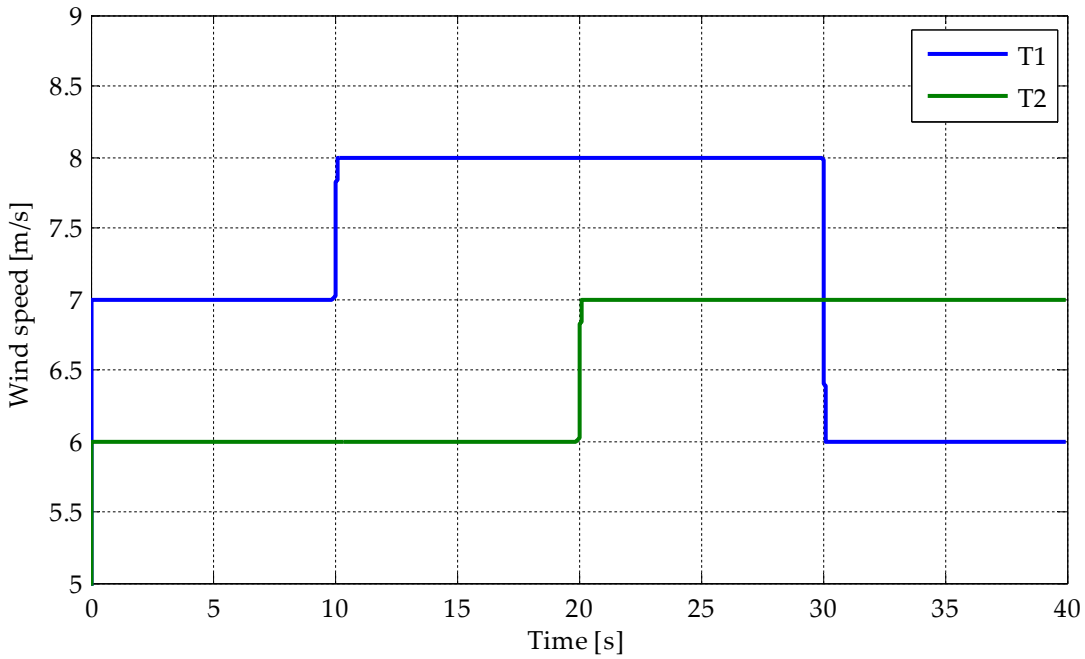

Figure 7-32: Step changes of wind speed applied to each turbine for the experimental validation of the simulation models.

7.4.1 Rectifier commutation

The commutation of the output current between the generator windings by the rectifier causes significant distortion of the generator terminal voltages and also the winding currents. To provide confirmation of the distortion present within the model, measurements of both the generator terminal voltage and winding current have been taken using a single turbine with a constant 7m/s wind speed.

The distortion of the winding currents in the simulation can be clearly observed in Figure 7-33; the feature that is of most interest is the commutation overlap between the outgoing and incoming winding currents. Also notable is the roughly trapezoidal shape of the currents over each conduction period. It can be observed, by comparing these currents with those measured experimentally on the test rig under equal input conditions in Figure 7-34, that the correlation with the simulation is good. In particular,

the lengths of the commutation overlap and waveform shapes closely match, highlighting both the general trapezoidal shape and the ripple harmonic caused by the sampling of the rectifier DC output current.

The distortion of the generator winding voltages in both simulation and experiment, which results from the commutation overlap, can be observed in Figure 7-35. The commutation overlap causes the windings involved to be effectively short circuited for its duration, which is reflected by the equality of the terminal voltages involved in the commutation during this period. It can be observed in Figure 7-35 that there is a general similarity between the voltages that occur at the terminals of the windings involved in the commutation, in both the simulation and test rig. In particular the terminal voltages while each winding is conducting, correlate well; although the peak voltages do not match perfectly. It is likely that the differences between the peaks are caused by the non-ideal construction of the test rig generators in contrast to the model generators which are mathematically ideal. In particular, the imperfect distribution of the stator windings within the test rig generators causes a miss-match between the simulation and test rig generator emfs, this effect is shown in Figure B-3 in the Appendix.

The principle effect of the voltage distortion, introduced by rectifier commutation, is the reduction of the voltage average at the output of the rectifier which contributes to the generator slip. It can be observed in Figure 7-36 that there is quite a significant difference between the average experimental and simulation rectifier output voltage, although the waveform shapes do bear some resemblance. The primary cause of the differences observed in Figure 7-36 is the imperfect construction of the test rig generator, as mentioned above, causing an error between the peak experimental and

simulation emfs, lowering the average DC output voltage by approximately 5V, as shown.

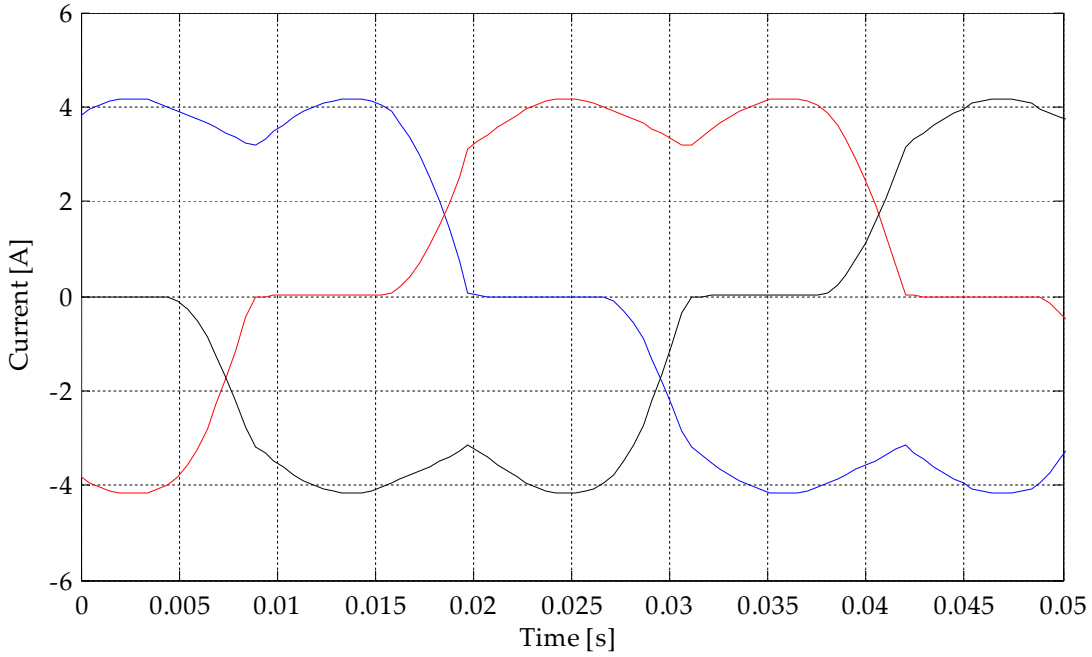

Figure 7-33: Simulated generator winding currents.

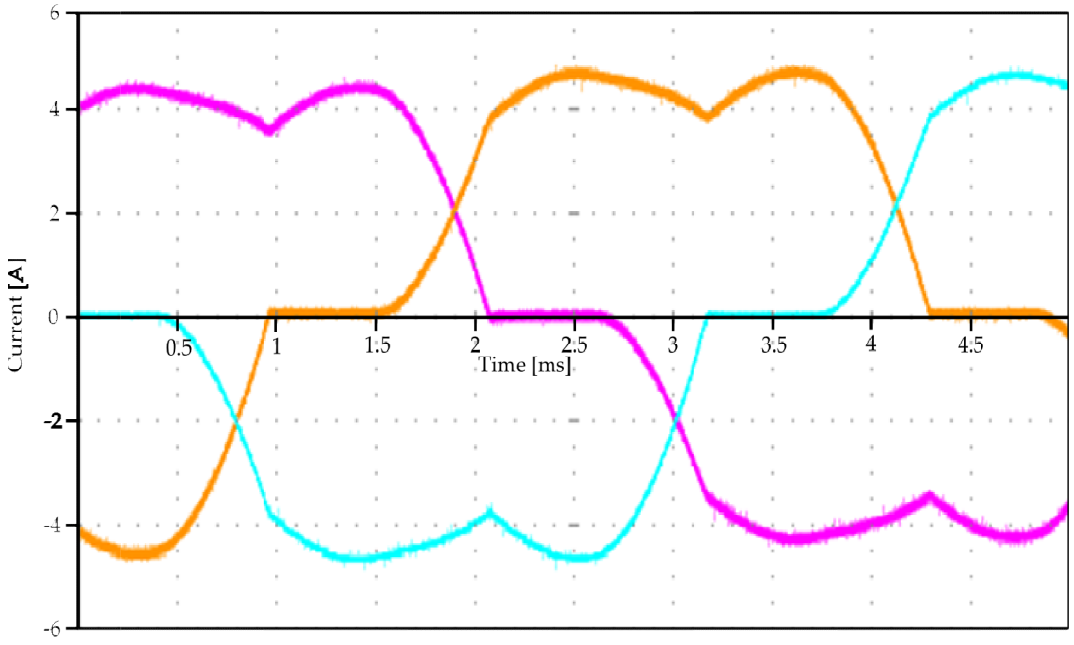

Figure 7-34: Experimental generator winding currents.

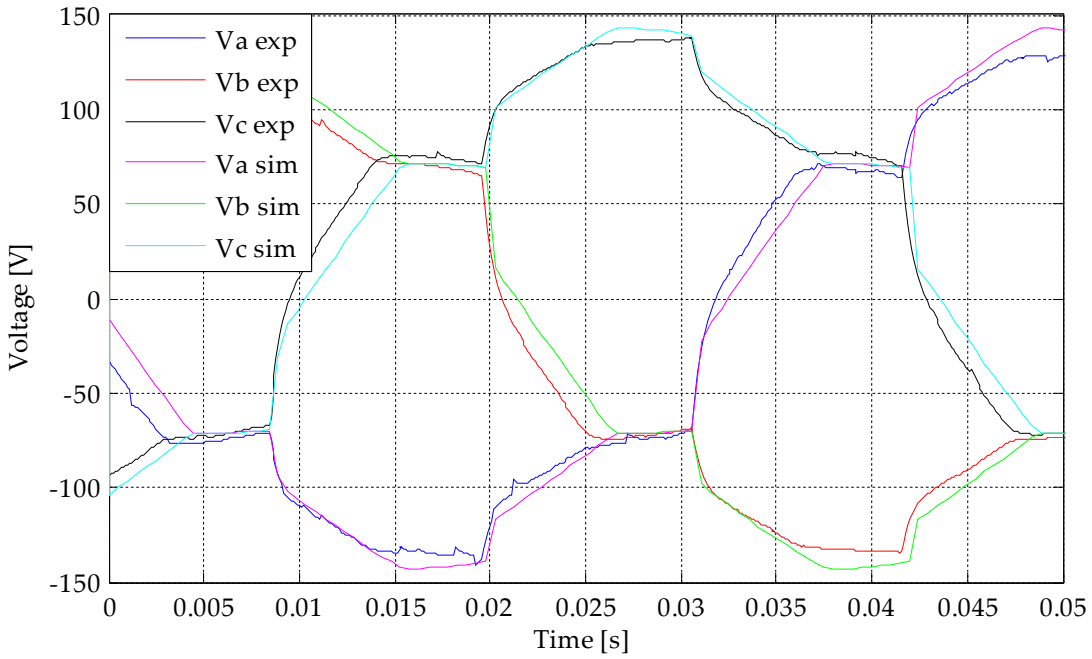

Figure 7-35: Experimental and simulated generator winding terminal voltages relative to neutral.

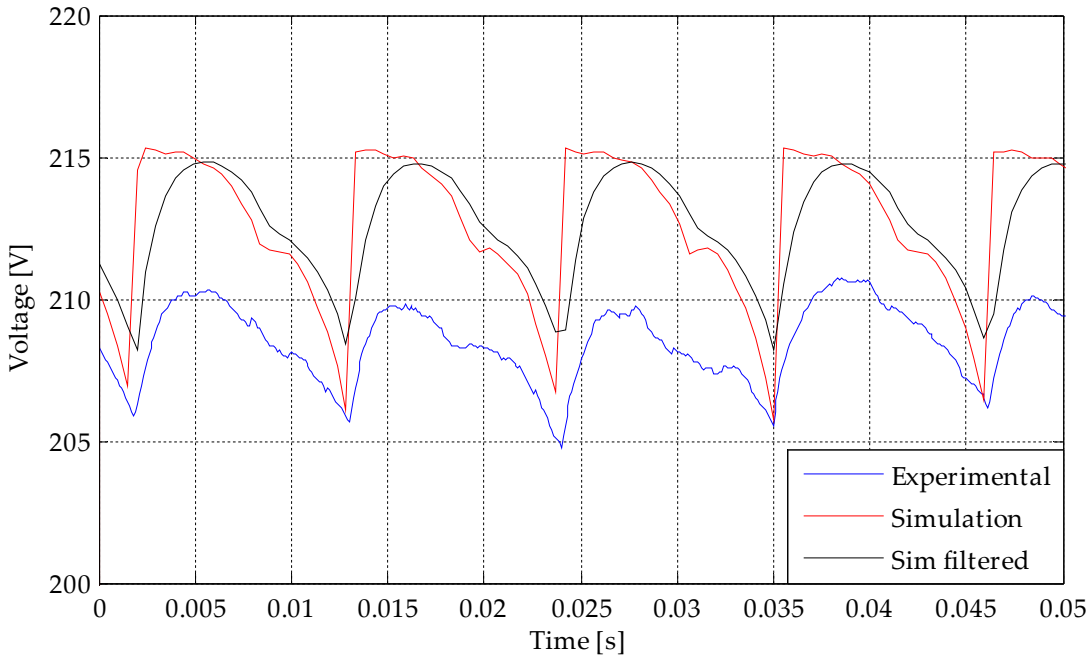

Figure 7-36: Experimental rectifier output voltage and the filtered and unfiltered simulation rectifier output voltage.

It should also be noted that the experimental measurement has been filtered to remove high frequency noise; this filtering causes the softening of the rising edge of the experimental waveform relative to the simulation; the impact of this filtering on the waveform rising edge is confirmed by the third waveform in Figure 7-36, where the same filtering has been applied to the simulation voltage.

The generator slip that occurs both experimentally and in simulation, in response to the first step change in Figure 7-32, can be observed in Figure 7-37 demonstrating that the correlation is generally quite good. There is however a slight steady state error that is again the result of the slight differences between the experimental and simulation rectifier emfs in Figure 7-36, therefore requiring a greater rotational speed to output the same power in the experimental case; the error however is approximately 1% slip, out of 27% slip overall and is therefore not significant. The transient responses of both the test rig and model generator slip also correlate well, with both reaching steady state within approximately the same time period (approximately 2.5 seconds).

On the whole the correlation of the winding current, generator terminal and rectifier voltage and generator slip measurements produced experimentally and by simulation are very good. This proves that the distortion of each caused by the commutation overlap of the rectifier observed in the simulations is representative of the distortion that results from the rectification of the output of a practical PM generator. It also proves that the reduction of the average rectifier output voltage, which results from this distortion, allows a significant amount of generator slip to occur experimentally as well as in simulation.

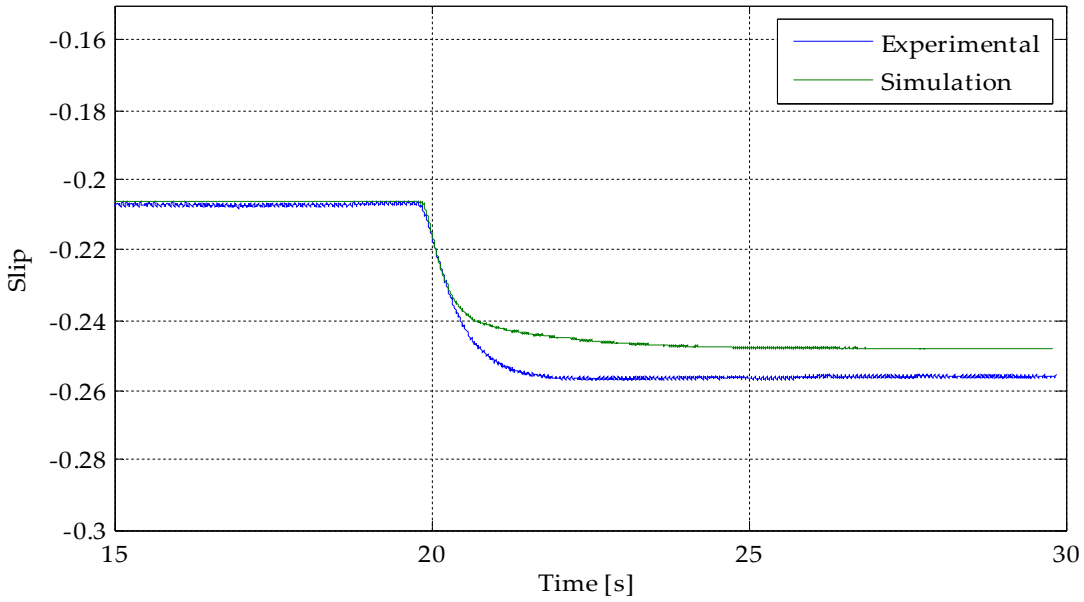

Figure 7-37: Experimental and simulated generator slip of a single turbine in response to a step increase of wind speed from 7m/s to 8m/s.

7.4.2 Harmonics

The effects of the high order harmonics that are introduced to the generator winding currents and voltages by the rectification process can be observed in Figure 7-33, Figure 7-34 and Figure 7-35. The rectification process also introduces harmonics to the voltage and current outputs from the rectifiers, as shown in Figure 7-36 and Figure 7-38, and also to the generator torque. (Demonstration of the harmonics present on the generator torque has not been possible experimentally and therefore has been omitted). It is shown in Figure 7-36 and Figure 7-38 that the resultant waveform shapes, caused by the presence of the high order harmonics, correlate well between the experimental results and those of the simulation; indicating that the experimental and simulation harmonic components are similar.

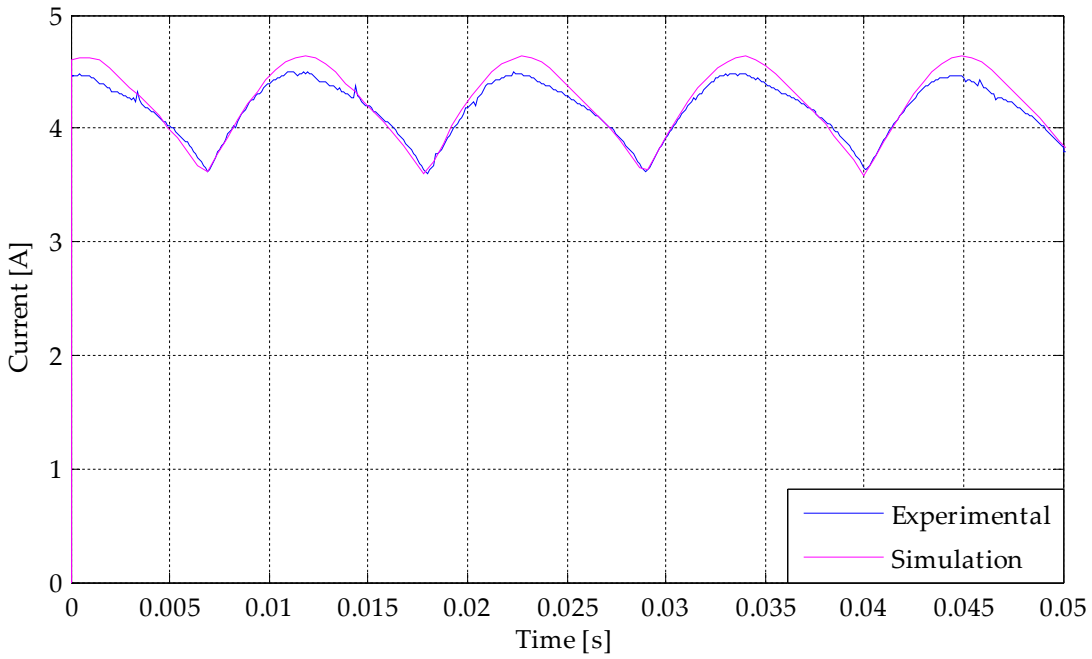

Figure 7-38: Experimental and simulated rectifier output currents.

The harmonic components of the rectifier output voltage and currents, first observed in Chapter 6, have a significant impact on both the voltage at the cluster common point and also on the aggregated current from all of the cluster turbines in the common cluster output cable. In particular, the impact of these harmonics is observed when the turbines are rotating at different speeds or when they are out of electrical phase with each other. When this is the case, the DC current harmonics produced by the generators superimpose within the cluster common output cable introducing a low frequency beat harmonic. To demonstrate the presence of this beat harmonic on the cluster common cable current, both in simulation and experimentally, the simulation is firstly used to provide a reference ideal measurement of the cluster output current where the turbines are rotating at the same speed (23.66 rad/s) and are electrically in phase with each other, shown in Figure 7-39. The operation of the generators in these conditions is unlikely to occur in reality because the wind speed incident on each of the turbines will not be the same.

Secondly, the generator rotational speeds are offset from each other (22.63rad/s and 21.24rad/s respectively) and further measurements of the current flowing through the cluster taken, shown in Figure 7-40.

Observing the current waveforms in the reference case reveals that when the generator speeds are equal, and the generators electrically in phase, the cluster output current exhibits a harmonic component with a magnitude that is the sum of the 6^{th} current harmonic components produced by the rectified outputs of both generators. Observing the same current in the second case, where the generator speeds are different, in Figure 7-40, reveals that there is a lower harmonic frequency beat, in addition to the 6^{th} harmonic component, as a result of the superposition of the different frequency 6^{th} harmonic components produced by each generator. By comparing the experimental and simulation cluster output current measurements in Figure 7-40, it is clear that the beat harmonic is a feature of the experimental system as well as the simulation models. The frequency of the beat harmonic component is equal to the difference between the 6^{th} harmonic components frequencies produced by each machine, calculated as 33.36rad/s (5.3Hz) in this case. The presence of this beat harmonic is also reflected on the cluster common point voltage, which is a function of the voltage drop across the common cable resistance as a result of the current flowing through it. It is shown in Figure 7-41 that both the experimental and simulation common point voltages exhibit the beat harmonic. The voltage beat harmonic component however does not affect the turbine output currents, as its magnitude is small, with respect to the voltage average.

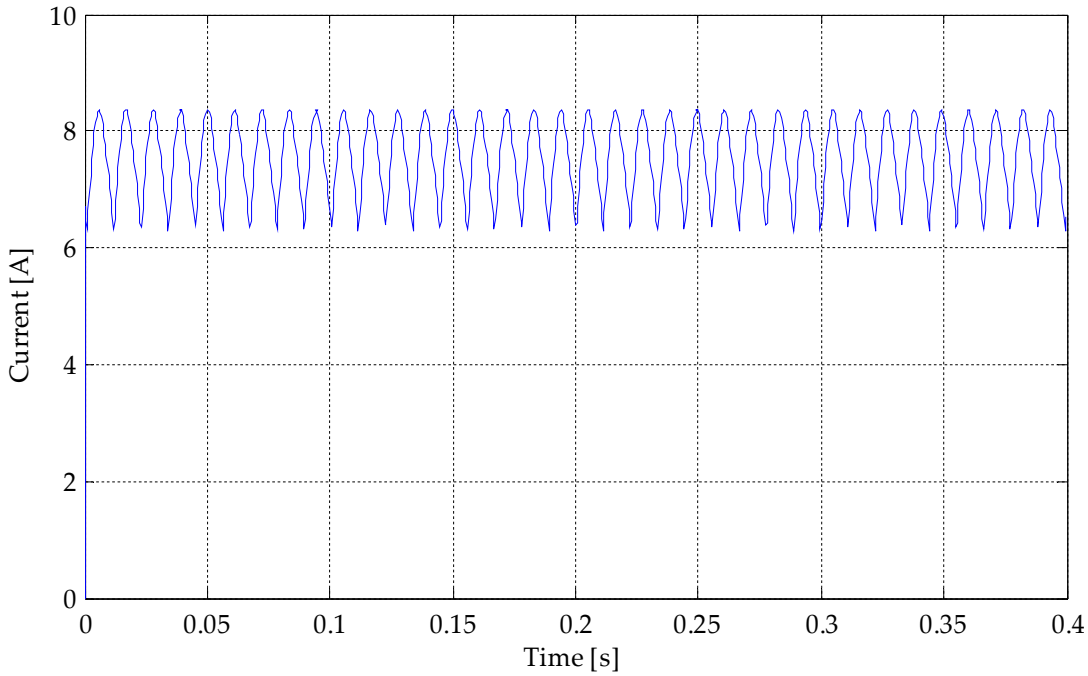

Figure 7-39: Simulated cluster output current, when both generators are rotating with the same speed, 23.66rad/s, and are in phase electrically.

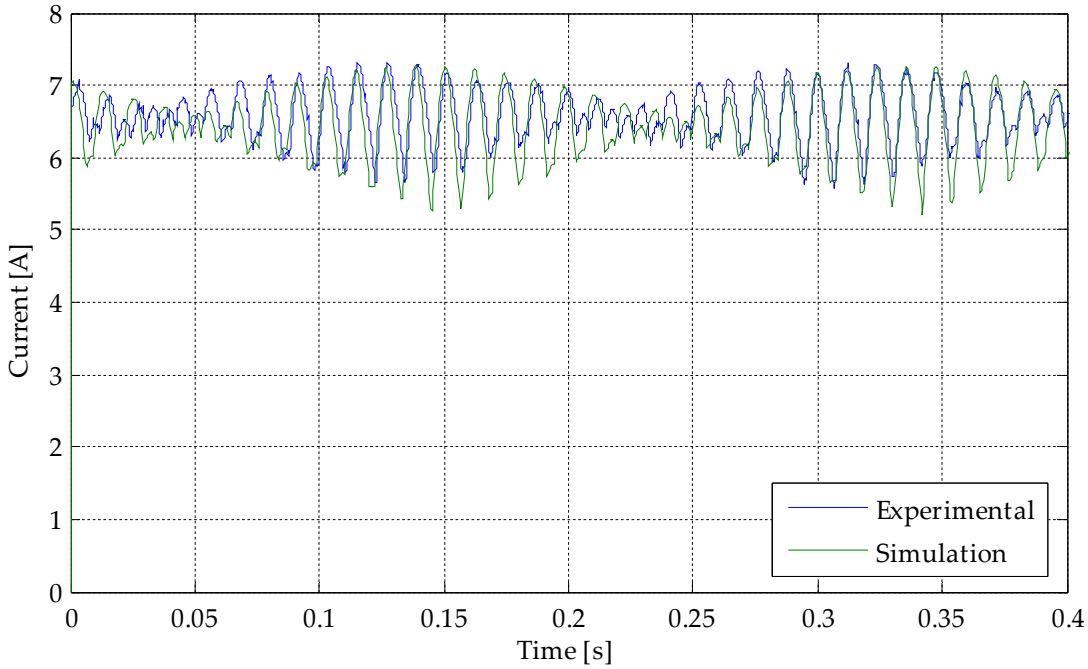

Figure 7-40: Experimental and simulated cluster output currents, when the rotational speeds of the generators are 22.63rad/s and 21.24rad/s respectively.

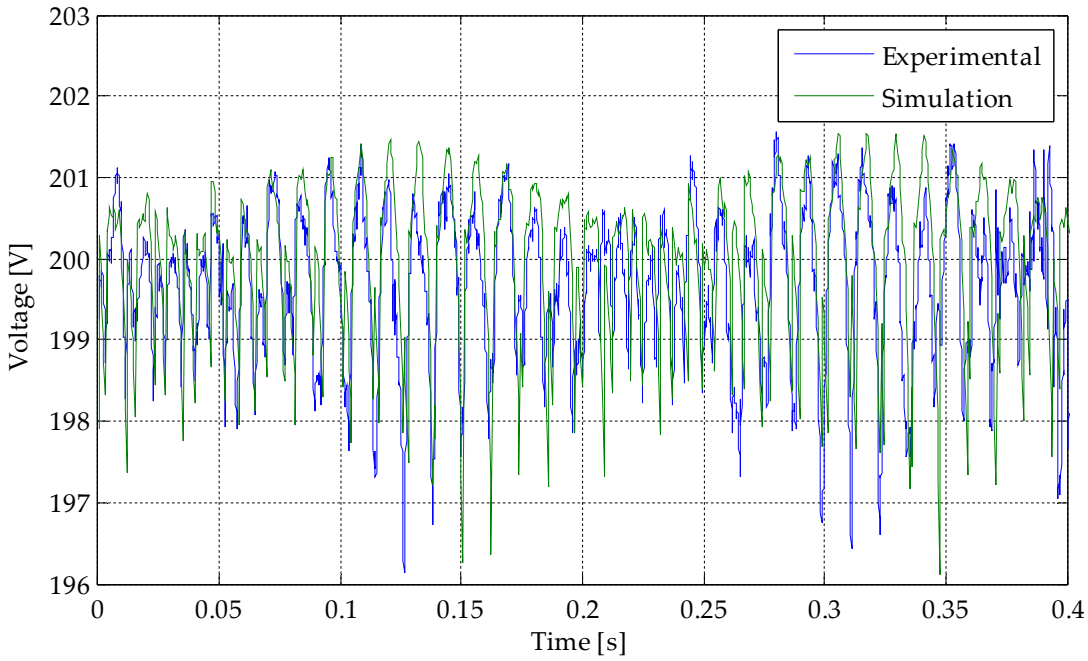

Figure 7-41: Experimental and simulated cluster common point voltage, when the rotational speeds of the generators are 22.63rad/s and 21.24rad/s respectively.

Interactions between turbines

The electrical clustering of multiple wind turbines causes interactions to occur when each is subject to a different wind speed. The interactions occur as a result of two factors: the response of the cluster controller to the change of the average wind speed across the cluster, and the change of the common point voltage as a result of the changing cluster output current flowing through the cluster common output cable. To verify the effect of each source of interaction experimentally, two scenarios are applied: firstly the cluster controller is given the freedom to vary its control voltage in response to changes of the cluster power output, and secondly the control voltage is held constant at 188.8V. In both cases the wind speed step changes shown in Figure 7-32 are applied and the rotational speed of each turbine used as an indicator of the interactions.

In response to the step changes of wind speed in the first case, it can be observed in Figure 7-42 and Figure 7-43 that the speed of the turbine whose wind speed increases, accelerates, and the speed of the second turbine and the cluster synchronous speed respond to a lesser extent. The response of the second wind turbine speed indicates that there is some degree of interaction between the turbines; this interaction is primarily caused by the action of the cluster controller to adjust the cluster synchronous speed to match the new average wind speed across the cluster. Comparing the experimental and simulation responses of this turbine reveals that the experimental response to the step changes is similar to the simulation. The interactions between the turbines can be separated into two stages: transient and steady state. The transient response includes the initial response of the turbine to the step change, and once it has settled to a steady state it enters stage two. Observation of each stage independently reveals that there are slight differences between the experimental and simulation responses. The transient differences are likely to be the result of errors between the experimental and modelled generator and drive shaft moments of inertia, and also the effect of extra filters included in the test rig to remove background measurement noise. The slight error between the steady state responses is likely to be caused by the imperfect test-rig generator emfs, which require the generators to rotate at slightly greater speeds to produce the same voltage.

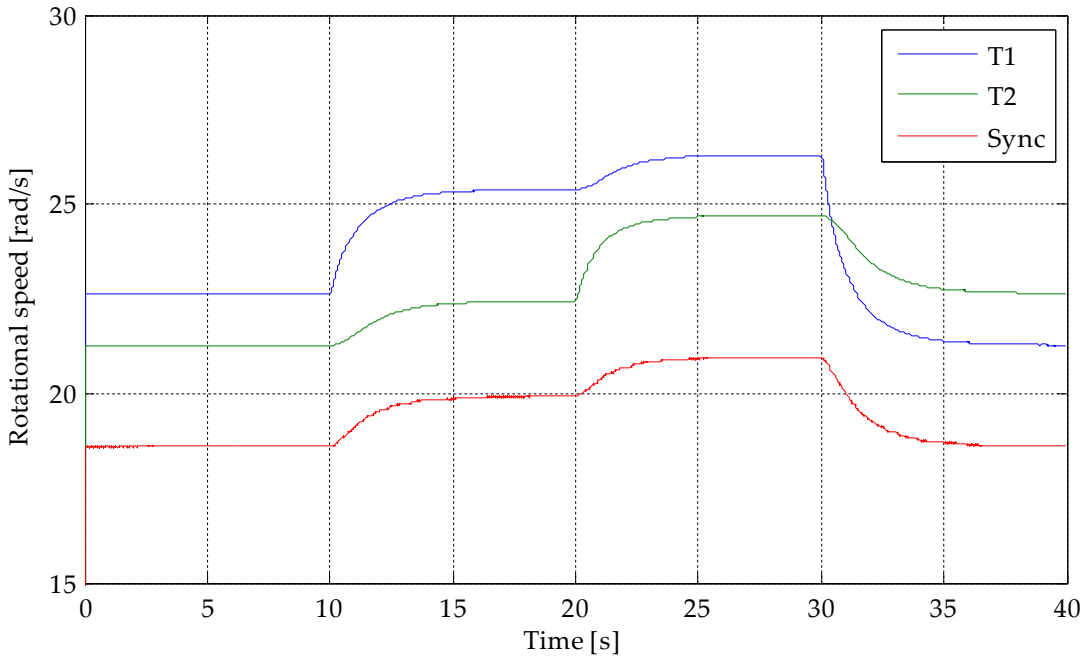

Figure 7-42: Simulation turbine and synchronous rotational speeds in response to step changes of wind speed.

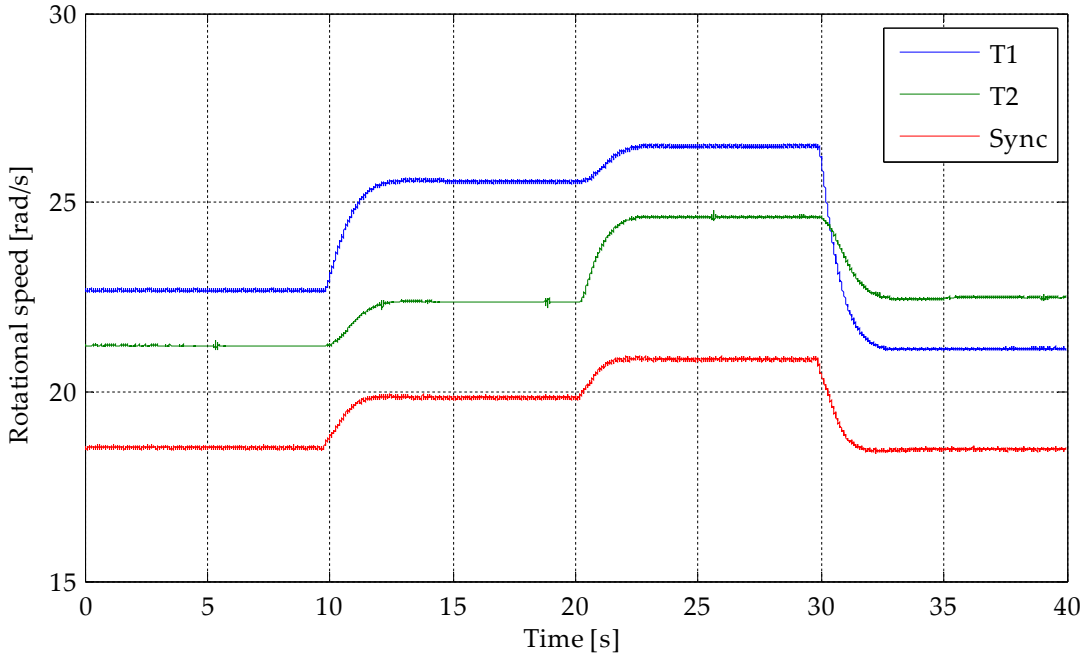

Figure 7-43: Experimental turbine and synchronous rotational speeds in response to step changes of wind speed.

In the second case, where the control voltage is held constant, the change of the turbine rotational and synchronous speeds in response to the wind speed step changes is more limited, as shown in Figure 7-44 and Figure 7-45, and therefore the interactions between the turbines are also more limited. The responses observed are the result of both the increase of generator slip in response to the increased generator power output and the increase of current magnitude through the cluster common cable. The effect of the changing output current is demonstrated to be small by the limited change of the synchronous speeds in either case; and the increase of generator slip is demonstrated by the change of rotational speed of the turbine which experiences the wind speed change. It is therefore demonstrated, by comparing the change of the synchronous speed and the change of rotational speed of the turbine that experiences the wind speed step, that the change of generator slip is the dominant cause of the rotational speed response in this case. This is confirmed by comparing the experimental and simulation responses of the system in this scenario.

The limitation of the interactions between the turbines observed in the second case, where the control voltage is constant, in comparison to the interactions in the first case, therefore confirms that the interactions between the turbines are predominately caused by the action of the system controller, as found in Chapter 6.

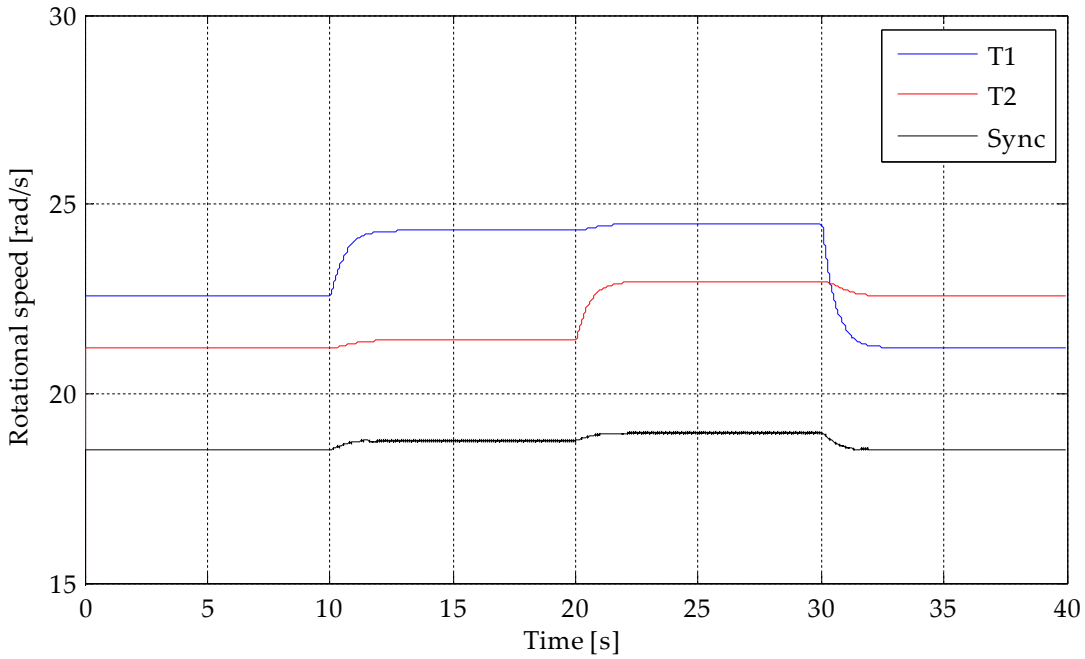

Figure 7-44: Simulated turbine rotational speeds in response to step changes of wind speed, where the cluster control voltage is held constant at 188.5V.

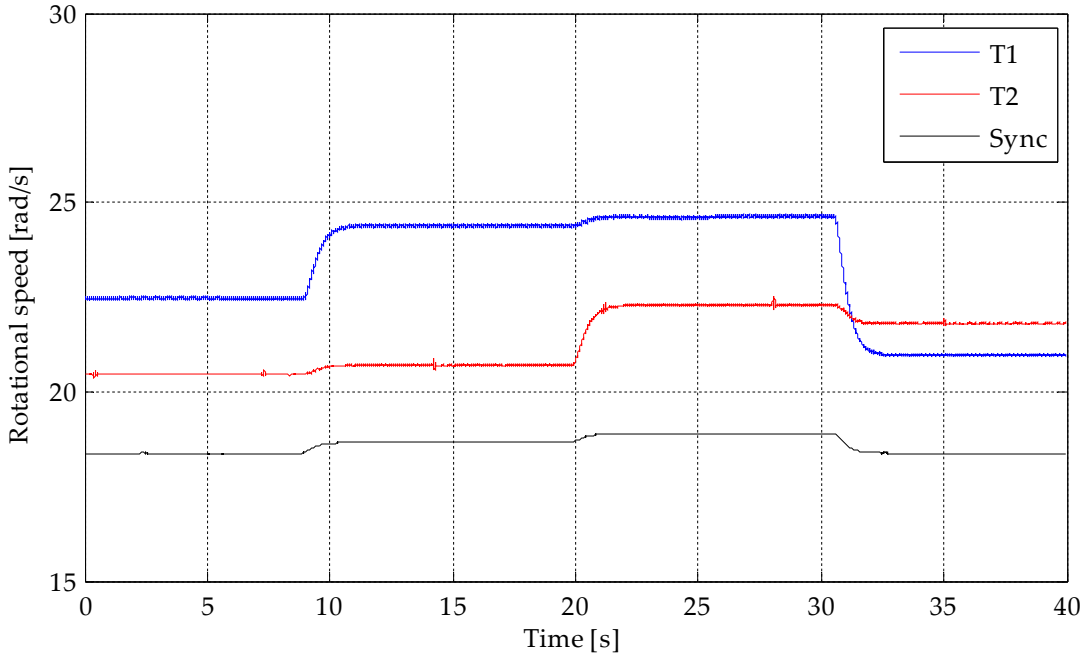

Figure 7-45: Experimental turbine rotational speeds in response to step changes of wind speed, where the cluster control voltage is held constant at 188.8V.

7.4.3 Continuously varying wind speeds

To demonstrate the experimental operation of the system in wind speed conditions that are representative of reality, the continuously varying wind speed profiles shown in Figure 7-46 have been fed in to test rig turbine rotor models. These profiles are different to those used in previous Chapters of this thesis but have been generated by the same method, with altered parameters to reflect the intended smaller dimensions of the test rig wind turbine rotors, given in Table 7-1; the effect of the smaller rotor dimensions is a reduced turbine rotor moment of inertia, which allows the turbine speeds to respond quicker to changes of wind speed.

It can be observed by comparing Figure 7-46 and Figure 7-47 that the changes of the rotational speed of each turbine follow the wind speed quite closely; it can also be observed that the cluster synchronous speed follows the average of the wind speeds. This demonstrates that the turbine speeds have the freedom to change according to their local wind speeds and also that the cluster controller action, to regulate the cluster synchronous speed, follows the change of the average wind speed across the cluster, as expected. The ability of each turbine rotational speed to follow its local wind speed is achieved by the variation of the generator slip; Figure 7-48 demonstrates the considerable variation of the generator slip, in response to the changing wind speeds, which facilitates the variation of the rotational speeds. The effectiveness of the rotational speed variation at optimising the power coefficient of the turbine rotors is shown in Figure 7-49; demonstrating that the variation of speed, allowed by the generator slip, keeps the power coefficient of each turbine within 4% of the 41.88% maximum. Finally, in Figure 7-50 the power output of the cluster is shown to follow the change of

the average wind speed across the cluster, similarly to the cluster synchronous speed which is driven by the change of the power output.

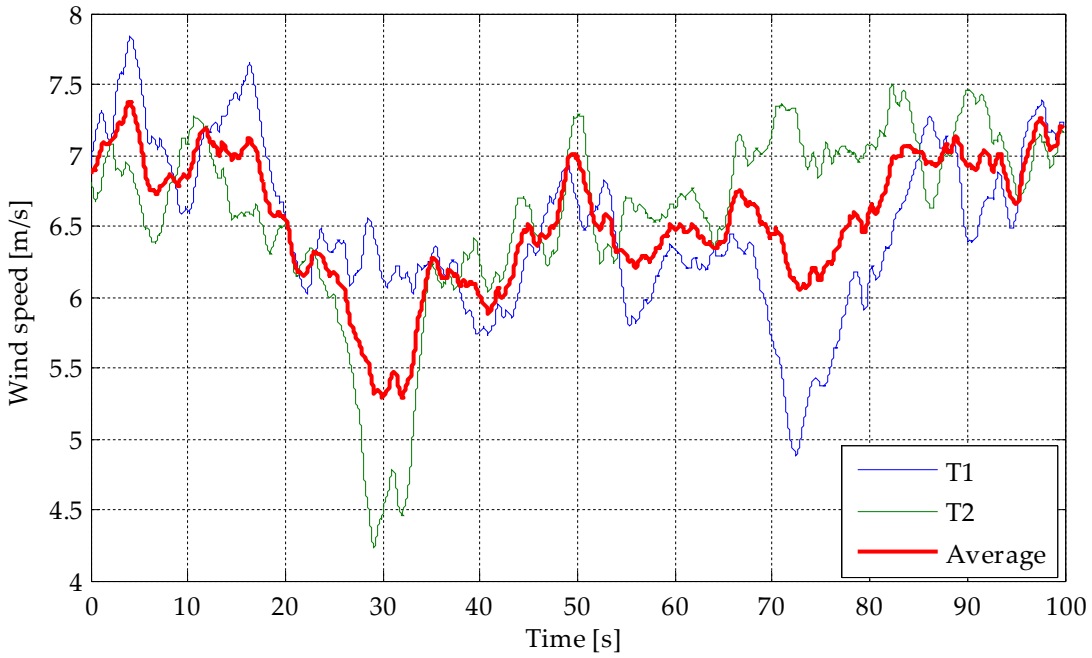

Figure 7-46: Continuously varying wind speed profiles used to demonstrate the experimental operation of the cluster based system in realistic wind conditions.

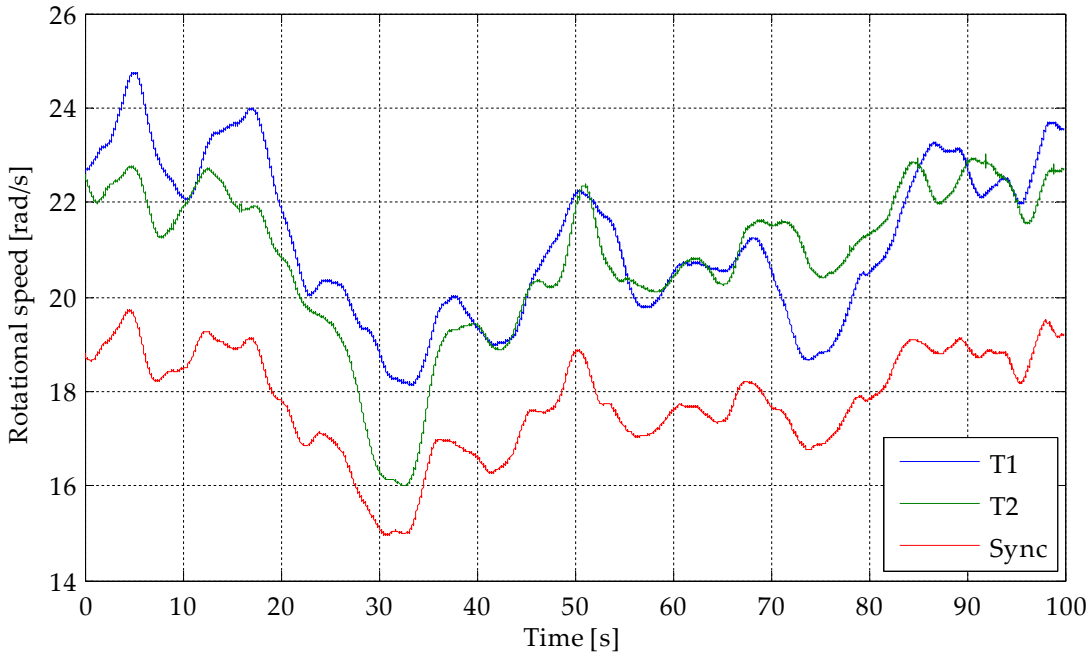

Figure 7-47: Rotational speed of each turbine along with the cluster synchronous speed, in response to the continuously varying wind speeds.

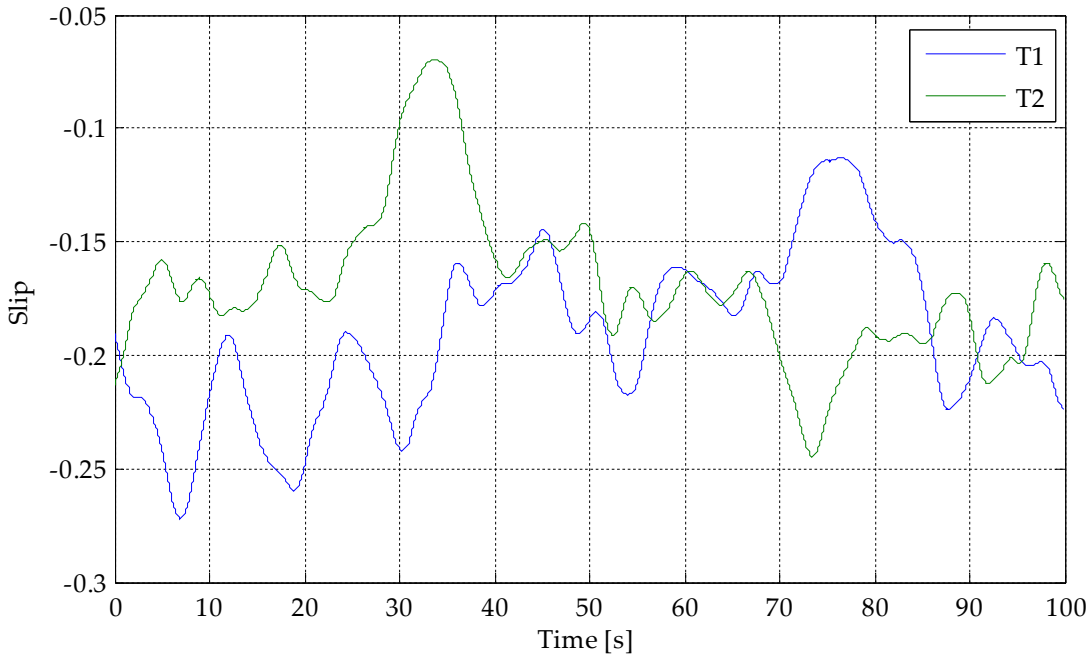

Figure 7-48: Generator slip of each turbine, in response to the continuously varying wind speeds.

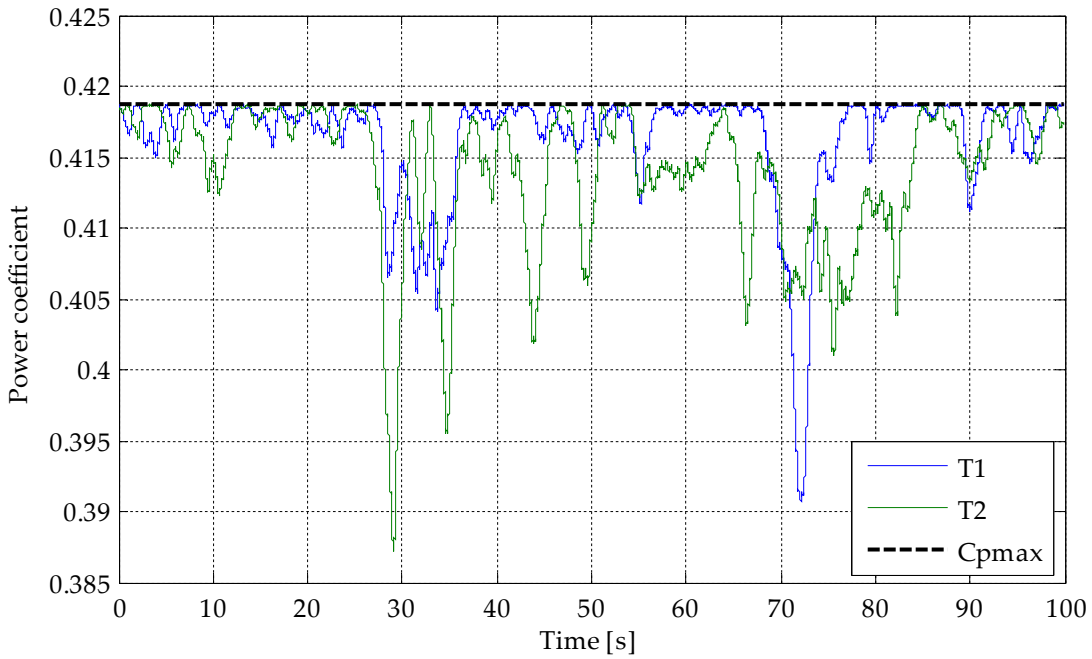

Figure 7-49: Turbine rotor power coefficient for each turbine in comparison to the Cpmax, in response to the continuously varying wind speeds.

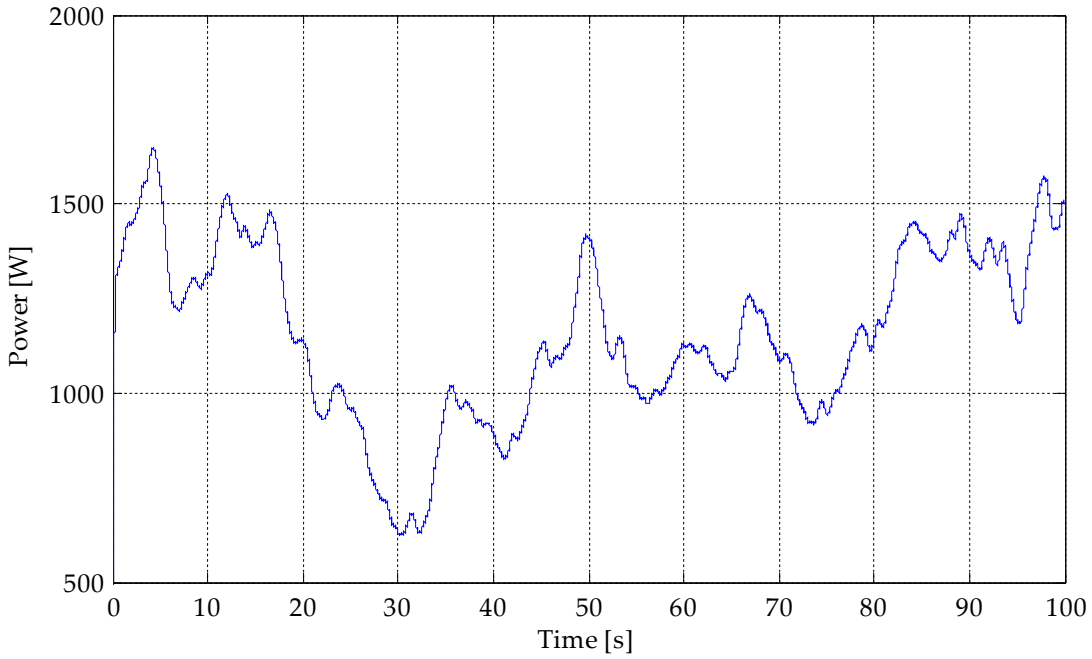

Figure 7-50: Cluster power output in response to the continuously varying wind speeds.

7.5 Conclusions and summary of practical considerations

Within this chapter the development of a laboratory scale practical implementation of a cluster based collection network, which is capable experimentally validating the operation of the system, has been detailed. A key component of the laboratory test rig is the DC converter; the design of the two conversion stages of this converter has been covered in detail along with their expected operational and control characteristics. To aid the selection of the converter component parameters and to confirm its capability to regulate the cluster DC voltage over the required range, a simulation model of the converter has also been developed in Matlab Simulink. The practical implementation of the converter, in conjunction with two small PM generators, has then been described in detail and the operation of the whole system verified.

To experimentally validate the operation of the cluster system, a simulation model of the scaled down test rig system has been used to provide the benchmark for comparison with the test-rig. Comparisons between the modelled system operation and that of the test-rig have been conducted in a number of input wind speed scenarios to validate the different operation aspects of the system. Initially the rectifier commutation process and the distortion it introduces to the generator winding voltages and currents and rectifier DC output current and voltages has been investigated. This investigation has demonstrated that there is good correlation between the experimental and simulation generator current and voltage waveforms throughout the commutation process, although the non-ideal construction of the test-rig generators is shown to cause some minor differences. Secondly, a constant wind speed and a step change have been applied to investigate the slip capability of the generators; this investigation has proven that the

amount of slip that occurs between the cluster synchronous speed (derived from the cluster common point voltage) and the turbine rotational speed, observed experimentally and in simulation are similar, although, as above, the imperfect construction of the test rig generators causes some minor errors.

In the previous chapters of this thesis it has been shown that the rectifier commutation process introduces a significant amount of higher order harmonic content to the generator winding currents and also to the rectifier output currents and voltages. The presence of these harmonic components has been confirmed here by the comparison of the experimental current waveforms with those observed in simulation. In addition, the introduction of a lower frequency beat harmonic to the cluster output current, as a result of the superposition of the DC output current harmonics from each turbine in the common cluster output cable, has been confirmed.

The interaction of the clustered turbines has also been investigated by observing the response of the test-rig turbines to step changes of wind speed, in two scenarios. This investigation has confirmed experimentally that the dominant cause of these interactions is the cluster controller; whose action causes all of the turbines in a cluster to respond to a change of wind speed on a single turbine.

Lastly, the operation of the experimental system under continuously varying wind speed conditions, representative of reality, has confirmed that the slip capability of the generators allows the rotational speeds of each turbine to vary in response local changes of wind speed. It is also proven that the combination of the controller action and variation of the turbine rotational speeds as a result of the generator slip, allows the turbine rotor power

coefficients to be kept within a small margin (4%) of the maximum, as the wind speed changes.

7.6 References

1. Mohan, N., T.M. Undeland, and W. Robbins, *Power Electronics - Converters, Applications and Design*. 3rd ed2003: John Wiley & Sons.
2. Semikron, *SemiTrans M IGBT Modules SKM 50GB123 D datasheet*.
3. Semikron, *Heat sink P3 data sheet*.

Chapter 8 Conclusions and Further Work

The work presented in this thesis provides a comprehensive study of the feasibility of electrically grouping large offshore wind turbines into clusters of up to five. The connection and operation of a group of turbines in an electrical cluster is motivated by the potential reduction of power electronic converter numbers within a wind farm, the subsequent simplification of the turbine subsystems and the reduction of the number of turbine failures it will allow; which are key considerations in the development and operation of distant offshore wind farms. The starting point for the work presented here is a study of the potential improvements to the availability of offshore wind turbines for the generation of electricity, which can be achieved in comparison to the status quo. Following on from this, a statistical study of the effect of requiring groups of adjacent wind turbines to rotate with equal speed has on their annual energy capture is conducted. Both of these studies aim to trade off the effects of clustering turbines on the two primary

operational economic factors of an offshore wind farm: the maintenance of the turbines and associated balance of plant, which presents substantial costs to a wind farm operator, and also the efficiency with which the turbines capture energy from the wind, which impacts directly upon the incoming revenue stream from the sale of the electrical energy generated.

The crux of the work presented here has been the investigation of potential technologies with which an electrical cluster of turbines could be implemented. Chapter 4 provides a comparison of three different potential technologies: induction generators with a variable frequency AC network, PM generators with a variable frequency AC network, and PM generators with passively rectified outputs and a multi-terminal DC network. This comparison is based upon the extensive simulation of these potential technologies to evaluate them in a range of operating conditions; the conclusion of which, in terms of energy transfer efficiency and operational performance, is that the third option offers the greatest operational benefits whilst maintaining a high level of efficiency, and is therefore the preferred choice.

The preferred technology is taken forward within the later chapters which investigate the commutation process of the passive rectifiers, how it can be exploited to provide generator slip, and how the exploitation of this property effects the harmonic emission of a rectifier and the energy losses within the system. Within this investigation the maximum generator slip that can be achieved by using a diode rectifier is determined, along with the effects of complementing it with additional resistance. The impact of different amounts of generator slip on the operation of clustered turbines, in terms of energy capture performance and the damping of mechanical drive train oscillations, is also determined by the simulation of the system using

simplified simulation models. The operation of the system when different wind speeds are incident on each turbine is further determined by investigating the interactions that occur between the turbines due to their parallel connection and collective control.

Finally, the operation of a cluster of wind turbines, based upon the rectification of their outputs and parallel connection by a DC electrical network, is experimentally verified using a laboratory scale test rig, consisting of two 2.5kW wind turbine emulator systems.

The investigations conducted in this thesis indicate that electrically clustering a group of five wind turbines in an offshore wind farm is a technically feasible approach to the electrical system design which reduces the required number of power electronic converters, simplifies the turbine subsystems and will reduce the number of turbine failures. In particular it is demonstrated that the implementation of such a system using PM generators, diode rectifiers and a variable voltage multi-terminal DC electrical network allows them to operate with variable speed and retain a significant degree of independence, allowing them to maintain high energy capture efficiencies when faced with continuously varying and different wind speeds to their neighbours.

8.1 Key findings

The key findings of the work conducted in this thesis are summarised as follows:

Chapter 3

- Reducing the number of power converters within a wind farm has been demonstrated to directly reduce the number of converter failures, from 83.76 failures/year to 16.75 failures/year for case study investigated;

therefore improving the availability of the turbines for energy production. It is also found however, that the greater loss of generating capacity associated with a single failure of a large converter negates the benefits of the improved availability on the annual energy production of the wind turbines (assuming the failure rates of the large and small converters are equal). It should also be noted therefore that the design of the larger power converters to have a higher fault tolerance and therefore lower failure rate, could be justified; which would bring further benefits to the availability of the clustered turbines and provide a positive energy production benefit.

- The potential energy capture loss that could occur as a result of operating a group of wind turbines with a common rotational speed is less than 0.25%, where the wind farm turbulence intensity is 9%, rising to 0.55% where the turbulence intensity is 15%. In addition, a greater proportion of energy is lost for wind farms with mean wind speeds between 7m/s and 8.5m/s, because the turbines spend proportionately more time operating within the variable speed region of their operating curves.
- The lower maintenance costs associated with the lower annual number of converter failures would be likely to offset the energy capture deficit introduced by the requirement for the clustered turbines to rotate with equal speeds.

Chapter 4

- The control of either the electrical frequency of an AC connected cluster of turbines or the voltage magnitude of a DC connected cluster, allows the single cluster converter to regulate the rotational speeds of the clustered turbines to follow the average wind speed across the cluster.

- The use of PM generators provides significant advantages in terms of energy transfer efficiency, with each of the two PM generator cases considered achieving 95% and 98% efficiency respectively; whereas the use of induction generators lowers the efficiency to between 87% and 90%, depending upon the size of the rotor winding resistance. The direct connection of PM generators to an AC network however will also require additional damper windings to achieve stable operation, adding complexity and cost to the generator design.
- The use of PM generators with diode rectifiers and a DC electrical network combines the high efficiency of the PM generators with the ability of the induction generators to provide generator slip; therefore allowing each turbine to retain a degree of independence from its neighbours, improving its energy capture efficiency from the wind. The rectification of the output of a PM generator also removes the requirement for additional damper windings within the machines.
- The use of passive rectifiers introduces significant harmonic components to the generator winding currents and therefore to the generator torque, and to the currents and voltages within the DC collection network.

Chapter 5

- The commutation overlap introduced by the rectification of a PM generators output distorts the generator terminal voltages and introduces harmonic components to the winding currents and torque.

  The distortion introduced to the terminal voltages is reflected onto the DC output voltage of the rectifier, lowering its average; the extent of which is a function of the generator rotational speed and also the turbine power output. This reduction allows for an increased voltage difference to arise between the cluster common point and the emf of the generator,

and therefore is a key contributor to the provision of generator slip. This voltage drop occurs without significantly increasing the losses in the system, but it does lower the power factor of the generator output due to the absorption of reactive power by the rectifier.

- The length of the commutation overlap, the reduction of DC voltage average, the harmonic component magnitudes and the power factor reduction can be predicted theoretically. Theoretical predictions of the currents, voltages and generator torque waveforms have been verified extensively against simulation results demonstrating a high degree of correlation.
- Theoretical prediction of the commutation voltage drop with power throughput allows the cluster to be controlled by regulating the common voltage so that it follows the power output of the cluster; therefore optimising the cluster synchronous speed for the average wind speed across the cluster.
- Predictions of the commutation voltage drop allow the PM generators and rectifiers to be represented by an equivalent ideal DC generator; therefore simplifying the system model and allowing the general behaviour of the system to be observed with greater clarity, without the presence of the harmonic components produced by the rectifier.

Chapter 6

- The generator slip capability of each turbine can be maximised by either increasing the generator winding inductance or adding resistance at the rectifier outputs. Increasing the generator winding inductance to 4.56mH allows the maximisation of the rectifier commutation overlap ($\pi/3$ radians), producing a maximum generator slip of 33%.

- Maximising the length of the rectifier commutation overlap will increase the reactive power consumption of the rectifier and therefore lower the generator output power factor to approximately 0.86. The increase in generator winding current associated with this reduction of power factor also causes a slight increase of the energy losses within the generator windings. In addition, it has been found that the maximisation of the commutation overlap length is advantageous to reducing the harmonic distortion of the generator winding currents and torque, by lowering the output power level at which the maximum generator winding current and torque Total Harmonic Distortion occurs.
- The additional resistance required to produce an equal amount of generator slip as the maximisation of the commutation overlap length is 24Ω; doubling this resistance to 48Ω allows the generator slip to be increased to 47%. A major drawback of adding resistance is the loss of energy it causes, which reduces the energy transfer efficiency of the system by 6% and 13%, for each value of resistance respectively. It is therefore preferred that the generator winding inductance be increased to achieve a greater amount of generator slip; therefore maintaining a high energy transfer efficiency and reducing the harmonic distortion of the generator currents and torque.
- It is demonstrated that the presence of generator slip improves the energy capture performance of the clustered wind turbines. In particular the greatest improvements of energy capture performance are observed by increasing the generator slip provision from a minimal amount to 13%, and from 13% to 26%; increasing the generator slip provision further to 34% however provides a comparatively smaller improvement of energy capture performance. Therefore the pursuit of the maximum amount of

generator slip is not warranted by the additional energy capture performance it provides, over the performance achieved by the slip that occurs as a result of the natural generator and transformer winding inductances.

- It is demonstrated theoretically and through the simulation of the wind turbine mechanical drive train dynamics that the provision of generator slip introduces a component of generator torque that is a function of the generator rotational speed, and is therefore capable of damping the natural oscillation of the wind turbine drive train.
- Simulation of the system indicates that the collective control of two wind turbines diminishes their individual ability to maintain the optimal rotational speed and rotor power coefficient for optimal energy capture from the wind. This occurs as a result of the cluster controller regulating the cluster synchronous speed according to the average of the turbine wind speeds. It is also proven that increasing the size of a cluster from two to five wind turbines does not further diminish the energy capture performance of the clustered turbines significantly.
- It has been proven through simulation that the parallel connection of turbines causes them to interact; the primary cause of which is the variation of the cluster common point voltage, which influences the current output and therefore generator torque produced by each turbine. The variation of the cluster common point voltage is affected by both the action of the cluster controller to regulate the cluster common point voltage according to the aggregate cluster power output, and the change of the voltage drop across the common output cable impedance. By removing the action of the controller it has been observed that the influence of the common cable voltage drop is small, and therefore the

action of the controller is the dominant cause of the interactions between the turbines.

Chapter 7

- The development of a bench scale test rig has allowed the operation of the system observed in simulation to be rigorously validated experimentally; in particular the rectifier commutation process and the ability of the generators to slip from the cluster synchronous speed. It is observed however that the imperfect construction of the test rig generators introduces some error between the experimental and simulation observations.
- The harmonic emission of the diode rectifiers has been correlated with the simulation observations further validating the theoretical predictions.
- The operation of the cluster system when the turbines are subject to continuously varying wind speeds, representative of reality, is demonstrated experimentally; proving that the capability of the generators to slip from the cluster synchronous speed allows the turbine rotational speeds to vary according to their local wind speed, therefore allowing them to maintain high energy capture efficiencies from the wind.

8.2 Contribution to knowledge

The connection of multiple adjacent offshore wind turbines in an electrical cluster is a novel approach to the design of a wind farm electrical collection network. This thesis provides the first comprehensive study of both the motivation and operation of such a system.

In particular this thesis provides the first comprehensive review of the potential methods for connecting multiple electrical generators, which are subject to significantly different input torques and required to rotate at different speeds, in parallel. The outcome of this review is carried forward by the rigorous investigation of the operating principles and resultant system characteristics of connecting multiple PM generators in parallel, by rectifying their outputs and using a multi-terminal DC electrical network.

Providing a degree of independence between the parallel connected wind turbines is advantageous to their operation; an innovative approach to the provision of this independence is proposed here by the production of generator slip by enlarging the voltage difference between the generator emfs and the cluster common point voltage. The work presented here also provides the first comprehensive study of the merits and pitfalls of producing generator slip either by exploiting the DC voltage distortion caused by the rectifier commutation overlap or by the introduction of additional DC resistance.

Finally, this thesis provides potentially the first experimental validation of the operational aspects of such a system, where the clustered turbines are subject to different and continuously varying wind speeds. In particular the presence of a degree of independence between the rotational speeds of adjacent turbines is confirmed.

8.3 Future work

The work conducted in this thesis has explored the major economic factors involved with the clustering of a number of turbines together, reviewed the potential technologies that could be used to implement such a system, and studied in depth the operation of a cluster of turbines where the outputs of PM generators are rectified and connected in parallel. At each stage of the work presented here a number of different avenues which could provide interesting further topics of research have been identified, as follows:

1. Through the partnership with an offshore wind farm operator the study of the availability improvements provided by the reduction of the number of power electronic converters within a wind farm could be enhanced. In particular the use of more comprehensive data describing the failure and repair rates of power electronic converters and the accessibility of turbines would be beneficial.
2. The development of a method for predicting the energy capture loss caused by limiting the rotational speed of multiple adjacent wind turbines to a common speed, which incorporates the power spectral density of wind speed variations and the coherence between the winds incident on adjacent wind turbines, would be worthwhile. The effects of introducing different amounts of generator slip, and therefore different degrees of turbine independence, may also prove interesting.
3. The further investigation of the advantages, in the context of a cluster collection network based on the rectification of the outputs of PM generators, of using alternative PM generator designs such as brushless DC generators and multi-phase generators, on the harmonics introduced to the generator winding currents and torque as

a result of the rectification process, may prove helpful to mitigating the harmonic emission of the rectifiers.

4. The review, investigation and development of potential methods of protecting the system components when faults occur within the turbines, the cluster electrical network and in the wider wind farm electrical system would be imperative to the successful implementation of such a system on a large scale.
5. The investigation of potential methods of providing damping to the wind turbine structure through the provision of a partial active control capability of generator torque, whilst maintaining the robustness and simplicity qualities of the passive rectifiers.
6. The investigation of the procedure through which a cluster of turbines could be used in conjunction with other adjacent clusters to provide black start capability and disturbance recovery support (voltage and frequency) to the wider electrical system.
7. The optimisation and refinement of the cluster converter topography to provide a fault tolerant and low maintenance converter that is low cost.

Appendix A Cluster Control Curve Script

Main Algorithm Script

```
clear

 %% Wind turbine parameters

%Cp vs lamba data for 5MW turbine produced using GH Bladed and NREL
5MW ref
Cp=[0,  0.0005, 0.0009, 0.0014, 0.0019, 0.0025, 0.0030, 0.0036,
0.0043, 0.0050, 0.0057, 0.0064, 0.0072, 0.0080, 0.0088, 0.0098,
0.0111, 0.0129, 0.0154, 0.0186, 0.0227, 0.0273, 0.0326, 0.0390,
0.0463, 0.0543, 0.0629, 0.0722, 0.0817, 0.0914, 0.1014, 0.1117,
0.1220, 0.1323, 0.1431, 0.1544, 0.1661, 0.1779, 0.1899, 0.2022,
0.2150, 0.2278, 0.2412, 0.2550, 0.2690, 0.2836, 0.2976, 0.3116,
0.3252, 0.3390, 0.3534, 0.3690, 0.3841, 0.3966, 0.4059, 0.4133,
0.4201, 0.4264, 0.4324, 0.4378, 0.4430, 0.4478, 0.4521, 0.4562,
0.4600, 0.4638, 0.4674, 0.4708, 0.4743, 0.4774, 0.4804, 0.4825,
0.4839, 0.4850, 0.4858, 0.4865, 0.4869, 0.4872, 0.4873, 0.4872,
0.4869, 0.4865, 0.4859, 0.4853, 0.4844, 0.4834, 0.4824, 0.4813,
0.4801, 0.4787, 0.4773, 0.4757, 0.4741, 0.4723, 0.4705, 0.4686,
0.4666, 0.4646, 0.4624, 0.4603, 0.4580, 0.4557, 0.4533, 0.4508,
0.4483, 0.4456, 0.4427, 0.4399, 0.4370, 0.4341, 0.4309, 0.4278,
0.4246, 0.4213, 0.4179, 0.4144, 0.4108, 0.4072, 0.4034, 0.3996,
0.3956, 0.3916, 0.3875, 0.3833, 0.3791, 0.3747, 0.3703, 0.3658,
0.3613, 0.3566, 0.3519, 0.3471, 0.3421, 0.3371, 0.3319, 0.3266,
0.3214, 0.3160, 0.3105, 0.3051, 0.2995, 0.2938, 0.2879, 0.2821,
0.2761, 0.2701, 0.2640, 0.2577, 0.2514, 0.2450];

TSR=[0, 0.1, 0.2, 0.3, 0.4, 0.5, 0.6, 0.7, 0.8, 0.9, 1, 1.1, 1.2,
1.3, 1.4, 1.5, 1.6, 1.7, 1.8, 1.9, 2, 2.1, 2.2, 2.3, 2.4, 2.5,
2.6, 2.7, 2.8, 2.9, 3, 3.1, 3.2, 3.3, 3.4, 3.5, 3.6, 3.7, 3.8, 3.9,
```

```
4, 4.1, 4.2, 4.3, 4.4, 4.5, 4.6, 4.7, 4.8, 4.9, 5, 5.1, 5.2, 5.3,
5.4, 5.5, 5.6, 5.7, 5.8, 5.9, 6, 6.1, 6.2, 6.3, 6.4, 6.5, 6.6, 6.7,
6.8, 6.9, 7, 7.1, 7.2, 7.3, 7.4, 7.5, 7.6, 7.7, 7.8, 7.9, 8, 8.1,
8.2, 8.3, 8.4, 8.5, 8.6, 8.7, 8.8, 8.9, 9, 9.1, 9.2, 9.3, 9.4, 9.5,
9.6, 9.7, 9.8, 9.9, 10, 10.1, 10.2, 10.3, 10.4, 10.5, 10.6, 10.7,
10.8, 10.9, 11, 11.1, 11.2, 11.3, 11.4, 11.5, 11.6, 11.7, 11.8,
11.9, 12, 12.1, 12.2, 12.3, 12.4, 12.5, 12.6, 12.7, 12.8, 12.9, 13,
13.1, 13.2, 13.3, 13.4, 13.5, 13.6, 13.7, 13.8, 13.9, 14, 14.1,
14.2, 14.3, 14.4, 14.5, 14.6, 14.7, 14.8, 14.9];


LamdaOpt=7.8;           %optimum tip speed ratio
Cpmax=0.487326;         %maximum power coefficienct
Airdens=1.225;          %Air density [kg/m^2]
r=63;                   %Turbine rotor radius [m]
area= pi*r^2;           %Turbine rotor area [m^2]
GearRatio=97;           %Gear box ratio
wmax = 1.267 * GearRatio;

NoMach=1;               %number of turbines in the cluster

%% Parameters for PM generator model
pp=2;                   %pole pairs
Ui=3115*sqrt(3);        %Rated line-line voltage
wnom= 1174*2*pi/60;     %Nominal rotational speed

K= Ui/(wnom*pp);        %Generator flux constant, based on line to
                        line voltage
Km=K/sqrt(3);           %Generator flux constant, based on line to
                        GND voltage

Lq=0.0016;              % Stator inductance
Ld=Lq;
R=0.002;                % Stator resistance
PhiF=Km;
Lad=Ld;
Laq=Lq;
Lld=0;                  %leakage inductance
Llq=0;

%% Line and device parameters
Rl1=0.0366*10;          %Common cable resistance, 10km, 500mmsq
                        conductor  [ohms]
Ll1=10*0.55e-3  ;       %Common cable inductance, 10km, 500mmsq
                        conductor  [H]
Rl2=0.0366*10;          %Branch line resistance, 10km, 500mmsq
                        conductor   [ohms]
Ll2=10*0.55e-3;         %Branch cable inductance, 10km, 500mmsq
                        conductor  [H]

Ron=0.002;              %Conduction resistance of all power
                        electronic devices [ohms]
Rpara=1000;             %Parasitic resistances at machine terminals
                        [ohms]
Vfwd=0.8;               %Diode forward voltage drop [V]

%% Transformer parameters
```

```
Lt1=2.3e-3;             %Primary winding inductnace [H]
Lt2=Lt1;                %Secondary winding inductnace [H]
Rt1=0.0363;             %Primary winding resistance [ohms]
Rt2=Rt1;                %Secondary winding resistance [ohms]
Vt1=3.315e3;            %Primary side voltage [V]
Vt2=33e3;               %Secondary side voltage [V]
Nt=Vt2/Vt1;             %Transformer ratio
Rtm=1089;               %Magnetising resistance [ohms]
Ltm=4.333;              %Magnetising inductances [H]

Lc=Lt2+(Lq+Lt1)*(Nt^2); %Generator and LV transformer inductance
                         referred to HV side [H]
Rc=Rt2+(R+Rt1)*(Nt^2);  %Generator and LV transformer resistance
                         referred to HV side [ohms]

Km=Km*Nt;               %Generator flux constant HV side (L-L)
K=K*Nt;                 %Generator flux constant HV side (L-Gnd)

RLVPara=Rtm*Rpara/(Rtm+Rpara);  % Combined parallel resistance[ohms]

%% initial conditions
w0=0.77;                %turbine rotational speed [rad/s]
Vdcinit=0.95*GearRatio*3*sqrt(3)*Km*w0*pp/pi;   %DC voltage [V}

%% mechanical systen parameters
Jgen=534.116;           %Generator intertia [kg.m^2]
Jturb=3.544e7;          %Turbine rotor inertia [kg.m^2]

Jcombined=Jgen+(Jturb/(GearRatio^2));       %combined generator and
turbine rotor inertia for when gearbox model is not present
Jgen=Jcombined;                             %include when gearbox
model is not present

%% Gearbox model parameters
N=97;                   %gear ratio
KwgLSS=8.676e8;         %low speed shaft stiffness (N/rad)
KwgHSS=KwgLSS/N^2;      %high speed shaft stiffness (Nm/rad)
Kwg=19601.4;
Kg=1e9;                 %gear contact stiffness  linear
stiffness(N/m)
Jg1=10;                 %gear wheel inertia
Jg2=10;                 %gear wheel inertia
r1=9.7;                 %LSSgear radius
r2=r1/N;                %HSSgear radius  ratio of r1:r2 give gear
ratio

%% other
Tsamp=1e-6;             %simulation sample time
run VControlCurve       %Calls control curve script
Km=Km/Nt;               %reverts Km to the pretransformer level so
                        it can be used in the model.
```

VcontrolCurve Script

```
%% set-up of paramenters
V=[1:0.05:11.4];
wturb=LamdaOpt*V/r;
wr=wturb*GearRatio;          %gen speed
Pwind=0.5*Airdens*area*(V.^3)*Cpmax;   %power in the wind

k=Km;                        %machine constant
E=k*wr*pp;                   %peak machine voltage
area= pi*r^2;                %rotor Swept area

%initialisation of arrays
It = zeros(1,length(wr));
Idc = zeros(1,length(wr));
VdcRectAverage  = zeros(1,length(wr));
VdcRect = zeros(1,length(wr));
VacR = zeros(1,length(wr));
VacD = zeros(1,length(wr));
VacAngDisp = zeros(1,length(wr));
VacDif = zeros(1,length(wr));
IaMag = zeros(1,length(wr));
alpha = zeros(1,length(wr));
delta = zeros(1,length(wr));
PLossAC = zeros(1,length(wr));
PparaLoss = zeros(1,length(wr));
Idcmth = zeros(1,length(wr));
Rv = zeros(1,length(wr));
VdcPcc= zeros(1,length(wr));
Vdccont= zeros(1,length(wr));
DcCurrentHarmPLossBranch = zeros(1,length(wr));
DcCurrentHarmPLossCommon = zeros(1,length(wr));
PlossElecSysBranch = zeros(1,length(wr));
PlossElecSysCommon = zeros(1,length(wr));
PoutPCC = zeros(1,length(wr));
PoutConv = zeros(1,length(wr));
wsync = zeros(1,length(wr));
slip = zeros(1,length(wr));
Requiv = zeros(1,length(wr));
Vmachdiff = zeros(1,length(wr));

IdcMthMag=0;

for y=1:length(wr)           %repeats process for every value of wr

  %% calculation of voltage curve for full switch model

     Id = zeros(1,200);
     a = zeros(1,200);
     d = zeros(1,200);
     VdcAveComm = zeros(1,200);
     VdcAveCommNew = zeros(1,200);
     VdcAve = zeros(1,200);
     VaRectrms = zeros(1,200);
     VacDiff = zeros(1,200);
     VangDisp = zeros(1,200);
     IarmsMag = zeros(1,200);
```

```
 VdcAveNew = zeros(1,200);
 IdcMth = zeros(1,200);
 Ploss = zeros(1,200);
 PlossPara = zeros(1,200);
 deltaId = zeros(1,200);

 Erms(y)=E(y)/sqrt(2);      %Converts to Rms

 %Calculates initial Vdcave, alpha (commutation start angle) and
 %delta (commutation length)when Idc =0
 [a(1), d(1), VdcAveComm(1), VdcAve(1)] =
  VdcRectAve(0, E(y), wr(y), Rc, Lc, pp, Ltm, Nt);

 %Calculates initial Idc
 Id(1)=Pwind(y)/VdcAve(1);
 %Calculates the magnitude of the mth harmonic component
 IdcMth(1)=Id(1)*IdcMthMag;
 %initial AC loss are zero
 Ploss(1)=0;

for i = 1:200         %Iteration loop for max 200 iterations

%Calculates Vdcave, alpha (commutation start angle) and delta
  (commutation length)
[a(i), d(i), VdcAveComm(i), VdcAve(i)] =
  VdcRectAve(Id(i),E(y), wr(y), Rc, Lc, pp, Ltm, Nt);

%breaks loop when commutation angle goes beyond pi/3 rad
if d(i)==10
       delta(y)=d(i);
       disp('Delta has gone beyond pi/3');
       wrfail=wr(y)
       break;
end

%Calculates AC losses due to harmonics on through AC resistance
[Ploss(i) TorqueAve(i) TorqueHarm(i) CurHarmMag(i,:)
  PHarmLoss(i,:)] = FuncACLoss(Id(i),d(i),a(i), VdcAveComm(i),
  RLVPara, Rc, IdcMth(i),Nt,pp,k);

%recalculates Idc taking into account AC losses
Id(i+1) = (Pwind(y)-Ploss(i))/VdcAveComm(i);


%calculates the difference between present and previous values
  of Idc
deltaId(i+1)=Id(i)-Id(i+1);

%outputs data if error between past and present Id is less than
  0.000001
if abs(deltaId(i+1))<0.000001

    It(y)=i;
    Idc(y)=Id(i);
    VdcRectAverage(y)=VdcAveComm(i);
    VdcRect(y)=VdcAve(i);
```

```
    CurrentHarmMag(y,:)=CurHarmMag(i,:);
    alpha(y)=a(i);
    delta(y)=d(i);
    PLossAC(y)=Ploss(i);
    PlossHarm(y,:)= PHarmLoss(i,:);
    Idcmth(y)=IdcMth(i);
    Rv(y)=(VdcAve(i)-VdcAveComm(i))/Id(i);
    Vcomm(y)=(VdcAve(i)-VdcAveComm(i));
    TorqueAverage(y)=TorqueAve(i);
    TorqueHarmonic(y)=TorqueHarm(i);

    break;

 end
end

%breaks loop when commutation angle goes beyond pi/3 rad
 if delta(y) ==10
    delta(y)=pi/3;
    break;
 end

 %% Calculates final values of control characteristic

 %VdcPCC voltage [V]
 VdcPcc(y) = (VdcRectAverage(y) - 2  *Vfwd - Idc(y) * (2 * Rl2 +
   Rex + 2 * Ron));
 %Vdc control voltage [V]
 Vdccont(y) = VdcPcc(y)- (NoMach * Idc(y) * 2 * Rl1);

 %power loss due to mth harmonic on the DC side. [W]
 DcCurrentHarmPLossBranch(y) = (Idcmth(y) / sqrt(2))^2 * (2 * Rl2
   + Rex + 2 * Ron);
 %power loss due to mth harmonic on the DC side between the PCC
   and the converter. [W]
 DcCurrentHarmPLossCommon(y) = (NoMach * Idcmth(y) / sqrt(2))^2 *
   (2 * Rl1);

 %power loss on the branches between machines and PCC [W]
 PlossElecSysBranch(y) = (Idc(y)^2 * (2 * Rl2 + Rex + 2 * Ron) +
   DcCurrentHarmPLossBranch(y));
 %power loss on the branches between the PCC and the converter
   [W]
 PlossElecSysCommon(y) = ((NoMach * Idc(y))^2 * (2 * Rl1) +
   DcCurrentHarmPLossCommon(y)) ;

 %power output measured at the PCC [W]
 PoutPCC(y) = NoMach * (Pwind(y) - PLossAC(y) -
   PlossElecSysBranch(y));
 %power output measured at the cluster converter [W]
 PoutConv(y) = PoutPCC(y) - PlossElecSysCommon(y);

 %synchnronous speed derived from VdcPCC [rad/s]
 wsync(y) = VdcPcc(y) *pi/ (k * pp * 3 * sqrt(3));
 %slip
 slip(y) = (wsync(y) - wr(y)) / wsync(y);
```

```
    %Power Factor
    PowerFactor(y) = cos((delta(y)-alpha(y))/2);
    %Power transfer efficiency [%]
    Eff(y) = (PoutPCC(y)/Pwind(y))*100;

    %equivalent resistance between the PCC and the machine internal
      voltage [ohms]
    Requiv(y) = 2 * Rc + 2 * Rl2 + Rex + 2 * Ron + Rv(y);
    %voltage drop due to stator resistance and virtual resistance
      [V]
    Vmachdiff(y) = (3 * E(y) * sqrt(3) / pi) -  VdcRectAverage(y);
    %Generator torque
    GenTorque(y)=Pwind(y)/wr(y);

    %Winding current total harmonic distortion [%]

      CurrentTHD(y)=100*(CurrentHarmMag(y,5)+CurrentHarmMag(y,7))/(C
      urrentHarmMag(y,1));
    %Generator torque total harmonic distortion [%]
    TorqueTHD(y)=100*(TorqueHarmonic(y)/sqrt(2))/TorqueAverage(y);


end
```

VdcRectAve Function

```
function [a, delta, VdcAveComm, VdcAve]=VdcRectAve(Id, VacRect, wr,
Rc, Lc, pp, Ltm, Nt)

w=wr*pp;                  %electrical frequency

%angle range, increment dramatically affects computation time
wt=[0:pi/2000:2*pi/3];
save=0;
delta=10;   %initial delta value

%determines angle alpha at which commutation begins <0 when Rc is
present.
a=asin(Id*Rc/(sqrt(3)*VacRect))  ;

%% determines commutation length
% to determine the commutation time i3 is calculated and the end of
the commutation is the point where i3=Id, the commutation length is
% recorded in del(y);
for x=1:length(wt)

    %Calculation of i3 (incoming phase current)
    wt1=wt(x) ;
    alpha=-a;
    t(x)=wt1/w;

    %Constituent parts of incoming winding current (i3)
```

```
    i3a(x) = (((sqrt(3)*VacRect*w)/(2*Lc*((Rc/Lc)^2+w^2)))-
    (Id/2))*exp(-Rc*t(x)/Lc);
    i3aa(x) = -(sqrt(3)*VacRect*Rc*sin(alpha) /
            (2*(Lc^2)*(w^2+(Rc/Lc)^2)))*exp(-Rc*t(x)/Lc);
    i3b(x) = ((sqrt(3)*VacRect)/(2*Lc*((Rc/Lc)^2+w^2)) * (-
             w*cos(wt1)+(Rc/Lc)*sin(wt1)));
    i3c(x)=(sqrt(3)*VacRect/(2*Lc))*((Rc*sin(alpha)*cos(wt1) /
      (Lc*w^2+Lc*(Rc/Lc)^2)) + (sin(alpha)*sin(wt1)/w)-
      (Rc^2*sin(alpha)*sin(wt1)/(Lc*Lc*w*(w^2+(Rc/Lc)^2))));
    i3d(x)=Id/2;

    %summation of all i3 parts
    i3(x)=i3a(x)+ i3aa(x)+i3b(x)+i3c(x)+i3d(x);

    i1(x)=Id-i3(x);       %i1 = outgoing phase current through diode
                              1, fed from phase a.


      %waits for the point where i3 = Id, which signifies the end
      %of the commutation and records the angle at which it occurs.
    if i3(x)>Id && save == 0
       delta=wt(x)-a;
       %del(y)=delta;
       save=1;
    end
end


%% Calculates average voltage

%Area 1 contribution...equations are split into three parts for ease
of
%programmeing.
A1a= VacRect*(-sin(-a)/2)+(Id*Rc*a/2);
A1b=-VacRect*((sqrt(3)/2)-sin(-a+(pi/3)));
A1c=Id*Rc*a ;
A1=A1a+A1b+A1c;

%area 2 contribution

A2a= VacRect*(sin(a)/2)+(Id*Rc*a/2);
A2b=-VacRect*((sqrt(3)/2)+sin(a-(pi/3)));
A2c=Id*Rc*a;
A2=A2a+A2b+A2c;

%Area 3 contribution to Vdc from above
A3a=VacRect*(sin(delta-pi/3)-sin(a-pi/3))-(Id*Rc*delta-Id*Rc*a);
A3b=-VacRect*(sin(delta)-sin(a))/2 + (Id*Rc*delta/2) - (Id*Rc*a/2);
A3=A3a+A3b;

%overall average rectifier output voltage including the commutation
volt drop
VdcAveComm=(3*sqrt(3)*VacRect/pi)-2*Id*Rc+((A1+A2-A3)*3/pi);
%overall average rectifier output voltage without the commutation
volt drop
VdcAve=(3*sqrt(3)*VacRect/pi)-2*Id*Rc+(A1+A2)*3/pi;
```

FuncACLoss function

```
function [PlossTotal TorqueAve TorqueHarm CurrentMag1
PlossAC]=FuncACLoss(Idc, d, alpha, VdcAve, Rpara, Rc, IDCmth, Nt,
pp, k)
%calculates the anticipated power loss in the stator winding
resistance due
%to each of the current harmonics
%based around initial work in FourierTrapezoidal.m


m=6;        %harmonic order of the DC current harmonic.

%Voltage on the AC side of the rectifier
VaRect=VdcAve*pi*2/(3*sqrt(6)*(cos(alpha)+cos(d)));

for n=1:50

    a0=0;

    % coefficents taking into account early start to commutation,
      alpha=finite
    %calculates the an components
    a1(n)=2*Idc*(sin(n*d)+sin(n*alpha)) *
   (sin(2*pi*n/3)+sin(n*pi/3))/(pi*(d+alpha)*n^2);
    %calculates the bn components
    b1(n)=2*Idc*(cos(n*alpha) -
    cos(n*d))*(sin(n*pi/3)+sin(2*n*pi/3))/(pi*(d+alpha)*n^2);
    %contribution to b due to 6th DC harmonic current compomemt
    bmth(n)= (IDCmth/(pi*(m-n))*(sin((m-n)*pi/3) +
    sin((m-n)*(2*pi/3)))) -
    (IDCmth/(pi*(m+n))*(sin((m+n)*pi/3)+sin((m+n)*(2*pi/3))));
    %Dc current harmonic component when n=m, to avoid NAN appearing
     in results.
    bmth(m)= -(IDCmth/(pi*(m+n))*(sin((m+n)*pi/3) +
            sin((m+n)*(2*pi/3))));

    %calculates the phase of each harmonic component, based on the
      simplified maths.
    d21(n)=atan((cos(n*alpha)-cos(n*d))/(sin(n*d)+sin(n*alpha)));

    %calculates the phase of each harmonic component, using the an
      and bn components produced above.
    CurrentPhase1(n)=(atan(b1(n)/a1(n)));

    %calculates the magnitude of each harmonic component.
    CurrentMag1(n)=sqrt(a1(n)^2+(b1(n))^2);
    %calculates the magnitude of each harmonic component.
    CurrentMag2(n)=sqrt(a1(n)^2+(b1(n)-bmth(n))^2);

    %current reactive component
    Iim(n)=CurrentMag1(n)*sin(CurrentPhase1(n));
    %current active component
    Ire(n)=CurrentMag1(n)*cos(CurrentPhase1(n));
```

```
    if CurrentMag1(n)< 1e-2
        CurrentMag1(n)=0;
    end

end

%Average torque magnitude
TorqueAve=3*pp*k*a1(1)/2;
%Harmonic torque component magnitude
TorqueHarm=3*pp*k*sqrt((a1(5)+a1(7))^2+(b1(5)+b1(7))^2)/2;

b=b1-bmth;      %includes b components due to dc current harmonic,
                %subtracts to change the phase of the harmonic by
                   180deg

IarmsSq=(CurrentMag2/sqrt(2)).^2;          %current harmonic
magnitudes squared
PlossAC=(3*IarmsSq*Rc);                    %Power loss due to each
current harmonic


PlossPara=3*((VaRect/Nt)^2)/Rpara;         %power lost in the
parasitic resistance


Plossmach=sum(PlossAC);                      %total power lost in
                                                 generator
PlossTotal=Plossmach+PlossPara;              %Overall power loss
CurrentPhase1=CurrentPhase1*180/pi;          %converts current phase
                                                 from rad to deg
```

Appendix B Test Rig Additional Information

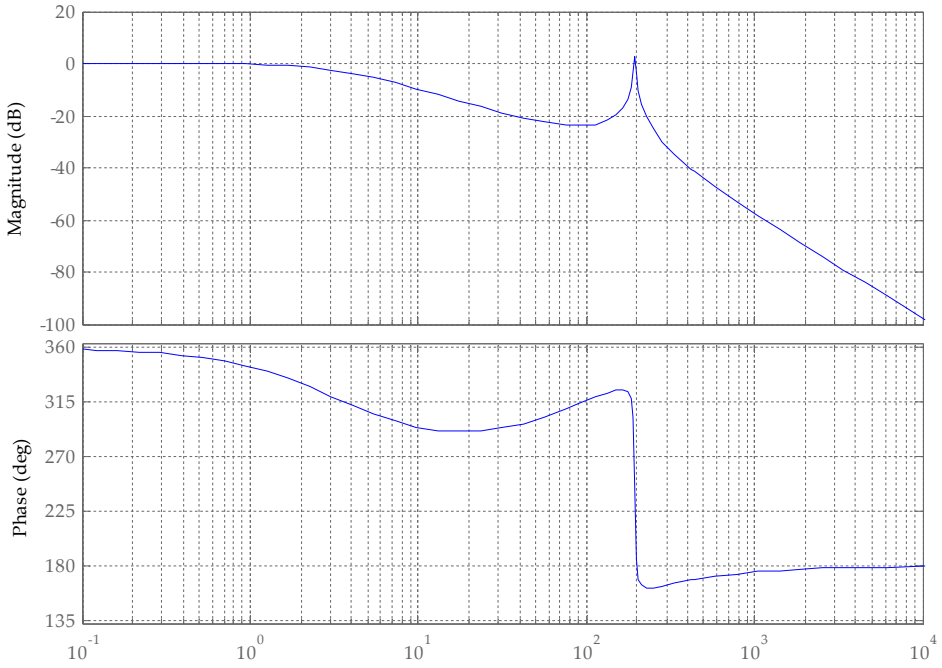

Figure B-1: Boost converter closed loop system bode plot.

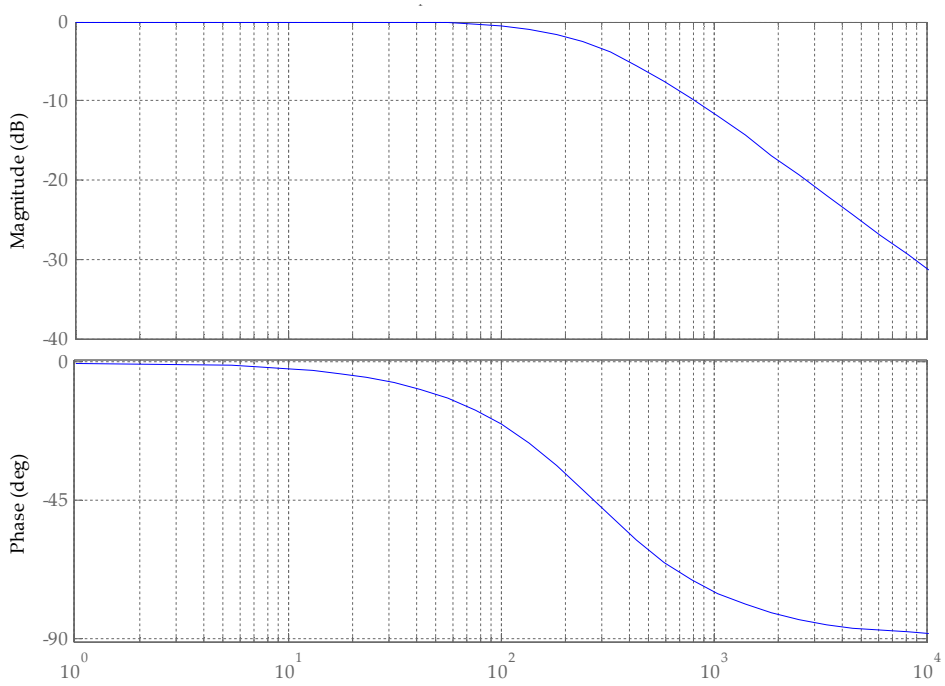

Figure B-2: Chopper converter closed loop system bode plot.

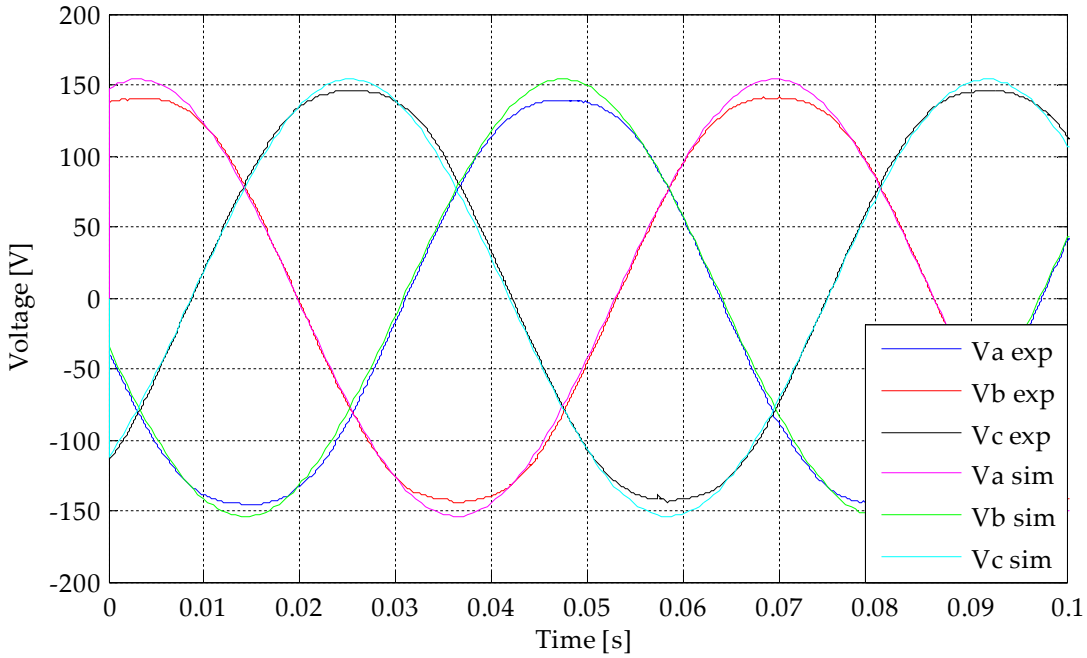

Figure B-3: Experimental and simulation generator emfs, measured when the generators are rotating at 23.66rad/s, demonstrating the effects of the imperfect distribution of the test rig generator stator windings.

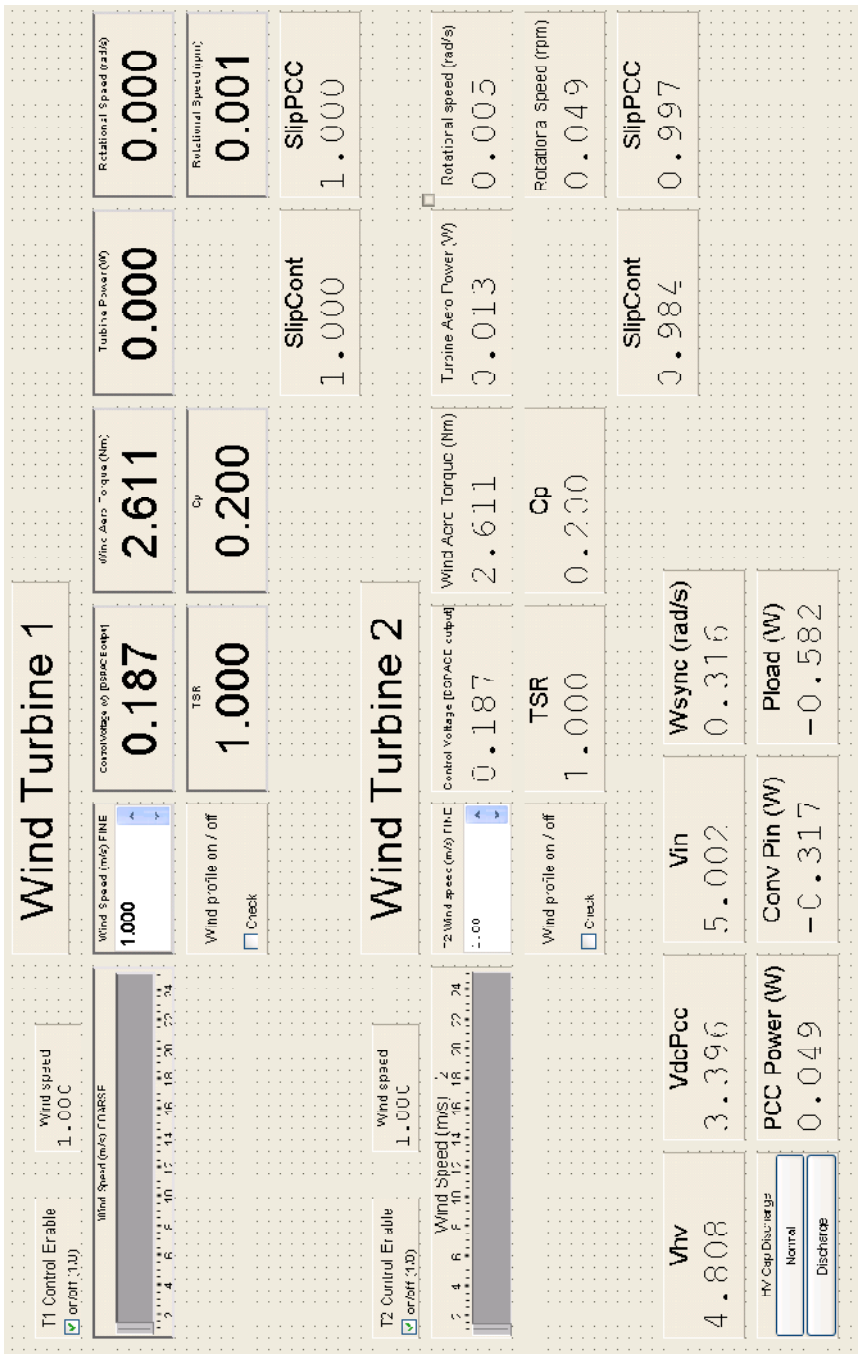

Figure B-4: Test-rig controller user interface, developed in dSPACE Controldesk for the operation of the system.

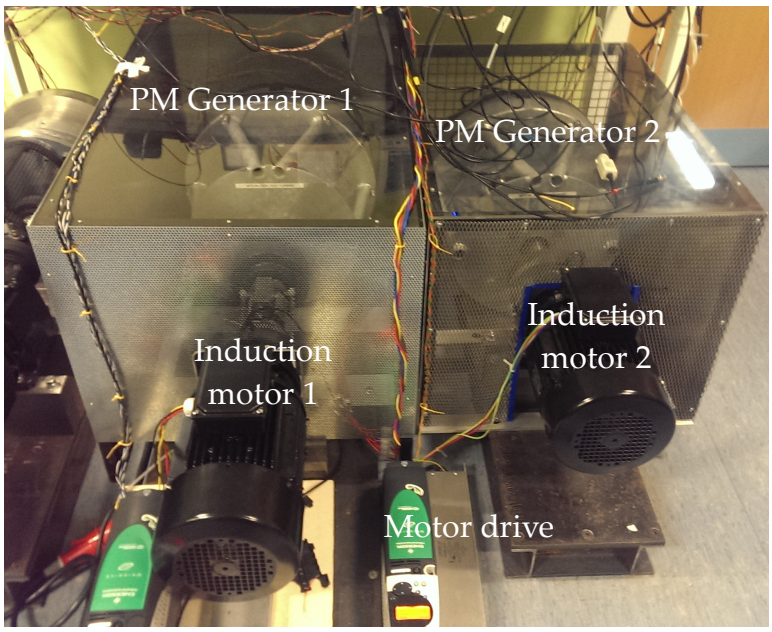

Figure B-5: Photograph of the 2.5kW PM generators driven by induction motors.

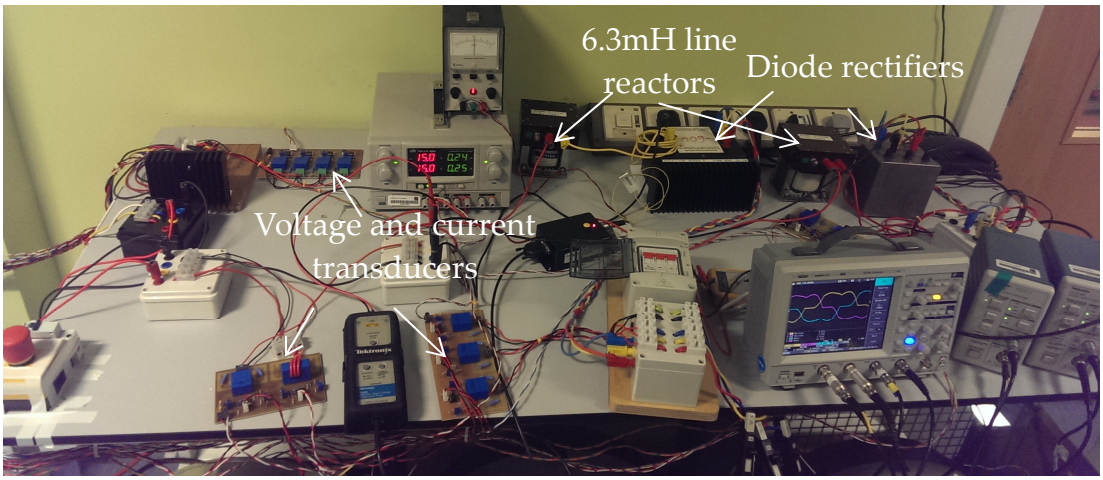

Figure B-6: Photograph showing the layout of the diode rectifiers with line reactors and voltage and current transducers.

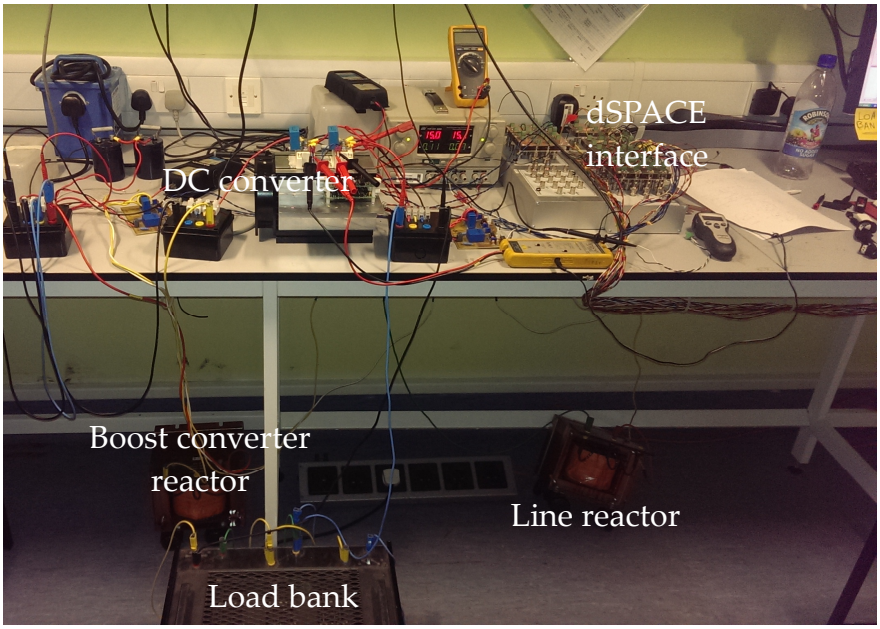

Figure B-7: Photograph showing the layout of the DC converter, reactors, load bank and dSPACE interface.